STUDIES ON TRANSITION METAL MACROCYCLIC COMPLEXES

by

Andrew J. Atkins

Ph.D Thesis

University of Edinburgh

1993

To my family

ACKNOWLEDGEMENTS

I would like to give my sincere thanks to Dr. Martin Schröder for all his help and thoughtful guidance during the course of this work. I am also very grateful to Drs. A.J.Blake and R.O.Gould for collecting the data for the X-ray structures in this thesis and for their invaluable advice in what to do with it. Many thanks to Drs. Martin Schröder and A.J.Blake for helping me assemble this work as well. I also wish to thank Drs. L.J.Yellowlees and R.E.P.Winpenny for helpful discussions on electrochemistry and e.s.r. spectroscopy respectively.

I would like to thank Drs. R.M.Potter and D.Thompson, from the Johnson-Matthey Technology Centre, for their input into this project and for their hospitality on visits to Sonning Common.

In addition I am indebted to the departmental analytical services, particularly Mr. J.R.A.Millar (for n.m.r.), Miss H.Grant (for n.m.r. and elemental analysis), Mr. A.T.Taylor (for mass spectral data), Miss E.Bell (for mass spectral data and elemental analysis) and to Mrs. E.MacDougall (elemental analysis).

I am extremely grateful to Dr. G.Reid, Dr A.Taylor and all other members of the "Schröder Group" for all their help, and who made Labs. 94 and 290 such enjoyable and good-humoured places to work.

I wish to acknowledge the S.E.R.C. and Johnson-Matthey p.l.c. for a CASE award and the latter for loans of platinum metals. I am also grateful to the University of Edinburgh for the use of their facilities.

Finally, many thanks to my family and friends who have supported and encouraged me throughout this period of studying, and whose contributions were particularly appreciated as the crises arose!

ABSTRACT

Chapter 1

An introduction to macrocyclic co-ordination chemistry and a discussion of the relevance of transition metal macrocycles and porphyrins to biological systems and catalysis is given. The general aims of the project are introduced.

Chapter 2

The co-ordination chemistry of the binucleating compartmental macrocycle 11,23-dimethyl-3,7,15,19-tetraazatricyclo[19.3.1.1^{9,13}] hexacosa-2,7,9,11,13(26),14,19,21(25),22,24-decaene-25,26-diol, ($\underline{1}H_2$), and its derivatives is reviewed with a discussion of synthetic routes to the complexes of ($\underline{1}H_2$). ($\underline{1}H_2$), ($C_{24}H_{28}N_4O_2$) is the Schiff-base product of the [2+2] condensation of 2,6-diformyl-4-methylphenol and 1,3-diaminopropane.

Chapter 3

The synthesis and characterisation of the protonated, metal-free macrocycle $[(\underline{1}H_4)]^{2+}$ as PF_6^- and BF_4^- salts are described. The single crystal structure of $[(\underline{1}H_4)](PF_6)_2$ reveals folding of the macrocycle in the uncomplexed state, to give extensive inter- and intra-molecular π-π interactions. Acidic protons were located on the four imino N-atoms and the zwitterionic nature of the molecule is reflected in the C-O$^-$ and C=NH$^+$- bond lengths [C-O = 1.278-1.284; C=N = 1.279-1.304Å]. The free ligand ($\underline{1}H_2$) was also synthesized but attempts to reduce $[(\underline{1}H_4)]^{2+}$ or isolate the dianion $(\underline{1})^{2-}$ were unsuccessful. The syntheses and characterisations of $[(\underline{2}H_4)]^{2+}$ and $[(\underline{5}H_4)]^{2+}$ (where ($\underline{2}H_2$) and ($\underline{5}H_2$) are the cyclic products of the condensation of 2,6-diformyl-4-methylphenol with 1,2-diaminoethane and 1,4-diaminobutane respectively) are also described and contrasted with

$[(\underline{1}H_4)]^{2+}$.

Chapter 4

The reaction of $[(\underline{1}H_4)](BF_4)_2$ with $[Ni(H_2O)_6](BF_4)_2$ in CH_3CN gives $[Ni_2(\underline{1})(CH_3CN)_4](BF_4)_2$. The single crystal structure of $[Ni_2(\underline{1})(CH_3CN)_4](BF_4)_2$ shows the incorporation of two octahedral Ni(II) centres within the planar macrocycle [Ni–Ni = 3.1355(8); Ni–O = 2.025–2.030; Ni–N = 2.015–2.024Å] and axial interactions with two CH_3CN ligands per Ni(II) centre [Ni–N = 2.122–2.143Å]. The reaction of $Ni(CH_3CO_2)_2$ with $[(\underline{1}H_4)](PF_6)_2$ in CH_3CN gives $[Ni_2(\underline{1})(CH_3CO_2)](PF_6)$ which dimerises in the solid state to give a Ni_4O_4 cubane-type structure (Ni–Ni = 3.0240–3.229; Ni–O = 2.031–2.168; Ni–N = 2.014–2.028Å). The two $(\underline{1})^{2-}$ macrocycles in $[Ni_2(\underline{1})(CH_3CO_2)]_2(PF_6)_2$ are slightly folded in order to avoid steric interactions with each other across the cube. Cyclic voltammetry of this compound reveals three reversible oxidations ($E_{\frac{1}{2}}$ = +0.81, +0.95, +1.15V) and two irreversible reductions (E_{pc} = −1.55, −1.89V, $0.20Vs^{-1}$, *vs.* Fc/Fc^+). The second oxidative process belongs to the daughter product of the first oxidation, which is consistent with an ECE mechanism. $[Pd(CH_3CO_2)_2]_3$ reacts with $[(\underline{1}H_4)](BF_4)_2$ to give $[Pd_2(\underline{1})](BF_4)_2$. The single crystal structure shows co-ordination of two square-planar Pd(II) ions in the planar macrocycle [Pd–Pd = 3.1514(6); Pd–O = 2.015–2.016; Pd–N = 1.979–1.993Å]. Reactions of Pt(II), Rh(III) and Rh(I) with $[(\underline{1}H_4)]^{2+}$ afford mixtures of products, including mononuclear and degraded ligand species.

Chapter 5

The reaction of 2,6-diformyl-4-methylphenol with $(CH_3)_2NCSCl$ in DMF followed by pyrolysis and NaOH hydrolysis gives 2,6-diformyl-4-methylthiophenol. The reaction of this with

1,3-diaminopropane and $Ni(CH_3CO_2)_2$ in CH_3CN yields $[Ni_2(\underline{22})]^{2+}$, where ($\underline{22}H_2$) is the thiophenol analogue of ($\underline{1}H_2$). The single crystal structure of $[Ni_2(\underline{22})](PF_6)_2.2DMF$ shows co-ordination of two distorted square-planar Ni(II) ions in a partially folded macrocycle [Ni-Ni = 3.163(4); Ni-S = 2.171-2.181; Ni-N = 1.906-1.927Å]. Cyclic voltammetry of $[Ni_2(\underline{22})]^{2+}$ shows one reversible oxidation ($E_{\frac{1}{2}}$ = +0.51V) and two reversible reductions ($E_{\frac{1}{2}}$ = -1.09, -1.58V *vs.* Fc/Fc^+). The structural and electrochemical properties of the Ni(II) complexes of $(\underline{1})^{2-}$ and $(\underline{22})^{2-}$ are discussed and contrasted.

Chapter 6

A study of the structures of $[Fe([9]aneS_3)_2]^{2+}$ (Fe-S = 2.2520-2.2657Å) and $[Fe([9]aneS_3)_2]^{3+}$ (Fe-S = 2.276-2.2846Å) provides good evidence for the π-acceptor properties of thioether ligands. Single crystal X-ray structures of $[Co([9]aneS_3)_2](BF_4)_2$ and $[Co([9]aneS_3)_2](PF_6)_2$ reveal a Jahn-Teller elongation and compression respectively and solid-state e.s.r. experiments are described which attempted to discover whether this deviation is due to a variation in temperature or counterion. The half-sandwich compound $[Fe([9]aneS_3)(dppv)Cl]^+$ was prepared from the reaction of $[Fe([9]aneS_3)Cl_3]$, $TlPF_6$ and dppv in CH_3NO_2. $[Fe([9]aneS_3)(CH_3CN)_3]^{2+}$ was also synthesized but is rapidly hydrolysed in air. Attempts to synthesize other half-sandwich complexes from $[Fe([9]aneS_3)(CH_3CN)_3]^{2+}$ by substitution of CH_3CN with other P-, N- and O-donor ligands were unsuccessful and gave $[Fe([9]aneS_3)_2]^{2+}$ as the product. Some reasons for the preferential formation of this compound are discussed.The synthesis of $[Co([9]aneS_3)(dppe)]^{2+}$ is described and an electrochemical study shows a reversible oxidation ($E_{\frac{1}{2}}$ = +0.09V) and reduction ($E_{\frac{1}{2}}$ = -0.71V *vs.*Fc/Fc^+) (assigned as Co(II)/Co(III) and Co(II)/Co(I) species respectively from *in situ* U.V. spectroscopy).

Chapter 7

The reaction of $[Fe(CH_3CN)_6]^{2+}$ with S_4 ligands (S_4 = [12]aneS_4, [14]aneS_4 and [16]aneS_4) in CH_3NO_2 gives readily hydrolysable $[Fe(S_4)(CH_3CN)_2]^{2+}$ species. Air-stable solid products $[Fe([12]aneS_4)(P-P)]^{2+}$ are obtained on reaction of $[Fe([12]aneS_4)(CH_3CN)_2]^{2+}$ with (P-P) ligands (P-P = dppe, dppm, dppv). A reversible oxidation ($E_{\frac{1}{2}}$ = +0.80→ +0.92V) and reduction ($E_{\frac{1}{2}}$ = −1.23→ −1.28V *vs.* Fc/Fc^+) are observed for all three $[Fe([12]aneS_4)(P-P)]^{2+}$ species, except for an irreversible reduction for $[Fe([12]aneS_4)(dppm)]^{2+}$ (E_{pc} = −1.36V). Insoluble $[Fe([18]aneS_6)]^{2+}$ and $[Fe([15]aneS_5)]^{2+}$ products were also prepared. The decomposition product of solvated $[Fe([12]aneS_4)(dppe)]^{2+}$, $[Fe(dppe)_2(CH_3CN)_2]^{2+}$, was characterised by X-ray crystallography.

TABLE OF CONTENTS

LIST OF FIGURES AND TABLES

CHAPTER 1

An Introduction to Macrocyclic Chemistry

1.1: Introduction

Macrocyclic complexes of transition metals have been the focus of a considerable amount of research in recent years[1-7]. This fact is a reflection of the important reactivities shown by the co-ordinated metal centres and also the relative kinetic inertness and thermodynamic stability of the metal-macrocycle unit. Macrocyclic complexes have therefore been used as models for metalloproteins[8-11] and as catalysts in their own right[12-15]. The functional properties of these compounds rely on the ability of macrocyclic complexes to stabilise unusual oxidation states of the metal centres, while restricting the labile co-ordination sites to specific environments[16]. This activity is characterised by the naturally occuring macrocycles based on the porphyrins.

The biological role of the porphyrin complexes includes the binding and activation of small substrate molecules at the axial sites of the metal centre e.g. O_2 transport with Fe-containing haemoglobin[17,18], or as electron carriers e.g. in cytochrome *c*[17,19]. Derivatives of porphyrin complexes also found in nature include Mg-containing chlorophyll[17,20,21] and Co-containing vitamin B_{12}[17,22,23] (See Figures 1.1-1.3). The porphyrin can occupy all the equatorial sites at the metal centre and is also able to tune the reactivity of the metal by its electronic and steric properties. For example, deoxyhaemoglobin contains a high spin Fe(II) ion bound in a square-pyramidal geometry to four porphyrin N-donors and an axially bonded imidazole ligand from histidine residue F8 from the protein backbone (Figure 1.4a)[17,18]. The high spin Fe(II) metal centre is too large to be bound in the plane of the porphyrin ring. On reacting with O_2, it is proposed that the Fe(II) centre is oxidised to Fe(III) and adopts a low spin state with an accompanying decrease in metal ion size[17,24]. The metal ion can then be incorporated within the equatorial plane of the porphyrin to give

a superoxo octahedral complex (Figure 1.4b). So in this case, the porphyrin dictates the site and nature of O_2 binding and the co-ordination geometries of the resulting Fe complexes. The binding of O_2 and peroxides at the vacant sites of Fe-porphyrin units also occurs in the functioning of the myoglobin, cytochrome oxidase, cytochrome P-450, catalase and peroxidase enzymes[17].

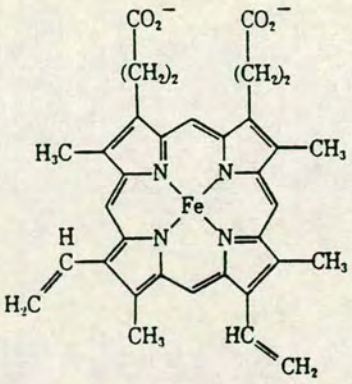

Figure 1.1 Porphyrin complex in Haemoglobin

Figure 1.2 Chlorin complex in Chlorophyll

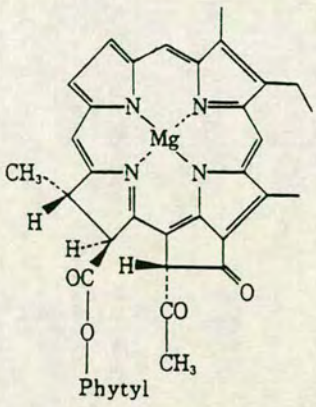

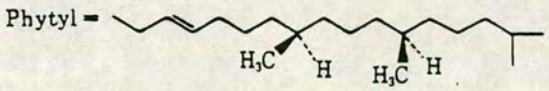

Figure 1.4 Proposed mechanism for O_2 binding in Haemoglobin

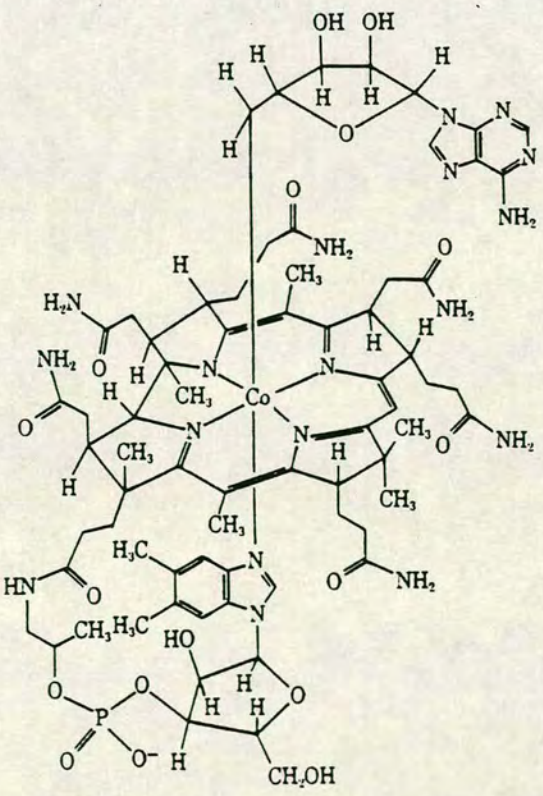

Figure 1.3 Corrin complex in Vitamin B_{12}

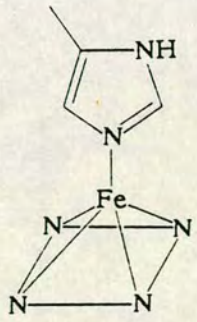

a) Deoxyhaemoglobin

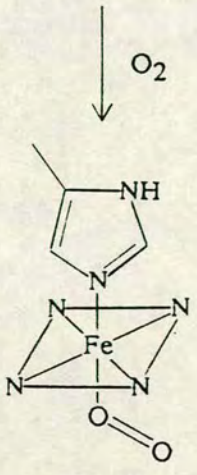

b) Oxyhaemoglobin

1.2: The Macrocyclic Effect

The most important feature of the porphyrin is its ring structure and this determines its kinetic inertness and thermodynamic stability that is attributed to the "macrocyclic effect". This term was first used by Margerum and Cabbiness[25] in their study of Cu(II) complexes with linear and macrocyclic tetramine ligands. They found that the macrocyclic Cu(II) complex of $Me_6[14]aneN_4$ had a stability constant that was 10^4 times greater than that of a linear analogue, 2,3,2-tet[25].

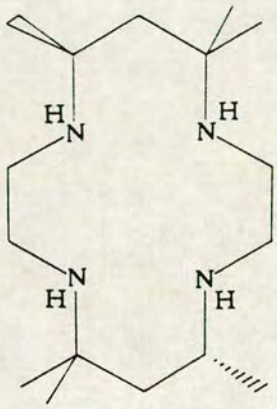

$Me_6[14]aneN_4$

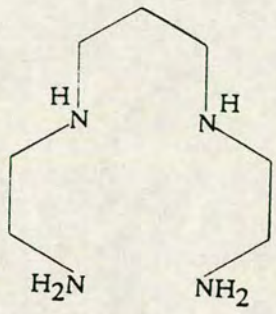

2,3,2-tet

The kinetic contribution to the macrocyclic effect is derived from the observation that macrocyclic complexes have relatively slow rates of formation and even slower rates of dissociation[26]. So for a reaction at equilibrium the stability constant is given by $K = k_f/k_d$, and a decrease of the dissociation rate, k_d, will raise the stability constant, K.

$$M_{(solv)} + L_{(solv)} \underset{k_d}{\overset{k_f}{\rightleftarrows}} ML_{(solv)}$$

The cause of the lowering of the rates of dissociation can be visualised as the difficulty in distorting the macrocyclic ring so that a metal-donor bond may dissociate (See Figure 1.5)[27]. For an acyclic system, such unfavourable strain for the sequential dissociation of the donor atoms does not occur.

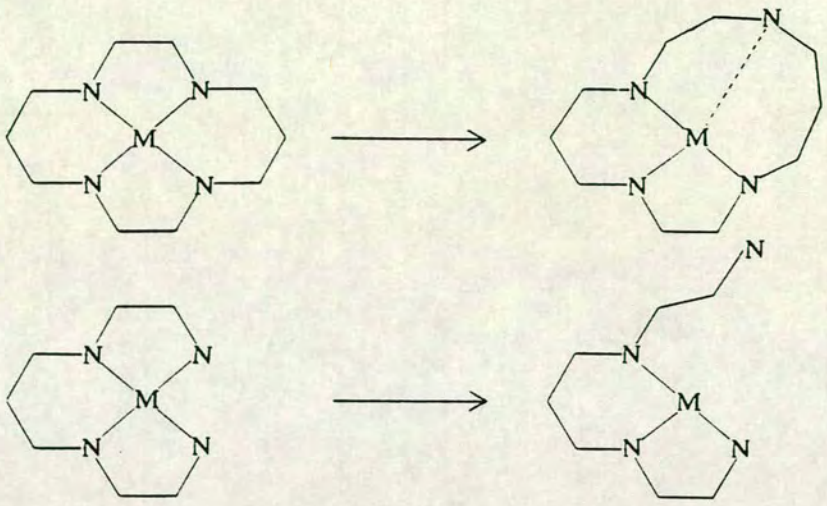

Figure 1.5 Comparison of the mechanisms of dissociation for macrocyclic and acyclic systems

The thermodynamic "macrocyclic effect" arises from the free energy gain ($\Delta G = \Delta H - T\Delta S$) for the metathesis reaction below:

$$L_{mac(solv)} + ML_{lin(solv)} \rightleftharpoons ML_{mac(solv)} + L_{lin(solv)}$$

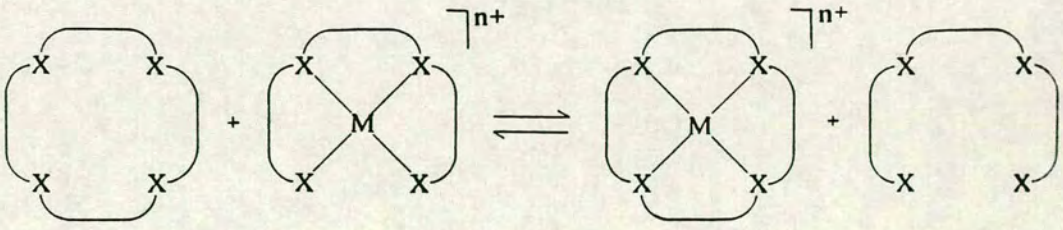

The dominant contributions to the energy gain can be from either the enthalpic or entropic term, depending on the system in question. For example, Margerum and Cabbiness[25], in their work on complexes of Cu(II) with tetramines, reported the macrocyclic effect to be primarily enthalpic in nature but Paoletti and others[28] have found that in complexes of Cu(II) with other polyamines the effect is dominated by entropic considerations. Recently,

Hancock and Martell[29] made a general conclusion that, provided there is no serious mismatch between the size of the metal ion and the macrocyclic cavity, there will always be a substantial contribution from enthalpy to the macrocyclic effect, with entropy sometimes contributing but usually to a lesser extent. To quantify the macrocyclic effect for specific systems however, the contributions from the enthalpic and entropic terms for each system have to be determined experimentally.

By considering the metal–ligand interactions as purely electrostatic, the various components of the ΔH and ΔS terms in the above reaction can be considered independently[30]. The entropic components include changes in solvation entropy of the cation and ligands, changes in the ligand internal entropy and changes in the translational entropy of the system. In particular, a significant entropic contribution to the macrocyclic effect is expected from an increase in the number of degrees of freedom on release of the linear ligand from complexation in the metathesis reaction. In a metal–free macrocyclic ligand there are considerably fewer internal degrees of freedom compared to an open–chain ligand. Therefore the entropy term in the free energy equation $\Delta G = \Delta H - T\Delta S$ is usually favourable.

The enthalpic term comprises of changes in solvation of the metal and ligands, interactions of some or all of the donor atoms of the ligand with the metal centre, repulsion effects between neighbouring atoms (including solvent molecules) and conformational changes of the ligand on complexation. For the first of these, Margerum and Hinz recognised that the acyclic ligand 2,3,2–tet had a greater solvation energy in H_2O than the macrocycle Me_6[14]aneN_4. Therefore the forward reaction of the above metathesis reaction had a favourable enthalpic term because of the release of the acyclic ligand into solution[31,32]. The enthalpic macrocyclic effect is not just dependent on solvation energies however, since large contributions have been found in

solvents of low dielectric constant too[29]. In these solvents, there can be an enthalpy gain on complexation due to the effective relief of dipole–dipole repulsions within the macrocycle[29,33]. Linear analogues do not experience the same dipole–dipole repulsions in the metal–free state, but can suffer larger increases in strain energy on complexation[34]. In such cases as these, a larger enthalpy gain is usually observed on complexation for the macrocycles than for open–chain analogues. However, the enthalpic basis for the macrocyclic effect is still subject to debate and is complicated by the varying significance of the contributing factors in different systems.

There have been recent reports of attempts to study the macrocyclic effect in the gas–phase, in order to investigate the intrinsic reactivities of macrocyclic ligands in the absence of solvent effects[35]. A strong macrocyclic effect has been observed on complexation of the alkali metals with the macrocyclic ligands [12]aneO_4 and [15]aneO_5 in comparison to their acyclic counterparts[35] and this is clearly an area for future development.

1.3: Pre–organisation in Macrocycles

Both the kinetic and thermodynamic properties of macrocyclic compounds can be influenced by any ligand conformation changes required for metal ion complexation. In particular, ligands requiring re–arrangement to bind with full donacity to a metal centre may suffer an increase in strain energy and hence show a diminished macrocyclic effect. Such ligands include [14]aneS_4[36]. [14]aneS_4 as a metal–free ligand adopts an *exo* conformation[36] and requires a stereochemical change to an *endo* conformation to bind a metal centre within the macrocyclic cavity (Figure 1.6). The *exo* conformation of [14]aneS_4 has been found to exist on complexation to certain metal centres, in $[Cl_2Hg([14]aneS_4)HgCl_2]$[37] and $[Cl_5Nb([14]aneS_4)NbCl_5$[38].

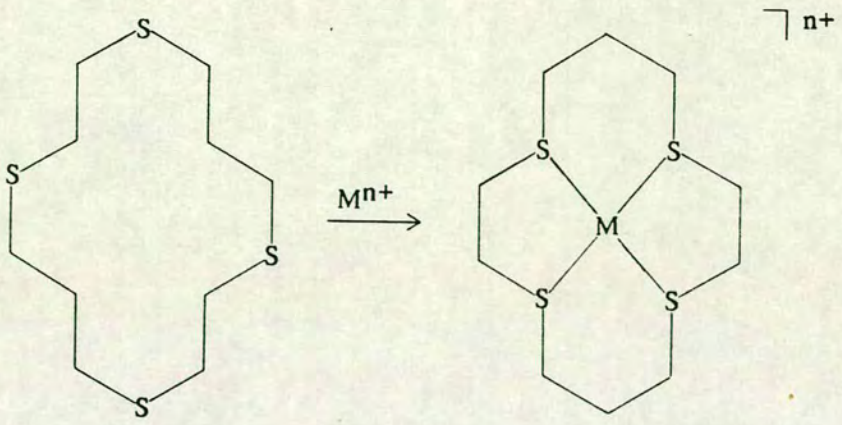

Figure 1.6 Re-organisation of [14]aneS_4 on co-ordination

Other macrocycles are considered pre-organised to co-ordinate to a metal centre. These ligands include the porphyrins and TAAB[27], which is shown in Figure 1.7. The metal-free ligands are constrained by unsaturation to the conformations observed in metal complexes of the ligand.

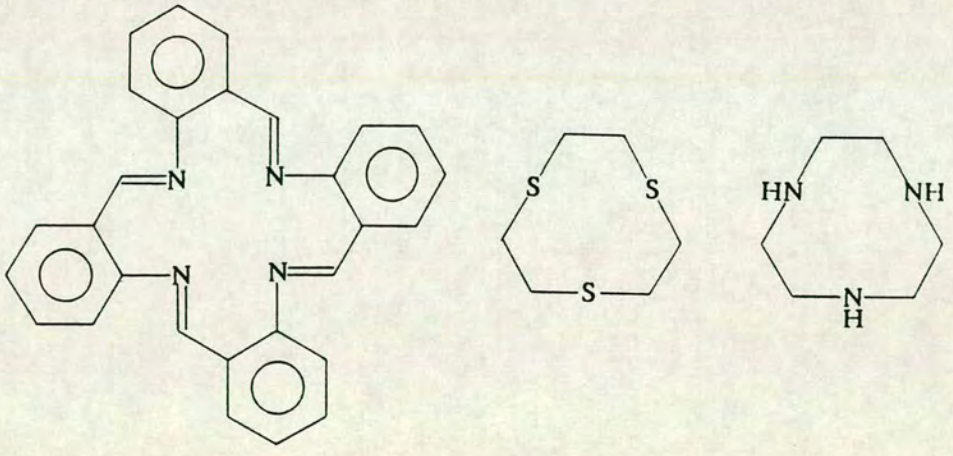

Figure 1.7 Ligands TAAB, [9]aneS_3 and [9]aneN_3

Pre-organisation for complexation is also observed in saturated small-ring macrocycles such as [9]aneS_3 and [9]aneN_3 (Figure 1.7). These are pre-organised to cap a face of a metal in an octahedral geometry as is shown in the single crystal X-ray structures (Figure 1.8) of the free ligand of [9]aneS_3[39] and a complex of [9]aneS_3, $[Fe([9]aneS_3)_2]^{2+}$ (see Section 6.2.2). The metal-free ligand is in an *endo* conformation, so that the lone pairs of

the S–donor atoms are directed to a point below the centre of the ring, which would be occupied by a metal centre on complexation.

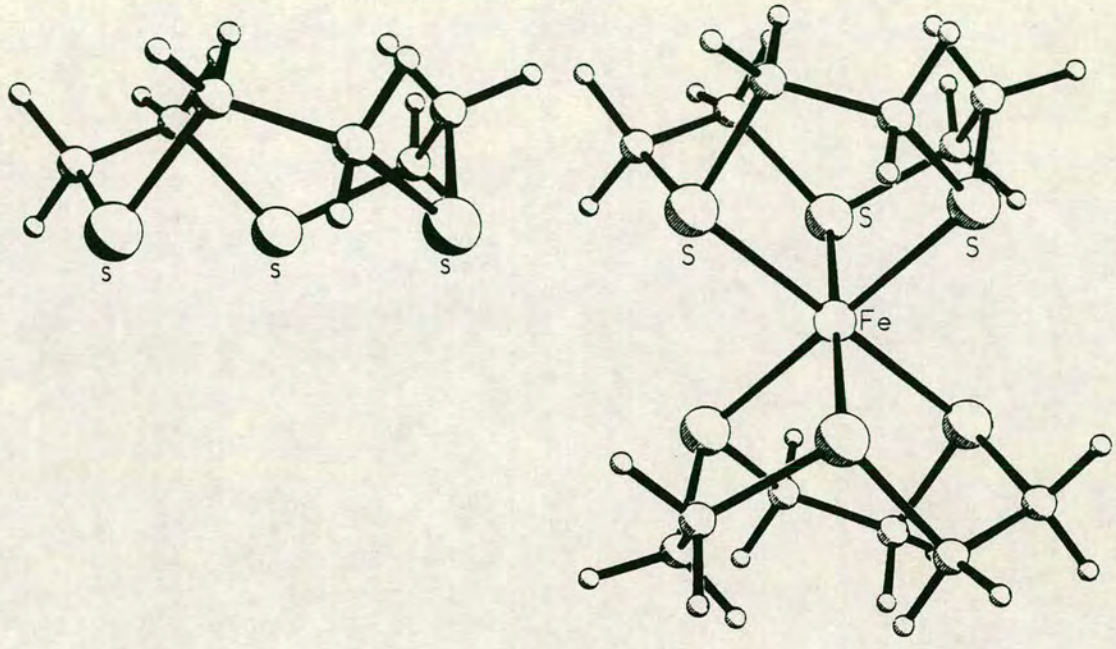

Figure 1.8 [9]aneS_3 and $[Fe([9]aneS_3)_2]^{2+}$

In the majority of work described in this thesis, we describe macrocycles that have well–defined stereochemical requirements, due to unsaturation and pre–organisation. In Chapter 7, complexes that show a high kinetic lability due to ligand flexibility, poor donacity and a mismatch of metal/ligand size will also be discussed.

1.4: Metal Complexes in Biological Systems

Transition metals are known to play a vital role in certain *in vivo* processes. The functions performed by metalloproteins include O_2 transport, electron transfer, acid/base catalysis, O_2 and N_2 reduction, detoxification and photosynthesis[17]. For these diverse tasks a number of elements have been used (particularly Mo, Mn, Fe, Ni, Cu and Zn) and also a variety of

co-ordination spheres. In addition to the macrocyclic porphyrin compounds already mentioned in Section 1.1, transition metals have been found co-ordinated directly to the amino-acid side chains within the protein structures. For enzymatic activity, the metal environments are typified by entatic (strained) states, so that the distortions in the preferred geometries of the metal ions lower the activation energies for the reaction pathways[40]. Examples of this phenomenon are given by the "blue-copper" proteins which have been characterised by an intense absorption in the visible spectrum near 600nm. which gives them their dramatic blue appearance[41,42]. This arises from a L → M charge transfer band from a cysteine (S^-) ligand to a Cu(II) centre which is in a very distorted tetrahedral N_2S_2 environment (Figure 1.9)[43]. "Blue-copper" proteins function in nature as oxidases and electron carriers[17].

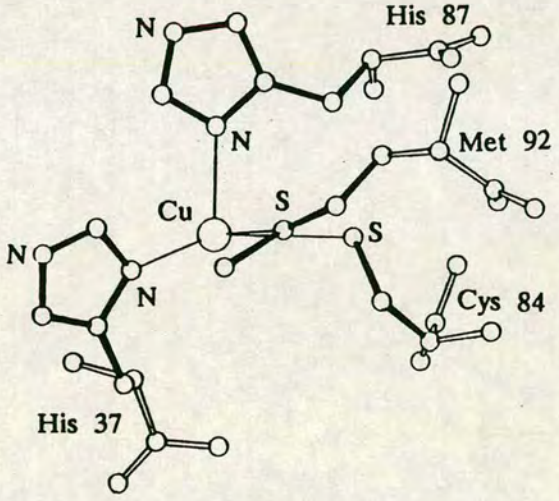

Figure 1.9 The Cu site in a "blue-copper" protein

The regulation of the stereochemical environment, the imposition of a well-defined donor set and the labilisation of specific sites on the metal centre are common features to both macrocyclic and bio-inorganic chemistry. Therefore macrocyclic complexes have been used extensively as models for the active sites of metalloproteins[8-11,44-50], whose detailed function or structure may be extremely difficult to elucidate. This expanding field of

research has been called "biomimicry" because it attempts to reproduce the behaviour of metalloproteins by metal complexes that can be prepared in the laboratory. Examples of functional models for O_2 binding by haemoglobin include the variety of "picket-fence"[51], "tailed picket-fence"[52,53], "strapped"[54], "capped"[55,56] and "pocket"[57] porphyrins (Figure 1.10). These have been designed to prevent the irreversible dimerisation process that usually occurs when a free iron-porphyrin complex combines with O_2. In biology this problem is avoided by the location of the active haem site in a cleft in the bulk of the protein.

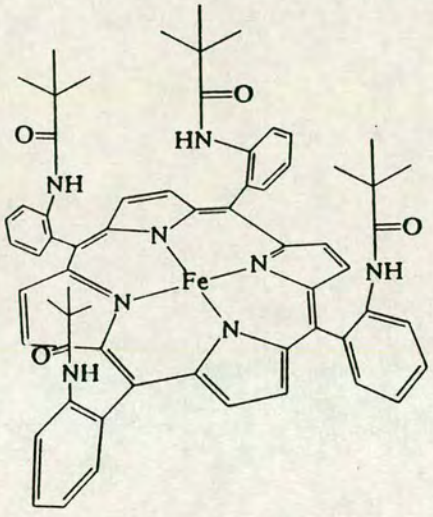

"picket-fence" porphyrin

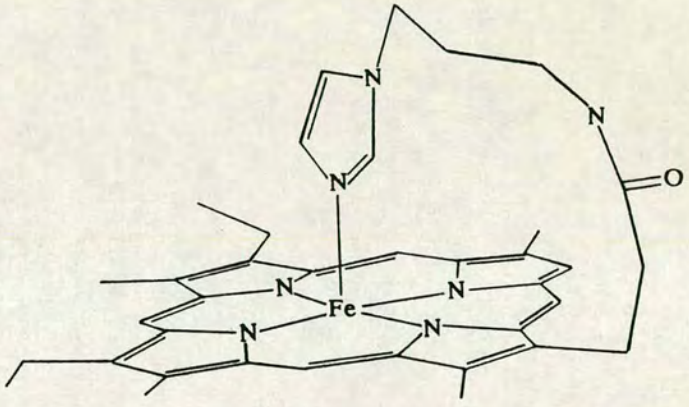

"strapped" porphyrin

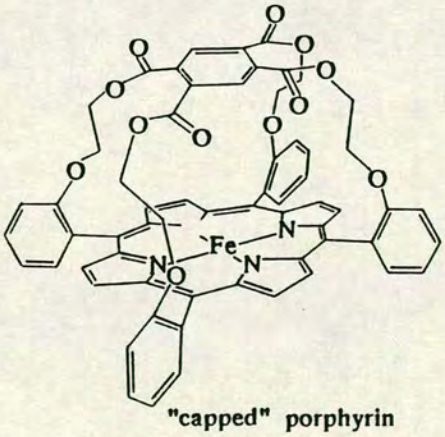

"capped" porphyrin

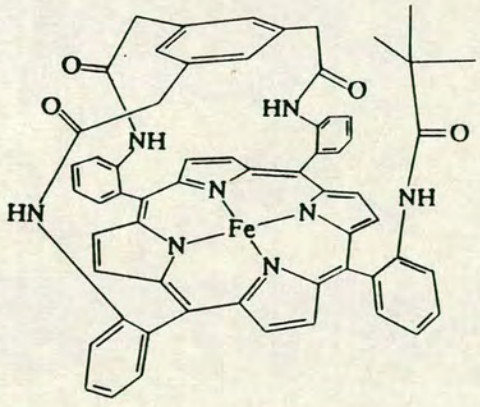

"picket pocket" porphyrin

Figure 1.10 Synthetic porphryins designed for reversible O_2 binding

Macrocyclic compounds have also been used to model non-porphyrinoid metalloproteins e.g. haemocyanin[11,58] and haemerythrin[59,60], which contain

two atoms of Cu and Fe per subunit respectively. Two macrocyclic compounds which attempt to mimic the behaviour of these O_2 carriers are shown in Figure 1.11[49,50].

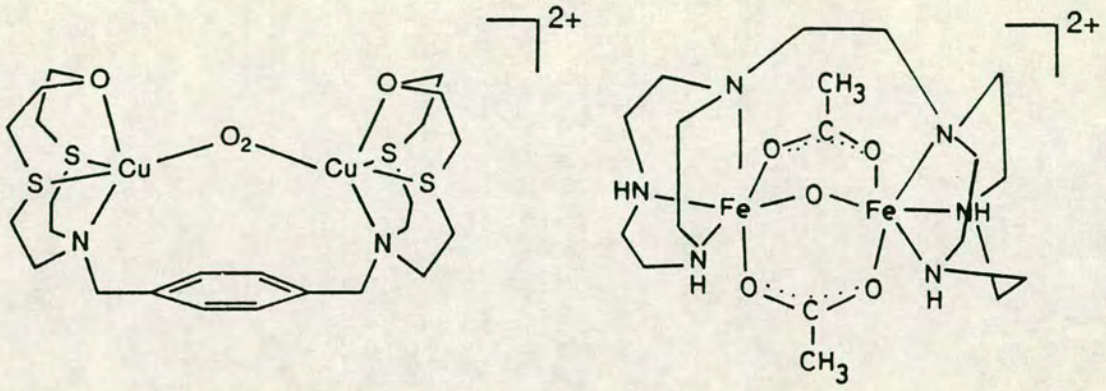

Figure 1.11 Models for haemocyanin[49] and haemerythrin[50]

Kimura *et al.*[61] have recently reported the macrocyclic complex $[Zn([12]aneN_3)(OH)]^+$ as a model for carbonic anhydrase (Figure 1.12). This model has a similar pK_a value to the natural Zn metalloprotein[62] and can reproduce the reversible hydration of CO_2, $CH_3CO_2CH_3$ hydrolysis and CH_3COH hydration behaviour of the enzyme[63]. The structural features of $[Zn([12]aneN_3)(OH)]^+$ also resemble the active site of carbonic anhydrase[64]. $[Zn([12]aneN_3)(OH)]^+$ can also model the function of phosphate esterases[65].

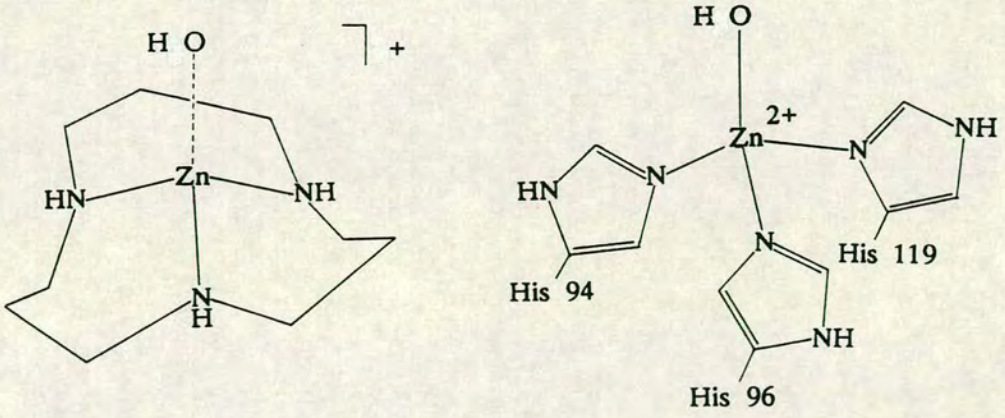

Figure 1.12 $[Zn([12]aneN_3)(OH)]^+$ and the active site of carbonic anhydrase

1.5: Macrocyclic Complexes in Catalysis

Macrocyclic complexes have the ability to stabilise unusual oxidation states at the co-ordinated metal centres[8,16]. This is a result of the increased thermodynamic stability of the metal-macrocycle unit and the restriction on the location and number of the labile sites at the metal centre. Decomposition or disproportionation routes to more common oxidation states may be therefore prevented or retarded. This property of macrocyclic compounds is appropriate for use as electrocatalysts and a range of macrocyclic compounds have been studied for potential activity in the activation of small substrate molecules such as CO_2[66-72], H_2[73-78], N_2O[79], N_2[80-84] and O_2[13-15,85-94].

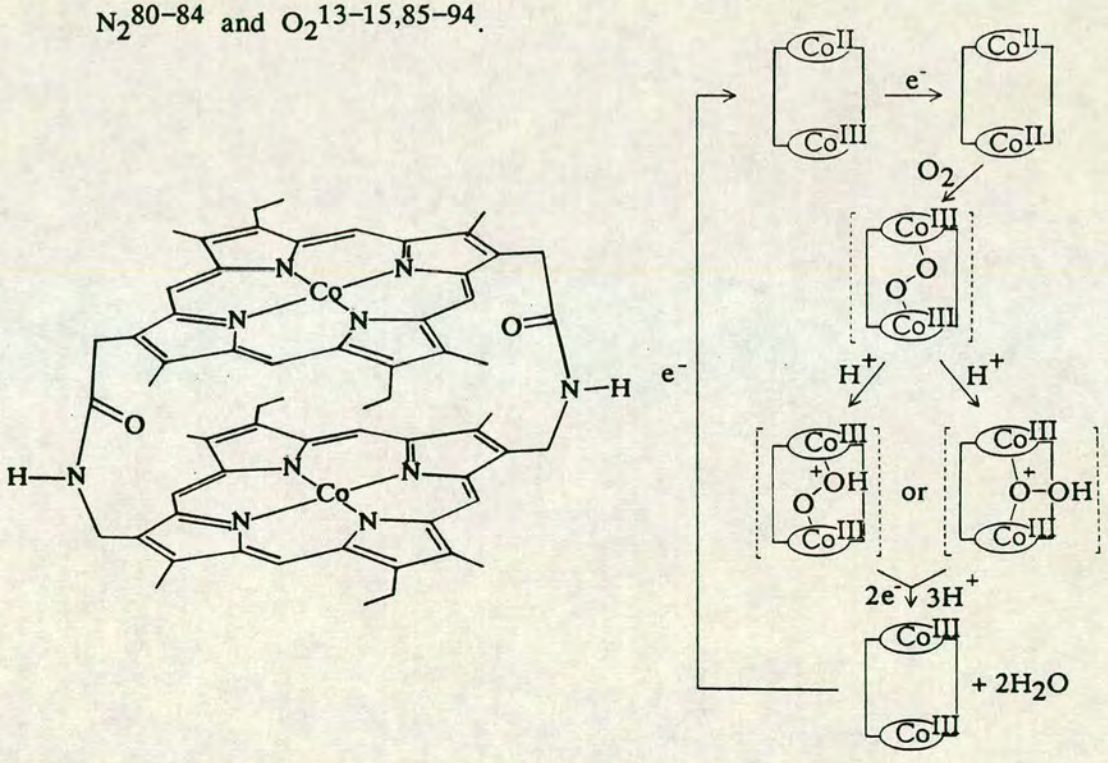

Figure 1.13 A cofacial [Co_2(diporphyrin)] and the proposed mechanism for O_2 reduction

The direct, four-electron reduction of O_2 to H_2O at unusually positive potentials has been achieved by a few macrocyclic electrocatalysts, which have potential application in fuel cell technology[14]. One of the successful systems, the cofacial [Co_2(diporphyrin)] [86] shown in Figure 1.13, uses two adjacent

metal centres to deliver sufficient electrons to produce the reduction step. The proposed mechanism for the four-electron reduction of O_2 is also shown in Figure 1.13[86]. A study of the importance of the metal-metal distance between the cofacial porphyrins for O_2 reduction has recently been reported[92].

A particular problem in the reduction of O_2 is to avoid the simpler two-electron reduction step to H_2O_2. This is undesirable since the peroxide species is a reactive product, causing degeneration of the catalyst and also the energy gain in this reduction process is much smaller. A novel method to overcome this has been reported by Shi and Anson[93], by the co-ordination of four $[Ru(NH_3)_5]^{2+}$ units to a monomeric Co(II) tetrakis(4-pyridyl)porphyrin. The four-electron reduction of O_2 is then accomplished by the rapid intramolecular transfer of electrons from the Ru(II) centres to O_2 molecules co-ordinated to the Co(II) centre. Lever *et al.*[94] have also recently reported a robust monomeric Co porphyrin complex which is resistant to H_2O_2 and can sequentially reduce O_2 to H_2O by two two-electron steps.

Saturated tetra-aza macrocyclic complexes with Ni and Co have been used to reduce CO_2 in H_2O to CO at accessible potentials[66,68,69,72]. With $[Ni([14]aneN_4)]^{2+}$, the reduction of CO_2 to CO occurs to the exclusion of the more common reduction of H_2O to H_2[68,69].

Another reaction of fundamental importance is the binding and activation of N_2[80-84]. The six-electron reduction of N_2 to NH_3 in a catalytic cycle has yet to be achieved, but Collman and co-workers[83,84] have reported the sequential oxidation of NH_3 to N_2, in a "retro N_2 fixation" process, using a cofacial [Ru_2 bis(porphyrin)]. This is shown in Figure 1.14 as a complex with N_2 but all the other intermediates (the N_2H_2, N_2H_4 and $2NH_3$ complexes) in the oxidation process have also been isolated and characterised[83,84]. The [Ru_2 bis(porphyrin)] unit can also bind H_2[77,78].

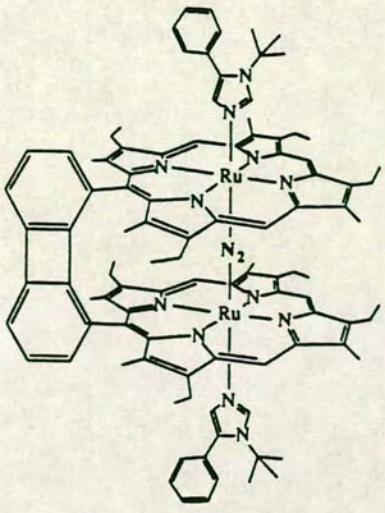

Figure 1.14 [Ru_2 bis(porphyrin)(N_2)(Im^*)$_2$]

The binding and activation of N_2 using thioether macrocycles has been reported by Yoshida and co-workers, with the complex [Mo(Me_8[16]aneS_4)(N_2)$_2$] shown in Figure 1.15[82].

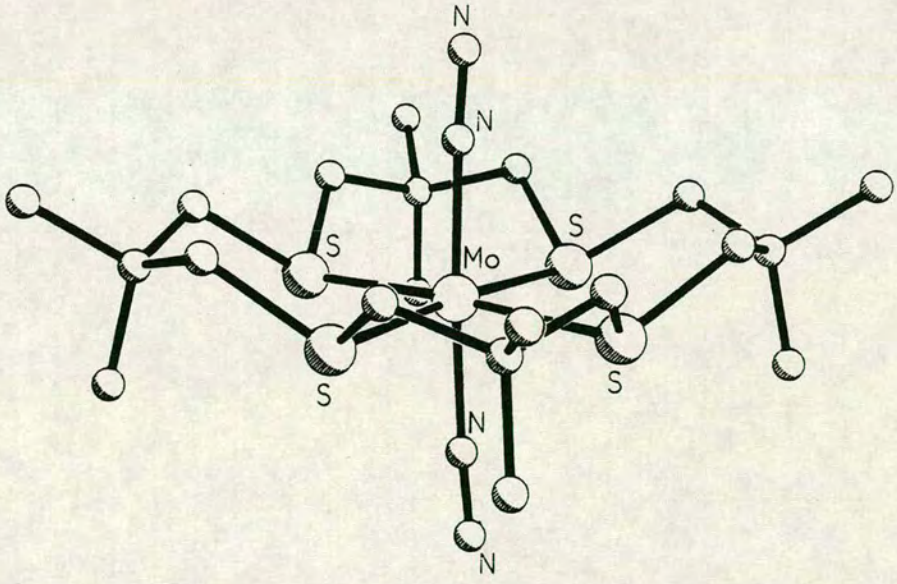

Figure 1.15 [Mo(Me_8[16]aneS_4)(N_2)$_2$]

The structure shows the two N_2 ligands to be bound end-on, in a mutually trans configuration. This compound will react with alkylating reagents such CH_3Br to give [Mo(Me_8[16]aneS_4)($N_2(CH_3)_2$)Br]Br (a methylated analogue of N_2H_2) while unsaturated hydrocarbons (C_2H_4, C_2H_2) simply substitute the N_2 ligands[95].

1.6: Binuclear Macrocyclic Complexes

Binuclear compounds have the potential to bind small molecule substrates in a number of arrangements not available ordinarily to mononuclear complexes. It is also possible to study magnetic interactions between the metal centres within a binuclear framework. By providing well-defined donor sets in close proximity for co-ordination to two metal centres, macrocyclic ligands can provide a useful means of synthesizing binuclear metal complexes. The donor atoms for the different metal sites can be in different macrocyclic rings, to give macropolycyclic ligands. Examples of these are the diporphyrins described in Section 1.5 and the saturated macropolycycles that are exemplified by the work of Lehn and co-workers[3] (see also Section 3.1 below). However, the ligands described in this thesis all contain the donor atoms within a single ring and a typical bonding arrangement for the binuclear macrocyclic complexes is shown schematically in Figure 1.16.

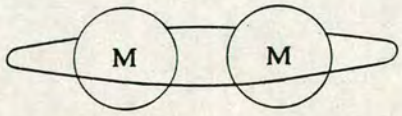

Figure 1.16 Schematic diagram of a binuclear macrocyclic complex

For classifying single-ring binucleating macrocyclic ligands, Groh[96] proposed that the complexes of these ligands fell into two types:

i) Compartmental ligands, in which at least one donor atom is shared between the two metal centres, to give a bridging donor set.

ii) Macrocyclic ligands in which the donor atoms co-ordinate to only one metal centre to form isolated donor sets.

Examples of two compartmental ligands are shown in Figure 1.17, which have N_4O_2 donor sets and the O-donors bridge the two macrocyclic cavities. The phenolic ligand ($\underline{1}H_2$)[97], its derivatives and their complexation reactions

will be described in detail in Chapters 2–5 of this thesis.

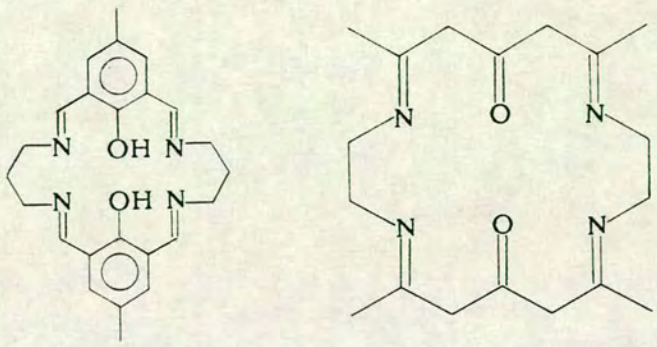

($\underline{1}H_2$)

Figure 1.17 Two compartmental binucleating ligands

The isolated donor set binucleating macrocycles are typified by the large ring crown ethers[98] and the crown thioethers[99–104], which are capable of fitting two metal centres within the macrocyclic cavities. Other examples of isolated donor set macrocycles are shown in Figure 1.18. The extensive chemistry of ligands containing Schiff–base groups has been reviewed[105,106] while ligands with large spaces between metal sites, such as [24]aneN_2S_4[107] have aroused considerable interest by their ability to incorporate bridging substrates between the metal centres[12,107].

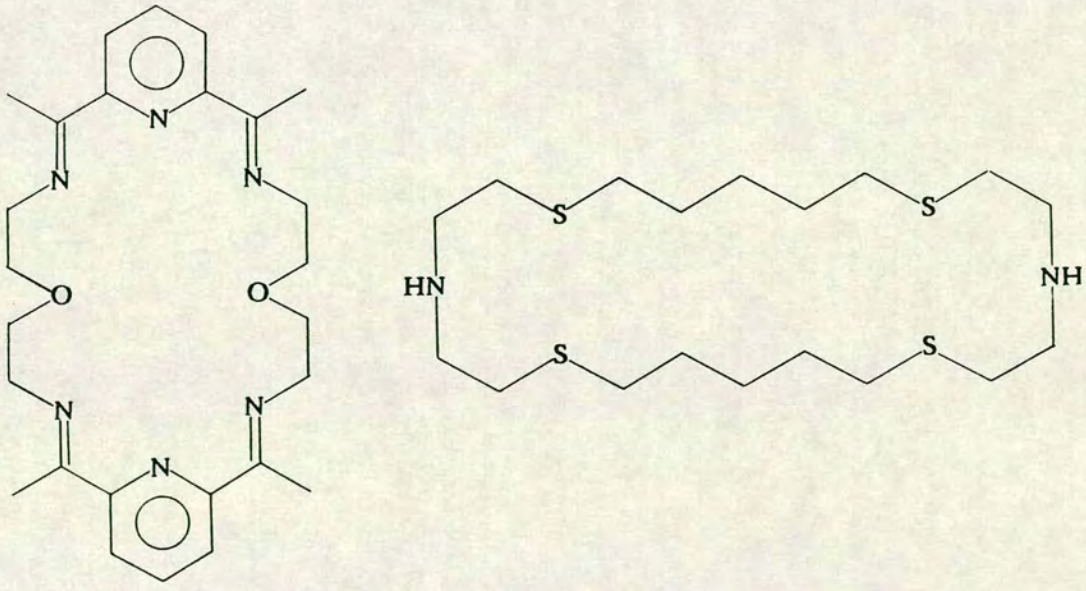

Figure 1.18 A Schiff–base binucleating macrocycle and [24]aneN_2S_4

Finally, binuclear macrocyclic complexes can be prepared using two or more unattached macrocycles. In their review in 1987, Wieghardt and Chaudhuri[7] have described the properties of [9]aneN$_3$, its derivatives and complexes. Of interest here are the binuclear complexes formed by [9]aneN$_3$ and the methylated ligand, Me$_3$[9]aneN$_3$, with bridging ligands between the two metal centres, as shown in Figure 1.19. The bridging ligands (X) are generally based on oxygen (O^{2-}, OH^-, SO_4^{2-}, CO_3^{2-} or RCO_2^-) and complexes where M = V, Cr, Mn, Fe, Co, Mo, Ru, Os and Rh have been structurally and electrochemically characterised[7,108]. Analogous species with bridging Cl^- ligands (M = Ni) have also been investigated[109–111].

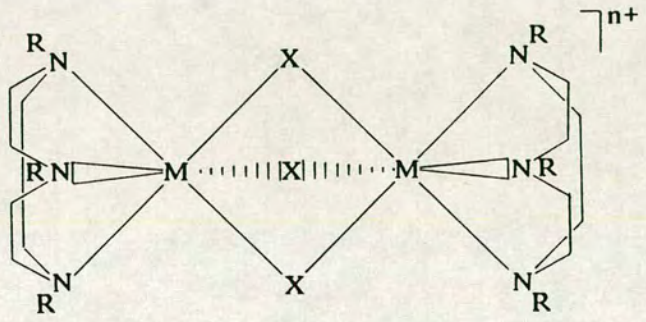

Figure 1.19 Binuclear complexes [([9]aneN$_3$)M(μ–X)$_3$M([9]aneN$_3$)]$^{n+}$

1.7: Aims of this Work

The major aim of the work in this thesis was to synthesise binuclear macrocyclic complexes of first, second and third row transition metals, with the metal centres either confined within a single binucleating ligand or linked by bridging species. For the first part of this programme, complexes of the compartmental ligand ($\underline{1}H_2$), shown in Figure 1.18, are suitable for such a study. Chapter 2 of this thesis is a review of the previous work that has been reported on complexes of this ligand and similar compounds. From this, we concluded that the majority of previous work had been directed towards binuclear Cu complexes of this ligand and that there was potential for a wider range of metal complexes to be prepared. In particular, we proposed to synthesize binuclear complexes of ($\underline{1}H_2$) with the platinum group metals, which have found extensive use in the hetero- and homo-geneous catalysis of small molecule substrates[112].

For the second part of this thesis, we proposed to investigate the complexation of Fe(II) and Co(II) with the thioether macrocycles, with respect to the possible formation of bridged binuclear species. We proposed to study these metal centres since the reactivities of Fe(II) with thioether ligands has not, to our knowledge, been extensively investigated[16].

CHAPTER 2

A Review of the Co-ordination Chemistry of the Binucleating Macrocyclic Ligand which is the Dianion of 11,23-Dimethyl-3,7,15,19-tetraazatricyclo[19.3.1.1^{9,13}] hexacosa-2,7,9,11,13(26),14,19,21(25),22,24-decaene-25,26-diol, (1)$^{2-}$

2.1: Introduction

In 1970, Robson and Pilkington[97] synthesised an important series of compounds of the form $[M_2(\underline{1})Cl_2]$ (M = Mn(II), Fe(II), Co(II), Ni(II), Cu(II), Zn(II)) where $(\underline{1})^{2-}$ is the dianion of the binucleating macrocyclic ligand in Figure 2.1. The complexes were formed by the condensation of equimolar amounts of 2,6-diformyl-4-methylphenol and 1,3-diaminopropane around two metal template ions. In the Cu(II) complex, $[Cu_2(\underline{1})Cl_2].6H_2O$, the Cl^- could be exchanged with $(SO_4)^{2-}$ by metathesis with Ag_2SO_4 to give $[Cu_2(\underline{1})](SO_4).2H_2O$. The complex $[Cu_2(\underline{1})](ClO_4)_2.2H_2O$ was also prepared using $[Cu(ClO_4)_2]$ as the starting material. Attempts to prepare the binuclear square-planar complex, $[Ni_2(\underline{1})]^{2+}$, gave predominantly monomeric products such as $[Ni(\underline{1}H_2)](ClO_4)_2$ [97].

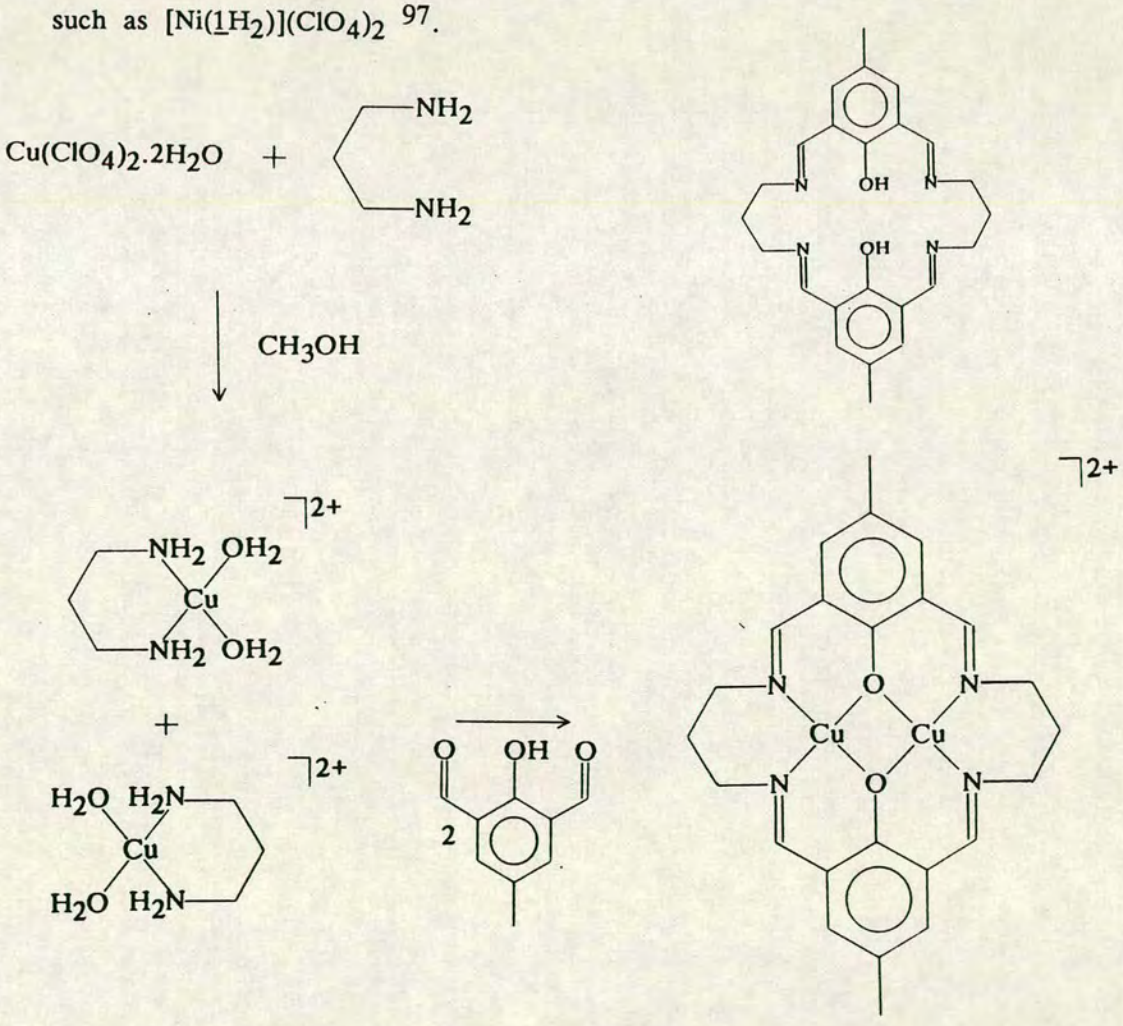

Figure 2.1 ($\underline{1}H_2$) and the template synthesis of $[Cu_2(\underline{1})]^{2+}$

2.2: Co-ordinative Flexibility of $(\underline{1})^{2-}$

From spectroscopic data, it was proposed that the ligand $(\underline{1})^{2-}$ imposed a square pyramidal geometry on the metal centres in the $[M_2(\underline{1})Cl_2]$ complexes, with the apical sites being occupied by Cl^- or solvent molecules[97]. Subsequent single crystal X-ray structure determinations of $[Cu_2(\underline{1})Cl_2]$ [113] and $[Cu_2(\underline{1})(H_2O)_2]^{2+}$ [3] showed this to be the case. However, the latter cationic species co-crystallizes with a molecule of $[Cu_2(\underline{1})(H_2O)_2(ClO_4)_2]$ in which the Cu(II) ions have pseudo-octahedral geometries with *trans*-axial interactions to ClO_4^- ions to give an overall composition $[Cu_2(\underline{1})(H_2O)_2][Cu_2(\underline{1})(H_2O)_2(ClO_4)_2](ClO_4)_2$ [114]. Both molecules are shown in Figure 2.2 with relevant bond distances and angles.

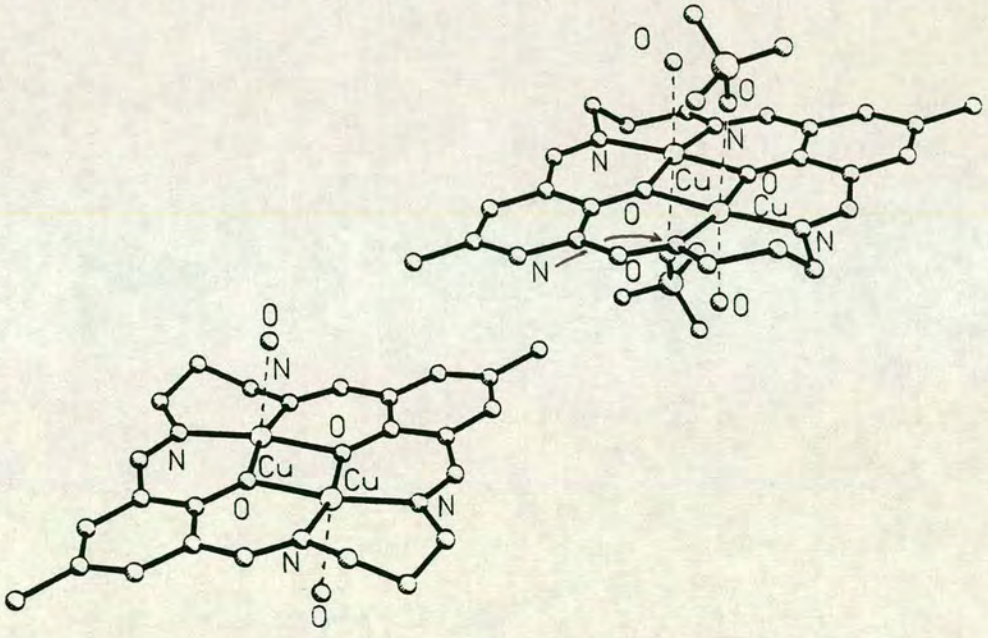

Figure 2.2 $[Cu_2(\underline{1})(H_2O)_2][Cu_2(\underline{1})(H_2O)_2(ClO_4)_2](ClO_4)_2$
a)$[Cu_2(\underline{1})(H_2O)_2]^{2+}$: Cu-$OH_2$ = 2.451(6); Cu-O = 1.970(6), 1.970(6); Cu-N = 1.986(8), 1.943(9); Cu-Cu = 3.096(3)Å; ∠Cu-O-Cu = 103.6(3)°.
b)$[Cu_2(\underline{1})(H_2O)_2(ClO_4)_2]$: Cu-$OH_2$ = 2.451(9); Cu-O = 1.989(6), 1.981(6); Cu-N = 1.956(8), 1.957(8); Cu-Cu = 3.091(3); Cu-$OClO_3$ = 2.589(10)Å; ∠Cu-O-Cu = 102.3(3)°.

On the basis of the initial evidence, Robson and co-workers suggested[116] that $(\underline{1})^{2-}$ may be able to impose a square-pyramidal geometry on metal ions which are unsuited to being five-co-ordinate and have a strong preference for

octahedral co-ordination e.g. Co(III). This was not found to be the case[116]. The binuclear complex $[Co_2(\underline{1})(CH_3OH)Br_2]$ has been synthesised and structurally characterised[115] and shows a CH_3OH molecule occupying a partially occupied octahedral position disordered between the two metal ions. Therefore one metal ion per molecule shows the predicted-square pyramidal geometry while the other metal ion is octahedral. Oxidation of this product with Br_2 yielded a number of products. Depending on reaction conditions, these include $[Co^{III}Co^{II}(\underline{1})(Br)_2(H_2O)_2]Br$, $\{[Co^{III}Co^{II}(\underline{1})(Br)_2(CH_3OH)]^+\}_2(Br^-)(Br_3^-)$, $[Co^{III}Co^{II}(\underline{1})(Br)_2(CH_3OH)_2](Br_3)$ and $[Co^{III}_2(\underline{1})(Br)_8].4CH_3OH$ [116]. The single crystal X-ray structure of $[Co^{III}Co^{II}(\underline{1})(Br)_2(H_2O)_2]Br$ showed two crystalline forms as two geometrical isomers[117]; both isomers contained one octahedral Co(II) and one octahedral Co(III) atom and both forms are shown in Figure 2.3, as A and B.

The geometries of the N_4O_2 donor sets in both isomers of $[Co^{III}Co^{II}(\underline{1})Br_2(H_2O)_2]Br$ are similar (Co-Co = 3.13Å) and it is possible to distinguish between the Co(III) and Co(II) centres by the fact that the N_2O_2 set around the Co(III) ion has contracted relative to that around the Co(II) atom[117]. In isomer A the preferential co-ordination of the Br^- ions to the Co(III) ion is also consistent with this assignment. Other important structural features are the equatorial co-ordination of the Co ions within the macrocycle (displacements of the Co ions out of the least mean-square N_4O_2 plane < 0.1Å) and the distortions of the macrocycle. In isomer B the ligand $(\underline{1})^{2-}$ is essentially flat, with the propylene side-arms being bent away from the bulkier Br^- ligands, in an *anti* arrangement. In isomer A, the propylene groups are *syn* to one another and the ligand adopts a bowl conformation with a dihedral angle between the phenoxy groups of 21.6°. This suggests that there is competition between the less-strained conformation of $(\underline{1})^{2-}$ in B and the co-ordination of the Br^- ions to the Co(III) centre in A.

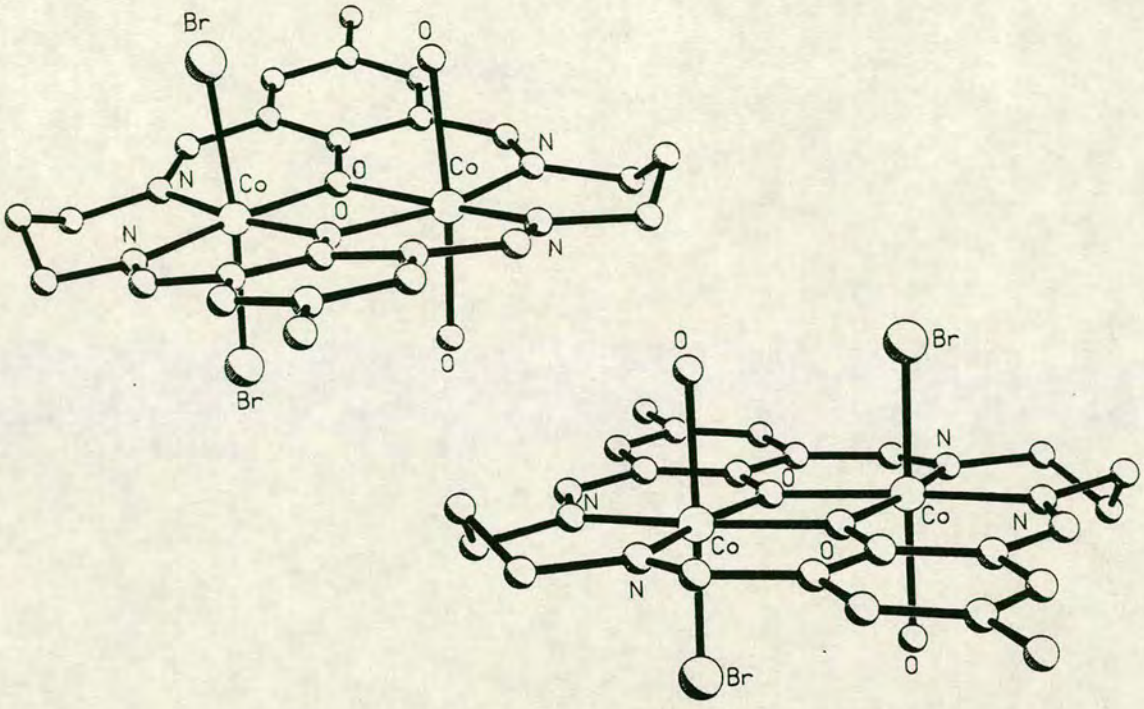

Fig 2.3 A and B Isomers of $[Co_2(\underline{1})Br_2(H_2O)_2]Br$
Isomer A (Orthorhombic): Co(III)–N = 1.94(2), 2.00(2); Co(II)–N = 2.11(2), 1.89(2); Co(III)–O = 1.98(1), 1.83(2); Co(II)–O = 2.13(2), 2.02(1); Co(III)–Br = 2.415(3), 2.426(3); Co(II)–OH_2 = 2.21(1), 2.09(2)Å; ∠Co–O–Co = 99.3(7), 108.9(8)°.
Isomer B (Monoclinic): Co(III)–N = 1.88(3), 1.95(3); Co(II)–N = 2.03(2), 2.02(3); Co(III)–O = 1.98(2), 1.97(1); Co(II)–O = 2.01(2), 2.02(2); Co(III)–Br = 2.380(4); Co(II)–Br = 2.647(5); Co(III)–OH_2 = 2.00(2); Co(II)–OH_2 = 2.17(2)Å; ∠Co–O–Co = 103.0(8), 103.5(7)°.

The single crystal X–ray structure of $[Co^{III}Co^{II}(\underline{1})(Br)_2(CH_3OH)_2](Br_3)$[116] shows a similar arrangement to isomer A of $[Co^{III}Co^{II}(\underline{1})(Br)_2(H_2O)_2]Br$ above, the major differences being the substitution of a $(Br_3)^-$ for a Br^- counterion and the co–ordination of CH_3OH onto the two axial sites of the Co(II) ion. The compound $[Co^{III}_2(\underline{1})Br_8].4CH_3OH$ does appear to be a genuine diamagnetic, binuclear Co(III) species but is very unstable, rapidly decomposing to a paramagnetic species (probably $\{[Co^{III}Co^{II}(\underline{1})(Br)_2(CH_3OH)]^+\}_2[Br^-][Br_3^-]$) via loss of Br_2 [116]. Further reaction of $[Co^{II}_2(\underline{1})(Br)_2].CH_3OH$ with Br_2 in boiling CH_3OH affords, in very low yield, red crystals of the protonated ligand as

$[(\underline{1}H_4)](Br_3)_2$. This is formed as a competition between acidic protons and the Co ions for the macrocyclic cavity, the HBr having been formed *in situ*. $[(\underline{1}H_4)](Br_3)_2$ was also synthesised in a metal-free reaction around a HBr template in CH_3OH, but only the i.r. spectrum and elemental analysis of this product was reported[116].

Robson and Williams[118] have also synthesized a binuclear Co(II) complex of $(\underline{1})^{2-}$, $\{Co^{II}_2(\underline{1})[S_2P(OC_2H_5)_2]_2\}$, which has two bridging ligands across the neighbouring axial sites of the octahedral metal centres. The single crystal X-ray structure of $\{Co^{II}_2(\underline{1})[S_2P(OC_2H_5)_2]_2\}$ is shown in Figure 2.4. There are two crystallographically distinct but chemically identical molecules per unit cell. The ligand $(\underline{1})^{2-}$ adopts a conformation similar to that of the B-isomer of $[Co^{III}Co^{II}(\underline{1})Br_2(H_2O)_2]Br$ shown above, with the propylene side-arms adopting *anti* arrangements.

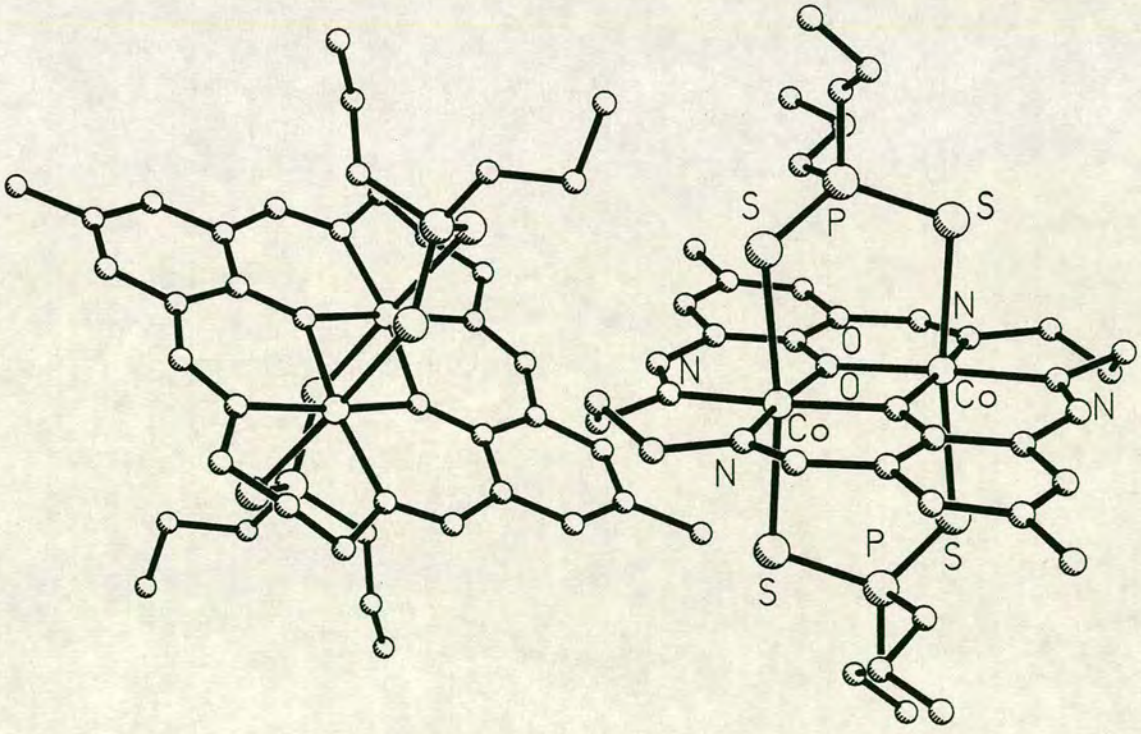

Figure 2.4 The two crystallographically unique molecules of

$\{Co^{II}_2(\underline{1})[S_2P(OC_2H_5)_2]_2\}$

The above complexes illustrate the ability of $(\underline{1})^{2-}$ to co-ordinate to both square-pyramidal and octahedral metal centres. Evidence for square-planar complexes with $(\underline{1})^{2-}$ and its derivatives was first reported by Okawa and Kida[119]. This was achieved via an important stepwise synthetic route to the binuclear complexes shown in Figure 2.5. With a stepwise synthetic method, it is possible to vary the length of the side-arms by use of the appropriate diamine and also to form heterobinuclear complexes (see Section 2.3). The complexes $[Cu_2(\underline{1})]Cl_2.H_2O$, $[Cu_2(\underline{2})]Cl_2.2H_2O$, $[Cu_2(\underline{3})]Cl_2.C_2H_5OH.2H_2O$, $[Cu_2(\underline{1})](SO_4).2H_2O$, $[Ni_2(\underline{2})]Cl_2.3H_2O$ and $[Ni_2(\underline{3})]Cl_2.2H_2O$ were prepared by this route[119], with the complexes of $(\underline{1})^{2-}$ being identical to those reported by Robson[97]. $[Ni_2(\underline{2})]Cl_2.3H_2O$ and $[Ni_2(\underline{3})]Cl_2.2H_2O$ were assigned as square-planar species on the basis of their diamagnetism and electronic spectra.

2.3: Electronic Properties of Complexes of $(\underline{1})^{2-}$

The major reason for the interest in binuclear compounds of $(\underline{1})^{2-}$ and its derivatives is that they provide a framework in which to study the electronic and magnetic properties of systems where two (or more) metals may interact. Of particular interest has been the role of the phenoxy ligands which are directly bonded to both metal centres and the importance of the angles about these bridging ligands[32]. Pilkington and Robson[97] reported variable temperature magnetic susceptibility data in the range 100-300K for the complexes $[M_2(\underline{1})Cl_2]$ (M = Cu, Ni, Co, Fe, Mn). A strong antiferromagnetic exchange interaction was found for the Cu(II) complex with only weak interactions being found for the other compounds. More extensive measurements were carried out at lower temperatures (285-4.2K)[120] and it was suggested that the trend of decreasing magnetic exchange across the series from Cu(II) to Mn(II) was caused by an increase in axial displacement by the

Figure 2.5 Stepwise synthesis of complexes of $(\underline{1})^{2-}$

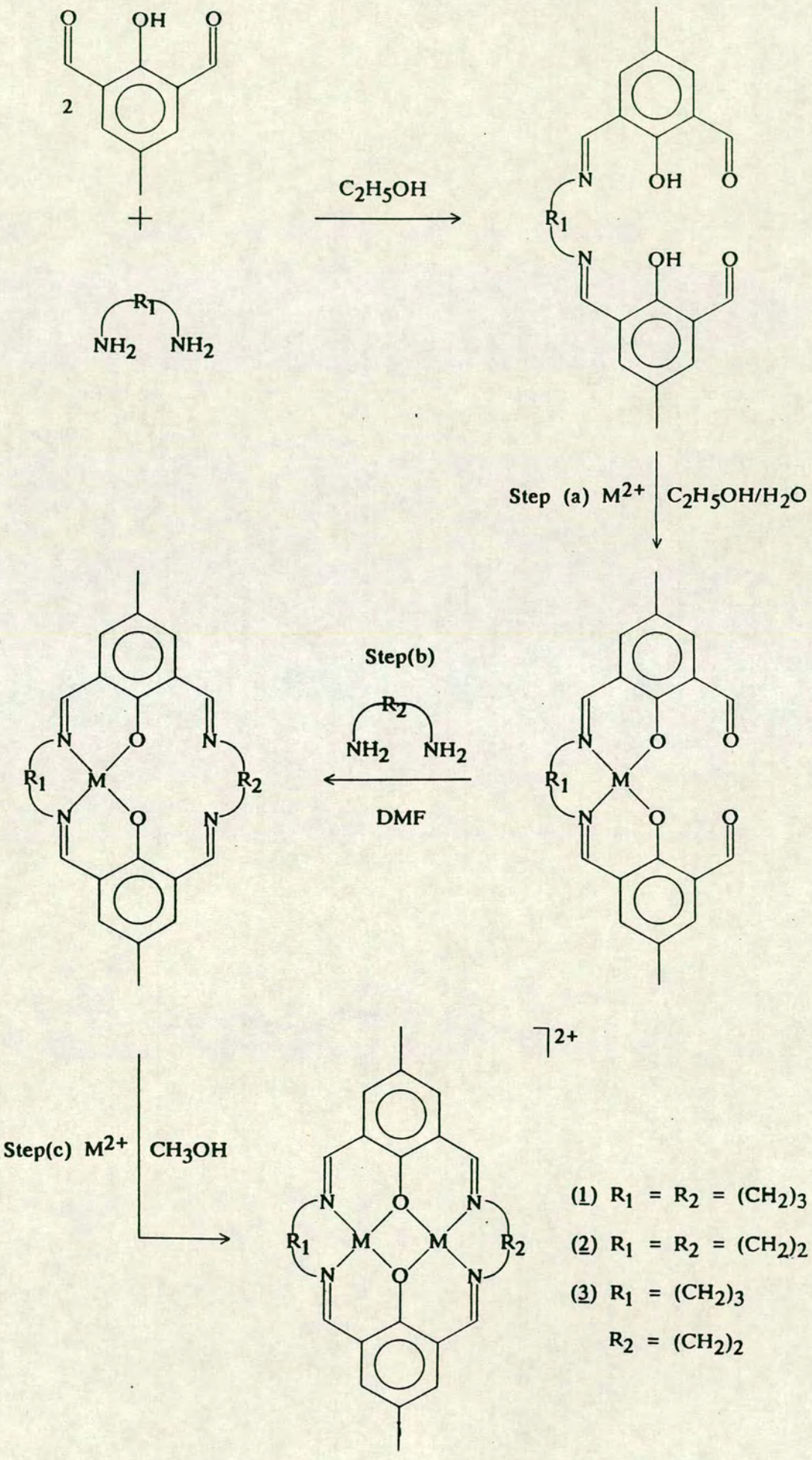

metal ions from the square-planar donor set[120]. This would reduce the overlap of the interacting metal $d_{x^2-y^2}$ orbitals with the *s* and *p* orbitals of the bridging O-atom. An increase in displacement from the ligand plane due to increasing metal ion size has been found across the series from Cu(II) to Mn(II)[113,25] and this is consistent with the above proposal.

To test this hypothesis, a series of binuclear high spin octahedral complexes of $(\underline{1})^{2-}$ were prepared by Gagné *et al.*[121], using a template synthesis about the appropriate metal(II) ion in the presence of base: $[Ni_2(\underline{1})(py)_4](BF_4)_2$, $[Co_2(\underline{1})(py)_4](BF_4)_2$, $[Fe_2(\underline{1})(py)_4](BF_4)_2$, $[Fe_2(\underline{1})(Im)_4](BF_4)_2$, $[Fe_2(\underline{1})(MeIm)_4](BF_4)_2$ and $[Fe_2(\underline{1})(MeNic)_4](BF_4)_2$, (py = pyridine, Im = imidazole, MeIm = 1-methylimidazole, MeNic = methyl ester of isonicotinic acid). To confirm the octahedral geometry for these complexes, a single crystal X-ray structure of $[Fe_2(\underline{1})(Im)_4](BF_4)_2$ was undertaken and is shown in Figure 2.6.

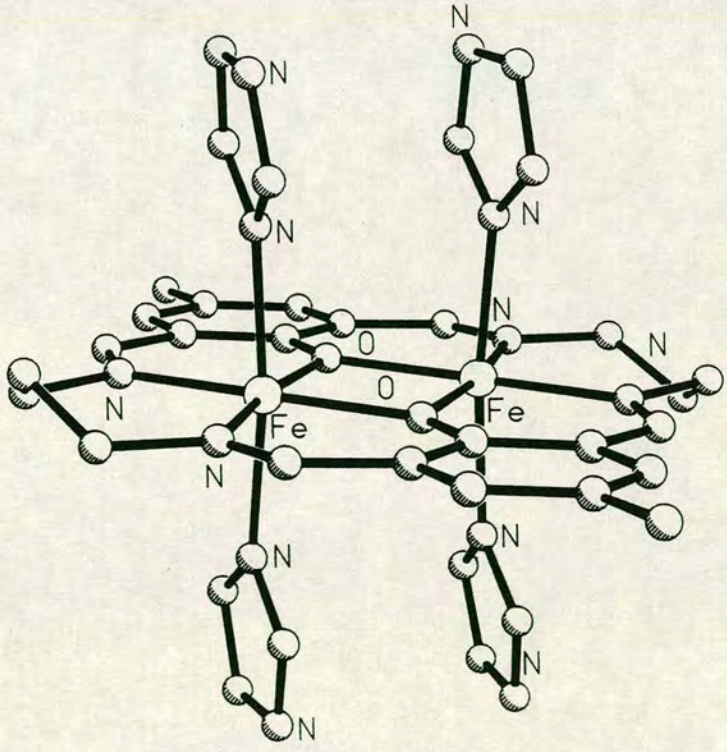

Figure 2.6 $[Fe_2(\underline{1})(Im)_4]^{2+}$
Fe-N = 2.088(6), 2.081(6); Fe-O = 2.092(5); $Fe-N_{(Im)}$ = 2.218(7); Fe-Fe = 3.117(2)Å; ∠Fe-O-Fe = 96.3(2)°.

The structure of $[Fe_2(\underline{1})(Im)_4]^{2+}$ shows the ligand $(\underline{1})^{2-}$ to be essentially planar except for the central carbons of the propylene groups, which are disordered about two positions. This disorder was also noted for the five-co-ordinate complexes $[Cu_2(\underline{1})Cl_2]$ and $[Co_2(\underline{1})Br_2]$ discussed previously[113,115]. In $[Fe_2(\underline{1})(Im)_4](BF_4)_2$, the two Fe(II) centres are only 0.011(1)Å out of the ligand plane.

For all complexes of the type $[M_2(\underline{1})(base)_4](BF_4)_2$ (base = py, Im, MeIm and MeNic), antiferromagnetic exchange was observed but little difference was found in the magnetic exchange interactions between these six-co-ordinate species and the corresponding five-co-ordinate species $[M_2(\underline{1})Cl_2]$ examined earlier[97,120]. It was suggested that the effect of the change in co-ordination geometry may be cancelled by the increase in ligand-field splitting expected for the six-co-ordinate complexes compared to the five-co-ordinate complexes. The fact that the ligand-field is significant in this study is shown in the series of $[Fe_2(\underline{1})(base)_4](BF_4)_2$ complexes[121], where the complexes with stronger axial bases (Im and MeIm) show weaker antiferromagnetic interactions than the complexes with weaker axial bases (py and MeNic). It was also suggested that the decrease in magnetic exchange interaction across the series Fe(II) to Ni(II) for the octahedral complexes is due to the increasing number of unpaired electrons[121].

Additional studies[24] on the influence of axial ligands on magnetic exchange reactions have been conducted on the complexes $[Cu_2(\underline{1})X_2]$, ($X = Cl^-$, Br^-, I^- and N_3^-). It is unusual that ligands that interact with orbitals that are orthogonal to the $d_{x^2-y^2}$ orbital should perturb the interactions of the $d_{x^2-y^2}$ orbital with the bridging O-atom. There is however a definite increase in the magnetic exchange integrals in the series $Cl < Br < N_3 < I$. The single crystal X-ray structures of $[Cu_2(\underline{1})Br_2]$ and $[Cu_2(\underline{1})I_2]$ show that the Cu(II) ions are in square-pyramidal environments,

similar to $[Cu_2(\underline{1})Cl_2]$, but with decreasing displacements from the ligand plane with increasing size of halide ligand.

Other evidence for metal–metal interactions in complexes of $(\underline{1})^{2-}$ and its derivatives has come from some extensive electrochemical studies on Cu complexes. In 1976, Addison briefly reported[122] the electrochemistry of $[Cu_2(\underline{8a})](ClO_4)_2$ and Gagné and co–workers studied the electrochemistry of $[Cu_2(\underline{1})](ClO_4)_2$ more extensively[123]. The latter workers showed that $[Cu_2(\underline{1})](ClO_4)_2$ can be reduced in well–defined, quasi–reversible, one–electron steps at −0.52V and −0.91V *vs.* NHE in DMF. The two reduction products could be isolated and characterised using controlled potential electrolysis. The mixed–valence species, $[Cu^{II}Cu^{I}(\underline{1})]^+$, is stable in oxygen–free solutions and reacts with CO to give $[Cu^{II}Cu^{I}(\underline{1})(CO)]^+$. Electronic spectroscopy indicates that the CO ligand is bound to the Cu(I) centre. The doubly–reduced species, $[Cu^{I}_2(\underline{1})]$, is a black, insoluble, crystalline material but can be solubilised by reacting it with CO to give $[Cu^{I}_2(\underline{1})(CO)_2]$. The single crystal X–ray structure of the mixed–valence $[Cu^{II}Cu^{I}(\underline{1})](ClO_4).0.5CH_3OH$ [124] (Figure 2.7) revealed distinct Cu co–ordination sites, with the Cu(II) ion in a square–planar geometry and the Cu(I) ion disordered between two nonequivalent distorted square–planar environments.

The ligand $(\underline{1})^{2-}$ in $[Cu^{II}Cu^{I}(\underline{1})]^+$ is basically planar with minor twisting and bending back of the phenyl groups. The distorted square–planar geometry about the Cu(I) ion is not the favoured tetrahedral co–ordination for Cu(I) complexes and the non–idealised co–ordination spheres are completed by axial interactions with aromatic carbon atoms in adjacent molecules. The structure of $[Cu^{II}Cu^{I}(\underline{1})]^+$ suggests that there is no facile thermal intramolecular electron transfer in the solid state and the intermolecular crystal packing forces are strong enough to ensure localized valence sites. However, electron–transfer in solution can be encouraged by the possibility of facile

geometric rearrangements including interactions with the solvent co-ordination sphere.

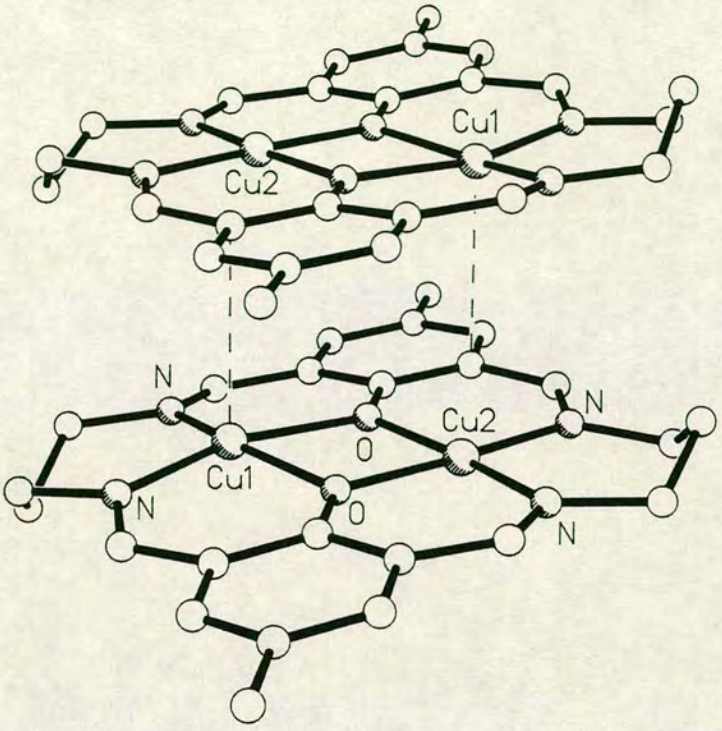

Figure 2.7 $[Cu^{II}Cu^{I}(\underline{1})]^{+}$
Cu(II)-N = 1.974(3), 1.979(3); Cu(II)-O = 1.967(2), 1.951(2)Å. Molecule a) (65%): Cu(I)-N = 1.974(4), 1.950(3); Cu(I)-O = 2.118(3), 2.127(3)Å; ∠Cu-O-Cu = 104.1(1), 104.4(1)°; Cu(I) displaced 0.15Å out of plane. Molecule b) (35%): Cu(I)-N = 2.059(4), 1.999(4); Cu(I)-O = 2.278(3), 2.240(3)Å; ∠Cu-O-Cu = 103.9(1), 105.8(1)°; Cu(I) displaced 0.65Å out of plane.

Even so, the macrocycle $(\underline{1})^{2-}$ cannot distort to accommodate tetrahedral co-ordination and a range of Cu complexes of derivatives of $(\underline{1})^{2-}$ have been synthesized in attempts to facilitate tetrahedral co-ordination and hence favour Cu(I) with respect to the Cu(II) state[125]. This work is summarised in Table 2.1. It can be seen that adjustments to the ligand structure cause subtle but significant variations in the reduction potentials, as does the solvent used (some slight discrepancies in the values by different groups may be due to the use of different reference and working electrodes). Some of the alterations to the ligand have been made to overcome the problem of insolubility of the

complex $[Cu^{I}Cu^{I}(\underline{1})]$. The most significant shift in reduction potential occurs for the ligand $(\underline{4d})^{2-}$ [128], which has two distorted tetrahedral cavities imposed on it by the two biphenylene side-arms. Placing additional donors in the side-arms[131], ligands $(\underline{6a})^{2-}$ and $(\underline{6b})^{2-}$, causes the two distinct reduction steps to coalesce to give a single two-electron reduction, $[Cu^{II}_2(\underline{6})]^{2+} \rightarrow [Cu^{I}_2(\underline{6})]$. Changes in the substitution at the imino groups and at the *para* position of the phenol seem to have a relatively weak effect on the first reduction potentials.

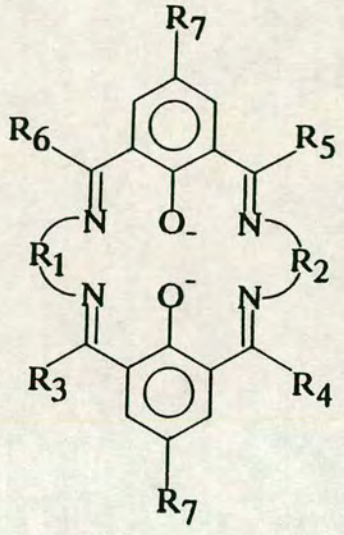

Figure 2.8 Variations on $(\underline{1})^{2-}$

The conproportionation constant, K_{con}, can be considered to be a measure of the stability of the mixed-valence species, $[Cu^{II}Cu^{I}L]^{+}$, with respect to dissociation to $[Cu^{II}_2L]^{2+}$ and $[Cu^{I}_2L]$ species. This is calculated by considering the separation between the standard electrode potentials of the $Cu^{II}Cu^{II}/Cu^{II}Cu^{I}$ and $Cu^{II}Cu^{I}/Cu^{I}Cu^{I}$ redox processes, ΔE, and using the expression

$$K_{con} = e\ (F\Delta E/RT)$$

where

$$[Cu^{II}_2(\underline{1})]^{2+} + [Cu^{I}_2(\underline{1})] \overset{K_{con}}{\leftrightarrows} 2[Cu^{II}Cu^{I}(\underline{1})]^{+}$$

It has been suggested[123,126] that the value of K_{con} can be correlated to

Table 2.1: Redox potentials for the two successive $Cu^{II}Cu^{II}/Cu^{II}Cu^{I}$ and $Cu^{II}Cu^{I}/Cu^{I}Cu^{I}$ reduction steps displayed by $[Cu_2L]^{2+}$

L	R_3	R_4	R_5	R_6	R_1	R_2	R_7	$E^{\cdot}_1$ (V)	$E^{\cdot}_2$ (V)	SOLV -ENT	K_{CON}	Ref.
$(\underline{1})^{2-}$	H	H	H	H	$(CH_2)_3$	$(CH_2)_3$	CH_3	-0.52	-0.91	DMF	3.9×10^6	11,14
$(\underline{1})^{2-}$	H	H	H	H	$(CH_2)_3$	$(CH_2)_3$	CH_3	-0.56	-0.91	DMF	5.6×10^5	15
$(\underline{1})^{2-}$	H	H	H	H	$(CH_2)_3$	$(CH_2)_3$	CH_3	-0.51	-	CH_3CN	-	15
$(\underline{1})^{2-}$	H	H	H	H	$(CH_2)_3$	$(CH_2)_3$	CH_3	-0.46	-0.94	DMSO	1.3×10^8	3
$(\underline{4a})^{2-}$	H	H	H	H	$(CH_2)_3$	$(CH_2)_3$	^tBu	-0.53	-0.92	DMF	4.3×10^6	16
$(\underline{4b})^{2-}$	H	H	H	H	a	a	^tBu	-0.55	-0.94	DMF	3.7×10^6	16
$(\underline{4c})^{2-}$	H	H	H	H	$(CH_2)_4$	$(CH_2)_4$	^tBu	-0.33	-0.81	DMF	1.2×10^8	16
$(\underline{4d})^{2-}$	H	H	H	H	b	b	^tBu	-0.23	-0.64	DMF	9.0×10^6	16
$(\underline{4e})^{2-}$	H	H	H	H	$(CH_2)_3$	a	^tBu	-0.54	-0.94	DMF	5.2×10^6	16
$(\underline{4f})^{2-}$	H	H	H	H	$(CH_2)_3$	b	^tBu	-0.38	-0.82	DMF	4.0×10^7	16
$(\underline{4g})^{2-}$	H	H	H	H	$(CH_2)_3$	$(CH_2)_4$	^tBu	-0.40	-0.92	DMF	7.1×10^8	16
$(\underline{5})^{2-}$	H	H	H	H	$(CH_2)_4$	$(CH_2)_4$	CH_3	-0.35	-0.81	DMSO	6.0×10^7	3
$(\underline{5})^{2-}$	H	H	H	H	$(CH_2)_4$	$(CH_2)_4$	CH_3	-0.29	-0.80	CH_3CN	4.3×10^8	3
$(\underline{6a})^{2-}$	H	H	H	H	c	c	Cl	-0.69	-0.69	DMSO	-	19
$(\underline{6b})^{2-}$	H	H	H	H	d	d	Cl	-0.79	-0.79	DMSO	-	19
$(\underline{7})^{2-}$	H	H	H	H	$(CH_2)_3$	$(CH_2)_3$	CF_3	-0.38	-0.72	DMF	5.6×10^5	18

a =

b =

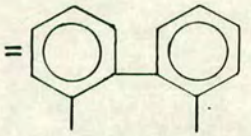

c =

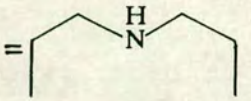

d =

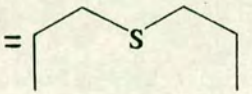

L	R_3	R_4	R_5	R_6	R_1	R_2	R_7	E°_1 (V)	E°_2 (V)	SOLV -ENT	K_{CON}	Ref.
$(\underline{8a})^{2-}$	CH_3	CH_3	CH_3	CH_3	$(CH_2)_3$	$(CH_2)_3$	CH_3	-0.44	-1.21	CH_3CN	1.1×10^{13}	10
$(\underline{8a})^{2-}$	CH_3	CH_3	CH_3	CH_3	$(CH_2)_3$	$(CH_2)_3$	CH_3	-0.46	-1.23	CH_3CN	1.2×10^{13}	15
$(\underline{8a})^{2-}$	CH_3	CH_3	CH_3	CH_3	$(CH_2)_3$	$(CH_2)_3$	CH_3	-0.52	-1.10	DMSO	6.6×10^{9}	3
$(\underline{8b})^{2-}$	CH_3	CH_3	CH_3	CH_3	$(CH_2)_4$	$(CH_2)_4$	CH_3	-0.33	-	CH_3CN	-	10
$(\underline{8c})^{2-}$	^nPr	^nPr	^nPr	^nPr	$(CH_2)_3$	$(CH_2)_3$	CH_3	-0.47	-1.25	CH_3CN	1.6×10^{13}	15
$(\underline{8c})^{2-}$	^nPr	^nPr	^nPr	^nPr	$(CH_2)_3$	$(CH_2)_3$	CH_3	-0.49	-1.04	DMSO	2.0×10^{9}	3
$(\underline{8d})^{2-}$	Ph	Ph	Ph	Ph	$(CH_2)_3$	$(CH_2)_3$	CH_3	-0.47	-1.02	CH_3CN	1.8×10^{9}	15
$(\underline{8d})^{2-}$	Ph	Ph	Ph	Ph	$(CH_2)_3$	$(CH_2)_3$	CH_3	-0.47	-1.02	DMF	1.7×10^{9}	17
$(\underline{8d})^{2-}$	Ph	Ph	Ph	Ph	$(CH_2)_3$	$(CH_2)_3$	CH_3	-0.53	-1.01	CH_2Cl_2	1.3×10^{8}	17
$(\underline{8e})^{2-}$	Ph	CH_3	Ph	CH_3	$(CH_2)_3$	$(CH_2)_3$	CH_3	-0.53	-1.23	CH_3CN	7.8×10^{11}	15
$(\underline{8f})^{2-}$	H	CH_3	CH_3	CH_3	$(CH_2)_3$	$(CH_2)_3$	CH_3	-0.43	-0.97	CH_3CN	1.4×10^{9}	17
$(\underline{8f})^{2-}$	H	CH_3	CH_3	CH_3	$(CH_2)_3$	$(CH_2)_3$	CH_3	-0.51	-0.96	CH_2Cl_2	5×10^{7}	17
$(\underline{8g})^{2-}$	H	CH_3	CH_3	Ph	$(CH_2)_3$	$(CH_2)_3$	CH_3	-0.42	-0.96	CH_3CN	1.1×10^{9}	17
$(\underline{8g})^{2-}$	H	CH_3	CH_3	Ph	$(CH_2)_3$	$(CH_2)_3$	CH_3	-0.51	-0.98	CH_2Cl_2	1.1×10^{8}	17
$(\underline{8h})^{2-}$	CH_3	CH_3	CH_3	Ph	$(CH_2)_3$	$(CH_2)_3$	CH_3	-0.44	-1.05	CH_3CN	2.5×10^{10}	17
$(\underline{8h})^{2-}$	CH_3	CH_3	CH_3	Ph	$(CH_2)_3$	$(CH_2)_3$	CH_3	-0.51	c.1.0	CH_2Cl_2	-	17
$(\underline{8i})^{2-}$	CH_3	CH_3	Ph	Ph	$(CH_2)_3$	$(CH_2)_3$	CH_3	-0.45	-1.42	CH_3CN	3×10^{9}	17
$(\underline{8i})^{2-}$	CH_3	CH_3	Ph	Ph	$(CH_2)_3$	$(CH_2)_3$	CH_3	-0.56	c.1.0	CH_2Cl_2	-	17
$(\underline{8j})^{2-}$	CH_3	CH_3	CH_3	CH_3	$(CH_2)_2$	$(CH_2)_2$	CH_3	-0.46	-1.20	DMSO	3.3×10^{12}	3

Table 2.2: E.s.r. data for $[Cu^{II}Cu^{I}L]^{+}$

L	R_3	R_4	R_5	R_6	R_1	R_2	R_7	T(K)	Lines	SOLVENT	T(K)	Lines	K_{CON}	Ref.
$(\underline{1})^{2-}$	H	H	H	H	$(CH_2)_3$	$(CH_2)_3$	CH_3	298	7	CH_2Cl_2	82	4	3.9×10^6	11,14
$(\underline{1})^{2-}$	H	H	H	H	$(CH_2)_3$	$(CH_2)_3$	CH_3	298	7	CH_3CN	77	4	3.9×10^6	11,14
$(\underline{1})^{2-}$	H	H	H	H	$(CH_2)_3$	$(CH_2)_3$	CH_3	298	7	CH_3OH	-	-	3.9×10^6	11,14
$(\underline{1})^{2-}$	H	H	H	H	$(CH_2)_3$	$(CH_2)_3$	CH_3	298	7	acetone	-	-	3.9×10^6	11,14
$(\underline{1})^{2-}$+CO	H	H	H	H	$(CH_2)_3$	$(CH_2)_3$	CH_3	298	4	CH_2Cl_2	79	4	3.9×10^6	11,14
$(\underline{1})^{2-}$	H	H	H	H	$(CH_2)_3$	$(CH_2)_3$	CH_3	15	1	solid	-	-	3.9×10^6	11,14
$(\underline{4a})^{2-}$	H	H	H	H	$(CH_2)_3$	$(CH_2)_3$	^tBu	298	7	e	105	4	4.3×10^6	16
$(\underline{4b})^{2-}$	H	H	H	H	a	a	^tBu	298	7	e	105	4	3.7×10^6	16
$(\underline{4c})^{2-}$	H	H	H	H	$(CH_2)_4$	$(CH_2)_4$	^tBu	298	7	e	105	4	1.2×10^8	16
$(\underline{4d})^{2-}$	H	H	H	H	b	b	^tBu	298	4	e	105	4	9.0×10^6	16
$(\underline{4e})^{2-}$	H	H	H	H	$(CH_2)_3$	a	^tBu	298	7	e	105	4	5.2×10^6	16
$(\underline{4f})^{2-}$	H	H	H	H	$(CH_2)_3$	b	^tBu	298	4	e	105	4	4.0×10^7	16
$(\underline{4g})^{2-}$	H	H	H	H	$(CH_2)_3$	$(CH_2)_4$	^tBu	298	4	e	105	4	7.1×10^8	16
$(\underline{5})^{2-}$	H	H	H	H	$(CH_2)_4$	$(CH_2)_4$	CH_3	298	7	CH_3CN	-	-	4.3×10^8	3
$(\underline{8a})^{2-}$	CH_3	CH_3	CH_3	CH_3	$(CH_2)_3$	$(CH_2)_3$	CH_3	298	4	CH_3CN	-	-	1.1×10^{13}	10
$(\underline{8a})^{2-}$	CH_3	CH_3	CH_3	CH_3	$(CH_2)_3$	$(CH_2)_3$	CH_3	298	4	CH_3CN	-	-	1.2×10^{13}	20
$(\underline{8c})^{2-}$	^nPr	^nPr	^nPr	^nPr	$(CH_2)_3$	$(CH_2)_3$	CH_3	298	4	CH_3CN	-	-	1.6×10^{13}	20
$(\underline{8d})^{2-}$	Ph	Ph	Ph	Ph	$(CH_2)_3$	$(CH_2)_3$	CH_3	298	4	CH_3CN	-	-	1.3×10^8	20
$(\underline{8f})^{2-}$	H	H	CH_3	CH_3	$(CH_2)_3$	$(CH_2)_3$	CH_3	298	4	CH_3CN	-	-	1.4×10^9	20

e = $(CH_3)_2CO$/toluene

the extent of delocalisation in the mixed-valence species, according to the Robin-Day classification[134]. Under this classification, all the compounds given in Table 2.1 would be completely delocalized "Class III" compounds, which have values of K_{con} in the range 10^6–10^{38}. This conclusion should be treated with caution.

More evidence for delocalisation in these systems has been obtained from e.s.r. spectroscopy at ambient and low temperatures. The results are summarised in Table 2.2. All the $[Cu^{II}Cu^{I}L]^+$ complexes show four line spectra at temperatures around 77K as frozen solutions, which is consistent with a completely localised system with a hyperfine coupling between the unpaired electron and a single Cu nucleus (for ^{63}Cu and ^{65}Cu, abundances 69.1 and 30.9 % respectively, I = 3/2). At room temperature, some complexes [with $(\underline{1})^{2-}$, $(\underline{4a})^{2-}$, $(\underline{4b})^{2-}$, $(\underline{4c})^{2-}$, $(\underline{4e})^{2-}$ and $(\underline{5})^{2-}$] show delocalised behaviour, with a seven line spectrum, which is consistent with the unpaired electron coupling to the two equivalent Cu nuclei. The compounds which show this feature tend to have lower values for K_{con}. Attempts have been made to find the transition temperatures in solution between these e.s.r. localised and delocalised spectra[123,128] in order to estimate the rate of electron exchange. Many difficulties were encountered including dimerisation at low temperatures and precipitation, but the coalescence temperature for $[Cu^{II}Cu^{I}(\underline{1})]^+$ was found to be approximately 200K[123], which gives an approximate value for the rate of electron exchange of $1.7 \times 10^{10} s^{-1}$ at 298K. Complexes $[Cu^{II}Cu^{I}(\underline{4d})]^+$, $[Cu^{II}Cu^{I}(\underline{4f})]^+$ and $[Cu^{II}Cu^{I}(\underline{4g})]^+$, which show localised behaviour at room temperature, were heated to 390K[128] but no transition to delocalised behaviour was observed. Solid state e.s.r. studies on $[Cu^{II}Cu^{I}(\underline{4})]^+$ have only yielded single line spectra, with broad features[128].

Electrochemical studies have also been carried out by Gagné *et al.* on heterobinuclear complexes of $(\underline{1})^{2-}$ [135,136]. These complexes were prepared

using the synthetic method developed by Okawa and Kida[119], whereby metal(II) ions can be co-ordinated stepwise, since they show an overwhelming preference for the N_2O_2 donor set as opposed to the O_4 donor set (Step (a) in Figure 2.4). With short reaction times, little scrambling to give homonuclear species was observed. Complexes of the form $[CuM(\underline{1})]^{2+}$ [M = Mn(II), Fe(II), Co(II), Ni(II) and Cu(II)] were synthesized and investigated electrochemically. In each case, a quasi-reversible Cu^{II}/Cu^{I} reduction was observed, at $E_{\frac{1}{2}} = -1.07V$ *vs.* Fc/Fc^+ in DMF, which was invariant with respect to the other co-ordinated metal ion. The one exception is the homobinuclear species, $[Cu_2(\underline{1})]^{2+}$, which is more readily reduced, at $E_{\frac{1}{2}} = -0.93V$ *vs.* Fc/Fc^+. This suggested, other factors being equal, that the homonuclear species $[Cu^{II}Cu^{I}(\underline{1})]^+$ existed as a resonance-stabilised species due to electron delocalisation. This apparent delocalisation energy was calculated to be $< 1kJmol^{-1}$ [136].

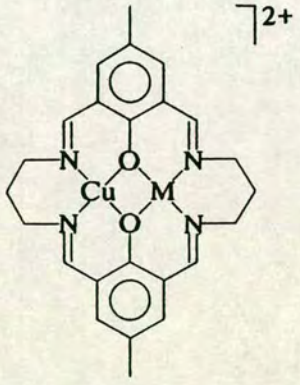

Figure 2.9 $[CuM(\underline{1})]^{2+}$

Recent interest in the electronic states of polynuclear manganese compounds[138-140], to mimic the behaviour of the manganese-containing protein Photosystem II (PS II)[141,142] that is active in photosynthesis, has resulted in the synthesis of a mixed-valence $Mn^{II}Mn^{III}$ complex of $(\underline{4a})^{2-}$ [143,144]. The single crystal X-ray structure of $[Mn^{II}Mn^{III}(\underline{4a})Cl_2Br].H_2O$ is shown in Figure 2.10.

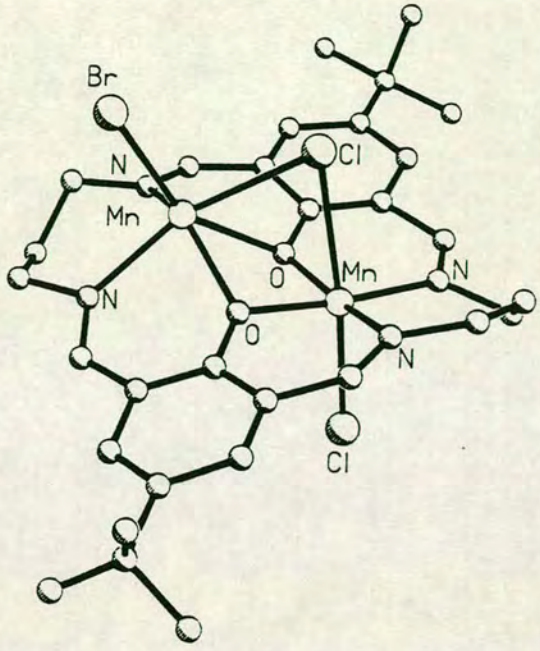

Figure 2.10 $[Mn^{II}Mn^{III}(\underline{4a})Cl_2Br]$
Mn1–Cl1 = 2.491(5); Mn1–Cl2 = 2.766(6); Mn1–O = 1.941(9), 1.931(10); Mn1–N = 1.973(13), 2.031(12); Mn2–Br = 2.514(4); Mn2–Cl2 = 2.763(5); Mn2–O = 2.386(11), 2.129(10); Mn2–N = 2.182(11), 2.236(17)Å; ∠Mn–O–Mn = 93.6(4), 102.5(4)°; Mn1–Mn2 = 3.168(3)Å.

$[Mn^{II}Mn^{III}(\underline{4a})Cl_2Br]$ [143,144] was synthesised by oxidation of $[Mn^{II}_2(\underline{4a})Cl_2]$ with Br_2 in H_2O and is another example of a valence-trapped species in the solid state. Contraction of the N_2O_2 donor set and the octahedral geometry indicate that Mn1 is the Mn^{III} ion, so Mn2 is assigned as Mn^{II}. To accommodate the distorted trigonal-prismatic geometry at Mn2, the metal ion is displaced 1.25Å out of the ligand plane, while an N-donor from the ligand $(\underline{4a})^{2-}$ lies 1.00Å out the plane of the other five donors. There is disorder between the Br and Cl1 atoms, which was modelled by fixing the occupancy of Br as 70% Br/30% Cl1 and the occupancy of Cl1 as 70% Cl1/30% Br. The single crystal X-ray structure of $[Mn^{II}_2(\underline{4a})Cl_2]$ was also reported for comparison and is analogous to that of $[Cu_2(\underline{1})Cl_2]$.

A cyclic voltammogram of $[Mn^{II}_2(\underline{4a})Cl_2]$ in CH_3CN shows two quasi-reversible oxidations at $E_{\frac{1}{2}}$ = +1.0 and +1.6V *vs.* Fc/Fc^+ [144]. This

gives a value for K_{con} of 1.7×10^{10} for the equilibrium

$$[Mn^{III}_2(\underline{4a})Cl_2]^{2+} + [Mn^{II}_2(\underline{4a})Cl_2] \overset{K_{con}}{\rightleftharpoons} 2[Mn^{III}Mn^{II}(\underline{4a})Cl_2]^{+}$$

E.s.r. spectra at 298K for $[Mn^{III}Mn^{II}(\underline{4a})Cl_2Br]$ show no signals, while in frozen glasses, the spectra are broad ($g \simeq 2.0$, 4.1, 5.4, 7.4 and 29.0) and difficult to assign, even at 7.5K. Hyperfine structure of transitions could be obscured by relaxation effects and contributions from excited states[144].

2.4: Complexes of $(\underline{1})^{2-}$ with Main Group Metals

The first report of the incorporation of a main group metal into $(\underline{1})^{2-}$ or its analogues was by Thompson and co-workers[145]. This was a synthesis of $(\underline{1})^{2-}$ about two Pb(II) templates to give $[Pb_2(\underline{1})](NO_3)_2.4H_2O$. This insoluble product was characterised by elemental analysis. This product was used for further reactions, including the reduction of $(\underline{1})^{2-}$ (see Section 2.5). The single crystal X-ray structure of $[Pb_2(\underline{1})](ClO_4)_2$ was reported later by Okawa *et al.*[146] and is shown in Figure 2.11.

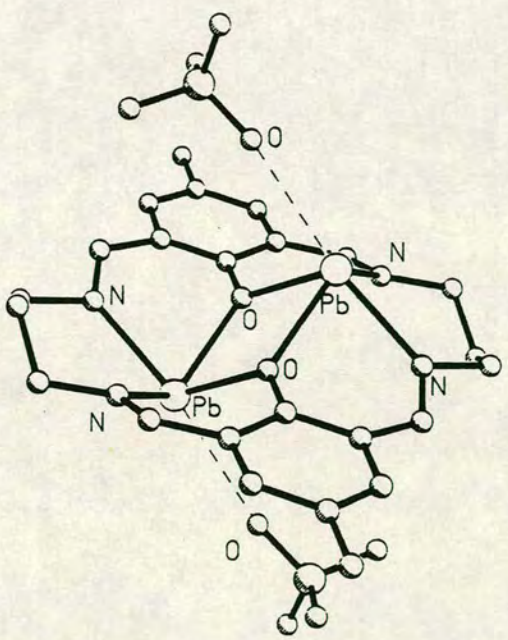

Figure 2.11 $[Pb_2(\underline{1})](ClO_4)_2$
Pb–O = 2.36(1), 2.37(1); Pb–N = 2.42(2), 2.48(2)Å; Distance of Pb(II) ion out of ligand plane = 1.28Å.

Each Pb(II) ion is seven co-ordinate, the co-ordination sphere being completed by three interactions with two ClO_4^- counterions. The macrocycle $(\underline{1})^{2-}$ adopts a planar conformation, except for the central carbons of the propylene groups. This complex illustrates the ability of Pb(II) ions to act as templating agents, particularly as the mismatch in metal ion/macrocycle hole size requires considerable flexibility in co-ordination. Further work has been carried out by this group on the synthesis of mixed Pb(II)/transition metal complexes of $(\underline{1})^{2-}$ and its derivatives[147] of the form $[Pb(ML)_2]^{2+}$ [M = Cu(II) and Ni(II)], using a stepwise synthesis. The ligands prepared in this way are (referring to Figure 2.8):

$(\underline{1})^{2-}$, $R_1 = (CH_2)_3$, $R_2 = (CH_2)_3$, $R_3 = R_4 = R_5 = R_6 = H$, $R_7 = CH_3$;

$(\underline{9a})^{2-}$, as $(\underline{1})^{2-}$ but $R_1 = (CH_2)_2$, $R_2 = (CH_2)_3$;

$(\underline{9b})^{2-}$, as $(\underline{1})^{2-}$ but $R_1 = (CH_2)_2$, $R_2 = (CH_2)_4$;

$(\underline{9c})^{2-}$, as $(\underline{1})^{2-}$ but $R_1 = (CH_2)_2$, $R_2 = (CH_2)_5$;

$(\underline{9d})^{2-}$, as $(\underline{1})^{2-}$ but $R_1 = (CH_2)_3$, $R_2 = (CH_2)_4$.

The compounds prepared were $\{Pb[Ni(\underline{9a})]_2\}^{2+}$, $\{Pb[Ni(\underline{9b})]_2\}^{2+}$, $\{Pb[Cu(\underline{1})]_2\}^{2+}$, $\{Pb[Cu(\underline{9a})]_2\}^{2+}$, $\{Pb[Cu(\underline{9b})]_2\}^{2+}$, $\{Pb[Cu(\underline{9c})]_2\}^{2+}$ and $\{Pb[Cu(\underline{9d})]_2\}^{2+}$ and the single crystal X-ray structure of $\{Pb[Cu(\underline{1})]_2\}(ClO_4)_2$.DMF is shown in Figure 2.12[147]. These complexes are the first examples of ligands with mixed, longer alkane chain side-arms, since the original stepwise synthesis gives poor results with diamines longer than 1,3-diaminopropane[147]. No evidence has been found for heteronuclear species of the type $[PbML]^{2+}$. It remains to be seen if the Pb(II) ion can undergo substitution reactions with other metal ions to give more heterobinuclear complexes.

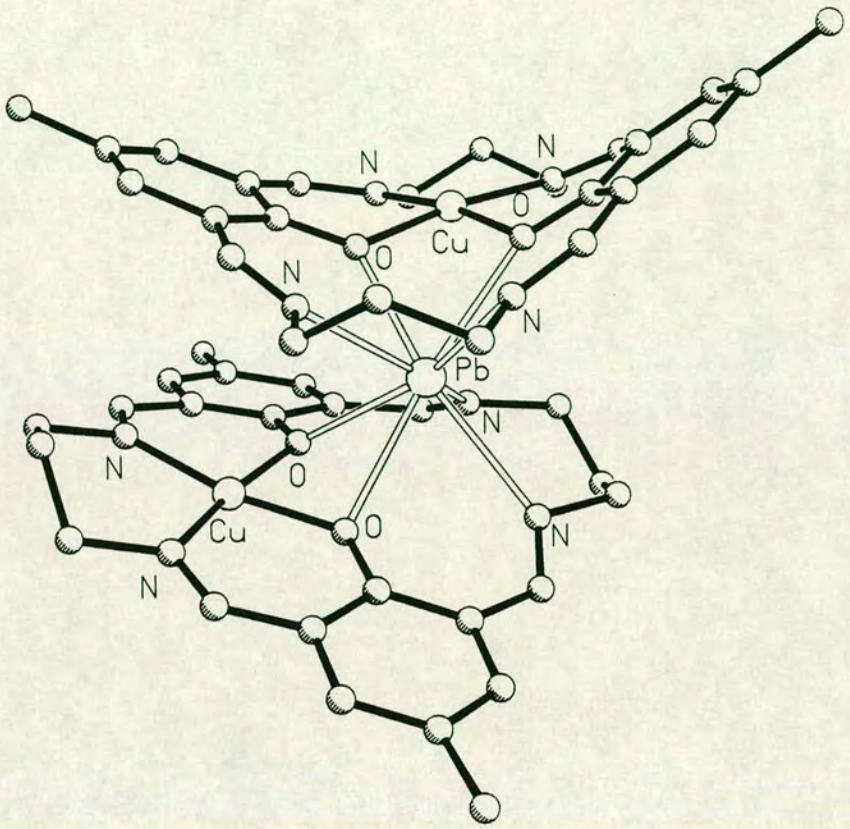

Figure 2.12 $\{Pb[Cu(\underline{1})]_2\}^{2+}$
Range of Pb–O distances = 2.49(1) – 2.67(1); Range of Pb–N distances = 2.63(1) – 2.71(1); Cu1–O = 1.94(1), 1.96(1); Cu1–N = 1.96(1), 1.97(1); Cu2–O = 1.91(1), 1.94(1); Cu2–N = 1.95(2), 1.99(1); Pb–Cu1 = 3.442(2); Pb–Cu2 = 3.424(2)Å.

These complexes are the first examples of ligands with mixed, longer alkane chain side–arms, since the original stepwise synthesis gives poor results with diamines longer than 1,3–diaminopropane[147]. No evidence has been found for heteronuclear species of the type $[PbML]^{2+}$. It remains to be seen if the Pb(II) ion can undergo substitution reactions with other metal ions to give more heterobinuclear complexes.

2.5: Reduced and Oxidised Derivatives of $(\underline{1})^{2-}$ and their Complexes

One further objective of the previous work on $(\underline{1})^{2-}$ has been to reduce the imino bonds in the macrocycle, to give a greater flexibility to the ligand framework and to change the co-ordinating properties of the donor set. It is also likely that the products from such a macrocycle would be less prone to undesirable side reactions and so give cleaner reactions. The first report of a reduced derivative of $(\underline{1})^{2-}$ was by Mandal and Nag[148] which has just two of the imino bonds reduced to secondary amines ($[Cu_2(\underline{10})](ClO_4)_2.2H_2O$ in Figure 2.13).

$(\underline{10a})^{2-}$ R = R' = H

$(\underline{10b})^{2-}$ R = R' = CH_3

$(\underline{10c})^{2-}$ R = Ph, R' = CH_3

$(\underline{10d})^{2-}$ R = R' = Ph

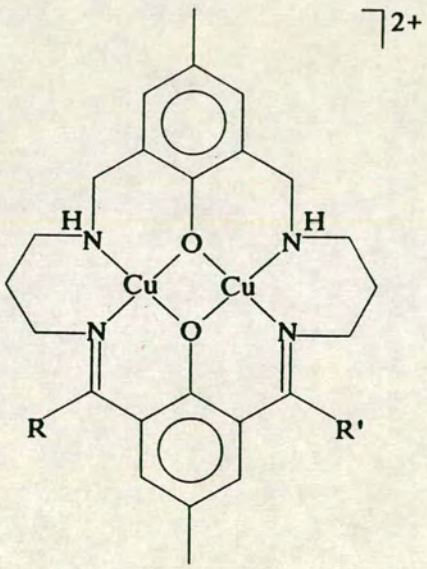

Figure 2.13 $[Cu_2(\underline{10})]^{2+}$

This compound was synthesised by a modification of the strategy developed by Okawa[119] and is summarised in Figure 2.14. The initial step, using two equivalents of 1,3-diaminopropane to one of 2,6-diformyl-4-methylphenol must be carried out at high dilution in order to obtain the desired acyclic product[149]. The electrochemical properties of $[Cu_2(\underline{10})]^{2+}$ will be discussed in conjunction with the fully reduced form later.

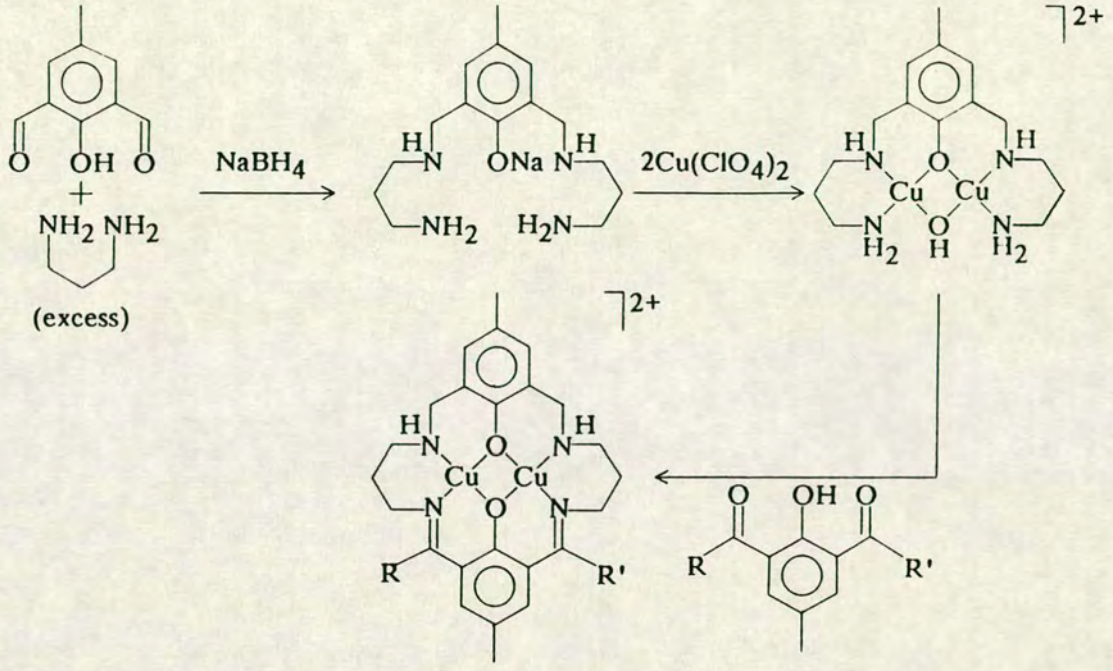

Figure 2.14 Synthesis of $[Cu_2(\underline{10})](ClO_4)_2$

The fully reduced form of ($\underline{1}H_2$), ($\underline{11}H_2$), has been isolated as the product of the reaction between a suspension of $[Pb_2(\underline{1})](NO_3)_2$ in a H_2O/CH_3OH mixture and $NaBH_4$ [145] and analysed by elemental analysis and ^1H n.m.r. spectroscopy. Reaction of ($\underline{11}H_2$) with two equivalents of $Cu(ClO_4)_2$ in aqueous NaOH gives the blue product $[Cu_2(\underline{11})(ClO_4)_2]$. The single crystal X-ray structure of $[Cu_2(\underline{11})(ClO_4)_2]$ [145] shows that the geometries at the Cu(II) ions are best described as severely distorted, axially elongated octahedra with the metal centres lying in the centre of the macrocyclic N_2O_2 plane. The axial positions are occupied by two bidentate ClO_4^- ligands. The single crystal X-ray structure of $[Cu_2(\underline{11})(CH_3OH)_2](ClO_4)_2$, which shows *trans*-axially co-ordinated CH_3OH molecules, has also been reported[150] and is shown in Figure 2.15. This structure shows that the saturation of the imino bonds allows the ligand $(\underline{11})^{2-}$ to twist and gives the complex a shorter metal-metal distance than any complex of $(\underline{1})^{2-}$. This increased interaction is reflected in the greater

antiferromagnetic exchange interactions found for these two complexes of $(\underline{11})^{2-}$ [145,150].

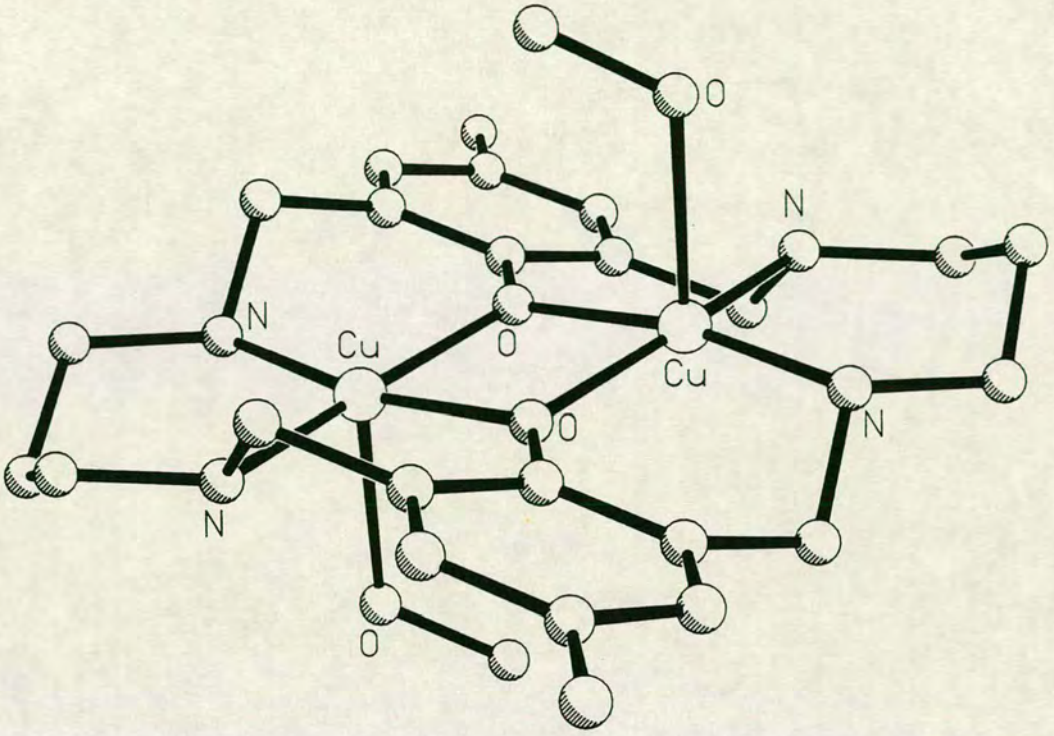

Figure 2.15 $[Cu_2(\underline{11})(CH_3OH)_2]^{2+}$
Cu–N = 1.989(4), 1.991(4); Cu–O = 1.9590(25), 1.963(3);
Cu–O–CH_3 = 2.413(4); Cu–Cu(a) = 3.088(1)Å; ∠Cu–O–Cu(a) = 103.88(12)°.

The electrochemical data[145] for the compounds $[Cu_2(\underline{1})]^{2+}$, $[Cu_2(\underline{10a})]^{2+}$ and $[Cu_2(\underline{11})]^{2+}$ are summarised in Table 2.3. The partially– and fully–reduced complexes show the first, one–electron reduction process occuring at progressively more negative potentials with increasing saturation of the macrocyclic ring. This is consistent with the enhanced stability of Cu(I) centres with unsaturated N–donors, as documented for mononuclear analogues[151]. The second, one–electron reduction process is surprisingly unaffected by the degree of unsaturation. Additionally, the complex $[Cu_2(\underline{11})]^{2+}$ shows two reversible, one–electron oxidations and $[Cu_2(\underline{10a})]^{2+}$ shows one oxidation. This behaviour of $[Cu_2(\underline{11})]^{2+}$, to give four, one–electron redox processes in a binuclear Cu system is unprecedented[145].

Table 2.3: Electrochemical data for $[Cu_2(\underline{11})]^{2+}$, $[Cu_2(\underline{10a})]^{2+}$ and $[Cu_2(\underline{1})]^{2+}$

	Step $Cu^{II}_2 \rightarrow Cu^{II}Cu^{I}$ (V)	Step $Cu^{II}Cu^{I} \rightarrow Cu^{I}_2$ (V)	K_{CON} (red.)	Step $Cu^{II}_2 \rightarrow Cu^{III}Cu^{II}$ (V)	Step $Cu^{III}Cu^{II} \rightarrow Cu^{III}_2$ (V)	K_{CON} (oxid.)
$[Cu_2(\underline{11})(ClO_4)_2]$	-0.76	-0.90	2.3×10^2	+1.19	+1.41	5.2×10^3
$[Cu_2(\underline{10a})](ClO_4)_2$	-0.58	-0.90	2.6×10^5	+1.34		
$[Cu_2(\underline{1})](ClO_4)_2$	-0.46	-0.94	1.3×10^8			

Reductions performed in DMSO, oxidations in CH_3CN

The value of K_{con} for the reaction

$$[Cu^{II}_2(\underline{11})]^{2+} + [Cu^{III}_2(\underline{11})]^{4+} \rightleftarrows 2[Cu^{III}Cu^{II}(\underline{11})]^{3+}$$

is 5.2×10^3, which is lower by orders of magnitude than those of the unsaturated, reduced complexes. Solution e.s.r. studies at 298K for both mixed-valence species of $(\underline{11})^{2-}$, $[Cu^{II}Cu^{I}(\underline{11})]^{+}$ and $[Cu^{III}Cu^{II}(\underline{11})]^{3+}$, show hyperfine interactions with just one Cu nucleus (four lines, for ^{63}Cu and ^{65}Cu, I = 3/2). This suggests that the Cu(III) centre in the oxidised species is low spin and the unpaired electron in both mixed-valence species is localised on the e.s.r. time scale[145].

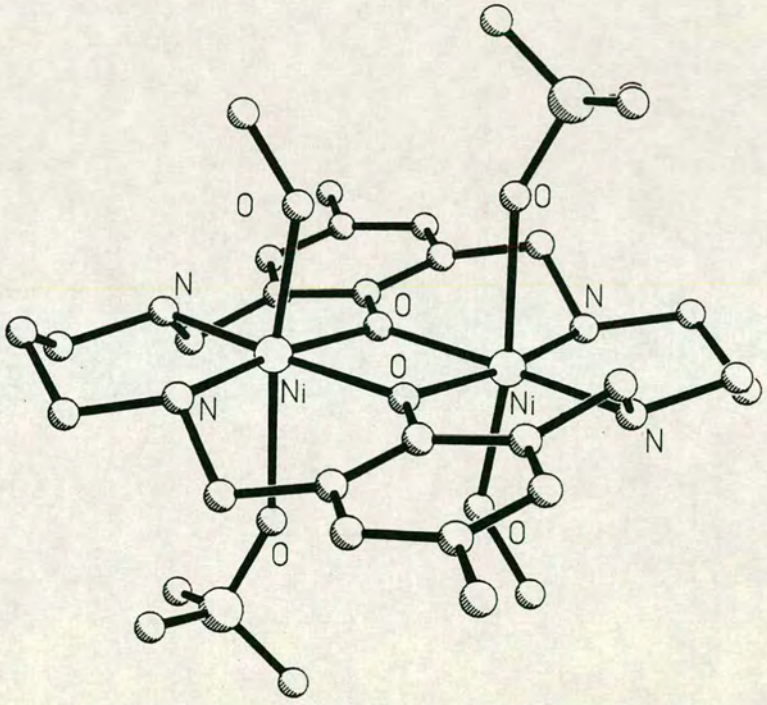

Figure 2.16 $[Ni_2(\underline{11})(CH_3OH)_2(ClO_4)_2]$
Ni-N = 2.064(3), 2.057(5); Ni-O = 2.028(4), 2.027(3);
Ni-O-ClO_3 = 2.411(5); Ni-OH-CH_3 = 2.105(5); Ni-Ni(a) = 3.135(2)Å;
∠Ni-O-Ni(a) = 101.3(1)°.

Nag and co-workers have also prepared binuclear Ni(II) complexes with ligand $(\underline{11})^{2-}$ [152,153]. Single crystal X-ray structures show that the Ni(II) centres in $[Ni_2(\underline{11})(CH_3OH)_2(ClO_4)_2]$ [152] (shown in Figure 2.16) have pseudo-octahedral geometries, while in $[Ni_2(\underline{11})(pyridine)_2](ClO_4)_2$ [153], the

Ni(II) ions have square-pyramidal co-ordination, with the pyridine ligands in *trans*-diaxial sites. In both complexes, the ligand $(\underline{11})^{2-}$ has a puckered conformation.

Cyclic voltammetry of $[Ni_2(\underline{11})(CH_3OH)_2(ClO_4)_2]$ in DMSO shows a quasi-reversible, one-electron reduction at $E_{\frac{1}{2}} = -1.8V$ *vs.* Fc/Fc^+ and a quasi-reversible reduction at $E_{\frac{1}{2}} = -2.1V$ *vs.*Fc/Fc^+, which are consistent with the formation of $[Ni^{II}Ni^{I}(\underline{11})]^+$ and $[Ni^{I}Ni^{I}(\underline{11})]$ respectively[152]. The latter species was not stable on the coulometric time scale. In CH_3CN, $[Ni_2(\underline{11})(CH_3OH)_2(ClO_4)_2]$ also shows two reversible oxidations ($E_{\frac{1}{2}} = +0.6$ and $+0.7V$ *vs.*Fc/Fc^+ respectively) which were found to be one-electron processes.

Okawa and co-workers[154] and Thompson and co-workers[155] have also reported the Cu(II) complexes of oxidised derivatives of $(\underline{1})^{2-}$, where two amido groups replace two of the imino groups (see Figure 2.17). Okawa *et al.* first reported the synthesis of $[Cu_2(\underline{12a})]$ [65] which is insoluble in most solvents. The single crystal X-ray structures of $[Cu_2(\underline{12b})]$ and $[Cu_2(\underline{12c})]$ were obtained[155] by adding $-(C_3H_7)$ and $-(C_6H_5)$ units to the macrocycle, which were sufficient to solubilise the neutral complexes. For both $[Cu_2(\underline{12b})]$ and $[Cu_2(\underline{12c})]$ very strong antiferromagnetic exchange is observed between the the metal centres[155].

$(\underline{12a})^{4-}$, n = 2, R = H

$(\underline{12b})^{4-}$, n = 2, R = C_3H_7

$(\underline{12c})^{4-}$, n = 3, R = C_6H_5

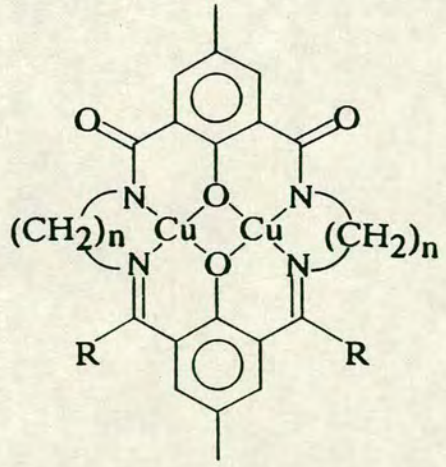

Figure 2.17 $[Cu_2(\underline{12})]$

2.6: Derivatives of $(\underline{1})^{2-}$ with Functionalised Side-arms

Recent developments in the chemistry of the derivatives of $(\underline{1})^{2-}$ have included the introduction of other functional groups in the diamine chain. Modifications of this sort have lead to the isolation of some higher nuclearity species (see below). The first example, however, was described by Gagné, Hendrickson and co-workers in 1985, as a binucleating, clathrochelate ligand, $(\underline{13})^{3-}$. This was synthesized by the condensation of three equivalents of 2,6-diformyl-4-methylphenol with two equivalents of tren [tris(aminoethyl)amine] about two metal templates[156]. The single crystal X-ray structure of $[FeCo(\underline{13})](BF_4)$ was reported and corrected[157], to show the complexation of the two metal centres in equivalent, highly distorted octahedral sites, with a Fe-Co distance of 3.07Å. Other complexes prepared with this ligand were $[Cu_2(\underline{13})]^+$, $[Fe_2(\underline{13})]^+$, $[Mn_2(\underline{13})]^+$ and $[MnFe(\underline{13})]^+$, and were found to be isostructural with $[FeCo(\underline{13})](BF_4)$.

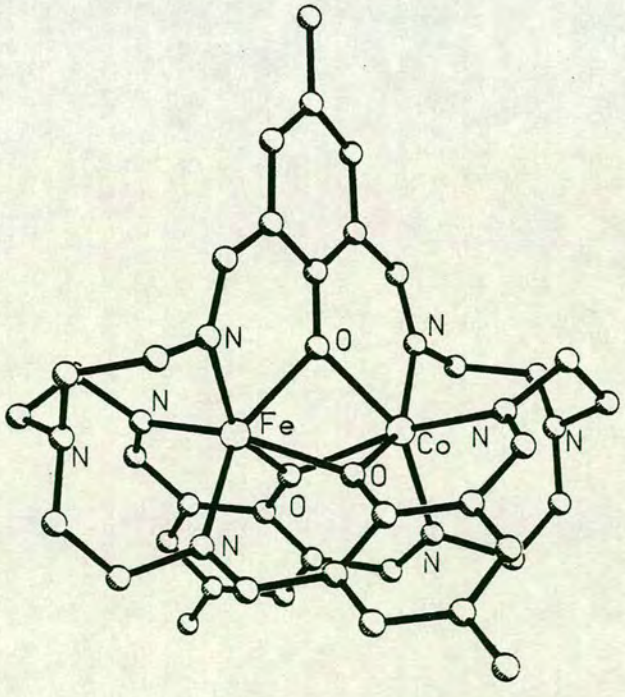

Figure 2.18 $[FeCo(\underline{13})]^+$

The inclusion of alkoxy groups in the side-chains has been a significant step in the co-ordinative properties of $(\underline{1})^{2-}$ and its derivatives. The design

of ligands with endogenous bridges as models for haemocyanin has been an important motive for this work. Fenton *et al.*[158] synthesised the compound $[Ba(\underline{14}H_4)(ClO_4)_2]$, where $(\underline{14}H_4)$ is the fully protonated ligand formed by the [2+2] condensation of 2,6-diacetyl-4-methylphenol with 1,3-diamino-2-propanol in the presence of one equivalent of $Ba(ClO_4)_2$. The single crystal X-ray structure of $[Ba(\underline{14}H_4)(ClO_4)_2]$ showed the ligand to have an unusual folded structure with just one Ba(II) ion co-ordinated above the potentially octadentate N_4O_4 cavity. This is an important example of a template synthesis around a non-transition metal ion.

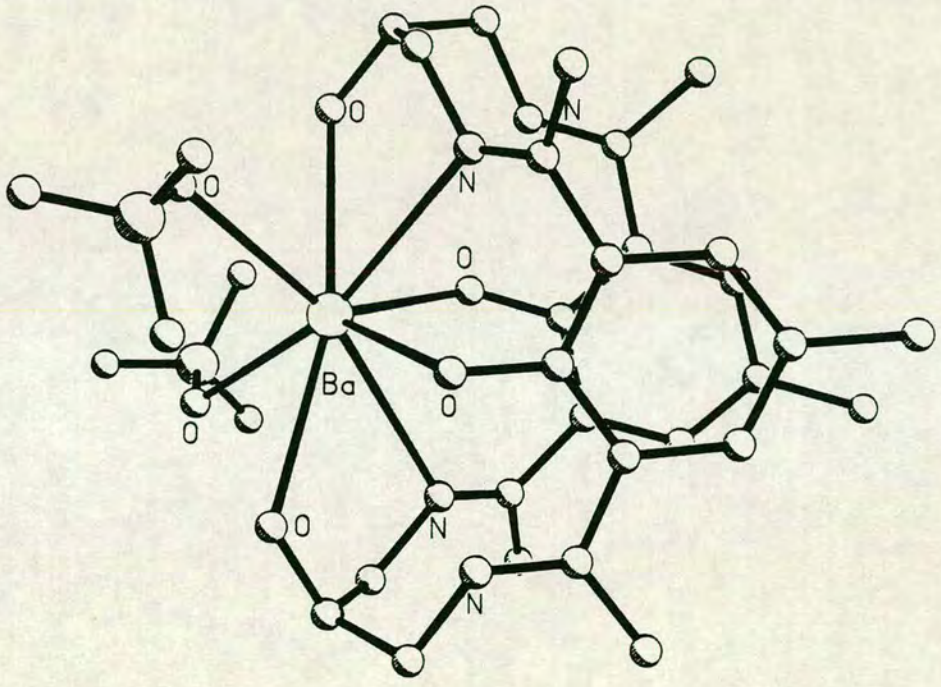

Figure 2.19 $[Ba(\underline{14}H_4)(ClO_4)_2]$

In $[Ba(\underline{14}H_4)(ClO_4)_2]$, two N-donors are hydrogen-bonded to adjacent phenol oxygens and are not bound to the metal ion. The co-ordination sphere of the Ba(II) is completed by interactions with two ClO_4^- counterions. The fact that this compound is mononuclear is probably due to the size of the Ba(II) centre (radius = 1.29Å)[159], which is too large for two metal centres to fit into the macrocyclic cavity. By comparison, the complexes $[Pb_2(\underline{14}H_2)(SCN)_2]$ and $[Sr_2(\underline{14}H_2)(ClO_4)_2]$ [158] are binuclear (radius of

Pb(II) = 1.06Å, radius of Sr(II) = 1.13Å).

A slightly different result was found by McKee and Tandon[160] with the complexation of $(\underline{15a}H_2)^{2-}$ with Pb(II) and Ba(II) salts. The Ba(II) complex was mononuclear, but with Pb(II), binuclear, mononuclear and demetallated compounds were formed. The binuclear complex, $[Pb_2(\underline{15a}H_2)](ClO_4)_2$, was the initial kinetic product of a reaction between equimolar quantities of 2,6-diformyl-4-methylphenol and 1,3-diamino-2-propanol in the presence of $Pb(ClO_4)_2$. On standing, this slowly converts to the two other forms. Single crystal X-ray structures of $[Pb_2(\underline{15a}H_2)](ClO_4)_2$, $[Pb(\underline{15a}H_4)](ClO_4)_2$ and $[(\underline{15a}H_6)(H_2O)_2](ClO_4)_2$ have been reported[160].

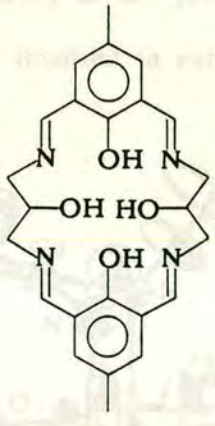

Figure 2.20 ($\underline{15a}H_4$)

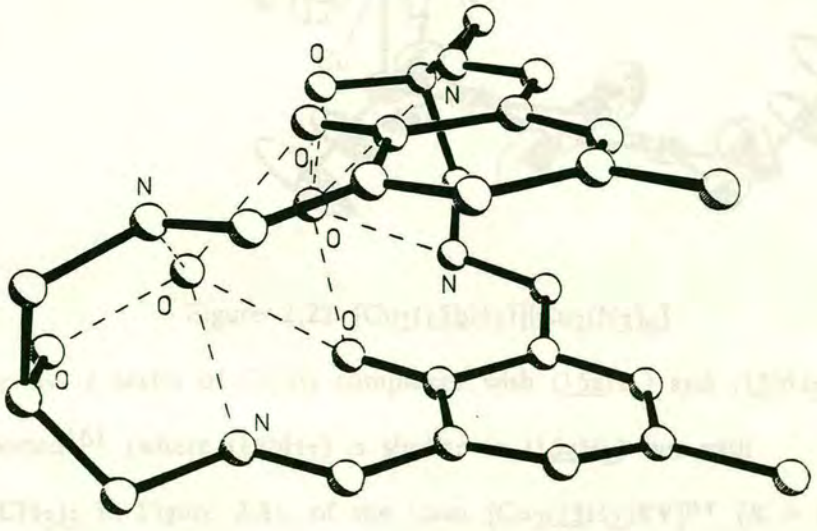

Figure 2.21 $[(\underline{15a}H_6)(H_2O)_2]^{2+}$

co-ordination to two Cu(II) ions in the square plane of the macrocycles, the macrocyclic side-arms can not distort sufficiently to interact with the metal centres, and so the secondary alcohol groups remain unco-ordinated. The single crystal X-ray structure of $[Cu_2(\underline{15b}H_2)][Cu_2(N_3)_6]$ [161], which has unusual polymeric, hexa-azide bridging interactions between the $[Cu_2(\underline{15b}H_2)]^{2+}$ units, is shown in Figure 2.22.

Using a ligand that has only one functionalised side-arm, Tuchagues and co-workers[162] have isolated and structurally characterised a binuclear manganese(II) complex, $[Mn_2(\underline{16}H)(CH_3CO_2)](ClO_4)$. This has the Mn(II) ions in essentially square-pyramidal geometries, but with axial interactions with the $CH_3CO_2^-$ groups in preference to the alcohols on the sidearms. The binuclear Mn_2 units stack in infinite chains, with bidentate $CH_3CO_2^-$ bridges. In the single crystal X-ray structure shown in Figure 2.23, the pendant alcohol groups are unco-ordinated and disordered between the two propylene chains, C11 and C11'.

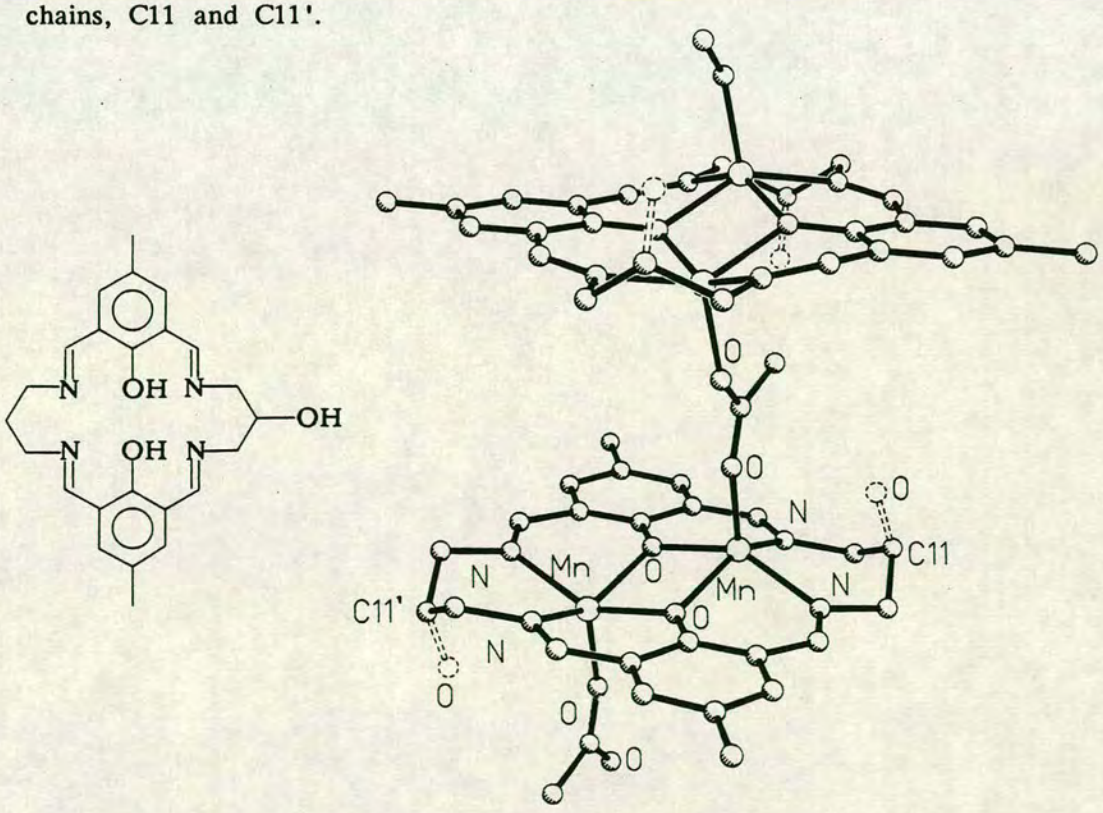

Figure 2.23 ($\underline{16}H_3$) and two units of the $[Mn_2(\underline{16}H)(CH_3CO_2)]^+$ chain

Similar unsymmetrical ligands have been used by Okawa *et al.*[163] in a development of their stepwise synthesis of macrocycles related to $(\underline{1})^{2-}$. They found that the ring closing step (Step (b) in Figure 2.5) with 1,3-diamino-2-propanol gave better results using Pb(II) salts as a templating ion. Heterobinuclear complexes of the form $[CuPb(\underline{16})]^{2+}$ could be prepared in this way, these species being unobtainable by other methods[163].

An important feature of these ligands is that the condensation reaction always proceeds to give a stereospecific product, with the pendant alcohol groups directed into the cavity of the macrocycle (as is to be expected from a template synthesis). This gives ligands like $(\underline{15a}H_2)^{2-}$ the potential to act as octadentate ligands. By including a μ_4-bridging donor in the centre of the cavity, McKee and Tandon have prepared a number of Cu_4 and Cu_8 complexes[164-166], and a mixed-valence $Mn^{II}_2Mn^{III}_2$ complex[167] with ligands such as $(\underline{15a})^{4-}$. A [3+3] condensation of three equivalents of 2,6-diformyl-4-methylphenol with three equivalents of 1,5-diamino-3-pentanol in the presence of $Cu(NO_3)_2$ gives a Cu_6 macrocyclic complex, which dimerises to form a Cu_{12} agglomerate[168].

Phenol groups can also be used as endogenous bridges in the side-arms, to ensure the *endo* conformation of the extra donor ligands. Robson and co-workers have designed a tetranucleating ligand using 2,6-bis(aminomethyl)-4-methylphenol as the diamine linkage[169]. The reaction of two equivalents of 2,6-bis(aminomethyl)-4-methylphenol with two equivalents of 2,6-diformyl-4-methylphenol in the presence of $Ni(CH_3CO_2)_2$ in CH_3OH gives $[Ni_4(\underline{17})(CH_3CO_2)_2(OH)(CH_3O\text{-}H\text{-}OCH_3)]$ [169] as a tetranuclear macrocyclic complex. An analogous Zn_4 macrocyclic complex can be prepared in the same way using $Zn(CH_3CO_2)_2$ [169]. Using $Cu(CH_3CO_2)_2$ as the templating agent, a hexanuclear $[Cu_6(\underline{17a})(CH_3CO_2)_2(OH)_2(CH_3OH)_2(H_2O)](BF_4)_2$ species is obtained, where

($\underline{17a}$)$^{6-}$ is a [3+3] condensation product[170]. The single crystal X-ray structure of [Ni_4($\underline{17}$)(CH_3CO_2)$_2$(OH)(CH_3O-H-OCH_3)], in Figure 2.23, shows that the ligand ($\underline{17}$)$^{4-}$ adopts a domed conformation and incorporates a μ_4-OH group in the centre of the structure. Reactions of this complex with N_3^- and CH_3O^- showed the [Ni_4($\underline{17}$)(OH)(CH_3O-H-OCH_3)]$^{2+}$ to be a stable unit, capable of undergoing substitution reactions[171]. The metal-free protonated ligand has also been synthesised[169], as an insoluble salt [($\underline{17}H_6$)]Cl_2. This can be reduced with $NaBH_4$, to give [($\underline{18}H_8$)]Cl_4, which is the amine analogue of the tetranucleating Schiff-base macrocycle[172]. The structure of the Zn_4 complex with ($\underline{18}$)$^{4-}$ has been reported[172].

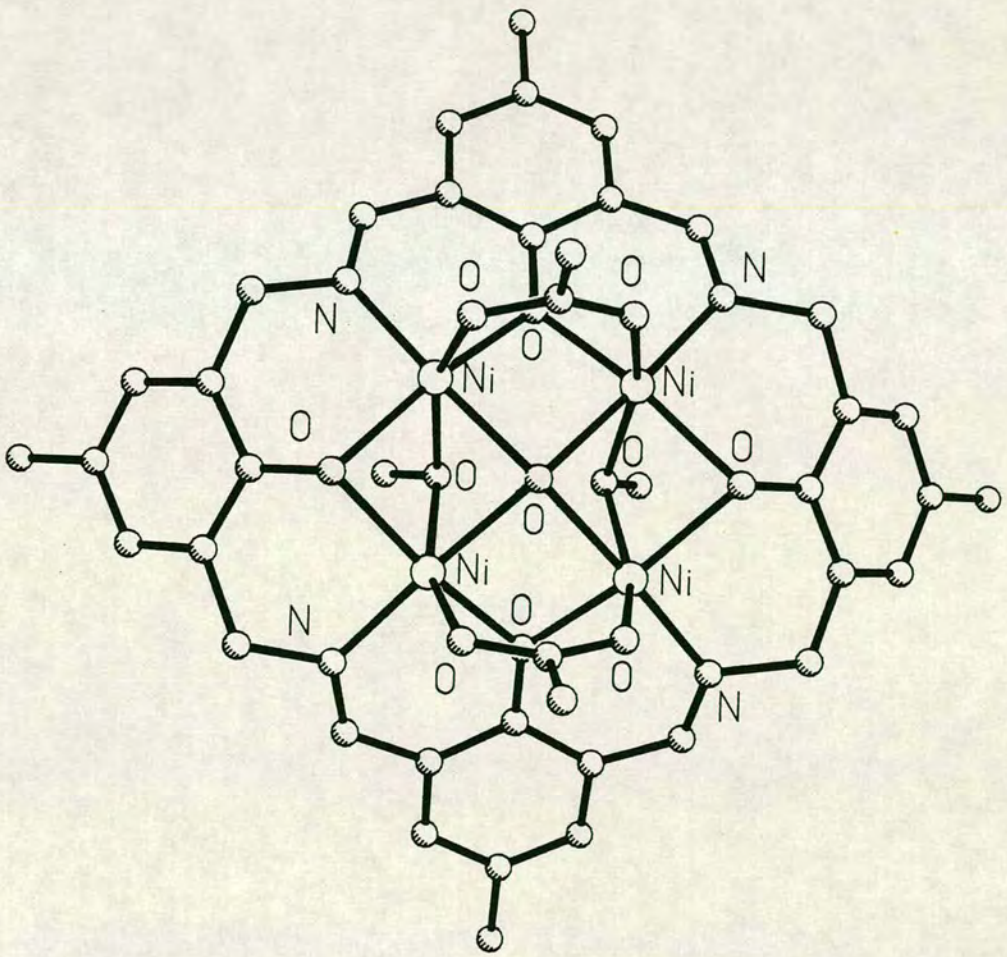

Figure 2.23 [Ni_4($\underline{17}$)(CH_3CO_2)$_2$(OH)(CH_3O-H-OCH_3)]

Attempts to prepare complexes of macrocycles with side-arms containing functional groups other than alkoxy and phenoxy groups have also been reported. Fenton and co-workers tried to incorporate two ether groups in a compartmental macrocycle[173], complexes with an amine group have been mentioned above as $[Cu_2(\underline{6})]^{2+}$ [131] and Okawa *et al.* have reported tetranuclear and binuclear complexes of ligands using 1,8-diamino-3,6-diaza-octane[174] and 1,9-diamino-3,7-diazanonane respectively[175] as the diamine linkage.

Finally, a Schiff-base macrocycle has been reported that is formed by the [2+2] condensation of two equivalents of 3-formyl-benzaldehyde with 1,5-diamino-3-azapentane[176]. The binuclear Cu(I) complex of this ligand has been found to react with O_2 to give the corresponding binuclear Cu(II) complex with bridging hydroxy and phenoxy donors (see Figure 2.25). This is the first example of a macrocyclic tyrosinase model, with the O_2 insertion step proceeding in 74% yield, as determined by the ratios of the dialdehyde products obtained by acidic degradation of the final Cu(II) complex.

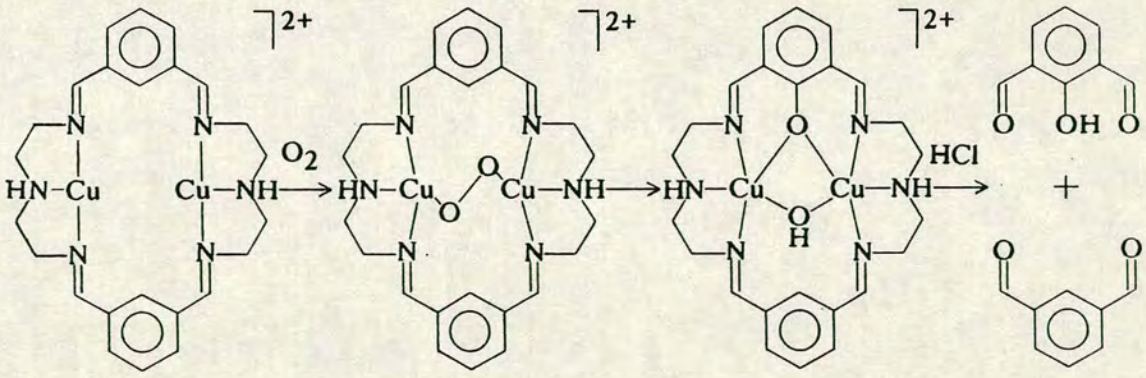

Figure 2.25 The hydroxylation of a Schiff-base macrocyclic ligand by O_2.

CHAPTER 3

The Synthesis and Characterisation of the Schiff-Base Macrocycles $(\underline{1})^{2-}$, $(\underline{2})^{2-}$ and $(\underline{5})^{2-}$

3.1: Introduction

A macrocyclic framework is a useful basis for synthesising binuclear metal complexes, since macrocyclic cavities can clearly define the metal binding sites and force the metal centres into close proximity. Once the metal complex is formed, the macrocycle could also act as a mediating group between the metal centres and create other specific, co-ordinatively labile sites on the metal centres. Moreover, since macrocyclic compounds show useful potential in the development of catalytic systems in general, binuclear species might be especially important, since the specific labile sites created on the metal centres can be fixed adjacent to one another.

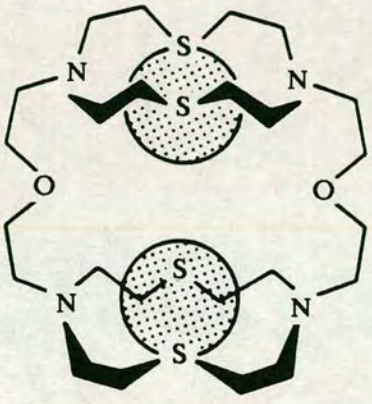

Figure 3.1 A binuclear complex using a macropolycyclic ligand

The predominant form of binuclear macrocyclic complexes reported in the literature have been dimeric porphyrinoid metal compounds, which have been mentioned in Chapter 1. Other examples of binuclear macrocyclic complexes are characterised by the work of Lehn[3,177] and Weiss[178] and co-workers on the synthesis of macropolycyclic ligands which can bind two metal centres in a face-to-face manner similar to the porphyrins (see Figure 3.1). At Edinburgh, the incorporation of two Cu(I)[103,104], Ag(I)[104], Au(I)[104] and Pd(II)[179] metal ions into the large ring macrocycles [24]aneS$_8$ and [28]aneS$_8$ has been achieved. The complexes [Pd$_2$([24]aneS$_8$)](PF$_6$)$_4$ and

$[Pd_2([28]aneS_8)](PF_6)_4$ are part of a series of studies we have undertaken on the complexation of the platinum metals with N–, O– and particularly S–donor macrocycles[6,16]. The binding of the platinum metals to macrocycles should give very inert species with versatile redox activities and may have special applications in catalytic chemistry.

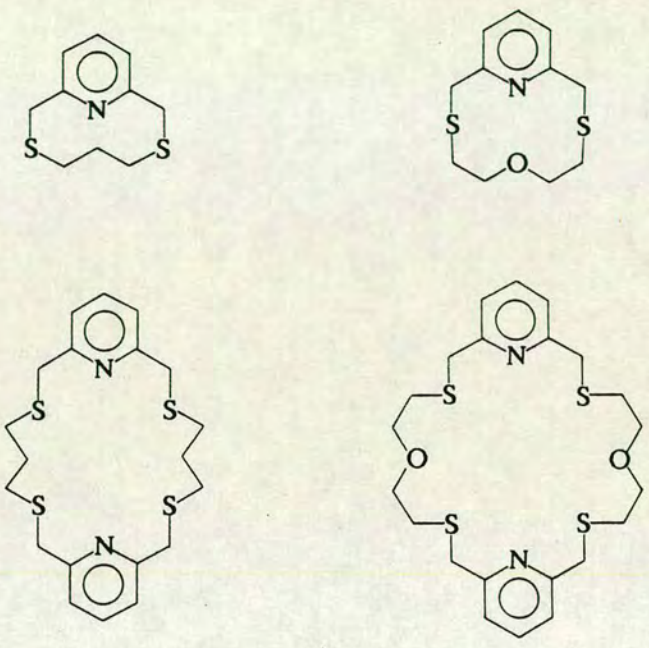

Figure 3.2 Pyridine–based macrocyclic ligands

Parker *et al.* have reported a number of binuclear macrocyclic complexes with Rh(I)[180–184], Pd(II)[180,181] and Pt(II)[181] centres, using pyridine–containing ligands, including those shown in Figure 3.2. The smaller ring macrocycles form complexes of the form $[RhL(CO)]_2^{2+}$ that dimerise with carbonyl bridges, while the hexa– and octa–dentate macrocycles are thought to incorporate two metal centres within the ring. Lawrance and co–workers[185] have also reported Ni(II) and Pd(II) binuclear complexes with a fully saturated macrocycle which has two bridging thiolates, shown in Figure 3.3. The synthesis of $[M_2(\underline{19})]^{2+}$ is also shown in Figure 3.3 and the formation of $[Pd_2(\underline{19})](ClO_4)_2$ is the first known example of Pd(II) ions acting as templating agents[185].

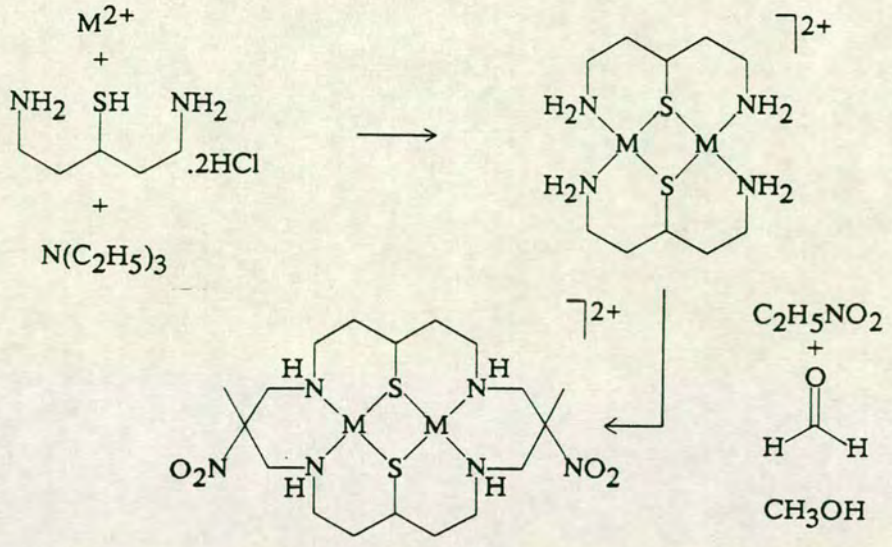

Figure 3.3 Synthesis of $[M_2(\underline{19})]^{2+}$ [M = Ni(II), Pd(II)]

The complexes of $(\underline{1})^{2-}$ and its derivatives reported in the literature have necessarily been limited to complexes of labile metal centres which are good templating agents. This is illustrated by the numerous examples reported containing Cu(II), a good templating ion. To overcome this limitation and to synthesize complexes of $(\underline{1})^{2-}$ with non-labile second and third row metal ions, metal insertion into the preformed ligand is required. In our previous work at Edinburgh with mononuclear macrocyclic complexes, we have found that template syntheses are generally unsuccessful with the platinum metals due to the relative stability of the intermediates formed in the template process[186]. Metal insertion into the preformed macrocycle, however, can yield good results. In order to synthesize binuclear complexes of $(\underline{1})^{2-}$ with Pd(II), Pt(II), Rh(I)/(III), Ir(III) and Ru(II)/(III), we proposed to undertake the synthesis of the unmetallated ligand. To our knowledge, there have been no previously reported, structurally characterised, binuclear complexes of the platinum group metals, where the metal centres are enclosed within the same macrocyclic ring. This is a major objective of our work with the macrocycle $(\underline{1})^{2-}$.

The protonated macrocyclic ligand, $[(\underline{1}H_4)](Br_3)_2$, has been prepared

previously in low yield by Robson and co-workers[116] by boiling $[Co_2(\underline{1})Br_2]$ in CH_3OH in an excess of Br_2. A compound with similar composition was obtained by the metal-free reaction of 2,6-diformyl-4-methylphenol with 1,3-diaminopropane in the presence of HBr in CH_3OH, followed by addition of excess Br_2. However, only the elemental analysis and i.r. spectrum of the highly insoluble $[(\underline{1}H_4)](Br_3)_2$ species was reported[116]. We proposed to repeat the metal-free synthesis of $[(\underline{1}H_4)]^{2+}$, but with metathesis of the counterion to PF_6^- or BF_4^- as the final step. A soluble and stable product should be obtained, which could be used for metal insertion reactions with any metal centres. Other derivatives of $(\underline{1})^{2-}$ in their protonated forms and in metal complexes could also be synthesised by this method. McKee and Tandon[160] remarked that the protonated ligand $[(\underline{15a}H_6)(H_2O)_2]^{2+}$ (see Figure 2.21) appeared to be the thermodynamically favoured product of a synthesis in the presence of a Pb(II) template and attributed this stability to the folded conformation that allowed intra- and inter-molecular π-interactions. The hydrogen-bonded H_2O molecules that occupy the cavity may also have a significant stabilising effect, particularly with the interactions of the alcohol pendant arms. The unfunctionalised ligand, $(\underline{1})^{2-}$, would not have these auxiliary interactions.

Robson and Pilkington[97] have reported that many attempts to isolate the metal-free ligand previous to the synthesis of $[(\underline{1}H_4)](Br_3)_2$ had been unsuccessful. Insoluble, gummy products were obtained, that did not give satisfactory analyses[1]. Transmetallation reactions are also a possible route to binuclear complexes of $(\underline{1})^{2-}$, using $[Pb_2(\underline{1})](NO_3)_2$ as a source of the ligand. The Pb(II) ions are expected to be readily replaced due to the size mismatch and displacement of the Pb(II) ions from the ligand cavity. However, it is likely that reactions with kinetically inert metals will give a mixture of products, through incomplete substitution of the Pb(II) metal ions.

3.2: Results and Discussion

3.2.1: The Synthesis of $[(\underline{1}H_4)]^{2+}$

Reaction of equimolar amounts of 2,6-diformyl-4-methylphenol and 1,3-diaminopropane with an excess of aqueous HBr in refluxing CH_3OH gave a red solution with varying amounts of an insoluble, yellow solid. On the basis of its insolubility and its i.r. spectrum, which shows C=O stretching vibrations, this latter yellow product is probably a polymer. Reducing the volume of solvent, followed by addition of excess NH_4PF_6 or $NaBF_4$ counterion gave an orange crystalline material. Recrystallisation of the orange solid from CH_3NO_2/diethyl ether by solvent or vapour diffusion gave a red crystalline product.

The i.r. spectrum of the product shows two close bands due to imine stretching vibrations (symmetric and asymmetric modes), coming at 1667 and 1645cm^{-1}. This is shifted from the two aldehyde C=O stretching vibrations of 2,6-diformyl-4-methylphenol, for which there are two bands at 1685 and 1665cm^{-1}. This shift and the absence of the characteristic band at 2870cm^{-1} due to the aldehydic C-H stretching vibration, shows that cyclisation has occured. Other strong bands present are at 1537cm^{-1}, which may be due to the C-O stretching vibration of the phenol, and at 1055cm^{-1} for the BF_4^- counterion or at 840 and 558cm^{-1} for the PF_6^- counterion. F.a.b. mass spectroscopy shows molecular ion peaks at M^+ = 405 and 551/493. These are assigned to $[(\underline{1}H_3)]^+$ and $[(\underline{1}H_4)](PF_6)^+/[(\underline{1}H_4)](BF_4)^+$ respectively. This evidence combined with elemental analytical data confirm the product as $[(\underline{1}H_4)](PF_6)_2$ or $[(\underline{1}H_4)](BF_4)_2$. In just one synthesis, smaller molecular ion peaks at M^+ = 607, 753 and 899 are observed, which correspond to the products of a minor [3+3] condensation, and are assigned as $[C_{36}H_{43}N_6O_3]^+$, $[C_{36}H_{44}N_6O_3](PF_6)^+$ and $[C_{36}H_{45}N_6O_3](PF_6)_2^+$ respectively. It is not known why this is unrepeatable.

Electronic spectroscopy of $[(\underline{1}H_4)]^{2+}$ in different solvents all give an absorption at $\lambda_{max.}$ = 432 nm., but with variable extinction coefficients [$\varepsilon_{max.}$ = 37,700$M^{-1}cm^{-1}$ in CH_3NO_2, 35,000 in $(CH_3)_2CO$, 33,800 in CH_3CN]. Also, the solutions of $[(\underline{1}H_4)]^{2+}$ in various solvents have visibly different colours [red in CH_3NO_2 and CH_3OH, orange in CH_3CN and yellow in $(CH_3)_2CO$)]. Although there is no apparent shift in $\lambda_{max.}$ in the electronic spectra, the visible differences are probably due to different band-shapes, with underlying bands to the main absorption causing the bulk differences. This suggests there are variations in the extent of the π-interactions in solution, caused by the polarities of the different solvents [dipole moments for solvents: μ = 3.84D (CH_3CN); μ = 3.44D (CH_3NO_2); μ = 2.88D [$(CH_3)_2CO$]; μ = 1.71D (CH_3OH)[244]]. Factors affecting the π-interactions could include the stabilisation of different conformers in solution and stabilisation of the excited states (from $\pi \rightarrow \pi^*$) with varying solvent polarity.

The ^1H n.m.r. spectrum of a crystalline sample of $[(\underline{1}H_4)](PF_6)_2$ measured at 298K in CD_3NO_2 is shown in Figure 3.4. Each major resonance peak can be assigned to a unique proton environment and are assigned below. However, each assigned peak appears to have an accompanying minor peak, at approximately 20% of the major peak's integration.

δ = 2.16p.p.m., Ph-C$\underline{H}_3$, 6H, singlet, minor peak at 2.30p.p.m.;

δ = 2.51p.p.m., C-C$\underline{H}_2$-C, 4H, broad singlet, minor peak at 2.27p.p.m;

δ = 4.20p.p.m., C-C$\underline{H}_2$-N, 8H, broad doublet, minor peak at 4.05p.p.m.;

δ = 7.37p.p.m., Ph-$\underline{H}$, 4H, singlet, minor peak at 7.70p.p.m.;

δ = 8.39p.p.m., Ph-C$\underline{H}$=N, doublet, J = 13Hz, minor peak at 8.55p.p.m.;

δ = 13.71p.p.m., N-$\underline{H}$, broad with shoulder.

The protons on the imino-carbons have a large coupling constant

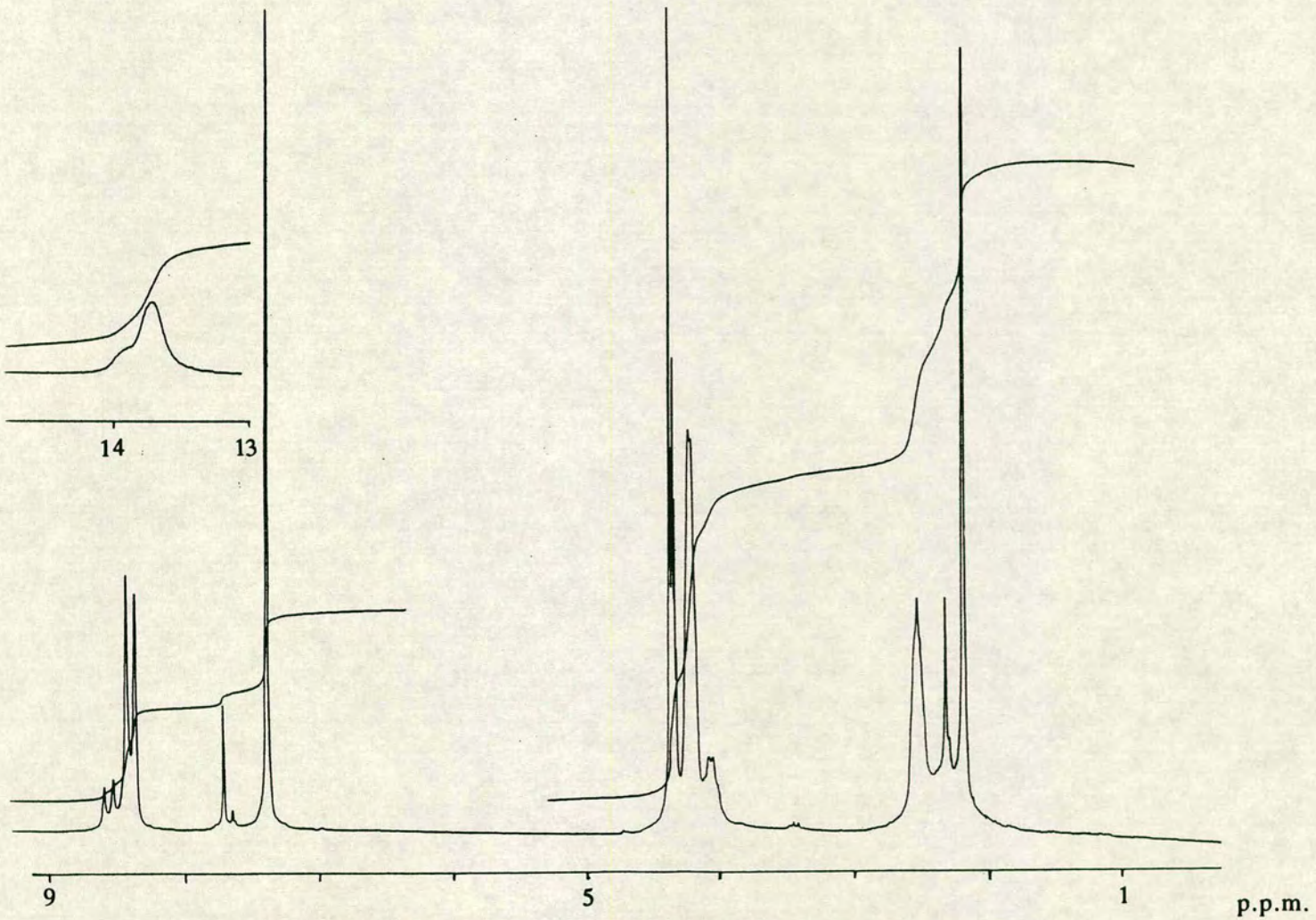

Figure 3.4 ^{1}H n.m.r. spectrum of $[(\underline{1}H_4)](PF_6)_2$ in CD_3NO_2

(J = 13Hz) with no other signal showing complementary splitting. The acidic protons on the N–atoms are *trans* to them across a C=N bond and could therefore give coupling constants of the appropriate magnitude. However, the signals due to the N–H protons are broad which might be due to rapid exchange on the n.m.r. timescale. These observations are consistent with intra–molecular exchange of the acidic protons, presumably between the phenoxy–oxygens and the imino–nitrogens. Coupling between protons that are exchanging intra–molecularly can be observed, but not if the exchange is inter–molecular. This intra–molecular exchange could also be the cause of the broadening observed for other signals. The appearence of the minor peaks then suggests that there are two species in solution, which differ by the locations of the acidic protons. At this temperature the two different species can be observed. An additional contribution to the broad signal observed for the acidic N–H protons might be that these protons are undergoing rapid relaxation, due to the quadrupole moment of ^{14}N (I = 1). If this fast relaxation is occuring, the coupling constant between the imino protons would be reduced in magnitude. Coupling constants for *trans* protons across a double bond are usually in the range J = 12–18Hz, so if quadrupolar relaxation is occuring, it is not significant.

The ^{13}C DEPT n.m.r. spectrum at 298K can be unambiguously assigned. Two methylene resonances occur at δ = 25.99 and 51.39p.p.m. which are assigned as C–$\underline{C}H_2$–C and N–$\underline{C}H_2$–C respectively. The Ph–$\underline{C}H_3$ resonance occurs at δ = 17.48p.p.m., the aromatic $\underline{C}$–H occurs at δ = 145.37p.p.m. and the imino carbon is at δ = 166.94p.p.m.

In order to ascertain the conformation of $[(\underline{1}H_4)](PF_6)_2$ in the crystalline state and possibly to locate the positions of the acidic protons, a single crystal X–ray structure determination of $[(\underline{1}H_4)](PF_6)_2$ was undertaken.

3.2.2: The Single Crystal X-ray Structure of $[(\underline{1}H_4)](PF_6)_2.CH_3NO_2$

Details of the structure solution are given in the Experimental Section. Bond lengths, angles and torsions are listed in Tables 3.1, 3.2 and 3.3 respectively. Two ORTEP plots showing the cationic structure are presented in Figures 3.5 and 3.6, and packing diagrams along two different axes are shown in Figures 3.7 and 3.8.

The structure of the $[(\underline{1}H_4)]^{2+}$ cation shows that the two aromatic rings are folded to give a dihedral angle between the calculated planes of conjugation of 13.90° and the distance between the centres of gravity of the planes is 3.601Å. For comparison, the separation between layers in graphite is 3.35Å [187]. $[(\underline{1}H_4)]^{2+}$ is a zwitterionic species, since all the imino-nitrogens are protonated (the hydrogens were located on a difference map and then fixed) and the phenolic oxygens are formally negatively charged. The bond lengths for the imino and phenolic groups are found to reflect this distribution of the protons and charge. The C-O bonds [1.278(5) and 1.284(6)Å] are short for a phenol C-OH bond (1.36Å)[244], suggesting significant delocalisation, and the imine bonds [C=N = 1.299(6), 1.287(6), 1.304(6) and 1.279(6)Å] are relatively long (av.C=N = 1.27Å)[244]. The intramolecular hydrogen bonding parameters and the distances within the cavity are shown in Table 3.4 and Figure 3.9. Consideration of the cavity distances suggest a further reason for the folding of $[(\underline{1}H_4)]^{2+}$. An unfolded structure would force the lone pairs of the phenoxy oxygens to be directed towards each other leading to strong electrostatic repulsions. Folding of the macrocyclic ligand minimises this. The cavity is further defined by the propylene groups which are completely ordered and show that all the hydrogen orientations on neighbouring carbons are staggered.

Packing diagrams of $[(\underline{1}H_4)](PF_6)_2.CH_3NO_2$ show that there are inter- as well as intra-molecular π-interactions. The aromatic systems of different

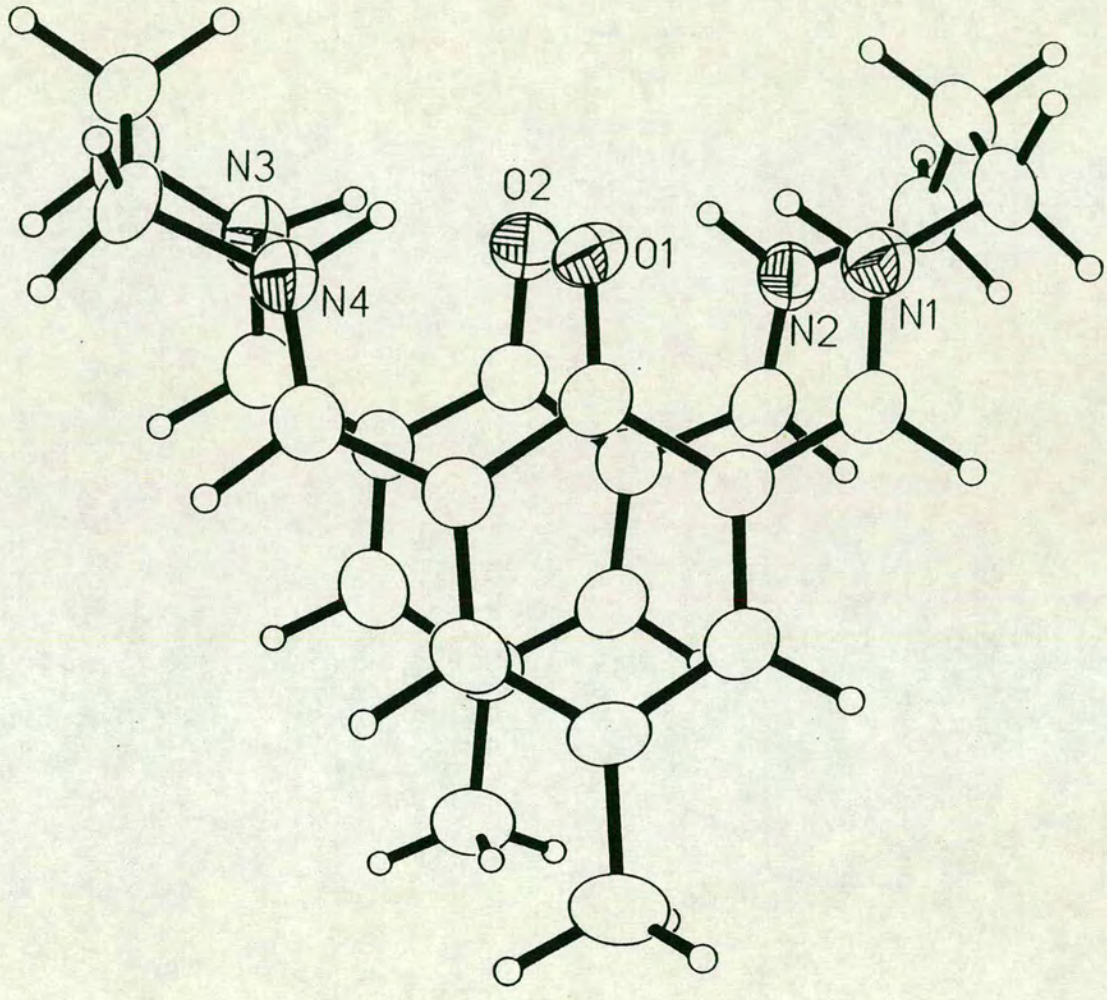

Figure 3.5 View of the single crystal X-ray structure of $[(\underline{1})H_4)]^{2+}$

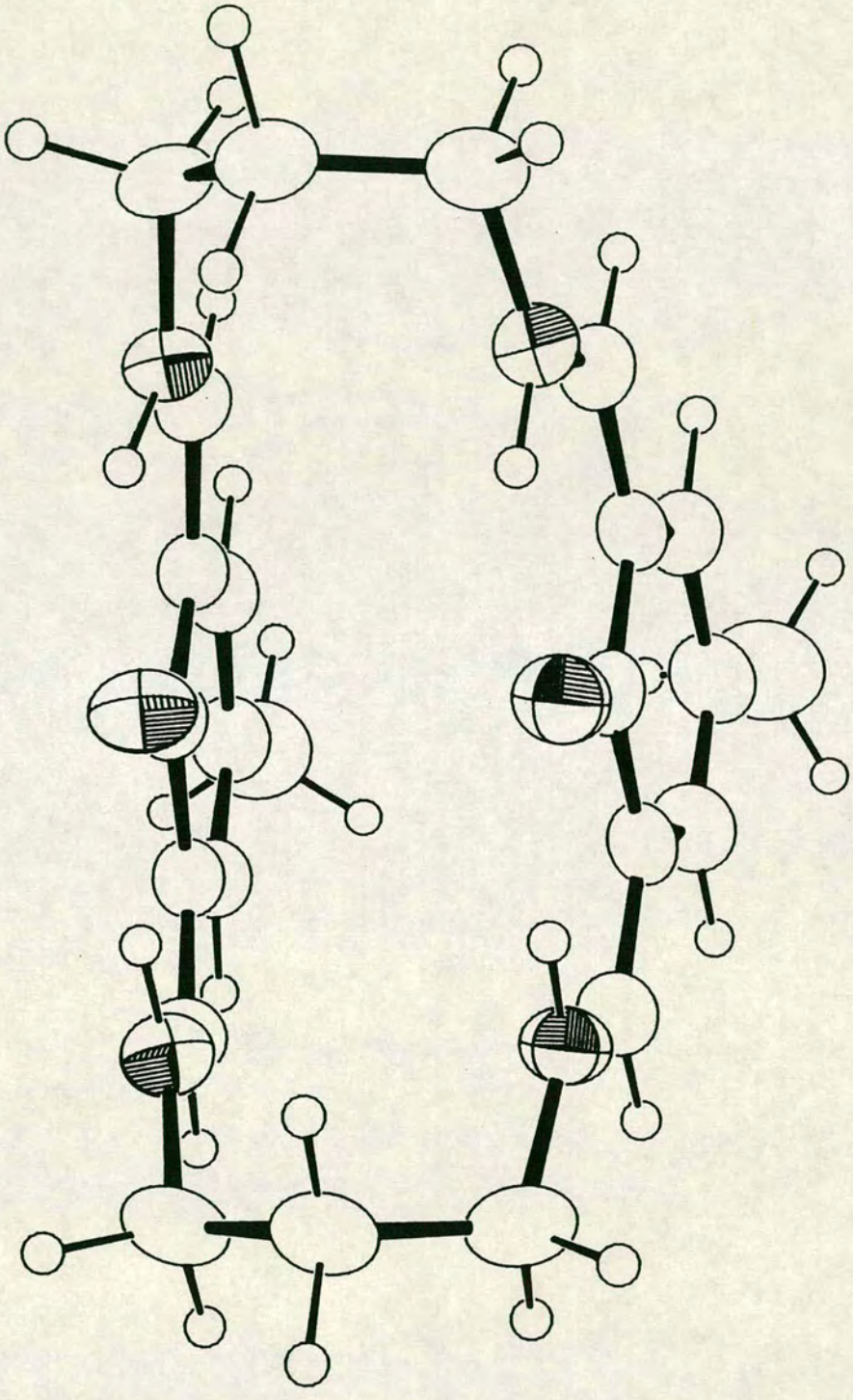

Figure 3.6 Alternative view of the single crystal X-ray structure of $[(\underline{1}H_4)]^{2+}$

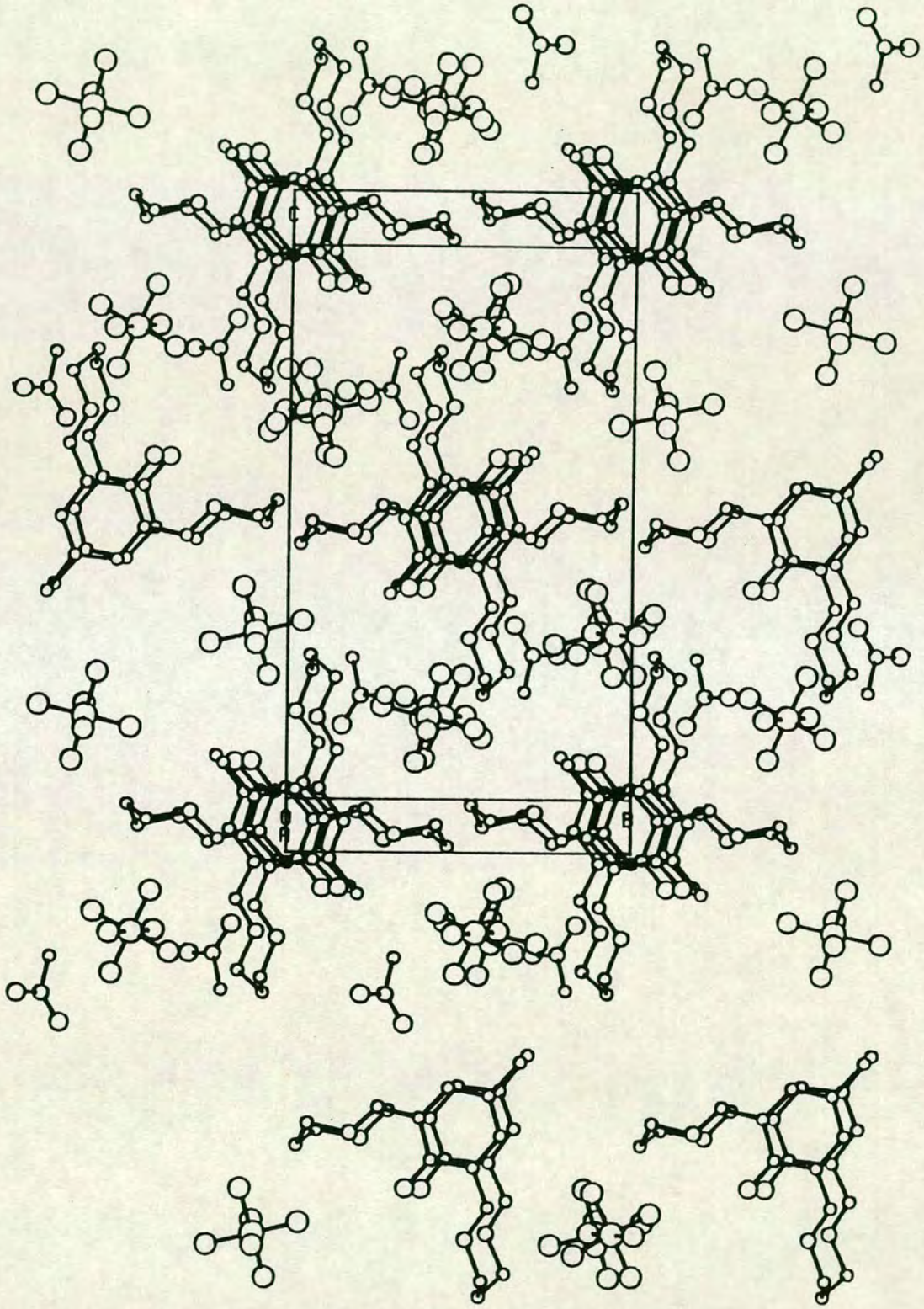

Figure 3.7 Packing diagram of $[(\underline{1}H_4)](PF_6)_2.CH_3NO_2$

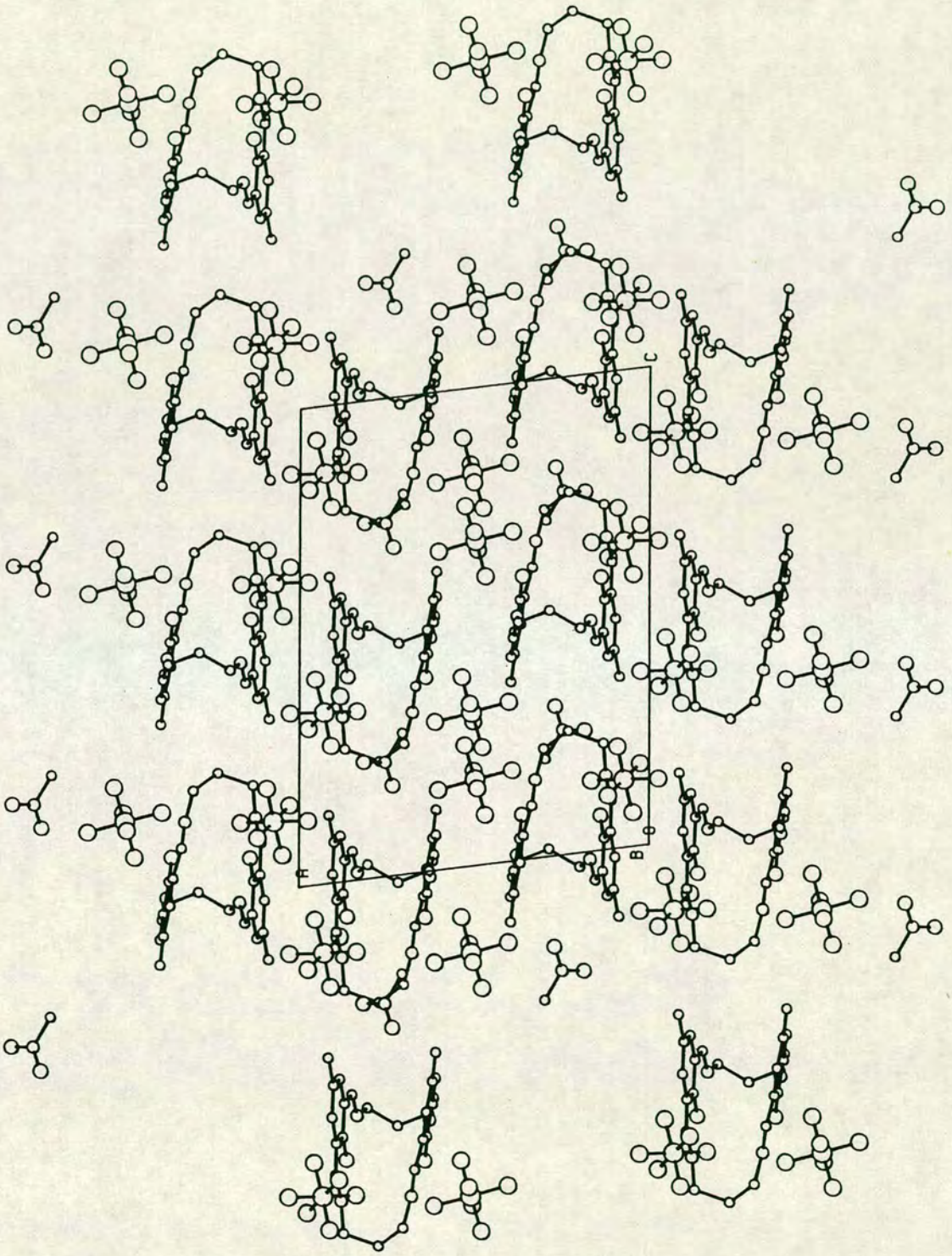

Figure 3.8 Packing diagram of $[(\underline{1}H_4)](PF_6)_2.CH_3NO_2$ along different axis

Table 3.1 Selected bond lengths (Å) of $[(\underline{1}H_4)](PF_6)_2.CH_3NO_2$

O(1) - C(1)	1.278(5)	C(4) - C(6)	1.391(7)
O(2) -C(13)	1.284(6)	C(6) - C(7)	1.394(6)
N(1) - C(8)	1.299(6)	C(7) - C(8)	1.416(6)
N(1) - C(9)	1.457(6)	C(9) -C(10)	1.524(7)
N(2) -C(11)	1.469(6)	C(10) -C(11)	1.510(7)
N(2) -C(12)	1.287(6)	C(12) -C(14)	1.432(7)
N(3) -C(20)	1.304(6)	C(13) -C(14)	1.431(6)
N(3) -C(21)	1.458(7)	C(13) -C(19)	1.433(6)
N(4) -C(23)	1.479(6)	C(14) -C(15)	1.397(7)
N(4) -C(24)	1.279(6)	C(15) -C(16)	1.380(7)
C(1) - C(2)	1.441(6)	C(16) -C(17)	1.537(8)
C(1) - C(7)	1.439(6)	C(16) -C(18)	1.383(7)
C(2) - C(3)	1.398(6)	C(18) -C(19)	1.396(7)
C(2) -C(24)	1.424(6)	C(19) -C(20)	1.410(7)
C(3) - C(4)	1.371(7)	C(21) -C(22)	1.526(7)
C(4) - C(5)	1.514(8)	C(22) -C(23)	1.508(7)

Table 3.2 Selected bond angles (°) of $[(\underline{1}H_4)](PF_6)_2.CH_3NO_2$

C(8) - N(1) - C(9)	124.6(4)	N(2) -C(11) -C(10)	111.4(4)
C(11) - N(2) -C(12)	125.0(4)	N(2) -C(12) -C(14)	123.0(4)
C(20) - N(3) -C(21)	124.1(4)	O(2) -C(13) -C(14)	122.2(4)
C(23) - N(4) -C(24)	125.3(4)	O(2) -C(13) -C(19)	121.6(4)
O(1) - C(1) - C(2)	121.8(4)	C(14) -C(13) -C(19)	116.1(4)
O(1) - C(1) - C(7)	122.2(4)	C(12) -C(14) -C(13)	120.2(4)
C(2) - C(1) - C(7)	115.9(4)	C(12) -C(14) -C(15)	119.1(4)
C(1) - C(2) - C(3)	119.8(4)	C(13) -C(14) -C(15)	120.6(4)
C(1) - C(2) -C(24)	120.7(4)	C(14) -C(15) -C(16)	122.8(5)
C(3) - C(2) -C(24)	119.5(4)	C(15) -C(16) -C(17)	121.6(5)
C(2) - C(3) - C(4)	123.9(4)	C(15) -C(16) -C(18)	117.1(5)
C(3) - C(4) - C(5)	122.3(4)	C(17) -C(16) -C(18)	121.2(5)
C(3) - C(4) - C(6)	116.9(4)	C(16) -C(18) -C(19)	123.1(5)
C(5) - C(4) - C(6)	120.8(4)	C(13) -C(19) -C(18)	120.2(4)
C(4) - C(6) - C(7)	122.8(4)	C(13) -C(19) -C(20)	120.6(4)
C(1) - C(7) - C(6)	120.6(4)	C(18) -C(19) -C(20)	119.2(4)
C(1) - C(7) - C(8)	120.7(4)	N(3) -C(20) -C(19)	124.2(4)
C(6) - C(7) - C(8)	118.7(4)	N(3) -C(21) -C(22)	111.5(4)
N(1) - C(8) - C(7)	123.4(4)	C(21) -C(22) -C(23)	116.3(4)
N(1) - C(9) -C(10)	112.7(4)	N(4) -C(23) -C(22)	112.4(4)
C(9) -C(10) -C(11)	116.1(4)	N(4) -C(24) - C(2)	124.5(4)

Table 3.3 Selected torsion angles (°) of $[(\underline{1}H_4)](PF_6)_2.CH_3NO_2$

C(9)	N(1)	C(8)	C(7)	-175.8(4)	C(1)	C(7)	C(8)	N(1)	-0.3(7)
C(8)	N(1)	C(9)	C(10)	123.2(5)	C(6)	C(7)	C(8)	N(1)	177.4(4)
C(12)	N(2)	C(11)	C(10)	-124.6(5)	N(1)	C(9)	C(10)	C(11)	-68.6(6)
C(11)	N(2)	C(12)	C(14)	174.7(4)	C(9)	C(10)	C(11)	N(2)	73.3(5)
C(21)	N(3)	C(20)	C(19)	-173.2(5)	N(2)	C(12)	C(14)	C(13)	-1.1(7)
C(20)	N(3)	C(21)	C(22)	108.9(5)	N(2)	C(12)	C(14)	C(15)	-179.1(5)
C(24)	N(4)	C(23)	C(22)	-137.4(5)	O(2)	C(13)	C(14)	C(12)	2.8(7)
C(23)	N(4)	C(24)	C(2)	-179.4(4)	O(2)	C(13)	C(14)	C(15)	-179.2(4)
O(1)	C(1)	C(2)	C(3)	-179.6(4)	C(19)	C(13)	C(14)	C(12)	-177.4(4)
O(1)	C(1)	C(2)	C(24)	3.0(7)	C(19)	C(13)	C(14)	C(15)	0.6(7)
C(7)	C(1)	C(2)	C(3)	2.6(6)	O(2)	C(13)	C(19)	C(18)	179.3(4)
C(7)	C(1)	C(2)	C(24)	-174.8(4)	O(2)	C(13)	C(19)	C(20)	-2.8(7)
O(1)	C(1)	C(7)	C(6)	178.7(4)	C(14)	C(13)	C(19)	C(18)	-0.5(7)
O(1)	C(1)	C(7)	C(8)	-3.6(7)	C(14)	C(13)	C(19)	C(20)	177.4(4)
C(2)	C(1)	C(7)	C(6)	-3.4(6)	C(12)	C(14)	C(15)	C(16)	177.8(5)
C(2)	C(1)	C(7)	C(8)	174.3(4)	C(13)	C(14)	C(15)	C(16)	-0.2(7)
C(1)	C(2)	C(3)	C(4)	-0.9(7)	C(14)	C(15)	C(16)	C(17)	179.6(5)
C(24)	C(2)	C(3)	C(4)	176.5(5)	C(14)	C(15)	C(16)	C(18)	-0.4(8)
C(1)	C(2)	C(24)	N(4)	-3.1(7)	C(15)	C(16)	C(18)	C(19)	0.5(8)
C(3)	C(2)	C(24)	N(4)	179.5(4)	C(17)	C(16)	C(18)	C(19)	-179.5(5)
C(2)	C(3)	C(4)	C(5)	179.8(5)	C(16)	C(18)	C(19)	C(13)	-0.1(7)
C(2)	C(3)	C(4)	C(6)	-0.1(7)	C(16)	C(18)	C(19)	C(20)	-177.9(5)
C(3)	C(4)	C(6)	C(7)	-0.9(7)	C(13)	C(19)	C(20)	N(3)	-1.2(7)
C(5)	C(4)	C(6)	C(7)	179.3(5)	C(18)	C(19)	C(20)	N(3)	176.6(5)
C(4)	C(6)	C(7)	C(1)	2.7(7)	N(3)	C(21)	C(22)	C(23)	-63.1(6)
C(4)	C(6)	C(7)	C(8)	-175.0(4)	C(21)	C(22)	C(23)	N(4)	73.9(5)

Table 3.4: Intramolecular hydrogen bonding parameters and distances within the cavity of $[(\underline{1}H_4)]^{2+}$

Atom N	Atom H	Atom O	Atom C	Distance H··O (Å)	Angle N-H··O(°)	Angle H··O-C(°)
N1	H1N	O1	C1	1.848(14)	132.3(11)	103.8(5)
N2	H2N	O2	C13	1.836(14)	131.2(11)	104.4(5)
N3	H3N	O2	C13	1.753(16)	142.9(14)	101.0(6)
N4	H4N	O1	C1	1.847(17)	134.9(14)	101.8(6)

Cavity distances (Å)

	N_1	N_2	N_3	N_4	O_1	O_2
N_1	-	3.040(6)	-	-	2.625(5)	-
N_2	3.040(6)	-	-	-	-	2.604(5)
N_3	-	-	-	2.994(6)	-	2.617(5)
N_4	-	-	2.994(6)	-	2.647(5)	-
O_1	2.625(5)	-	-	2.647(5)	-	3.261(5)
O_2	-	2.604(5)	2.617(5)	-	3.261(5)	-

Figure 3.9 Labelling of atoms in the cavity of $[(\underline{1}H_4)]^{2+}$

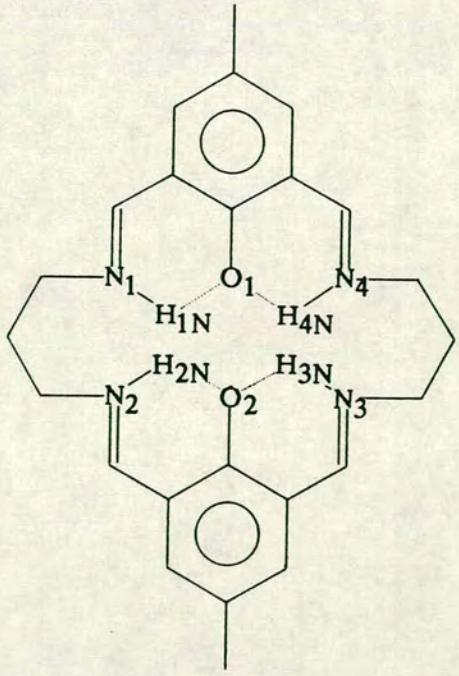

molecules are approximately parallel and stack on top of one another. The view perpendicular to the aromatic rings (Figure 3.7) is directed down these columns and shows that the phenoxy oxygens of different molecules are in *anti* positions relative to each other.

The gross structure of $[(\underline{1}H_4)](PF_6)_2$ has similarities to the structure of the metal-free macrocycle, $[(\underline{15a}H_6)](ClO_4)_2$, reported by McKee and Tandon[160] (see Figure 2.21) and also to the mononuclear Ba(II) complex, $[Ba(\underline{14}H_4)](ClO_4)_2$, by Fenton *et al*[158], (see Figure 2.19). For $[(\underline{15a}H_6)]^{2+}$, however, the cavity hydrogen atoms were not found and the macrocyclic cavity is occupied by two H_2O molecules. The phenolic C-O bond length of $[(\underline{15a}H_6)]^{2+}$ is similar to that of $[(\underline{1}H_4)]^{2+}$, but the C=N bonds are significantly longer[160]. In $[Ba(\underline{14}H_4)]^{2+}$, the metallated and protonated imino bonds are comparable to those of $[(\underline{1}H_4)]^{2+}$, but the phenol bonds are longer[158]. The structure of $[(\underline{15a}H_6)]^{2+}$ is folded so that the aromatic, conjugated planes are at an angle of 7° to each other and in $[Ba(\underline{14}H_4)]^{2+}$ the angle is 2°. Both of the previously reported structures have crystallographically imposed C_2 symmetry. In $[(\underline{1}H_4)](PF_6)_2$, however, there is one molecule of $[(\underline{1}H_4)]^{2+}$ per asymmetric unit.

We have therefore synthesized the macrocycle $[(\underline{1}H_4)]^{2+}$ by a template condensation about acidic protons that are derived from aqueous HBr in CH_3OH. The synthesis of $[(\underline{1}H_4)]^{2+}$ has been attempted using aqueous HBF_4 in CH_3OH but the products isolated were oils which could not be purified further. However, the protonation of the Schiff-base appears to be vital to the stability of the resultant compound.

3.2.3: Reactions of $[(\underline{1}H_4)]^{2+}$

In addition to studying the complexation reactions of $(\underline{1})^{2-}$, it was proposed that the protonated macrocycle, $[(\underline{1}H_4)]^{2+}$, may be a convenient source of the fully reduced ligand $(\underline{11})^{2-}$. Reactions were conducted to ascertain this. The reaction of $[(\underline{1}H_4)](PF_6)_2$ with an excess of $NaBH_4$ in C_2H_5OH gave a product whose i.r. spectrum shows no imine stretching vibrations. The f.a.b. mass spectrum of the solid suggests a mixture of products had been obtained, including a peak at $M^+ = 413$, which could be assigned to $[(\underline{11}H_3)]^+$. It is probable that the product, which is soluble in non-polar organic solvents such as $CHCl_3$, does contain some $[\underline{11}H_2]$ but the purification procedures described in Section 3.4.5 were insufficient to isolate the pure compound.

Additional reduction reactions were attempted with NaH (60% in mineral oil). The reaction of a solution of $[(\underline{1}H_4)](PF_6)_2$ in dry CH_3CN with ten equivalents of NaH caused effervescence and an orange to yellow colour change. On standing, a small amount of a yellow gummy solid was precipitated. The i.r. spectrum of the solid shows very broad peaks and the strongest absorption occurrs at $1625cm^{-1}$, which suggest that there are some unreduced imine bonds. The f.a.b. mass spectrum of the solid suggests a mixture of products had been obtained, including a peak at $M^+ = 413$, which is tentatively assigned to $[(\underline{11}H_3)]^+$. From these results, we conclude that $[(\underline{1}H_4)]^{2+}$ does react vigorously with reducing agents, but to give a variety of products, some of them possibly polymers due to their insolubility. It is probable that the reduced ligand $(\underline{11}H_2)$ can be prepared from the reduction of $[(\underline{1}H_4)]^{2+}$, but this was not investigated further.

We also proposed that the dianionic species $(\underline{1})^{2-}$ might be isolated, for example, as a disodium salt. Reactions were carried out in dry CH_3OH using stoichiometric or excess amounts of $NaOCH_3$. No evidence for dianionic

$[Na_2(\underline{1})]$ was obtained by f.a.b. mass spectroscopy. A reaction in dry CH_3CN with four equivalents of NaH to one of $[(\underline{1}H_4)](PF_6)_2$ gave a yellow, insoluble product, and the i.r. spectrum of this solid shows that no PF_6^- is present. No other analysable data was obtained. A solution of $[(\underline{1}H_4)](PF_6)_2$ in CH_3OH was added to an ion-exchange column (AG50) that had been previously washed with NaOH. It was not possible to remove the red band corresponding to $[(\underline{1}H_4)]^{2+}$ from the resin. We conclude from this series of reactions that a species such as $[Na_2(\underline{1})]$ is not readily isolatable from $[(\underline{1}H_4)]^{2+}$ and that the most successful route to complexation reactions is through *in situ* deprotonation and metallation of $[(\underline{1}H_4)]^{2+}$ in the presence of a metal ion in solution (see Chapter 4).

It is relevant to note here that imine groups bonded to metal centres or protons are deactivated towards hydrolysis by OH^- or cleavage by other nucleophiles. Removal of the protecting cation may liberate a very labile, neutral imine species. Relatively few metal-free Schiff-base species have been reported in the literature[188-194], presumably for this very reason. An example of the activity of Schiff-base compounds is given by Martell[176] with an isolated Schiff-base ligand formed by condensation of two equivalents of 3-formyl-benzaldehyde with 1,5-diamino-3-azapentane. The single crystal X-ray structure of the ligand shows that intramolecular nucleophilic attack by the amines of the side-arms has occurred at two of the imine groups, thus contracting the macrocyclic ring and forming two extra five-membered rings (see Figure 3.10)[176]. It is postulated that an equilibrium exists in solution between the two isomeric forms but only the fully expanded form is obtained on addition of Cu(I) ions, to give the binuclear complex. Ring contraction/expansion by Schiff-base macrocycles has also been noted by Fenton *et al.*[195] (using alcohol groups in the side-arms), Nelson *et al.*[196] and Okawa *et al.*[175], but only in the presence of metal ions.

Intramolecular reactions such as that shown in Figure 3.10 give stable products, but if the nucleophile comes from an external source, then fission of the Schiff-base species is likely to occur. Since $(\underline{1})^{2-}$ has no internal nucleophiles, unprotected imine bonds in $(\underline{1})^{2-}$ could react with a large number of nucleophilic species to give unpredictable and variable reactions.

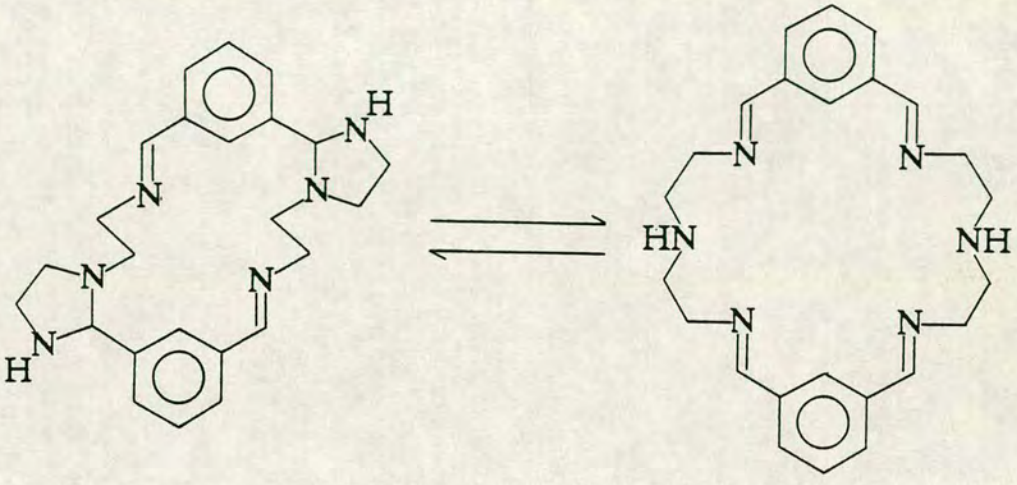

Figure 3.10 Macrocyclic ring contraction in a Schiff-base ligand

3.2.4: The Synthesis of ($\underline{1}H_2$)

We have also attempted to synthesize the neutral species ($\underline{1}H_2$). The reaction of equimolar amounts of 1,3-diaminopropane and 2,6-diformyl-4-methylphenol in THF at high dilution ($0.12 mol.dm^{-3}$) gave a yellow solution. Reduction of the volume of solvent and the slow addition of diethyl ether produced a yellow, waxy solid, which was recrystallised from CH_2Cl_2/diethyl ether. The i.r. spectrum of the yellow solid shows two strong bands at 1637 and $1598 cm^{-1}$, both of which may be tentatively assigned as C=N stretching vibrations. There are also broad features in the 3000 to $2000 cm^{-1}$ range which suggest that there are still some amine impurities in the yellow product. Elemental analytical data also indicate that the yellow

product is not pure (found C = 69.0; H = 7.55; N = 12.82%. Calculated for $[C_{24}H_{28}N_4O_2].\frac{1}{2}THF$: C = 70.9; H = 7.32; N = 12.72%). The f.a.b. spectrum of the yellow product shows a molecular ion peak at $M^+ = 405$, which can be assigned as $[(\underline{1}H_3)]^+$. A small peak is also found at $M^+ = 607$, which is due to the [3+3] condensation product $[C_{36}H_{43}N_6O_3]^+$. With the above data, we conclude that the yellow product does contain $(\underline{1}H_2)$. The electronic spectrum of the yellow product in CH_2Cl_2 solution is very different to that of the protonated $[(\underline{1}H_4)](PF_6)_2$, showing absorptions at $\lambda_{max.}$ = 426 and 346 nm. ($\epsilon_{max.}$ = 970 and 8,550 respectively). In particular the extinction coefficients are smaller by one or two orders of magnitude.

The ^1H n.m.r. of $(\underline{1}H_2)$ in $CDCl_3$ at 298K in Figure 3.11 shows resonances that are broadened, especially those for the aromatic and imino protons. The cause of this broadening is not known. It is tentatively suggested that, by analogy to $[(\underline{1}H_4)]^{2+}$, exchange of the phenolic protons could be occurring since the resonances due to O–H are not found in the region 0.00 → 15.00p.p.m. and may be so broad as to disappear. Other assignments are made below.

δ = 2.10p.p.m., C–HC<u>H</u>–C, 2H, doublet of doublets, J = 6Hz.;

δ = 2.22p.p.m., C–<u>H</u>CH–C, 2H, doublet of doublets, J = 5Hz.;

δ = 2.26p.p.m., Ph–C<u>H</u>$_3$, 6H, singlet;

δ = 4.20p.p.m., C–C<u>H</u>$_2$–N, 8H, doublet of doublets, J = 6Hz.;

δ = 7.42p.p.m., Ph–<u>H</u>, 4H, broad;

δ = 8.53p.p.m., Ph–C<u>H</u>=N, 4H, broad;

In ^{13}C n.m.r. of $(\underline{1}H_2)$ in $CDCl_3$, the imino carbon is not observed at chemical shifts < 185p.p.m. and the resonance at 134.00p.p.m. due to the aromatic <u>C</u>H is visibly broadened. Other assignments are given in the Experimental Section 3.4.7.

Figure 3.11 ^{1}H n.m.r. spectrum of ($\underline{1}H_2$) in $CDCl_3$

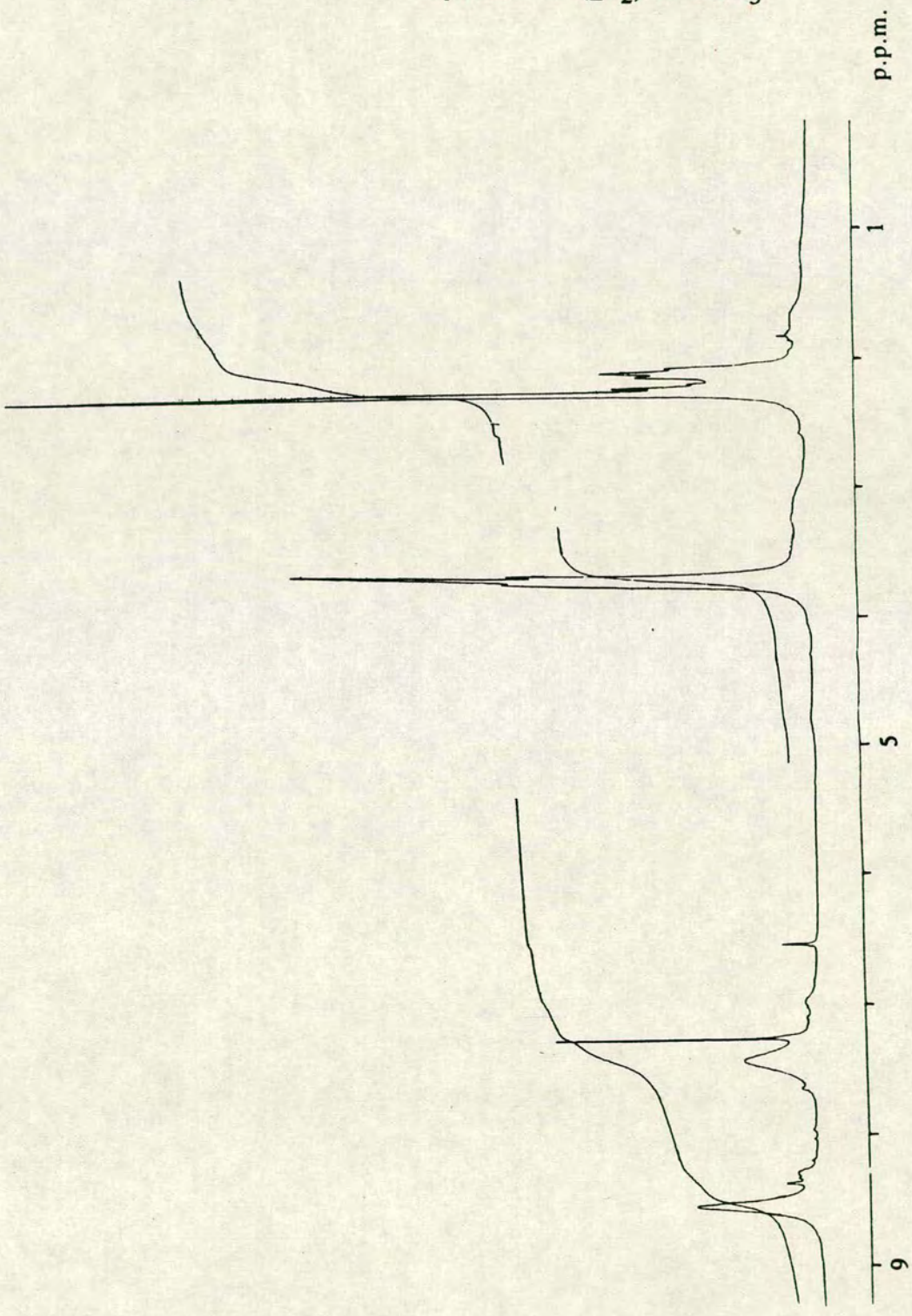

3.2.5: The Synthesis of $[(\underline{2}H_4)]^{2+}$ and $[(\underline{5}H_4)]^{2+}$

Both $(\underline{2})^{2-}$ and $(\underline{5})^{2-}$ have been synthesised previously in template reactions in the presence of labile metal ions, to give $[Ni_2(\underline{2})]Cl_2$[119], $[Cu_2(\underline{2})]Cl_2$[119] and $[Cu_2(\underline{5})(ClO_4)_2]$[114]. The single crystal X-ray structures of $[Cu_2(\underline{5})(ClO_4)_2]$[114] and $[Cu_2(\underline{8j})(H_2O)_2](BF_4)_2$[197], where $(\underline{8j})^{2-}$ is a methylated analogue of $(\underline{2})^{2-}$, have been reported. Comparison of the structure of $[Cu_2(\underline{5})(ClO_4)_2]$ with that of $[Cu_2(\underline{1})(H_2O)_2][Cu_2(\underline{1})(H_2O)_2(ClO_4)_2](ClO_4)_2$ [114], shows that the extension of the side-arms from a $-(CH_2)_3-$ to a $-(CH_2)_4-$ group has relatively little effect on the Cu-ligand interactions. In $[Cu_2(\underline{8j})(H_2O)_2]^{2+}$, however, the macrocyclic cavity is considerably contracted, giving shorter Cu-N, Cu-O and Cu-Cu bond distances (average Cu-O and Cu-N distances < 1.92Å, Cu-Cu distance = 2.847(4)Å)[197]. We proposed that the protonated Schiff-base macrocycles $[(\underline{2}H_4)](BF_4)_2$ and $[(\underline{5}H_4)](PF_6)_2$ could be prepared by a similar method to $[(\underline{1}H_4)](PF_6)_2$, using equimolar amounts of 1,2-diaminoethane or 1,4-diaminobutane respectively with 2,6-diformyl-4-methylphenol in refluxing CH_3OH. After preparation of the free, protonated ligands $[(\underline{2}H_4)]^{2+}$ and $[(\underline{5}H_4)]^{2+}$, metal ions other than Cu(II) could be inserted into the macrocycles. We proposed that the effect of the side-arm chain length could then be investigated; whether the above Cu(II) complexes are typical for these ligands or if the ligand $(\underline{5})^{2-}$ can give an expanded macrocyclic cavity and so accommodate a larger metal ion.

$[(\underline{2}H_4)]^{2+}$ in CH_3OH gave a dark red solution and on addition of excess $NaBF_4$ a yellow powder precipitated immediately. Recrystallisation of the yellow powder from CH_3NO_2/diethyl ether by vapour diffusion in bulk gave a red crystalline material. An i.r. spectrum of this compound shows strong, broad bands around 1650cm^{-1}, assigned to two C=N stretching vibrations, a strong band at 1540cm^{-1}, tentatively assigned to a C-O phenoxide stretching

vibration and also a strong, broad band for the BF_4^- counterion at $1058cm^{-1}$. F.a.b. mass spectroscopy shows peaks at $M^+ = 378$ and 466, which are assigned to $[(\underline{2}H_4)]^+$ and $[(\underline{2}H_5)](BF_4)^+$ respectively. In the f.a.b. mass spectra of crude products of $[(\underline{2}H_4)](BF_4)_2$, an additional peak at $M^+ = 566$ is also observed. The peak at $M^+ = 566$ may be assigned to the product of a [3+3] condensation, which has been also found to occur in the synthesis of $[(\underline{1}H_4)]^{2+}$. This evidence together with elemental analytical data confirm that the product is $[(\underline{2}H_4)](BF_4)_2$.

$[(\underline{5}H_4)]^{2+}$ in CH_3OH gave a yellow solution and on addition of excess NH_4PF_6, a yellow solid precipitated slowly. Recrystallisation of the yellow solid from CH_3NO_2 gave a yellow, crystalline material. The i.r. spectrum of this compound shows two close, strong bands at $1655cm^{-1}$ assigned to two C=N stretching vibrations, a strong band at $1535cm^{-1}$ tentatively assigned to a C–O phenoxide stretching vibration and strong bands at 844 and $558cm^{-1}$ due to the PF_6^- counterion. A f.a.b. mass spectrum of the product shows molecular ion peaks at $M^+ = 433$ and 580, assigned to $[(\underline{5}H_3)]^+$ and $[(\underline{5}H_4)](PF_6)^+$ respectively. This evidence together with elemental analytical confirm that the product is $[(\underline{5}H_4)](PF_6)_2$.

$[(\underline{1}H_4)](PF_6)_2$, $[(\underline{2}H_4)](BF_4)_2$ and $[(\underline{5}H_4)](PF_6)_2$ show absorptions in the U.V./visible region at $\lambda_{max.} = 432$, 431 and 430nm. respectively in their electronic spectra. This suggests that the conjugated systems in all three ligands are the same. The extinction coefficients decrease in the series $[(\underline{1}H_4)]^{2+} > [(\underline{5}H_4)]^{2+} > [(\underline{2}H_4)]^{2+}$ (in CH_3CN 33,790, 23,830 and $5,570M^{-1}cm^{-1}$ respectively) for this absorption.

3.3: Conclusions

Three Schiff-base macrocycles, $[(\underline{1}H_4)](PF_6)_2$, $[(\underline{2}H_4)](BF_4)_2$ and $[(\underline{5}H_4)](PF_6)_2$, have been synthesized in their protonated forms. The single crystal X-ray structure of $[(\underline{1}H_4)](PF_6)_2$ was determined and shows that the metal-free ligand $[(\underline{1}H_4)]^{2+}$ has a folded structure in the solid-state, with $\pi-\pi$ interactions stabilising this conformation. The variation in carbon chain side-arm length in $[(\underline{1}H_4)]^{2+}$, $[(\underline{2}H_4)]^{2+}$ and $[(\underline{5}H_4)]^{2+}$ may lead to different complexation properties due to different cavity sizes. However, the cavity can only be elongated along the carbon chain and the conjugated imine-phenol system will have approximately similar dimensions for all three ligands.

3.4: Experimental

3.4.1: Synthesis of 2,6-diformyl-4-methylphenol

2,6-Diformyl-4-methylphenol was prepared by a modified route from that reported by Ullman and Brittner[198] and then Gagné *et al*[136]. The reaction scheme is summarised in Figure 3.12. To a solution of NaOH (20.0g) in H_2O ($80cm^3$) was added 43.2g (0.4 mole) of 4-methylphenol. The mixture was stirred for 30 minutes until a clear, golden-brown solution was obtained. Stirring was continued while a 35% solution of CH_2O ($84cm^3$, 0.88 mole) in H_2O was added. The yellow solution was allowed to stand for 48 hours, after which time a white solid had precipitated. This was filtered and washed with saturated NaCl solution ($160cm^3$). Further crops of white precipitate were obtained by allowing the filtrate to stand further. The white precipitate was dried under suction.

The dried product, [Na(2,6-dimethylol-4-methylphenolate)], was transferred to a $1dm^3$, 3-necked round-bottomed flask and a solution of NaOH (1.2g in $300cm^3$ of H_2O) was added. The white suspension was stirred with an overhead stirrer for 30 mins. and *p*-toluenesulphonyl chloride (98.8g,

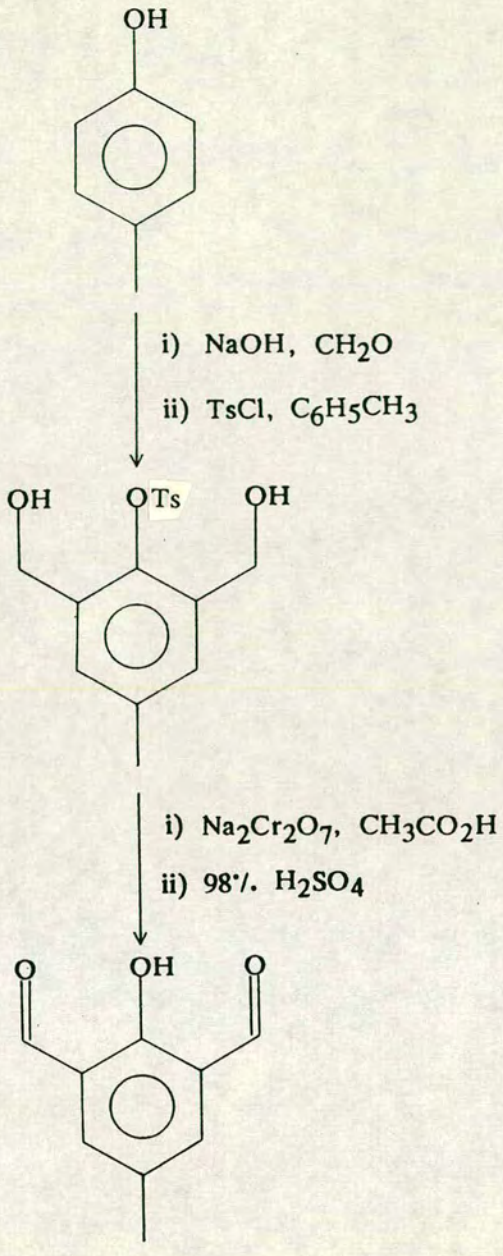

Ts = *p*–Toluene sulphonyl

Figure 3.12 Synthesis of 2,6–diformyl–4–methylphenol

0.52mole) suspended in 200cm^3 of toluene, was added. The white mixture was stirred for 24 hours to give a white solid and a biphasic, colourless solution. The white solid, 2,6-dimethylol-4-methyltosylphenol, was filtered and dried *in vacuo*. Yield at this stage = 75.8g, 56%.

The dried white solid, 2,6-dimethylol-4-methyltosylphenol, was placed in a 1l, 3-necked, round-bottomed flask that was equipped with an overhead condenser and a 500cm^3 dropping funnel. Glacial CH_3CO_2H (90cm^3) was added and the product dissolved with stirring. $Na_2Cr_2O_7$ (66.6g) was dissolved in 200cm^3 of glacial CH_3CO_2H with heating and placed in the dropping funnel (N.B. $K_2Cr_2O_7$ should not be used since it is less soluble in CH_3CO_2H than the Na^+ salt). The $Na_2Cr_2O_7$ solution was added dropwise to the refluxing, stirred solution of 2,6-dimethylol-4- methyltosylphenol over two hours and the refluxing was continued for 15 minutes after the final addition. The green mixture was allowed to cool overnight to give a brown solid and green solution. The solid, 2,6-diformyl-4-methyltosylphenol, was filtered and washed with H_2O to give a pale green solid which was dried under suction. 2,6-Diformyl-4-methyltosylphenol was added slowly to 180cm^3 of 98% H_2SO_4 in a 1dm^3 beaker with stirring to give a very dark solution which was stirred with cooling in an ice bath for 1 hour. Ice was slowly added to the stirring solution until the total volume reached 800cm^3. The brown suspension was allowed to stand overnight and the brown precipitate was filtered, washed with cold H_2O and dried *in vacuo*. Recrystallisation from toluene gave a brown crystalline solid. Overall yield = 13.23g (20%). Care should be taken when handling this compound since contact with the skin causes a yellow stain which lasts for several days. Elemental analysis: found C = 65.4; H = 5.00%. Calculated for $C_9H_8O_3$: C = 65.8; H = 4.87%. F.a.b. mass spectrum (3-NOBA matrix): found M^+ = 165. Calculated for $C_9H_9O_3^+$, M^+ = 165. I.r. spectrum (KBr disc): 3026w, 2924w, 2870m, 2739w, 1823w,

1685vs, 1665vs, 1604s, 1459s, 1405s, 1333m, 1302s, 1258s, 1215s, 1158m, 1022w, 963s, 800m, 807m, 748s, 716m, 626s, 561m, 547m, 474m cm^{-1}. U.V./vis. spectrum [$(CH_3)_2CO$]: $\lambda_{max.}$ = 352nm.

3.4.2: Synthesis of [(1H4)]$(PF_6)_2$

2,6-Diformyl-4-methylphenol (394.2mg, 2.4mmol.) was dissolved in 200cm^3 of CH_3OH and 1,3-diaminopropane (0.2cm^3, 2.4mmol.) was added with stirring. The clear green/yellow solution was stirred for 1 minute and 48% HBr solution in H_2O (0.3cm^3) was added. The solution was stirred and heated to reflux to give a red solution and allowed to cool slowly. Any yellow insoluble material present was filtered off at this stage. Addition of an excess of NH_4PF_6 with stirring gave an orange precipitate on cooling at 253K. This was filtered, washed with diethyl ether and recrystallised from CH_3NO_2/diethyl ether. Yield = 800mg, 88%. Elemental analysis: found C = 39.5; H = 4.41; N = 8.83%; found also C = 40.2; H = 4.62; N = 9.08%. Calculated for $[C_{24}H_{30}N_4O_2](PF_6)_2.CH_3NO_2$: C = 39.6; H = 4.39; N = 9.25%. F.a.b. mass spectrum (3-NOBA matrix): found M^+ = 405, 551. Calculated for: $[C_{24}H_{29}N_4O_2]^+$, M^+ = 405; $[C_{24}H_{30}N_4O_2](PF_6)^+$, M^+ = 551. I.r. spectrum (KBr disc): 3400br, 2930w, 1668vs, 1645vs, 1535vs, 1460w, 1375w, 1338w, 1305w, 1234m, 1212w, 1122m, 1037w, 989w, 838vs, 741w, 665w, 558s, 469w, 434w cm^{-1}. U.V./vis. spectrum: (in CH_3NO_2) $\lambda_{max.}$ = 431nm. ($\varepsilon_{max.}$ = 37,720$M^{-1}cm^{-1}$); [in $(CH_3)_2CO$] $\lambda_{max.}$ = 431nm. ($\varepsilon_{max.}$ = 35,000$M^{-1}cm^{-1}$); (in CH_3CN) $\lambda_{max.}$ = 432nm. ($\varepsilon_{max.}$ = 33,790$M^{-1}cm^{-1}$), 267 (28,520), 250 (41,660,), 211 (39,610). ^1H n.m.r. spectrum (200.13MHz, CD_3NO_2, 298K): δ = 2.16p.p.m. (s, C$\underline{H}_3$, major, 6H), 2.30 (s, C$\underline{H}_3$, minor); 2.27 (s, C-C$\underline{H}_2$-C, minor), 2.51 (s, C-C$\underline{H}_2$-C, major, 4H); 4.02-4.08 (m, C-C$\underline{H}_2$-N, minor), 4.18-4.22 (m, C-C$\underline{H}_2$-N, major, 8H); 7.37 (s, Ar-$\underline{H}$, major, 4H), 7.70 (s, Ar-$\underline{H}$, minor);

8.39 (d, J = 13Hz, C<u>H</u>=N, major, 4H), 8.55 (d, J = 13Hz, C<u>H</u>=N, minor); 13.73 (br with shoulder upfield, N<u>H</u>). ^{13}C DEPT n.m.r. spectrum (50.32MHz, CD_3NO_2, 298K): δ = 17.48p.p.m. (Ph-<u>C</u>H_3); 25.99 (C-<u>C</u>H_2-C, major), 28.63 (C-<u>C</u>H_2-C, minor); 48.13 (N-<u>C</u>H_2-C, minor), 51.39 (N-<u>C</u>H_2-C, major); 145.37 (aromatic <u>C</u>H); 166.94 (<u>C</u>=N, major), 167.66 (<u>C</u>=N, minor).

3.4.3: Synthesis of $[(\underline{1}H_4)](BF_4)_2$

$[(\underline{1}H_4)](BF_4)_2$ was synthesized by the same method as $[(\underline{1}H_4)](PF_6)_2$ but using excess $NaBF_4$ instead of NH_4PF_6. Elemental analysis: found C = 47.7; H = 5.15; N = 9.15%. Calculated for $[C_{24}H_{30}N_4O_2](BF_4)_2$: C = 49.7; H = 5.21; N = 9.66%. F.a.b. mass spectrum (3-NOBA matrix): found M^+ = 405, 493. Calculated for: $[C_{24}H_{29}N_4O_2]^+$, M^+ = 405; $[C_{24}H_{30}N_4O_2](BF_4)^+$, M^+ = 493. I.r. spectrum (KBr disc): 3422br m, 2953w, 1667vs, 1643vs, 1537vs, 1460m, 1378w, 1342m, 1308m, 1236m, 1212w, 1124m, 1055vs, 993m, 902w, 869m, 843m, 792w, 780w, 665w, 558w, 521w, 469w, 429w cm^{-1}.

3.4.4.: Single Crystal X-ray Structure of $[(\underline{1}H_4)](PF_6)_2.CH_3NO_2$

Vapour diffusion of diethyl ether into a solution of the compound in CH_3NO_2 gave red crystals of crystallographic quality.

Crystal Data:

$[C_{24}H_{30}N_4O_2](PF_6)_2.CH_3NO_2$ M = 757.35. Monoclinic, space group $P2_1/c$, a = 14.4770(6), b = 11.2662(12), c = 20.0823(20)Å, β = 97.213(7)°, V = 3250Å^3 (by least-squares refinement on diffraction angles for 26 reflections measured at $\pm\omega$ [$24 < 2\theta < 26°$, λ = 0.71073Å]), Z = 4, D_c = 1.548gcm^{-3}, T = 298K. Crystal dimensions 0.36 x 0.28 x 0.24mm^3, μ(Mo-Kα) = 0.235mm^{-1}, F(000) = 1552.

Data Collection and Processing:

Stöe STADI-4 four-circle diffractometer, ω-2θ scan mode using the learnt-profile method[199]. Graphite-monochromated Mo-Kα radiation; 5313 reflections measured ($2\theta_{max.}$ = 45°, h −15 → 15, k 0 → 12, l 0 → 21), 4250 unique data (R_{int} = 0.07), giving 4250 with $F > 4\sigma(F)$. No significant crystal decay, no absorption correction.

Structure Analysis and Refinement:

The structure was solved by direct methods[200] and successive cycles of least-squares refinement and difference Fourier synthesis[201] identified the positions of all the atoms. The crystal lattice was found to contain one CH_3NO_2 molecule per cation. Anisotropic thermal parameters were refined for the C, N, O, P and F atoms. H atoms were located from a difference map and included in fixed, calculated positions. The weighting scheme $w^{-1} = \sigma^2(F) + 0.000487F^2$ gave satisfactory agreement analyses. At final convergence, R = 0.0578, R_w = 0.0791, S = 1.337 for 455 independent parameters, and the final difference Fourier synthesis shows no feature above 0.43 or below −0.29eÅ^{-3}.

Atomic scattering factors were inlaid[201], molecular geometry calculations utilised *CALC*[202] and figures were produced by *ORTEP*-II[203].

3.4.5: Reduction of $[(\underline{1}H_4)](PF_6)_2$

$[(\underline{1}H_4)](PF_6)_2$ (31.6mg, 0.045mmol.) was dissolved in freshly distilled C_2H_5OH (5cm^3). $NaBH_4$ (125mg) was dissolved in C_2H_5OH (10cm^3) and added dropwise with stirring. The mixture rapidly decolourized. After stirring for 2 hours at room temperature, excess dilute HCl acid was added dropwise, each addition being delayed until the effervescence had subsided. A white

solid was initially precipitated which redissolved on adding more acid. H_2O ($20cm^3$) was added to the clear, colourless solution and the volume of solvent was reduced to $20cm^3$. Dilute aqueous NH_3 ($7cm^3$) was added dropwise to the stirring mixture to give an alkaline solution and a white solid was precipitated. Extraction of the solid with $CHCl_3$ was unsuccessful. The white solid was filtered, washed with H_2O and recrystallised from $CHCl_3$/hexane. I.r. spectrum ($CHCl_3$ solution): 3390br, 2961m, 2929m, 2871m, 1718w, 1600w, 1488m, 1456m, 1406m, 1367m, 1329m, 1306w, 1265m, 1233m, 1160s, 1123m, 1094m, 1034m and 1010m cm^{-1}. F.a.b. mass spectrum (3-NOBA matrix): found M^+ = 245, 413, 451, 468, 490. Calculated for: $[C_{24}H_{37}N_4O_2]^+$, M^+ = 413; other peaks, assignment unknown.

$[(\underline{1}H_4)](PF_6)_2$ (42.0mg, 0.055mmol) was dissolved in freshly distilled CH_3CN ($10cm^3$). NaH (60% in mineral oil, 22.5mg, 0.56mmol) was added as a suspension in CH_3CN ($10cm^3$). The clear solution rapidly turned yellow with effervescence. The solution was stirred for 2 hours as a yellow gummy solid was precipitated in low yield. This was filtered and washed with diethyl ether. I.r. spectrum (KBr disc): 3600-3200br, 2963w, 2925w, 2850w, 1631br m, 1488w, 1463m, 1444m, 1250w, 1203w, 1088w, 1038w, 975w, 850m, 825m and 700-500br cm^{-1}. F.a.b. mass spectrum (3-NOBA matrix): found M^+ = 413, 427. Calculated for: $[C_{24}H_{37}N_4O_2]^+$, M^+ = 413; $[C_{24}H_{35}N_4O_2(H_2O)]^+$, M^+ = 427. A satisfactory elemental analysis for this compound was not obtained.

3.4.6: Attempted isolation of $[Na_2(\underline{1})]$

$[(\underline{1}H_4)](PF_6)_2$ (30mg, 0.04mmol) was dissolved in dry, degassed CH_3CN ($5cm^3$) and NaH (60% in mineral oil, 6.4mg, 0.16mmol) was added. After stirring for two hours under N_2, the orange solution had turned yellow with a

small amount of yellow solid being precipitated. The solution was filtered and after reducing the volume, diethyl ether was added to the yellow solution and the mixture cooled. A yellow gummy solid was precipitated which was filtered, washed with diethyl ether and dried *in vacuo*. I.r. spectrum of yellow solid (KBr disc): 3500–3300br, 2915w, 2900w, 2820w, 1633m, 1615w, 1517w, 1467m, 1458m, 1440w, 1405w, 1390w, 1350w, 1268w, 1222w, 1110w, 1061w, 1040w, 988w, 961w, 912w, 868w, 842w, 815w, 786w, 672w, 556w and 493w cm^{-1}. F.a.b. mass spectra (3–NOBA matrix): (positive ion) found M^+ = 405, 427. Calculated for: $[C_{24}H_{29}N_4O_2]^+$, M^+ = 405; $[C_{24}H_{35}N_4O_2(H_2O)]^+$, M^+ = 427. (negative ion) Found M^- = 369, assignment unknown. A satisfactory elemental analysis was not obtained for this compound.

$[(\underline{1}H_4)](PF_6)_2$ (39.2mg, 0.05mmol) was added to freshly distilled CH_3OH (15cm^3) to give an orange suspension. A standardised (0.108M) $NaOCH_3$ solution in CH_3OH (2cm^3, 0.22mmol) was added and a clear, orange solution was obtained on stirring. The volume of the solvent was reduced, diethyl ether was added and a brown solid was obtained. The product was filtered, washed with diethyl ether and dried *in vacuo*. I.r. spectrum (KBr disc): 3500–3000br, 2732w, 1636s, 1529w, 1454m, 1379m, 1270w, 1126w, 1008s, 844m and 563w cm^{-1}. F.a.b. mass spectrum (3–NOBA matrix): found M^+ = 413. Calculated for $[C_{24}H_{37}N_4O_2]^+$, M^+ = 413. A satisfactory elemental analysis was not obtained for this compound.

The above reaction was repeated but using an excess of $NaOCH_3$ solution (8cm^3, 0.88mmol). A gummy, brown solid was obtained. I.r. spectrum (KBr disc): 3600–3200br, 1653br m, 1551w, 1489w, 1375w, 1271s, 1186w, 1163w, 1081w, 1017w, 930w, 895w and 841m cm^{-1}. F.a.b. mass

spectrum (3-NOBA matrix): found M^+ = 413, 482. Calculated for: $[C_{24}H_{37}N_4O_2]^+$, M^+ = 413; $[Na_3C_{24}H_{37}N_4O_2]^+$, M^+ = 482. A satisfactory elemental analysis was not obtained for this compound.

3.4.7: Synthesis of [($\underline{1}H_2$)]

2,6-Diformyl-4-methylphenol (197mg, 1.2mmol) was dissolved in THF ($100cm^3$) and 1,3-diaminopropane ($0.1cm^3$, 1.2mmol) was added. The yellow solution was refluxed for one hour to give an orange/yellow solution and a small amount of colourless particles. The solution was filtered and the volume of solvent was reduced to $5cm^3$. Diethyl ether was added until the solution became turbid and the mixture was cooled. An orange, waxy solid was obtained which was filtered, washed with diethyl ether and dried. The orange product was recrystallised from CH_2Cl_2/diethyl ether and dried *in vacuo*. Yield = 140mg, 30%. Elemental analysis: found C = 69.0; H = 7.55; N = 12.82%. Calculated for $[C_{24}H_{28}N_4O_2].\frac{1}{2}$THF: C = 70.9; H = 7.32; N = 12.72%. F.a.b. mass spectrum (3-NOBA matrix): found M^+ = 405, 607. Calculated for: $[C_{24}H_{29}N_4O_2]^+$, M^+ = 405; $[C_{36}H_{43}N_6O_3]^+$, M^+ = 607. I.r. spectrum (KBr disc): 3414br, 2919m, 2836m, 1637s, 1598m, 1458m, 1369m, 1308w, 1253m, 1159w, 1111w, 1033w, 973w, 867w, 800w, 759w, 641w, 568w and 471w cm^{-1}. U.V./vis. spectrum (CH_2Cl_2): $\lambda_{max.}$ = 426nm. ($\varepsilon_{max.}$ = $970M^{-1}cm^{-1}$), 346 (8550). ^1H n.m.r. spectrum (200.13MHz, $CDCl_3$, 298K): δ = 2.10p.p.m. (dd, J = 6Hz, C-$\underline{H}$CH-C, 2H); 2.21 (dd, J = 5Hz, C-HC$\underline{H}$-C, 2H); 2.26 (s, Ph-C$\underline{H}_3$, 6H); 3.71 (dd, J = 6Hz, N-C$\underline{H}_2$-C, 8H); 7.42 (br s, Ph-$\underline{H}$, 4H); 8.53 (br s, C$\underline{H}$=N, 4H). ^{13}C DEPT n.m.r. spectrum (50.32MHz, $CDCl_3$, 298K): δ = 20.14p.p.m. (Ph-$\underline{C}H_3$); 31.73 (C-$\underline{C}H_2$-C); 58.06 (br, N-$\underline{C}H_2$-C); 134.00 (aromatic $\underline{C}$H). No other peaks found < 180p.p.m.

3.4.8: Synthesis of $[(\underline{2}H_4)](BF_4)_2$

2,6-Diformyl-4-methylphenol (245.0mg, 1.5mmol) was dissolved in distilled CH_3OH ($40cm^3$) and 1,2-diaminoethane ($0.1cm^3$, 1.5mmol) was added. A yellow suspension was formed. A solution of 48% HBr ($0.2cm^3$) in H_2O was added and the mixture heated to reflux. A red/orange solution was obtained with a small amount of brown particles, which were filtered and the solution was allowed to cool. Addition of an excess of $NaBF_4$ precipitated a orange solid, which was filtered, washed with diethyl ether and recrystallised from CH_3NO_2/diethyl ether. Yield = 248mg, 49%. Elemental analysis: found C = 47.4; H = 5.05; N = 8.89%. Calculated for $[C_{22}H_{26}N_4O_2](BF_4)_2$: C = 47.9; H = 4.75; N = 10.2%. F.a.b. mass spectrum (3-NOBA matrix): found M^+ = 378, 466, 566. Calculated for: $[C_{22}H_{26}N_4O_2]^+$, M^+ = 378; $[C_{22}H_{27}N_4O_2](BF_4)^+$, M^+ = 466; $[C_{33}H_{38}N_6O_3]^+$, M^+ = 566. I.r. spectrum (KBr disc): 3442br, 2931m, 1650s, 1540s, 1449m, 1383m, 1334m, 1294m, 1223s, 1058br s, 928m, 880m, 944s, 802m, 783w, 703w, 664w, 595w, 558m, 522m and 466w cm^{-1}. U.V./vis. spectrum (CH_3CN): $\lambda_{max.}$ = 431nm. ($\varepsilon_{max.}$ = $5,570M^{-1}cm^{-1}$); 251 (12,590); 220 (18,720).

3.4.9: Synthesis of $[(\underline{5}H_4)](PF_6)_2$

2,6-Diformyl-4-methylphenol (200.7mg, 1.22mmol) was dissolved in dry CH_3OH ($200cm^3$) and 1,4-diaminobutane (115mg, 1.30mmol) was added. The yellow suspension was stirred for 5 minutes and a solution of 48% HBr ($0.5cm^3$) in H_2O was added. The mixture was heated to reflux and a clear yellow solution was obtained. The solution was allowed to cool and an excess of NH_4PF_6 was added. On cooling at 253K, a yellow precipitate appeared and this was filtered, washed with diethyl ether and dried *in vacuo*. Further crops of the yellow solid were obtained by adding diethyl ether to the mother liquor. The yellow solid was recrystallised from CH_3NO_2. Yield = 128mg,

29%. Elemental analysis: found C = 42.9; H = 4.90; N = 8.17%. Calculated for $[C_{26}H_{34}N_4O_2](PF_6)_2$: C = 43.1; H = 4.73; N = 7.73%. F.a.b. mass spectrum (3-NOBA matrix): found M^+ = 433, 579. Calculated for: $[C_{26}H_{33}N_4O_2]^+$, M^+ = 433; $[C_{26}H_{34}N_4O_2](PF_6)^+$, M^+ = 579. I.r. spectrum (KBr disc): 3054m, 2944m, 2870m, 1654s, 1535s, 1470m, 1454m, 1387m, 1357m, 1328m, 1307m, 1284w, 1256w, 1220s, 1199m, 1132m, 1096w, 1047m, 1031m, 1007w, 987w, 937m, 844br s, 754m, 740w, 696w, 675w, 556s, 506w, 464w, 440m and 415m cm^{-1}. U.V./vis. spectrum (CH_3CN): $\lambda_{max.}$ = 430nm. ($\epsilon_{max.}$ = 23,830$M^{-1}cm^{-1}$); 322 (3,090); 258 (28,970); 222 (27,360).

CHAPTER 4

The Synthesis and Characterisation of Complexes of Macrocycles $(\underline{1})^{2-}$, $(\underline{2})^{2-}$ and $(\underline{5})^{2-}$ with Ni(II), Pd(II), Pt(II) and Rh(III)/(I)

4.1: Introduction

The co-ordination chemistry of the ligand $(\underline{1})^{2-}$ reported in the literature is dominated by complexes with Cu(II)[125]. This is due to the fact that Cu(II) is a very good templating ion and that the resultant complexes are suitable for studying Cu-Cu interactions in binuclear complexes. With the availibility of the protonated ligand $[(\underline{1}H_4)]^{2+}$, however, the possibility of synthesizing complexes with other metals, particularly with the second and third row transition metals is increased. Considering the square-planar array of N- and O-donors in the ligand $(\underline{1})^{2-}$, we proposed that complexes of the Ni triad (Ni, Pd and Pt) would be most readily inserted into the macrocyclic cavity and give dipositive complexes of the form $[M_2(\underline{1})]^{2+}$. The fact that these species will be charged is important since it has been noted that the neutral complexes $[Cu^{I}_2(\underline{1})]$ [123] and $[Cu^{II}_2(\underline{12a})]$[154] (see Section 2.5) are insoluble in common solvents; it seemed likely to us that other neutral metal complexes with $(\underline{1})^{2-}$ and its derivatives would probably give similarly insoluble products.

There have been no structurally characterised complexes of $(\underline{1})^{2-}$ with metals from the Ni triad reported in the literature. Robson and Pilkington have described the synthesis of the paramagnetic, square-pyramidal complex $[Ni_2(\underline{1})Cl_2]$[97] and Gagné and co-workers[121] reported the synthesis of the paramagnetic, octahedral complex $[Ni_2(\underline{1})(pyridine)_4](BF_4)_2$ and compared its electronic and magnetic properties with $[Fe_2(\underline{1})(pyridine)_4](BF_4)_2$ and $[Co_2(\underline{1})(pyridine)_4](BF_4)_2$ [121]. However, Robson and Pilkington[97] also reported that the attempted preparation of $[Ni_2(\underline{1})](ClO_4)_2$, using a template synthesis about $Ni(ClO_4)_2$, yielded a mixture of two products: mononuclear $[Ni(\underline{1}H_2)](ClO_4)_2.2H_2O$ and a green species that was probably a binuclear complex. In $[Ni(\underline{1}H_2)](ClO_4)_2.2H_2O$, the Ni(II) ion was assigned a square-pyramidal environment with an axial H_2O ligand and unco-ordinated

ClO_4^- counterions. Okawa and Kida[119] have synthesized $[Ni_2(\underline{2})Cl_2]$ and $[Ni_2(\underline{3})Cl_2]$ in CH_3OH but could not synthesize the binuclear complex of $(\underline{1})^{2-}$. On the basis of spectroscopic data, they concluded that $[Ni_2(\underline{2})Cl_2]$ and $[Ni_2(\underline{3})Cl_2]$ were diamagnetic, square-planar species even in pyridine solution. Additionally they suggested that an increase in length of both side-arms of the macrocycle to $-(CH_2)_3-$ groups would give $(\underline{1})^{2-}$ a larger macrocyclic cavity than $(\underline{2})^{2-}$ or $(\underline{3})^{2-}$, and the resulting decrease in ligand field would destabilise low spin Ni(II). On this basis we expected that any Ni(II) complexes of $(\underline{1})^{2-}$ would be paramagnetic, as the ligand-field strength of $(\underline{1})^{2-}$ is too small to cause spin-pairing of electrons in the e_g 3d-orbitals of Ni(II). A binuclear Pd(II) or Pt(II) complex with $(\underline{1})^{2-}$, however, would be a low spin, square-planar compound due to the larger spin-orbit coupling constants of the second and third row transition elements.

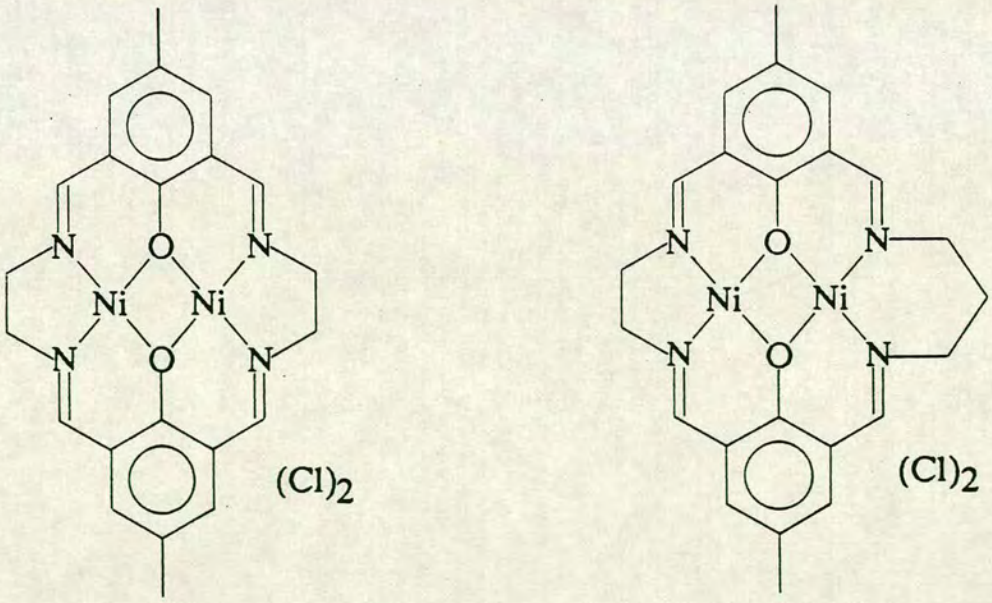

Figure 4.1 $[Ni_2(\underline{2})]Cl_2$ and $[Ni_2(\underline{3})]Cl_2$

4.2: Results and Discussion

This chapter describes the syntheses of Ni(II), Pd(II) and Rh(III) complexes of the ligand $(\underline{1})^{2-}$ and describes attempts to synthesize the corresponding Pt(II), Ru(II) and Rh(I) complexes. The synthesis of $[Ni_2(\underline{2})]^{2+}$ and the attempted synthesis of $[Pt_2(\underline{5})]^{2+}$ are also described. A novel cubane-type structure has been discovered for the complex $[Ni_2(\underline{1})(CH_3CO_2)]_2(PF_6)_2$ in the solid-state but there is no conclusive evidence that this agglomerate is present in solution. The electrochemical properties of some of the above complexes have also been studied.

4.2.1: The Synthesis of $\{[Ni_2(\underline{1})](BF_4)_2\}_n$

The reaction of two equivalents of $[Ni(H_2O)_6](BF_4)_2$ with one equivalent of $[(\underline{1}H_4)](BF_4)_2$ in refluxing C_2H_5OH in the presence of $N(C_2H_5)_3$ gave a red precipitate. The i.r. spectrum of this product shows strong bands at 1629 and 1084cm^{-1}, which are assigned to the stretching vibrations of a co-ordinated C=N group and B-F bonds respectively. The f.a.b. mass spectrum of the red solid shows a molecular ion peak at M^+ = 518, corresponding to $[^{58}Ni_2(\underline{1})]^+$ and also a peak at M^+ = 684 with the expected isotope patterns for a binuclear Ni compound. This evidence combined with elemental analytical data confirm the product of the initial reaction to be $[Ni_2(\underline{1})](BF_4)_2$.

The peak in the f.a.b. mass spectrum at M^+ = 684 is assigned to an adduct of $[Ni_2(\underline{1})]^{2+}$ and 3-nitrobenzoate ($O_2CC_6H_4NO_2^-$, molecular weight = 166). We propose that the 3-nitrobenzoic acid is derived from the solvating matrix used in performing the mass spectrum experiment (3-nitrobenzyl alcohol). It is possible that 3-nitrobenzyl alcohol, even with a deactivated benzene ring, is oxidised in air to give the benzoic acid derivative. The 3-nitrobenzoic acid thus formed reacts with $[Ni_2(\underline{1})]^{2+}$ to give

$[Ni_2(\underline{1})(O_2CC_6H_4NO_2)]^{2+}$. From the compounds described in Sections 4.2.7 and 4.2.8 below, it can be seen that a carboxylic group can bridge the two Ni(II) centres in $[Ni_2(\underline{1})]^{2+}$, and the bridged species is more soluble than $[Ni_2(\underline{1})](BF_4)_2$. When the f.a.b. mass spectrum of the same sample of $[Ni_2(\underline{1})](BF_4)_2$ was carried out in a DMF/glycerol matrix, no peak at $M^+ = 684$ was observed. This is consistent with the previously observed peak at $M^+ = 684$ being due to an adduct of 3-nitrobenzoate and $[Ni_2(\underline{1})]^{2+}$. However, the spectrum obtained using DMF/glycerol as the matrix is of considerably poorer quality and in addition to the peak at $M^+ = 518$, shows a peak at $M^+ = 462$, corresponding to mononuclear $[^{58}Ni(\underline{1}H_2)]^+$. Therefore the following spectra are run in 3-NOBA, since the spectra are of better quality and still show peaks due to $[Ni_2(\underline{1})]^+$.

The red precipitate of $[Ni_2(\underline{1})](BF_4)_2$ was soluble in DMSO, sparingly soluble in DMF and insoluble in boiling CH_3CN, C_2H_5OH and CH_3NO_2. A red, oily solid which was isolated from the red solution of the reaction mixture contained small amounts of $[Ni_2(\underline{1})]^{2+}$, as determined by f.a.b. mass spectroscopy. We propose that the initial insoluble red solid contains aggregrates of $[Ni_2(\underline{1})](BF_4)_2$ which are formed by the parallel stacking of $[Ni_2(\underline{1})]^{2+}$ units in infinite chains. Therefore, each Ni(II) ion is in an octahedral environment completed by axial interactions with the phenoxy groups of two neighbouring ligand molecules. Only strongly co-ordinating solvents, like DMSO and to a lesser extent DMF, are capable of breaking these interactions to give soluble $[Ni_2(\underline{1})]^{2+}$ species. It is also possible that there may be H_2O or OH^- groups within the aggregates that assist this packing, particularly as the percentage of hydrogen in the elemental analysis is high for the proposed formulation. To investigate this, a portion of the red solid was boiled in C_2H_5OH that had been acidified with HBF_4 in H_2O (48%), in an attempt to cleave any OH^- bridges present. No reaction was

observed.

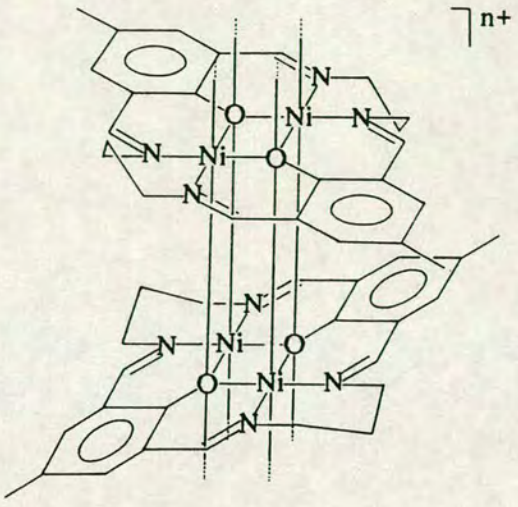

Figure 4.2 Proposed solid-state structure of $\{[Ni_2(\underline{1})](BF_4)_2\}_n$

We suspect that intermolecular stacking interactions occurs between $[Ni_2(\underline{1})]^{2+}$ molecules since stacking interactions have been documented for mononuclear Ni(II) complexes of acyclic Schiff base ligands. These mononuclear complexes, exemplified by $Ni(Me\text{-}sal)_2$, are analogous to Ni(II) complex of $(\underline{1})^{2-}$, because the donor sets around the Ni(II) ions are identical. Holm and other workers[204] have reported that the neutral Schiff-base complex $Ni(Me\text{-}sal)_2$ is diamagnetic in the solid-state at room temperature, partially paramagnetic in chloroform and fully paramagnetic in pyridine solutions. The fully paramagnetic behaviour of $Ni(Me\text{-}sal)_2$ in pyridine (μ = 3.1B.M.) is readily explained in terms of the association of two pyridine molecules per nickel to give a six-co-ordinate complex. The partial paramagnetism of $Ni(Me\text{-}sal)_2$ (μ = 1.1-2.2B.M.) in ostensibly nonco-ordinating solvents was best accounted for in terms of dimerisation and aggregation processes similar to that described above. Other possible explanations, that there was a mixture of tetrahedral and planar species in solution[205-207], or that a weak axial perturbation by solvent molecules of the

planar molecules lowered a triplet state to within thermal range[208,209], required that the spectral and magnetic properties would be independent of solvent concentration at a fixed temperature. Measurements carried out in chloroform and benzene solutions at 297K, however, showed a definite increase in magnetic moment with increasing concentration[210]. The proposed association to aggregates would decrease the tetragonality of the ligand field and so stabilize a triplet ground state for the Ni(II) centres. It has not been demonstrated whether the partially paramagnetic species are dimers (Ni(II) ions being five-co-ordinate) or larger (Ni(II) ions octahedral or five-co-ordinate). Ni(Me-sal)$_2$ also shows changes from diamagnetic to paramagnetic behaviour in the solid-state in the temperature range 100-350K (diamagnetic) to 473K (paramagnetic)[211]. The buff-coloured paramagnetic material is insoluble and has the same elemental analyses as the soluble, green, diamagnetic starting material.

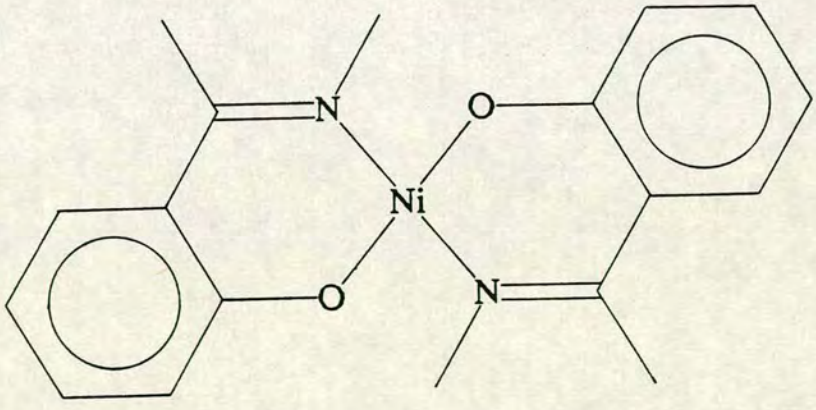

Figure 4.3 Ni(Me-sal)$_2$

We propose that the red, insoluble [Ni$_2$(1)](BF$_4$)$_2$ is paramagnetic, but unfortunately insufficient sample could be prepared to take a measurement of its magnetic moment. We have attempted to synthesize [Ni$_2$(1)](BF$_4$)$_2$ at room temperature in case the aggregation is caused by refluxing in C_2H_5OH. However, stirring a solution of two equivalents of [Ni(H$_2$O)$_6$](BF$_4$)$_2$ with one

equivalent of $[(\underline{1}H_4)](BF_4)_2$ in C_2H_5OH in the presence of excess $N(C_2H_5)_3$ at room temperature for 48 hours gave a mixture of products, including $[Ni_2(\underline{1})](BF_4)_2$, $[Ni(\underline{1}H_2)](BF_4)_2$ and unreacted ligand (from the i.r. and f.a.b. mass spectra).

The electronic spectra of $[Ni_2(\underline{1})](BF_4)_2$ in different solvents show that there is a solvent dependence for the positions of the bands. In DMSO, peaks occur at $\lambda_{max.}$ = 470 and 318nm; in DMF, $\lambda_{max.}$ = 462 and 317nm. and in CH_3CN (a solution of the oily, red material isolated from the reaction solution), $\lambda_{max.}$ = 445, 380 and 246nm. This supports the claim that significant solvent interactions are required to solubilise the $[Ni_2(\underline{1})](BF_4)_2$ species. The bands are assigned as charge-transfer bands due to their intensities, although the $\varepsilon_{max.}$ values quoted in section 4.4.2a are probably inaccurate as even in DMSO, residual insoluble solids were present in the solutions. The solutions were too low in concentration to observe d → d transitions.

4.2.2: Cyclic Voltammetry of $[Ni_2(\underline{1})](BF_4)_2$ in DMSO

Cyclic voltammetry of $[Ni_2(\underline{1})](BF_4)_2$ measured in DMSO (0.1M $NBu^n{}_4BF_4$ supporting electrolyte) at Pt electrodes at 298K reveals one irreversible reduction at E_{pc} = −1.56V (scan rate = $0.15Vs^{-1}$) and −1.60V ($0.50Vs^{-1}$) and two irreversible oxidations at E_{pa} = +0.13V ($0.10Vs^{-1}$) and +0.15V ($0.30Vs^{-1}$) and E_{pa} = +0.35V ($0.10Vs^{-1}$) and +0.37V ($0.30Vs^{-1}$) (all *vs.* Fc/Fc^+). Heating the solution to 353K caused small shifts in E_{pc} and E_{pa} for the first reduction and oxidation processes, the second oxidation became broadened and a second reduction appeared, at E_{pc} = −1.87V ($0.18Vs^{-1}$) and −1.92V ($0.60Vs^{-1}$) *vs.* Fc/Fc^+. It has been previously established that the ligand $(\underline{1})^{2-}$ does not show redox activity within these potentials[145] so these four processes are tentatively assigned as two one-electron reductions,

corresponding to

$[Ni^{II}_2(\underline{1})]^{2+} \rightarrow [Ni^{II}Ni^{I}(\underline{1})]^{+}$ and

$[Ni^{II}Ni^{I}(\underline{1})]^{+} \rightarrow [Ni^{I}_2(\underline{1})]$

and two one-electron oxidations, corresponding to

$[Ni^{II}_2(\underline{1})]^{2+} \rightarrow [Ni^{II}Ni^{III}(\underline{1})]^{3+}$ and

$[Ni^{II}Ni^{III}(\underline{1})]^{3+} \rightarrow [Ni^{III}_2(\underline{1})]^{4+}$.

Importantly the irreversiblility of these processes suggests that the redox products of $[Ni_2(\underline{1})]^{2+}$ are unstable, which react further to give unidentified products.

4.2.3: The Synthesis of $[Ni_2(\underline{1})(CH_3CN)_4](BF_4)_2$

The reaction of two equivalents of $[Ni(H_2O)_6](BF_4)_2$ with one equivalent of $[(\underline{1}H_4)](BF_4)_2$ with excess 1,8-bis(dimethylamino)naphthalene in refluxing CH_3CN under N_2 gave an amber solution that gave a yellow solid on addition of diethyl ether. This was recrystallised from CH_3CN/diethyl ether or CH_3NO_2/diethyl ether by vapour diffusion to give a brown crystalline solid. The i.r. spectrum of this solid shows strong bands at 1643 and 1059cm^{-1} which are assigned to the stretching vibrations of a co-ordinated C=N group and B-F bonds respectively. There are also weak bands at 1929 and 1820cm^{-1} which are tentatively assigned to co-ordinated C=N stretching vibrations. The f.a.b. mass spectrum of the product shows peaks at M^+ = 518 and 684, which are assigned to $[Ni_2(\underline{1})]^+$ and $[Ni_2(\underline{1})(O_2CC_6H_4NO_2)]^+$ respectively. The elemental analytical data agrees best with the formulation $[Ni_2(\underline{1})(CH_3CN)_2(H_2O)](BF_4)_2$ which incorporates only two CH_3CN ligands per molecule and also a H_2O molecule.

When single crystals of the brown product were grown for X-ray diffraction, it was found that the crystals lost solvent very readily in air leading to disintegration of the crystals. It was therefore concluded that the

compound, probably $[Ni_2(\underline{1})(CH_3CN)_4](BF_4)_2$, was unstable when isolated from its mother liquor and decomposed by loss of CH_3CN. When handled in an oil drop at 195K, the crystals were stable for at least 5 minutes, so it appeared that the instability of $[Ni_2(\underline{1})(CH_3CN)_4](BF_4)_2$ was due to thermal decomposition at room temperatures. Due to the lack of structurally characterised Ni(II) complexes with $(\underline{1})^{2-}$, the single crystal structure determination was undertaken. Additionally, we felt that low temperature X-ray diffraction was the best method for characterising the compound.

4.2.4: The Single Crystal X-Ray Structure of $[Ni_2(\underline{1})(CH_3CN)_4](BF_4)_2$

Details of the structure solution are given in the Experimental Section. Selected bond lengths, angles and torsions are listed in Tables 4.1, 4.2 and 4.3 respectively. Two views of the cation $[Ni_2(\underline{1})(CH_3CN)_4]^{2+}$ are shown in Figures 4.4 and 4.5.

The structure of $[Ni_2(\underline{1})(CH_3CN)_4]^{2+}$ shows the macrocycle to be essentially flat with only the middle carbons of the propylene chains deviating from the ligand plane of $(\underline{1})^{2-}$. A centre of inversion is located in the centre of the cation, so the two Ni(II) ions are identical. Each Ni(II) centre is in an octahedral environment and are co-ordinated to two imine N-donors [Ni-N(1) = 2.024(4), Ni-N(2) = 2.015(4)Å], two bridging phenoxy O-donors [Ni-O(1) = 2.030(3), 2.025(3)Å] and two axial CH_3CN ligands [Ni-N(3) = 2.143(4), Ni-N(4) = 2.122(4)Å]. The Ni-Ni separation is 3.136(1)Å. This metal-metal distance is similar to the Cu(II)-Cu(II) distance [3.091(3)Å] found in $[Cu_2(\underline{1})(H_2O)_2(ClO_4)_2]$ [114] and the Fe(II)-Fe(II) distance [3.117(3)Å] found in $[Fe_2(\underline{1})(imidazole)_4]^{2+}$ [121], where the metal centres are also in octahedral environments and located in the ligand plane. The Ni(II)-N bond lengths from the metal centre to the ligand $(\underline{1})^{2-}$ are shorter by approximately 0.10Å than the Ni(II)-N distances from the metal to

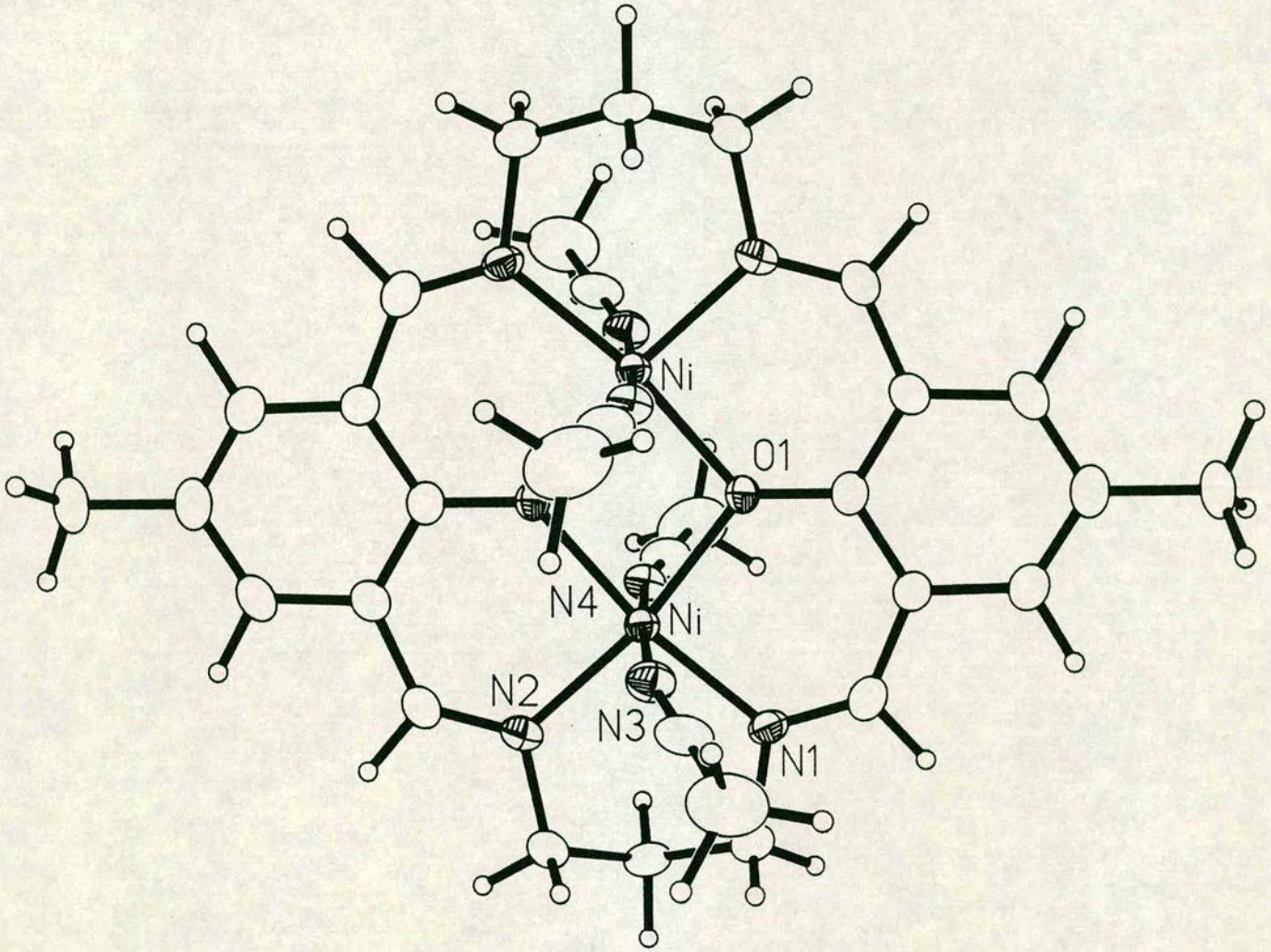

Figure 4.4 View of the single crystal X-ray structure of $[Ni_2(\underline{1})(CH_3CN)_4]^{2+}$

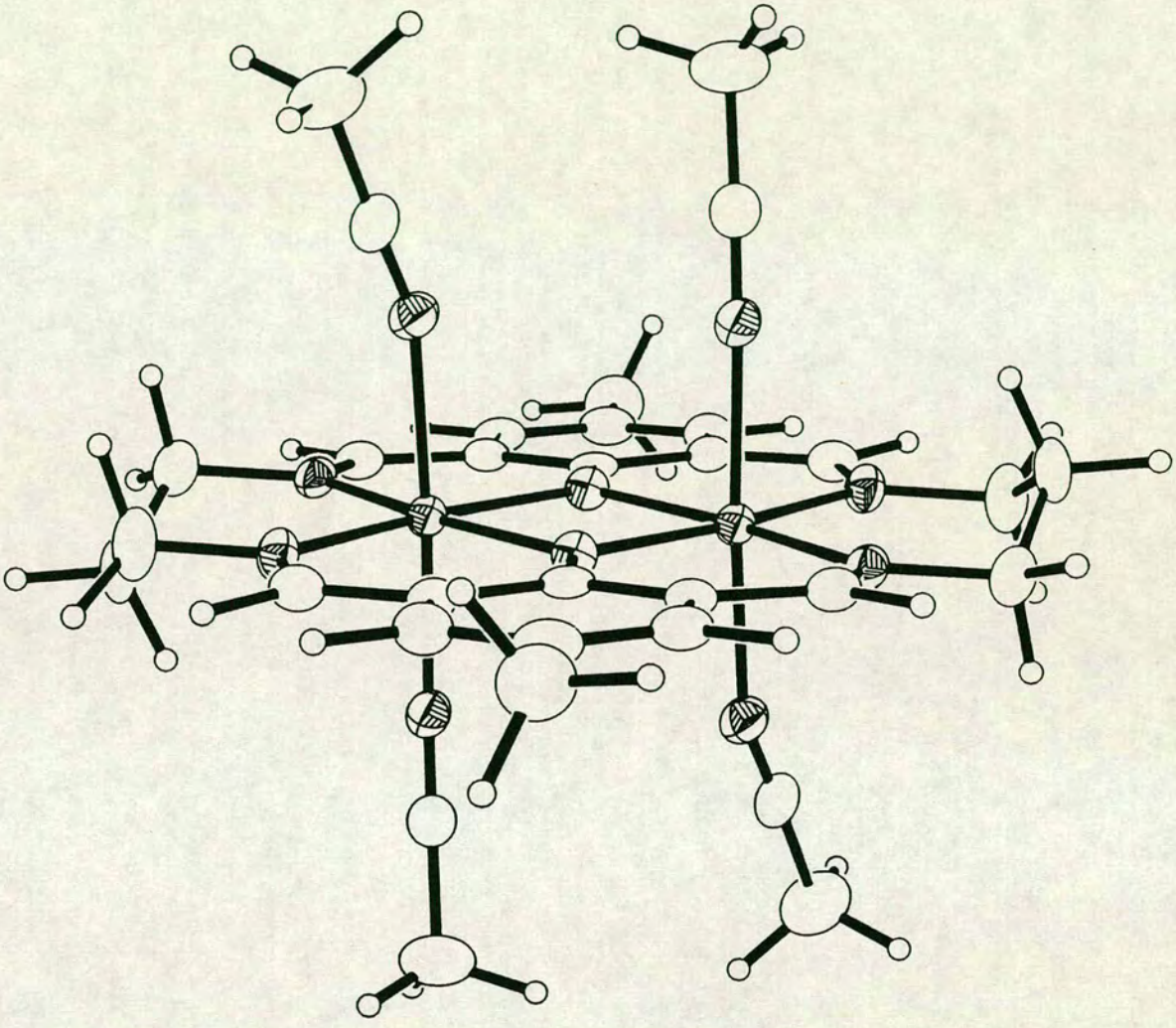

Figure 4.5 Alternative view of the single crystal X-ray structure of $[Ni_2(\underline{1})(CH_3CN)_4]^{2+}$

Table 4.1 Selected bond lengths (Å) of $[Ni_2(\underline{1})(CH_3CN)_4]^{2+}$

Ni	- O(1)	2.030(3)	C(2)	- C(3)	1.413(6)
Ni	- N(1)	2.024(4)	C(2)	-C(12')	1.447(6)
Ni	- N(2)	2.015(4)	C(3)	- C(4)	1.378(7)
Ni	- N(3)	2.143(4)	C(4)	- C(5)	1.513(7)
Ni	- N(4)	2.122(4)	C(4)	- C(6)	1.381(7)
Ni	-Ni(')	3.1355(8)	C(6)	- C(7)	1.406(6)
Ni	-O(1')	2.025(3)	C(7)	- C(8)	1.454(6)
O(1)	- C(1)	1.311(5)	C(9)	-C(10)	1.524(7)
N(1)	- C(8)	1.278(6)	C(10)	-C(11)	1.525(7)
N(1)	- C(9)	1.484(6)	N(3)	-C(13)	1.134(6)
N(2)	-C(11)	1.477(6)	C(13)	-C(14)	1.451(8)
N(2)	-C(12)	1.281(6)	N(4)	-C(15)	1.128(6)
C(1)	- C(2)	1.420(6)	C(15)	-C(16)	1.451(8)
C(1)	- C(7)	1.429(6)			

Table 4.2 Selected bond angles (°) of $[Ni_2(\underline{1})(CH_3CN)_4]^{2+}$

O(1)	- Ni	- N(1)	91.60(14)	O(1)	- C(1)	- C(2)	121.3(4)
O(1)	- Ni	- N(2)	169.63(13)	O(1)	- C(1)	- C(7)	121.3(4)
O(1)	- Ni	- N(3)	91.76(14)	C(2)	- C(1)	- C(7)	117.4(4)
O(1)	- Ni	- N(4)	88.12(13)	C(1)	- C(2)	- C(3)	119.7(4)
O(1)	- Ni	-O(1')	78.68(12)	C(1)	- C(2)	-C(12')	125.3(4)
N(1)	- Ni	- N(2)	98.75(15)	C(3)	- C(2)	-C(12')	115.0(4)
N(1)	- Ni	- N(3)	86.29(15)	C(2)	- C(3)	- C(4)	123.2(4)
N(1)	- Ni	- N(4)	89.15(15)	C(3)	- C(4)	- C(5)	121.6(4)
N(1)	- Ni	-O(1')	170.28(14)	C(3)	- C(4)	- C(6)	116.8(4)
N(2)	- Ni	- N(3)	89.52(15)	C(5)	- C(4)	- C(6)	121.5(4)
N(2)	- Ni	- N(4)	91.42(15)	C(4)	- C(6)	- C(7)	123.4(4)
N(2)	- Ni	-O(1')	90.97(13)	C(1)	- C(7)	- C(6)	119.5(4)
N(3)	- Ni	- N(4)	175.43(15)	C(1)	- C(7)	- C(8)	125.9(4)
N(3)	- Ni	-O(1')	94.24(14)	C(6)	- C(7)	- C(8)	114.7(4)
N(4)	- Ni	-O(1')	90.22(13)	N(1)	- C(8)	- C(7)	127.9(4)
Ni	- O(1)	- C(1)	128.9(3)	N(1)	- C(9)	-C(10)	112.4(4)
Ni	- O(1)	-Ni(')	101.32(13)	C(9)	-C(10)	-C(11)	114.0(4)
C(1)	- O(1)	-Ni(')	129.5(3)	N(2)	-C(11)	-C(10)	111.7(4)
Ni	- N(1)	- C(8)	124.1(3)	N(2)	-C(12)	-C(2')	128.2(4)
Ni	- N(1)	- C(9)	121.6(3)	Ni	- N(3)	-C(13)	157.2(4)
C(8)	- N(1)	- C(9)	114.2(4)	N(3)	-C(13)	-C(14)	178.3(5)
Ni	- N(2)	-C(11)	119.5(3)	Ni	- N(4)	-C(15)	166.5(4)
Ni	- N(2)	-C(12)	124.3(3)	N(4)	-C(15)	-C(16)	178.7(5)
C(11)	- N(2)	-C(12)	116.2(4)				

Table 4.3 Selected torsion angles (°) of $[Ni_2(\underline{1})(CH_3CN)_4]^{2+}$

C(9)	- N(1)	- C(8)	- C(7)	-175.3(4)	C(12')	- C(2)	- C(3)	- C(4)	-178.6(4)
C(8)	- N(1)	- C(9)	-C(10)	-153.0(4)	C(1)	- C(2)	-C(12')	-N(2')	0.6(8)
C(12)	- N(2)	-C(11)	-C(10)	139.8(4)	C(3)	- C(2)	-C(12')	-N(2')	179.4(4)
C(11)	- N(2)	-C(12)	-C(2')	175.0(4)	C(2)	- C(3)	- C(4)	- C(5)	178.7(4)
O(1)	- C(1)	- C(2)	- C(3)	178.8(4)	C(2)	- C(3)	- C(4)	- C(6)	0.8(7)
O(1)	- C(1)	- C(2)	-C(12')	-2.5(7)	C(3)	- C(4)	- C(6)	- C(7)	-0.7(7)
C(7)	- C(1)	- C(2)	- C(3)	-1.3(6)	C(5)	- C(4)	- C(6)	- C(7)	-178.7(4)
C(7)	- C(1)	- C(2)	-C(12')	177.4(4)	C(4)	- C(6)	- C(7)	- C(1)	-0.4(7)
O(1)	- C(1)	- C(7)	- C(6)	-178.7(4)	C(4)	- C(6)	- C(7)	- C(8)	-179.6(4)
O(1)	- C(1)	- C(7)	- C(8)	0.4(7)	C(1)	- C(7)	- C(8)	- N(1)	-4.9(8)
C(2)	- C(1)	- C(7)	- C(6)	1.3(6)	C(6)	- C(7)	- C(8)	- N(1)	174.2(5)
C(2)	- C(1)	- C(7)	- C(8)	-179.5(4)	N(1)	- C(9)	-C(10)	-C(11)	-69.8(5)
C(1)	- C(2)	- C(3)	- C(4)	0.2(7)	C(9)	-C(10)	-C(11)	- N(2)	76.9(5)

CH_3CN ligands. The metal–nitrile bonds are long for Ni(II)–$NCCH_3$ (average distances are in the range 2.03–2.12Å [212]) which is consistent with the observation that the metal–nitrile bonds are relatively weak and the CH_3CN ligands are readily lost. Importantly, the structure shows that there are no other solvent molecules incorporated in the crystal lattice, so the disintegration of the crystals in air is due to actual decomposition of the $[Ni_2(\underline{1})(CH_3CN)_4]^{2+}$ cation.

The view shown in Figure 4.4 also shows that the Ni–N≡C angle is significantly deviated from the expected linear geometry, particularly ∠Ni–N(3)–C(13)= 157.2(4)°. Deviations from linearity are very common in nitrile complexes, but are usually only 180±10° [213]. Examples which show deviations greater than 170° are often explained on the basis of sp^2 contributions to the electronic state of N and are then often designated as weak π–donors, rather than the usual weak π–acceptors[214]. Both of the C≡N bonds in the CH_3CN ligands of $[Ni_2(\underline{1})(CH_3CN)_4]^{2+}$ are of average length for a co–ordinated C≡N group (usually 1.11–1.15Å [213]). Packing forces and steric interactions are also implicated in deviations from the linear co–ordination of nitriles. A space filling diagram of $[Ni_2(\underline{1})(CH_3CN)_4]^{2+}$ is shown in Figure 4.6 and shows that if the CH_3CN ligands were both co–ordinated linearly, the CH_3CN methyl groups would probably experience steric repulsions. Bending of the Ni(II)–N bond relieves these interactions. The different values of the observed Ni–N≡C angles [157.2(4), 166.5(4)°] are probably caused by the displacement of the middle carbon of the propylene groups from the macrocyclic ligand plane. Therefore, the more linear Ni–CH_3CN group is forced towards this linearity by the central propylene hydrogen which is displaced towards it. This is shown by the short distance of the central propylene H atom to $CH_3C\underline{N}$ (2.77Å), which is the shortest non–bonded distance to the denoted nitrogen atom. We propose, then, that

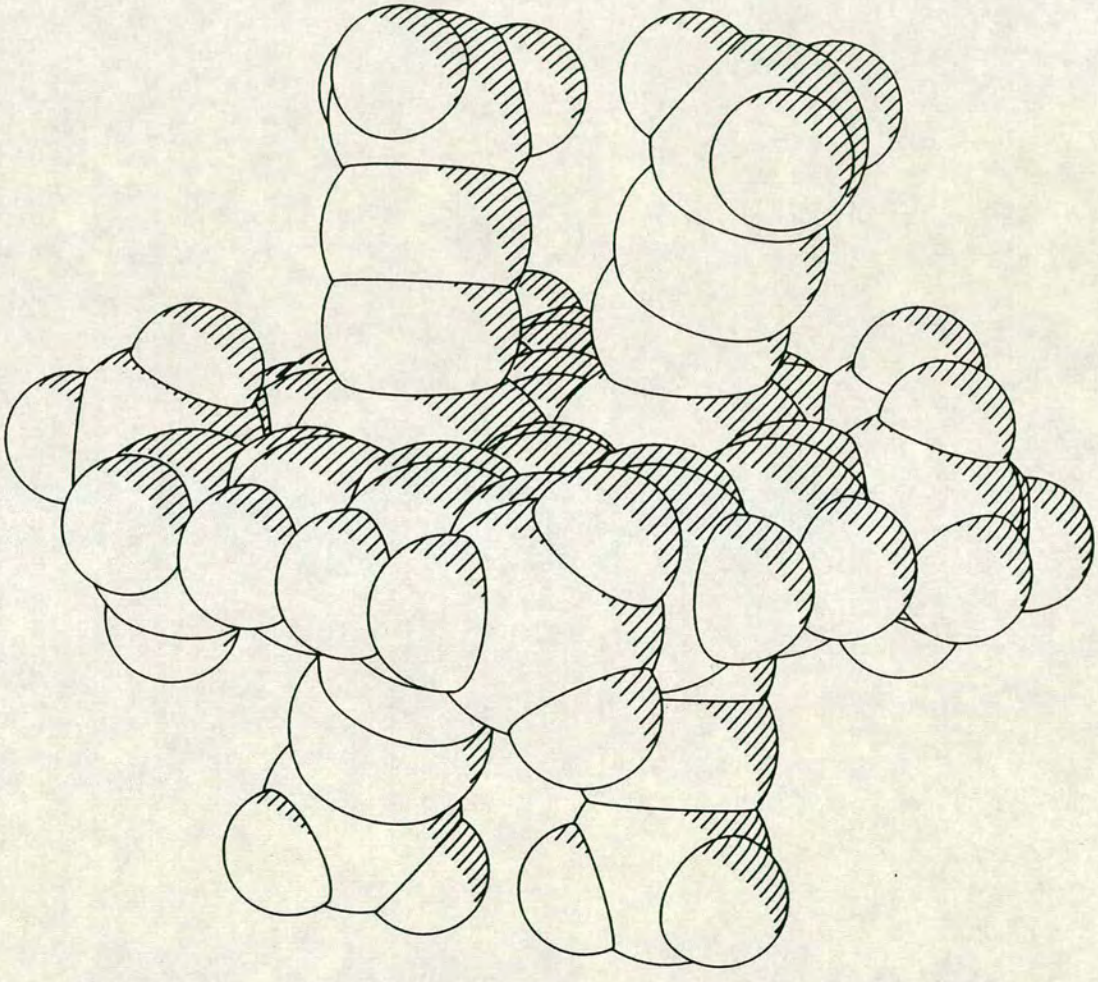

Figure 4.6 Space filling diagram of $[Ni_2(\underline{1})(CH_3CN)_4]^{2+}$

the non-linearity of the Ni(II)-$NCCH_3$ groups and perhaps the instability of the complex is caused primarily by steric interactions of the axial ligands with each other.

The single crystal X-ray structure of $[Ni_2(\underline{1})(CH_3CN)_4](BF_4)_2$ confirms the conclusion of Okawa and Kida[119], that Ni(II) ions will adopt an octahedral geometry when co-ordinated to ligand $(\underline{1})^{2-}$. This is because the macrocyclic cavity does not give a sufficiently strong ligand-field to enforce a square-planar geometry on the Ni(II) centre. The CH_3CN ligands that are bound in the axial sites of the octahedral Ni(II) then experience steric repulsions on bonding to the metal centres. CH_3CN is a relatively non-bulky monodentate ligand and so the fact that even this ligand has steric interactions could be a serious hindrance to the synthesis of other octahedral binuclear Ni(II) complexes of $(\underline{1})^{2-}$. Two strategies could be used to avoid this problem. They are to resynthesize the $[Ni_2(\underline{2})]^{2+}$ species which was first prepared by Okawa and Kida[119], where the proposed Ni(II) environments are square-planar, or to use a single chelating ligand, such as a carboxylate, that could bridge the adjacent axial sites in $[Ni_2(\underline{1})]^{2+}$. These studies are described later in Sections 4.2.6 and 4.2.7 respectively.

4.2.5: Alternative Synthetic Routes to $[Ni_2(\underline{1})(solvent)_4]^{2+}$ (solvent = CH_3CN, H_2O)

We have also prepared the binuclear Ni(II) complexes of the form $[Ni_2(\underline{1})(solvent)_4]^{2+}$ by the reaction of the neutral form of the ligand, $(\underline{1}H_2)$, with two equivalents of $Ni(CH_3CO_2)_2$ and excess $N(C_2H_5)_3$ in refluxing CH_3CN. The yield is low, however, and gives a mixture of products. This is shown in the f.a.b. mass spectrum in 3-nitrobenzyl alcohol of the isolated product which shows peaks at M^+ = 519, 537, 578, 685 and 703. These are assigned to $[^{58}Ni_2(\underline{1})]^+$, $[^{58}Ni_2(\underline{1}H)(H_2O)]^+$, $[^{58}Ni_2(\underline{1}H)(CH_3CO_2)]^+$,

$[^{58}Ni_2(\underline{1}H)(O_2CC_6H_4NO_2)]^+$ and $[^{58}Ni_2(\underline{1}H)(O_2CC_6H_4NO_2)(H_2O)]^+$ respectively, where $O_2CC_6H_4NO_2^-$ is derived from the oxidation of 3-nitrobenzyl alcohol. Except for differences due to the use of different counterions, the i.r. spectrum of the isolated product of the reaction is similar to that obtained for $[Ni_2(\underline{1})(CH_3CN)_4](BF_4)_2$ in air. In particular, the C=N stretching vibration at $1640cm^{-1}$ is closest to the previous value of $1643cm^{-1}$ quoted for the C=N stretching vibration of $[Ni_2(\underline{1})(CH_3CN)_4]^{2+}$. On the basis of the elemental analysis and the above data, the major product of the reaction is assigned as $[Ni_2(\underline{1})(solvent)_4](CH_3CO_2)_2$ where (solvent) is a mixture of H_2O and CH_3CN ligands.

A product that also contained $[Ni_2(\underline{1})(solvent)_4]^{2+}$ was prepared by the transmetallation reaction between $[Pb_2(\underline{1})](NO_3)_2$ and two equivalents of $[Ni(H_2O)_6](BF_4)_2$ in refluxing CH_3CN. A yellow solid was obtained on addition of diethyl ether to the reaction solution and the f.a.b. mass and i.r spectra obtained for this compound were similar to those of $[Ni_2(\underline{1})(solvent)_4](BF_4)_2$ (solvent = H_2O or CH_3CN). For details of this data see section 4.4.2e. The transmetallation appeared to proceed readily, with the preferential insertion of Ni(II) into the macrocyclic ligand, displacing the larger Pb(II) ions. There are a number of examples of related ligands undergoing transmetallations[215-218] in the literature but to our knowledge, there have been no previous transmetallation reactions reported with $[Pb_2(\underline{1})]^{2+}$. Further examples of transmetallations with $[Pb_2(\underline{1})]^{2+}$ will be given in Sections 4.2.11 and 4.2.19.

4.2.6: The Synthesis of $[Ni_2(\underline{2})](BF_4)_2$

The reaction of $[Ni(CH_3CN)_6](BF_4)_2$ [219] with $[(\underline{2}H_4)](BF_4)_2$ in the presence of excess $N(C_2H_5)_3$ under N_2 in refluxing CH_3CN gave a red solution. Addition of diethyl ether to the solution gave a red solid. The f.a.b.

mass spectrum of this solid shows peaks at M^+ = 490, 509 and 579, which are assigned to $[^{58}Ni_2(\underline{2})]^+$, $[^{58}Ni_2(\underline{2}H)(H_2O)]^+$ and $[^{58}Ni_2(\underline{2}H_2)](BF_4)^+$ respectively. The i.r. spectrum shows strong bands at 1623, 1563 and 1058cm^{-1} and are assigned to C=N, C–O and B–F stretching vibrations respectively. The bands at 1623 and 1563cm^{-1} compare well with the values previously quoted by Okawa and Kida[119] for the complex $[Ni_2(\underline{2})]Cl_2$, which shows bands at 1633 and 1565cm^{-1}. They assigned the latter band to a skeletal vibration of the benzene ring, but Mandal and Nag[127] concluded, on further studies, that the band around 1560cm^{-1} is due to the C–O stretching vibration. On the basis of the above and elemental analytical data, the red product was assigned as $[Ni_2(\underline{2})](BF_4)_2$. The electronic spectrum of the complex in CH_3CN shows bands at 386, 290 and 243nm. and these are assigned as charge–transfer bands because of the magnitude of their extinction coefficients ($\varepsilon_{max.}$ = 5,100, 12,000, 22,200 $M^{-1}cm^{-1}$ respectively).

4.2.7: The Synthesis of $[Ni_2(\underline{1})(CH_3CO_2)](PF_6)$

The reaction of $Ni(CH_3CO_2)_2$ with $[(\underline{1}H_4)](PF_6)_2$ in the presence of excess $N(C_2H_5)_3$ in refluxing CH_3CN gave a green solution, which on careful addition of diethyl ether gave a green, crystalline solid. The f.a.b. mass spectrum in 3–nitrobenzyl alcohol of the green solid shows peaks at M^+ = 518, 577 and 684. No other peaks were found up to M^+ = 1600. These peaks are assigned to $[^{58}Ni_2(\underline{1})]^+$, $[^{58}Ni_2(\underline{1})(CH_3CO_2)]^+$ and $[^{58}Ni_2(\underline{1})(O_2CC_6H_4NO_2)]^+$ respectively. The green solid shows strong bands in the i.r. spectrum at 1648, 1575, 1417 and 843cm^{-1} and these are assigned to C=N, C–O, bridging O–C–O and P–F stretching vibrations respectively. This data, together with elemental analytical figures, confirms the product to be $[Ni_2(\underline{1})(CH_3CO_2)](PF_6)$.

$[Ni_2(\underline{1})(CH_3CO_2)](PF_6)$ can also be synthesized by the reaction of

$[Ni(H_2O)_6](BF_4)_2$ with $[(\underline{1}H_4)](BF_4)_2$ and $(CH_3CO)_2O$ in the presence of excess $N(C_2H_5)_3$ in refluxing CH_3CN. This green product gives identical spectra to the reaction above, except for a band in the i.r. spectrum for B–F stretching vibrations was observed at $1038cm^{-1}$, and the band at $843cm^{-1}$ due to P–F stretching vibrations was absent. The $CH_3CO_2^-$ ligand in $[Ni_2(\underline{1})(CH_3CO_2)]^+$ in the second synthesis is derived from the hydrolysis of $(CH_3CO_2)_2O$, which was originally added to remove H_2O from the reaction mixture.

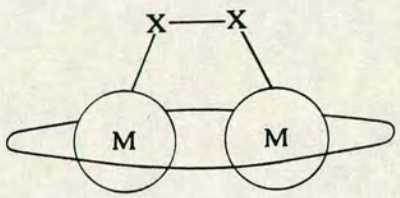

Figure 4.7 Proposed binding of substrates by $[M_2(\underline{1})]^{n+}$

The i.r. spectrum of $[Ni_2(\underline{1})(CH_3CO_2)]^+$ suggests that the $CH_3CO_2^-$ ligand is bridging the two Ni(II) ions, since no bands due to free C=O stretching vibrations are observed and the band at $1417cm^{-1}$ is typical for a $CH_3CO_2^-$ group bridging two metal centres[220]. The presence of a bridging ligand is significant, since the original conception of $(\underline{1})^{2-}$ was that it could position two metal centres sufficiently close so that a small substrate (such as O_2, N_2 or alkenes) could be bound to both metal centres simultaneously. Robson proposed[97,221] that co-ordination in the manner shown in Figure 4.7 might activate the bridging substrates to give catalytically useful reactions. To date, no example of this kind of binding or reactivity with such small molecules has been observed.

A number of the compounds discussed in Chapter 2 have bridging ligands, including $CH_3CO_2^-$ [167–169,171,172] and ClO_4^- [114,145,165,166]. The mixed-valence compound $[Mn_2(\underline{4a})Cl_2Br]$[143,144] has a single atom Cl bridge,

but this is exceptional since the trigonal-prismatic Mn^{II} ion is displaced by 1.25Å out of the macrocyclic plane (see Figure 2.10). Recently, the compound $\{[Cu_2(\underline{15b})][Cu_2(N_3)_6]\}_n$ was reported[161], which has the two octahedral Cu(II) centres which are co-ordinated in the plane of the macrocycle $(\underline{15b})^{2-}$ bridged by two $[(N_3)Cu(N_3)]^-$ bridges (see Figure 2.22). There is only one example of the two metal centres in a complex of $(\underline{1})^{2-}$ being bridged by a bidentate ligand; that is $\{Co_2(\underline{1})[S_2P(OC_2H_5)_2]_2\}$ [118] (see Figure 2.4). The Co(II) centres are octahedral and are bridged by the two $[S_2P(OC_2H_5)_2]^-$ chelates. The latter two complexes, $\{[Cu_2(\underline{15b})][Cu_2(N_3)_6]\}_n$ and $\{Co_2(\underline{1})[S_2P(OC_2H_5)_2]_2\}$, have two chelating ligands per macrocyclic unit and the metal ions incorporated in the macrocycle can adopt octahedral geometries. In the compound $[Ni_2(\underline{1})(CH_3CO_2)](PF_6)$, however, there is only one bridging ligand per macrocyclic unit and it is not clear what the co-ordination geometry at the Ni(II) ions would be. It might be possible for the two Ni(II) ions to be *cis*-diaxially bound to the bridging $CH_3CO_2^-$, in an arrangement like that shown in Figure 4.7. However, any mutual displacements of the Ni(II) ions out of the macrocyclic plane towards the $CH_3CO_2^-$ bridge would cause severe perturbations in the sp^2 bonding orbitals of the bridging phenoxide ligands. The single crystal X-ray structure determination of $[Ni_2(\underline{1})(CH_3CO_2)](PF_6)$ was therefore undertaken, to discover the co-ordination geometries of the Ni(II) ions and the binding mode of the $CH_3CO_2^-$ bridge.

4.2.8: The Single Crystal X-ray Structure of $[Ni_2(\underline{1})(CH_3CO_2)]_2(PF_6)_2.2CH_3CN.CH_3NO_2$

Details of the structure solution are given in the Experimental Section. Selected bond lengths, angles and torsions are listed in Tables 4.4, 4.5 and 4.6 respectively. A view of the cation $[Ni_2(\underline{1})(CH_3CO_2)]_2^{2+}$ is shown in

Figure 4.8 and the central $Ni_4O_8N_8$ unit is shown in Figure 4.9.

The single crystal X-ray structure of $[Ni_2(\underline{1})(CH_3CO_2)]_2(PF_6)_2$ shows that the $[Ni_2(\underline{1})(CH_3CO_2)]^+$ units have dimerised to give a central Ni_4O_4 cube, with stacking interactions like those proposed for $[Ni_2(\underline{1})]^{2+}$ in Section 4.2.1. There is a crystallographic two-fold axis passing through the centres of the "open" faces of the cube. Each Ni(II) centre is in a distorted octahedral environment, being bonded to two imino nitrogens, two bridging phenoxy oxygens of the macrocycle $(\underline{1})^{2-}$, a carboxylic oxygen of the bridging $CH_3CO_2^-$ group and a phenoxy oxygen from $(\underline{1})^{2-}$ from the other half of the dimer. The Ni-O distances vary from 2.031(3) and 2.035(3)Å for the Ni-$OCOCH_3$ bonds, 2.080(3), 2.095(3), 2.099(3) and 2.081(3)Å for the Ni-O(macrocycle) bonds, and 2.152(3) and 2.168(3)Å for the Ni-O bonds to the neighbouring macrocycle. The Ni-Ni distance [3.0240(9)Å] within the macrocycle is approximately 0.1Å shorter than the Ni-Ni distance [3.136(1)Å] in $[Ni_2(\underline{1})(CH_3CN)_4]^{2+}$. The four Ni-Ni vectors describe a distorted tetrahedron with two sides approximately 3.02Å long and four sides approximately 3.22Å long. This is shown in Figure 4.10, together with the superimposed oxygen tetrahedron of the phenoxy oxygens, which has sides of approximately 2.70, 2.78 or 2.84Å.

The macrocycle $(\underline{1})^{2-}$ in $[Ni_2(\underline{1})(CH_3CO_2)]_2^{2+}$ is non-planar and the angle between the normals to the planes defined by the two phenol groups is 76°. There are probably two reasons for this. Firstly, the bending avoids steric interactions with the macrocycle in the other half of the molecule. Secondly, the phenoxy oxygens are closer to the centre of the Ni_4O_4 cube than the Ni(II) ions (from the dimensions of the O_4 tetrahedron in Figure 4.10) and to achieve this geometry the macrocycle $(\underline{1})^{2-}$ must fold. The two $CH_3CO_2^-$ and $(\underline{1})^{2-}$ groups in $[Ni_2(\underline{1})(CH_3CO_2)]_2^{2+}$ are orientated at 90° to each other, so there is no possibility for intramolecular $\pi-\pi$ interactions

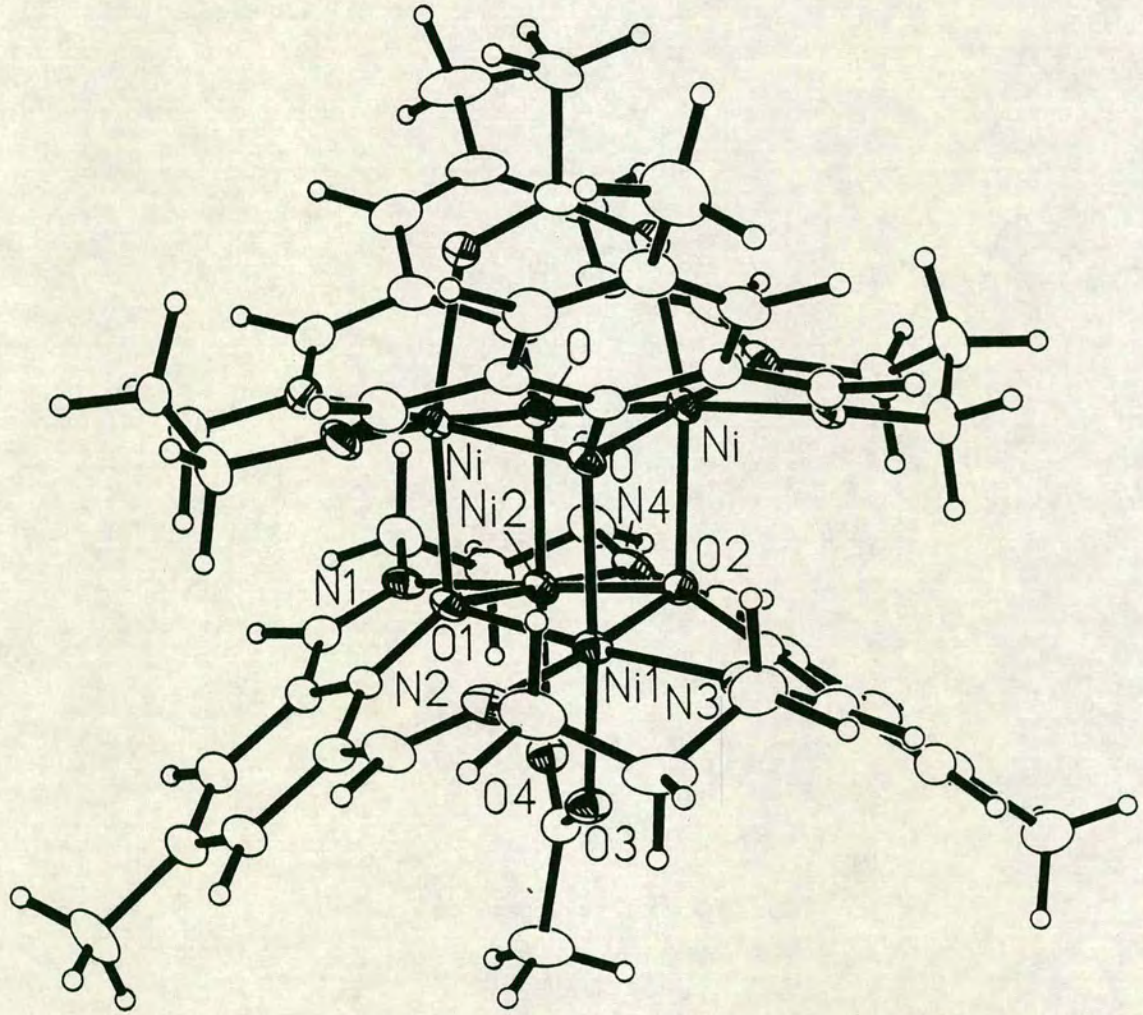

Figure 4.8 View of the single crystal X-ray structure of $[Ni_2(\underline{1})(CH_3CO_2)]_2^{2+}$

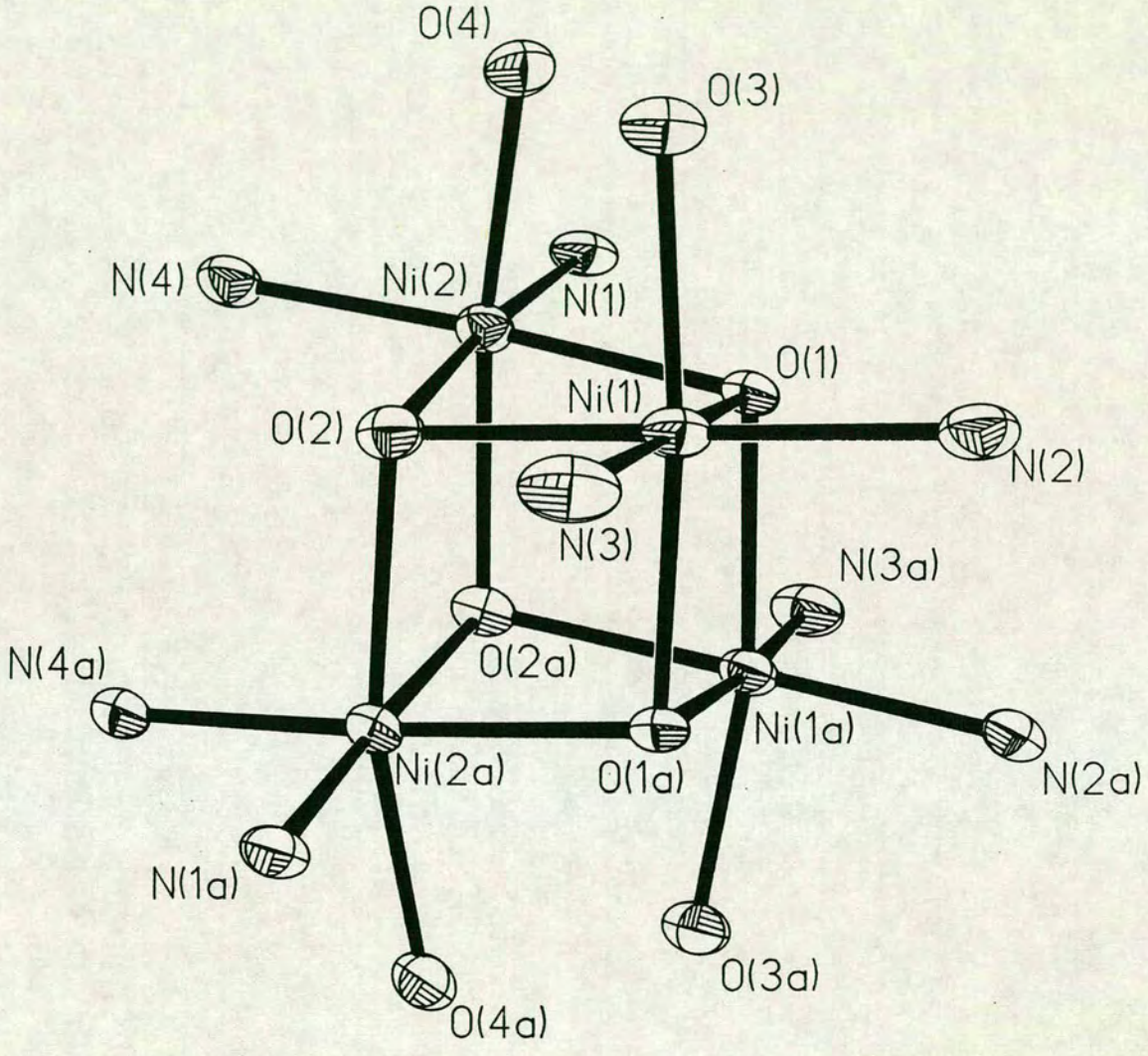

Figure 4.9 The central $Ni_4O_8N_8$ unit of $[Ni_2(\underline{1})(CH_3CO_2)]_2^{2+}$

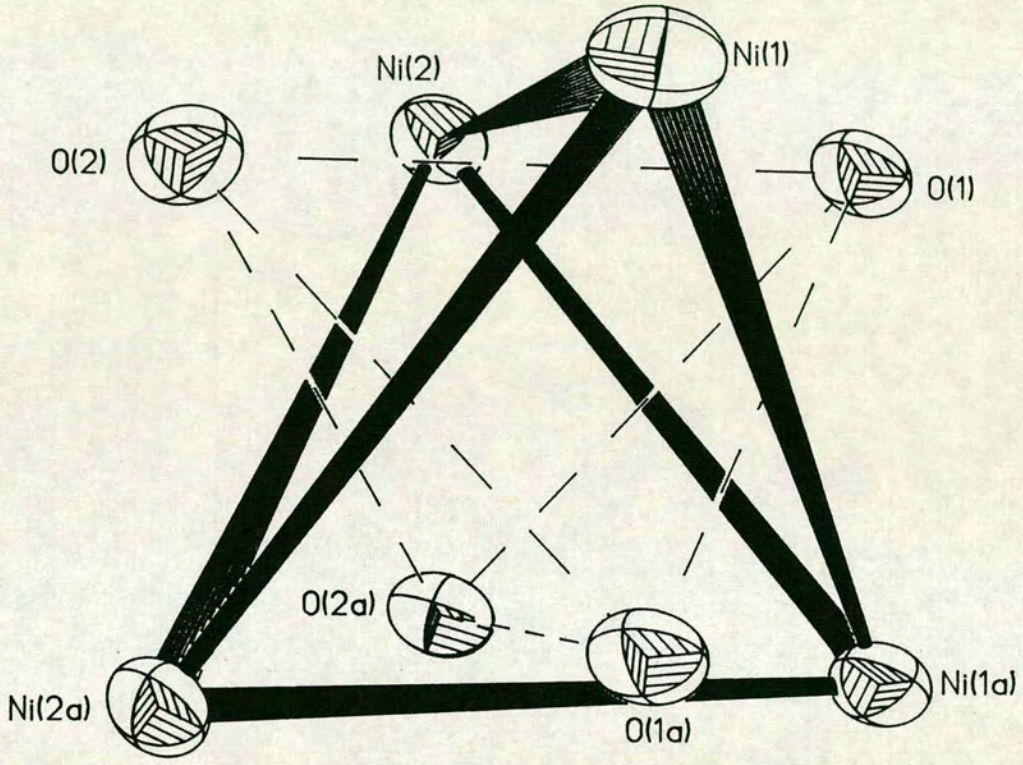

Figure 4.10 The superimposed Ni_4 and O_4 tetrahedra of $[Ni_2(\underline{1})(CH_3CO_2)]_2^{2+}$

Table 4.4 Selected bond lengths (Å) of $[Ni_2(\underline{1})(CH_3CO_2)]_2^{2+}$

Ni(1) -Ni(2)	3.0240(9)	C(5) - C(7)	1.375(7)
Ni(1) - O(1)	2.080(3)	C(7) - C(8)	1.408(7)
Ni(1) - N(2)	2.027(4)	C(8) - C(9)	1.453(7)
Ni(1) - N(3)	2.014(4)	C(9) - N(2)	1.273(7)
Ni(1) - O(2)	2.095(3)	N(2) -C(10)	1.482(7)
Ni(1) - O(3)	2.031(3)	C(10) -C(11)	1.520(8)
Ni(1) -Ni(1a)	3.2069(9)	C(11) -C(12)	1.525(8)
Ni(1) -Ni(2a)	3.2234(9)	C(12) - N(3)	1.465(7)
Ni(1) -O(1a)	2.152(3)	N(3) -C(13)	1.282(7)
Ni(2) - O(1)	2.099(3)	C(13) -C(14)	1.456(7)
Ni(2) - N(1)	2.028(4)	C(14) -C(15)	1.425(7)
Ni(2) - O(2)	2.081(3)	C(14) -C(16)	1.400(8)
Ni(2) - N(4)	2.027(4)	C(15) - O(2)	1.352(6)
Ni(2) - O(4)	2.035(3)	C(15) -C(20)	1.408(7)
Ni(2) -Ni(1a)	3.2234(9)	C(16) -C(17)	1.390(8)
Ni(2) -Ni(2a)	3.2290(9)	C(17) -C(18)	1.515(9)
Ni(2) -O(2a)	2.168(3)	C(17) -C(19)	1.389(8)
O(1) - C(1)	1.360(5)	C(19) -C(20)	1.408(7)
C(1) - C(2)	1.412(7)	C(20) -C(21)	1.451(7)
C(1) - C(8)	1.418(7)	C(21) - N(4)	1.281(6)
C(2) - C(3)	1.453(7)	N(4) -C(22)	1.473(7)
C(2) - C(4)	1.402(7)	C(22) -C(23)	1.523(7)
C(3) - N(1)	1.268(6)	C(23) -C(24)	1.514(7)
N(1) -C(24)	1.481(7)	O(3) -C(25)	1.271(6)
C(4) - C(5)	1.386(7)	O(4) -C(25)	1.262(6)
C(5) - C(6)	1.521(8)	C(25) -C(26)	1.510(8)

Table 4.5 Selected bond angles (°) of $[Ni_2(\underline{1})(CH_3CO_2)]_2^{2+}$

O(1)	-Ni(1) - N(2)	89.55(14)	C(6)	- C(5) - C(7)	121.9(5)
O(1)	-Ni(1) - N(3)	175.19(15)	C(5)	- C(7) - C(8)	122.6(5)
O(1)	-Ni(1) - O(2)	85.65(12)	C(1)	- C(8) - C(7)	119.7(4)
O(1)	-Ni(1) - O(3)	88.62(13)	C(1)	- C(8) - C(9)	125.5(4)
O(1)	-Ni(1) -O(1a)	81.41(12)	C(7)	- C(8) - C(9)	114.8(4)
N(2)	-Ni(1) - N(3)	94.76(17)	C(8)	- C(9) - N(2)	126.7(5)
N(2)	-Ni(1) - O(2)	175.17(14)	Ni(1)	- N(2) - C(9)	121.1(3)
N(2)	-Ni(1) - O(3)	91.18(15)	Ni(1)	- N(2) -C(10)	122.0(3)
N(2)	-Ni(1) -O(1a)	97.10(14)	C(9)	- N(2) -C(10)	116.2(4)
N(3)	-Ni(1) - O(2)	90.01(15)	N(2)	-C(10) -C(11)	111.8(4)
N(3)	-Ni(1) - O(3)	93.40(15)	C(10)	-C(11) -C(12)	113.4(4)
N(3)	-Ni(1) -O(1a)	95.93(15)	C(11)	-C(12) - N(3)	111.8(4)
O(2)	-Ni(1) - O(3)	89.25(12)	Ni(1)	- N(3) -C(12)	122.1(3)
O(2)	-Ni(1) -O(1a)	81.67(12)	Ni(1)	- N(3) -C(13)	120.7(4)
O(3)	-Ni(1) -O(1a)	166.96(13)	C(12)	- N(3) -C(13)	116.7(4)
O(1)	-Ni(2) - N(1)	89.66(14)	N(3)	-C(13) -C(14)	127.6(5)
O(1)	-Ni(2) - O(2)	85.55(12)	C(13)	-C(14) -C(15)	125.2(5)
O(1)	-Ni(2) - N(4)	175.24(14)	C(13)	-C(14) -C(16)	114.6(5)
O(1)	-Ni(2) - O(4)	88.04(12)	C(15)	-C(14) -C(16)	120.1(5)
O(1)	-Ni(2) -O(2a)	81.23(12)	C(14)	-C(15) - O(2)	120.9(4)
N(1)	-Ni(2) - O(2)	174.76(14)	C(14)	-C(15) -C(20)	117.8(4)
N(1)	-Ni(2) - N(4)	94.89(16)	O(2)	-C(15) -C(20)	121.3(4)
N(1)	-Ni(2) - O(4)	91.88(14)	Ni(1)	- O(2) -Ni(2)	92.79(12)
N(1)	-Ni(2) -O(2a)	96.21(14)	Ni(1)	- O(2) -C(15)	117.7(3)
O(2)	-Ni(2) - N(4)	89.85(14)	Ni(1)	- O(2) -Ni(2a)	98.24(13)
O(2)	-Ni(2) - O(4)	90.08(12)	Ni(2)	- O(2) -C(15)	117.8(3)
O(2)	-Ni(2) -O(2a)	80.98(12)	Ni(2)	- O(2) -Ni(2a)	98.92(13)
N(4)	-Ni(2) - O(4)	93.20(14)	C(15)	- O(2) -Ni(2a)	125.0(3)
N(4)	-Ni(2) -O(2a)	96.86(14)	C(14)	-C(16) -C(17)	122.3(5)
O(4)	-Ni(2) -O(2a)	166.49(12)	C(16)	-C(17) -C(18)	120.5(5)
Ni(1)	- O(1) -Ni(2)	92.70(12)	C(16)	-C(17) -C(19)	117.3(5)
Ni(1)	- O(1) - C(1)	117.5(3)	C(18)	-C(17) -C(19)	122.2(5)
Ni(1)	- O(1) -Ni(1a)	98.50(13)	C(17)	-C(19) -C(20)	122.6(5)
Ni(2)	- O(1) - C(1)	116.6(3)	C(15)	-C(20) -C(19)	119.9(5)
Ni(2)	- O(1) -Ni(1a)	98.61(13)	C(15)	-C(20) -C(21)	125.7(4)
C(1)	- O(1) -Ni(1a)	126.4(3)	C(19)	-C(20) -C(21)	114.3(4)
O(1)	- C(1) - C(2)	121.0(4)	C(20)	-C(21) - N(4)	127.0(5)
O(1)	- C(1) - C(8)	121.3(4)	Ni(2)	- N(4) -C(21)	121.1(3)
C(2)	- C(1) - C(8)	117.8(4)	Ni(2)	- N(4) -C(22)	121.8(3)
C(1)	- C(2) - C(3)	125.6(4)	C(21)	- N(4) -C(22)	116.7(4)
C(1)	- C(2) - C(4)	119.9(4)	N(4)	-C(22) -C(23)	112.5(4)
C(3)	- C(2) - C(4)	114.5(4)	C(22)	-C(23) -C(24)	114.0(4)
C(2)	- C(3) - N(1)	127.3(4)	N(1)	-C(24) -C(23)	111.5(4)
Ni(2)	- N(1) - C(3)	120.8(3)	Ni(1)	- O(3) -C(25)	127.1(3)
Ni(2)	- N(1) -C(24)	122.1(3)	Ni(2)	- O(4) -C(25)	127.0(3)
C(3)	- N(1) -C(24)	116.5(4)	O(3)	-C(25) - O(4)	126.7(4)
C(2)	- C(4) - C(5)	122.5(5)	O(3)	-C(25) -C(26)	116.0(4)
C(4)	- C(5) - C(6)	120.7(5)	O(4)	-C(25) -C(26)	117.3(4)
C(4)	- C(5) - C(7)	117.4(5)			

Table 4.6 Selected torsion angles (°) of $[Ni_2(\underline{1})(CH_3CO_2)]_2^{2+}$

O(1)	C(1)	C(2)	C(3)	0.8(7)	C(11)	C(12)	N(3)	C(13)	-124.8(5)
O(1)	C(1)	C(2)	C(4)	-178.9(4)	C(12)	N(3)	C(13)	C(14)	-180.0(5)
C(8)	C(1)	C(2)	C(3)	179.9(4)	N(3)	C(13)	C(14)	C(15)	16.4(9)
C(8)	C(1)	C(2)	C(4)	0.2(7)	N(3)	C(13)	C(14)	C(16)	-165.6(5)
O(1)	C(1)	C(8)	C(7)	-179.7(4)	C(13)	C(14)	C(15)	O(2)	0.8(8)
O(1)	C(1)	C(8)	C(9)	1.0(7)	C(13)	C(14)	C(15)	C(20)	178.7(5)
C(2)	C(1)	C(8)	C(7)	1.2(7)	C(16)	C(14)	C(15)	O(2)	-177.1(5)
C(2)	C(1)	C(8)	C(9)	-178.1(5)	C(16)	C(14)	C(15)	C(20)	0.8(7)
C(1)	C(2)	C(3)	N(1)	19.2(8)	C(13)	C(14)	C(16)	C(17)	-179.6(5)
C(4)	C(2)	C(3)	N(1)	-161.2(5)	C(15)	C(14)	C(16)	C(17)	-1.5(8)
C(1)	C(2)	C(4)	C(5)	-2.9(7)	C(14)	C(15)	C(20)	C(19)	-0.9(7)
C(3)	C(2)	C(4)	C(5)	177.4(5)	C(14)	C(15)	C(20)	C(21)	-180.0(5)
C(2)	C(3)	N(1)	C(24)	177.4(5)	O(2)	C(15)	C(20)	C(19)	177.0(4)
C(3)	N(1)	C(24)	C(23)	-126.4(5)	O(2)	C(15)	C(20)	C(21)	-2.0(8)
C(2)	C(4)	C(5)	C(6)	-176.2(5)	C(14)	C(16)	C(17)	C(18)	-177.8(5)
C(2)	C(4)	C(5)	C(7)	4.0(8)	C(14)	C(16)	C(17)	C(19)	2.2(8)
C(4)	C(5)	C(7)	C(8)	-2.5(8)	C(16)	C(17)	C(19)	C(20)	-2.4(8)
C(6)	C(5)	C(7)	C(8)	177.6(5)	C(18)	C(17)	C(19)	C(20)	177.7(5)
C(5)	C(7)	C(8)	C(1)	0.0(7)	C(17)	C(19)	C(20)	C(15)	1.8(8)
C(5)	C(7)	C(8)	C(9)	179.3(5)	C(17)	C(19)	C(20)	C(21)	-179.1(5)
C(1)	C(8)	C(9)	N(2)	-17.0(8)	C(15)	C(20)	C(21)	N(4)	-16.2(8)
C(7)	C(8)	C(9)	N(2)	163.7(5)	C(19)	C(20)	C(21)	N(4)	164.7(5)
C(8)	C(9)	N(2)	C(10)	-179.9(5)	C(20)	C(21)	N(4)	C(22)	-179.4(5)
C(9)	N(2)	C(10)	C(11)	125.8(5)	C(21)	N(4)	C(22)	C(23)	128.6(5)
N(2)	C(10)	C(11)	C(12)	70.4(6)	N(4)	C(22)	C(23)	C(24)	70.8(5)
C(10)	C(11)	C(12)	N(3)	-71.8(6)	C(22)	C(23)	C(24)	N(1)	-71.0(5)

between neighbouring macrocycles within the same molecule. Packing diagrams, however, show that intermolecular long-range $\pi-\pi$ interactions between different molecules may be present in two dimensions.

There have been a number of Ni(II) complexes reported in the literature that contain a Ni_4O_4 cubane structure[222-239], the simplest being $[Ni_4(OH)_4]^{4+}$ [224,230,231,233]. One of the best studied is $[Ni_4(OCH_3)_4(o\text{-}OC_6H_4CHO)_4(C_2H_5OH)_4]$[222,225,226], which is shown in Figure 4.11. The oxygen vertices in the cube are provided by CH_3O^- anions and the remaining co-ordination sites are provided by the C_2H_5OH and bidentate salicylaldehyde ligands. From the single crystal X-ray structure[226], it can be seen that the geometry of the Ni_4O_4 cube is similar to that of $[Ni_2(\underline{1})(CH_3CO_2)]_2^{2+}$. The magnetic properties of the compound $[Ni_4(OCH_3)_4(o\text{-}OC_6H_4CHO)_4(C_2H_5OH)_4]$ were investigated in the temperature range 6-300K[222,226] and it was found that there was a weak, intramolecular, ferromagnetic exchange interaction between the Ni(II) ions. In a related compound, $[Ni_4(OCH_3)_4(\text{acetylacetonate})_4(CH_3OH)_4]$ [228,229], Ginsberg has proposed that intermolecular ferromagnetic interactions were present as well.

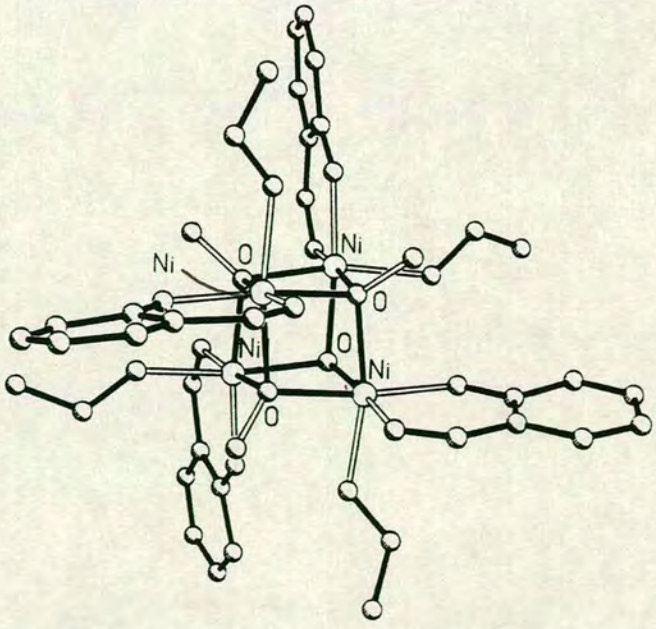

Figure 4.11 $[Ni_4(OCH_3)_4(o\text{-}OC_6H_4CHO)_4(C_2H_5OH)_4]$

All the previously structurally characterised Ni_4O_4 cubane-type compounds are believed to keep this structure in solution as well as in the solid-state. Two of the previously reported compounds[236,238] have bridging ligands across most of the sides of the cube which are expected to keep the cubane structure intact. $[Ni_2(\underline{1})(CH_3CO_2)]_2^{2+}$, however, has a entirely unbridged set of four faces of the Ni_4O_4 cube which could be cleaved more readily. There is no evidence in the f.a.b. mass spectrum of $[Ni_2(\underline{1})(CH_3CO_2)]_2(PF_6)_2$ for the tetranuclear $[Ni_2(\underline{1})(CH_3CO_2)]_2^{2+}$ species; only a peak for $[Ni_2(\underline{1})(CH_3CO_2)]^+$ at $M^+ = 518$ is observed. However, there is no colour change on dissolving crystalline $[Ni_2(\underline{1})(CH_3CO_2)]_2(PF_6)_2$ in solvents which have non-oxygen donors (e.g. CH_3CN). If the cube were being cleaved in solution, a non-O-donor co-ordinating *trans* to the $CH_3CO_2^-$ group might be expected to give a colour change. Furthermore, the crystal structure shows that the cubane-type structure is stable in the presence of the solvents CH_3CN and CH_3NO_2, although packing effects could be dominant here. In the absence of more evidence, we tentatively propose that the dimerised form of $[Ni_2(\underline{1})(CH_3CO_2)]^+$ is maintained in solution as well as the solid-state.

To our knowledge, all previously reported compounds containing a Ni_4O_4 cubane structure have either OH^- or alkoxy groups as the O-vertices in the cube. $[Ni_2(\underline{1})(CH_3CO_2)]_2(PF_6)_2$ is therefore the first example of the incorporation of phenoxy O-ligands within a Ni_4O_4 cube. This is significant since the bonding orbitals of the oxygen donors in a cubane structure should be sp^3 hybridised, while those of a phenolic oxygen are expected to be sp^2 hybridised. In $[Ni_2(\underline{1})(CH_3CO_2)]_2(PF_6)_2$, the angles around the O-donors of the cube are not strictly tetrahedral, but vary in the range 92.7° (for ∠Ni(1)-O(1)-Ni(2) within the macrocycle) to 126.4° (for ∠C(1)-O(1)-Ni(1a)). The C-O bond length in $(\underline{1})^{2-}$ is also lengthened to an average value of

1.36Å in $[Ni_2(\underline{1})(CH_3CO_2)]_2(PF_6)_2$, as compared to the value of 1.31Å in $[Ni_2(\underline{1})(CH_3CN)_4]^{2+}$ and 1.28Å in $[(\underline{1}H_4)]^{2+}$. This lengthening of the C–O bond is consistent with a gradual change from sp^2 hybridisation to sp^3 hybridisation at the oxygen atom and a corresponding decrease in the π–interactions of the oxygen atom with the aromatic ring.

$[Ni_2(\underline{1})(CH_3CO_2)]_2(PF_6)_2$ is also the first example of a macrocyclic complex containing a Ni_4O_4 cube. McKee and Shepard[215,216] have synthesized a complex of a Schiff–base macrocycle $[Mn_4(\underline{20})](ClO_4)_4$ which incorporates a cubane Mn_4O_4 unit and is shown in Figure 4.12. The macrocycle $(\underline{20})^{4-}$ is completely folded so there is one macrocyclic ligand per Mn_4O_4 core and each Mn(II) ion is seven–co–ordinate with approximate pentagonal–bipyramidal geometry.

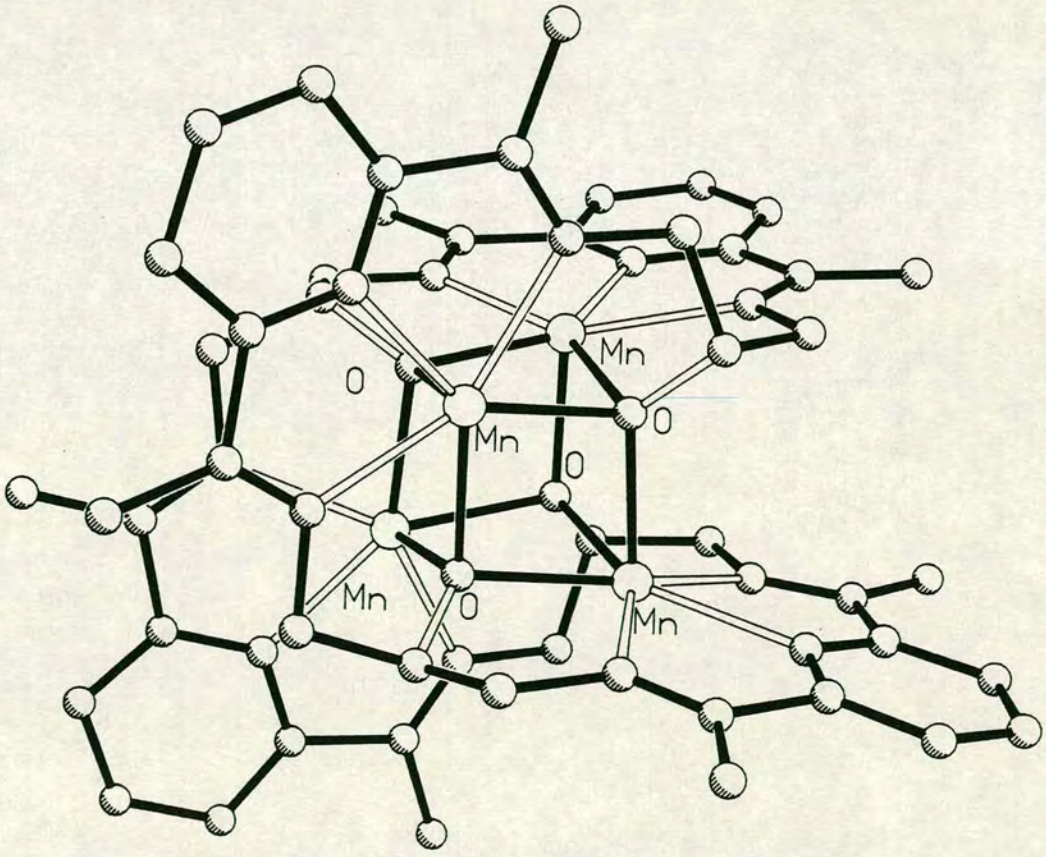

Figure 4.12 $[Mn_4(\underline{20})]^{4+}$

Additionally, three of the copper complexes mentioned in Chapter 2[165,166,168], with ligands such as $(\underline{15a})^{2-}$ incorporating hydroxy groups in the side-arms, show interactions in the solid-state between the copper ions of one molecule with the oxygen ligands of another. This results in the dimerisation of the macrocyclic complexes, although none of these compounds have a cubane-type structure.

An important aspect of the structure of $[Ni_2(\underline{1})(CH_3CO_2)]_2^{2+}$ is that it gives clear evidence that Schiff-base complexes of Ni(II) can have intermolecular interactions in the manner suggested in Figure 4.2. In $[Ni_2(\underline{1})(CH_3CO_2)]_2^{2+}$, the co-ordination of the $CH_3CO_2^-$ groups in the axial positions prevents further aggregation and the resulting dimeric complex is soluble in organic solvents. In the absence of these bridging ligands, polymerisation could occur, to give insoluble products (see Section 4.2.1). Robson *et al.* have reported the tetranuclear Ni(II) complex[240,241] of the binucleating, acyclic ligand $(\underline{21})^{3-}$, which is shown in Figure 4.13. These workers propose that the Ni(II) complex $[Ni_2(\underline{21})(OH)]_2(CH_3CO_2)_2(H)_2$ is isostructural with the Co complex $[Co_2(\underline{21})(OH)(CH_3CO_2)]_2$, the structure of which has been determined by X-ray crystallography[240] and is shown in Figure 4.14. The complex shows stacking interactions similar to those described above. However, with the ligand $(\underline{21})^{3-}$ it appears that a cubane-type structure is unfavoured for theNi(II) and Co complexes, possibly because the aminophenolare O-atoms of $(\underline{21})^{3-}$ rather than the bridging phenolate O-atoms are preferentially involved in stacking interactions. By using the aminophenolate O-atoms for the intermolecular interactions, all phenolate O-atoms can remain sp^2 hybridised and maintain π-interactions with the aromatic rings. As in $[Ni_2(\underline{1})(CH_3CO_2)]_2^{2+}$, the presence of the bridging $CH_3CO_2^-$ groups may be restricting the extent of polymerisation, to give discrete, molecular species which are soluble in organic solvents.

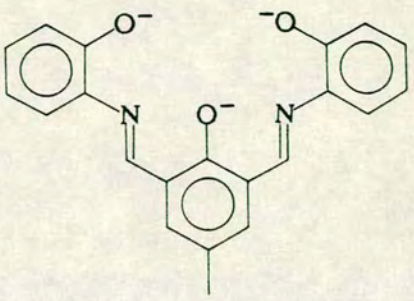

Figure 4.13 Ligand $(\underline{21})^{3-}$

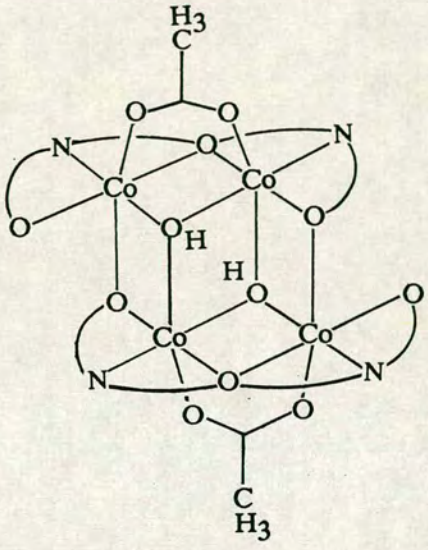

Figure 4.14 $[Co_2(\underline{21})(OH)(CH_3CO_2)]_2$

4.2.9: Cyclic Voltammetry of $[Ni_2(\underline{1})(CH_3CO_2)]_2(PF_6)_2$ in CH_3CN

Cyclic voltammetry of $[Ni_2(\underline{1})(CH_3CO_2)]_2(PF_6)_2$ measured in CH_3CN (0.1M $NBu^n_4BF_4$ supporting electrolyte) at Pt electrodes at 298K reveals three oxidative and two rather ill-defined reductive processes. The reductions are irreversible, even at 251K, and occur at E_{pc} = −1.55V (scan rate = $0.20Vs^{-1}$) and −1.71V ($0.45Vs^{-1}$) and E_{pc} = −1.89V ($0.20Vs^{-1}$) and −1.92V ($0.45Vs^{-1}$) *vs.* Fc/Fc^+ at 298K. The oxidative processes are more complicated. Scanning to +1.55V *vs.* Fc/Fc^+ at scan rates from 0.70 to $0.21Vs^{-1}$ gives three anodic peaks but only two cathodic peaks on the return

wave. The oxidation at the most positive potential ($E_{\frac{1}{2}}$ = +1.15V *vs.* Fc/Fc^+) appears to be reversible at all scan rates. At slow scan rates at 298K, the return waves for the first two oxidations coalesce, to give a reduction wave at an average position for the two return waves (see Figure 4.15a). At faster scan rates and lower temperatures (251K), two return waves are observed, with the return wave for the first oxidation becoming more prominent as the temperature is lowered and the scan rate increases (see Figure 4.15b). This gives two reversible oxidations at $E_{\frac{1}{2}}$ = +0.81V and $E_{\frac{1}{2}}$ = +0.95V. This data is consistent with the formation of a daughter product (A^+) of $[Ni_2(\underline{1})(CH_3CO_2)]_2(PF_6)_2$ after the first oxidation at $E_{\frac{1}{2}}$ = +0.81V. This daughter product then undergoes the second oxidation at $E_{\frac{1}{2}}$ = +0.95V. At fast scan rates or at lower temperatures, insufficient A^+ is generated to give a return cathodic wave for the second process. However, at slow scan rates, all the $[Ni_2(\underline{1})(CH_3CO_2)]_2(PF_6)_2$ near the electrode surface is converted to A^+ and so the cathodic waves for A^+ and $[Ni_2(\underline{1})(CH_3CO_2)]_2(PF_6)_2$ coalesce at a potential which is approximately the mean position of the return waves of the first two oxidations. This behaviour, therefore, is consistent with an ECE mechanism.

$$O + e^- \leftrightarrows R \qquad R \leftrightarrows Y \qquad Y + e^- \leftrightarrows Z$$

Multiple electron transfer with intervening chemical reaction, the ECE mechanism

It is not known if the third oxidation at $E_{\frac{1}{2}}$ = +1.15V is due to a daughter product of A^+, since the potential gap between the two processes is too large for the third oxidation to be affected by scan rate. Each of the peak heights for the three oxidations are equal, we tentatively propose that each oxidation process corresponds to a one-electron transfer. At present, we

are unable to suggest what any of the products of the electrochemical reactions are, although the formation of intermediate Ni(III) species seems likely.

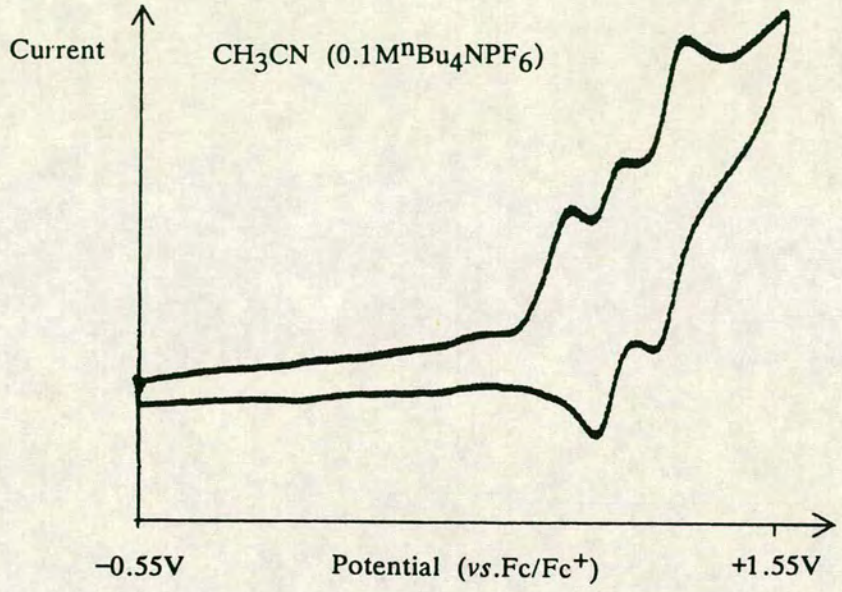

Figure 4.15a The Oxidative Cyclic Voltammogram of $[Ni_2(\underline{1})(CH_3CO_2)]_2(PF_6)_2$ at 298K and scan rate = $0.21Vs^{-1}$

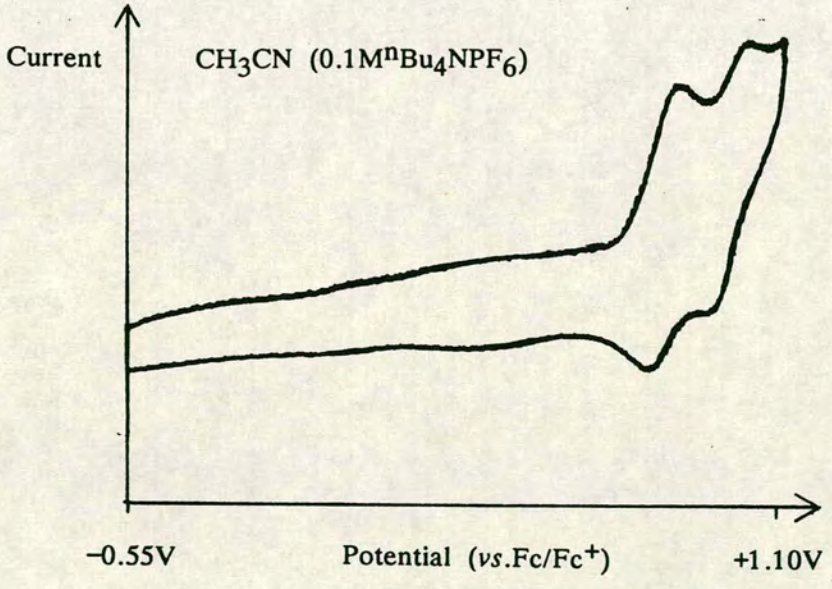

Figure 4.15b The Oxidative Cyclic Voltammogram of $[Ni_2(\underline{1})(CH_3CO_2)]_2(PF_6)_2$ at 251K and scan rate = $0.33Vs^{-1}$

4.2.10: The Synthesis of $[Pd(\underline{1})](BF_4)_2$

The reaction of two equivalents of $Pd(CH_3CO_2)_2$ with $[(\underline{1}H_4)](BF_4)_2$ in the presence of an excess of $N(C_2H_5)_3$ in a mixture of CH_2Cl_2/CH_3CN gave a yellow precipitate on stirring. The complex was recrystallised from CH_3CN/diethyl ether or CH_3NO_2/diethyl ether. The i.r. spectrum of the yellow compound shows strong bands at 1624, 1573 and 1054cm^{-1}, which are assigned to co-ordinated C-O and C=N stretching vibrations and B-F stretching vibrations respectively. The observation of these bands suggest that complexation of the Pd(II) ions by the ligand $(\underline{1})^{2-}$ has occurred. The f.a.b. mass spectrum of the yellow complex shows peaks at M^+ = 616 and 702, which are assigned as the molecular ion peaks with the correct isotope distributions, for $[^{106}Pd_2(\underline{1}H_2)]^+$ and $[^{106}Pd_2(\underline{1}H)](BF_4)^+$ respectively. This evidence combined with elemental analytical data confirms the assignment of the product as $[Pd_2(\underline{1})](BF_4)_2$.

The ^1H n.m.r. of $[Pd_2(\underline{1})](BF_4)_2$ in CD_3CN shows resonances for all the proton environments except that for the aldehydic protons, which were not observed at chemical shifts up to 15.00p.p.m. The protons on the $-CH_2CH_2CH_2-$ side-arms show coupling with ^3J = 7Hz. However, the pattern of a triplet for the central $-CH_2-$ group and a quartet for the other $-CH_2-$ groups also requires coupling of the outer $-CH_2-$ groups to the aldehydic protons of approximately ^4J = 7Hz. This evidence, together with the fact that the resonance due to the aromatic protons is a broad multiplet, suggests that if the resonance due to the aldehydic proton was observed, a complex, broadened pattern might be expected. Running the spectrum again at higher frequencies might give better definition of the peaks and allow the resonance to be observed. The ^{13}C DEPT spectrum can be assigned unambiguously, with resonances due to all hydrogen-bearing carbons being observed. Of particular note is the resonance due to the imino carbon

(-HC=N-), observed at 163.98p.p.m.

The synthesis of $[Pd_2(\underline{1})](BF_4)_2$ can also be achieved in good yield by the reaction of two equivalents of $[Pd(CH_3CN)_4](BF_4)_2$ (prepared by the method of Thomas and Sen[242]) with $[(\underline{1}H_4)](BF_4)_2$ in the presence of excess $N(C_2H_5)_3$ in refluxing CH_3CN under N_2. On reducing the volume of solvent, a yellow solid was obtained that was recrystallised from CH_3NO_2/diethyl ether. This compound gives identical i.r. and f.a.b. mass spectra to the yellow product described above. Elemental analytical data also confirms the assignment of this product as $[Pd_2(\underline{1})](BF_4)_2$. An impure sample of $[Pd_2(\underline{1})]^{2+}$ was also synthesized by the transmetallation of $[Pb_2(\underline{1})](NO_3)_2$ with two equivalents of $Pd(CH_3CO_2)_2$ in refluxing CH_3CN. This compound was obtained as a NO_3^- salt which was insoluble in common solvents. The i.r. spectrum of this product shows strong bands at 1624, 1572 and 1385cm^{-1} which are assigned as co-ordinated C-O and C=N stretching vibrations and a O-NO_2 stretching vibration respectively. The f.a.b. mass spectrum of this compound, however, shows a number of peaks suggest the presence of other products. The most intense peak is at M^+ = 614, assigned to a molecular ion peak $[^{106}Pd_2(\underline{1})]^+$, but there are other, less intense peaks at M^+ = 511, 676, 716 and 778, which are assigned to $[^{106}Pd(\underline{1}H_3)]^+$, $[^{106}Pd_2(\underline{1})](NO_3)^+$, $[^{106}Pd^{208}Pb(\underline{1})]^+$ and $[^{106}Pd^{208}Pb(\underline{1})](NO_3)^+$ respectively. This evidence suggests that the Pd(II) insertion into the macrocycle was incomplete, but that the major product is still the desired complex. There is therefore a clear preference by the macrocycle $(\underline{1})^{2-}$ for the Pd(II) ions rather than Pb(II). The preferential formation of $[Pd_2(\underline{1})]^{2+}$ in the presence of Pb(II) ions may be due to a good match between the stereochemical requirements of the Pd(II) centres and the macrocycle $(\underline{1})^{2-}$, since the macrocycle can provide a well-defined square-planar array of donors for the d^8 metal centre. Okawa and co-workers[146] have shown that in the complex $[Pb_2(\underline{1})](ClO_4)_2$, the

Pb(II) ions are considerably displaced from the macrocyclic cavity (by 1.28Å).

Interestingly there are, to our knowledge, no structurally characterised complexes of the platinum group metals, where two metal ions are enclosed within a single macrocyclic ring. In order to confirm the structure of the Pd(II) complex of $(\underline{1})^{2-}$, a single crystal X-ray structural determination of $[Pd_2(\underline{1})](BF_4)_2$ was undertaken.

4.2.11: The Single Crystal X-Ray Structure of $[Pd_2(\underline{1})](BF_4)_2.2CH_3NO_2$

Details of the structure solution are given in the Experimental Section. Selected bond lengths, angles and torsions are listed in Tables 4.7, 4.8 and 4.9 respectively. Two views of the macrocyclic complex are shown in Figures 4.16 and 4.17 and a packing diagram is presented in Figure 4.18.

The single crystal X-ray structure of $[Pd_2(\underline{1})](BF_4)_2$ shows that two Pd(II) centres can be perfectly accommodated within the two compartments of $(\underline{1})^{2-}$ and the cationic molecule adopts a very flat conformation. A centre of inversion is located at the centre of the $[Pd_2(\underline{1})]^{2+}$ unit so the Pd(II) centres are in identical environments. Each Pd(II) ion is co-ordinated to two bridging phenoxy oxygens [Pd-O = 2.016(4) and 2.015(4)Å] and two imino nitrogens [Pd-N = 1.979(5) and 1.993(5)Å] and the Pd-Pd distance is 3.1514(6)Å. The central $-CH_2-$ groups of the propylene side-arms are the only deviation from planarity, as shown by Figure 4.17, which suggests that Pd(II) ions fit well into the planar array of the N_2O_2 donors offered by $(\underline{1})^{2-}$. However, the N_2O_2 cavity does not form a strictly square-donor set; this is demonstrated by the angles subtended at the Pd(II) ion by the N- and O-ligands [$\angle$N(1)-Pd-N(2) = 96.36(18), $\angle$O(1)-Pd-O(1a) = 77.13(15) and $\angle$O(1)-Pd-N(1) = 93.30(17)$^{\circ}$]. Also, the angle subtended at the bridging phenoxy O-ligands are 102.88(16)$^{\circ}$. There are no axial interactions of the metal ions with the included solvent. The packing diagram presented in

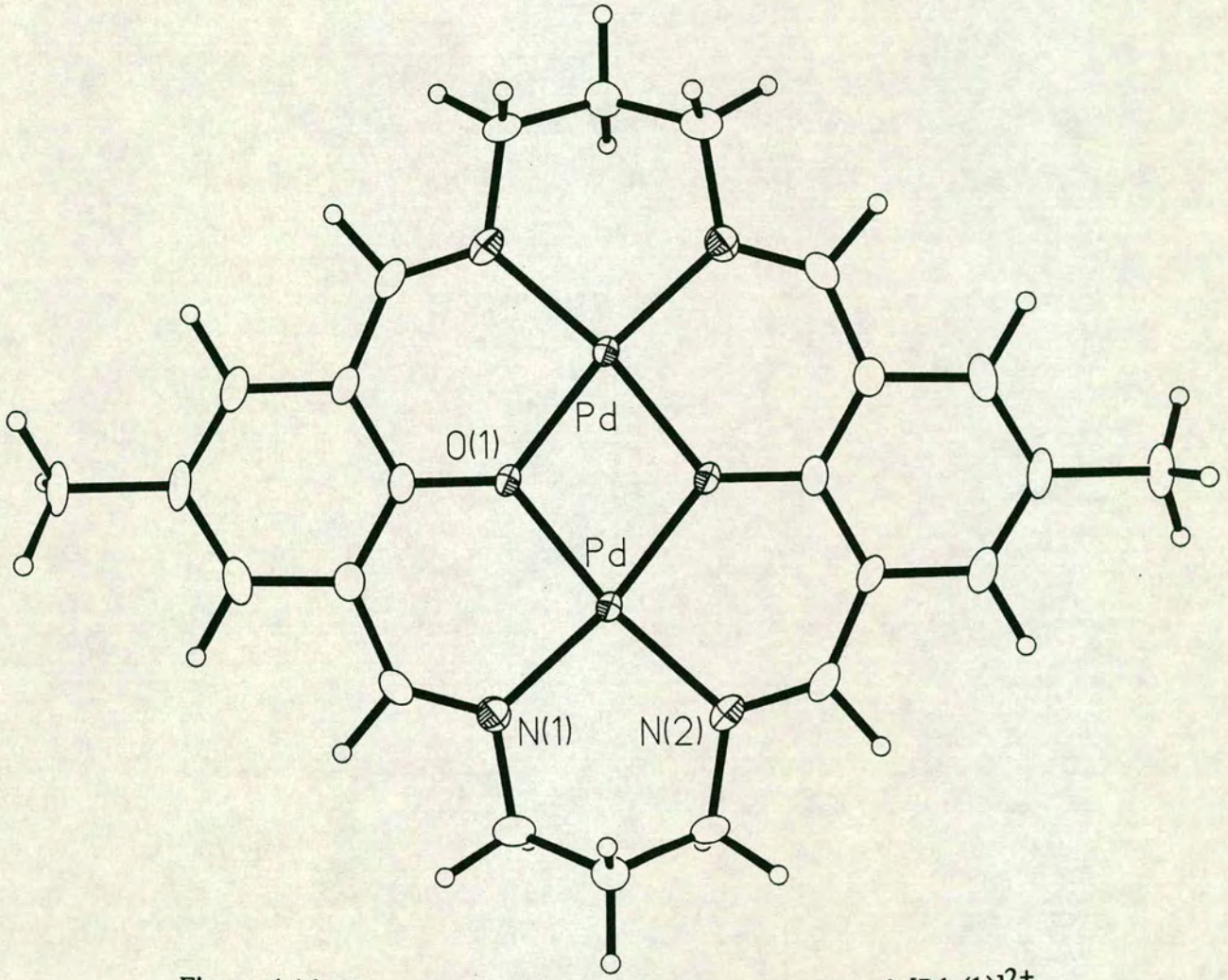

Figure 4.16 View of the single crystal X-ray structure of $[Pd_2(\underline{1})]^{2+}$

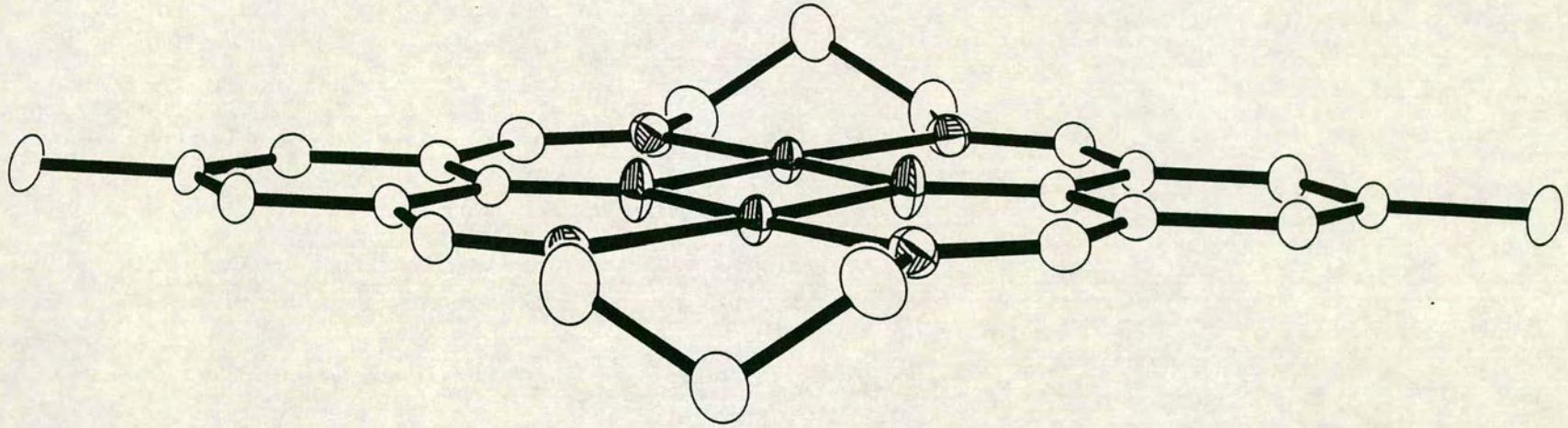

Figure 4.17 Alternative view of the single crystal X-ray structure of $[Pd_2(\underline{1})]^{2+}$

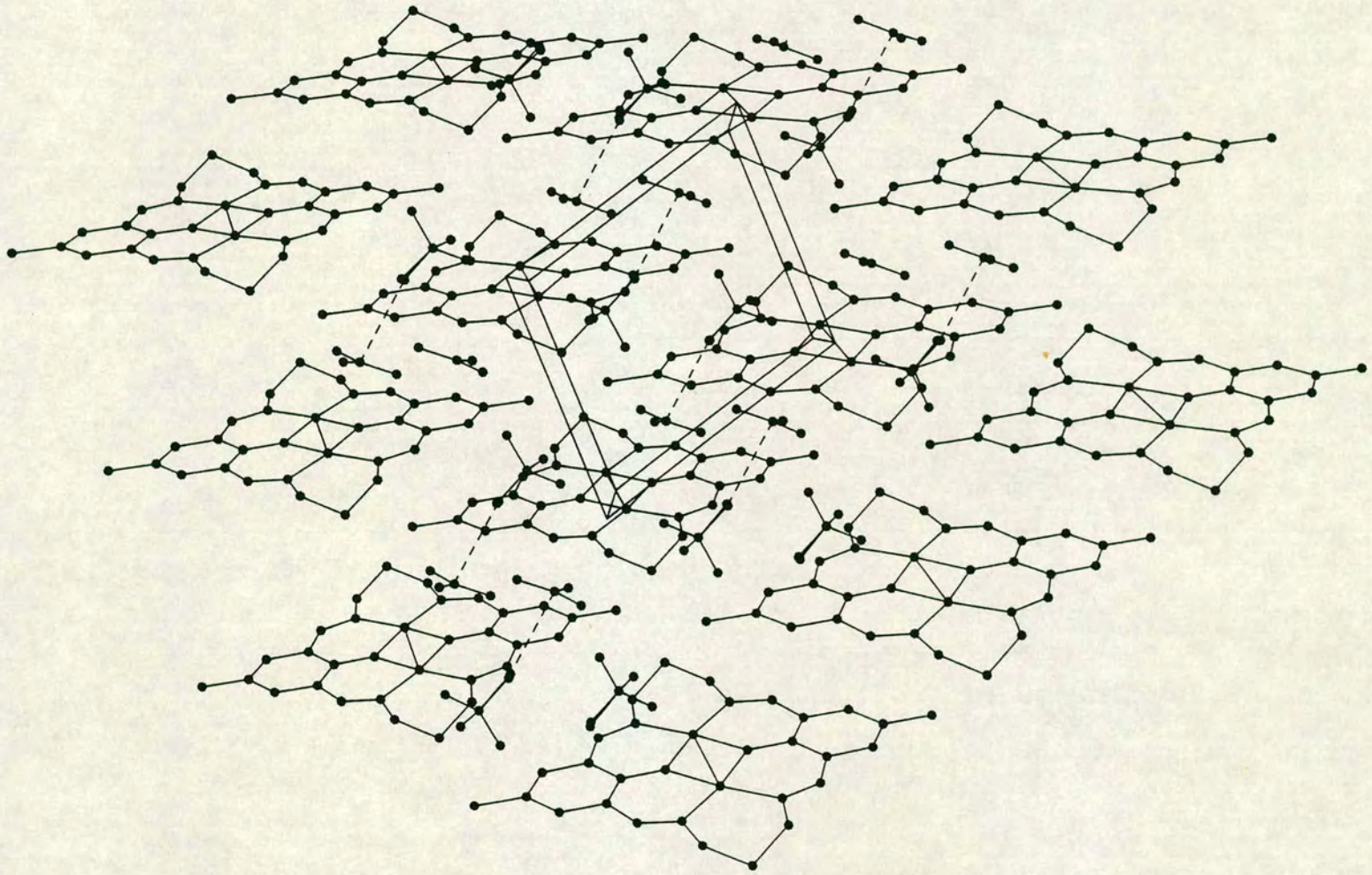

Figure 4.18 Packing diagram of $[Pd_2(\underline{1})](BF_4)_2.2CH_3NO_2$

Table 4.7 Selected bond lengths (Å) of $[Pd_2(\underline{1})](BF_4)_2$

Pd	- O(1)	2.016(4)	C(1)	- C(7)	1.396(7)
Pd	- N(1)	1.981(4)	C(2)	- C(3)	1.400(8)
Pd	- N(2)	1.993(4)	C(2)	-C(12a)	1.450(8)
Pd	-Pd(a)	3.1511(6)	C(3)	- C(4)	1.381(8)
Pd	-O(1a)	2.014(4)	C(4)	- C(5)	1.517(8)
O(1)	- C(1)	1.355(6)	C(4)	- C(6)	1.382(8)
N(1)	- C(8)	1.298(7)	C(6)	- C(7)	1.410(8)
N(1)	- C(9)	1.485(7)	C(7)	- C(8)	1.442(8)
N(2)	-C(11)	1.472(7)	C(9)	-C(10)	1.506(8)
N(2)	-C(12)	1.283(7)	C(10)	-C(11)	1.520(8)
C(1)	- C(2)	1.409(7)			

Table 4.8 Selected bond angles (°) of $[Pd_2(\underline{1})](BF_4)_2$

O(1) -	Pd	- N(1)	93.30(17)	C(2) - C(1) - C(7)	120.0(5)
O(1) -	Pd	- N(2)	170.34(17)	C(1) - C(2) - C(3)	118.7(5)
O(1) -	Pd	-O(1a)	77.13(15)	C(1) - C(2) -C(12a)	125.6(5)
N(1) -	Pd	- N(2)	96.36(18)	C(3) - C(2) -C(12a)	115.8(5)
N(1) -	Pd	-O(1a)	170.33(17)	C(2) - C(3) - C(4)	122.3(5)
N(2) -	Pd	-O(1a)	93.21(17)	C(3) - C(4) - C(5)	121.4(5)
Pd	- O(1)	- C(1)	127.9(3)	C(3) - C(4) - C(6)	118.2(5)
Pd	- O(1)	-Pd(a)	102.88(16)	C(5) - C(4) - C(6)	120.4(5)
C(1)	- O(1)	-Pd(a)	129.2(3)	C(4) - C(6) - C(7)	121.8(5)
Pd	- N(1)	- C(8)	122.2(4)	C(1) - C(7) - C(6)	119.0(5)
Pd	- N(1)	- C(9)	122.6(4)	C(1) - C(7) - C(8)	125.9(5)
C(8)	- N(1)	- C(9)	115.2(5)	C(6) - C(7) - C(8)	115.1(5)
Pd	- N(2)	-C(11)	122.9(4)	N(1) - C(8) - C(7)	130.0(5)
Pd	- N(2)	-C(12)	121.1(4)	N(1) - C(9) -C(10)	112.3(5)
C(11)	- N(2)	-C(12)	115.9(5)	C(9) -C(10) -C(11)	111.2(5)
O(1)	- C(1)	- C(2)	119.3(5)	N(2) -C(11) -C(10)	112.8(5)
O(1)	- C(1)	- C(7)	120.7(5)	N(2) -C(12) -C(2a)	131.5(5)

Table 4.9 Selected torsion angles (°) of $[Pd_2(\underline{1})](BF_4)_2$

C(9) - N(1) - C(8) - C(7)	-178.9(5)	C(12a)- C(2) - C(3) - C(4)	179.5(5)
C(8) - N(1) - C(9) -C(10)	-146.2(5)	C(1) - C(2) -C(12a)-N(2a)	-1.9(10)
C(12) - N(2) -C(11) -C(10)	149.5(5)	C(3) - C(2) -C(12a)-N(2a)	178.7(6)
C(11) - N(2) -C(12) -C(2a)	178.7(6)	C(2) - C(3) - C(4) - C(5)	179.1(5)
O(1) - C(1) - C(2) - C(3)	-179.0(5)	C(2) - C(3) - C(4) - C(6)	-0.6(8)
O(1) - C(1) - C(2) -C(12a)	1.6(8)	C(3) - C(4) - C(6) - C(7)	0.5(8)
C(7) - C(1) - C(2) - C(3)	0.6(8)	C(5) - C(4) - C(6) - C(7)	-179.2(5)
C(7) - C(1) - C(2) -C(12a)	-178.7(5)	C(4) - C(6) - C(7) - C(1)	0.2(8)
O(1) - C(1) - C(7) - C(6)	178.9(5)	C(4) - C(6) - C(7) - C(8)	178.6(5)
O(1) - C(1) - C(7) - C(8)	0.7(8)	C(1) - C(7) - C(8) - N(1)	0.9(10)
C(2) - C(1) - C(7) - C(6)	-0.8(8)	C(6) - C(7) - C(8) - N(1)	-177.4(6)
C(2) - C(1) - C(7) - C(8)	-178.9(5)	N(1) - C(9) -C(10) -C(11)	-73.1(6)
C(1) - C(2) - C(3) - C(4)	0.0(8)	C(9) -C(10) -C(11) - N(2)	71.5(6)

Figure 4.18 shows that due to the planarity of the macrocyclic complex, inter-molecular stacking of the aromatic rings occurs between adjacent cations, but not so that the Pd(II) ions of one molecule can interact with the phenoxy donors of a neighbouring one. This is in direct contrast with the proposed structure of $\{[Ni_2(\underline{1})](BF_4)_2\}_n$ described in Figure 4.2 above. The stacking in $[Pd_2(\underline{1})](BF_4)_2$ is staggered to give infinite two-dimensional sheets of the cationic species, with the BF_4^- counterions and CH_3NO_2 molecules occupying interstitial sites.

4.2.12: An Electrochemical Study on $[Pd_2(\underline{1})]^{2+}$

Considering the planarity of the $[Pd_2(\underline{1})]^{2+}$ species in the solid-state, we were interested to investigate the redox chemistry of this compound, particularly with the possibility of reductive coupling at negative potentials. At Edinburgh, we have used spectroelectrochemical and e.s.r. techniques to investigate the reactions of reduced Pd-macrocyclic complexes and have obtained evidence for the rapid dimerisation of Pd(I) species in solution on electrogeneration[179]. We therefore proposed that the complex $[Pd_2(\underline{1})]^{2+}$ may exhibit similar behaviour, due to the possibility of the close approach of the reduced Pd centres, and the stereochemical flexibility of the ligand $(\underline{1})^{2-}$, as demonstrated by the varied redox behaviour of the Cu complexes with this ligand described in Chapter 2.

Cyclic voltammetry of $[Pd_2(\underline{1})](BF_4)_2$ measured at 298K in CH_3CN (0.1M $NBu^n_4BF_4$ supporting electrolyte) at Pt electrodes shows two irreversible reductions at E_{pc} = -1.04V (scan rate = $0.63Vs^{-1}$) and -0.97V ($0.2Vs^{-1}$) and E_{pc} = -2.18V ($0.63Vs^{-1}$) and -2.15V ($0.2Vs^{-1}$) *vs.* Fc/Fc^+. A broad, irreversible oxidation is observed at E_{pa} = +0.89V ($0.5Vs^{-1}$) *vs.* Fc/Fc^+. Cooling the solution to 238K gave no change in the irreversibility of the processes and precipitation of $[Pd_2(\underline{1})]^{2+}$ was observed.

A quantitative investigation of the first reduction was undertaken. Coulometry of $[Pd_2(\underline{1})](BF_4)_2$, measured at −1.15V *vs.* Fc/Fc^+, 298K in CH_3CN (0.1M $NBu^n{}_4BF_4$ supporting electrolyte) at a Pt basket confirmed this to be a one-electron process (n = 0.95 electrons). During electrolysis the brown solution became cloudy with the formation of an insoluble precipitate. Due to these insolubility problems, a spectroelectrochemical investigation of the first reduction process was impossible. Considering the relative sizes of the two reduction peaks, we tentatively propose that the second process is a demetallation reaction, with the concomitant transfer of three or four electrons to deposit Pd metal from the macrocyclic complex.

4.2.13: The Attempted Synthesis of a Mixed Ni(II)/Pd(II) Complex of $(\underline{1})^{2-}$

The reaction of one equivalent of $Pd(CH_3CO_2)_2$ with $[(\underline{1}H_4)](BF_4)_2$ in CH_3CN with 2.2 equivalents of 1,8-bis(dimethylamino)naphthalene gave a brown suspension. Addition of one equivalent of $[Ni(H_2O)_6](BF_4)_2$ and a further 2.2 equivalents of 1,8-bis(dimethylamino)naphthalene gave a brown solution and a dark, insoluble precipitate on stirring. An i.r. spectrum of the dark solid shows no evidence for the presence of the ligand and from its appearence and properties, it was concluded that the precipitate was Pd metal. A brown solid was isolated from the reaction solution, and a f.a.b. mass spectrum of this solid shows peaks at M^+ = 518 and, in small amounts, 616 and 701. These are assigned as molecular ion peaks, with the correct isotope patterns, for $[^{58}Ni_2(\underline{1})]^+$, $[^{106}Pd_2(\underline{1}H_2)]^+$ and $[^{106}Pd_2(\underline{1})](BF_4)^+$ respectively. There is no evidence for the mixed Ni(II)/Pd(II) complex $[^{58}Ni^{106}Pd(\underline{1})]^+$ at M^+ = 566 or the mononuclear complexes $[^{58}Ni(\underline{1}H_2)]^+$ and $[^{106}Pd(\underline{1})H_2]^+$. We therefore tentatively suggest that $[Ni(H_2O)_6]^{2+}$ can reduce Pd(II) to Pd(0) in a basic solution, but the binuclear complex, $[Pd_2(\underline{1})]^{2+}$, is sufficiently inert to remain unreduced.

4.2.14: The Attempted Syntheses of Pt(II) Complexes of $(\underline{1})^{2-}$

There are a greater number of macrocyclic complexes of Pd(II) reported in the literature than of Pt(II), which is a reflection of the greater kinetic inertness of Pt(II) metal ions compared to Pd(II)[16,243]. Formally, the ionic sizes of Pd(II) and Pt(II) are very similar[244] and so the synthesis of a binuclear Pt(II) complex of $(\underline{1})^{2-}$ may be thermodynamically possible. However, the third-row transition metals are considerably less reactive than the second-row elements and the more forcing conditions required to react a heavier metal centre may cause difficulties in the synthesis of $[Pt_2(\underline{1})]^{2+}$.

Two equivalents of $[PtCl_2(PhCN)_2]$[245] with $[(\underline{1}H_4)](BF_4)_2$ in the presence of excess 1,8-bis(dimethylamino)naphthalene in CH_3CN was refluxed vigorously for 24 hours under N_2 to give a brown solution. On addition of diethyl ether, a dark solid was obtained in low yield. A Pt mirror was also deposited on the reaction vessel. The dark solid proved to be difficult to redissolve and vigourous heating in air caused more metallic solids to be precipitated. The i.r. spectrum of the dark solid shows only a strong band at 1029cm^{-1}, which is assigned as a B-F stretching vibration. A band of medium intensity is observed at 1618cm^{-1}, which may be due to a weak co-ordinated C=N stretching vibration. The f.a.b. mass spectrum of the dark product does show very small peaks at M^+ = 598 and 791 which have the correct isotope distributions for assignments to $[^{195}Pt(\underline{1}H)]^+$ and $[^{195}Pt_2(\underline{1}-H)]^+$ respectively. This suggests that $[Pt_2(\underline{1})]^{2+}$ can be synthesized but the insertion of two Pt(II) centres into $(\underline{1})^{2-}$ does require even more forcing conditions.

The above reaction was repeated with the addition of two equivalents of $TlPF_6$ per Pt(II) ion in order to activate the metal centre, and using the PF_6^- salt of $[(\underline{1}H_4)]^{2+}$ and $N(C_2H_5)_3$ as the base. After removal of the grey TlCl precipitate by centrifugation, a brown solution was obtained, from which

a brown solid was isolated on addition of diethyl ether. The f.a.b. mass spectrum of the brown solid shows a peak at M^+ = 350 for residual $[^{205}TlPF_6]^+$, and also peaks at M^+ = 407 and 597, which are assigned to $[(\underline{1})H_5]^+$ and $[^{195}Pt(\underline{1})]^+$ respectively. The i.r. spectrum of the brown solid shows strong bands at 1621, 1553, 1455 and 845cm^{-1}. The last band may be assigned to a P–F stretching vibration and the others are tentatively assigned to the C=N and C–O stretching vibrations of the macrocycle and the benzene ring vibrations of a PhCN group. The data obtained from this reaction suggests again that the insertion of two Pt(II) ions into $(\underline{1})^{2-}$ has not been achieved, even with the activation of the metal centre by the removal of Cl^- in the form of TlCl. Kimura and co-workers[246] have reported the use of a reductant ($Na_2S_2O_3$ in H_2O) to activate Pt(II) for complexation to a tetraaza macrocycle. This reductant is not suitable for the reactions with $(\underline{1})^{2-}$, since a basic, aqueous solution would cause hydrolysis of the free macrocyclic ligand. In investigative reactions with other reductants such as Zn mesh in the reaction mixture for $[Pt_2(\underline{1})]^{2+}$, we observed the reduction of the Pt(II) to Pt metal. Repeating the above reactions in a higher boiling solvent, DMF, was also attempted but degradation of the ligand $(\underline{1})^{2-}$ is observed in the i.r. spectra of the products, by the removal of the absorptions due to C=N and C–O stretching vibrations.

4.2.15: The Attempted Synthesis of a Pt(II) Complex of $(\underline{5})^{2-}$

From the crystal structure of $[Pd_2(\underline{1})]^{2+}$ described in Section 4.2.11, it can be seen that the angles subtended at the Pd(II) centres by the bridging phenoxy donors are significantly less than 90°. It is possible that Pt(II) can not tolerate this bonding angle and so Pt(II) complexes are not readily formed with the ligand $(\underline{1})^{2-}$. We proposed that the complexation of two Pt(II) ions may be more readily achieved with ligand $(\underline{5})^{2-}$ due to the longer

side-arms of the ligand which would create a larger hole size in $(\underline{5})^{2-}$ compared to $(\underline{1})^{2-}$. The relatively acute angle subtended by the phenoxy O-donors observed in $[Pd_2(\underline{1})]^{2+}$ might then be avoided. A macrocycle with a less constrained macrocyclic cavity such as $(\underline{5})^{2-}$ might also facilitate the formation of a binuclear complex of Pt(II).

The reaction of two equivalents of $[PtCl_2(PhCN)_2]$[245] with $[(\underline{5}H_4)](PF_6)_2$ in the presence of excess 1,8-bis(dimethylamino)naphthalene in refluxing CH_3CN gave an orange precipitate. The f.a.b. mass spectrum of this solid only shows peaks due to the 3-NOBA matrix. The i.r. spectrum shows strong bands at 1637 and 1532cm^{-1}, which could be tentatively assigned to co-ordinated C=N and C-O stretching vibrations respectively. Importantly, however, there are no strong absorptions found in the region for counterion vibrations, which might suggest that any Pt(II) ions co-ordinated to $(\underline{5})^{2-}$ still have bound Cl^- ions. This initial reaction can only suggest that if the binuclear Pt(II) complex of $(\underline{5})^{2-}$ can be formed, it requires more forcing conditions than those above.

4.2.16: The Syntheses of Rh(III) Complexes of $(\underline{1})^{2-}$

In contrast to Pd(II) and Pt(II), there have been relatively few complexes of Rh(III) with Schiff-base ligands reported in the literature. West *et al.*[247,248] have described the synthesis of [RhCl(salen)(pyridine)] [salen = the dianion of *N*,*N*'-ethylenebis(salicylaldimine)] which on reduction with $NaBH_4$ or sodium amalgam reacts with a number of acyl and alkyl halides to form a series of derivatives of the form [R-Rh(salen)(pyridine)]. West and Rogers[249] have also reported the synthesis of $[Rh(salen)(pyridine)_2](PF_6)$ which reacts with alkyl halides in a similar fashion to [RhCl(salen)(pyridine)]. To our knowledge, the only other Rh complex with a Schiff-base ligand that has been reported is a dimeric Rh(II) complex of

N,N'-o-phenylenebis(salicylaldimine) which can react explosively with air[250]. We therefore proposed that the synthesis of Rh(III) complexes with $(\underline{1})^{2-}$ might give some novel and potentially reactive compounds.

Reaction of two equivalents of $RhCl_3.3H_2O$ with $[(\underline{1}H_4)](BF_4)_2$ in the presence of excess $N(C_2H_5)_3$ in degassed, refluxing CH_3CN under N_2 initially gave a brown solution and solid. Two equivalents of $TlBF_4$ per Rh(III) ion were added and and the mixture was refluxed under N_2 to give a TlCl precipitate and a red solution. On removal of the TlCl by centrifugation, a red oil was obtained from the red solution on addition of diethyl ether. Addition of H_2O to the red oil gave an orange solid. The Tl(I) was added after the $RhCl_3$ had been allowed to react with $(\underline{1})^{2-}$, since we suspect, from previous reactions, that the Tl(I) ion can interfere with the complexation of the desired metal ion with $(\underline{1})^{2-}$. Complexation of Tl(I) with $(\underline{1})^{2-}$ is even a possibility, although we have obtained no direct evidence for this.

The i.r. spectrum of the orange solid shows strong bands at 1628 and 1084cm^{-1}, which are assigned to a co-ordinated C=N stretching vibration and a B-F stetching vibration respectively. No clear Rh-Cl stretching vibrations are observed at frequencies down to 250cm^{-1}. The f.a.b. mass spectrum of the orange solid shows peaks at M^+ = 608, 643, 678 and 715, which have the correct isotope distributions for and are assigned to $[^{103}Rh_2(\underline{1})]^+$, $[^{103}Rh_2{}^{35}Cl(\underline{1})]^+$, $[^{103}Rh_2{}^{35}Cl_2(\underline{1})]^+$ and $[^{103}Rh_2{}^{35}Cl_2{}^{37}Cl(\underline{1})]^+$ respectively. The elemental analytical data suggests that if the compound is pure, there is a considerable amount of solvent in the product. These spectroscopic and analytical data suggest that the orange product contains some solvated $[Rh_2(\underline{1})Cl_2](BF_4)_2$.

To ascertain whether Rh(III) complexes of $(\underline{1})^{2-}$ could be formed without using Tl(I) as an activating agent, a reaction was carried out using Zn mesh as an activating agent. West and Rogers[249] have used Zn in their

synthesis of [Rh(salen)(pyridine)$_2$](PF$_6$) and propose that Zn acts as a two-electron reductant to form transient and more labile Rh(II) or Rh(I) species. The reaction of two equivalents of $RhCl_3.3H_2O$ with [(1H$_4$)](PF$_6$)$_2$ in the presence of $N(C_2H_5)_3$ and a catalytic amount of Zn mesh in degassed, refluxing CH_3CN gave a yellow suspension. On removal of the $N(C_2H_5)_3$ by washing with H_2O, an orange solid was obtained that was recrystallised from CH_3CN/diethyl ether. The i.r. spectrum of this orange product shows strong bands at 1627, 1551 and 843cm^{-1}, which are assigned as co-ordinated C-O and C=N stretching vibrations and P-F stretching vibrations respectively. This establishes that the product is positively charged since there is counterion present. The f.a.b. mass spectrum of the orange product shows small peaks at M^+ = 678 and 715, which are assigned as $[^{103}Rh_2{}^{35}Cl_2(1)]^+$ and $[^{103}Rh_2{}^{35}Cl_2{}^{37}Cl(1)]^+$ respectively. Elemental analysis data indicate that there is a considerable non-organic component in the product which is not removed by recrystallisation, but that the macrocyclic complex is present in small amounts (C : H : N ratio = 6 : 8 : 1, percentage of compound containing C, H and N = 21%).

We have also established that $RhCl_3.3H_2O$ reacts with $(1)^{2-}$ in the absence of any activating agents. The reaction of two equivalents of $RhCl_3.3H_2O$ with [(1H$_4$)](BF$_4$)$_2$ in the presence of $N(C_2H_5)_3$ in degassed, refluxing C_2H_5OH under N_2 gave a brick-red solid. The i.r. spectrum of this solid shows strong bands at 1627, 1548 and 1456cm^{-1}, which are assigned to co-ordinated C=N and C-O stretching vibrations and an unknown. Importantly there is no absorption for the BF_4^- counterion and we tentatively suggest that this insoluble species is [Rh_2Cl_4(1)]. In order to obtain a product that could be studied electrochemically without the interference of a Cl^- ion, the insoluble brick-red solid was reacted with 4 equivalents of $TlBF_4$ in CH_3CN, to give a clear, brown solution and copious amounts of TlCl precipitate.

Although a number of different solvent systems were tried, it was impossible to obtain a solid material from the clear, brown solution. Oils and gums only were formed.

An incompletely transmetallated Rh(III) complex can be synthesized by reacting two equivalents of $RhCl_3.3H_2O$ with $[Pb_2(\underline{1})](NO_3)_2$ in refluxing CH_3CN to give an orange solid and solution. Removal of the solid, addition of excess PF_6^- and diethyl ether to the solution gave an orange solid. The f.a.b. mass spectrum of this orange solid shows peaks at M^+ = 405, 506, 541, 577, 678 and 715, which are assigned to $[(\underline{1})H_3]^+$, $[^{103}Rh(\underline{1}H)]^+$, $[^{103}Rh^{35}Cl(\underline{1}H)]^+$, $[^{103}Rh^{35}Cl_2(\underline{1}H_2)]^+$, $[^{103}Rh_2{}^{35}Cl_2(\underline{1})]^+$ and $[^{103}Rh_2{}^{35}Cl_2{}^{37}Cl(\underline{1})]^+$ respectively. This shows that some substitution of the Pb(II) ions in $[Pb_2(\underline{1})]^{2+}$ has occurred. In the i.r. spectrum of the orange solid, however, the band that is assigned to the C=N stretching vibration is observed at an anomalously high value ($1664cm^{-1}$) for a metal complex of $(\underline{1})^{2-}$. This value, in fact, is similar to the value for the C=N stretching vibration of $[(\underline{1}H_4)]^{2+}$. The implication of this is not clear. Other strong bands in the i.r. spectrum of the orange solid are observed at 1554, 1401 and $834cm^{-1}$, which are assigned to a co-ordinated C–O, an unknown and a P–F stretching vibration.

These reactions of Rh(III) with $(\underline{1})^{2-}$ indicate that the metal ion will complex with the macrocycle, but the products of the reactions can not be unambiguously assigned. It appears that often a number of products are obtained with a varying number of co-ordinated Cl^- ligands. Even in the attempt to synthesize $[Rh_2(\underline{1})Cl_2]^{2+}$, when two equvalents of Tl(I) were present per Rh(III) ion, the f.a.b. mass spectrum of the compound still shows peaks for a compound containing 3 Cl^- ligands. In a f.a.b. mass spectrum experiment, where pressures in the ion chamber are as low as 10^{-3} atmospheres, molecular collisions are unlikely to occur and so this eliminates

the possibility of Cl^- exchange. In addition to the problem of actually complexing Rh(III) to $(\underline{1})^{2-}$, there has been documentation of Rh(III) ions participating in reactions with the bases $N(C_2H_5)_3$ [251] and 1,8-bis(dimethylamino)naphthalene[252]. For example, $[RhCl_3(DMSO)_3]$ will dehydrogenate $N(C_2H_5)_3$ to form enamine complexes thus[251]:

$$[RhCl_3(DMSO)_3] + N(C_2H_5)_3 \rightarrow [RhCl_3(DMSO)_2(\sigma\text{-}CH_2CH{=}N(C_2H_5)_2] + H_2$$

It is unlikely that reactions such as these are specific to $[RhCl_3(dmso)_3]$, so there are also problems in the complexation reactions with $(\underline{1})^{2-}$ with the unpredictable reactivity of the Rh(III) centres. It has not been possible to find a more suitable base which will not react with the solvated Rh(III) nor attack the macrocyclic imine bonds. We have also remarked above on the reactivity of the reported complexes of Rh(III) with Schiff-base ligands. The problems with the complexation of Rh(III) with $(\underline{1})^{2-}$, have therefore been in isolating pure products, avoiding unwanted side-reactions and the irreproducibility of the reactions.

4.2.17: The Synthesis of Rh(I) Complexes of $(\underline{1})^{2-}$

The complexation of two Rh(I) centres in close proximity in a macrocyclic framework is of particular interest for potential catalytic processes. Parker and co-workers[180-184] have reported some binuclear complexes using macrocycles with pyridine, amine and thioether donors, containing the Rh(I) centres either within a single binucleating ligand or by the coupling of two mononuclear units. This coupling can occur through two bridging carbonyl ligands or through a weak, unsupported, metal-metal interaction which has been observed in the solid-state only[184]. In Section 4.2.11 it has been shown that $(\underline{1})^{2-}$ can accomodate two square-planar, d^8, second-row transition metal centres and we proposed that the ligand $(\underline{1})^{2-}$ might be able to complex two

Rh(I) centres in the neighbouring compartmental sites, offering a novel donor set for Rh(I).

Reaction of one equivalent of $[Rh(CO)_2Cl]_2$ with $[(\underline{1}H_4)](PF_6)_2$ in the presence of 1,8-bis(dimethylamino)naphthalene in $(CH_3)_2CO$ at room temperature under N_2 afforded a brown solid and brown solution. Further crops of the brown solid were obtained from the mother liquor on allowing the reaction mixture to stand. The f.a.b. mass spectrum of the brown solid shows peaks at M^+ = 508 and 609, which are assigned to $[^{103}Rh(\underline{1})]^+$ and $[^{103}Rh_2(\underline{1})]^+$ respectively. This suggested that the Rh(I) ions had inserted cleanly into the macrocycle $(\underline{1})^{2-}$, to give an insoluble product. This insolubility was not unexpected, since the neutral binuclear Cu(I) complex of $(\underline{1})^{2-}$, $[Cu_2(\underline{1})]$ [123], is also insoluble in common solvents, presumably through extensive stacking of the molecules. However, the i.r. spectrum of the brown solid shows very strong bands at 2079 and 2002cm^{-1}, which are indicative of the asymmetric and symmetric stretches of two terminally bound carbonyl ligands. No evidence for these ligands being present has been obtained in the f.a.b. mass spectrum of the brown solid. Other significant information from the i.r. spectrum are the bands at 1621 and 1547cm^{-1}, assigned to co-ordinated C=N and C-O stretching vibrations and the absence of the strong absorption of the PF_6^- counterion. Elemental analysis data do not agree with the formulation $[Rh_2(\underline{1})]$ for the product and are consistently very low in nitrogen (typically C = 39.0, H = 5.67, N = 4.34%; expected for $[Rh_2(\underline{1})]$: C = 47.4, H = 4.31, N = 9.21%). It is possible that the metal centres are catalysing a polymerisation of the ligand $(\underline{1})^{2-}$, by an oxidative addition mechanism, but in the absence of further data, it is not clear what is occuring.

4.3: Conclusions

A number of novel, binuclear macrocyclic complexes have been described in this chapter, including the first structurally characterised complex of one of the platinum metals with a binucleating macrocyclic ligand. The co-ordination chemistry of Ni(II) with $(\underline{1})^{2-}$ has shown a tendency for polynuclear aggregation, which has been previously reported for other Ni(II) complexes with Schiff-bases. By using $CH_3CO_2^-$ as a chelating cap to prevent aggregation, a macrocyclic compound containing a Ni_4O_4 cubane structure has been characterised. However, the aim of synthesizing binuclear complexes of the platinum metals has been, overall, hampered by the need for vigorous reaction conditions to activate the metal centres and to insert them into a relatively constrained environment. This has caused difficulties in reaction reproducibility and by the contamination of the desired products with those of side-reactions.

4.4: Experimental

4.4.1: Synthesis of $[Pb_2(\underline{1})](NO_3)_2$

$[Pb_2(\underline{1})](NO_3)_2$ was prepared by the method of Mandal and Nag[145]. $Pb(CH_3CO_2)_2.3H_2O$ (285mg, 0.75mmol) and $Pb(NO_3)_2$ (248mg, 0.75mmol) were dissolved in DMF ($1cm^3$) and this solution was added to a CH_3OH solution ($5cm^3$) of 2,6-diformyl-4-methylphenol (246mg, 1.50mmol). The addition of 1,3-diaminopropane ($0.125cm^3$, 1.50mmol) followed immediately. The mixture was refluxed in air for 8 hours, by which time a yellow precipitate had formed. The mixture was cooled, filtered, washed with CH_3OH and $CHCl_3$ and dried *in vacuo*. Yield = 436mg, 62%. Elemental analysis: found C = 31.3; H = 3.10; N = 7.94%. Calculated for $[Pb_2(C_{24}H_{26}N_4O_2)](NO_3)_2.3CH_3OH$: C = 31.3; H = 3.40; N = 8.10%. F.a.b. mass spectrum (3-NOBA matrix): found M^+ = 406, 611. Calculated

for: $[C_{24}H_{30}N_4O_2]^+$, M^+ = 406; $[^{208}Pb(C_{24}H_{27}N_4O_2)]^+$, 611. I.r. spectrum (KBr disc): 2934w, 2853w, 1636s, 1560m, 1447m, 1385s, 1298s, 1255m, 1239m, 1192m, 1123m, 1064m, 1030w, 981w, 927w, 872w, 823w, 805w and 769w cm^{-1}.

4.4.2: Syntheses of Ni(II) Complexes of $(1)^{2-}$

4.4.2a: Synthesis of $[Ni_2(1)](BF_4)_2$

$[Ni(H_2O)_6](BF_4)_2$ (50.0mg, 0.15mmol) was dissolved in distilled C_2H_5OH (10cm^3) and $[(1H_4)](BF_4)_2$ (40.0mg, 0.07mmol) was added. A solution of $N(C_2H_5)_3$ in C_2H_5OH (0.180M, 4cm^3, 0.72mmol) was added dropwise into the stirring solution, which became an orange colour. The solution was refluxed for 4 hours and a red solid and solution was obtained. The red solid was filtered off and dried *in vacuo*. The red solution was reduced in volume and diethyl ether was added. A red, oily solid was precipitated, which was filtered, washed with diethyl ether and dried *in vacuo*. Yield of initial red solid = 24mg, 49%. Elemental analysis: found C = 41.9; H = 5.03; N = 7.53%. Calculated for $[Ni_2(C_{24}H_{26}N_4O_2)](BF_4)_2$: C = 41.6; H = 3.78; N = 8.08%. F.a.b. mass spectrum (3-NOBA matrix): found M^+ = 518, 684. Calculated for: $[^{58}Ni_2(C_{24}H_{26}N_4O_2)]^+$, M^+ = 518; $[^{58}Ni_2(C_{24}H_{26}N_4O_2)(O_2CC_6H_4NO_2)]^+$, M^+ = 684. (DMF/Glycerol matrix): found M^+ = 462, 518. Calculated for: $[^{58}Ni(C_{24}H_{28}N_4O_2)]^+$, M^+ = 462; $[^{58}Ni_2(C_{24}H_{26}N_4O_2)]^+$, M^+ = 518. I.r. spectrum (KBr disc): 3405br, 2922w, 1629s, 1543m, 1495w, 1451m, 1340w, 1315m, 1242w, 1194w, 1084br, 964w, 870w, 834w, 772w, 556w, 522w and 472w cm^{-1}. U.V./vis. spectrum (in DMSO): $\lambda_{max.}$ = 470nm. ($\varepsilon_{max.}$ = 1,500$M^{-1}cm^{-1}$), 318 (1,700). (in DMF): $\lambda_{max.}$ = 462nm. ($\varepsilon_{max.}$ = 700$M^{-1}cm^{-1}$), 317 (800). (in CH_3CN): $\lambda_{max.}$ = 445, 380 and 246nm.

4.4.2b: Synthesis of $[Ni_2(\underline{1})(CH_3CN)_4](BF_4)_2$

$[Ni(H_2O)_6](BF_4)_2$ (85.8mg, 0.25mmol), $[(\underline{1}H_4)](BF_4)_2$ (69.9mg, 0.12mmol) and 1,8-bis(dimethylamino)naphthalene (120.0mg, 0.56mmol) were dissolved in dry, distilled CH_3CN ($10cm^3$) and refluxed for 2 hours under N_2. The clear, amber solution was filtered to remove a little solid material, evaporated down to $5cm^3$ and diethyl ether was added. A yellow precipitate was obtained which was filtered, washed with diethyl ether, CH_2Cl_2 and H_2O and dried *in vacuo*. Recrystallisation from CH_3CN/diethyl ether or CH_3NO_2/diethyl ether by vapour diffusion gave a brown, crystalline material. Yield = 48mg, 50%. Elemental analysis: found C = 41.9; H = 4.48; N = 10.8%. Calculated for $[Ni_2(C_{24}H_{26}N_4O_2)(CH_3CN)_2](BF_4)_2.H_2O$: C = 42.4; H = 4.32; N = 10.6%. Also calculated for $[Ni_2(C_{24}H_{26}N_4O_2)(CH_3CN)_2](BF_4)_2.2H_2O$: C = 41.4; H = 4.47; N = 10.4%. F.a.b. mass spectrum (3-NOBA matrix): found M^+ = 518, 684. Calculated for: $[^{58}Ni_2(C_{24}H_{26}N_4O_2)]^+$, M^+ = 518; $[^{58}Ni_2(C_{24}H_{26}N_4O_2)(O_2CC_6H_4NO_2)]^+$, M^+ = 684. I.r. spectrum (KBr disc): 3490br, 3067w, 2927m, 1949w, 1820w, 1643s, 1557s, 1465s, 1414m, 1364w, 1334m, 1284m, 1240m, 1225m, 1196m, 1135m, 1059br s, 931m, 877w, 829m, 766s, 633m, 584m, 532m, 521m and 470m cm^{-1}. U.V./vis. spectrum (CH_3CN): $\lambda_{max.}$ = 376nm. ($\varepsilon_{max.}$ = $900M^{-1}cm^{-1}$); 284 (11,800); 274 (11,000). ^1H n.m.r. spectrum (80.13MHz, $(CD_3)_2CO$, 298K): gave only broad peaks.

4.4.2c: Single Crystal X-ray Structure of $[Ni_2(\underline{1})(CH_3CN)_4](BF_4)_2$

Vapour diffusion of diethyl ether into a solution of the complex in CH_3NO_2 gave brown crystals of crystallographic quality. To prevent crystal degradation as a result of solvent loss, a brown block was transferred from its cold mother liquor into a drop of mineral oil at 195K and mounted on the

diffractometer which was equipped with an Oxford Cryosystems low-temperature device[253] operating at 150K.

Crystal Data:

$[Ni_2(C_{24}H_{26}N_4O_2)(CH_3CN)_4](BF_4)_2$ M = 857.64. Monoclinic, space group $P2_1/n$, a = 10.419(4), b = 9.029(3), c = 19.798(9)Å, β = 93.40(3)°, V = 1859Å^3 (by least-squares refinement on diffraction angles for 25 reflections measured at $\pm\omega$ [$26 < 2\theta < 28°$, λ = 0.71073Å]), Z = 2, D_c = 1.532gcm^{-3}, T = 150K. Crystal dimensions 0.23 x 0.31 x 0.39mm^3, μ(Mo-Kα) = 1.097mm^{-1}, F(000) = 880.

Data Collection and Processing:

Stöe STADI-4 four-circle diffractometer, ω-2θ scan mode using the learnt-profile method[199]. Graphite-monochromated Mo-Kα radiation; 3435 reflections measured ($2\theta_{max.}$ = 45°, h -11 → 11, k 0 → 9, l 0 → 21), 2337 unique data (R_{int} = 0.05), giving 2123 with $F > 4\sigma(F)$. No significant crystal decay, no absorption correction.

Structure Analysis and Refinement:

The Ni-Ni vector was located using a Patterson synthesis[201], and successive cycles of least-squares refinement and difference Fourier synthesis[201] identified the positions of all of the atoms. During refinement some disorder of the BF_4^- was observed. This was modelled successfully using partial occupancies of two sets of 4 F atom positions (occupancies of different sets = 88 and 12%). Anisotropic thermal parameters were refined for the Ni, C, N, O, B and for the major F positions. H atoms were located from a difference map and included in fixed, calculated positions. The methyl groups of the CH_3CN ligands required treatment as rigid groups. The weighting

scheme $w^{-1} = \sigma^2(F) + 0.000140F^2$ gave satisfactory agreement analyses. At final convergence, $R = 0.0456$, $R_w = 0.0580$, $S = 1.096$ for 282 independent parameters, and the final difference Fourier synthesis showed no feature above +0.65 or below $-0.45e\text{Å}^{-3}$.

Atomic scattering factors were inlaid[201], except for Ni[254], molecular geometry calculations utilised *CALC*[202] and figures were produced by *SHELXTL PC*[255].

4.4.2d: Reaction of ($\underline{1}H_2$) with Ni(II)

$Ni(CH_3CO_2)_2.4H_2O$ (52.3mg, 0.21mmol) and ($\underline{1}H_2$) (40.5mg, 0.10mmol) were mixed in degassed CH_3CN under N_2. The ligand ($\underline{1}H_2$) appeared to be insoluble in CH_3CN so $N(C_2H_5)_3$ (0.07ml, 0.50mmol) was added. The solution became an orange colour and was heated overnight under N_2. A brown solid and solution were obtained. The solid was filtered, washed with CH_2Cl_2 and diethyl ether and dried *in vacuo*. Only oily products could be obtained from the brown solution. Yield of brown solid = 15mg. Elemental analysis: found C = 43.9; H = 5.56; N = 6.53%. Calculated for $[Ni_2(C_{24}H_{26}N_4O_2)](CH_3CO_2)_2.8H_2O$: C = 43.0; H = 6.19; N = 7.16%. F.a.b mass spectrum (3-NOBA matrix): found M^+ = 519, 537, 578, 685, 703. Calculated for: $[^{58}Ni_2(C_{24}H_{27}N_4O_2)]^+$, M^+ = 519; $[^{58}Ni_2(C_{24}H_{27}N_4O_2)(H_2O)]^+$, M^+ = 537; $[^{58}Ni_2(C_{24}H_{27}N_4O_2)(CH_3CO_2)]^+$, M^+ = 578; $[^{58}Ni_2(C_{24}H_{27}N_4O_2)(O_2CC_6H_4NO_2)]^+$, M^+ = 685; $[^{58}Ni_2(C_{24}H_{27}N_4O_2)(O_2CC_6H_4NO_2)(H_2O)]^+$, M^+ = 703. I.r. spectrum (KBr disc): 3384br, 2922w, 1640s, 1559s, 1456m, 1410s, 1339w, 1281w, 1256w, 1234w, 1123w, 1099w, 1036w, 972w, 917w, 875w, 823w, 774w, 757w, 669w, 634w, 566w, 500w and 472w cm^{-1}.

4.4.2e: Transmetallation of $[Pb_2(\underline{1})](NO_3)_2$ with Ni(II)

$[Pb_2(\underline{1})](NO_3)_2$ (52.7mg, 0.06mmol) and $[Ni(H_2O)_6](BF_4)_2$ (40.0mg, 0.12mmol) were refluxed in CH_3CN (10ml) for 5 hours to give a green solution and a pale yellow solid. The pale yellow solid was filtered and dried. The green solution was evaporated down to $3cm^3$ and diethyl ether was added to give a yellow solid. This was filtered and recrystallised from CH_3NO_2/diethyl ether to give a yellow/brown solid. Yield = 35mg. F.a.b mass spectrum (3-NOBA matrix): found M^+ = 461, 518, 537, 684. Calculated for: $[^{58}Ni(C_{24}H_{27}N_4O_2)]^+$, M^+ = 461; $[^{58}Ni_2(C_{24}H_{26}N_4O_2)]^+$, M^+ = 518; $[^{58}Ni_2(C_{24}H_{27}N_4O_2)(H_2O)]^+$, M^+ = 537; $[^{58}Ni_2(C_{24}H_{26}N_4O_2)(O_2CC_6H_4NO_2)]^+$, M^+ = 684. I.r. spectrum (KBr disc): 3504br, 2918m, 1642s, 1545s, 1486w, 1450m, 1433w, 1412w, 1384w, 1359w, 1335w, 1274m, 1237m, 1198w, 1060br s, 947w, 907w, 872m, 848m, 815w, 780w, 771w, 671w, 578w, 558w, 521w and 502w cm^{-1}.

4.4.3: Complexation of $(\underline{2})^{2-}$ with Ni(II)

$[Ni(CH_3CN)_6](BF_4)_2$ (prepared by the method of Underhill *et al.*[219]) (as a 0.115M CH_3CN solution, $2cm^3$, 0.23mmol) was added to a degassed, dry CH_3CN solution (10ml) of $[(\underline{2}H_4)](BF_4)_2$ (60.2mg, 0.11mmol). $N(C_2H_5)_3$ ($0.25cm^3$, 1.80mmol) was added and the red solution was refluxed for 2 hours under N_2. A small amount of brown solid was formed which was filtered off to leave a clear, red solution. The volume of solvent was reduced and diethyl ether was added to give a brown solid. This was filtered, recrystallised from CH_3NO_2/diethyl ether and dried *in vacuo*. Yield = 33mg, 45%. Elemental analysis: found C = 39.0; H = 3.73; N = 7.75%. Calculated for $[Ni_2(C_{22}H_{22}N_4O_2)](BF_4)_2$: C = 39.7; H = 3.33; N = 8.42%. F.a.b. mass spectrum (3-NOBA matrix): found M^+ = 490, 509, 579. Calculated for: $[^{58}Ni_2(C_{22}H_{22}N_4O_2)]^+$, M^+ = 490; $[^{58}Ni_2(C_{22}H_{23}N_4O_2)(H_2O)]^+$, M^+ = 509;

$[^{58}Ni_2(C_{22}H_{24}N_4O_2)](BF_4)^+$, M^+ = 579. I.r. spectrum (KBr disc): 3406br, 2922w, 1623s, 1563s, 1457s, 1396w, 1318s, 1236m, 1218w, 1178w, 1058br s, 962w, 877m, 818w, 770w, 756m, 730w, 666w, 632w, 569w, 547w, 534w, 521w, 452w and 414m cm^{-1}. U.V./vis. spectrum (CH_3CN): $\lambda_{max.}$ = 386nm. ($\epsilon_{max.}$ = 5,100$M^{-1}cm^{-1}$); 290sh (12,000); 243 (22,200).

4.4.4a: Synthesis of $[Ni_2(\underline{1})(CH_3CO_2)](PF_6)$

$Ni(CH_3CO_2)_2$ (36.6mg, 0.15mmol) and $[(\underline{1}H_4)](PF_6)_2$ (48.8mg, 0.07mmol) were dissolved in distilled CH_3CN (10cm^3) and $N(C_2H_5)_3$ (0.05cm^3, 0.36mmol) was added dropwise. On addition of the $N(C_2H_5)_3$, the solution immediately became a brown colour. The solution was refluxed under N_2 for 24 hours to give a green solution and a small amount of pale solid. The solution was filtered, the volume of solvent reduced and diethyl ether was added until the solution became turbid. Cooling the solution at 253K gave a green crystalline solid, which was recrystallised from CH_3NO_2/diethyl ether or CH_3CN/diethyl ether and dried *in vacuo*. Yield = 35mg, 70%. Elemental analysis: found C = 42.2; H = 4.51; N = 7.25%. Calculated for $[Ni_2(C_{24}H_{26}N_4O_2)(CH_3CO_2)](PF_6)$: C = 43.1; H = 4.04; N = 7.74%. F.a.b. mass spectrum (3-NOBA matrix): found M^+ = 518, 577, 684. Calculated for: $[^{58}Ni_2(C_{24}H_{26}N_4O_2)]^+$, M^+ = 518; $[^{58}Ni_2(C_{24}H_{26}N_4O_2)(CH_3CO_2)]^+$, M^+ = 577; $[^{58}Ni_2(C_{24}H_{26}N_4O_2)(O_2CC_6H_4NO_2)]^+$, M^+ = 684. I.r. spectrum (KBr disc): 3648w, 3424br, 2929w, 2867w, 1648s, 1575s, 1447m, 1417m, 1368w, 1348w, 1310m, 1279w, 1264w, 1241m, 1197m, 1128m, 1078m, 1046w, 967w, 931w, 843s, 803m, 773m, 740w, 674w, 618w, 590w, 558m, 520w, 498w, 478w, 450w and 407w cm^{-1}. U.V./vis. spectrum (CH_3CN): $\lambda_{max.}$ = 377nm. ($\epsilon_{max.}$ = 12,850$M^{-1}cm^{-1}$).

4.4.4b: Alternative Synthesis of $[Ni_2(\underline{1})(CH_3CO_2)]^+$

$[Ni(H_2O)_6](BF_4)_2$ (57.8mg, 0.17mmol) and $[(\underline{1}H_4)](BF_4)_2$ (46.0mg, 0.08mmol) were dissolved in CH_3CN ($5cm^3$) and a 0.180M solution of $N(C_2H_5)_3$ in C_2H_5OH ($5cm^3$, 0.9mmol) was added dropwise with stirring. $(CH_3CO)_2O$ (approximately $0.5cm^3$) was added and the yellow solution was refluxed under N_2 for 3 hours. A green solution was obtained that was reduced in volume and added to excess diethyl ether to give a green solid. Recrystallisation from CH_3CN/diethyl ether gave a green crystalline material. Yield =29mg, 55%. F.a.b. mass spectrum (3-NOBA matrix): found M^+ = 518, 577, 684. Calculated for: $[^{58}Ni_2(C_{24}H_{26}N_4O_2)]^+$, M^+ = 518; $[^{58}Ni_2(C_{24}H_{26}N_4O_2)(CH_3CO_2)]^+$, M^+ = 577; $[^{58}Ni_2(C_{24}H_{26}N_4O_2)(O_2CC_6H_4NO_2)]^+$, M^+ = 684. I.r. spectrum (KBr disc): 3424br, 2939m, 2878w, 1648s, 1575s, 1475m, 1447s, 1417s, 1308m, 1243m, 1038br s, 886w, 849w, 804m, 773m, 673w, 589w and 522m cm^{-1}.

4.4.4c: Single Crystal X-ray structure of

$\{[Ni_2(\underline{1})(CH_3CO_2)](PF_6)\}_2.2CH_3CN.CH_3NO_2$

Vapour diffusion of diethyl ether into a solution of the complex in CH_3CN gave green crystals of crystallographic quality. To prevent crystal degradation as a result of solvent loss, a green block was transferred from its cold mother liquor into a drop of mineral oil at 195K and mounted on the diffractometer which was equipped with an Oxford Cryosystems low-temperature device[253] operating at 150K.

Crystal Data:

$\{[Ni_2(\underline{1})(CH_3CO_2)](PF_6)\}_2.2CH_3CN.CH_3NO_2$ M = 1590.92. Monoclinic, space group $C_{2/c}$, a = 22.540(7), b = 19.983(8), c = 15.418(5)Å, β = 109.74(3)°, V = 6535Å^3 (by least-squares refinement on diffraction angles for

25 reflections measured at $\pm\omega$ [$30 \leq 2\theta \leq 32^{\circ}$, $\lambda = 0.71073$Å]), $Z = 4$, $D_c = 1.616 gcm^{-3}$, $T = 150K$. Crystal dimensions 0.90 x 0.50 x 0.30mm^3, μ(Mo-Kα) = $1.284 mm^{-1}$, $F(000) = 3264$.

Data Collection and Processing:

Stöe STADI-4 four-circle diffractometer, ω-2θ scan mode using the learnt-profile method[199]. Graphite-monochromated Mo-Kα radiation; 4422 reflections measured ($2\theta_{max.} = 45^{\circ}$, h $-24 \rightarrow 24$, k $0 \rightarrow 21$, l $0 \rightarrow 16$), 4276 unique data ($R_{int} = 0.000$), giving 3444 with $F > 4\sigma(F)$. No significant crystal decay, no absorption correction.

Structure Analysis and Refinement:

The Ni-Ni vector was located using a Patterson synthesis[201], and successive cycles of least-squares refinement and difference Fourier synthesis[201] identified the positions of all other atoms. During refinement disorder of the PF_6^- was observed. Thirteen F positions were found with a variety of occupancies and these were fixed in proportion to the refined occupancies (66% $\rightarrow$ 24%). The crystal lattice was found to contain 2 CH_3CN molecules per cation and one CH_3NO_2 per cation which was located on a symmetry axis. It is probable that this CH_3NO_2 molecule is disordered but no other positions were found. Anisotropic thermal parameters were refined for the Ni, C, N, O, P and the F atoms with occupancies > 50%. For the C and N atoms of the CH_3NO_2 that were lying on the symmetry axis, two anisotropic parameters per atom could not be refined. H atoms were located from a difference map and included in fixed, calculated positions. The weighting scheme $w^{-1} = \sigma^2(F) + 0.000157F^2$ gave satisfactory agreement analyses. At final convergence, $R = 0.0417$, $R_w = 0.0528$, $S = 1.297$ for 464 independent parameters, and the final difference Fourier synthesis showed no

feature above +0.78 or below $-0.61 e\text{Å}^{-3}$.

Atomic scattering factors were inlaid[201], except for Ni[254], molecular geometry calculations utilised *CALC*[202] and figures were produced by *SHELXTL PC*[255].

4.4.5: Synthesis of Pd(II) complexes with $(\underline{1})^{2-}$

4.4.5a: Synthesis of $[Pd(\underline{1})](BF_4)_2$

$[Pd(CH_3CO_2)_2]_3$ (57.0mg, 0.25mmol) was dissolved in dry CH_2Cl_2 ($10cm^3$) and added to a CH_3CN solution ($5cm^3$) of $[(\underline{1}H_4)](BF_4)_2$ (70.0mg, 0.12mmol). $N(C_2H_5)_3$ ($0.08cm^3$, 0.56mmol) was added and a yellow precipitate rapidly formed. The mixture was stirred overnight and a yellow precipitate and brown solution were obtained. The yellow solid was filtered, washed with CH_2Cl_2, recrystallised from CH_3CN/diethyl ether and dried *in vacuo*. Yield = 72mg, 75%. Elemental analysis: found C = 35.5; H = 3.61; N = 6.50%. Calculated for $[Pd_2(C_{24}H_{26}N_4O_2)](BF_4)_2$: C = 36.5; H = 3.32; N = 7.10%. F.a.b. mass spectrum (3-NOBA matrix): found M^+ = 616, 702. Calculated for: $[^{106}Pd_2(C_{24}H_{28}N_4O_2)]^+$, M^+ = 616; $[^{106}Pd_2(C_{24}H_{27}N_4O_2)](BF_4)^+$, M^+ = 702. I.r. spectrum (KBr disc): 3464br, 2925w, 1624s, 1573s, 1469m, 1439m, 1418m, 1375w, 1328s, 1287w, 1246w, 1197w, 1054br s, 840m, 752m, 652m, 533w, 522m and 400w cm^{-1}. U.V./vis. spectrum (CH_3CN): $\lambda_{max.}$ = 370nm. ($\varepsilon_{max.}$ = $11{,}150M^{-1}cm^{-1}$), 266 (54,700). ^1H n.m.r. spectrum (200.13MHz, CD_3CN, 298K): δ = 1.16p.p.m. (t, J = 7Hz, C-C$\underline{H}_2$-C, 4H); 2.75 (s, Ph-C$\underline{H}_3$, 6H); 2.96 (dd, J = 7Hz, N-C$\underline{H}_2$-C, 8H); 7.20-7.70 (m, Ph-$\underline{H}$, 4H). No other peaks found < 15.00p.p.m. ^{13}C DEPT n.m.r. spectrum (50.32MHz, CD_3CN, 298K): δ = 7.91p.p.m. (Ph-$\underline{C}H_3$); 45.50 (C-$\underline{C}H_2$-C); 58.68 (N-$\underline{C}H_2$-C); 144.63 (aromatic $\underline{C}$-H); 163.98 (-$\underline{C}$H=N).

4.4.5b: Alternative Synthesis of $[Pd_2(\underline{1})](BF_4)_2$

$[Pd(CH_3CN)_4](BF_4)_2$ [242] (48.2mg, 0.11mmol) and $[(\underline{1}H_4)](BF_4)_2$ (30.0mg, 0.05mmol) were dissolved in distilled, degassed CH_3CN ($10cm^3$) under N_2 to give an orange solution. $N(C_2H_5)_3$ ($0.10cm^3$, 0.72mmol) was added and the solution was refluxed for 4 hours under N_2 to give a yellow solid and brown solution. The volume of solvent was reduced to $5cm^3$ and diethyl ether was added. The yellow solid formed was filtered, washed with diethyl ether and recrystallised from CH_3NO_2. The brown crystalline solid obtained was dried *in vacuo*. Yield = 33mg, 80%. Elemental analysis: found C = 36.3; H = 3.55; N = 7.80%. Calculated for $[Pd_2(C_{24}H_{26}N_4O_2)](BF_4)_2.CH_3NO_2.\frac{1}{2}C_4H_{10}O$: C = 36.6; H = 3.86; N = 7.90%. F.a.b. mass spectrum (3-NOBA matrix): found M^+ = 616, 702. Calculated for: $[^{106}Pd_2(C_{24}H_{28}N_4O_2)]^+$, M^+ = 616; $[^{106}Pd_2(C_{24}H_{27}N_4O_2)](BF_4)^+$, M^+ = 702. I.r. spectrum (KBr disc): 3422br, 2926w, 1624s, 1572m, 1545m, 1498w, 1450m, 1419w, 1384w, 1328m, 1286w, 1244w, 1195w, 1116m, 1057br s, 962w, 882w, 840m, 752w, 668w, 652w, 612w, 560w, 533w, 522w and 404w cm^{-1}.

4.4.5c: Single Crystal X-ray Structure of $[Pd_2(\underline{1})](BF_4)_2.2CH_3NO_2$

Vapour diffusion of diethyl ether into a solution of the complex in CH_3NO_2 gave brown crystals of crystallographic quality. To prevent crystal degradation as a result of solvent loss, a brown tablet was transferred from its cold mother liquor into a drop of mineral oil at 195K and mounted on the diffractometer which was equipped with an Oxford Cryosystems low-temperature device[253] operating at 150K.

Crystal Data:

$[Pd_2(C_{24}H_{26}N_4O_2)](BF_4)_2.2CH_3NO_2$ M = 911.03. Triclinic, space group

$P\bar{1}$, a = 7.545(4), b = 8.566(4), c = 13.057(7)Å, α = 101.30(4), β = 94.82(3), γ = 102.92(3)°, V = 799.2Å^3 (by least-squares refinement on diffraction angles for 26 reflections measured at $\pm\omega$ [24 < 2θ < 28°, λ = 0.71073Å]), Z = 1, D_c = 1.892gcm^{-3}, T = 150K. Crystal dimensions 0.23 x 0.19 x 0.12mm^3, μ(Mo-Kα) = 1.205mm^{-1}, F(000) = 452.

Data Collection and Processing:

Stöe STADI-4 four-circle diffractometer, ω-2θ scan mode using the learnt-profile method[199]. Graphite-monochromated Mo-Kα radiation; 2700 reflections measured ($2\theta_{max.}$ = 45°, h -8 → 8, k -9 → 9, l 0 → 14), 2045 unique data (R_{int} = 0.024), giving 1950 with $F > 4\sigma(F)$. No significant crystal decay, no absorption correction.

Structure Analysis and Refinement:

The Pd atom was located using a Patterson synthesis[201], and successive cycles of least-squares refinement and difference Fourier synthesis[201] identified the positions of all other atoms. During refinement some disorder of the BF_4^- anion was observed. This was modelled by using two superimposed, idealised BF_4^- units, centred at the same boron atom, and allowing the occupancies of the different tetrahedra to refine. At convergence, the occupancies of the two BF_4^- groups were 89 and 11%. The crystal lattice was found to contain two CH_3NO_2 molecules per cation. Anisotropic thermal parameters were refined for Pd, C, N, O, B and F (major positions). H atoms were located from a difference map and included in fixed, calculated positions. The weighting scheme $w^{-1} = \sigma^2(F) + 0.000056F^2$ gave satisfactory agreement analyses. At final convergence, R = 0.0342, R_w = 0.0413, S = 1.129 for 251 independent parameters, and the final difference Fourier synthesis showed no feature above +0.77 or below

$-0.89eÅ^{-3}$.

Atomic scattering factors were inlaid[201], except for Pd[254], molecular geometry calculations utilised *CALC*[202] and figures were produced by *SHELXTL PC*[255].

4.4.5d: Transmetallation of $[Pb_2(\underline{1})](NO_3)_2$ by Pd(II)

$[Pb_2(\underline{1})](NO_3)_2$ (113.0mg, 0.12mmol) and $[Pd(CH_3CO_2)_2]_3$ (57.0mg, 0.25mmol) were refluxed in CH_3CN ($10cm^3$) for 4 hours under N_2. A yellow solid and solution were obtained and the yellow solid was filtered, washed with diethyl ether and dried *in vacuo*. Yield = 155mg. $[Pd_2(\underline{1})](NO_3)_2$ was insoluble in common organic solvents and H_2O. F.a.b. mass spectrum (3-NOBA matrix): found M^+ = 511, 614, 676, 716, 778. Calculated for: $[^{106}Pd(C_{24}H_{29}N_4O_2)]^+$, M^+ = 511; $[^{106}Pd_2(C_{24}H_{26}N_4O_2)]^+$, M^+ = 614, $[^{106}Pd_2(C_{24}H_{26}N_4O_2)](NO_3)^+$, M^+ = 676; $[^{106}Pd^{208}Pb(C_{24}H_{26}N_4O_2)]^+$, M^+ = 716; $[^{106}Pd^{208}Pb(C_{24}H_{26}N_4O_2)](NO_3)^+$, M^+ = 778. I.r. spectrum (KBr disc): 3426br, 2926w, 1624s, 1572s, 1385br s, 1328s, 1248w, 1198w, 1119m, 1015w, 937w, 840m, 752w, 663m, 618w and 524w cm^{-1}.

4.4.6: Attempted Synthesis of $[PdNi(\underline{1})](BF_4)_2$

$[Pd(CH_3CO_2)_2]_3$ (24.4mg, 0.11mmol) and $[(\underline{1}H_4)](BF_4)_2$ (60.0mg, 0.10mmol) were dissolved in CH_3CN and 1,8-bis(dimethylamino)naphthalene (46.5mg, 0.22mmol) was added. The solution was gently heated under N_2 for 30 minutes and then stirred for 2 hours. To the brown suspension formed, $[Ni(H_2O)_6](BF_4)_2$ (37.0mg, 0.11mmol) and 1,8-bis(dimethylamino)naphthalene (46.5mg, 0.22mmol) were added. The mixture was heated gently for 30 minutes and then stirred for 24 hours. A very dark, fine solid and a brown solution was formed which was filtered and the dark solid washed with

CH_3CN. The CH_3CN washings and brown solution were evaporated to $5cm^3$ and diethyl ether was added. A brown solid was obtained which was filtered, washed with diethyl ether, recrystallised from CH_3CN/diethyl ether and dried *in vacuo*. F.a.b. mass spectrum (3-NOBA matrix): found M^+ = 518, 616, 701. Calculated for: $[^{58}Ni_2(C_{24}H_{26}N_4O_2)]^+$, M^+ = 518; $[^{106}Pd_2(C_{24}H_{28}N_4O_2)]^+$, M^+ = 616; $[^{106}Pd_2(C_{24}H_{26}N_4O_2)](BF_4)^+$, M^+ = 701. I.r. spectrum (KBr disc): 3472br, 3001w, 1625s, 1576m, 1517w, 1472s, 1412w, 1377w, 1329w, 1300w, 1280w, 1225m, 1196w, 1031br s, 841s, 781s, 584br, 522m, 476br, and 414m cm^{-1}.

4.4.7: Synthesis of Pt(II) Complexes with $(1)^{2-}$

4.4.7a: Attempted Syntheses of $[Pt_2(1)]^{2+}$

$[PtCl_2(PhCN)_2]$ [245] (47.6mg, 0.14mmol) was dissolved in CH_3CN ($10cm^3$) and $[(1H_4)](BF_4)_2$ (38.0mg, 0.06mmol) and 1,8-bis(dimethylamino)naphthalene (94.0mg, 0.44mmol) were added. The initial yellow solution was refluxed vigorously for 24 hours under N_2 to give a brown solution. The solution was reduced in volume, diethyl ether was added and a dark green solid was obtained. This was filtered from the brown filtrate, washed with diethyl ether and dried *in vacuo*. Metallic Pt was deposited on the side of the reaction vessel. Yield = 23mg, 37%. F.a.b. mass spectrum (3-NOBA matrix): found M^+ = 598, 791 (very small). Calculated for: $[^{195}Pt(C_{24}H_{27}N_4O_2)]^+$, M^+ = 598; $[^{195}Pt_2(C_{24}H_{25}N_4O_2)]^+$, M^+ = 791. I.r. spectrum (KBr disc): 3470br s, 3001w, 2923w, 2102w, 1618m, 1576w, 1553w, 1516w, 1472m, 1411w, 1378w, 1300w, 1226w, 1029br s, 841m, 781m, 612br and 522m cm^{-1}.

4.4.7b:

$[PtCl_2(PhCN)_2]$ [245] (80.0mg, 0.17mmol), $TlPF_6$ (121.3mg, 0.35mmol), $[(\underline{1}H_4)](PF_6)_2$ (55.9mg, 0.08mmol) and $N(C_2H_5)_3$ (0.10cm^3, 0.72mmol) were refluxed for 12 hours in CH_3CN (10cm^3) under N_2. After cooling, a grey precipitate and brown solution were obtained. The grey precipitate was removed by centrifugation (CARE: thallium salt!) and the brown solution was reduced in volume to 5cm^3 and diethyl ether was added. The brown solid obtained was filtered, washed with diethyl ether and dried *in vacuo*. Yield = 23mg, 30%. F.a.b. mass spectrum (3-NOBA matrix): found M^+ = 350, 407, 597. Calculated for: $[^{205}TlPF_6]^+$, M^+ = 350; $[C_{24}H_{31}N_4O_2]^+$, M^+ = 407; $[^{195}Pt(C_{24}H_{26}N_4O_2)]^+$, M^+ = 597. I.r. spectrum (KBr disc): 3638w, 3371w, 3214w, 2940w, 1621s, 1600sh, 1553s, 1455s, 1401m, 1339w, 1307w, 1237m, 1206w, 1038w, 845s, 764w, 740w, 705w and 558s cm^{-1}.

4.4.8: **Attempted Synthesis of a Pt(II) Complex of $(\underline{5})^{2-}$**

$[PtCl_2(PhCN)_2]$ (80.3mg, 0.17mmol), $[(\underline{5}H_4)](PF_6)_2$ (58.0mg, 0.08mmol) and 1,8-bis(dimethylamino)naphthalene (107.0mg, 0.50mmol) were dissolved in CH_3CN (15cm^3) and refluxed for 24 hours. An orange solid was precipitated which was filtered, washed with diethyl ether and dried. F.a.b. mass spectrum (CH_3CN/3-NOBA matrix): matrix peaks only observed. I.r. spectrum (KBr disc): 3454br, 2920w, 1637s, 1532s, 1450m, 1386w, 1332w, 1305w, 1260w, 1220w, 1194w, 1030w, 986w, 840m, 765w, 668w, 559w and 504w cm^{-1}.

4.4.9: Synthesis of Rh(III) Complexes of $(\underline{1})^{2-}$

4.4.9a: Attempted Synthesis of $[Rh_2Cl_2(\underline{1})](BF_4)_2$

$RhCl_3.3H_2O$ (37.0mg, 0.14mmol) and $[(\underline{1}H_4)](BF_4)_2$ (37.0mg, 0.06mmol) were placed in degassed CH_3CN ($10cm^3$) and $N(C_2H_5)_3$ ($0.15cm^3$, 1.00mmol) was added. The brown mixture was refluxed under N_2 for 3 hours to give a brown solution and solid. On cooling, $TlBF_4$ (82.0mg, 0.28mmol) was added and refluxed for 6 hours. The grey precipitate obtained was removed by centrifugation (CARE: thallium salt!) to give a clear, red solution. The solution was reduced in volume to $5cm^3$ and added to diethyl ether. A red oil was obtained that, on attempted recrystallisation from CH_2Cl_2/hexane, gave another red oil. H_2O was added and an orange precipitate and solution was obtained. The orange solution was removed by filtration and the orange solid was recrystallised from CH_3CN/diethyl ether. Yield = 21mg. Elemental analysis: found C = 31.9; H = 4.05; N = 6.91%. Calculated for $[Rh_2Cl_2(C_{24}H_{26}N_4O_2)](BF_4)_2.CH_3CN.5H_2O$: C = 31.7; H = 4.00; N = 7.12%. F.a.b. mass spectrum (3-NOBA matrix): found M^+ = 608, 643, 678, 715. Calculated for: $[^{103}Rh_2(C_{24}H_{26}N_4O_2)]^+$, M^+ = 608; $[^{103}Rh_2{}^{35}Cl(C_{24}H_{26}N_4O_2)]^+$, M^+ = 643; $[^{103}Rh_2{}^{35}Cl_2(C_{24}H_{26}N_4O_2)]^+$, M^+ = 678; $[^{103}Rh_2{}^{35}Cl_2{}^{37}Cl(C_{24}H_{26}N_4O_2)]^+$, M^+ = 715. I.r. spectrum (KBr disc): 3432br, 2925w, 1628s, 1568m, 1465m, 1438m, 1320m, 1279w, 1244w, 1123m, 1084s, 834w, 756w, 647w, 568w, 522w, 442w and 416w cm^{-1}. U.V./vis. spectrum (CH_3CN): $\lambda_{max.}$ = 395nm. ($\varepsilon_{max.}$ = $4,200M^{-1}cm^{-1}$).

4.4.9b: Attempted Synthesis of $[Rh_2Cl_4(\underline{1})]$

$[(\underline{1}H_4)](PF_6)_2$ (68.5mg, 0.09mmol), Zn mesh (1.3mg, 0.02mmol) and $N(C_2H_5)_3$ ($0.10cm^3$, 0.72mmol) were mixed in degassed CH_3CN under N_2 to give a yellow suspension. $RhCl_3.3H_2O$ (50.0mg, 0.19mmol) was added and the mixture was refluxed under N_2 for 5 hours. A yellow suspension was obtained

that was evaporated to dryness and washed with 2 x 20cm^3 distilled H_2O. The yellow supernatant was removed by filtration to leave an orange solid that was recrystallised from CH_3CN/diethyl ether and dried *in vacuo*. Yield = 66mg, 75%. F.a.b mass spectrum (3-NOBA matrix): found M^+ = 678, 715. Calculated for: $[^{103}Rh_2{}^{35}Cl_2(C_{24}H_{26}N_4O_2)]^+$, M^+ = 678; $[^{103}Rh_2{}^{35}Cl_2{}^{37}Cl(C_{24}H_{26}N_4O_2)]^+$, M^+ = 715. I.r. spectrum (KBr disc): 3428br, 2928w, 1627s, 1551s, 1466m, 1323m, 1283m, 1239m, 1119w, 1087w, 1042w, 843s, 754w, 646w, 558s and 522w cm^{-1}.

4.4.9c: Attempted Synthesis of $[Rh_2(1)(CH_3CN)_4](BF_4)_4$

$[(1H_4)](BF_4)_2$ (37.0mg, 0.06mmol), $RhCl_3.3H_2O$ (37.0mg, 0.14mmol) and $N(C_2H_5)_3$ (0.180M solution in C_2H_5OH, 2cm^3, 0.36mmol) were stirred in degassed C_2H_5OH (5cm^3) under N_2 and refluxed for 96 hours under N_2. A brick-red solid was obtained which was filtered and washed with diethyl ether. I.r spectrum (KBr disc): 3450br, 2932w, 1627s, 1548s, 1456s, 1317w, 1242w, 1150w, 1117w, 1084w, 1033w, 867w, 817w, 767w and 550br w cm^{-1}. The brick-red solid was added to degassed CH_3CN (10cm^3) with $TlBF_4$ (81.5mg, 0.28mmol) and the mixture was refluxed under N_2 for 96 hours. The grey solid that was formed was removed by centrifugation (CARE: thallium salt!) to leave a clear, brown solution. Attempts to isolate solid material from this solution resulted in unanalysable oils.

4.4.9d: Attempted Transmetallation of $[Pb_2(1)](NO_3)_2$ with Rh(III)

$[Pb_2(1)](NO_3)_2$ (69.7mg, 0.07mmol) and $RhCl_3.3H_2O$ (40.0mg, 0.15mmol) were refluxed in dry, degassed CH_3CN (5cm^3) under N_2 for 5 hours to give an orange solid and solution. The orange solid was removed by filtration and excess NH_4PF_6 was added to the solution. The solution was evaporated down to 5cm^3 and diethyl ether was added to give an orange

solid. This was filtered, washed with diethyl ether, recrystallised from CH_3CN/diethyl ether and dried *in vacuo*. Yield = 45mg. F.a.b. mass spectrum (3-NOBA matrix): found M^+ = 405, 506, 541, 577, 678, 715. Calculated for: $[C_{24}H_{29}N_4O_2]^+$, M^+ = 405; $[^{103}Rh(C_{24}H_{27}N_4O_2)]^+$, M^+ = 506; $[^{103}Rh^{35}Cl(C_{24}H_{27}N_4O_2)]^+$, M^+ = 541; $[^{103}Rh^{35}Cl_2(C_{24}H_{28}N_4O_2)]^+$, M^+ = 577; $[^{103}Rh_2{}^{35}Cl_2(C_{24}H_{26}N_4O_2)]^+$, M^+ = 678; $[^{103}Rh_2{}^{35}Cl_2{}^{37}Cl(C_{24}H_{26}N_4O_2)]^+$, M^+ = 715. I.r. spectrum (KBr disc): 3334m, 3147br, 3037m, 1664s, 1554s, 1437m, 1401s, 1278w, 1238w, 1119w, 834s, 558s and 406w cm^{-1}.

4.4.10: Synthesis of Rh(I) Complexes of $(\underline{1})^{2-}$

$[(\underline{1}H_4)](PF_6)_2$ (52.2mg, 0.07mmol), $[Rh(CO)_2Cl]_2$ (30.6mg, 0.07mmol) and 1,8-bis(dimethylamino)naphthalene (160.0mg, 0.75mmol) were added to degassed $(CH_3)_2CO$ ($5cm^3$) and stirred under N_2 for 90 minutes, with occasional degassing of the solution. A brown suspension was formed that was filtered under N_2 to give a brown solid and brown solution. Further crops of the brown solid were obtainable by allowing the brown solution to stand. The brown solid was washed with degassed diethyl ether and dried *in vacuo*. Yield = 37mg. F.a.b. mass spectrum (3-NOBA matrix): found M^+ = 508, 609. Calculated for: $[^{103}Rh(C_{24}H_{29}N_4O_2)]^+$, M^+ = 508; $[^{103}Rh_2(C_{24}H_{27}N_4O_2)]^+$, M^+ = 609. I.r. spectrum (KBr disc): 3448br, 2922w, 2079vs, 2002vs, 1621s, 1547s, 1450m, 1400w, 1310w, 1236w, 1130w, 1045w, 840w, 766w, 615w, 558w and 521w cm^{-1}.

CHAPTER 5

The Synthesis and Characterisation of the Ni(II) Complex of the Ligand $(\underline{22})^{2-}$, the Thiophenolate Analogue of $(\underline{1})^{2-}$

5.1: Introduction

In Chapters 2, 3 and 4 of this thesis complexes of ligand $(\underline{1})^{2-}$ with first, second and third row transition metal ions have been described. The complexed metal ions can adopt a range of co-ordination geometries, indicating that the binucleating ligand $(\underline{1})^{2-}$ can be co-ordinatively flexible. The co-ordination modes of ligand $(\underline{1})^{2-}$ have been further extended by the inclusion of additional donor groups such as phenols and alcohols in the side-arms of $(\underline{1})^{2-}$. This work is discussed in Section 2.6 above. We proposed that the binucleating framework of $(\underline{1})^{2-}$ could be manipulated further by exchanging the phenoxy O-donors for thiophenolate S-donors to give the macrocyclic ligand $(\underline{22})^{2-}$. The modified donor set would give an increased scope for potential binuclear metal complexes, particularly with respect to our aim of synthesizing binuclear complexes of the platinum group metals. We proposed that the less polarising thiophenolate ligands would bind the "softer" second and third row metals more strongly than the phenoxy O-donors, with the square-planar array of donors being particularly suited for complexation with d^8, low spin metal centres.

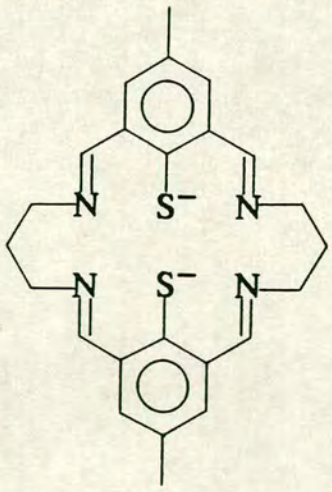

Figure 5.1 $(\underline{22})^{2-}$

There are numerous examples in the literature of thiophenolate ligands co-ordinating to metal centres[256]. We concluded from these reports that

complexes of the thiophenolate bridged ligand, $(\underline{22})^{2-}$, will have significantly different chemical properties to the complexes of $(\underline{1})^{2-}$. This is a result of the different electron configurations, orbital hybridisations and orbital availabilities at the bridging S- or O-donor atoms[256]. For example, iron-sulphur-cubane clusters containing thiophenolate ligands, such as $[\{(SPh)_3Fe_3MoS_4\}_2(\mu\text{-}SPh)_3]^{3-}$ [257], show two sequential one-electron electrochemical reductions and the reduced species $[\{(SPh)_3Fe_3MoS_4\}_2(\mu\text{-}SPh)_3]^{5-}$ can liberate H_2 from thiophenol[258]. This reactivity is dependent on the basic properties of the co-ordinated thiophenolate and is illustrative of the fact that the availability of electron density at S-donors is generally greater than at O-donors of analogous phenolate complexes[259]. This is rationalised in terms of the S-atom being less able to transfer electron density to the metal atom by π-donation and the lesser delocalisation of thiophenols than phenols due to poor overlap of the S(3p) orbital with the ring π-orbitals. There is also the possibility of thiophenolate donors possessing greater π-accepting properties than phenolates.

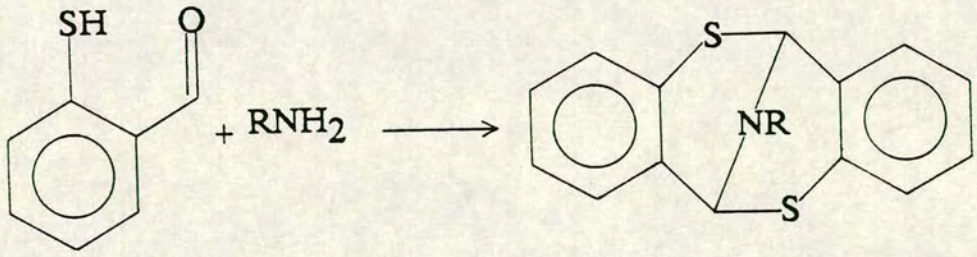

Figure 5.2 Cyclic condensation product of tsalen

In contrast to phenols, thiophenols can undergo redox reactions at the S-heteroatom, by either a one-electron oxidation to give a coupled disulphide or four- and six-electron oxidations to sulphonic acid derivatives. These oxidations are generally undesirable side-reactions in the formation of metal complexes of thiophenolates, but complexes have been formed with intact disulphide bridges acting as ligands[260]. Difficulties with unwanted redox reactions have been reported with the synthesis of metal complexes with *o*-mercaptobenzaldehyde and *o*-mercaptobenzaldimines[261-267]. The *o*-mercaptobenzaldimines include the thiophenol analogue of salen (tsalen) and West and co-workers have isolated the Fe(II)[265,268,269], Co(II)/(III)[262,270] and Cu(II)[264] complexes with tsalen. In the synthesis of [Co(tsalen)][262], West and Corrigan found that the presence of the templating Co(II) ion was essential before addition of the diamine, since the free tsalen ligand would rapidly react to form a bicyclic product[263] shown in Figure 5.2. Solutions of [Fe(tsalen)] in pyridine are unstable in air and [Fe(tsalen)] reacts with CO to form a monocarbonyl complex [Fe(tsalen)(CO)(pyridine)] and with O_2 to form the Fe(III) μ-oxo-bridged [{Fe(tsalen)}$_2$O](pyridine)[265,271].

The Ni(II) complexes with thiophenolate ligands are of particular interest, since a Ni(II) site with predominantly S-ligands has been implicated in the function of CO dehydrogenase (CODH). CODH catalyzes the reversible reduction of CO_2 to CO and the synthesis of acetyl coenzyme A [272] in certain autotrophic bacteria.

The complex [Ni(tsalen)] and its derivatives have been reported[266,267,273] and the single crystal X-ray structure of [Ni(tsalen)] [267] shows the Ni(II) co-ordinated to a square-plane arrangement of two thiophenolate S- and two imine N-donors, in an analogous fashion to [Ni(salen)]. The formation of cyclic product shown in Figure 5.2 does not compete with the formation of the [Ni(tsalen)] complex since the

complexation reaction occurs so rapidly. However, the crystals of [Ni(tsalen)] were obtained using a novel synthesis that avoided isolation of the free *o*-mercaptobenzaldehyde by protecting the thiophenol groups with $-C(CH_3)_3$ (Figure 5.3)[267]. The reaction of the protected tsalen ligand with $Ni(CH_3CO_2)_2$ removed the protecting group *in situ* to form the metal complex.

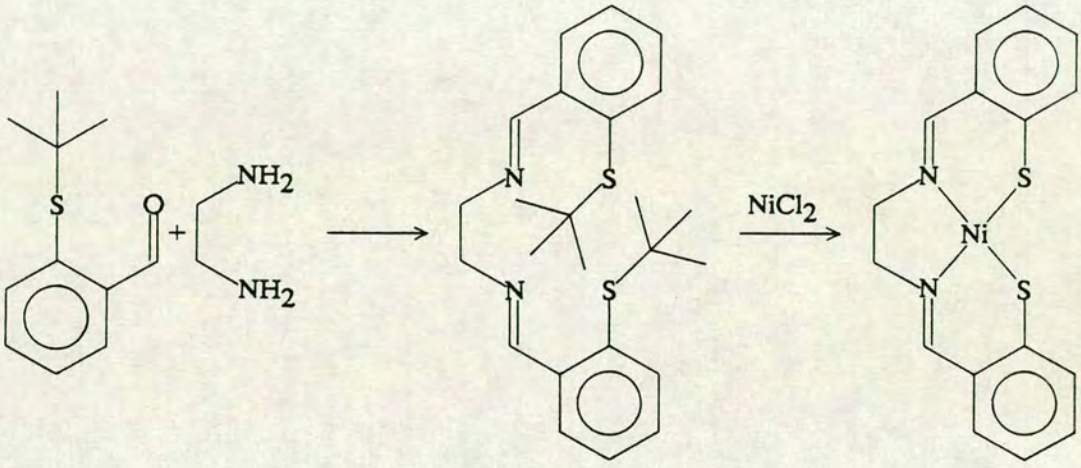

Figure 5.3 Synthesis of [Ni(tsalen)]

Fenton *et al.* have also reported the successful synthesis of $[Ni(Me_2tsalen)]$[266] forming $[Ni\{1-(2-mercaptophenyl)ethanone\}_2]$ before the addition of the diamine, by the method of West[262]. With Cu(II), however, $[Cu\{1-(2-mercaptophenyl)ethanone\}_2]$ could not be formed[266] and white crystals of the disulphide were obtained. This is presumably as a result of the oxidation of 1-(2-mercaptophenyl)ethanone by the reduction of Cu(II) to Cu(I).

Robson and co-workers[274-278] have synthesised a series of Ni(II), Cu(II) and Pd(II) binuclear compounds with acyclic ligands $(\underline{23})^{n-}$ (Figure 5.4) that are based on the thiophenol analogues of $(\underline{21})^{3-}$ (in Section 4.2.8 above). The ligands have a single, bridging thiophenolate bonding to both metal centres and a variety of sidearms have been employed with O- [274-277],

N- [278] and S-donors[275]. The vacant co-ordination site is occupied by a range of bridging ligands (X) such as pyrazolate$^-$, iminazolate$^-$, thiolate$^-$, halide$^-$, N_3^-, NO_2^- and $CH_3CO_2^-$. The ligands have been prepared by the reaction of 2,6-diformyl-4-methyl-*N*,*N*-dimethylcarbamoylthiophenol with two equivalents of the appropriate amine reagent for the side-arms, to give the S-protected ligand precursor. The metal complexes are formed by reaction of a metal(II) salt with the S-protected ligand precursor with S-deprotection occuring *in situ*. The Cu(II) complexes synthesised by this method are the first binuclear Cu(II) complexes reported in the literature with bridging thiolates[279,280].

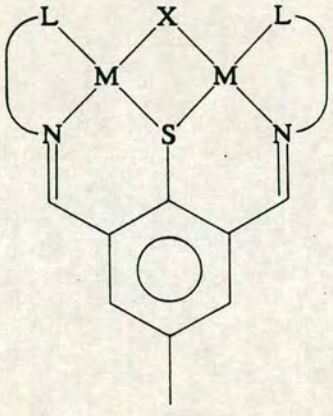

M = Ni^{2+}, Cu^{2+}, Pd^{2+}

X = RCO_2^-, halide$^-$, N_3^-, dppm, RO^-, OH^-, NO_2^-,

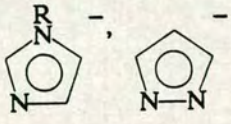

L = N, O and S donors

Figure 5.4 $[M_2(\underline{23})X]^{n+}$

We proposed that the macrocyclic ligand $(\underline{22})^{2-}$ could be synthesised either by a template synthesis around two metal ions or as the protonated or neutral free ligand species, using 2,6-diformyl-4-methyl-*N*,*N*-dimethylcarbamoylthiophenol as a starting material. The stereochemical requirements of $(\underline{22})^{2-}$ will be different from those of $(\underline{1})^{2-}$ and changes in the ring structure and in the size of the macrocyclic cavity are expected. In particular, the longer C-S bonds and the larger S-atoms of $(\underline{22})^{2-}$ have to

be accommodated within the macrocyclic framework without prohibitive ring strain and electronic and steric interactions in the macrocyclic cavity. However, in Chapter 3, we have reported the folded structure of the free ligand $[(\underline{1}H_4)]^{2+}$ which illustrates the flexibility of the macrocyclic structure about the propylene side-arms. Folding of $(\underline{22})^{2-}$, as observed for $[\underline{1}H_4]^{2+}$, would relieve the steric crowding within the macrocyclic cavity. Partial folding of the macrocycle $(\underline{1})^{2-}$ has also been reported in Chapter 4 for the complex $[Ni_2(\underline{1})(CH_3CO_2)]_2^{2+}$. Non-planar conformations of $(\underline{22})^{2-}$ might be further encouraged by the preference of thiophenolates for a pyramidal geometry about the S-donors, in comparison to the trigonal-planar geometries which are usually (but not exclusively) found about phenolate O-donors. Finally, we proposed that the ligand $(\underline{22})^{2-}$ might also be synthesised in an oxidised form ($\underline{22}$), with a disulphide bridge coupling the two S-atoms. This could still be used for complexation reactions, by oxidatively adding low oxidation-state metal centres across the disulphide group on co-ordination to the imino ligands. Reactions of this type have been described by West[269], in the synthesis of [Fe(tsalen)] using $Fe(CO)_5$, and by other workers[281,282].

5.2: Results and Discussion

5.2.1: The Synthesis of 2,6-diformyl-4-methyl-*N*,*N*-dimethylcarbamoylthiophenol

2,6-Diformyl-4-methyl-*N*,*N*-dimethylcarbamoylthiophenol was prepared by the conversion of phenols to thiophenols first described by Newman and Karnes[283] and by the method of Robson[284]. The synthesis is shown schematically in Figure 5.5. The reaction of 2,6-diformyl-4-methylphenol with *N*,*N*-dimethylthiocarbamoyl chloride proceeds in good yield in basic DMF, to give 2,6-diformyl-4-methyl-*N*,*N*-dimethylthiocarbamoylphenol. The f.a.b. mass spectrum of this product shows peaks at M^+ = 252, 218 and 178 which are

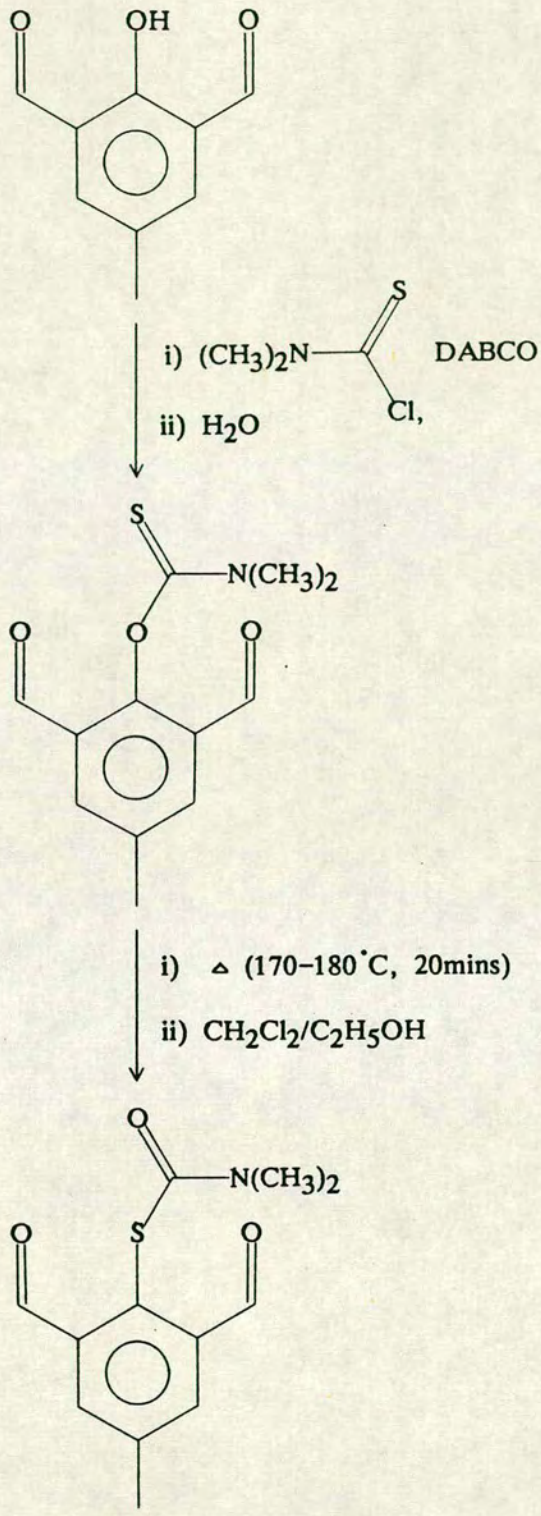

Figure 5.5 Synthesis of 2,6–diformyl–4–methyl–*N*,N–dimethylcarbamoylthiophenol

assigned to $[C_{12}H_{14}NO_3S]^+$ (the molecular ion, MH^+), $[C_{12}H_{12}NO_3]^+$ ($[M-SH_2]^+$) and $[C_{10}H_8O_3]^+$ ($[M-NC_2H_6S]^+$ respectively. These peaks are consistent with being the breakdown products of 2,6-diformyl-4-methyl-*N*,*N*-dimethylthiocarbamoylphenol. The i.r. spectrum of 2,6-diformyl-4-methyl-*N*,*N*-dimethylthiocarbamoylphenol shows a number of strong bands. There is only one absorption due to a C=O stretching vibration, at 1683cm^{-1}, and absorptions at 1548 and 1193cm^{-1} are characteristic of O-aryl dialkylthiocarbonates[283]. The synthesis of 2,6-diformyl-4-methyl-*N*,*N*-dimethylcarbamoylthiophenol was continued without further characterisation of 2,6-diformyl-4-methyl-*N*,*N*-dimethylthiocarbamoylphenol.

The pyrolysis of 2,6-diformyl-4-methyl-*N*,*N*-dimethylthiocarbamoylphenol at 443-453K under N_2 gave a very dark melt, which on recrystallisation from CH_2Cl_2/CH_3CH_2OH gave yellow needles. The f.a.b. mass spectrum of this yellow product shows peaks at M^+ = 252 and 72, which are assigned to $[C_{12}H_{14}NO_3S]^+$ and $[C_3H_6NO]^+$ ($[M-C_9H_8O_2S]^+$) respectively. The e.i. mass spectrum shows these peaks and an additional peak at M^+ = 179 which is assigned to $[C_9H_7O_2S]^+$. These peaks are consistent with being the breakdown products of 2,6-diformyl-4-methyl-*N*,*N*-dimethylcarbamoylthiophenol. The i.r. spectrum of the yellow needles shows two C=O stretching vibrations, at 1688 and 1664cm^{-1}, which are assigned to the aldehydic and carbamoyl C=O stretching vibrations respectively. The characteristic absorptions in the regions 1560-1530 and 1230-1190cm^{-1} for O-aryl dialkylthiocarbonates are now absent. This data, together with elemental analysis data, confirm that the pyrolysis rearrangement had gone to completion and the product to be 2,6-diformyl-4-methyl-*N*,*N*-dimethylcarbamoylthiophenol.

The ^1H n.m.r. of 2,6-diformyl-4-methyl-*N*,*N*-dimethylcarbamoylthiophenol in $CDCl_3$ at 298K can be readily assigned to the

proposed structure (see Section 5.4.1). Interestingly, the methyl resonances for $-N-(C\underline{H}_3)_2$ are observed as a broadened doublet. This behaviour is often observed for protons adjacent to amide groups and is attributed to resticted rotation about the amido N–C bond. The canonical forms of a general amide group shown in Figure 5.6 describe the source of this restricted rotation because of the partial double-bond character to the N–C bond.

Figure 5.6 Canonical structures of an amide

Carbon: 1, δ = 20.90;

2a and 2b, δ = 37.06 and 37.20;

3, 4, 5, 6, δ = 131.75, 133.85, 138.05 and 140.86;

7, δ = 163.64;

8, δ = 190.22.

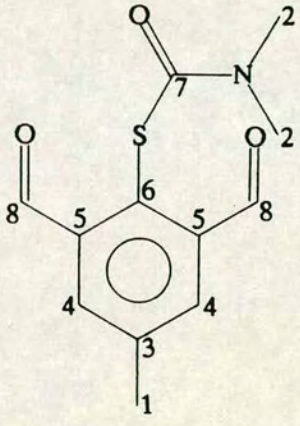

Figure 5.7 2,6–Diformyl–4–methyl–*N*,*N*–dimethylcarbamoylthiophenol and ^{13}C n.m.r. assignments

The ^{13}C n.m.r. of 2,6–diformyl–4–methyl–*N*,*N*–dimethylcarbamoylthiophenol in $CDCl_3$ at 298K adds further evidence to the proposal of restricted rotation about the amido N–C bond, by the appearence of two close resonances at 37.20 and 37.06p.p.m. which are assigned to two

distinct carbon environments in the $-N-(\underline{C}H_3)_2$ group. Other assignments from the ^{13}C n.m.r. for 2,6-diformyl-4-methyl-*N*,*N*-dimethylcarbamoylthiophenol are shown in Figure 5.7.

The mechanism of the rearrangement of O-aryl dimethylthiocarbamates has been discussed[283] and the conversion of O-*p*-nitrophenyl dimethylthiocarbamate to S-*p*-nitrophenyl dimethylthiocarbamate has been shown to be a first-order reaction[283]. This indicates that the rearrangement is an intramolecular process. It has also been found[283] that compounds with electron-withdrawing groups in *para* positions on the phenyl rings rearrange more readily than those with electron-donating groups. On the basis of this evidence the mechanism in Figure 5.8 has been proposed[283]. It is also noteworthy that 2-(acetylphenyl)phenol required protection as a ketal for the phenol → thiophenol rearrangement to occur[283], while 2,6-diformyl-4-methylphenol can undergo the rearrangement with no protection.

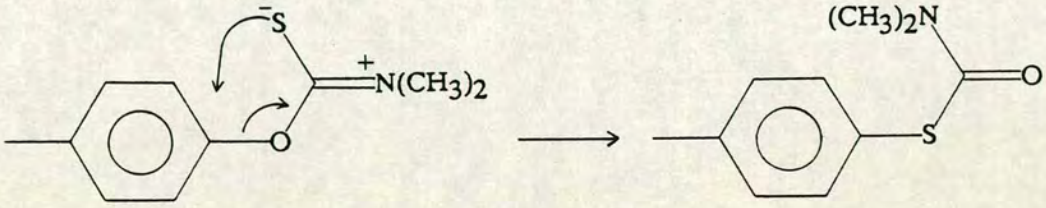

Figure 5.8 Proposed mechanism for phenol → thiophenol rearrangement

5.2.2: The Synthesis of 2,6-diformyl-4-methylthiophenol

In order to synthesize the free ligand ($\underline{22}H_2$) or protonated ligand $[(\underline{22}H_4)]^{2+}$, we thought that it might be necessary to deprotect 2,6-diformyl-4-methyl-*N*,*N*-dimethylcarbamoylthiophenol by removal of the carbamoyl species. However, being uncertain whether this was a necessary step, we attempted syntheses of the unmetallated ligand and of the complexed

ligand $(\underline{22})^{2-}$ (in template reactions) with both 2,6-diformyl-4-methylthiophenol and 2,6-diformyl-4-methyl-*N*,*N*-dimethylcarbamoylthiophenol. Robson[284] appears never to have isolated the free thiophenol, since complexation reactions with Ni(II), Pd(II) or Cu(II) and ligands derived from 2,6-diformyl-4-methyl-*N*,*N*-dimethylcarbamoylthiophenol deprotect the thiophenolate *in situ* to form the complexes $[M_2(\underline{22})X]^{n+}$ as described in Section 5.1. Newman and Karnes[283] reported that thiophenols could be generated from the *N*,*N*-dimethylcarbamoylthiophenols by reaction with NaOH, but no experimental procedures were given. Details of the preparation of 2,6-diformyl-4-methylthiophenol are given in Section 5.4.2 and are discussed here.

The reaction of 2,6-diformyl-4-methyl-*N*,*N*-dimethylcarbamoylthiophenol with an excess of NaOH in CH_3OH under N_2 gave a clear orange solution. Acidification of the solution with aqueous HCl under N_2 gave a gummy white precipitate, which was extracted into CH_2Cl_2 under N_2. A white precipitate was obtained on addition of hexane to the CH_2Cl_2 solution. Recrystallisation of the white precipitate from C_6H_6/hexane gave off-white needles. The e.i. mass spectrum of the off-white needles shows peaks at M^+ = 180, 152 and 118 which are assigned as $[C_9H_8O_2S]^+$ (M^+), $[C_8H_8OS]^+$ ($[M-CO]^+$) and $[C_8H_6O]^+$ ($[M-CH_2OS]^+$) respectively. The i.r. spectrum of the off-white needles shows only one strong band for a C=O stretching vibration, at $1683cm^{-1}$ implying that the carbomoyl protecting group had been removed. The very weak absorption at $2737cm^{-1}$ is tentatively assigned to a S-H stretch. This evidence, together with elemental analytical data, confirm the product to be 2,6-diformyl-4-methylthiophenol. The deprotection was not attempted in air, so it is unknown which, if any, of the products are air-sensitive.

The ^1H n.m.r. spectrum of 2,6-diformyl-4-methylthiophenol in $CDCl_3$ at

298K also confirms, by the absence of the $-C\underline{H}_3$ protons from the spectrum, that the $-CO-N(CH_3)_2$ group has been removed. The spectrum also shows broadened and complicated structures for the S–H and Ar–H resonances. In the ^{13}C n.m.r. spectrum of 2,6–diformyl–4–methylthiophenol, multiplets are also observed in the aromatic C and C=O regions. The assignments for the ^1H and ^{13}C n.m.r. are made in Section 5.4.2. It is not clear whether the complicated resonances are due to second–order effects or impurities, although the same sample was used to obtain the n.m.r. spectra and the elemental analysis.

5.2.3: The Attempted Syntheses of $[(22H_4)]^{2+}$

Attempts to synthesize $[(22H_4)]^{2+}$ as a metal–free ligand were made using 2,6–diformyl–4–methyl–*N*,*N*–dimethylcarbamoylthiophenol or 2,6–diformyl–4–methylthiophenol as the starting material. The reaction of one equivalent of 2,6–diformyl–4–methyl–*N*,*N*–dimethylcarbamoylthiophenol with one equivalent of 1,3–diaminopropane in refluxing CH_3OH in the presence of HBr (48% in H_2O) gave a red/brown solution. No precipitate was obtained on addition of excess $NaBF_4$ and cooling. The solution was evaporated down to dryness and a brown solution was obtained on extraction with CH_3NO_2. Addition of diethyl ether to the brown solution gave a brown solid. The f.a.b. mass spectrum of the brown solid shows peaks at M^+ = 199, 352 and 436 (weak), which are assigned as $[C_9H_{11}O_3S]^+$, an unknown product and, possibly $[(22H_2)]^+$ respectively. The i.r. spectrum of the brown solid shows a large number of absorptions for O–H and N–H stretching vibrations at 3426 and 2600–2400cm^{-1} respectively and there is no strong absorption for C=N stretching vibrations. This data, and the lack of elemental analytical data that agree with the proposed formulation $[(22H_4)](BF_4)_2$, suggest that significant amounts of $[(22H_4)](BF_4)_2$ had not been formed in this reaction.

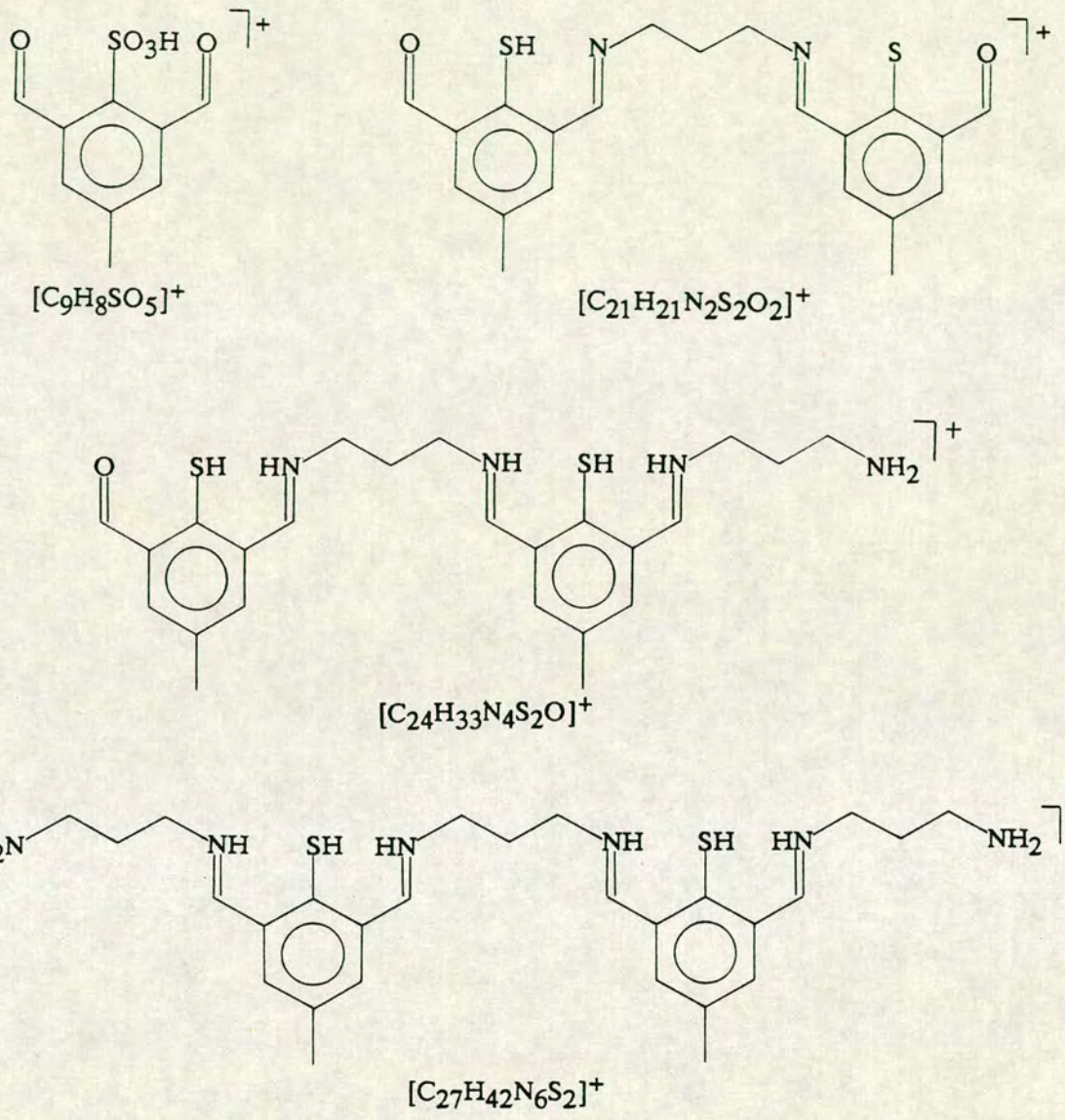

Figure 5.9 Possible acyclic products from the condensation of 2,6-diformyl-4-methylthiophenol and 1,3-diaminopropane in acidic CH_3OH

Using one equivalent of 2,6-diformyl-4-methylthiophenol and one equivalent of 1,3-diaminopropane in refluxing CH_3OH with excess HBr (48% in H_2O), a brown precipitate was obtained. No change was observed on addition of an excess of NH_4PF_6. The brown mixture was evaporated to dryness and a brown solution was obtained on extraction with CH_3NO_2. Addition of diethyl ether to the brown solution gave a gummy brown solid.

The f.a.b. mass spectrum of this brown solid indicates that a number of products had been formed, with peaks being observed at M^+ = 228, 381, 457, 514 and 527. These are assigned to the products $[C_9H_8SO_5]^+$, $[C_{21}H_{21}N_2S_2O]^+$, $[C_{24}H_{33}N_4S_2O]^+$, $[C_{27}H_{42}N_6S_2]^+$ and $[C_{21}H_{22}N_2S_2O](PF_6)^+$ respectively, the proposed structures of which are shown in Figure 5.9. If these suggested products are correct, then cyclisation has not occurred and only acyclic products have been obtained. The i.r. spectrum of the brown product only shows a strong absorption at 845cm^{-1}, which is assigned to P–F stretching vibrations, although there are other weaker absorptions at 1654 and 1555cm^{-1}, which are tentatively assigned to C=N and C–O stretching vibrations. On the basis of this data, it is concluded that condensation reactions with 2,6–diformyl–4–methylthiophenol and 1,3–diaminopropane do occur, but under these conditions give acyclic products of varying length. Manipulation of the reaction conditions, such as high dilution, slow addition of reactants or use of a different acidic medium are strategies that are potential improvements on the synthetic method.

5.2.4: The Attempted Synthesis of (22H$_2$)

The reaction of one equivalent of 2,6–diformyl–4–methylthiophenol with 1,3–diaminopropane in refluxing THF under N_2 gave a brown solution. An orange solid was obtained on addition of diethyl ether to the brown solution. The f.a.b. mass spectrum of this orange solid shows peaks at M^+ = 400 and 616 which are assigned as $[C_{21}H_{20}N_2S_2O_2]^+$ and $[C_{33}H_{32}N_4S_3O_2]^+$ respectively and are shown in Figure 5.10. The i.r. spectrum of the orange product has only a medium absorption in the C=N stretching region, at 1636cm^{-1}, and no strong bands at other frequencies. From this evidence, we suggest that acyclic products of varying length have again been prepared.

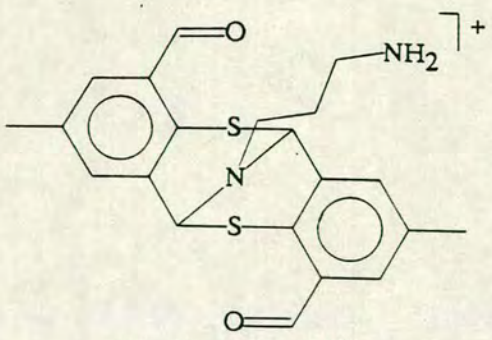

$[C_{21}H_{20}N_2S_2O_2]^+$

Figure 5.10 Possible product from the condensation of 2,6-diformyl-4-methylthiophenol and 1,3-diaminopropane in THF

The results obtained from attempted syntheses of $[\underline{22}H_4]^{2+}$ and $[(\underline{22}H_2)]$ indicate that the 2,6-diformyl-4-methylthiophenol with 1,3-diaminopropane does not undergo cyclic condensations as readily as 2,6-diformyl-4-methylphenol with 1,3-diaminopropane. This might be due to the increase in size of the bridging donor atom, which would be positioned in the centre of the macrocyclic cavity, on going from O to S. The increase in C-X bond length (X = O, S), when X = S, may also cause difficulties in the assembling of the cyclic structure. Robson and Hughes[274] have proposed that, provided that the entire system remains close to co-planar, substitution of the central O-donors for S-donors in $(\underline{1})^{2-}$ will have the following three consequences (shown diagramatically in Figure 5.11):

a) the angle subtended by co-ordinated protons or metal centres at the bridging S-donors (∠M-S-M) will be increased beyond the 100-110° observed with bridging O-atoms;

b) the metal-metal distances will be considerably increased from those observed for $[M_2(\underline{1})]^{n+}$;

c) the angle subtended at the co-ordinated protons or metal centres by the bridging S-donors (∠S-M-S) will be more acute than those observed for $[M_2(\underline{1})]^{n+}$.

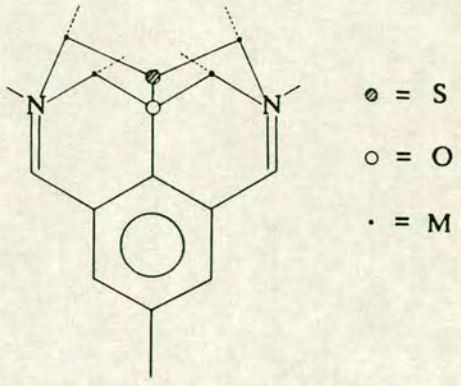

Figure 5.11 Implications of substituting bridging S–donors for O–donors in planar $(\underline{1})^{2-}$

However, Robson and Hughes stressed[274] that the planarity imposed on this model is unrealistic for bridging thiolates, which prefer pyramidal geometries about the S–atom. The resulting deviation from planarity will reduce the ∠M–S–M angle and cause strain in the side–arms, particularly angle strain at the imine nitrogens. On consideration of these arguments, we proposed that a macrocyclic ligand with 2,6–diformyl–4–methylthiophenol might be more readily obtained using $-C_4H_8-$ chains as the side–arms, rather than $-C_3H_6-$ groups. This would have the effect of increasing the macrocyclic cavity–size to accommodate the larger S–atoms, and of increasing the conformational flexibility of the side–arms.

5.2.5: The Attempted Synthesis of $[(\underline{24}H_4)](PF_6)_2$

The reaction of one equivalent of 2,6–diformyl–4–methylthiophenol with one equivalent of 1,4–diaminobutane in the presence of HBr (48% in H_2O) in refluxing CH_3OH gave a yellow solution. Addition of excess NH_4PF_6 and diethyl ether to the solution gave a yellow crystalline precipitate. The f.a.b. mass spectrum of this yellow solid shows peaks assignable to the 3–NOBA/CH_3CN matrix only. The i.r. spectrum of the yellow solid shows a strong band at 1399cm^{-1} which is tentatively assigned to the stretching vibrations of a $-SO_3-$ group. A large amount of H_2O also appears to be

included in the sample. The probable product of the reaction is, therefore, the sulphonic acid derivative of 2,6-diformyl-4-methylthiophenol, which has formed by aerial oxidation of the thiophenol in refluxing CH_3OH. It is possible that $[(\underline{24}H_4)](PF_6)_2$ might still be prepared using this synthesis but with the rigorous exclusion of air. The required experiments could not be performed, however, due to shortage of time.

5.4.6: The Attempted Syntheses of $[Pb_2(\underline{22})]^{2+}$

The use of main-group metals as templating agents has been well-established in the preparation of Schiff-base macrocycles[145,146,158,160]. For the synthesis of $(\underline{22})^{2-}$, we proposed that Pb(II) might be an ideal non-transition metal template, since a large number of compounds of Pb(II) with thiolates have been reported in the literature[295]. Therefore, a similar synthesis to that of Nag *et al.*[145] for $[Pb_2(\underline{1})](NO_3)_2$ was attempted. The reaction of one equivalent of 2,6-diformyl-4-methyl-*N,N*-dimethylcarbamoylthiophenol with one equivalent of 1,3-diaminopropane in the presence of $Pb(NO_3)_2$ and $Pb(CH_3CO_2)_2$ in refluxing DMF/CH_3OH gave a brown solid. The f.a.b. mass spectrum of this brown solid shows only peaks due to the 3-NOBA matrix. It is noted that in the f.a.b. mass spectrum of $[Pb_2(\underline{1})]^{2+}$, only peaks for the demetallated ligand and mononuclear Pb(II) salt were observed. However, in the above reaction, even the thiophenol analogues of these peaks are not seen. The i.r. spectrum of the brown solid shows absorptions at 1636 and 1384cm^{-1} which are tentatively assigned to C=N and N-O stretching vibrations. However, these bands do not have the intensities expected for these absorptions. The brown product could not be purified further due to its insolubility.

In order to obtain a more soluble product, a reaction to obtain a PF_6^- salt was performed. The reaction of one equivalent of

2,6-diformyl-4-methylthiophenol with one equivalent of 1,3-diaminopropane in the presence of one equivalent of $Pb(CH_3CO_2)_2$ in refluxing CH_3OH gave a orange suspension. Excess NH_4PF_6 was added to the suspension and an orange solid was precipitated. The orange solid was insoluble in common organic solvents. The f.a.b. mass spectrum of this orange solid shows only peaks due to the 3-NOBA matrix. The i.r. spectrum of the orange solid shows unidentified strong bands at 1044 and 983cm^{-1} and no strong absorption around 1620-1660cm^{-1}. Further characterisation was not attempted, since there is no evidence for $(\underline{22})^{2-}$ or its Pb(II) complex having been formed.

5.2.7: The Attempted Synthesis of $[Cu_2(\underline{22})](PF_6)_2$

To our knowledge, there are no reported attempts to synthesize complexes of $(\underline{22})^{2-}$ by template syntheses around transition metal centres. This is somewhat surprising considering the number of complexes of $(\underline{1})^{2-}$ which have been reported using this method. This fact may be due to complications with thiolates when using the most common templating agent, Cu(II), as a template (see Section 5.1). However, Robson and co-workers[275] have successfully isolated binuclear Cu(II) complexes with a bridging thiophenolate with acyclic ligands derived from 2,6-diformyl-4-methyl-*N*,*N*-dimethylcarbamoylthiophenol. This is unusual since Cu(II) centres are generally sufficiently oxidising to oxidise thiophenols to disulphides. Using 2,6-diformyl-4-methyl-*N*,*N*-dimethylcarbamoylthiophenol, the Cu(II) complexes can be prepared presumably because the substituents in the *ortho* positions to the thiophenol prevent the formation of disulphides due to their steric bulk. We therefore investigated whether $(\underline{22})^{2-}$ could be synthesized about Cu(II) templates using 2,6-diformyl-4-methyl-*N*,*N*-dimethylcarbamoylthiophenol as a starting material.

The reaction of one equivalent of 2,6-diformyl-4-methyl-*N*,*N*-dimethylcarbamoylthiophenol with one equivalent of 1,3-diaminopropane and $Cu(CH_3CO_2)_2.H_2O$ in the presence of excess NH_4PF_6 in refluxing $(CH_3)_2CO$ gave a very dark solution. Initially only very dark, viscous oils could be obtained from the reaction mixture. Washing the oil with H_2O formed a brown solid which could be collected. The f.a.b. mass spectrum of this brown solid shows a peak at $M^+ = 371$ which cannot be assigned in conjunction with the remaining data. The i.r. spectrum of the brown product shows strong bands at 1654 and 842cm^{-1}, which are assigned to C=N and P-F stretching vibrations respectively. Elemental analytical data indicate that $[Cu_2(\underline{22})](PF_6)_2$ has not been formed (found C = 43.1, H = 5.43, N = 6.40%; calculated for $[Cu_2(\underline{22})](PF_6)_2$: C = 33.8; H = 3.08; N = 6.58%. Approximate C : H : N ratio for the brown solid, 8 : 12 : 1; expected for $[Cu_2(\underline{22})](PF_6)_2$, 6 : 6.5 : 1). From this data and considering the difficulties in obtaining a solid product, the nature of this product cannot be determined.

5.2.8: The Attempted Synthesis of $[Ni_2(\underline{22})](PF_6)_2$ from 2,6-diformyl-4-methyl-*N*,*N*-dimethylcarbamoylthiophenol

The reaction of one equivalent of 2,6-diformyl-4-methyl-*N*,*N*-dimethylcarbamoylthiophenol with one equivalent of 1,3-diaminopropane and $Ni(CH_3CO_2)_2.4H_2O$ in the presence of excess NH_4PF_6 in refluxing $(CH_3)_2CO$ gave a red solution. On addition of diethyl ether to the red solution, a dark viscous oil was obtained, from which solid products could not be obtained initially. Washing the oil with H_2O gave a brown solid. The f.a.b. mass spectrum of the brown solid shows peaks at $M^+ = 72$ and 641 (weak), which are assigned as $[(CH_3)_2NCO]^+$ and tentatively $[^{58}Ni_2(\underline{22})(DMF)(H_2O)]^+$, as the latter has the correct isotope distribution

pattern for a binuclear Ni(II) species. The i.r. spectrum of the brown solid shows strong bands at 1657 and 845cm^{-1}, which are assigned to C=N and P–F stretching vibrations respectively. The i.r. spectrum of this brown product is similar to the brown solid described in Section 5.2.7. Elemental analytical data do not agree with a formulation for the product of $[Ni_2(\underline{22})](PF_6)_2$ (found C = 41.7, H = 6.00, N = 5.69%; calculated for $[Ni_2(\underline{22})](PF_6)_2$: C = 34.2; H = 3.11; N = 6.65%. Approximate C : H : N ratio for the brown solid, 17 : 29 : 2; expected for $[Ni_2(\underline{22})](PF_6)_2$, 6 : 6.5 : 1).

5.2.9: The Synthesis of $[Ni_2(\underline{22})](PF_6)_2$ from 2,6–diformyl–4–methylthiophenol

The reaction of one equivalent of 2,6–diformyl–4–methylthiophenol with one equivalent of 1,3–diaminopropane and two equivalents of $Ni(CH_3CO_2)_2.4H_2O$ in the presence of excess NH_4PF_6 in refluxing CH_3CN gave a red suspension. A small amount of pink solid was removed by filtration and diethyl ether was added to the red filtrate. A red solid was obtained that was recrystallised from CH_3CN/diethyl ether or CH_3NO_2/diethyl ether.

The f.a.b. mass spectrum of the red solid shows peaks at M^+ = 551 and 696 which are assigned, with the correct isotope distributions, as $[^{58}Ni_2(\underline{22}H)]^+$ and $[^{58}Ni_2(\underline{22}H)](PF_6)^+$ respectively. The i.r. spectrum of the red solid shows strong bands at 1557 and 838cm^{-1}, which are assigned to benzene ring and P–F stretching vibrations respectively. An absorption is observed in the region expected for a C=N stretching vibration, at 1632cm^{-1}, but is not as intense as bands for the C=N stretching vibration of complexes of $(\underline{1})^{2-}$. This reduction in intensity may be due to distortion of the imine bonds in $[Ni_2(\underline{22})]^{2+}$. This evidence, together with elemental analytical data, confirm the product to be $[Ni_2(\underline{22})](PF_6)_2$. The synthesis of $[Ni_2(\underline{22})]^{2+}$ described above suggests that $[Ni_2(\underline{22})]^{2+}$ is synthesized more successfully from

the unprotected thiophenol, not from 2,6-diformyl-4-methyl-*N*,*N*-dimethylcarbamoylthiophenol. However the reason for this is not clear.

The ^1H n.m.r. of $[Ni_2(\underline{22})](PF_6)_2$ in CD_3CN at 298K can be readily assigned to the proposed complex on the grounds of the chemical shifts and signal integrations of the observed resonances. The resonances due to the $-C\underline{H}_2-$ and $-C\underline{H}=N-$ protons are broadened and can not be resolved at the operating frequency (80.13MHz). Obtaining the spectrum at higher applied frequencies might give better resolution. For the assignments, see Section 5.4.11 below.

In order to determine the co-ordination geometry imposed on the Ni(II) centres by ligand $(\underline{22})^{2-}$, the single crystal X-ray structure of $[Ni_2(\underline{22})](PF_6)_2$ was undertaken.

5.2.10: The Single Crystal X-ray Structure of $[Ni_2(\underline{22})](PF_6)_2.2DMF$

Details of the structure solution and refinement are given in the Experimental Section. Tables of relevant bond lengths, angles and torsions are given in Tables 5.1, 5.2 and 5.3 respectively. A view of the cation $[Ni_2(\underline{22})]^{2+}$ is shown in Figure 5.12 and the interactions of $[Ni_2(\underline{22})]^{2+}$ with the included DMF molecules are shown in Figure 5.13.

The single crystal structure of $[Ni_2(\underline{22})](PF_6)_2$ shows that the complex is located on a crystallographic two-fold axis, so the two Ni(II) positions within the complex are equivalent. Each Ni(II) ion is directly bonded to two bridging thiophenolate S-donors [Ni-S = 2.181(6), Ni-S(a) = 2.171(6)Å] and two imine N-donors [Ni-N(1) = 1.927(15), Ni-N(2) = 1.906(15)Å] and there are additional interactions with O-donors from the DMF molecules which are included in the crystal lattice [Ni-O(1s) = 2.644(15)Å]. The co-ordination geometries about the Ni(II) centres are therefore distorted square-planar, since

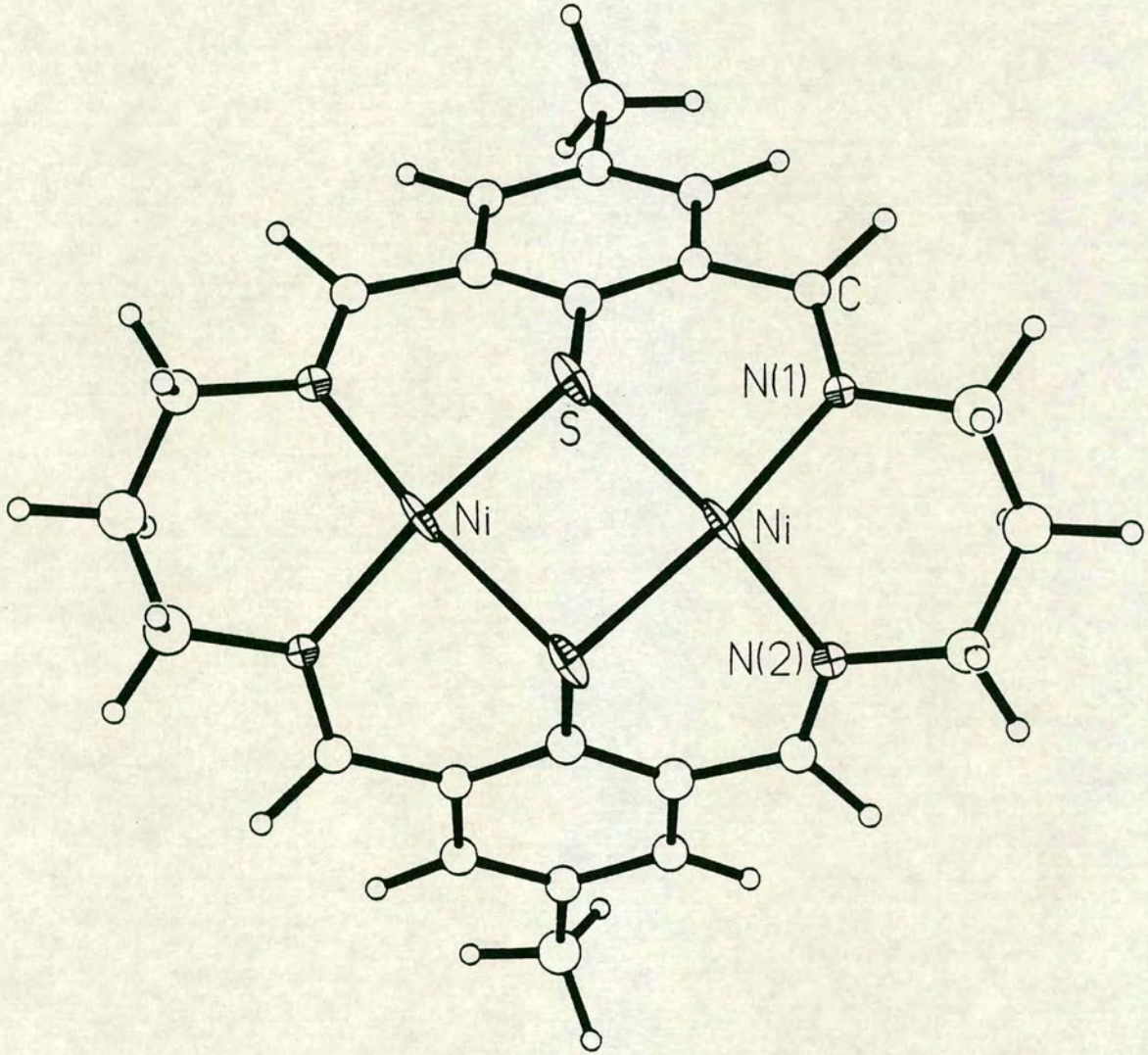

Figure 5.12 A view of the single crystal X-ray structure of $[Ni_2(\underline{22})]^{2+}$

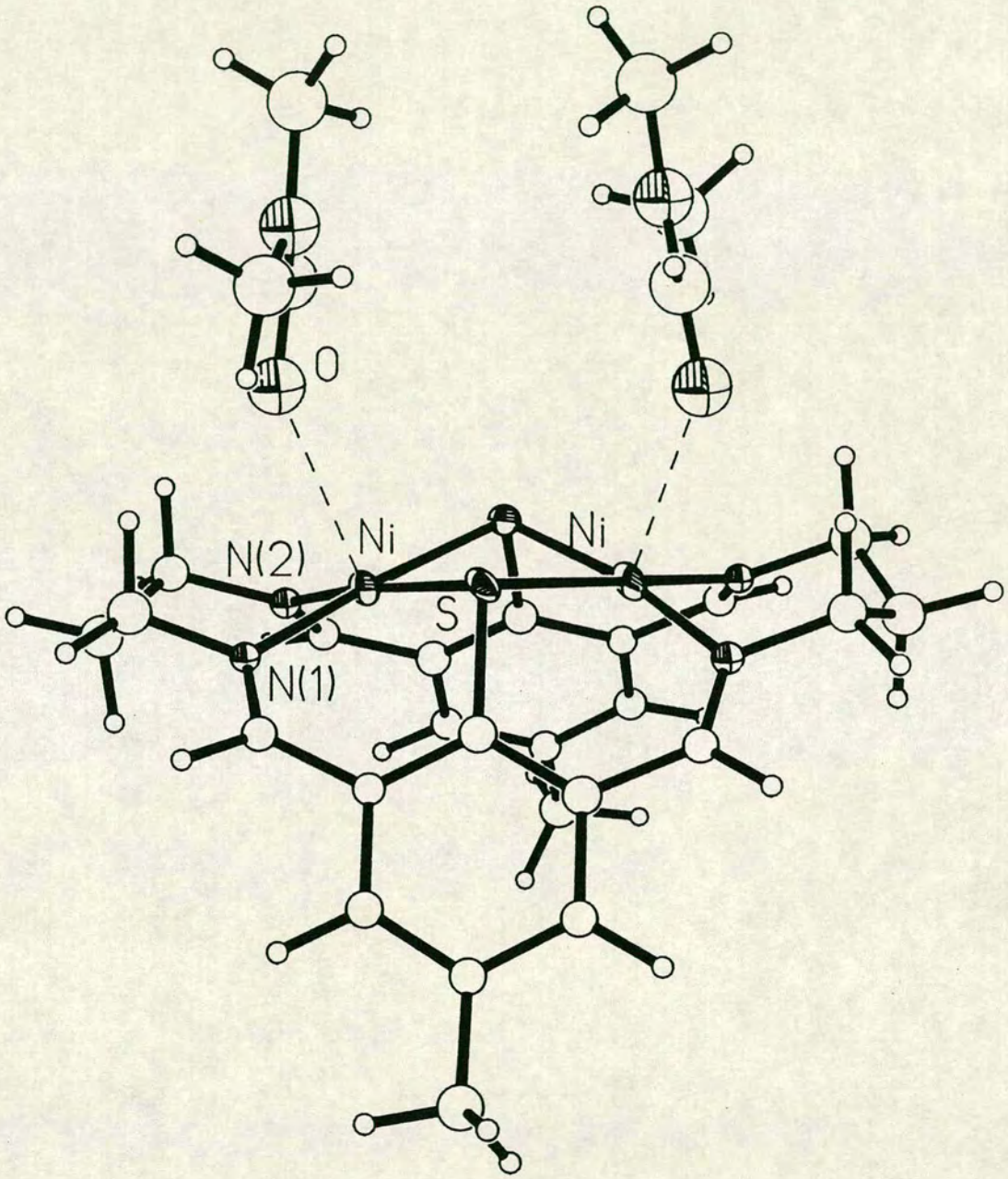

Figure 5.13 The single crystal X-ray structure of $[Ni_2(\underline{22})]^{2+}$ showing the interactions with DMF molecules

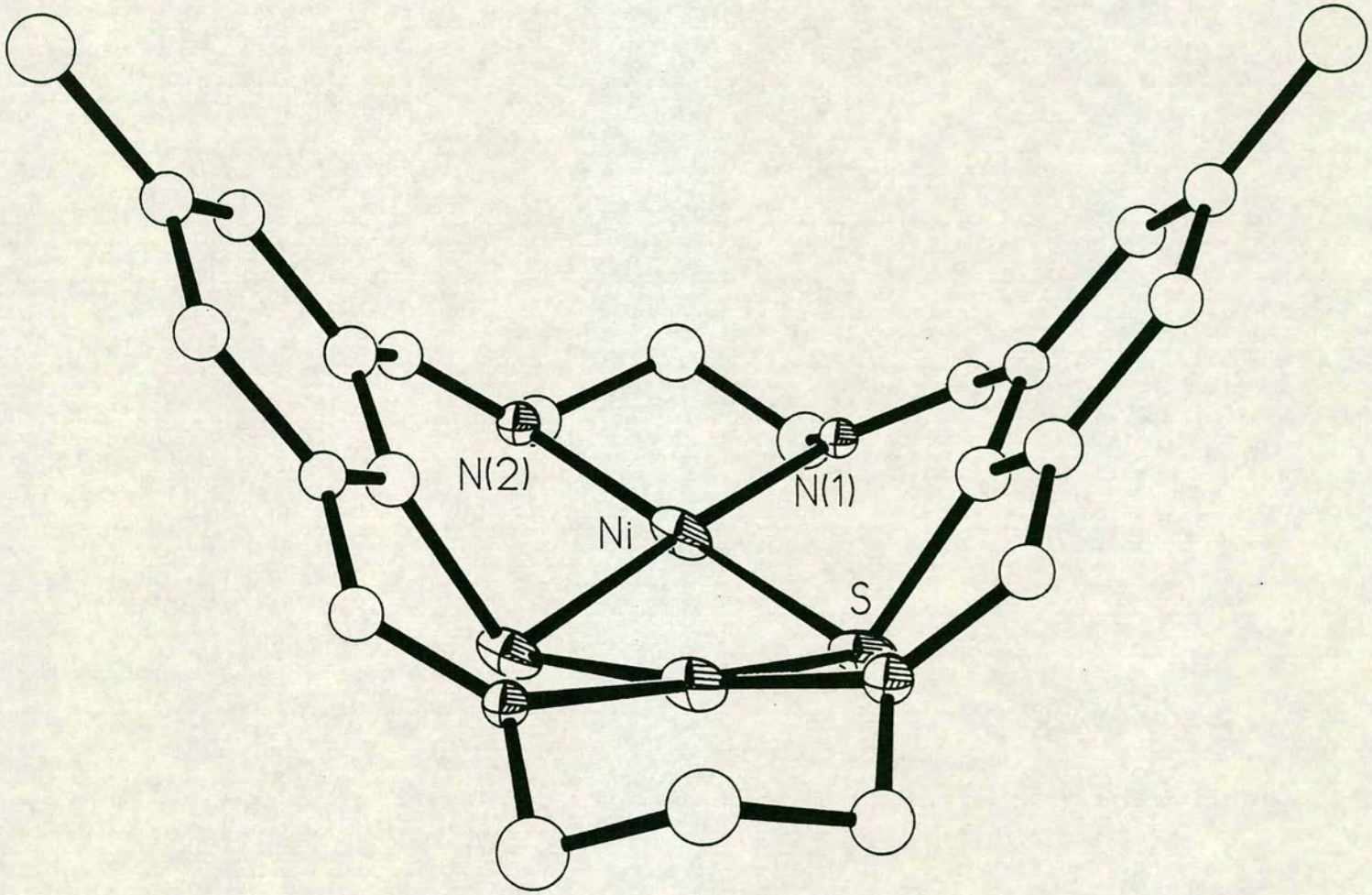

Figure 5.16 Alternative view of the single crystal X-ray structure of $[Ni_2(\underline{22})]^{2+}$

Table 5.1 Selected bond lengths (Å) of $[Ni_2(\underline{22})]^{2+}$

Ni	- S	2.181(6)	C(9)	- N(1)	1.282(24)
Ni	- N(1)	1.927(15)	N(1)	-C(10)	1.48(3)
Ni	- N(2)	1.906(15)	C(10)	-C(11)	1.47(3)
Ni	-Ni(a)	3.163(4)	C(11)	-C(12)	1.50(3)
Ni	- S(a)	2.171(6)	C(12)	- N(2)	1.47(3)
S	- C(1)	1.771(20)	C(4)	- C(5)	1.39(3)
C(1)	- C(2)	1.40(3)	C(5)	- C(6)	1.49(3)
C(1)	- C(8)	1.40(3)	C(5)	- C(7)	1.39(3)
C(2)	- C(3)	1.46(3)	C(7)	- C(8)	1.43(3)
C(2)	- C(4)	1.45(3)	C(8)	- C(9)	1.43(3)
C(3)	-N(2a)	1.279(24)			

Table 5.2 Selected bond angles (°) of $[Ni_2(\underline{22})]^{2+}$

S	-	Ni	-	N(1)	91.2(5)	C(4)	-	C(5)	-	C(6)	120.5(17)
S	-	Ni	-	N(2)	170.7(5)	C(4)	-	C(5)	-	C(7)	119.1(18)
S	-	Ni	-	S(a)	82.60(21)	C(6)	-	C(5)	-	C(7)	120.3(17)
N(1)	-	Ni	-	N(2)	94.2(6)	C(5)	-	C(7)	-	C(8)	122.2(18)
N(1)	-	Ni	-	S(a)	173.5(5)	C(1)	-	C(8)	-	C(7)	119.0(17)
N(2)	-	Ni	-	S(a)	91.6(5)	C(1)	-	C(8)	-	C(9)	123.8(17)
Ni	-	S	-	C(1)	99.3(7)	C(7)	-	C(8)	-	C(9)	117.1(16)
Ni	-	S	-Ni(a)		93.24(22)	C(8)	-	C(9)	-	N(1)	125.2(17)
C(1)	-	S	-Ni(a)		101.6(7)	Ni	-	N(1)	-	C(9)	125.5(13)
S	-	C(1)	-	C(2)	120.7(15)	Ni	-	N(1)	-C(10)		115.1(12)
S	-	C(1)	-	C(8)	119.7(14)	C(9)	-	N(1)	-C(10)		119.3(16)
C(2)	-	C(1)	-	C(8)	119.3(18)	N(1)	-C(10)		-C(11)		110.0(17)
C(1)	-	C(2)	-	C(3)	124.4(18)	C(10)	-C(11)		-C(12)		112.6(18)
C(1)	-	C(2)	-	C(4)	121.2(18)	C(11)	-C(12)		-	N(2)	113.6(16)
C(3)	-	C(2)	-	C(4)	114.2(17)	Ni	-	N(2)	-C(12)		115.0(12)
C(2)	-	C(3)	-N(2a)		125.1(17)	Ni	-	N(2)	-C(3a)		126.8(13)
C(2)	-	C(4)	-	C(5)	119.0(17)	C(12)	-	N(2)	-C(3a)		118.2(16)

Table 5.3 Selected torsion angles (°) of $[Ni_2(\underline{22})]^{2+}$

S	-	C(1)	-	C(2)	- C(3)	-1.8(28)	C(4)	-	C(5)	- C(7)	- C(8)	5.4(29)
S	-	C(1)	-	C(2)	- C(4)	173.5(15)	C(6)	-	C(5)	- C(7)	- C(8)	-178.4(18)
C(8)	-	C(1)	-	C(2)	- C(3)	-175.4(18)	C(5)	-	C(7)	- C(8)	- C(1)	-4.0(29)
C(8)	-	C(1)	-	C(2)	- C(4)	-0.2(29)	C(5)	-	C(7)	- C(8)	- C(9)	178.5(18)
S	-	C(1)	-	C(8)	- C(7)	-172.4(14)	C(1)	-	C(8)	- C(9)	- N(1)	33.3(30)
S	-	C(1)	-	C(8)	- C(9)	4.9(26)	C(7)	-	C(8)	- C(9)	- N(1)	-149.3(19)
C(2)	-	C(1)	-	C(8)	- C(7)	1.3(28)	C(8)	-	C(9)	- N(1)	-C(10)	177.3(18)
C(2)	-	C(1)	-	C(8)	- C(9)	178.6(18)	C(9)	-	N(1)	-C(10)	-C(11)	-120.5(19)
C(1)	-	C(2)	-	C(3)	-N(2a)	-25.9(31)	N(1)	-C(10)		-C(11)	-C(12)	-68.7(22)
C(4)	-	C(2)	-	C(3)	-N(2a)	158.6(19)	C(10)	-C(11)		-C(12)	- N(2)	67.0(22)
C(1)	-	C(2)	-	C(4)	- C(5)	1.6(29)	C(11)	-C(12)		- N(2)	-C(3a)	122.4(19)
C(3)	-	C(2)	-	C(4)	- C(5)	177.3(17)	C(12)	-	N(2)	-C(3a)	-C(2a)	175.5(17)
C(2)	-	C(4)	-	C(5)	- C(6)	179.7(18)	O(1S)	-C(1S)		-N(1S)	-C(2S)	-176.1(21)
C(2)	-	C(4)	-	C(5)	- C(7)	-4.1(28)	O(1S)	-C(1S)		-N(1S)	-C(3S)	-6.0(35)

the Ni(II) ions are displaced by approximately 0.1Å out of the least squares plane defined by the N_2S_2 donor set. The angle between the two square planes defined by the N_2S_2 arrays about Ni and Ni(a) is 144.4°. The metal–metal distance in $[Ni_2(\underline{22})]^{2+}$ [Ni–Ni(a) = 3.163(4)Å] is similar to those observed in the macrocyclic complexes of $(\underline{1})^{2-}$ noted in Chapters 2 and 4 above, which suggests that there is a well–defined metal–metal distance that can be accommodated by two bridging phenolate or thiophenolate donors within the Schiff–base macrocyclic framework.

In order to accommodate the co–ordination geometries about the Ni(II) ions in $[Ni_2(\underline{22})]^{2+}$, the macrocycle $(\underline{22})^{2-}$ adopts a folded conformation (angle between the aromatic rings in $(\underline{22})^{2-}$ = 72.5°). Importantly, this folding allows the bridging thiophenolate S–donors to form a Ni_2S_2 ring which is *syn–endo* in form[256], and the geometries about the S–atoms are pyramidal [∠Ni–S–C(1) = 99.3(7), ∠Ni(a)–S–C(1) = 101.6°]. This contrasts with most structures known for the complexes of $(\underline{1})^{2-}$, where the geometries about the bridging phenolate O–donors are trigonal planar ($[Ni_2(\underline{1})(CH_3CO_2)]_2^{2+}$ described in Section 4.2.8 being an exception). The folded conformation of ligand $(\underline{22})^{2-}$ also permits a lengthening of the S··S distance within the macrocycle [S··S(a) = 2.872(20)Å]. If $(\underline{22})^{2-}$ were to adopt a planar conformation, the S··S distance would become prohibitively short, as suggested originally by Robson and Hughes[274].

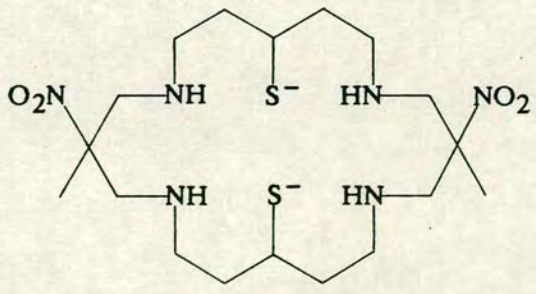

Figure 5.14 The macrocyclic ligand $(\underline{19})^{2-}$

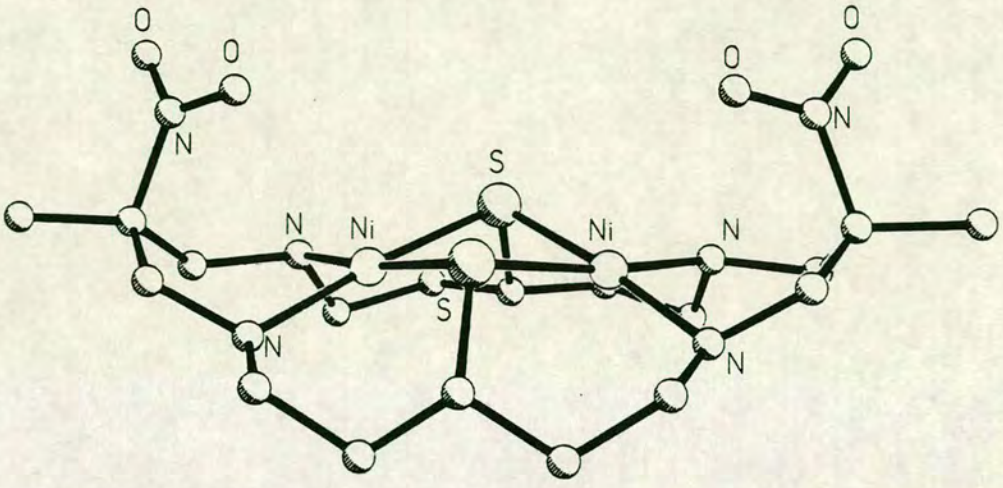

Figure 5.15 $[Ni_2(\underline{19})]^{2+}$

The Ni(II) complex of the binucleating macrocycle $(\underline{19})^{2-}$ shown in Figure 5.14, which also has bridging thiophenolate S-donors, has been reported recently by Lawrance and co-workers[185]. The template synthesis of this ligand was described above in Section 3.1 and Figure 3.3. The X-ray structure of $[Ni_2(\underline{19})](NO_2)_2$ shows that the ligand $(\underline{19})^{2-}$ also has a partially folded structure, so that the Ni_2S_2 unit is the *syn-endo* isomer and gives a S··S distance within the macrocycle of 2.813(5)Å (see Figure 5.15). These structural features are similar to those are observed in the complex $[Ni_2(\underline{22})]^{2+}$.

The folding of the macrocycle $(\underline{22})^{2-}$ in $[Ni_2(\underline{22})]^{2+}$, however, does not occur solely about the saturated propylene side-arms. This is seen in another view of $[Ni_2(\underline{22})]^{2+}$ in Figure 5.16. This view shows that the C=N bonds within the macrocycle are bent out of the planes of the aromatic benzene rings and towards the Ni(II) ions. This aids the folding of the macrocycle and suggests that there is some strain within the macrocyclic ring. The distortion of the imine bonds out of the conjugated system may explain the loss of intensity that is observed for the C=N stretching vibration in the i.r. spectrum of the compound. It is concluded that the folding and strain within the

macrocycle is a result of the incorporation of the thiophenolate S-donors within the macrocyclic cavity. Robson and co-workers have also found distortions in the C=N bonds of complexes of the form $[M_2(\underline{23})]^{n+}$ [277,278] (see Figure 5.4 above) and in one case[278], cleavage of the C=N bond occurs to give a mononuclear compound containing one imine bond and one free aldehyde.

It is interesting to note the differences between the Ni(II) complexes of the macrocyclic ligands $(\underline{1})^{2-}$ and $(\underline{22})^{2-}$, which are due to the steric and electronic differences between bridging phenolate O- and thiophenolate S-donors. For $[Ni_2(\underline{22})]^{2+}$, the Ni(II) ions adopt distorted square-planar co-ordination geometries, whereas the complexes of Ni(II) with $(\underline{1})^{2-}$ are either octahedral or square-pyramidal[97]. Thus, we have obtained evidence for the greater electron density on the S-donor of thiophenolates in comparison to phenolates and maybe also for the potential of S-donors to act as π-acceptor ligands. Even in the presence of a potentially bidentate $CH_3CO_2^-$ ligand, the Ni(II) centre in $(\underline{22})^{2-}$ remains square-planar. In contrast, the macrocycle $(\underline{1})^{2-}$ can not exert a sufficiently strong ligand-field to force Ni(II) into a square-planar geometry.

The ligand conformations of the Ni(II) complexes of $(\underline{1})^{2-}$ and $(\underline{22})^{2-}$ are also important. In $[Ni_2(\underline{1})(CH_3CN)_4]^{2+}$, the ligand $(\underline{1})^{2-}$ can adopt a planar conformation, even though there are steric repulsions between the axial ligands. The ligand $(\underline{1})^{2-}$ in $[Ni_2(\underline{1})(CH_3CO_2)]_2^{2+}$, however, folds to allow the phenolate O-donors to interact with additional octahedral Ni(II) centres. In comparison to this, there is evidence that the folding of $(\underline{22})^{2-}$ in $[Ni_2(\underline{22})]^{2+}$ is caused by strain within the macrocycle itself, in order to accommodate the larger S-donors within the macrocyclic cavity.

5.2.11: Cyclic Voltammetry of $[Ni_2(\underline{22})](PF_6)_2$ in CH_3CN

Cyclic voltammetry of $[Ni_2(\underline{22})](PF_6)_2$ measured in CH_3CN (0.1M $NBu^n_4BF_4$ supporting electrolyte) at Pt electrodes at 298K reveals one oxidative and two reductive processes. The oxidation is reversible (at scan rates from 0.50 to $0.20Vs^{-1}$) and occurs at $E_{\frac{1}{2}}$ = +0.51V *vs.* Fc/Fc^+. The two reductions are also reversible (at scan rates from 0.46 to $0.15Vs^{-1}$) and are observed at $E_{\frac{1}{2}}$ = −1.09 and −1.58V *vs.* Fc/Fc^+. The peak heights for all three processes are approximately equal and on this basis, we tentatively assign the two reductions and the oxidation as one-electron steps. Further experiments are required to confirm this assignment.

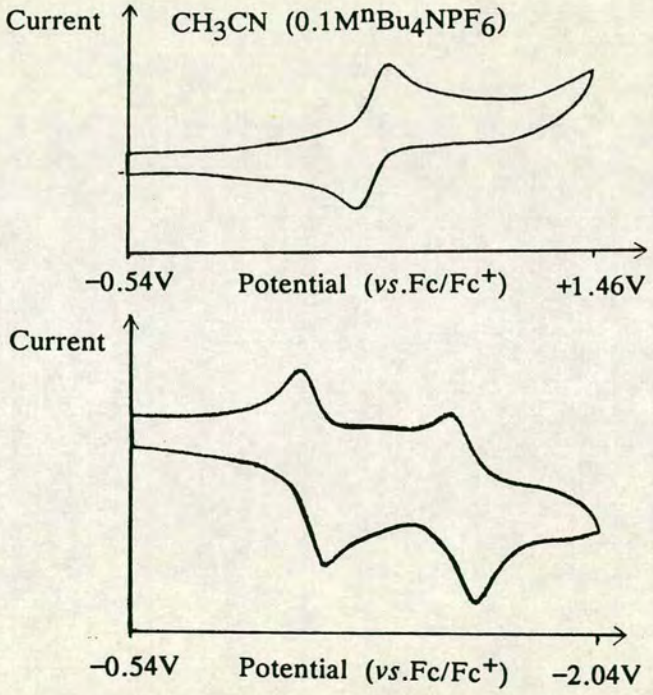

Figure 5.17 The oxidative and reductive cyclic voltammograms of $[Ni_2(\underline{22})](PF_6)_2$

It is relevant to remark here on the differences observed in the electrochemical behaviour between $[Ni_2(\underline{22})](PF_6)_2$ and $[Ni_2(\underline{1})(CH_3CO_2)]_2(PF_6)_2$ (see Section 4.2.9). The oxidative and reductive processes for $[Ni_2(\underline{22})]^{2+}$ occur at less extreme potentials than for $[Ni_2(\underline{1})(CH_3CO_2)]_2{}^{2+}$, which is probably a reflection of the electronic properties of the thiophenolate S-donors in $(\underline{22})^{2-}$. We conclude, therefore

that the ligand $(\underline{22})^{2-}$ can stabilise both the Ni(I) and the Ni(III) oxidation states more than the ligand $(\underline{1})^{2-}$ can. However, the electrochemical response of the ligand $(\underline{22})^{2-}$ has not yet been investigated, and so the possibility of the reduction or oxidation of $(\underline{22})^{2-}$ must not be overlooked.

5.3: Conclusions and Further Work

The synthesis of the Ni(II) complex of a novel N_4S_2 macrocycle $(\underline{22})^{2-}$ has been achieved by a template synthesis using 2,6-diformyl-4-methylthiophenol and 1,3-diaminopropane around two Ni(II) centres. It has not been possible to isolate the free or protonated forms of the ligand $(\underline{22})^{2-}$ as yet. The single crystal X-ray structure of $[Ni_2(\underline{22})](PF_6)_2.2DMF$ shows that $(\underline{22})^{2-}$ can impose a distorted square-planar geometry on the Ni(II) centres, which is in contrast to the octahedral geometries found for Ni(II) with the N_4O_2 macrocycle $(\underline{1})^{2-}$. Although there is some evidence for strain within the macrocyclic ring of $(\underline{22})^{2-}$, there is considerable scope for the synthesis of more complexes of macrocycle $(\underline{22})^{2-}$ with a range of transition metal centres. Furthermore, the folding of the macrocycle $(\underline{22})^{2-}$ in $[Ni_2(\underline{22})]^{2+}$ might be more readily achieved on reduction of the imine bonds to give four amine groups. This would give a more flexible macrocycle, which could accommodate a variety of co-ordination geometries and hence a range of transition metal centres.

5.4: Experimental

5.4.1: Synthesis of 2,6-diformyl-4-methyl-*N*,*N*-dimethylcarbamoylthiophenol

2,6-Diformyl-4-methyl-*N*,*N*-dimethylcarbamoylthiophenol was prepared by the method of Robson[284], which is described in detail here. In a 3-necked, $100cm^3$, round-bottomed flask fitted with a condenser, 2,6-diformyl-4-methylphenol (3.00g, 18.30mmol) and

1,4-diazabicyclo[2.2.2]octane (DABCO, 4.00g, 35.66mmol) were dissolved in dry, degassed DMF ($30cm^3$) to give a brown solution. *N*,*N*-dimethylthiocarbamoyl chloride (3.35g, 27.0mmol) was added and the mixture heated at 348K (± 5K) for two hours under N_2, to give a yellow solid and a brown solution. The mixture was poured into an ice-water mixture ($30cm^3$) and stirred to give a yellow slurry. This product was filtered and washed with H_2O, dilute $HCl_{(aq.)}$, H_2O, $Na_2CO_{3(aq.)}$ and H_2O and dried over P_2O_5 *in vacuo*. Yield = 4.60g, 100%. F.a.b. mass spectrum (3-NOBA matrix): found M^+ = 252, 218, 176. Calculated for: $[C_{12}H_{14}NO_3S]^+$, M^+ = 252; $[C_{12}H_{12}NO_3]^+$, M^+ = 218; $[C_{10}H_8O_3]^+$, M^+ = 176. I.r. spectrum (KBr disc): 3356w, 3044w, 2930m, 2884m, 2771w, 1829w, 1722m, 1683s, 1594s, 1548s, 1464s, 1393s, 1277s, 1235s, 1193s, 1170s, 1138s, 1107s, 1052m, 1002w, 985w, 934s, 890m, 826m, 748w, 716s, 693s, 628w, 582w, 550s, 505m and 442m cm^{-1}.

The dried yellow solid, 2,6-diformyl-4-methyl-*N*,*N*-dimethylthiocarbamoylphenol was placed in a Schlenk tube fitted with a condenser and heated using an oil-bath at 443-453K for 20-25 minutes under N_2. A little yellow solid sublimed up the tube and this was later removed. The majority of the solid gave a dark brown melt which solidified on cooling. This was dissolved in CH_2Cl_2 and C_2H_5OH was added until the brown solution became turbid. On further cooling at 253K, yellow needles were obtained which were filtered cold and dried *in vacuo*. Yield = 2.77g, 60%. Elemental analysis: found C = 56.6; H = 5.54; N = 5.24%. Calculated for $C_{12}H_{13}NO_3S$: C = 57.3; H = 5.21; N = 5.57%. F.a.b. mass spectrum (3-NOBA): found M^+ = 252, 72. Calculated for: $[C_{12}H_{14}NO_3S]^+$, M^+ = 252; $[C_3H_6NO]^+$, M^+ = 72. E.i. mass spectrum: found M^+ = 251, 179, 72. Calculated for: $[C_{12}H_{13}NO_3S]^+$, M^+ = 251; $[C_9H_7O_2S]^+$, M^+ = 179; $[C_3H_6NO]^+$, M^+ = 72. I.r. spectrum (KBr disc): 2932w, 2866w,

1824w, 1688s, 1664s, 1592m, 1563m, 1466w, 1445w, 1405m, 1388m, 1357s, 1284m, 1257m, 1230m, 1158w, 1106m, 1057m, 932m, 907m, 889m, 734w, 710w, 702m, 678m, 652m, 617w, 548m, 524m, 486w and 450w cm^{-1}. ^{1}H n.m.r. spectrum (80.13MHz, $CDCl_3$, 298K): δ = 2.44p.p.m. (s, Ph–C<u>H</u>$_3$, 3H); 3.02–3.15 (br d, N–C<u>H</u>$_3$, 6H); 7.98 (s, Ph–<u>H</u>, 2H); 10.49 (s, –C<u>H</u>=O, 2H). ^{13}C n.m.r. spectrum (50.32MHz, $CDCl_3$, 298K): δ = 20.90; 37.06; 37.20; 131.75; 133.85; 138.05; 140.86; 163.64; 190.22p.p.m. (see Figure 5.7 for assignments).

<u>5.4.2</u>: Synthesis of 2,6–diformyl–4–methylthiophenol

All the below procedures were performed in Schlenk apparatus under N_2. Degassed CH_3OH (25cm^3) was placed in a 3–necked, 100cm^3 round–bottomed flask and N_2 was bubbled through the solvent. 2,6–diformyl–4–methyl–*N*,*N*–dimethylcarbamoylthiophenol (384.0mg, 1.53mmol) was dissolved in the CH_3OH and NaOH (0.2g, 5.0mmol) was added. Within five minutes, an orange solution was obtained and this was heated under N_2 for 4 hours. The orange suspension was evaporated to dryness to give an orange solid and degassed H_2O (20cm^3) was added to give an orange suspension. The aqueous suspension was washed with 2 x 75cm^3 CH_2Cl_2. The orange suspension was acidified dropwise with dilute $HCl_{(aq.)}$ (5cm^3) with stirring and a gummy, white precipitate was formed immediately. The white solid was extracted into 2 x 20cm^3 CH_2Cl_2 to give a yellow organic layer and a clear colourless aqueous phase. The CH_2Cl_2 solution was dried over $MgSO_4$ for an hour and filtered to give a clear yellow solution. The volume of solvent was reduced to ca.15cm^3 and n–hexane was added to give a white precipitate. This was filtered in air and recrystallised from benzene/hexane. Yield = 202mg, 75%. Elemental analysis: found C = 59.6; H = 5.14%. Calculated for: $C_9H_8O_2S$: C = 60.0; H = 4.47%. E.i. mass spectrum: found

M^+ = 180, 152, 118. Calculated for: $[C_9H_8O_2S]^+$, M^+ = 180; $[C_8H_8OS]^+$, M^+ = 152; $[C_8H_6O]^+$, M^+ = 118. I.r. spectrum (KBr disc): 3421br w, 2923m, 2857w, 2737w, 1686s, 1598m, 1560m, 1445m, 1383m, 1285m, 1216m, 1097s, 1033m, 873m, 773w, 722w, 549w and 404w cm^{-1}. ^1H n.m.r. spectrum (80.13MHz, $CDCl_3$, 298K): δ = 2.42p.p.m. (s, Ph–C<u>H</u>$_3$, 3H); 3.48–3.74 (m, S<u>H</u>, 1H); 7.52–7.74 (br, Ph–<u>H</u>, 2H); 10.40 (s, –C<u>H</u>=O, 2H). ^{13}C n.m.r. spectrum (50.32MHz, $CDCl_3$, 298K): δ = 20.54p.p.m. (Ph–<u>C</u>H$_3$); 125–140 (m, aromatic <u>C</u>); 204.50 (m, <u>C</u>H=O).

<u>5.4.3</u>: Attempted synthesis of $[(\underline{22}H_4)](BF_4)_2$

2,6–Diformyl–4–methyl–*N*,*N*–dimethylcarbamoylthiophenol (500.0mg, 2.00mmol) was dissolved in CH_3OH (100cm^3) and HBr (48% aqueous solution, 1.0cm^3) was added dropwise. 1,3–Diaminopropane (0.17cm^3, 2.00mmol) was added and the solution was heated for 45 minutes under N_2 to give a red/brown solution. Excess $NaBF_4$ was added and the solution allowed to cool. The solution was evaporated to dryness and the brown solid was washed with diethyl ether. The remaining brown solid was filtered and heated in CH_3NO_2 to give a brown solution and a pale solid. The brown solution was filtered off and diethyl ether was added. A brown solid was obtained that was dried *in vacuo*. Yield = 40mg. F.a.b. mass spectrum (3–NOBA matrix): found M^+ = 199, 352, 436 (small). Calculated for: $[C_9H_{11}O_3S]^+$, M^+ = 199; unknown, M^+ = 352; $[C_{24}H_{28}N_4S_2]^+$, M^+ = 436. I.r. spectrum (KBr disc): 3426br s, 3017br s, 2798w, 2600–2400br, 1635m, 1547w, 1466m, 1306w, 1070br s, 886w, 772w, 534m and 522m cm^{-1}. A satisfactory elemental analysis was not obtained for this product.

5.4.4: Attempted synthesis of $[(\underline{22}H_4)](PF_6)_2$

2,6-Diformyl-4-methylthiophenol (108.2mg, 0.60mmol) was added to degassed CH_3OH ($50cm^3$) and HBr (48% aqueous solution, $0.05cm^3$) was added to give a clear yellow solution. 1,3-Diaminopropane ($0.05cm^3$, 0.60mmol) was added and an immediate brown coloration was observed. The solution was refluxed for ten minutes under N_2 and a brown precipitate started to appear. The reaction mixture was cooled and excess NH_4PF_6 was added. The solution was evaporated to dryness to give an oily brown solid and CH_3NO_2 was added to extract the product. The brown solution obtained was evaporated to $5cm^3$ and diethyl ether was added. A gummy brown solid was obtained, which was filtered washed with diethyl ether and cold CH_3OH and dried *in vacuo*. F.a.b. mass spectrum (3-NOBA/CH_3CN matrix): found M^+ = 228, 381, 527, 457, 514. Calculated for: $[C_9H_8SO_5]^+$, M^+ = 228; $[C_{21}H_{21}N_2S_2O]^+$, M^+ = 381; $[C_{21}H_{22}N_2S_2O](PF_6)^+$, M^+ = 527; $[C_{24}H_{33}N_4S_2O]^+$, M^+ = 457; $[C_{27}H_{42}N_6S_2]^+$, M^+ = 514. I.r. spectrum (KBr disc): 3425br, 2929w, 1654m, 1555m, 1522w, 1442w, 1384w, 1342w, 1194w, 1110w, 1065w, 845s, 740w, 668w and 558m cm^{-1}.

5.4.5: Attempted synthesis of $[(\underline{22}H_2)]$

2,6-Diformyl-4-methylthiophenol (50.0mg, 0.28mmol) was dissolved in degassed THF ($25cm^3$) to give a yellow solution. 1,3-Diaminopropane ($0.023cm^3$, 0.28mmol) was added and an immediate red coloration of the solution occurred. The solution was refluxed for an hour under N_2, allowed to cool and filtered. The brown solution was evaporated down to $5cm^3$ and diethyl ether was added. An orange solid appeared and this was filtered, washed with diethyl ether and dried *in vacuo*. F.a.b. mass spectrum (3-NOBA/CH_3CN matrix): found M^+ = 400, 616. Calculated for: $[C_{21}H_{20}N_2S_2O_2]^+$, M^+ = 400; $[C_{33}H_{32}N_4S_3O_2]^+$, M^+ = 616. I.r. spectrum

(KBr disc): 3384br, 2934m, 2856m, 1636m, 1510w, 1437m, 1366w, 1212w, 1152w, 1110m, 1066m, 1037m, 959w, 869w, 770w, 679w, 551w and 463w cm^{-1}.

5.4.6: Attempted synthesis of $[(\underline{24}H_4)](PF_6)_2$

2,6-Diformyl-4-methylthiophenol (113.0mg, 0.63mmol) and 1,4-diaminobutane (55.0mg, 0.62mmol) were dissolved in degassed CH_3OH ($200cm^3$) and HBr (48% in aqueous solution, $1.5cm^3$) was added to give a clear yellow solution. The solution was refluxed for 30 minutes and allowed to cool. Excess NH_4PF_6 was added and the yellow solution was evaporated in air to $5cm^3$. A yellow crystalline precipitate formed on further cooling and the mixture was centrifuged, the yellow solid isolated, washed with diethyl ether and dried *in vacuo*. F.a.b. mass spectrum (3-NOBA/CH_3CN matrix): only matrix peaks observed. I.r. spectrum (KBr disc): 3120br s, 1636br, 1399s, 1234m, 1052m, 860w, 744w and 484w cm^{-1}.

5.4.7: Attempted synthesis of $[Pb_2(\underline{22})](NO_3)_2$

2,6-Diformyl-4-methyl-*N*,*N*-dimethylcarbamoylthiophenol (60.3mg, 0.24mmol) was dissolved in hot CH_3OH ($5cm^3$) and added to this was a DMF solution of $Pb(NO_3)_2$ (39.7mg, 0.12mmol) and $Pb(CH_3CO_2)_2.3H_2O$ (45.5mg, 0.12mmol). 1,3-Diaminopropane ($0.02cm^3$, 0.24mmol) was added and the dark brown solution was heated overnight in air. The brown precipitate formed was filtered, washed with CH_3OH and $CHCl_3$ and dried *in vacuo*. F.a.b. mass spectrum (3-NOBA matrix): only matrix peaks observed. I.r. spectrum (KBr disc): 3420br, 2919m, 1636m, 1437m, 1384m, 1222w, 1058w, 869w and 683w cm^{-1}.

5.4.8: Attempted synthesis of $[Pb_2(22)](PF_6)_2$

2,6-Diformyl-4-methylthiophenol (164.0mg, 0.91mmol), 1,3-diaminopropane ($0.08cm^3$, 0.96mmol) and $Pb(CH_3CO_2)_2.3H_2O$ (364.0mg, 0.96mmol) were mixed in CH_3OH under N_2 and refluxed overnight to give an orange suspension. The mixture was cooled and excess NH_4PF_6 was added. The orange solid was filtered, washed with H_2O and diethyl ether, but could not be recrystallised since it was not soluble in any common organic solvents. F.a.b. mass spectrum (3-NOBA matrix): matrix peaks only observed. I.r. spectrum (KBr disc): 3426br, 2923w, 1636br, 1576w, 1432w, 1044s, 983s, 845m, 728w, 693w, 668w, 573m, 539m and 419w cm^{-1}.

5.4.9: Attempted synthesis of $[Cu_2(22)](PF_6)_2$

2,6-Diformyl-4-methyl-*N*,*N*-dimethylcarbamoylthiophenol (60.3mg, 0.24mmol), $Cu(CH_3CO_2)_2.H_2O$ (47.9mg, 0.24mmol) and NH_4PF_6 (160.0mg, 1.00mmol) were heated in $(CH_3)_2CO$ ($20cm^3$) to give a clear green solution. 1,3-Diaminopropane ($0.02cm^3$, 0.24mmol) was added and the solution immediately became a dark blue colour. The solution was heated for 3 hours and a very dark solution was obtained. The solution was evaporated down to ca.$5cm^3$ and diethyl ether was added. A dark, viscous oil was obtained which was isolated, washed with diethyl ether, dried *in vacuo* and washed with H_2O. Washing the brown oil with H_2O caused a brown solid to form which was filtered and dried. Yield = 24mg. Elemental analysis: found C = 43.1, H = 5.43, N = 6.40%. F.a.b. mass spectrum (3-NOBA matrix): found 371. Calculated for: $[^{63}CuC_{15}H_{24}N_4SO]^+$, M^+ = 371. I.r. spectrum (KBr disc): 3637m, 3426br, 2970m, 1707w, 1654s, 1445m, 1376m, 1258w, 1166w, 1104w, 1054w, 842s, 740w, 689w and 558s cm^{-1}.

5.4.10: Attempted synthesis of $[Ni_2(\underline{22})](PF_6)_2$

2,6-Diformyl-4-methyl-*N*,*N*-dimethylcarbamoylthiophenol (60.3mg, 0.24mmol) and $Ni(CH_3CO_2)_2.4H_2O$ (59.7mg, 0.24mol) were heated in $(CH_3)_2CO$ ($20cm^3$) to give a brown suspension. 1,3-Diaminopropane ($0.02cm^3$, 0.24mmol) and NH_4PF_6 (160mg, 1.00mmol) were added and the solution was heated for 3 hours to give a clear, red solution. The solution was evaporated down to ca.$5cm^3$ and diethyl ether was added. A dark, viscous oil was obtained which was isolated, washed with diethyl ether, dried *in vacuo* and washed with H_2O. Washing the brown oil with H_2O caused a brown solid to form which was filtered and dried again. Yield = 31mg. Elemental analysis: found C = 41.7, H = 6.00, N = 5.69%. F.a.b. mass spectrum (3-NOBA): found M^+ = 72, 641. Calculated for: $[(CH_3)_2NCO]^+$, M^+ = 72; $\{^{58}Ni_2(C_{24}H_{26}N_4S_2)[(CH_3)_2NCHO](H_2O)\}^+$, M^+ = 641. I.r. spectrum (KBr disc): 3630m, 3279br, 2965m, 1707m, 1657s, 1440m, 1377m, 1261m, 1101m, 1020m, 845s, 740m, 688w and 558s cm^{-1}.

5.4.11: Synthesis of $[Ni_2(\underline{22})](PF_6)_2$

2,6-Diformyl-4-methylthiophenol (69mg, 0.38mmol) and $Ni(CH_3CO_2)_2.4H_2O$ (200mg, 0.80mmol) were dissolved in CH_3CN ($20cm^3$) to give a brown solution. 1,3-Diaminopropane ($0.032cm^3$, 0.38mmol) and NH_4PF_6 (400mg, 2.4mmol) were added and the solution was refluxed for 24 hours to give a red suspension. On cooling a small amount of pink solid precipitated which was removed by filtration. The red solution was evaporated to ca.$5cm^3$ and diethyl ether was added. The red solid that was formed was filtered, washed with diethyl ether and dried. Recrystallisation from CH_3CN/diethyl ether or CH_3NO_2/diethyl ether gave red crystals. Yield = 89mg, 56%. Elemental analysis: found C = 30.8, H = 3.62, N = 6.59%; calculated for $[Ni_2(C_{24}H_{26}N_4S_2)](PF_6)_2$: C = 34.2, H = 3.11,

N = 6.65%. F.a.b. mass spectrum (3-NOBA/CH_3CN matrix): found M^+ = 551, 696. Calculated for: $[^{58}Ni_2(C_{24}H_{27}N_4S_2)]^+$, M^+ = 551; $[^{58}Ni_2(C_{24}H_{26}N_4S_2)](PF_6)^+$, M^+ = 696. I.r. spectrum (KBr disc): 3422br, 2950w, 1632m, 1593w, 1557s, 1444m, 1403m, 1378m, 1361w, 1300m, 1277w, 1200w, 1132w, 1073m, 952w, 838s, 740w, 709w, 656w and 557s cm^{-1}. U.V./vis. spectrum (CH_3CN): $\lambda_{max.}$ = 513nm. ($\varepsilon_{max.}$ = 1,510$M^{-1}cm^{-1}$); 251 (39,370). ^1H n.m.r. spectrum (80.13MHz, CD_3CN, 298K): δ = 2.55p.p.m. (s, $C\underline{H}_3$, 6H); 2.84 (br d, J = 12Hz, C-$C\underline{H}_2$-C, 4H); 4.49 (br m, N-$C\underline{H}_2$-C, 8H); 7.61 (d, J = 0.5Hz, Ar-$\underline{H}$, 4H); 9.80 (br, $C\underline{H}$=N, 4H).

5.4.12: Single Crystal X-ray Structure of $[Ni_2(\underline{22})](PF_6)_2.2(CH_3)_2NCHO$

Vapour diffusion of diethyl ether into a solution of the complex in CH_3CN/DMF gave red crystals of crystallographic quality. To prevent crystal degradation as a result of solvent loss, a red block was transferred from its cold mother liquor into a drop of mineral oil at 195K and mounted on the diffractometer which was equipped with an Oxford Cryosystems low-temperature device[253] operating at 150K.

Crystal Data:

$[Ni_2C_{24}H_{26}N_4S_2](PF_6)_2.2(CH_3)_2NCHO$ M = 988.02. Monoclinic, space group $C_{2/c}$, a = 24.50(3), b = 10.004(12), c = 18.218(24)Å, β = 120.23(5)°, V = 3858Å^3 (by least-squares refinement on diffraction angles for 27 reflections measured at $\pm\omega$ [$20 < 2\theta < 26°$, λ = 0.71073Å]), Z = 4, D_c = 1.701gcm^{-3}, T = 150K. Crystal dimensions 0.35 x 0.23 x 0.08mm^3, μ(Mo-Kα) = 1.261mm^{-1}, F(000) = 2016.

Data Collection and Processing:

Stöe STADI-4 four-circle diffractometer, ω-2θ scan mode using the

learnt-profile method[199]. Graphite-monochromated Mo-Kα radiation; 2790 reflections measured ($2\theta_{max.}$ = 45°, h −26 → 18, k 0 → 10, l 0 → 23), 2127 unique data (R_{int} = 0.1553), giving 1543 with $F > 4\sigma(F)$. No significant crystal decay, no absorption correction.

Structure Analysis and Refinement:

The Ni atoms were located using a Patterson synthesis[201], and successive cycles of least-squares refinement and difference Fourier synthesis[201] identified the positions of all other non-H atoms. At isotropic convergence, final correction for absorption was made using *DIFABS*[285] (maximum absorption correction = 1.246, minimum absoption correction = 0.595). The crystal lattice was found to contain two DMF molecules per cation. Anisotropic thermal parameters were refined for Ni, S, P and F but the C and N atoms could only be refined isotropically. H atoms were located from a difference map and included in fixed, calculated positions. The weighting scheme $w^{-1} = \sigma^2(F) + 0.003949F^2$ gave satisfactory agreement analyses. At final convergence, R = 0.1263, R_w = 0.1676, S = 1.195 for 167 independent parameters, and the final difference Fourier synthesis showed no feature above +1.386 or below −1.728eÅ^{-3}.

Atomic scattering factors were inlaid[201], except for Ni[254], molecular geometry calculations utilised *CALC*[202] and figures were produced by *SHELXTL PC*[255].

CHAPTER 6

The Synthesis and Characterisation of Fe(II) and Co(II) Complexes of the Thioether Macrocycle [9]aneS_3

6.1: Introduction

The Edinburgh group has studied extensively the co-ordination chemistry of the thioether macrocycles, with metal ions from all rows of the transition block and some main-group elements. The work up to 1990 has been reviewed[6]. Particular emphasis has been placed on the binding of the platinum group metals which had been poorly represented in the field of macrocyclic chemistry[6,16]. The choice of thioether donors for binding to the platinum metals was instigated by the compatibility of the soft S-donor ligands with the soft platinum group metal centres. This, together with the stereochemical requirements of the macrocyclic ligands, has resulted in the stabilisation of some unusual oxidation states for these metal centres, notably Rh(II)[16,286], Pd(III)[287-289] and Pt(III)[289,290] as mononuclear $[M([9]aneS_3)_2]^{n+}$ complexes. However, we have had less success with the isolation and characterisation of complexes of thioether macrocycles with metal ions from the middle to early transition elements to date and Chapters 6 and 7 in this thesis will describe attempts to synthesize compounds with a range of thioether macrocycles and Fe(II) and Co(II) centres.

Thioethers have been considered to be relatively poor donor ligands, compared to phosphines and amines[291], but the incorporation of thioethers into a macrocyclic ring considerably enhances the stability of the thioether-metal complex. The reasons for this stability are threefold:

i) the chelate effect;

ii) the macrocyclic effect;

iii) the macrocycles are sterically efficient so that the alkyl chains attached to the S-donor atoms do not experience steric repulsions.

An important advantage that thioethers have over phosphine and amine ligands is that thioethers have the potential to act as either π-acceptors or π-donors, according to the requirements of the co-ordinated metal centre.

This is possible because an sp^3-hybridised S-donor has two lone pairs, one for σ-bonding and the other potentially for π-donation; in addition to this, the 3d-orbitals on S-donors may be of the correct symmetry and energy to be able to accept electron density from the metal centre, thus acting as π-acceptors[291,292].

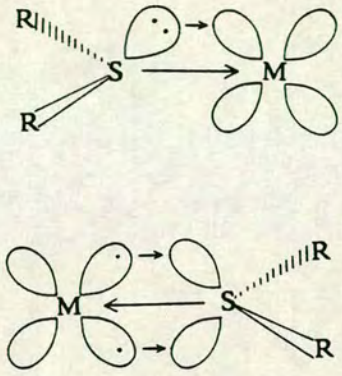

Figure 6.1 π-donor and π-acceptor properties of thioethers

We have obtained important evidence for the π-acceptor properties of thioethers by comparing the single crystal X-ray structures of $[Fe([9]aneS_3)_2](ClO_4)_2$ (described in this thesis) and $[Fe([9]aneS_3)_2](ClO_4)_3$[292] and these compounds will be discussed in Section 6.2.1 below. By incorporating versatile ligands such as thioethers into a metal complex, it may be possible for the metal ion to undergo a series of redox processes, with the range of oxidation states being stabilised by the appropriate π-interactions with the thioether ligands. For example, a hypothetical Fe-thioether complex might be able to undergo a progressive two-electron oxidation Fe(I) → Fe(II) → Fe(III) with the corresponding change in the thioether S-donors from π-acceptor to π-donor properties. Such a complex would be ideal as a catalytic centre for the activation of small substrate molecules, if vacant co-ordination sites could be incorporated into the Fe-thioether macrocyclic complex. We proposed therefore to undertake the synthesis of Fe(II)-thioether macrocyclic complexes of the form of

half-sandwich compounds $[Fe([9]aneS_3)XYZ]^{n+}$ (X, Y, Z = other mono- or bi-dentate ligands).

6.1.1: Half-sandwich complexes of [9]aneS$_3$

The thioether macrocyclic ligand [9]aneS$_3$ is considered to be pre-organised for facial co-ordination to a metal centre[29,293]. The solid-state structure of [9]aneS$_3$[293] shows that the molecule adopts an *endo* conformation, with the bonding lone pairs of the S-donors directed towards the centre of the macrocyclic ring. This is in contrast to the larger ring thioether macrocycles described later in Chapter 7. This pre-organisation of [9]aneS$_3$ for facial co-ordination can give increased stabilities of the complexes of [9]aneS$_3$ relative to the larger ring thioether macrocycles[294,311]. This facial binding mode of [9]aneS$_3$ is analogous to that of a number of other facially capping ligands which have been studied extensively, particularly those based on a cyclopentadienyl ($C_5R_5^-$) framework[295]. Research on Fe complexes using one $C_5R_5^-$ ligand as a protecting group for an octahedral face has been particularly fruitful and is exemplified by the work of Davies and co-workers[296].

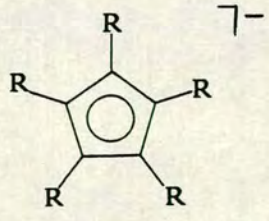

Cp^-, R = H; Cp^{*-}, R = CH_3

Cyclopentadienyl ligands

There have been only two half-sandwich complexes of [9]aneS$_3$ with Fe reported in the literature, $[Fe([9]aneS_3)(C_5H_5)]^+$ [297] and $[Fe([9]aneS_3)Cl_3]$[298]. Reactions with $[Fe([9]aneS_3)Cl_3]$ will be described below in Section 6.2.3. $[Fe([9]aneS_3)(C_5H_5)]^+$ was prepared by the reaction of

[9]aneS$_3$ with an equimolar amount of [Fe(C$_5$H$_5$)I(CO)$_2$] in CH$_3$CN and red crystals were obtained[297]. A single crystal X-ray structure of [Fe([9]aneS$_3$)(C$_5$H$_5$]$^+$ [297] shows the Fe(II) ion is sandwiched between C$_5$H$_5^-$ and [9]aneS$_3$ ligands and is shown in Figure 6.2. Cyclic voltammetry of [Fe([9]aneS$_3$)(C$_5$H$_5$)]$^+$ in CH$_3$CN/Bu$^n_4$NPF$_6$ shows a reversible one-electron oxidation at $E_{\frac{1}{2}}$ = +0.44V *vs.* Fc/Fc$^+$, which is assigned to a Fe(II)/Fe(III) couple[297]. This oxidation occurs at an intermediate value between those of [Fe([9]aneS$_3$)$_2$]$^{2+}$ and [Fe(C$_5$H$_5$)$_2$].

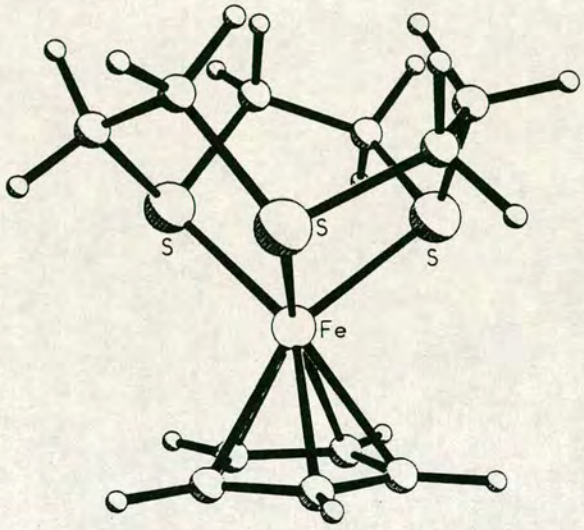

Figure 6.2 [Fe([9]aneS$_3$)(C$_5$H$_5$)]$^+$

A series of half-sandwich compounds with [9]aneS$_3$ have been prepared with the other members of the Fe triad, that is Ru(II)[294,299] and Os(II)[299]. The stoichiometries of the piano-stool products of the form [Ru([9]aneS$_3$)Y$_2$Z] depend on the starting materials, reaction conditions and the tertiary phospine used, to give [Ru([9]aneS$_3$)X$_2$(PR$_3$)], [Ru([9]aneS$_3$)X(PR$_3$)$_2$]$^+$ [X = Cl, Br; PR$_3$ = PPh$_3$, P(C$_2$H$_5$)Ph$_2$], [Ru([9]aneS$_3$)Cl(PR$_3$)$_2$]$^+$ [PR$_3$ = P(C$_2$H$_5$)$_2$Ph, P(CH$_3$)$_2$Ph] and [Ru([9]aneS$_3$)Cl(DMSO)$_2$]$^+$ [299]. Chiral complexes of the form [Ru([9]aneS$_3$)XYZ] have also been prepared and structurally characterised, namely [Ru([9]aneS$_3$)Cl(CO)(PPh$_3$)]$^+$ [300] and [Ru([9]aneS$_3$)Cl(NCCH$_3$)(PPh$_3$)]$^+$ [299]. In the latter compound, the CH$_3$CN

ligand may be substituted with a number of other monodentate ligands, such as thiophene and PR_3[300,301]. The single crystal X-ray structure of $[Os([9]aneS_3)H(CO)(PPh_3)]^+$ has also been determined[299].

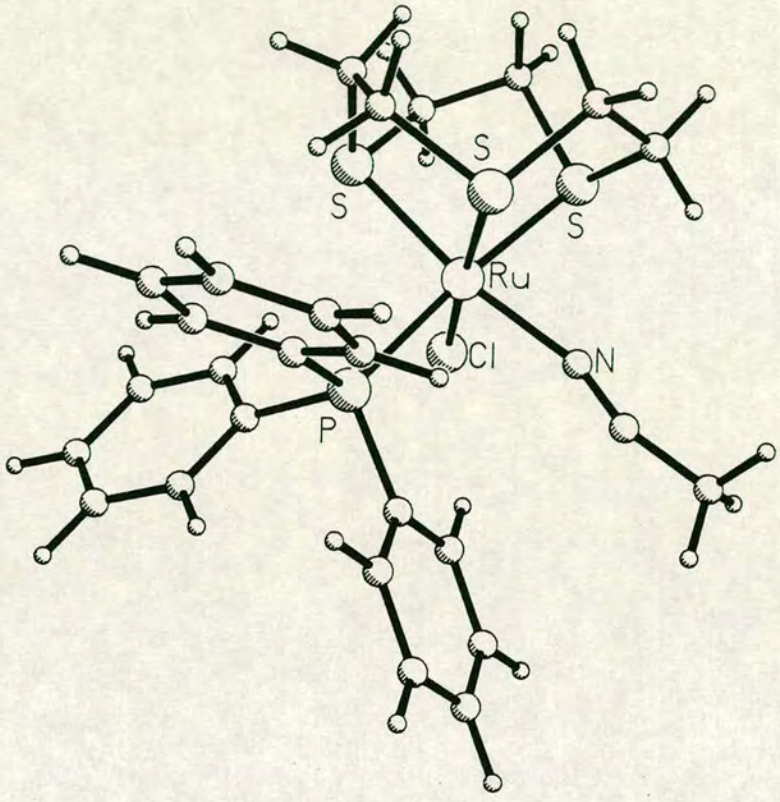

Figure 6.3 $[Ru([9]aneS_3)Cl(NCCH_3)(PPh_3)]^+$

A number of half-sandwich complexes with $[9]aneS_3$ have been reported where the metal centre is five- [302] or four-co-ordinate[300]. These are with Ni(II) and Pd(II) ions respectively. Of particular interest here are the series of complexes $[Ni([9]aneS_3)(diphosphine)]^{2+}$ (diphosphine = bidentate phosphines shown in Figure 6.4), which can be used to electrochemically and chemically generate genuine Ni(I) species[302]. The single crystal X-ray structures of $[Ni([9]aneS_3)(diphosphine)]^{2+}$ [diphosphine = $Ph_2PCH_2PPh_2$, $Ph_2PC_2H_4PPh_2$, $(C_6H_{11})_2PC_2H_4P(C_6H_{11})_2$, $CH_3C(CH_2PPh_2)_3$] all show distorted square-pyramidal stereochemistries with bond lengths $Ni-S_{apical}$ = 2.38-2.65, $Ni-S_{basal}$ = 2.22-2.24 and Ni-P = 2.17-2.22Å. The

single crystal X-ray structure of $[Ni([9]aneS_3)(Ph_2PC_2H_4PPh_2)]^{2+}$ is shown in Figure 6.5[302].

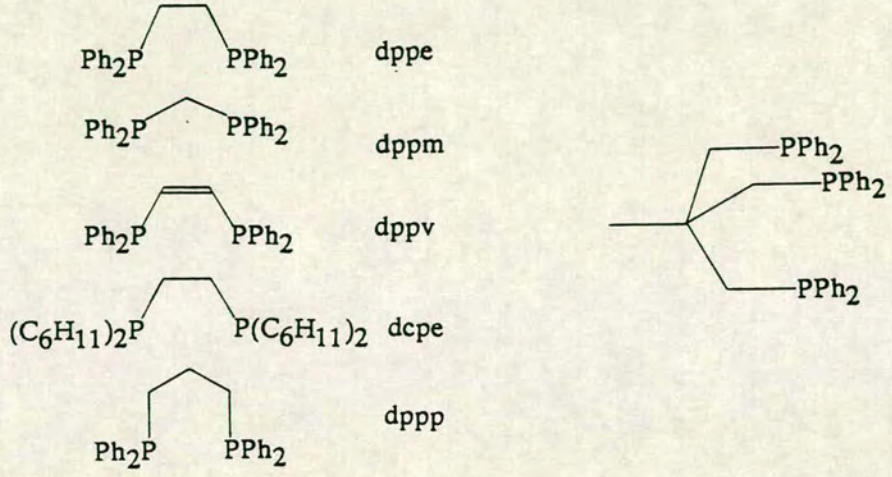

Figure 6.4 Bidentate phosphines (diphosphine) and the tridentate phosphine (triphos) used in this work

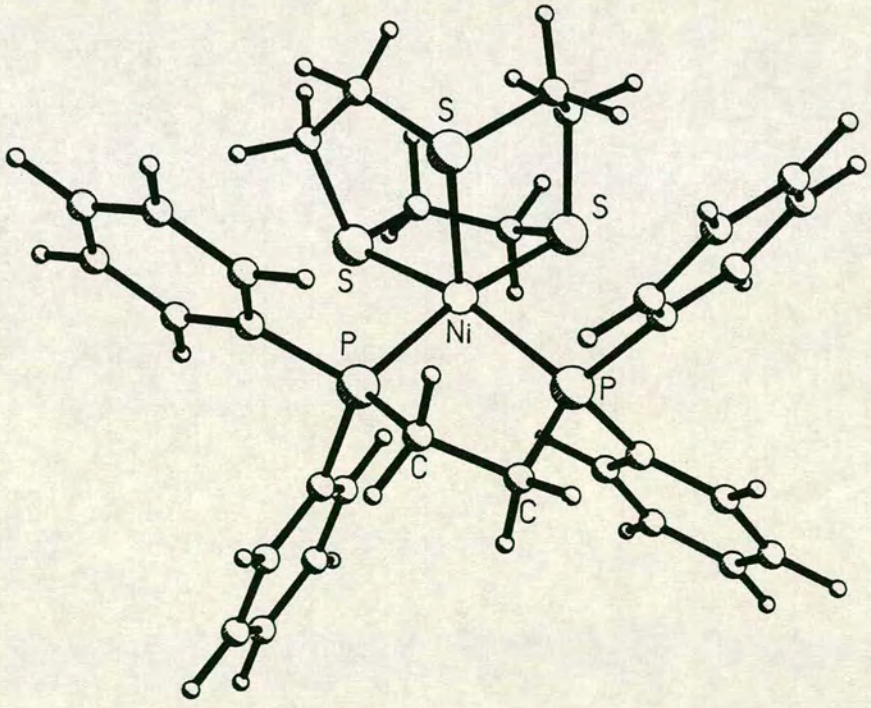

Figure 6.5 $[Ni([9]aneS_3)(Ph_2PC_2H_4PPh_2)]^{2+}$

The one-electron reductions in $CH_3CN/Bu^n_4NPF_6$ of the $[Ni([9]aneS_3)(diphosphine)]^{2+}$ species occur in the range $E_{\frac{1}{2}}$ = –0.77 to

−0.96V *vs.* Fc/Fc^+., the most anodic value $E_{\frac{1}{2}}$ = −0.77V being obtained for $[Ni([9]aneS_3)(Ph_2PCH_2PPh_2)]^{2+}$. All reduction processes were followed using *in situ* U.V./visible spectroscopy and the e.s.r. spectra of the reduction products were examined. On the basis of this data, the products $[Ni([9]aneS_3)(diphosphine)]^+$ were assigned as d^9 metal-centred radical cations, probably with square-pyramidal geometries[302]. The $[Ni([9]aneS_3)(diphosphine)]^+$ species formed adducts with CO and $[Ni([9]aneS_3)(diphosphine)]^{2+}$ was regenerated on re-oxidation. No reaction was observed between $[Ni([9]aneS_3)(diphosphine)]^+$ and CO_2. Considering that the half-sandwich complexes $[Ni([9]aneS_3)(diphosphine)]^{2+}$ can be readily synthesized and reduced to $[Ni([9]aneS_3)(diphosphine)]^+$ species at relatively anodic potentials, we proposed to undertake the synthesis of the Co(II) and Fe(II) analogues of $[Ni([9]aneS_3)(diphosphine)]^{2+}$. We proposed that these Co(II) and Fe(II) analogues might still show a readiness to undergo one-electron reductions to M(I) similar to $[Ni([9]aneS_3)(diphosphine)]^{2+}$, but might also exhibit well-defined one-electron oxidations to the M(III) state. If this is the case, then the $[M([9]aneS_3)(diphosphine)]^{2+}$ species could possibly be used as two-electron reductants or oxidants for small molecule substrates in a catalytic cycle. The electrochemical properties of any $[M([9]aneS_3)(diphosphine)]^{2+}$ species synthesized was therefore examined.

6.1.2: Binuclear complexes containing [9]aneS$_3$

The reaction of equimolar amounts of $NiCl_2.6H_2O$ and $[9]aneS_3$ gives the binuclear compound $[([9]aneS_3)Ni(\mu\text{-}Cl)_3Ni([9]aneS_3)]^+$ [110,302]. The single crystal X-ray structure of $[([9]aneS_3)Ni(\mu\text{-}Cl)_3Ni([9]aneS_3)]^+$ is shown in Figure 6.6 and shows that the octahedral Ni(II) centres are triply Cl^- bridged, so that the Ni-Ni distance is 2.9211(20)Å. Triple Cl^- bridges are common for some metals, particularly Ru and Os[303], but not Ni(II). We

therefore proposed to investigate whether bridged binuclear structures such as this are a common structural motif in the complexes of [9]aneS$_3$, by attempting to synthesize Fe(II) or Fe(III) analogues of [([9]aneS$_3$)Ni(μ–Cl)$_3$Ni([9]aneS$_3$)]$^+$. Bridged binuclear structures are a recurring feature in the co–ordination chemistry of [9]aneN$_3$ and Me$_3$[9]aneN$_3$[7,108], especially with carboxylate and μ–O bridges. Therefore complexation reactions with Fe(II) and [9]aneS$_3$ in the presence of the potentially bridging ligand $CH_3CO_2^-$ was also attempted.

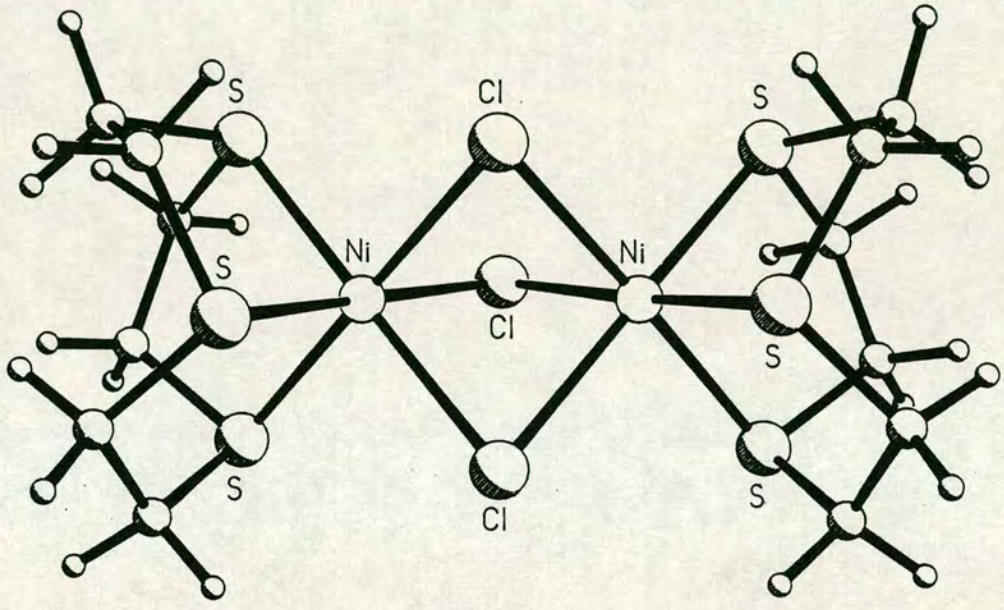

Figure 6.6 [([9]aneS$_3$)Ni(μ–Cl)$_3$Ni([9]aneS$_3$)]$^+$

6.2: Results and Discussion

6.2.1: The Synthesis of [Fe([9]aneS$_3$)$_2$](ClO$_4$)$_2$

[Fe([9]aneS$_3$)$_2$](ClO$_4$)$_2$ was prepared as described by Wieghardt *et al.*[298], by the reaction of two equivalents of [9]aneS$_3$ with Fe(ClO$_4$)$_3$.6H$_2$O in CH$_3$OH. The pink precipitate obtained from this reaction was recrystallized by vapour diffusion of diethyl ether into a CH$_3$NO$_2$/DMF solution of the pink precipitate. The f.a.b. mass spectrum of the pink solid shows peaks at M$^+$ = 415 and 515, which are assigned as [^{56}Fe([9]aneS$_3$)([9]aneS$_3$–H)]$^+$ and

$[^{56}Fe([9]aneS_3)_2](ClO_4)^+$ respectively. The i.r. spectrum and elemental analytical data confirm the assignment of the product as $[Fe([9]aneS_3)_2](ClO_4)_2$. Wieghardt *et al.*[298] have also prepared $[Fe([9]aneS_3)_2](ClO_4)_2$ using $FeCl_2.4H_2O$ as the Fe(II) starting material, followed by metathesis of the counterion with $NaClO_4$. Therefore, the same Fe(II) product, $[Fe([9]aneS_3)_2]^{2+}$, is obtained using either Fe(II) or Fe(III) starting materials, which is a measure of the stability of the low spin d^6 species $[Fe([9]aneS_3)_2]^{2+}$.

The single crystal X-ray structure of $[Fe([9]aneS_3)_2](PF_6)_2$ has been determined previously[298]. However, the counterion used in the Fe(III) complex $[Fe([9]aneS_3)_2]^{3+}$ [292] was ClO_4^-, since the oxidation from $[Fe([9]aneS_3)_2]^{2+}$ to $[Fe([9]aneS_3)_2]^{3+}$ was accomplished in aqueous concentrated $HClO_4$ [292]. Therefore to be able to compare the structures of $[Fe([9]aneS_3)_2]^{2+}$ and $[Fe([9]aneS_3)_2]^{3+}$ with complete confidence, we decided it was necessary to determine the structure of $[Fe([9]aneS_3)_2](ClO_4)_2$ by X-ray crystallography.

6.2.2: The Single Crystal X-ray Structure of $[Fe([9]aneS_3)_2](ClO_4)_2.2DMF$

Details of the structure solution and refinement are given in the Experimental Section. Tables of relevant bond lengths, angles and torsions are given in Tables 6.1, 6.2 and 6.3 respectively. A view of the cation $[Fe([9]aneS_3)_2]^{2+}$ is shown in Figure 6.7 and for comparison the structure of the $[Fe([9]aneS_3)_2]^{3+}$ cation (determined at Edinburgh)[292] is shown in Figure 6.8.

The single crystal X-ray structure of $[Fe([9]aneS_3)_2](ClO_4)_2$ shows there are discreet $[Fe([9]aneS_3)_2]^{2+}$ cations, ClO_4^- anions and two included DMF molecules per $[Fe([9]aneS_3)_2]^{2+}$ unit in the crystal. The Fe(II) ion occupies a crystallographic inversion centre and is in an octahedral environment of six

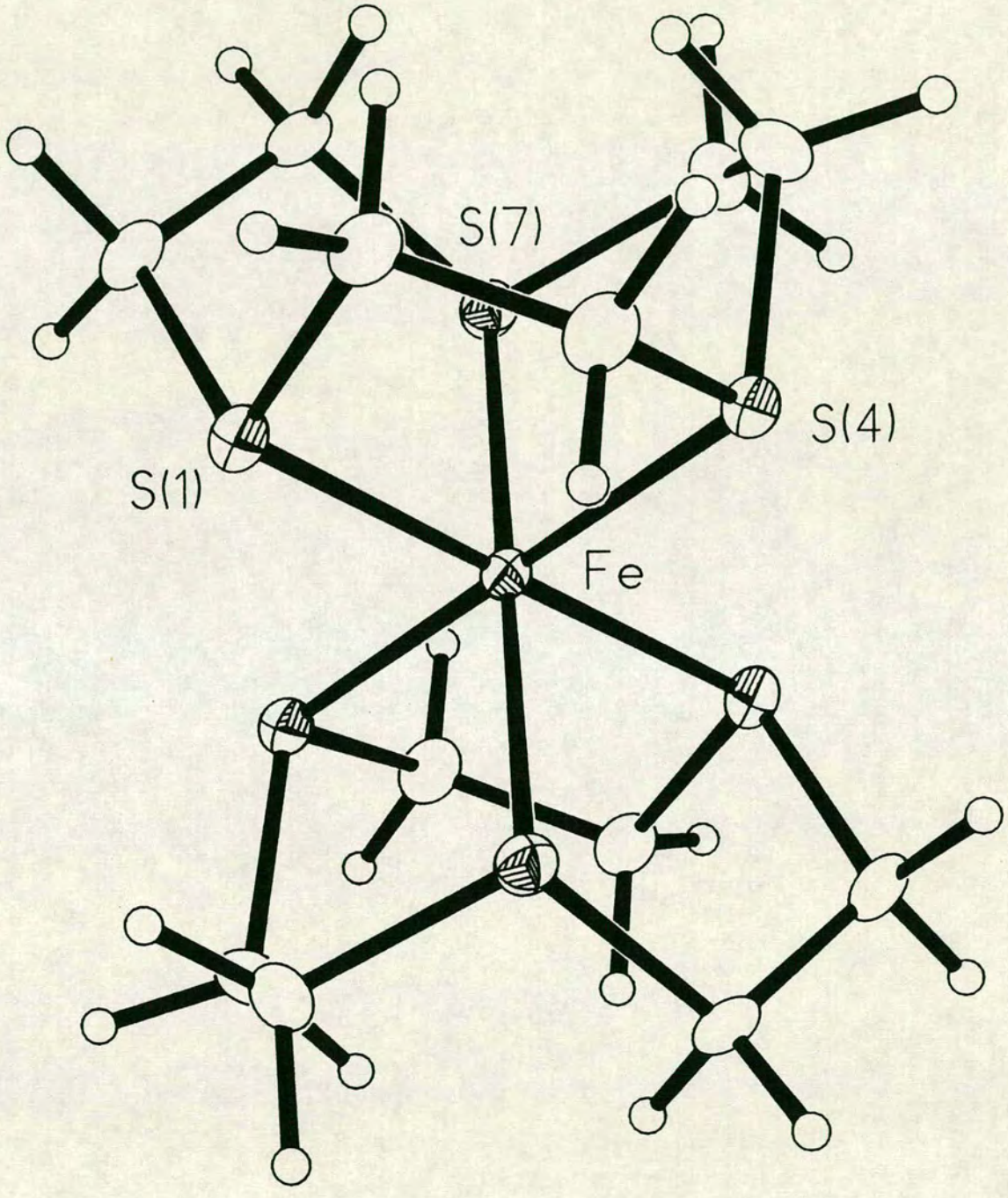

Figure 6.7 View of the single crystal X-ray structure of $[Fe([9]aneS_3)_2]^{2+}$

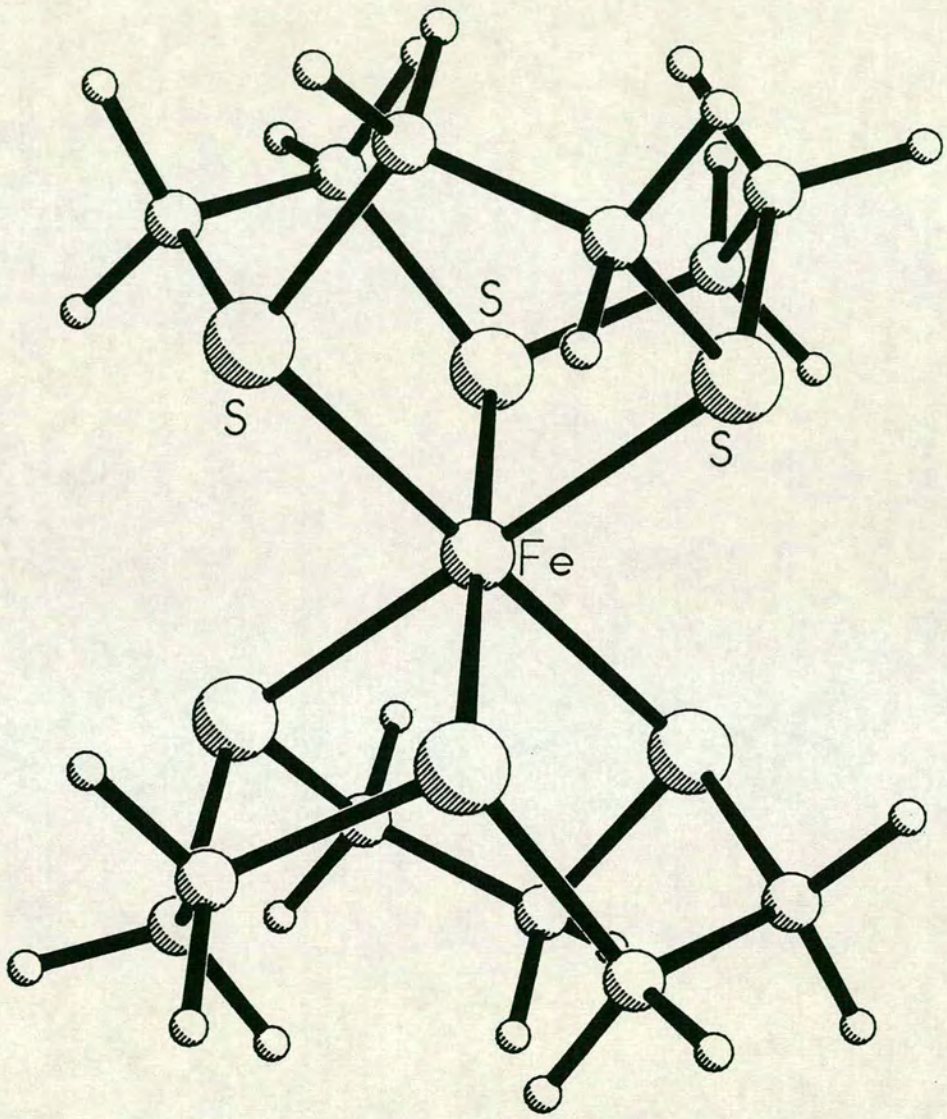

Figure 6.8 $[Fe([9]aneS_3)_2]^{3+}$

Table 6.1 Selected bond lengths (Å) of $[Fe([9]aneS_3)_2]^{2+}$

Fe - S(1)	2.2657(7)	C(3) - S(4)	1.820(3)
Fe - S(4)	2.2538(7)	S(4) - C(5)	1.831(3)
Fe - S(7)	2.2520(7)	C(5) - C(6)	1.519(4)
S(1) - C(2)	1.831(3)	C(6) - S(7)	1.824(3)
S(1) - C(9)	1.830(3)	S(7) - C(8)	1.842(3)
C(2) - C(3)	1.526(4)	C(8) - C(9)	1.520(4)

Table 6.2 Selected bond angles (°) of $[Fe([9]aneS_3)_2]^{2+}$

S(1) - Fe - S(4)	89.803(24)	Fe - S(4) - C(5)	105.26(9)
S(1) - Fe - S(7)	89.568(24)	C(3) - S(4) - C(5)	101.59(13)
S(4) - Fe - S(7)	90.236(24)	S(4) - C(5) - C(6)	111.12(19)
Fe - S(1) - C(2)	105.34(9)	C(5) - C(6) - S(7)	112.70(19)
Fe - S(1) - C(9)	102.38(9)	Fe - S(7) - C(6)	102.06(9)
C(2) - S(1) - C(9)	101.02(13)	Fe - S(7) - C(8)	105.89(9)
S(1) - C(2) - C(3)	110.33(19)	C(6) - S(7) - C(8)	101.95(13)
C(2) - C(3) - S(4)	112.63(19)	S(7) - C(8) - C(9)	110.06(19)
Fe - S(4) - C(3)	102.66(9)	S(1) - C(9) - C(8)	112.17(19)

Table 6.3 Selected torsion angles (°) of $[Fe([9]aneS_3)_2]^{2+}$

C(9) - S(1) - C(2) - C(3)	-136.60(20)	S(4) - C(5) - C(6) - S(7)	47.75(24)
C(2) - S(1) - C(9) - C(8)	64.69(21)	C(5) - C(6) - S(7) - C(8)	66.29(22)
S(1) - C(2) - C(3) - S(4)	49.00(24)	C(6) - S(7) - C(8) - C(9)	-136.48(19)
C(2) - C(3) - S(4) - C(5)	66.07(22)	S(7) - C(8) - C(9) - S(1)	49.38(23)
C(3) - S(4) - C(5) - C(6)	-134.55(20)		

S-donors provided by two facially co-ordinated [9]aneS$_3$ ligands. The Fe-S bond lengths are Fe-S(1) = 2.2657(7), Fe-S(4) =2.2538(7) and Fe-S(7) = 2.2520(7)Å, all of which are shorter than the Fe-S bond lengths observed for $[Fe([9]aneS_3)_2]^{3+}$: for $[Fe([9]aneS_3)_2](ClO_4)_3$, Fe-S(1) = 2.280(3); Fe-S(4) = 2.2846(25); Fe-S(7) = 2.276(3)Å[292]. The lengthening of the Fe-S bonds from $[Fe([9]aneS_3)_2]^{2+}$ to $[Fe([9]aneS_3)_2]^{3+}$ is good structural evidence for the π-acceptor properties of the thioether S-donors. In the absence of any π-interactions, it would be expected that the bond lengths would decrease on oxidation from Fe(II) to Fe(III) because of the increase of cation charge and the decrease in ionic radius of the metal centre. This conclusion is corroborated by the observation that the Fe-N bonds of $[Fe([9]aneN_3)_2]^{2+}$ shorten on oxidation to $[Fe([9]aneN_3)_2]^{3+}$: for $[Fe([9]aneN_3)_2]^{2+}$, average Fe-N bond length = 2.03(1)[304]; for $[Fe([9]aneN_3)_2]^{3+}$, Fe-N = 1.99(1)[304]. The opposite effect is observed on oxidation of $[Fe([9]aneS_3)_2]^{2+}$ to $[Fe([9]aneS_3)_2]^{3+}$ [292]. The elongation of the Fe-S bonds on oxidation is therefore caused by the removal of an electron from the bonding t_{2g} orbitals which then weakens the Fe $\rightarrow$ S π-back-bonding.

The lengthening of Fe-ligand bonds on oxidation of Fe(II) to Fe(III) has been noted for the low spin Fe(II) and Fe(III) complexes of other π-acceptor ligands, such as CN^- [305,306], 2,2-bipyridine[307,308] and phenanthroline[309,310]. These are shown in Table 6.4, with those of $[Fe([9]aneS_3)_2]^{2+}$ and $[Fe([9]aneS_3)_2]^{3+}$ for comparison.

6.2.3: The Synthesis and Attempted Activation of $[Fe([9]aneS_3)Cl_3]$

$[Fe([9]aneS_3)Cl_3]$ was prepared as described by Wieghardt *et al.*[298], by the reaction of one equivalent of [9]aneS$_3$ with $FeCl_3.6H_2O$ in CH_3OH. A red crystalline precipitate was obtained immediately, that was insoluble in all

Table 6.4: Structural data for low spin Fe(II) and Fe(III) complexes with [9]aneS_3 CN^-, 2,2-bipyridine and 1,10-phenanthroline

	Average Fe-L bond distance (Å)			
	Fe(II)-N	Fe(III)-N	Fe(II)-S	Fe(III)-S
Ligand				
[9]aneS_3	-	-	2.2572	2.280
CN^-	1.902	1.934	-	-
2,2-bipy	1.956	1.961	-	-
phen	1.97	1.973	-	-

common organic solvents. The i.r. spectrum of the insoluble red precipitate indicates the presence of the macrocycle [9]aneS$_3$, by the absorptions at 1440 and 1403cm^{-1}, which are assigned as C–S stretching vibrations and C–H deformations respectively. The strong absorption at 323cm^{-1} is assigned as a Fe–Cl stretching vibration and confirms the presence of the bound Cl$^-$ ligands. This evidence, together with elemental analytical data confirm the product to be [Fe([9]aneS$_3$)Cl$_3$].

Prolonged heating of [Fe([9]aneS$_3$)Cl$_3$] in polar organic solvents [CH$_3$OH, CH$_3$CN and (CH$_3$)$_2$CO] and H$_2$O gave a pink precipitate, which was identified as [Fe([9]aneS$_3$)$_2$]$^{2+}$ by i.r. and f.a.b. mass spectroscopy. We concluded then that a Cl–bridged species analogous to [([9]aneS$_3$)Ni(μ–Cl)$_3$Ni([9]aneS$_3$)]$^+$ [110] is not readily formed by Fe(III) and [9]aneS$_3$. Cl$^-$ bridged species can not be synthesized from FeCl$_2$.4H$_2$0 and [9]aneS$_3$ either[298] so we propose that the chemistry of [9]aneS$_3$ with Fe(II) and Fe(III) is dominated by the apparently thermodynamically favoured product [Fe([9]aneS$_3$)$_2$]$^{2+}$. It appears that the product [Fe([9]aneS$_3$)Cl$_3$] can only be isolated because of its insolubility and is prepared as the the kinetic product of the reaction between FeCl$_3$ with [9]aneS$_3$. [Fe([9]aneS$_3$)Cl$_3$] was also heated in C$_2$H$_5$OH in the presence of another facially co–ordinating ligand, triphos [(Ph$_2$PCH$_2$)$_3$CCH$_3$], in an attempt to trap any [Fe([9]aneS$_3$)(solvent)$_3$]$^{2+}$ species that might be briefly formed. The product of the reaction, however, was [Fe([9]aneS$_3$)$_2$]$^{2+}$ once more.

We have also attempted to activate [Fe([9]aneS$_3$)Cl$_3$] by chemical means, particularly Cl$^-$ abstraction by Tl$^+$ salts. The reaction of [Fe([9]aneS$_3$)Cl$_3$] with one equivalent of TlBF$_4$ in the presence of excess PR$_3$ [PR$_3$ = PPh$_3$, P(C$_6$H$_{11}$)$_3$] in CH$_3$OH still gave a pink precipitate of [Fe([9]aneS$_3$)$_2$]$^{2+}$ even when the reaction mixture was maintained at 273K. With a bidentate phosphine, however, evidence has been obtained for a half–sandwich

compound of Fe(II) and [9]aneS$_3$.

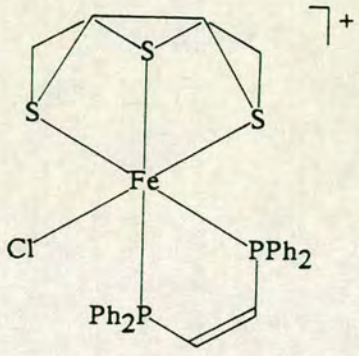

Figure 6.9 Proposed structure of [Fe([9]aneS$_3$)(dppv)Cl]$^+$

The reaction of [Fe([9]aneS$_3$)Cl$_3$] with two equivalents of TlPF$_6$ in the presence of dppv at room temperature rapidly gave a green solution and copious amounts of a white precipitate of TlCl. Addition of diethyl ether gave a green/brown solid, which was recrystallised by vapour diffusion of diethyl ether into CH_3NO_2 to give a brown solid. The f.a.b. mass spectrum of this brown solid shows peaks at M^+ = 486 and 666, which are assigned, with the correct isotope distribution patterns, as [^{56}Fe(dppv–H)^{35}Cl]$^+$ and [^{56}Fe([9]aneS$_3$)(dppv)^{35}Cl(–H)]$^+$ respectively. On the basis of this data and the i.r. spectrum of the brown solid, we tentatively assign the brown solid as [Fe([9]aneS$_3$)(dppv)Cl](PF$_6$). However the elemental analytical data shows that the compound was impure. The f.a.b. mass spectrum of the initial crude green/brown product shows additional peaks at M^+ = 848 and 883, which are assigned as [^{56}Fe(dppv)$_2$]$^+$ and [^{56}Fe(dppv)$_2$^{35}Cl]$^+$ respectively. Fortunately, the impurity that these peaks suggest, [Fe(dppv)$_2$Cl](PF$_6$), could be removed by recrystallisation. However, on repeated recrystallisations of the brown solid from CH_3NO_2/diethyl ether, small amounts of pink crystals appeared which have been identified as [Fe([9]aneS$_3$)$_2$](PF$_6$)$_2$. This suggests that the compound [Fe([9]aneS$_3$)(dppv)Cl](PF$_6$) slowly decomposes in solution to

$[Fe([9]aneS_3)_2](PF_6)_2$ and this impurity may be the cause of the disagreement between the elemental analytical data and the proposed formulation. A small amount of $[Fe([9]aneS_3)_2](PF_6)_2$ in the analysed sample would depress the percentages of both carbon and hydrogen (found C = 43.8; H = 3.79%. Calculated for $[Fe([9]aneS_3)(dppv)Cl](PF_6)$: C = 47.3; H = 4.21%. Calculated for $[Fe([9]aneS_3)_2](PF_6)_2$: C = 20.4; H = 3.42%). Further work is required for a full characterisation of this compound.

6.2.4: The Attempted Syntheses of $CH_3CO_2^-$ Bridged Fe Complexes with [9]aneS$_3$

The reaction of equimolar amounts of $Fe(CH_3CO_2)_2$ and [9]aneS$_3$ in dry CH_3CN under an inert atmosphere gave a pink precipitate of $[Fe([9]aneS_3)_2]^{2+}$, which was characterised by i.r. and f.a.b. mass spectroscopy. Repeating the reaction in dry CH_3OH gave a brown precipitate of the common basic carboxylate of Fe, $[Fe_3O(CH_3CO_2)_6]^+$. $[Fe_3O(CH_3CO_2)_6]^+$ was identified by i.r. spectroscopy by comparison with the spectrum of a commercial sample. These reactions persuaded us that Fe salts are unlikely to form $CH_3CO_2^-$ bridged dimers with [9]aneS$_3$ (at least under the conditions used here); this contrasts with the numerous examples known for $CH_3CO_2^-$ bridged dimers with Fe salts with [9]aneN$_3$ and Me$_3$[9]aneN$_3$[7,108]. Reasons for this behaviour of Fe complexes with [9]aneS$_3$ will be discussed later in Section 6.2.6.

6.2.5: The Synthesis of $[Fe([9]aneS_3)(CH_3CN)_3](BF_4)_2$

We have discovered that the solvated material $[Fe(CH_3CN)_6](BF_4)_2$ is a useful starting material for synthesizing thioether macrocyclic complexes of Fe(II) (see also Chapter 7). The CH_3CN ligands are readily replaced by thioether S-donors, provided H_2O is excluded from the reaction vessel. The

reactions described below involving $[Fe(CH_3CN)_6](BF_4)_2$ and its derivatives therefore have to be performed under N_2 in Schlenk apparatus using dried solvents.

$[Fe(CH_3CN)_6](BF_4)_2$ was prepared by the method of Underhill *et al.*[219], by the oxidation of Fe metal to Fe(II) in CH_3CN using $NOBF_4$ as the oxidising agent. The NO formed in the reaction can be removed during the experiment by evacuating the Schlenk tube. $[Fe(CH_3CN)_6](BF_4)_2$ is very deliquescent and rapidly dissolves on contact with air. However, solutions of $[Fe(CH_3CN)_6](BF_4)_2$ in CH_3NO_2 and CH_3CN can be stored cold under N_2 for several weeks. The compound $[Fe(CH_3CN)_6](BF_4)_2$ could not be fully characterised due to this reactivity with H_2O in the air but was used as a colourless solid as described in the literature[219].

The reaction of equimolar amounts of $[Fe(CH_3CN)_6](BF_4)_2$ and [9]aneS_3 in dry CH_3NO_2 under N_2 rapidly gave an intense purple solution, which decolourised immediately on exposure to air. Attempts to isolate a solid material from the purple solution by the addition of diethyl ether appeared to give pink $[Fe([9]aneS_3)_2](BF_4)_2$. We are not sure whether the formation of $[Fe([9]aneS_3)_2]^{2+}$ occurred because of attempting to isolate a solid material from the purple solution or due to accidental exposure to air during the characterisation procedure. We propose, however, that $[Fe([9]aneS_3)_2](BF_4)_2$ is not the initial product of the reaction of $[Fe(CH_3CN)_6]^{2+}$ and [9]aneS_3, since $[Fe([9]aneS_3)_2](BF_4)_2$ is not very soluble in CH_3NO_2 and gives a pale pink solution. Considering the stoichiometry of the reaction, we propose that $[Fe([9]aneS_3)(CH_3CN)_3](BF_4)_2$ is the kinetic product between equimolar amounts of $[Fe(CH_3CN)_6](BF_4)_2$ and [9]aneS_3 in CH_3NO_2. Unfortunately the only data we could obtain on the purple solution was a U.V./visible spectrum in CH_3NO_2 which shows an absorption at $\lambda_{max.}$ = 544nm. ($\varepsilon_{max.}$ = $54M^{-1}cm^{-1}$) and a shoulder to the solvent absorption band at

$\lambda \approx 390$nm. ($\varepsilon = 40$). Interestingly, performing the same reaction in CH_3CN gave a pink precipitate of $[Fe([9]aneS_3)_2](BF_4)_2$. This suggests that any $[Fe([9]aneS_3)(CH_3CN)_3]^{2+}$ formed in CH_3CN rapidly disproportionates to $[Fe([9]aneS_3)_2]^{2+}$ and $[Fe(CH_3CN)_6]^{2+}$. In CH_3NO_2 this disproportionation does not happen because the CH_3NO_2 solvent dilutes the liberated CH_3CN molecules on forming $[Fe([9]aneS_3)(CH_3CN)_3]^{2+}$ and CH_3NO_2 is too poor a ligand for Fe(II) to substitute a co-ordinated [9]aneS$_3$ ligand. $[Fe(CH_3CN)_6](BF_4)_2$ is insoluble in CH_2Cl_2 or THF and does not react with solutions of [9]aneS$_3$ in these solvents. On the evidence available, we propose that the purple solution contains the half-sandwich complex $[Fe([9]aneS_3)(CH_3CN)_3](BF_4)_2$, but we have little data to confirm this assignment.

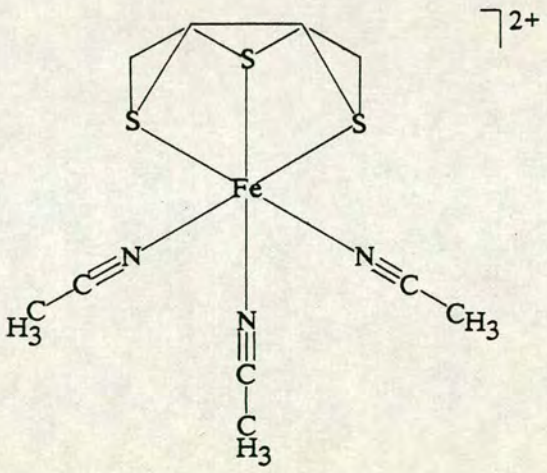

Figure 6.10 Proposed structure of $[Fe([9]aneS_3)(CH_3CN)_3]^{2+}$

6.2.6: Reactions of $[Fe([9]aneS_3)(CH_3CN)_3](BF_4)_2$ with Phosphine, Amine, $CH_3CO_2^-$ and Organometallic Ligands

Due to the difficulty in obtaining data on the half-sandwich complex $[Fe([9]aneS_3)(CH_3CN)_3](BF_4)_2$, we proposed that it might be possible to stabilise the $(Fe-[9]aneS_3)^{2+}$ unit by replacing some or all of the CH_3CN ligands in $[Fe([9]aneS_3)(CH_3CN)_3](BF_4)_2$ by other, possibly chelating ligands.

A series of reactions were attempted by stirring $[Fe([9]aneS_3)(CH_3CN)_3](BF_4)_2$ in CH_3NO_2 under N_2 with CH_3NO_2 solutions of monodentate (PPh_3), bidentate (dppe, dppv) and tridentate (triphos) phophines and $(Bu^n_4N)CH_3CO_2$. All the experiments yielded pink products that were characterised as $[Fe([9]aneS_3)_2](BF_4)_2$, by i.r. and f.a.b. mass spectroscopy. Reactions of $[Fe([9]aneS_3)(CH_3CN)_3](BF_4)_2$ with dppe and dppv in CH_3NO_2 at 253K also gave pink precipitates of $[Fe([9]aneS_3)_2](BF_4)_2$. The other products of the reactions with dppe and dppv are $[Fe(dppe)_2(CH_3CN)_2](BF_4)_2$ and $[Fe(dppv)_2(CH_3CN)_2](BF_4)_2$ respectively and their characterisation is given in Chapter 7. We propose that these reactions proceed similarly to that of $[Fe([9]aneS_3)(CH_3CN)_3](BF_4)_2$ in CH_3CN described in Section 6.2.5, by disproportionation of $[Fe([9]aneS_3)(CH_3CN)_3](BF_4)_2$ to give $[Fe([9]aneS_3)_2](BF_4)_2$ and a product of $[Fe(CH_3CN)_6](BF_4)_2$ with the other ligands. The driving force for these reactions is probably the formation of the thermodynamically favoured product $[Fe([9]aneS_3)_2](BF_4)_2$.

The reaction of $[Fe([9]aneS_3)(CH_3CN)_3](BF_4)_2$ with $CH_3NH\text{–}NH_2$ in CH_3NO_2 and under N_2 gave a brown solution and a brown solid was obtained on addition of diethyl ether. On exposure to air this product deliquesced very rapidly and could not be characterised. $[Fe([9]aneS_3)(CH_3CN)_3](BF_4)_2$ did not react with CO, cyclohex–1–ene, benzene, cyclo–octa–1,5–diene, excess $NaBH_4$ or elemental sulphur in CH_3NO_2 under N_2.

The conclusion we drew from this series of reactions was that half–sandwich compounds of $[9]aneS_3$ with Fe(II) are difficult to prepare due to their relative instability with respect to the formation of $[Fe([9]aneS_3)_2](BF_4)_2$. The rapid formation of $[Fe([9]aneS_3)_2](BF_4)_2$ at low temperatures (253K) suggests that $[Fe([9]aneS_3)_2](BF_4)_2$ is the favoured

product both thermodynamically and kinetically. Hancock and co-workers have reported molecular mechanics calculations[311] on the complexes $[M([9]aneS_3)_2]^{2+}$ and $[M([9]aneN_3)_2]^{2+}$ (M = Fe, Co, Ni), by considering the total strain energy of the complexes as a function of the covalent radius of the metal ion. They concluded that the most significant factor influencing the strain energies of the complexes was the non-bonded repulsions between the two facially co-ordinated ligands. The strain energies were calculated to be lower for the $[M([9]aneS_3)_2]^{2+}$ than the corresponding $[M([9]aneN_3)_2]^{2+}$ complexes and this was attributed to the longer M-S bonds which reduce steric crowding in the $[M([9]aneS_3)_2]^{2+}$ complexes. This has the result that the best-fit covalent radius for a metal ion co-ordinated as $[M([9]aneS_3)_2]^{2+}$ is 1.27Å, which is much shorter than the 1.40Å value for $[M([9]aneN_3)_2]^{2+}$. These calculations are shown graphically in Figure 6.11.

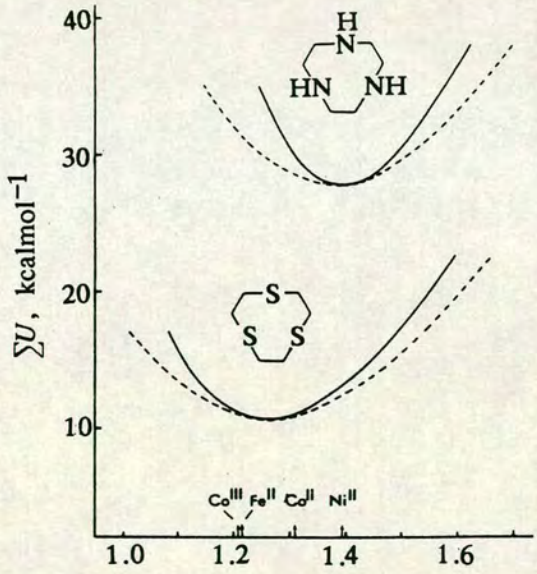

Figure 6.11 A graph of the calculated total strain energies, ΣU, of the complexes $[M([9]aneS_3)_2]^{2+}$ and $[M([9]aneN_3)_2]^{2+}$ against the covalent radii of the metal ions M = Fe, Co, Ni[311]

The graph shows that the $[M([9]aneS_3)_2]^{2+}$ complex with the lowest strain energy is $[Fe([9]aneS_3)_2]^{2+}$, while for the $[M([9]aneN_3)_2]^{2+}$ complexes

the best-fit metal ion is the larger Ni(II) ion in $[Ni([9]aneN_3)_2]^{2+}$. The implication of this is that $[Fe([9]aneS_3)_2]^{2+}$ is both kinetically inert and a thermodynamically favoured product[311]. These calculations may partly explain why it is possible to synthesize a chloro-bridged Ni(II) complex with [9]aneS$_3$, $[([9]aneS_3)Ni(\mu\text{-}Cl)_3Ni([9]aneS_3)]^+$, and $CH_3CO_2^-$ bridged Fe(II) complexes with [9]aneN$_3$[7], but half-sandwich Fe(II) complexes of [9]aneS$_3$ are very difficult to prepare.

6.2.7: The Synthesis of $[Co([9]aneS_3)_2](PF_6)_2$

The synthesis of $[Co([9]aneS_3)_2](PF_6)_2$ has been described by Glass *et al.*[293] We have developed a simpler synthetic procedure and this is given below. The reaction of $CoCl_2.6H_2O$ with two equivalents of [9]aneS$_3$ in CH_3CN gave an immediate blue precipitate, which on addition of H_2O dissolved to give a pale purple solution. The addition of excess NH_4PF_6 and removal of solvent gave a purple crystalline solid. The f.a.b. mass spectrum of the purple solid shows peaks at M^+ = 419 and 564, which are assigned to $[^{59}Co(C_6H_{12}S_3)_2]^+$ and $[^{59}Co(C_6H_{12}S_3)_2](PF_6)^+$ respectively. The i.r. spectrum and elemental analytical figures for the purple solid also confirm the assignment of the complex as $[Co([9]aneS_3)_2](PF_6)_2$.

6.2.8: The Single Crystal X-ray Structure of $[Co([9]aneS_3)_2](PF_6)_2.2CH_3NO_2$

Details of the structure solution and refinement are given in the Experimental Section. Tables of relevant bond lengths, angles and torsions are given in Tables 6.4, 6.5 and 6.6 respectively. A view of the cation of $[Co([9]aneS_3)_2](PF_6)_2$ is shown in Figure 6.12.

The single crystal X-ray structure of $[Co([9]aneS_3)_2](PF_6)_2$ shows distorted octahedral co-ordination at the metal ion and the structures of the PF_6^- counterion and included CH_3NO_2 solvent molecules are unremarkable.

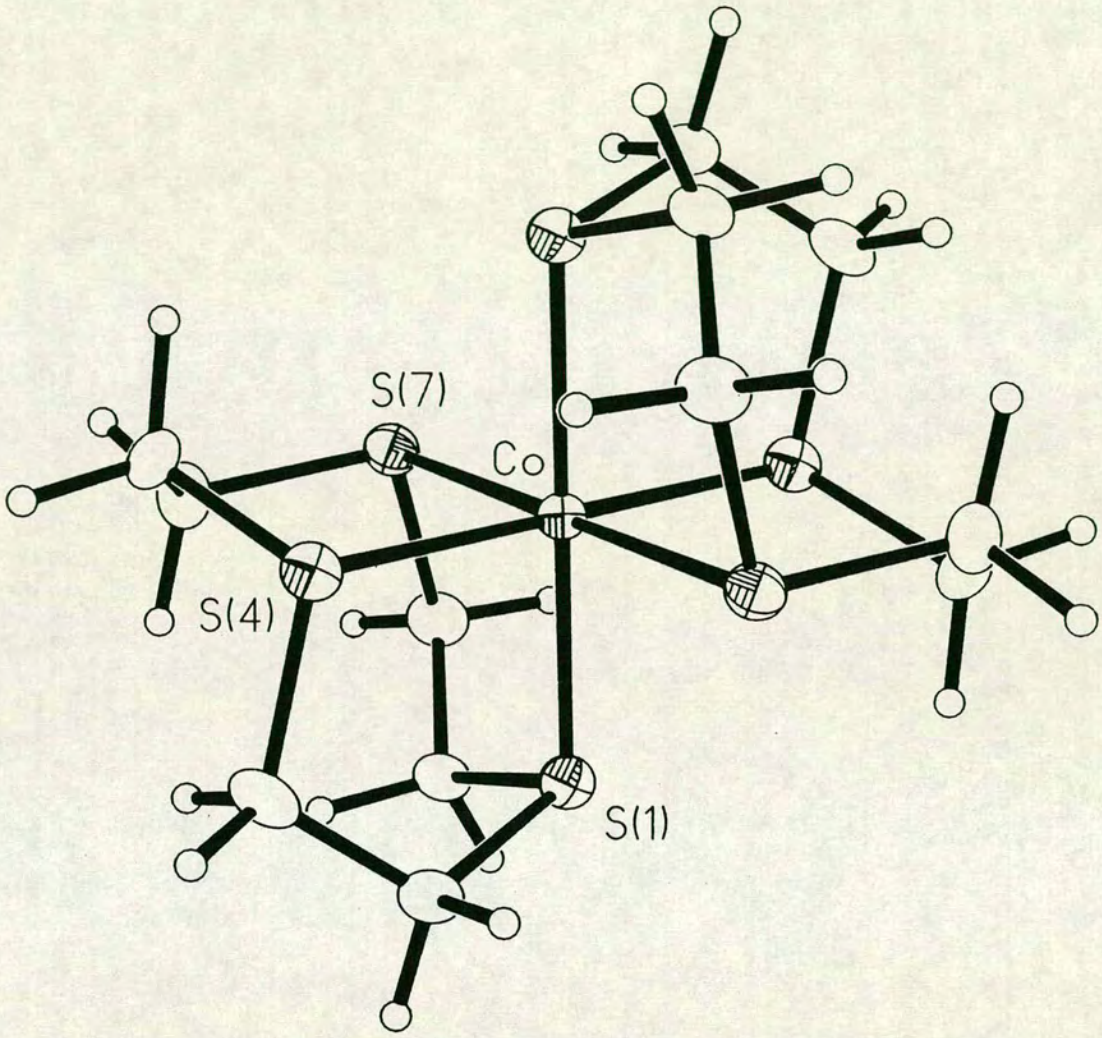

Figure 6.12 View of the single crystal X-ray structure of $[Co([9]aneS_3)_2]^{2+}$

Table 6.5 Selected bond lengths (Å) of $[Co([9]aneS_3)_2](PF_6)_2$

Co - S(1)	2.2649(22)	C(3) - S(4)	1.830(9)
Co - S(4)	2.2796(23)	S(4) - C(5)	1.831(9)
Co - S(7)	2.4298(23)	C(5) - C(6)	1.508(13)
S(1) - C(2)	1.816(9)	C(6) - S(7)	1.847(9)
S(1) - C(9)	1.820(9)	S(7) - C(8)	1.819(9)
C(2) - C(3)	1.513(12)	C(8) - C(9)	1.531(12)

Table 6.6 Selected bond angles (°) of $[Co([9]aneS_3)_2](PF_6)_2$

S(1) - Co - S(4)	90.25(8)	Co - S(4) - C(5)	102.6(3)
S(1) - Co - S(7)	89.39(8)	C(3) - S(4) - C(5)	102.5(4)
S(4) - Co - S(7)	88.61(8)	S(4) - C(5) - C(6)	113.2(6)
Co - S(1) - C(2)	101.2(3)	C(5) - C(6) - S(7)	111.7(6)
Co - S(1) - C(9)	106.1(3)	Co - S(7) - C(6)	101.7(3)
C(2) - S(1) - C(9)	102.8(4)	Co - S(7) - C(8)	98.6(3)
S(1) - C(2) - C(3)	113.8(6)	C(6) - S(7) - C(8)	103.3(4)
C(2) - C(3) - S(4)	110.9(6)	S(7) - C(8) - C(9)	114.8(6)
Co - S(4) - C(3)	104.5(3)	S(1) - C(9) - C(8)	113.0(6)

Table 6.7 Selected torsion angles (°) of $[Co([9]aneS_3)_2](PF_6)_2$

C(9) - S(1) - C(2) - C(3)	-65.4(7)	S(4) - C(5) - C(6) - S(7)	-53.6(8)
C(2) - S(1) - C(9) - C(8)	133.0(6)	C(5) - C(6) - S(7) - C(8)	133.9(6)
S(1) - C(2) - C(3) - S(4)	-49.1(8)	C(6) - S(7) - C(8) - C(9)	-62.2(7)
C(2) - C(3) - S(4) - C(5)	134.8(6)	S(7) - C(8) - C(9) - S(1)	-48.9(8)
C(3) - S(4) - C(5) - C(6)	-62.2(7)		

The metal centre occupies a crystallographic inversion centre, so the two [9]aneS$_3$ ligands are in identical environments. The octahedral co-ordination of the Co(II) metal ion is distorted by a tetragonal elongation along one axis [Co-S(1) = 2.2649(22), Co-S(4) = 2.2796(23), Co-S(7) = 2.4298(23)Å], as is expected for a Jahn-Teller distorted low spin d^7 octahedral metal centre.

The single crystal X-ray structure of $[Co([9]aneS_3)_2]^{2+}$ has been previously reported as a BF_4^- salt[293]. However, the structure of $[Co([9]aneS_3)_2](BF_4)_2$ is unusual since the Jahn-Teller distorted Co(II) centre is tetragonally compressed [Co-S(1) = 2.356(6), Co-S(4) = 2.240(7), Co-S(7) = 2.367(5)Å][293]. This is in direct contrast to the structure of $[Co([9]aneS_3)_2](PF_6)_2$ that we have determined. We therefore proposed to establish the cause of the structural variations in $[Co([9]aneS_3)_2]^{2+}$. Both structures contain two molecules of CH_3NO_2 per dication, so the most significant difference between the two structures is in the anion. It is also relevant to note here that our structure determination was carried out at 150K but the temperature at which the structure of $[Co([9]aneS_3)_2](BF_4)_2$ by Glass *et al.* was determined is not reported[293]. Significantly, the average of one of the short bonds and the elongated bond in the PF_6^- structure is approximately 2.35Å. This value is close to the two longer bond lengths in the BF_4^- structure. Therefore, it is possible that the two longer Co-S distances in the "compressed", BF_4^- structure are really dynamical averages of one elongated and one short (ca.2.26Å) bond length (as observed in the PF_6^- structure). A dynamic average of a Jahn-Teller distortion is more likely to be observed if the $[Co([9]aneS_3)_2](BF_4)_2$ structure had been determined at ambient temperatures. In order to ascertain whether the differences in the two $[Co([9]aneS_3)_2]^{2+}$ structures are due to counterion or temperature effects, we proposed to undertake an e.s.r. study of $[Co([9]aneS_3)_2](BF_4)_2$ and $[Co([9]aneS_3)_2](PF_6)_2$.

6.2.9: An E.s.r Study of $[Co([9]aneS_3)_2](BF_4)_2$ and $[Co([9]aneS_3)_2](PF_6)_2$

The fluid solution e.s.r. spectra of $[Co([9]aneS_3)_2](BF_4)_2$ and $[Co([9]aneS_3)_2](PF_6)_2$ in CH_3NO_2 at 293K are identical and show isotropic signals with g_{iso} = 2.10 and hyperfine coupling to ^{59}Co (I = 7/2, 100%) producing octets with A_{iso} = 40.2G (Figures 2.13 and 2.14).

The e.s.r spectra of $[Co([9]aneS_3)_2](BF_4)_2$ and $[Co([9]aneS_3)_2](PF_6)_2$ in CH_3NO_2 as frozen glasses at 77K are shown in Figures 2.15 and 2.16 respectively. There are slight differences between the spectra but both are tentatively analysed as anisotropic signals with g tensor values corresponding to a d_z2 ground state. If these are axial signals then the preliminary assignments are: for $[Co([9]aneS_3)_2](BF_4)_2$, $g_\perp$ = 2.13 ($A_\perp$ = 73.3G); $g_{||}$ = 2.04 ($A_{||}$ = 38.3G). For $[Co([9]aneS_3)_2](PF_6)_2$, $g_\perp$ = 2.12 ($A_\perp$ = 73.2G); $g_{||}$ = 2.04 ($A_{||}$ = 38.3G). The components show hyperfine coupling to the ^{59}Co nucleus and the octet patterns for the signals cause problems for analysing these spectra, so these assignments are only tentative. Computer simulations of the spectra are currently being undertaken at the University of Manchester.

To investigate possible $[Co([9]aneS_3)_2]^{2+}$–counterion interactions in the solid–state, e.s.r. powder spectra of $[Co([9]aneS_3)_2](BF_4)_2$ and $[Co([9]aneS_3)_2](PF_6)_2$ were required. The $[Co([9]aneS_3)_2]^{2+}$ species were suspended in a diamagnetic host to dilute the paramagnetism of the d^7 Co^{II} compounds and good quality powder spectra were obtained using 2% $[Co([9]aneS_3)_2](BF_4)_2$ in $[Fe([9]aneS_3)_2](BF_4)_2$ and 2% $[Co([9]aneS_3)_2](PF_6)_2$ in $[Fe([9]aneS_3)_2](PF_6)_2$. $[Fe([9]aneS_3)_2]^{2+}$ (see Section 6.2.1) was chosen as the host because of the identical nuclear charges and similar sizes of the Fe(II) and Co(II) cations. The powders were obtained by dissolving crystalline samples of the appropriate $[Co([9]aneS_3)_2]^{2+}$ and

Figure 6.13 Solution e.s.r. spectrum of $[Co([9]aneS_3)_2](BF_4)_2$

CH_3NO_2 fluid solution at 298K

Centre field 3300G

Sweep width 2000G

9.68GHz

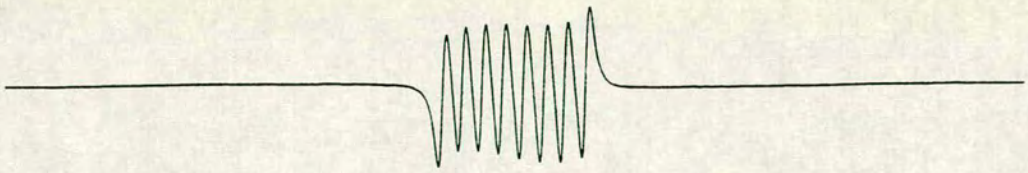

Figure 6.14 Solution e.s.r. spectrum of $[Co([9]aneS_3)_2](PF_6)_2$

CH_3NO_2 fluid solution at 298K

Centre field 3300G

Sweep width 2000G

9.68GHz

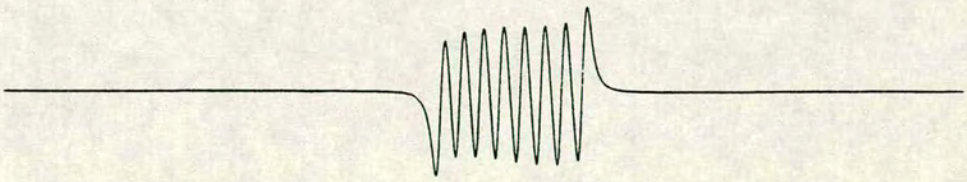

Figure 6.15 Frozen glass e.s.r. spectrum of $[Co([9]aneS_3)_2](BF_4)_2$

CH_3NO_2 frozen glass at 77K

Centre field 3300G

Sweep field 2000G

9.35GHz

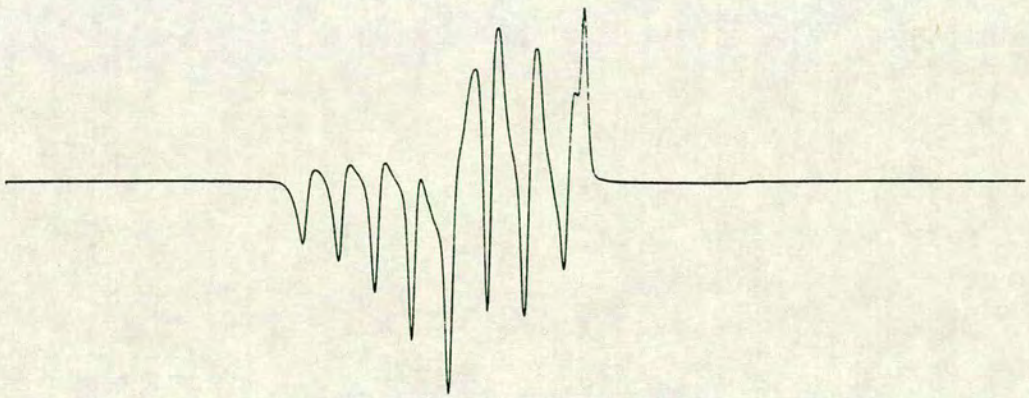

Figure 6.16 Frozen glass e.s.r. spectrum of $[Co([9]aneS_3)_2](PF_6)_2$

CH_3NO_2 frozen glass at 77K

Centre field 3300G

Sweep field 2000G

9.35GHz

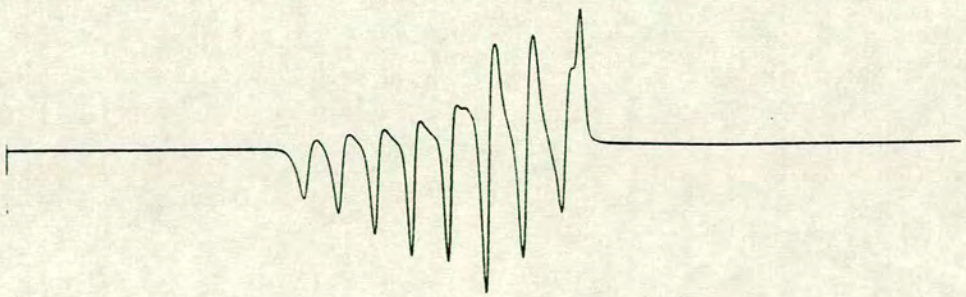

Figure 6.17 Powder e.s.r. spectrum of $[Fe([9]aneS_3)_2](BF_4)_2$ doped with 2% $[Co([9]aneS_3)_2](BF_4)_2$ at 293K

Centre field 3300G

Sweep field 2000G

9.35GHz

Figure 6.18 Powder e.s.r. spectrum of $[Fe([9]aneS_3)_2](PF_6)_2$ doped with 2% $[Co([9]aneS_3)_2](PF_6)_2$ at 293K

Centre field 3300G

Sweep field 2000G

9.36GHz

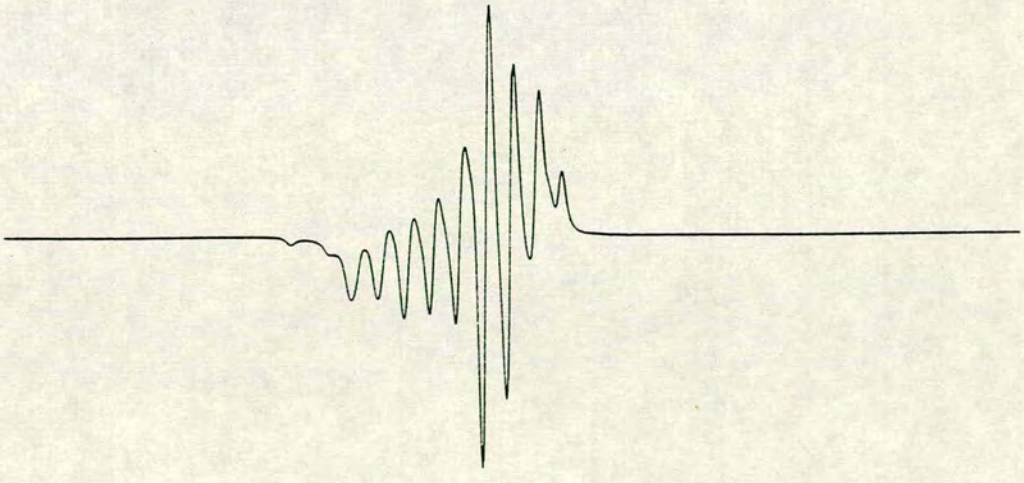

Figure 6.19 Powder e.s.r. spectrum of $[Fe([9]aneS_3)_2](BF_4)_2$ doped with 2% $[Co([9]aneS_3)_2](BF_4)_2$ at 77K

Centre field 3300G

Sweep field 2000G

9.35GHz

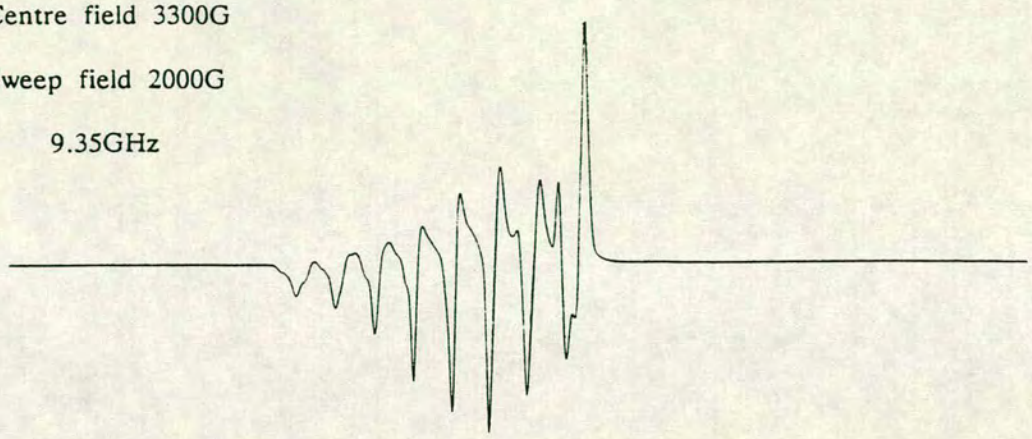

Figure 6.20 Powder e.s.r. spectrum of $[Fe([9]aneS_3)_2](PF_6)_2$ doped with 2% $[Co([9]aneS_3)_2](PF_6)_2$ at 77K

Centre field 3300G

Sweep field 2000G

9.36GHz

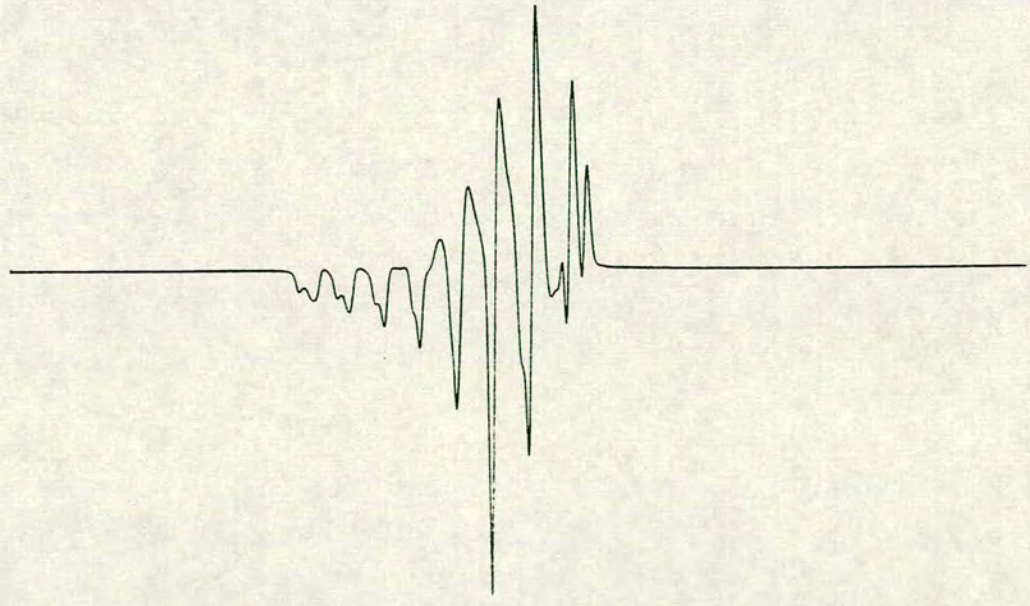

Figure 6.21 Second derivative of powder e.s.r. spectrum of $[Fe([9]aneS_3)_2)](BF_4)_2$ doped with 2% $[Co([9]aneS_3)_2](BF_4)_2$ at 77K

Centre field 3300G

Sweep field 2000G

9.35GHz

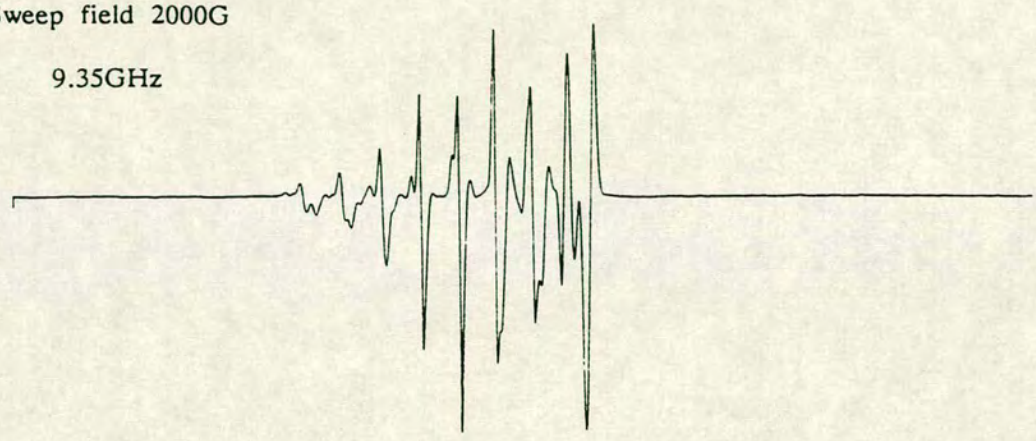

Figure 6.22 Second derivative of powder e.s.r. spectrum of $[Fe([9]aneS_3)_2)](PF_6)_2$ doped with 2% $[Co([9]aneS_3)_2](PF_6)_2$ at 77K

Centre field 3300G

Sweep field 2000G

9.36GHz

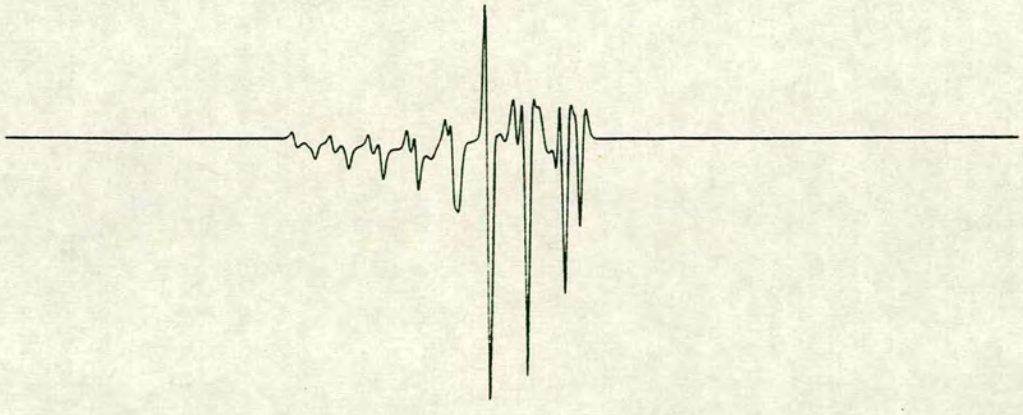

$[Fe([9]aneS_3)_2]^{2+}$ salts in CH_3NO_2 and filtering the resultant solution into diethyl ether.

The e.s.r. powder spectra of the doped samples show anisotropic signals and show distinct differences between the BF_4^- and PF_6^- salts both at room temperature and at 77K. The powder spectra of $[Co([9]aneS_3)_2](BF_4)_2$ and $[Co([9]aneS_3)_2](PF_6)_2$ at 293K are shown in Figures 6.17 and 6.18 respectively and the powder spectra of $[Co([9]aneS_3)_2](BF_4)_2$ and $[Co([9]aneS_3)_2](PF_6)_2$ at 77K are shown in Figures 6.19 and 6.20 respectively. Second derivative spectra at 77K for $[Co([9]aneS_3)_2](BF_4)_2$ and $[Co([9]aneS_3)_2](PF_6)_2$ are shown in Figures 6.21 and 6.22. Again, the spectra are very complicated and even tentative assignments have been possible only for some of the g tensor components at 293K. These are: for 2% $[Co([9]aneS_3)_2](BF_4)_2$ in $[Fe([9]aneS_3)_2](BF_4)_2$, $g_1 = 2.13$ ($A_1 = 68.5G$); $g_2 = 2.11$ ($A_2 = 68.9G$); g_3 unknown. For 2% $[Co([9]aneS_3)_2](PF_6)_2$ in $[Fe([9]aneS_3)_2](PF_6)_2$, $g_1 = 2.14$ ($A_1 = 72.0G$); $g_2 = 2.07$ ($A_2 = 48.3G$); g_3 unknown. These spectra are also being simulated at the University of Manchester and we hope to obtain more data on receipt of this information.

This study is at an early stage and definite conclusions can not yet be drawn. However it does appear to us that there are differences between the BF_4^- and PF_6^- salts of $[Co([9]aneS_3)]^{2+}$ in the solid-state at both room temperature and 77K, suggesting dependence of the electronic states of the low spin d^7 Co(II) ions on the counterion present. At this stage, speculation on the nature of this dependence is not possible.

6.2.10: The Synthesis of $[Co([9]aneS_3)(dppe)](PF_6)_2$

The reaction of equimolar amounts of $[Co(dppe)_2Cl]Cl$ (prepared by the method of Horrocks *et al.*[312]) and $[9]aneS_3$ in CH_2Cl_2 in the presence of two equivalents of $TlPF_6$ under N_2 gave brown and white precipitates. The

precipitates were removed by centrifugation from the reaction mixture and addition of CH_3CN to the solid mixture dissolved the brown solid to leave copious amounts of white TlCl. The brown CH_3CN solution produced a brown crystalline solid on vapour diffusion with diethyl ether. Fractional recrystallisation of the brown solid from CH_3CN/diethyl ether by vapour diffusion enabled the removal of a pink side product, which was identified as $[Co([9]aneS_3)_2](PF_6)_2$. The f.a.b. mass spectrum of the brown solid shows peaks at M^+ = 457, 476, 609, 637, 656 and 782, which are assigned as $[^{59}Co(dppe)]^+$, $[^{59}Co(dppe)(H_3O)]^+$, $[^{59}Co([9]aneS_3)(dppe)(-C_2H_4)]^+$, $[^{59}Co([9]aneS_3)(dppe)]^+$, $[^{59}Co([9]aneS_3)(dppe)(H_3O)]^+$ and $[^{59}Co([9]aneS_3)(dppe)](PF_6)^+$ respectively. This evidence, together with the i.r. spectrum and elemental analytical data, confirms the product to be $[Co([9]aneS_3)(dppe)](PF_6)_2$.

The half-sandwich complex $[Co([9]aneS_3)(dppe)](PF_6)_2$ has been successfully prepared only in CH_2Cl_2; reactions of $[Co(dppe)_2Cl]Cl$ with [9]*ane*S_3 in CH_3CN, CH_3OH or CH_3NO_2 yielded the starting material $[Co(dppe)_2Cl]^+$ and $[Co([9]aneS_3)_2]^{2+}$. We propose that the successful preparation of $[Co([9]aneS_3)(dppe)](PF_6)_2$ is due to its low solubility in CH_2Cl_2, which prevents the decomposition of the product to $[Co([9]aneS_3)_2](PF_6)_2$. Furthermore, we have not been able to prepare other diphosphine analogues of $[Co([9]aneS_3)(dppe)](PF_6)_2$ with dppv and dppm. Importantly, it has been reported that the diphosphine starting materials $[Co(dppv)_2Cl]^+$ [313,314] and $[Co(dppm)_2Cl]^+$ [313] have significantly different reactivities to $[Co(dppe)_2Cl]^+$. $[Co(dppe)_2Cl]^+$ has been shown to interconvert rapidly between two forms to give an equilibrium mixture in common organic solvents[315]. The two isomers of $[Co(dppe)_2Cl^+$ are either red, square-pyramidal or green, trigonal-bipyramidal, both of which have been structurally characterised (see Figure 6.23)[315]. Significantly, the mechanism

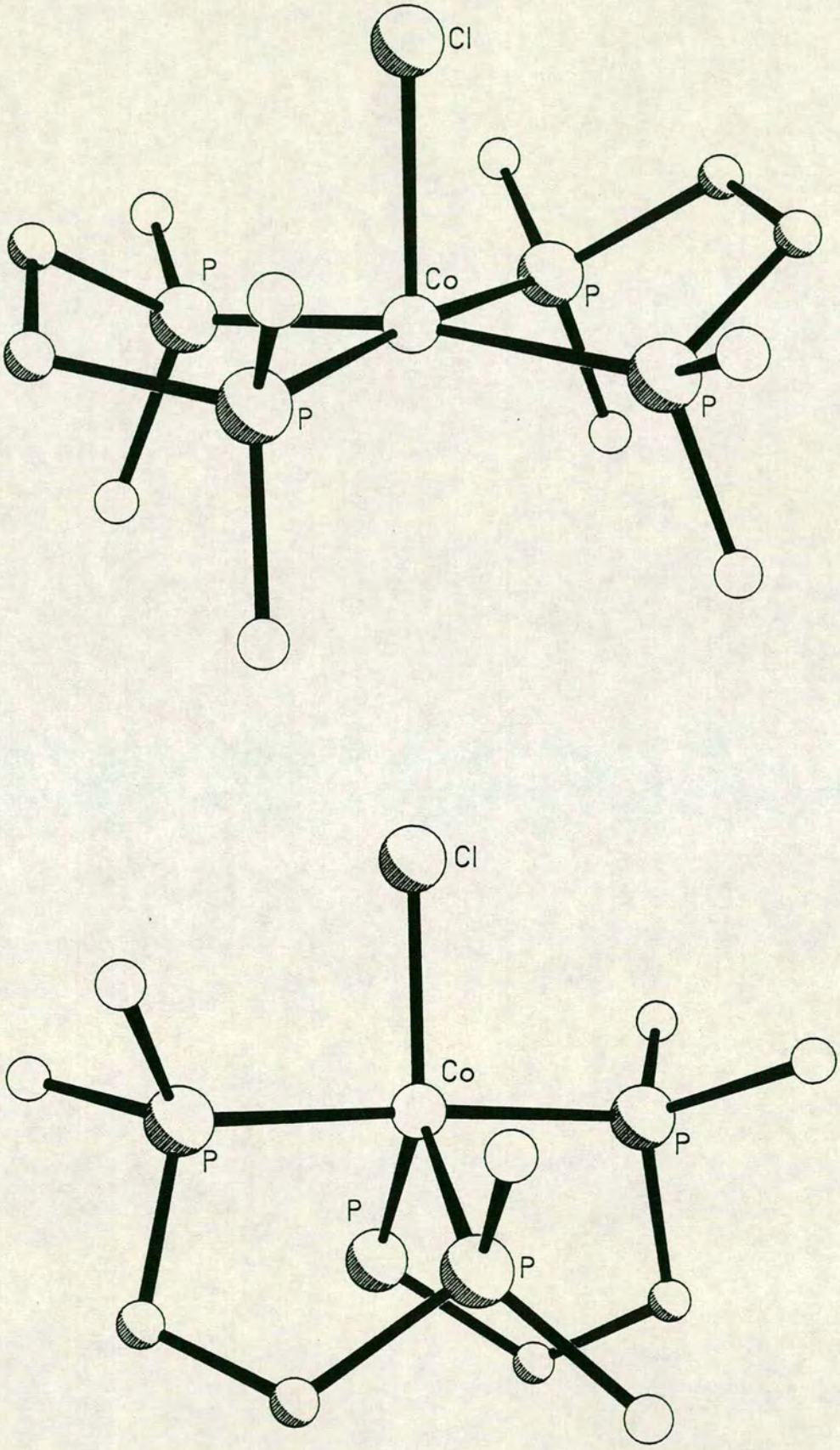

Figure 6.23 Two isomers of $[Co(dppe)_2Cl]^+$

(Phenyl rings omitted for clarity)

proposed for the isomerisation was a dissociative one[315], with one end of a phosphine ligand dissociating followed by the formation of either isomer. Molecular models indicate considerable steric hindrance to reorganisation by non-dissociative conformation changes[315]. Therefore a straightforward mechanism for substitution reactions to, for example, $[Co([9]aneS_3)(dppe)](PF_6)_2$ can be formulated. In contrast to this, $[Co(dppv)_2Cl]^+$ and $[Co(dppm)_2Cl]^+$ are expected to be stereochemically rigid, because of the alkene planarity of the dppv ligand and the "ring strain" of the dppm ligand on co-ordination respectively[313]. This suggested to us that the dppv and dppm ligands of the $[Co(diphosphine)_2X]^+$ complexes are considerably more difficult to substitute than dppe ligands are. Evidence for this dichotomy is given by a known series of Co(III) complexes, $[Co(dppv)_2X_2]^+$, [X = Cl^-, Br^-, NCO^-, N_3^-, NCS^-, NO^- and $\frac{1}{2}(O_2^{2-})$][332], whereas the analogous dppe complexes are unstable. Since the Rh(III) analogues of these complexes, $[Rh(diphosphine)_2X_2]^+$ are very stable with both dppv and dppe, Gray *et al.*[314] suggested that the cause of the instability of the $[Co^{III}(dppe)_2X_2]^+$ species is predominantly steric. Unfortunately, the dppp form of $[Co(diphosphine)_2Cl]^+$, which might be similar to $[Co(dppe)_2Cl]^+$, can not be synthesized[312].

The solution e.s.r. spectrum of $[Co([9]aneS_3)(dppe)](PF_6)_2$ in CH_3NO_2 at 293K shows a signal which is not easily rationalised (see Figure 2.24). The sample used was analytical pure, so impurities are not expected. However there appear to be two g components, rather than the expected isotropic signal. An eight-line signal is observed at g = 2.09 and with a hyperfine coupling to ^{59}Co (I = 7/2, 100%) of A = 40.4G. This is admittedly similar to the e.s.r. solution spectrum of $[Co([9]aneS_3)_2]^{2+}$. There is also a three-line signal at g = 2.22 with a (super)hyperfine coupling (possibly to two ^{31}P nuclei, I = 1/2, 100%) of A = 20.2G. We do not know how to interpret

Figure 6.24 Solution e.s.r. spectrum of $[Co([9]aneS_3)(dppe)](PF_6)_2$

CH_3NO_2 fluid solution at 298K

Centre field 3300G

Sweep field 2000G

9.68GHz

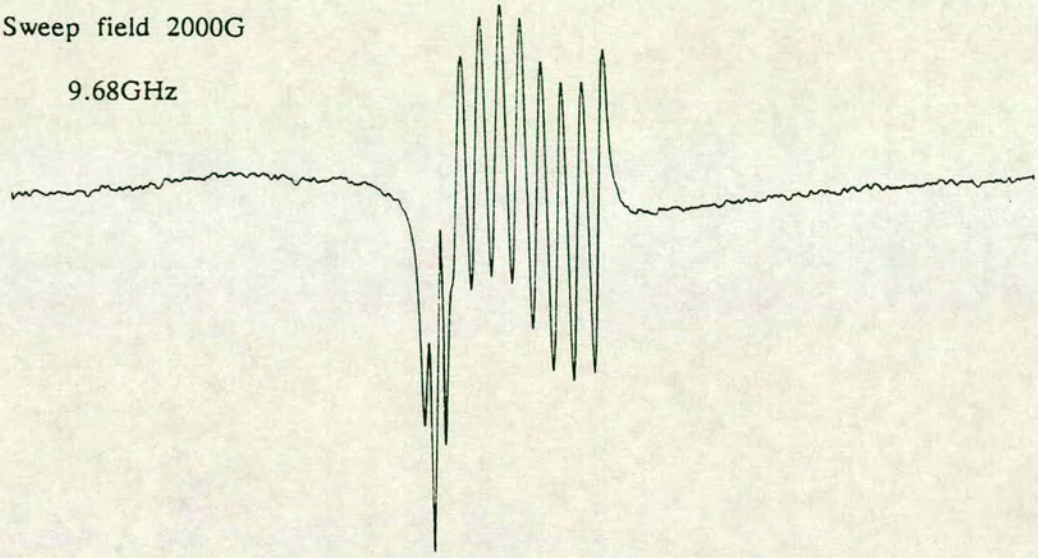

Figure 6.25 Frozen glass e.s.r. spectrum of $[Co([9]aneS_3)(dppe)](PF_6)_2$

CH_3NO_2 frozen glass at 77K

Centre field 3300G

Sweep field 2000G

9.35GHz

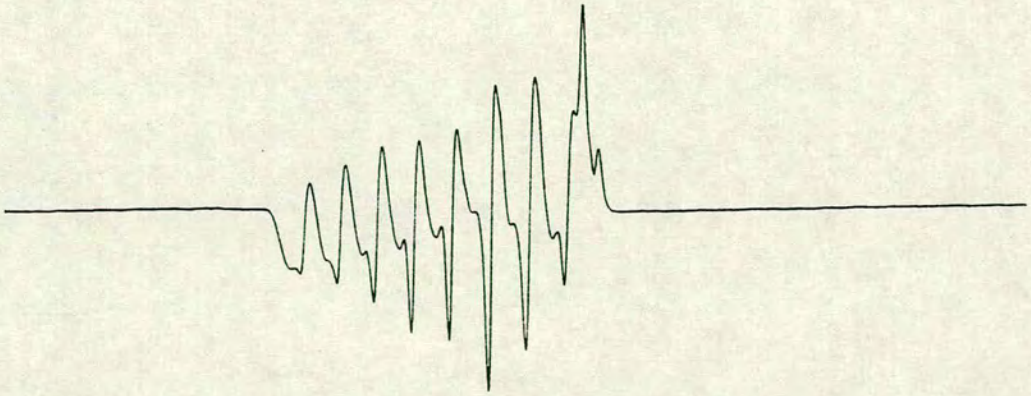

even this tentative analysis. Incidently, a solution spectrum of $[Co(dppe)_2Cl]Cl$ in CH_3NO_2 at 293K gave no signal. Simulation of the spectrum of $[Co([9]aneS_3)(dppe)](PF_6)_2$, which is currently being undertaken, may prove to be informative.

The frozen glass e.s.r. spectrum of $[Co([9]aneS_3)(dppe)](PF_6)_2$ in CH_3NO_2 at 77K (shown in Figure 2.25) is also difficult to interpret. An anisotropic signal is observed which appears to have three g tensor components, although only two can be identified. These two are tentatively assigned as: $g_1 = 2.13$ ($A_1 = 73.4G$); $g_2 = 2.09$ ($A_2 = 75.5G$). Similarly to$[Co([9]aneS_3)_2]^{2+}$, the e.s.r. frozen glass spectrum of $[Co([9]aneS_3)(dppe)]^{2+}$ at 77K is difficult to analyse because of the proximity of the different g tensor components and the broad eight-line pattern observed for each of these g values. Further work is required on these spectra.

6.2.11: An Electrochemical Study of $[Co([9]aneS_3)(dppe)](PF_6)_2$

Cyclic voltammetry of $[Co([9]aneS_3)(dppe)](PF_6)_2$ measured at 298K in CH_3CN (0.1M $Bu^n_4NPF_6$ supporting electrolyte) at Pt electrodes, shows one reversible oxidation at $E_{\frac{1}{2}} = +0.09V$ *vs.* Fc/Fc^+ and one reversible reduction at $E_{\frac{1}{2}} = -0.71V$ *vs.* Fc/Fc^+. A quantitative investigation of the oxidation process was undertaken. Coulometry of $[Co([9]aneS_3)(dppe)](PF_6)_2$, measured at +0.35V *vs.* Fc/Fc^+, 298K in CH_3CN (0.1M $Bu^n_4NPF_6$ supporting electrolyte) at a Pt basket, confirmed that the oxidation corresponds to a one-electron process (n = 0.97 electrons). During bulk electrolysis the solution changed from a pale yellow to a darker yellow colour. Controlled potential electrolysis at 298K, −0.50V regenerated the original Co(II) starting material quantitatively.

To investigate the nature of the product from the oxidation of $[Co([9]aneS_3)(dppe)](PF_6)_2$, the one-electron oxidation was followed at +0.35V

vs. Fc/Fc^+, 245K in CH_3CN by *in situ* U.V./visible spectroscopy using an O.T.T.L.E. system. The oxidation occurs isosbestically (λ_{iso} = 316nm.), with the loss of intensity of the absorption band at $\lambda_{max.}$ = 305nm and concommitant growth of a new band at $\lambda_{max.}$ = 351nm. The electronic spectrum observed during the oxidation is shown in Figure 6.26. Regeneration of the Co(II) starting material at −0.50V, 245K occurs quantitatively. Assuming that the oxidation is metal-based, corresponding to the oxidation state change Co(II) → Co(III), the shift of the charge-transfer band to higher wavelengths (305 → 351nm.) leads us to assign the absorption band as due to metal-to-ligand charge-transfer.

A quantitative investigation of the reduction process was also undertaken. Coulometry of $[Co([9]aneS_3)(dppe)](PF_6)_2$, measured at −1.00V *vs.* Fc/Fc^+, 298K in CH_3CN (0.1M $Bu^n_4NPF_6$ supporting electrolyte) at a Pt basket, confirmed that the reduction corresponds to a one-electron process (n = 0.95 electrons). During bulk electrolysis the solution changed from a pale yellow to an orange colour. The e.s.r. spectrum (measured at 77K, CH_3CN glass) of the orange solution shows no signal. Controlled potential electrolysis at 298K, 0.00V did not regenerate the original Co(II) starting material quantitatively, although a yellow coloured solution was obtained.

To investigate the nature of the product from the reduction of $[Co([9]aneS_3)(dppe)](PF_6)_2$, the one-electron reduction was followed at −1.15V *vs.* Fc/Fc^+, 245K in CH_3CN by *in situ* U.V./visible spectroscopy using an O.T.T.L.E. system. The reduction occurs isosbestically (λ_{iso} = 274, 344nm.), with the loss of intensity of the absorption band at $\lambda_{max.}$ = 305nm and concommitant growth of a new band at $\lambda_{max.}$ = 253nm. The electronic spectrum observed during the reduction is shown in Figure 6.27. The Co(II) starting material could not be regenerated at 0.00V, 245K. On the basis of this data from the reduction process, we conclude that the electrogenerated

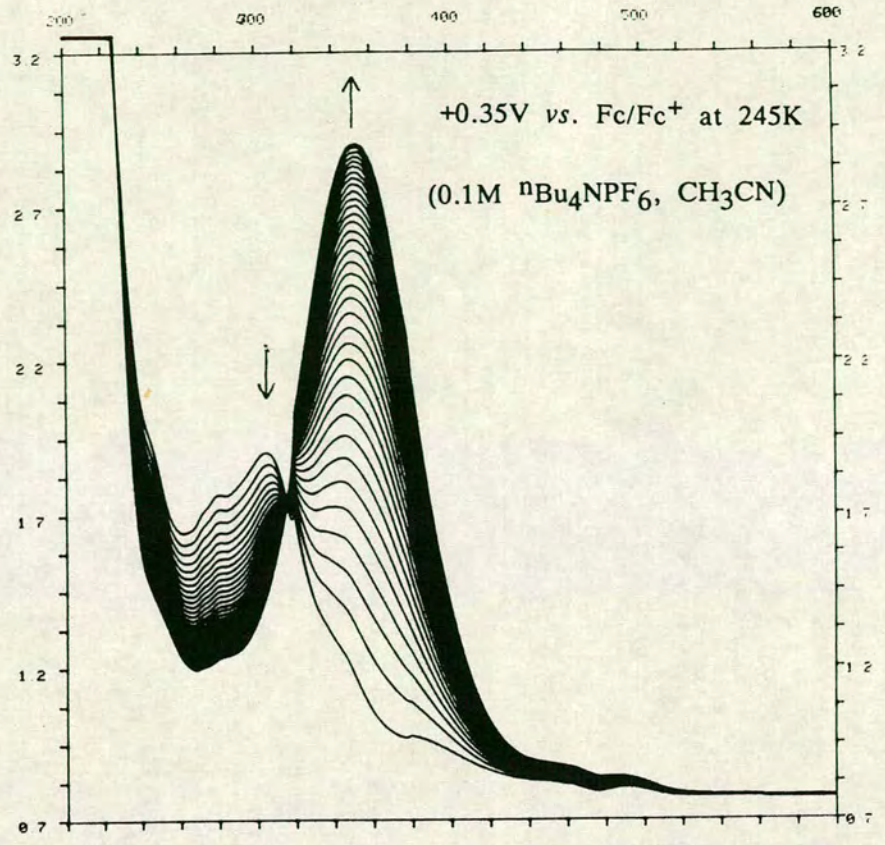

Figure 6.26 Electronic spectrum showing oxidation of [Co([9]aneS$_3$)(dppe)](PF$_6$)$_2$

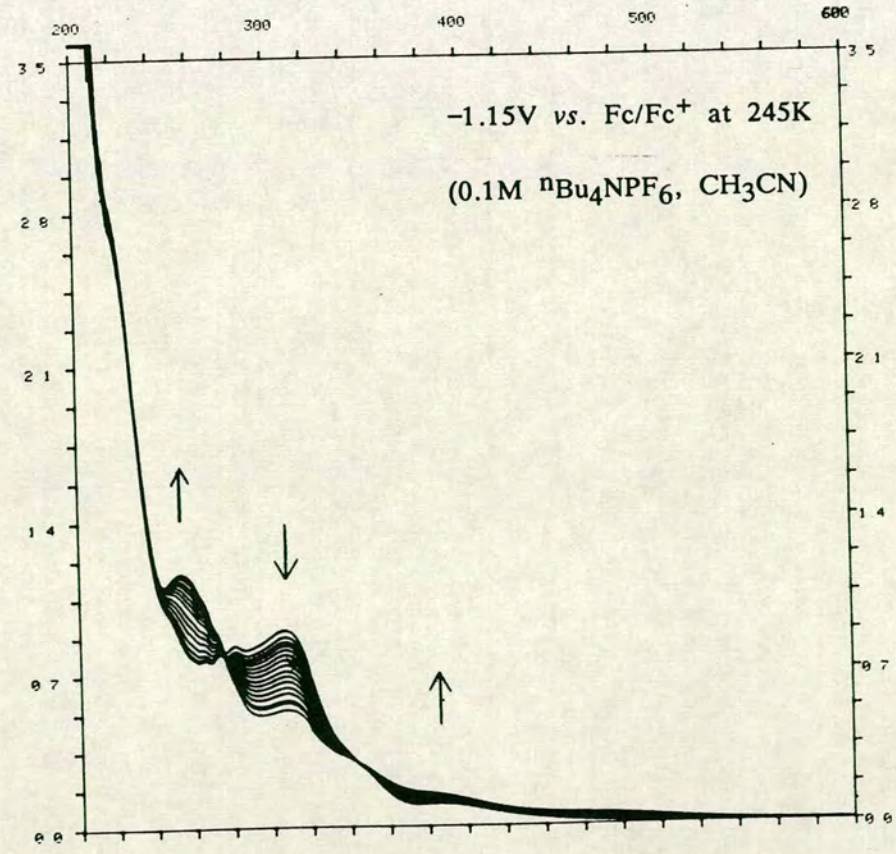

Figure 6.27 Electronic spectrum showing reduction of [Co([9]aneS$_3$)(dppe)](PF$_6$)$_2$

species is only stable on the C.V. timescale and longer experiments, even at low temperatures, lead to the decomposition of the reduction product.

One remarkable aspect of the electrochemical behaviour of $[Co([9]aneS_3)(dppe)](PF_6)_2$ is the proximity of the oxidative and reductive processes (ΔE = 0.80V). There is therefore only a small potential range for this ligand system that stabilises the Co(II) oxidation state.

6.3: Conclusions

In this Chapter, the reactions of Fe(II), Fe(III) and Co(II) centres with $[9]aneS_3$ have been investigated with the aim of preparing half-sandwich and binuclear complexes. We have prepared the half-sandwich compounds $[Fe([9]aneS_3)Cl(dppv)](PF_6)$, $[Fe([9]aneS_3)(CH_3CN)_3](BF_4)_2$ and $[Co([9]aneS_3)(dppe)](PF_6)_2$ and the electrochemical properties of the last compound were examined. $[Co([9]aneS_3)(dppe)](PF_6)_2$ undergoes a reversible one-electron oxidation (at $E_{\frac{1}{2}}$ = +0.09V *vs.* Fc/Fc^+) and a reversible one-electron reduction (at $E_{\frac{1}{2}}$ = −0.71V *vs.* Fc/Fc^+) and these redox processes were followed using the O.T.T.L.E. spectroelectrochemical technique. $[Fe([9]aneS_3)(CH_3CN)_3](BF_4)_2$ is very unstable with respect to hydrolysis and attempts to stabilise the $(Fe-[9]aneS_3)^{2+}$ unit by the co-ordination of other ligands were unsuccessful. However, the overwhelming feature of these reactions is the driving force for the formation of the bis$[9]aneS_3$ complexes, $[Fe([9]aneS_3)_2]^{2+}$ and $[Co([9]aneS_3)_2]^{2+}$. These stable octahedral species appear to be kinetically and thermodynamically favoured products and any half-sandwich complexes of $[9]aneS_3$ decompose readily to form these $[M([9]aneS_3)_2]^{2+}$ products. We decided further investigation of these complexes was warranted. On examination of the crystal structures of $[Fe([9]aneS_3)_2]^{2+}$ and $[Fe([9]aneS_3)_2]^{3+}$ [292], we have obtained good structural evidence for the π-acceptor properties of the thioether ligands. A

study of the properties of the $[Co([9]aneS_3)_2](PF_6)_2$ and $[Co([9]aneS_3)_2](BF_4)_2$ complexes was also undertaken and reveals unusual stereochemical behaviour for these low spin, d^7, Jahn–Teller distorted species. The crystal structures and solid–state e.s.r. spectra of the BF_4^- and PF_6^- salts of $[Co([9]aneS_3)_2]^{2+}$ suggest that there may be a counterion and temperature dependence on the extent and perhaps direction of the distortion from ideal octahedral geometries. However, these studies are at a preliminary stage and we are not able to draw any firm conclusions as yet.

No evidence for binuclear bridged species with Fe(II), Fe(III) or Co(II) and $[9]aneS_3$ was obtained under the reaction conditions described in the Experimental Section.

6.4: Experimental

6.4.1: Synthesis of $[Fe([9]aneS_3)_2](ClO_4)_2$

$Fe(ClO_4)_3.6H_2O$ (51mg, 0.11mmol) was dissolved in CH_3OH ($3cm^3$) and added to a solution of $[9]aneS_3$ (40mg, 0.22mmol) in CH_3OH ($5cm^3$) with stirring. The orange solution was refluxed for 20 hours and a pink precipitate appeared. The mixture was allowed to cool and the pink precipitate was filtered, washed with cold C_2H_5OH and diethyl ether and dried in air. Yield = 57mg, 84%. Elemental analysis: found C = 23.4; H = 4.00%. Calculated for $[Fe(C_6H_{12}S_3)_2](ClO_4)_2$: C = 23.4; H = 3.93%. F.a.b. mass spectrum (3–NOBA matrix): found M^+ = 415, 515. Calculated for: $[^{56}Fe(C_6H_{12}S_3)(C_6H_{11}S_3)]^+$, M^+ = 415; $[^{56}Fe(C_6H_{12}S_3)_2](ClO_4)^+$, M^+ = 515. I.r. spectrum (KBr disc): 3423m, 3346s, 2982w, 2964w, 2952w, 2932w, 2914m, 1437m, 1411m, 1397m, 1289w, 1235w, 1142s, 1110s, 1088s, 991m, 911m, 833m, 821m, 685w, 658w, 637m, 625m, 498w, 465w, 441w and 365w cm^{-1}. U.V./vis. spectrum (H_2O): $\lambda_{max.}$ = 525nm. ($\epsilon_{max.}$ = $60M^{-1}cm^{-1}$), 396 (60).

6.4.2: Single Crystal X-ray Structure of $[Fe([9]aneS_3)_2](ClO_4)_2.2DMF$

Vapour diffusion of diethyl ether into a solution of the complex in CH_3NO_2/DMF gave pink crystals of crystallographic quality. To prevent crystal degradation as a result of solvent loss, a pink tablet was transferred from its cold mother liquor into a drop of mineral oil at 195K and mounted on the diffractometer which was equipped with an Oxford Cryosystems low-temperature device[253] operating at 150K.

Crystal Data:

$[Fe(C_6H_{12}S_3)_2](ClO_4)_2.2(CH_3)_2NCOH$ M = 761.61. Orthorhombic, space group P_{cab} (Alt. P_{bca}, No.61), a = 9.1893(26), b = 15.353(4), c = 21.279(6)Å, V = 3002Å^3 (by least-squares refinement on diffraction angles for 47 reflections measured at $\pm\omega$ [$30 \leq 2\theta \leq 32^\circ$, λ = 0.71073Å]), Z = 4, D_c = 1.685gcm^{-3}, T = 150K. Crystal dimensions 0.19 x 0.47 x 0.54mm^3, μ(Mo-Kα) = 1.133mm^{-1}, F(000) = 1584.

Data Collection and Processing:

Stöe STADI-4 four-circle diffractometer, ω-2θ scan mode using the learnt-profile method[199]. Graphite-monochromated Mo-Kα radiation; 2268 reflections measured ($2\theta_{max.}$ = 45°, h 0 → 9, k 0 → 16, l 0 → 22), 1905 unique data (R_{int} = 0.000), giving 1767 with $F > 5\sigma(F)$. No significant crystal decay, no absorption correction.

Structure Analysis and Refinement:

The Fe atom was located using a Patterson synthesis[201], and successive cycles of least-squares refinement and difference Fourier synthesis[201] identified the positions of all other atoms. The crystal lattice was found to contain two DMF molecules per cation. During refinement, disorder of the

methyl groups of the DMF molecules was observed which was modelled successfully using two orientations for the methyl groups, giving two hydrogen positions per hydrogen atom (occupancy of each hydrogen position = 50%). Anisotropic thermal parameters were refined for Fe, C, S, Cl, O and N atoms. H atoms were located from a difference map and included in fixed, calculated positions. The weighting scheme $w^{-1} = \sigma^2(F) + 0.000172F^2$ gave satisfactory agreement analyses. At final convergence, R = 0.0265, R_w = 0.0389, S = 1.272 for 192 independent parameters, and the final difference Fourier synthesis showed no feature above +0.404 or below $-0.346e\text{Å}^{-3}$.

Atomic scattering factors were inlaid[201], except for Fe[254], molecular geometry calculations utilised *CALC*[202] and figures were produced by *SHELXTL PC*[255].

6.4.3: Synthesis of [Fe([9]aneS$_3$)Cl$_3$]

[Fe([9]aneS$_3$)Cl$_3$] was prepared by the method of Wieghardt *et al.*[298]. To a solution of [9]aneS$_3$ (100mg, 0.55mmol) in CH_3OH (10cm^3), a solution of $FeCl_3.6H_2O$ (150mg, 0.55mmol) in CH_3OH (5cm^3) was added dropwise. A red crystalline solid precipitated immediately, which was filtered, washed with CH_3OH and diethyl ether and dried in air. Yield = 151mg, 80%. Elemental analysis: found C = 21.2; H = 3.56%. Calculated for [Fe($C_6H_{12}S_3$)Cl_3]: C = 21.0; H = 3.53%. F.a.b. mass spectrum (3-NOBA matrix): only matrix peaks found. I.r. spectrum (KBr disc): 2972w, 2958w, 2921w, 1440m, 1403s, 1285w, 1246w, 1182w, 1129w, 930w, 896m, 825m and 323s cm^{-1}.

6.4.4: Reaction of [Fe([9]aneS$_3$)Cl$_3$] with triphos

[Fe([9]aneS$_3$)Cl$_3$] (30mg, 0.09mmol) and triphos {[(C$_6$H$_5$)$_2$PCH$_2$]$_3$CCH$_3$} (55mg, 0.09mmol) were stirred overnight at room temperature in C$_2$H$_5$OH (20cm^3) under N$_2$. No change from the original red suspension was observed. The suspension was then refluxed for two hours and a pink precipitate appeared. This was filtered, washed with C$_2$H$_5$OH and diethyl ether and dried *in vacuo*. F.a.b. mass spectrum (3-NOBA matrix): found M$^+$ = 416. Calculated for: [Fe(C$_6$H$_{12}$S$_3$)$_2$]$^+$, M$^+$ = 416. I.r. spectrum (KBr disc): 2975w, 2960w, 2938w, 2917w, 1438m, 1412s, 1402s, 1291w, 1238w, 1134w, 1116w, 1012w, 942w, 911m, 830m, 684w, 666w, 500w and 367w cm^{-1}.

6.4.5: Reaction of [Fe([9]aneS$_3$)Cl$_3$] with triphenylphosphine

[Fe([9]aneS$_3$)Cl$_3$] (25mg, 0.07mmol) was suspended in CH$_3$OH (15cm^3) under N$_2$ and P(C$_6$H$_5$)$_3$ (38mg, 0.14mmol) was added. On dissolution of the P(C$_6$H$_5$)$_3$, TlBF$_4$ (20mg, 0.07mmol) was added and the mixture was refluxed for 4 hours. The white precipitate which was formed was removed by centrifugation and on cooling the remaining solution precipitated pink crystals. These were filtered, washed with diethyl ether and dried in air. F.a.b. mass spectrum (3-NOBA matrix): found M$^+$ = 416. Calculated for: [Fe([9]aneS$_3$)$_2$]$^+$, M$^+$ = 416. I.r. spectrum (KBr disc): 3400br, 2980w, 2962w, 2945w, 2912m, 1438m, 1411s, 1400s, 1293w, 1237w, 1060br s, 944m, 912m, 832m, 685w, 666w, 534w, 523w, 500w and 367w cm^{-1}.

6.4.6: Reaction of [Fe([9]aneS$_3$)Cl$_3$] with tricyclohexylphosphine

Method as for 6.4.4 but with P(C$_6$H$_{11}$)$_3$ (39mg, 0.14mmol), with the same results.

6.4.7: Reaction of [Fe([9]aneS$_3$)Cl$_3$] with triphenylphosphine at 273K

Method as for 6.4.4 but with stirring in an ice bath for 2 days, with the same results.

6.4.8: Reaction of [Fe([9]aneS$_3$)Cl$_3$] with dppv

[Fe([9]aneS$_3$)Cl$_3$] (38.3mg, 0.11 mmol) was stirred in CH_3NO_2 (5cm^3) with dppv (44.3mg, 0.11mmol) to give a red suspension. $TlPF_6$ (80.0mg, 0.23 mmol) was added and the mixture was stirred at room temperature for 30 mins. A green solution and white precipitate was formed and the precipitate was removed by centrifugation. A green/brown solution was obtained which was evaporated to 3cm^3 and diethyl ether was added. A green/brown solid was precipitated which was filtered, recrystallised from CH_3NO_2/diethyl ether by vapour diffusion to give a brown solid and dried *in vacuo*. Elemental analysis: found C = 43.8; H = 3.79%. Calculated for [Fe($C_6H_{12}S_3$)($C_{26}H_{22}P_2$)Cl](PF_6): C = 47.3; H = 4.21%. F.a.b. mass spectrum (CH_3CN/3-NOBA matrix): found M^+ = 486, 666. Calculated for: [^{56}Fe($C_{26}H_{21}P_2$)Cl]$^+$, M^+ = 486; [Fe($C_6H_{12}S_3$)($C_{26}H_{22}P_2$)Cl](-H)$^+$, M^+ = 666. I.r. spectrum (KBr disc): 3432w, 3002w, 1708m, 1484w, 1436m, 1414w, 1365w, 1314w, 1225w, 1192w, 1135w, 1098w, 998w, 839s, 741w, 696m, 598w, 558s, 526w, 484w and 419w cm^{-1}.

6.4.9: Reactions of [Fe(CH_3CO_2)$_2$] with [9]aneS$_3$

[Fe(CH_3CO_2)$_2$] (from Strem Chemicals, 30mg, 0.17mmol) was suspended in dry, distilled CH_3CN (5cm^3) under N_2 and 5 drops of $(CH_3CO)_2O$ were added. A degassed solution of [9]aneS$_3$ (31mg, 0.17mmol) in CH_3CN (10cm^3) was added and the mixture was refluxed overnight. A pink precipitate of [Fe([9]aneS$_3$)$_2$]$^{2+}$ was obtained which was filtered and characterised using i.r. and f.a.b. mass spectroscopy.

$[Fe(CH_3CO_2)_2]$ (38mg, 0.22mmol) and [9]aneS_3 (40mg, 0.22mmol) were placed in a Schlenk tube under N_2 and degassed CH_3OH ($10cm^3$) was added. The mixture was refluxed for one hour under N_2 and a brown solid was precipitated. This brown solid was shown to be $[Fe_3O(CH_3CO_2)_6]^+$ by i.r. and f.a.b. mass spectroscopy.

The procedures 6.4.10 - 6.4.25 were carried out in Schlenk apparatus and under N_2 unless otherwise stated. Solids were handled and i.r and n.m.r. samples were prepared in an Aldrich Glove-bag under N_2. CH_3CN was distilled under N_2 over P_2O_5, CH_2Cl_2 was distilled under N_2 over CaH_2 and diethyl ether was dried with Na wire before use.

6.4.10: Synthesis of $[Fe(CH_3CN)_6](BF_4)_2$

$[Fe(CH_3CN)_6](BF_4)_2$ was prepared by the method of Underhill *et al.*[219]. An excess of Fe powder was placed in a Schlenk tube under N_2 and dry, distilled CH_3CN ($10cm^3$) was added. $NOBF_4$ (398mg, 3.41mmol) was added to the suspension and the mixture was stirred for 2 hours whilst evacuating the Schlenk tube to give a colourless solution. More CH_3CN was added if required. The solution was filtered, the volume of solvent was reduced to approximately $3cm^3$ and an excess of diethyl ether was added. A grey/white solid was precipitated, that was filtered, washed with diethyl ether and dried *in vacuo*. Yield = 688mg, 85%. The compound $[Fe(CH_3CN)_6](BF_4)_2$ could not be characterised by conventional techniques, because it was very hygroscopic and it decomposed by absorption of H_2O from air. Data available: U.V./vis. spectrum (CH_3CN): $\lambda_{max.}$ = 290nm. ($\varepsilon_{max.}$ = $13M^{-1}cm^{-1}$)

6.4.11: Synthesis of $[Fe([9]aneS_3)(CH_3CN)_3](BF_4)_2$

$[Fe(CH_3CN)_6](BF_4)_2$ (116mg, 0.24mmol) was dissolved in CH_3NO_2 ($5cm^3$) to give a colourless solution. A solution of $[9]aneS_3$ (44mg, 0.24mmol) in CH_3NO_2 ($15cm^3$) was added dropwise with stirring to give a dark purple solution. A small portion of this solution was removed by syringe, evaporated to near dryness and an excess of diethyl ether was added. A pink precipitate was obtained which was shown to be $[Fe([9]aneS_3)_2](BF_4)_2$ by i.r. spectroscopy. The purple solution could be used for further reactions but a solid was not isolatable. U.V./visible spectrum (CH_3NO_2): $\lambda_{max.}$ = 544nm. ($\epsilon_{max.}$ = $54M^{-1}cm^{-1}$), shoulder to solvent absorption band at $\lambda \approx$ 390nm. (40).

The following reactions were attempted, but gave $[Fe([9]aneS_3)_2]^{2+}$, unidentifiable products or no reaction was observed. The synthetic procedure was to add the dry reagent (in equivalents as shown) as a solution or solid to a solution of $[Fe([9]aneS_3)(CH_3CN)_3](BF_4)_2$ in CH_3NO_2 under N_2. The solid products were isolated by adding an excess of diethyl ether to the CH_3NO_2 solution, filtering and drying *in vacuo*.

Reagent	Products
6.4.12: $[9]aneN_3$ (CH_3NO_2)	Pink $[Fe([9]aneS_3)_2]^{2+}$
6.4.13: CH_3NHNH_2 (CH_3NO_2)	Brown air-sensitive solid
6.4.14: $4xP(C_6H_5)_3$ (CH_3NO_2)	Pink $[Fe([9]aneS_3)_2]^{2+}$
6.4.15: dppe (CH_3NO_2)	Pink $[Fe([9]aneS_3)_2]^{2+}$ and red $[Fe(dppe)_2(CH_3CN)_2]^{2+}$
6.4.16: dppe (CH_3NO_2, 253K)	Pink $[Fe([9]aneS_3)_2]^{2+}$ and red $[Fe(dppe)_2(CH_3CN)_2]^{2+}$
6.4.17: dppv (CH_3NO_2, 253K)	Pink $[Fe([9]aneS_3)_2]^{2+}$ and red $[Fe(dppv)_2(CH_3CN)_2]^{2+}$

6.4.18: triphos (CH_3NO_2)	Pink $[Fe([9]aneS_3)_2]^{2+}$
6.4.19: $S_{(solid)}$	No reaction
6.4.20: $(NBu^n_4)CH_3CO_2$	Pink $[Fe([9]aneS_3)_2]^{2+}$
6.4.21: $CO_{(g)}$	No reaction
6.4.22: $Cyclohexene_{(l)}$	No reaction
6.4.23: $Benzene_{(l)}$	No reaction
6.4.24: $Cyclooctadiene_{(l)}$	No reaction
6.4.25: $NaBH_{4(s)}$	No reaction

The products $[Fe([9]aneS_3)_2](BF_4)_2$, $[Fe(dppe)_2(CH_3CN)_2](BF_4)_2$ and $[Fe(dppv)_2(CH_3CN)_2](BF_4)_2$ were characterised by i.r. and f.a.b. mass spectroscopy.

6.4.26: Synthesis of $[Co([9]aneS_3)_2](PF_6)_2$

$CoCl_2.6H_2O$ (53mg, 0.22mmol) was dissolved in CH_3CN ($4cm^3$) and a solution of [9]aneS$_3$ (40mg, 0.22mmol) in CH_3CN ($4cm^3$) was added. The solution was stirred under N_2 to give a blue precipitate. H_2O ($8cm^3$) was added to the mixture and the blue solid dissolved to give a pale purple solution. NH_4PF_6 was added to the solution, the volume of solvent was reduced and a purple crystalline solid was obtained on cooling. The purple solid was filtered, washed with cold H_2O and recrystallised from CH_3NO_2/diethyl ether by vapour diffusion. Yield = 50mg, 64%. Elemental analysis: found C = 20.2; H = 3.56%. Calculated for $[Co([9]aneS_3)_2](PF_6)_2$: C = 20.3; H = 3.41%. F.a.b. mass spectrum (3-NOBA matrix): found M^+ = 419, 564. Calculated for: $[^{59}Co(C_6H_{12}S_3)_2]^+$, M^+ = 419; $[^{59}Co(C_6H_{12}S_3)_2](PF_6)^+$, M^+ = 564. I.r. spectrum (KBr disc): 3535m, 3445m, 3375m, 3024w, 2999w, 2952w, 1452m, 1441w, 1424m, 1414m, 1307w, 1290w, 1188w, 1179w, 1144w, 1012w, 938w, 840s, 744w, 671w, 625w, 558s and 492w cm^{-1}.

6.4.27: Single Crystal X-ray Structure of $[Co([9]aneS_3)_2](PF_6)_2.2CH_3NO_2$

Vapour diffusion of diethyl ether into a solution of the complex in CH_3NO_2 gave purple crystals of crystallographic quality. To prevent crystal degradation as a result of solvent loss, a purple block was transferred from its cold mother liquor into a drop of mineral oil at 195K and mounted on the diffractometer which was equipped with an Oxford Cryosystems low-temperature device[253] operating at 150K.

Crystal Data:

$[Co(C_6H_{12}S_3)_2](PF_6)_2.2CH_3NO_2$ M = 831.66. Monoclinic, space group $P2_1/a$, a = 9.518(3), b = 15.011(4), c = 10.496(7)Å, β = 101.11(3)°, V = 1472Å^3 (by least-squares refinement on diffraction angles for 42 reflections measured at $\pm\omega$ [$25 < 2\theta < 32°$, λ = 0.71073Å]), Z = 2, D_c = 1.876gcm^{-3}, T = 150.0K. Crystal dimensions 0.19 x 0.27 x 0.08mm^3, μ(Mo-Kα) = 1.200mm^{-1}, F(000) = 842.

Data Collection and Processing:

Stöe STADI-4 four-circle diffractometer, ω-2θ scan mode using the learnt-profile method[199]. Graphite-monochromated Mo-Kα radiation; 2539 reflections measured ($2\theta_{max.}$ = 45°, h -10 → 10, k -2→ 16, l 0 → 11), 1759 unique data (R_{int} = 0.049), giving 1377 with $F > 4\sigma(F)$. No significant crystal decay, no absorption correction.

Structure Analysis and Refinement:

The Co atom was located using a Patterson synthesis[201], and successive cycles of least-squares refinement and difference Fourier synthesis[201] identified the positions of all other atoms. The crystal lattice was found to contain two CH_3NO_2 molecules per cation. Anisotropic thermal parameters

were refined for Co, C, S, P, F, N and O atoms. H atoms were located from a difference map and included in fixed, calculated positions. The weighting scheme $w^{-1} = \sigma^2(F) + 0.001998F^2$ gave satisfactory agreement analyses. At final convergence, $R = 0.0651$, $R_w = 0.0827$, $S = 1.097$ for 190 independent parameters, and the final difference Fourier synthesis showed no feature above +1.245 or below $-0.981 e\text{Å}^{-3}$.

Atomic scattering factors were inlaid[201], except for Co[254], molecular geometry calculations utilised *CALC*[202] and figures were produced by *SHELXTL PC*[255].

6.4.28: Synthesis of [Co(dppe)$_2$Cl]Cl

[Co(dppe)$_2$Cl]Cl was prepared as described by Horrocks *et al.*[312]. Dppe (400mg, 1.00mmol) was dissolved in $(CH_3)_2CHOH$ (13cm^3) under N_2 and a solution of $CoCl_2.6H_2O$ (120mg, 0.50mmol) in $(CH_3)_2CHOH$ (7cm^3) was added. The mixture was refluxed under N_2 for 45 minutes to give a dark suspension. On cooling, a green solid was obtained, which was filtered, dried in air and recrystallised from C_2H_5OH/H_2O. Further crops of the green solid were obtained by allowing the solution to stand. Overall yield = 360mg, 78%. Elemental analysis: found C = 66.1; H = 5.45%. Calculated for $[Co(C_{26}H_{24}P_2)_2Cl]Cl$: C = 67.5; H = 5.19%. F.a.b. mass spectrum (3-NOBA matrix): found M^+ = 399, 457, 492, 508, 813, 855, 890, 925. Calculated for: $[C_{26}H_{25}P_2]^+$, M^+ = 399; $[^{59}Co(C_{26}H_{24}P_2)]^+$, M^+ = 457; $[^{59}Co(C_{26}H_{24}P_2)^{35}Cl]$, M^+ = 492; $[^{59}Co(C_{26}H_{24}P_2O)^{35}Cl]^+$, M^+ = 508; $[^{59}Co(C_{20}H_{19}P_2)(C_{26}H_{24}P_2)^{35}Cl]^+$, M^+ = 813; $[^{59}Co(C_{26}H_{24}P_2)_2]^+$, M^+ = 855; $[^{59}Co(C_{26}H_{24}P_2)_2{}^{35}Cl]^+$, M^+ = 890; $[^{59}Co(C_{26}H_{24}P_2)_2{}^{35}Cl_2]^+$, M^+ = 925. I.r. spectrum (KBr disc): 3450br, 3084w, 1602w, 1587w, 1499m, 1448s, 1400w, 1350w, 1332w, 1290w, 1207w, 1177w, 1115m, 1108w, 1087w,

1043w, 1015w, 930w, 893w, 872w, 831w, 756m, 711s, 632w, 545s, 531m, 496m, 477w, 457w, 437w, 404w, 337w and 332w cm^{-1}.

6.4.29: Synthesis of $[Co(dppm)_2Cl]Cl$

Method as for 6.4.30, but using dppm (100mg, 0.26mmol) and $CoCl_2.6H_2O$ (37mg, 0.16mmol) and reducing the volume of solvent accordingly. Yield = 64mg, 55%. Elemental analysis: found C = 66.4; H = 4.74%. Calculated for $[Co(C_{25}H_{22}P_2)_2Cl]Cl$: C = 66.8; H = 4.94%. F.a.b. mass spectrum (3-NOBA matrix): found M^+ = 385, 443, 478, 862. Calculated for: $[C_{25}H_{23}P_2]^+$, M^+ = 385; $[^{59}Co(C_{25}H_{22}P_2)]^+$, M^+ = 443; $[^{59}Co(C_{25}H_{22}P_2)^{35}Cl]^+$, M^+ = 478; $[^{59}Co(C_{25}H_{22}P_2)_2Cl]^+$, M^+ = 862. I.r. spectrum (KBr disc): 3404br, 3053w, 1588w, 1483m, 1436s, 1352w, 1333w, 1311w, 1159s, 1123s, 1097s, 1026w, 998w, 924w, 785m, 739s, 692s and 565s cm^{-1}.

6.4.30: Synthesis of $[Co(dppv)_2Cl]Cl$

Method as for 6.4.30, but using dppv (100mg, 0.25mmol) and $CoCl_2.6H_2O$ (32mg, 0.13mmol) and reducing the volume of solvent accordingly. Yield = 76mg, 63%. Elemental analysis: found C = 65.3; H = 4.77%. Calculated for $[Co(dppv)_2Cl]Cl$: C = 67.7; H = 4.81%. F.a.b. mass spectrum (3-NOBA matrix): found M^+ = 397, 455, 490, 851, 886. Calculated for: $[C_{26}H_{23}P_2]^+$, M^+ = 397; $[^{59}Co(C_{26}H_{22}P_2)]^+$, M^+ = 455; $[^{59}Co(C_{26}H_{22}P_2)^{35}Cl]^+$, M^+ = 490; $[^{59}Co(C_{26}H_{22}P_2)_2]^+$, M^+ = 851; $[^{59}Co(C_{26}H_{22}P_2)_2{}^{35}Cl]^+$, M^+ = 886. I.r. spectrum (KBr disc): 3450br, 3051w, 1584w, 1572w, 1482s, 1434s, 1312w, 1276w, 1190w, 1169w, 1093s, 1026w, 999m, 845w, 739s, 692s, 617w, 597w, 551s, 515s and 473m cm^{-1}.

6.4.31: Synthesis of $[Co(dppe)([9]aneS_3)](PF_6)_2$

$[Co(dppe)_2Cl]Cl$ (113mg, 0.12mmol) was dissolved in CH_2Cl_2 ($2cm^3$) and to this solution was added dropwise a solution of $[9]aneS_3$ (22mg, 0.12mmol) in CH_2Cl_2 ($5cm^3$). $TlPF_6$ (88mg, 0.25mmol) was added as a solid and the mixture stirred under N_2 for 3 hours at 298K. A mixture of brown and white precipitates and a green supernatant formed and these were separated by centrifugation. CH_3CN ($5cm^3$) was added to the mixture of precipitates and a brown solution over a white precipitate was obtained. The white solid was removed by centrifugation and diethyl ether was added to the brown CH_3CN solution by vapour diffusion to give a brown solid. The brown solid was filtered, recrystallised from CH_3CN/diethyl ether to give brown crystals and dried *in vacuo*. Yield = 63mg, 61%. Elemental analysis: found C = 41.7; H = 4.04%. Calculated for $[Co(C_{26}H_{24}P_2)(C_6H_{12}S_3)](PF_6)_2$: C = 41.4; H = 3.91%. F.a.b. mass spectrum (3-NOBA matrix): found M^+ = 457, 476, 609, 637, 656, 782. Calculated for: $[^{59}Co(C_{26}H_{24}P_2)]^+$, M^+ = 457; $[^{59}Co(C_{26}H_{24}P_2)(H_3O)]^+$, M^+ = 476; $[^{59}Co(C_{26}H_{24}P_2)(C_6H_{12}S_3)(-C_2H_4)]^+$, M^+ = 609; $[^{59}Co(C_{26}H_{24}P_2)(C_6H_{12}S_3)]^+$, M^+ = 637; $[^{59}Co(C_{26}H_{24}P_2)(C_6H_{12}S_3)(H_3O)]^+$, M^+ = 656; $[^{59}Co(C_{26}H_{24}P_2)(C_6H_{12}S_3)](PF_6)^+$, M^+ = 782. I.r. spectrum (KBr disc): 3082w, 3020w, 2983w, 2937w, 1587w, 1573w, 1485w, 1450w, 1442m, 1418w, 1345w, 1336w, 1312w, 1240w, 1185w, 1165w, 1139w, 1107m, 1026w, 998w, 989w, 836s, 760m, 751m, 740w, 725w, 709m, 696m, 682w, 662w, 558s, 530m, 492m, 474w, 438w, 425w, 386w and 371w cm^{-1}. U.V./vis. spectrum (CH_3CN): $\lambda_{max.}$ = 470nm. ($\varepsilon_{max.}$ = $220M^{-1}cm^{-1}$), 382 (620), 305 (4,400), 281 (4,000).

CHAPTER 7

The Complexation of Fe(II) with [12]aneS$_4$, [14]aneS$_4$, [16]aneS$_4$, [15]aneS$_5$ and [18]aneS$_6$ Thioether Macrocycles

7.1: Introduction

The synthesis and complexation reactions of thioether macrocycles have been widely reported in the literature[6]. In Edinburgh, particular emphasis has been placed on the complexation of first, second and third row metals on the right-hand side of the transition metal block[6,16,316-324]. Surprisingly, however, few complexes have been reported with metal ions from the Fe triad (Fe, Ru and Os) with thioether macrocycles larger than [9]aneS_3[6]. In particular, reports of the complexation of Fe with thioether donors are very rare, which is in contrast with the prolific chemistry of Fe with sulphides and thiolates[256]. We proposed, therefore, to undertake a study of the reactions of the tetra-, penta- and hexa-thioether macrocycles with Fe(II), in the hope of utilising the macrocyclic effect to stabilise any complexes that are formed.

To our knowledge, there have been three examples reported in the literature of Fe(II) bonded to large ring macrocycles incorporating thioether donors. Busch *et al.*[325] reported the Mössbauer spectra of a number of macrocyclic complexes of Fe(II) and Fe(III), including $[Fe([14]aneS_4)(CH_3CN)_2](BF_4)_2$. They proposed that the [14]aneS_4 ligand was bound equatorially to the low spin Fe(II) centre, with the octahedral co-ordination sphere being completed by two axial CH_3CN ligands. No further characterisation or synthesis of this compound was given. $[Fe([14]aneS_4)(CH_3CN)_2]^{2+}$ has been reported again by Leigh and co-workers[326] very recently, as a salt with a $[FeI_4]^{2-}$ counterion. $[Fe([14]aneS_4)(CH_3CN)_2][FeI_4]$ was prepared by refluxing anhydrous FeI_2 in CH_3CN with [14]aneS_4 and was assigned a *trans* stereochemistry once more, although the C≡N stretching vibrations in the i.r. spectrum of the compound were not observed. The Mössbauer spectrum of $[Fe([14]aneS_4)(CH_3CN)_2][FeI_4]$ was consistent with low spin octahedral Fe(II). No reaction was observed if anhydrous $FeCl_2$ or $FeBr_2$ is used in place of

FeI_2.

Leigh and co-workers have also reported[326,327] the single crystal X-ray structure of $[Fe([16]aneS_4)]I_2$ and the Mössbauer spectra of this and the Br^- analogue, $[Fe([16]aneS_4)]Br_2$. On the basis of this and magnetic data, the compounds are formulated as square-planar high spin Fe(II) complexes. The cause of this unusual structure is ascribed to the mismatch between the ring-size of the $[16]aneS_4$ and Fe(II), which forces longer than normal Fe-S bonds on the system. The interactions of the Fe(II) centres with I^- ions were thought to be largely ionic in nature, on the basis of the bond lengths. The structure of $[Fe([16]aneS_4)]I_2$ is shown in Figure 7.1.

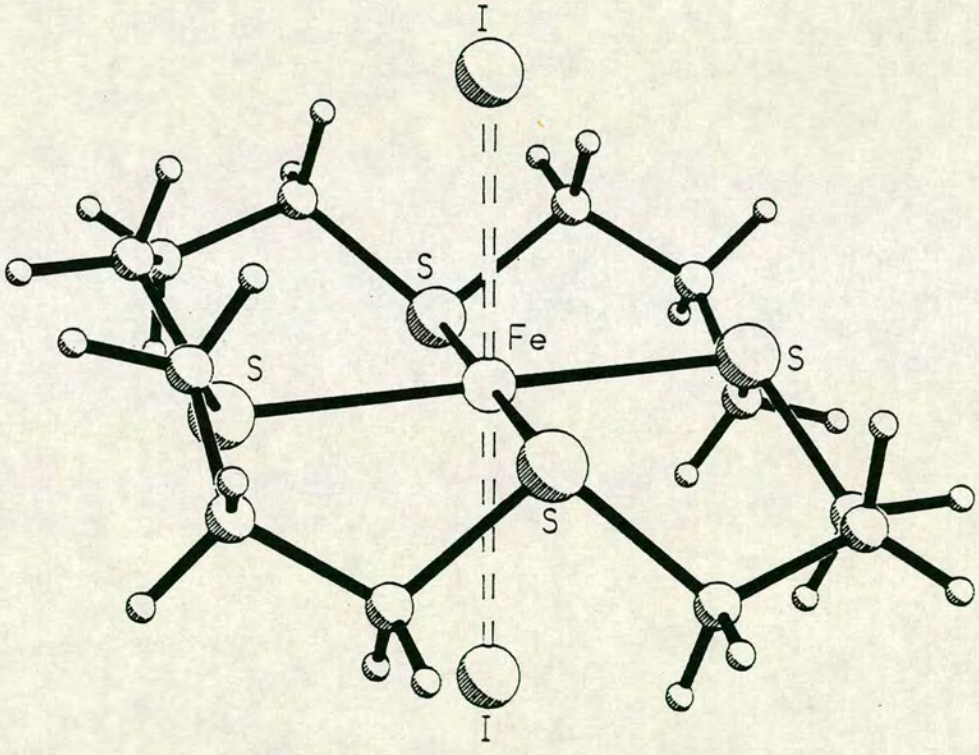

Figure 7.1 $[Fe([16]aneS_4)]I_2$

Finally, the complex $[Fe([18]aneN_2S_4)](BPh_4)_2$ has been synthesized and structurally characterised at Edinburgh[179,319]. The crystal structure of $[Fe([18]aneN_2S_4)](BPh_4)_2$ shows octahedral co-ordination at the low spin Fe(II) centre by four S- and two N-donors, in a similar fashion to the

Cu(II) and Ni(II) analogues. Although prepared from a hydrated Fe(II) salt, $FeCl_2.4H_2O$, the complex $[Fe([18]aneN_2S_4)]^{2+}$ is readily hydrolysed in aqueous solution. From this and the evidence from the above compounds, we concluded that Fe–thioether compounds are generally unstable towards hydrolysis and so anhydrous conditions would be required to synthesize Fe(II) complexes of the larger ring thioether macrocycles.

7.2: Results and Discussion

Preliminary experiments showed that hydrated Fe(II) salts do not react with the tetra– and penta–thioether macrocycles. Therefore the anhydrous Fe(II) starting material $[Fe(CH_3CN)_6](BF_4)_2$ (described in Chapter 6) was used for the following complexation reactions.

7.2.1: The Synthesis of $[Fe([12]aneS_4)(CH_3CN)_2](BF_4)_2$, $[Fe([14]aneS_4)(CH_3CN)_2](BF_4)_2$ and $[Fe([16]aneS_4)(CH_3CN)_2](BF_4)_2$

The reaction of a colourless CH_3NO_2 solution of $[Fe(CH_3CN)_6](BF_4)_2$ with an equimolar amount of $[12]aneS_4$ (dissolved in CH_3NO_2) under N_2 gave an intense blue solution. Analogous reactions using equimolar quantities of $[14]aneS_4$ or $[16]aneS_4$ with $[Fe(CH_3CN)_6](BF_4)_2$ gave intensely coloured purple and blue/green solutions respectively. All these solutions decolourised on exposure to air suggesting decomposition of the macrocyclic complex. The decomposition was verified by cooling the colourless aerified solutions which caused precipitation of the free macrocycle. Addition of anhydrous diethyl ether to the intensely coloured solutions gave blue, purple and blue/green solids for the reactions involving $[12]aneS_4$, $[14]aneS_4$ and $[16]aneS_4$ respectively. The solid products all decomposed readily in air but could be stored under N_2. I.r. spectra, obtained as hexachlorobutadiene (HCBD) mulls and prepared under N_2, indicate that the macrocycle is present in the

coloured solids, since C–H and C–S stretching vibrations are observed at 2960–2850 and 1430cm^{-1} respectively. Strong absorptions at 1060cm^{-1} in the i.r. spectra of the solids are also present and are assigned as B–F stretching vibrations. Little other direct evidence for these compounds could be obtained because of their instability in air, but we tentatively assign the products as [Fe([12]aneS$_4$)(CH$_3$CN)$_2$](BF$_4$)$_2$, [Fe([14]aneS$_4$)(CH$_3$CN)$_2$](BF$_4$)$_2$ and [Fe([16]aneS$_4$)(CH$_3$CN)$_2$](BF$_4$)$_2$.

The i.r spectra of [Fe([12]aneS$_4$)(CH$_3$CN)$_2$](BF$_4$)$_2$ and [Fe([14]aneS$_4$)(CH$_3$CN)$_2$](BF$_4$)$_2$ also show weak absorptions in the region 2330–2250cm^{-1}. For [Fe([12]aneS$_4$)(CH$_3$CN)$_2$](BF$_4$)$_2$, two weak bands at 2285 and 2265cm^{-1} are observed and these are tentatively assigned as symmetric and asymmetric C≡N stretching vibrations. This suggests that the CH$_3$CN ligands are *cis* to each other in [Fe([12]aneS$_4$)(CH$_3$CN)$_2$](BF$_4$)$_2$ and the [12]aneS$_4$ macrocycle has a folded conformation about two faces of the Fe(II) octahedron. For [Fe([14]aneS$_4$)(CH$_3$CN)$_2$](BF$_4$)$_2$, only a weak, broad band in the region 2330–2250cm^{-1} is observed and this may be due to a C≡N stretching vibration. Both Busch[325] and Leigh[326] and co-workers have assigned this compound with a *trans* stereochemistry previously. Presumably [Fe([16]aneS$_4$)(CH$_3$CN)$_2$](BF$_4$)$_2$ also has a *trans* configuration but no i.r. spectrum could be obtained for the blue/green solid since it decomposed even under N$_2$. All colour was lost within 24 hours from a 30mg sample of [Fe([16]aneS$_4$)(CH$_3$CN)$_2$](BF$_4$)$_2$ that was sealed and stored under N$_2$. [Fe([12]aneS$_4$)(CH$_3$CN)$_2$](BF$_4$)$_2$ and [Fe([14]aneS$_4$)(CH$_3$CN)$_2$](BF$_4$)$_2$ both decompose as solids rapidly in air but could be stored under N$_2$ for weeks. This stability pattern is also observed with the CH$_3$NO$_2$ solutions of [Fe([12]aneS$_4$)(CH$_3$CN)$_2$](BF$_4$)$_2$, [Fe([14]aneS$_4$)(CH$_3$CN)$_2$](BF$_4$)$_2$ and [Fe([16]aneS$_4$)(CH$_3$CN)$_2$](BF$_4$)$_2$. [Fe([16]aneS$_4$)(CH$_3$CN)$_2$](BF$_4$)$_2$ decomposes instantaneously on exposure to air, while [Fe([12]aneS$_4$)(CH$_3$CN)$_2$](BF$_4$)$_2$ and

$[Fe([14]aneS_4)(CH_3CN)_2](BF_4)_2$ decompose in a few minutes in air. The decomposition in air of a solution of $[Fe([12]aneS_4)(CH_3CN)_2](BF_4)_2$ in CH_3NO_2 was followed by U.V./visible spectroscopy, but no intermediates during decomposition could be identified. The U.V./visible spectrum of $[Fe([12]aneS_4)(CH_3CN)_2](BF_4)_2$ in CH_3NO_2 shows a single absorption at $\lambda_{max.}$ = 590nm. and the magnitude of the extinction coefficient suggests that this is a d → d transition ($\epsilon_{max.} = 120M^{-1}cm^{-1}$). No other absorptions are observed within the solvent range. For $[Fe([14]aneS_4)(CH_3CN)_2](BF_4)_2$ and $[Fe([16]aneS_4)(CH_3CN)_2](BF_4)_2$, two absorptions are observed in their U.V./visible spectra, at $\lambda_{max.}$ = 537 and 394nm. and $\lambda_{max.}$ = 581 and 426nm. respectively; all of these are assigned as d → d transitions.

To investigate whether the complex $[Fe([12]aneS_4)(CH_3CN)_2](BF_4)_2$ was interacting with the N_2 atmosphere of the reaction, the synthesis of $[Fe([12]aneS_4)(CH_3CN)_2](BF_4)_2$ was carried out under Ar. This gave an identical blue product to that obtained under N_2; we conclude therefore that $[Fe([12]aneS_4)(CH_3CN)_2](BF_4)_2$ does not interact with N_2. Importantly, $[Fe([12]aneS_4)(CH_3CN)_2](BF_4)_2$ does not react with dry $O_{2(g)}$, so the decomposition of $[Fe([12]aneS_4)(CH_3CN)_2](BF_4)_2$ in air is caused by its reaction with moisture in the atmosphere. $[Fe([12]aneS_4)(CH_3CN)_2](BF_4)_2$ is insoluble in CH_2Cl_2 and THF and decomposes in C_2H_5OH and CH_3OH. We decided to investigate the chemistry of $[Fe([12]aneS_4)(CH_3CN)_2](BF_4)_2$ quite thoroughly and a number of reactions of $[Fe([12]aneS_4)(CH_3CN)_2](BF_4)_2$ with other ligands were carried out and are described below.

$[Fe([12]aneS_4)(CH_3CN)_2](BF_4)_2$ was chosen in preference to the other two tetrathioether macrocyclic complexes, since it shows a slightly greater stability than $[Fe([14]aneS_4)(CH_3CN)_2](BF_4)_2$ and there is also the possibility of stabilising the Fe–thioether unit with bidentate ligands. The *trans* configurations of $[Fe([14]aneS_4)(CH_3CN)_2](BF_4)_2$ and

$[Fe([16]aneS_4)(CH_3CN)_2](BF_4)_2$ would not allow this co-ordination mode (see, however, Section 7.2.4). We also proposed that the *cis* stereochemistry of $[Fe([12]aneS_4)(CH_3CN)_2](BF_4)_2$ might encourage the formation of bridged binuclear species with bridging ligands.

7.2.2: The Synthesis of $[Fe([15]aneS_5)(CH_3CN)](BF_4)_2$

The reaction of a CH_3NO_2 solution of $[Fe(CH_3CN)_6](BF_4)_2$ with one equivalent of a solution of $[15]aneS_5$ in CH_3NO_2 under N_2 gave a purple solution. Addition of anhydrous diethyl ether gave a purple solid that would not redissolve in a similar volume of CH_3NO_2 in which the synthesis was performed. The purple solid was sparingly soluble in CH_3NO_2 and CH_3CN but decomposed slowly in air. The i.r. spectrum (as a KBr disc) of the purple solid shows absorptions at 2960–2850 and 1436cm^{-1} which are assigned to C–H and C–S stretching vibrations respectively. Strong absorptions at 1094, 1060 and 1032cm^{-1} are also observed which are assigned to different B–F stretching vibrations. The appearence of a number of B–F stretching vibrations in the i.r. spectrum suggests that the BF_4^- counterion is co-ordinating to the $[Fe([15]aneS_5)]^{2+}$ unit and may be causing the reduced solubility of the isolated solid. There are also weak absorptions in the i.r. spectrum of the purple solid at 2100–2060cm^{-1}, which are tentatively assigned to C≡N stretching vibrations. No elemental analytical data could be obtained due to the decomposition of the purple solid in air. On the basis of the i.r. spectrum alone, we tentatively assign the purple solid as $[Fe([15]aneS_5)(CH_3CN)](BF_4)_2$ but the stereochemistry of the product is unknown. The U.V./visible spectrum of the initial air-sensitive reaction solution in CH_3NO_2 shows two absorptions, at $\lambda_{max.}$ = 531 and 400nm. ($\epsilon_{max.}$ = 230 and 230$M^{-1}cm^{-1}$ respectively).

7.2.3: The Synthesis of $[Fe([18]aneS_6)](X)_2$ ($X = BF_4^-$, ClO_4^-)

The reaction of a CH_3NO_2 solution of $[Fe(CH_3CN)_6](BF_4)_2$ under N_2 with one equivalent of $[18]aneS_6$ gave a fine purple precipitate on stirring. This purple precipitate was air-stable but insoluble in all common organic solvents and H_2O. The i.r. spectrum of this purple solid shows absorptions for C-H, C-S and B-F stretching vibrations at 2860-2850, 1435 and 1060cm^{-1} respectively. This data and elemental analytical data confirm the product as $[Fe([18]aneS_6)](BF_4)_2$.

The $[Fe([18]aneS_6)]^{2+}$ cation can also be synthesized by the reaction of equimolar amounts of $Fe(ClO_4)_3.6H_2O$ and $[18]aneS_6$ in refluxing CH_3OH. This is the only successful complexation reaction known to us between a large ring thioether macrocycle and a hydrated Fe salt. However, the product was obtained as a fine purple precipitate, which is insoluble in common organic solvents and H_2O. The i.r. spectrum and elemental analytical data confirm this product as $[Fe([18]aneS_6)](ClO_4)_2$. Attempts to solubilise the product using BPh_4^- as counterion were unsuccessful. We suspect that $[Fe([18]aneS_6)](ClO_4)_2$ can be isolated only because of its insolubility and we propose that the compound is a kinetic product in the reaction mixture. Black and McLean[328] noted that the Co(II) and Ni(II) complexes of $[18]aneS_6$ also had low solubilities as ClO_4^- salts; soluble $[Co([18]aneS_6)]^{2+}$ and $[Ni([18]aneS_6)]^{2+}$ species were only obtained using picrate as the counterion[328].

7.2.4: The Synthesis of $[Fe([12]aneS_4)(dppe)](BF_4)_2$

The reaction of equimolar amounts of $[Fe([12]aneS_4)(CH_3CN)_2](BF_4)_2$ and dppe as CH_3NO_2 solutions under N_2 gave a purple air-sensitive solution. Addition of anhydrous diethyl ether gave a purple crystalline precipitate and was recrystallised from CH_2Cl_2/diethyl ether. The purple solid was air-stable

but rapidly hydrolysed in H_2O. The f.a.b. mass spectrum of the purple solid shows peaks at M^+ = 666, 694, 713 and 781 which are assigned to $[Fe([12]aneS_4)(dppe)-(C_2H_4)]^+$, $[Fe([12]aneS_4)(dppe)]^+$, $[Fe([12]aneS_4)(dppe)](H_3O)^+$ and $[Fe([12]aneS_4)(dppe)](BF_4)^+$ respectively. This data, together with the i.r. spectrum and elemental analytical data confirm the product as $[Fe([12]aneS_4)(dppe)](BF_4)_2$.

The U.V./visible spectrum of $[Fe([12]aneS_4)(dppe)](BF_4)_2$ in CH_2Cl_2 shows two absorptions at $\lambda_{max.}$ = 521 ($\varepsilon_{max.}$ = 270$M^{-1}cm^{-1}$) and 270nm. (16,000) which are assigned as a d → d transition and charge-transfer band respectively. The fact that only one band is observed below 300nm. suggested to us that the *cis* stereochemistry of the $[Fe([12]aneS_4)]^{2+}$ unit has been maintained on complexation to the bidentate diphosphine[329]. In the ^1H n.m.r. spectrum of $[Fe([12]aneS_4)(dppe)](BF_4)_2$ in CD_3NO_2, shown in Figure 7.2 , three broad resonances are observed at 2.00-2.20, 2.90-3.40 and 7.50-7.90p.p.m., which integrate correctly for assignments to P-C$\underline{H}_2$-, C$\underline{H}_2$(macrocycle) and aromatic-$\underline{H}$ protons respectively. The broad nature of the resonances may be concealing more detail. The ^{13}C DEPT spectrum of $[Fe([12]aneS_4)(dppe)](BF_4)_2$ in CD_3NO_2 shows three CH_2 resonances at 27.69, 32.21 and 42.79p.p.m. and three CH resonances at 128.74, 131.10 and 131.44p.p.m. These are assigned as P-$\underline{C}H_2$-, S-$\underline{C}H_2$-CH_2-S, S-CH_2-$\underline{C}H_2$-S and three $\underline{C}$-H from the phenyl rings respectively. The peak at 27.69p.p.m. appears as a doublet of doublets with equivalent couplings of 13.5Hz, due to the coupling of the ^{13}C nuclei to two ^{31}P nuclei (I = ½, 100% abundance). The ^{31}P n.m.r. spectrum of $[Fe([12]aneS_4)(dppe)](BF_4)_2$ shows just one singlet at 57.28p.p.m.

Interestingly, the reaction of equimolar amounts of $[Fe([14]aneS_4)(CH_3CN)_2](BF_4)_2$ and dppe also gave a purple air-sensitive solution, which on addition of diethyl ether gave a slightly air-sensitive purple

Figure 7.2 ^{1}H n.m.r. spectrum of $[Fe([12]aneS_4)(dppe)](BF_4)_2$ in CD_3NO_2

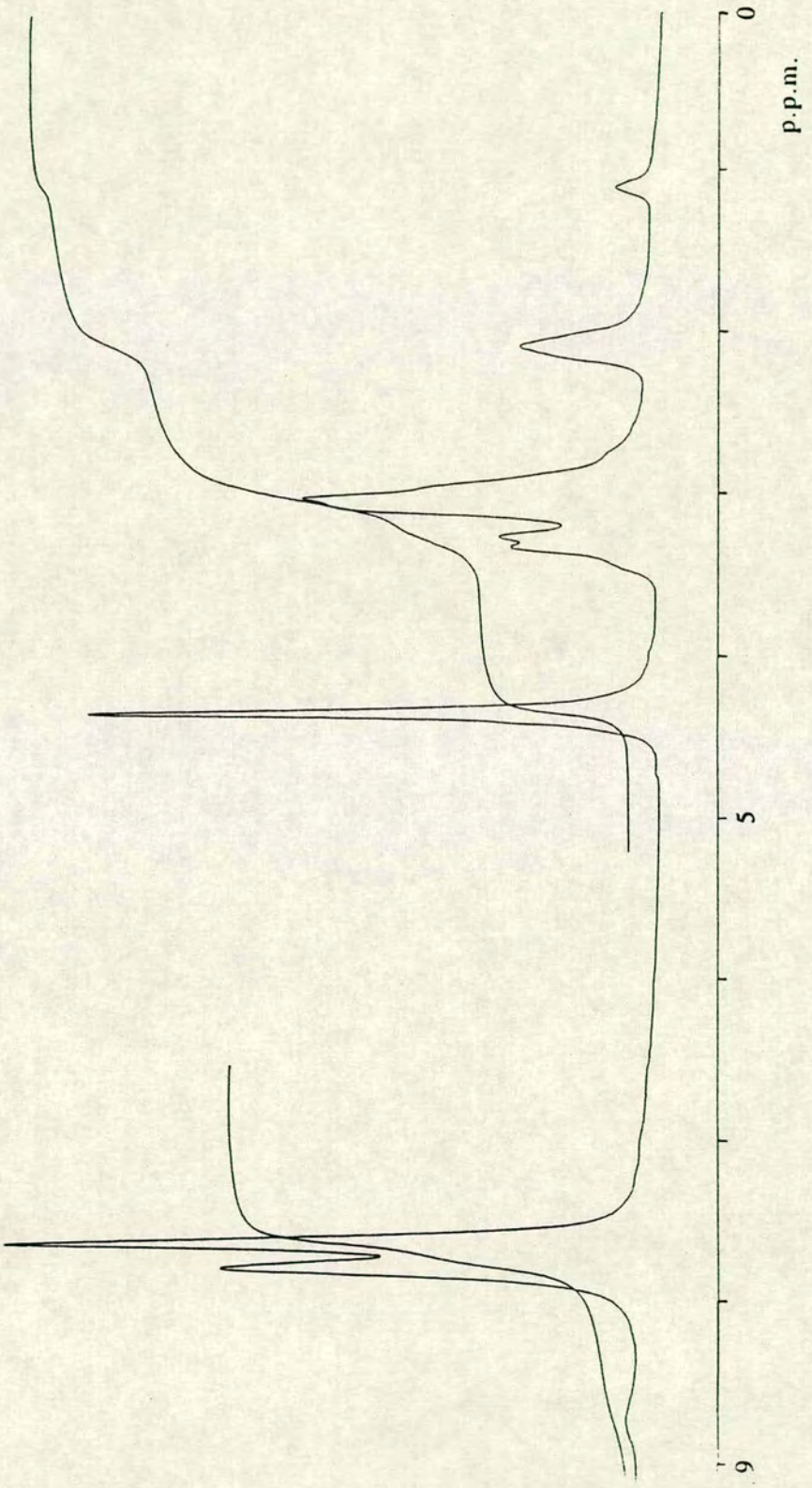

solid. The f.a.b. mass spectrum of this solid shows peaks at M^+ = 722, 741, 809, 852 and 871. These are assigned to $[Fe([14]aneS_4)(dppe)]^+$, $[Fe([14]aneS_4)(dppe)](H_3O)^+$, $[Fe([14]aneS_4)(dppe)](BF_4)^+$, $[Fe(dppe)_2]^+$ and $[Fe(dppe)_2(H_3O)]^+$. This evidence, together with the i.r. spectrum and elemental analytical data, confirm that the product contains some $[Fe([14]aneS_4)(dppe)](BF_4)_2$. The formation of the bis-diphosphine complexes are discussed later in Section 7.2.9. However on the basis of this evidence we propose that the $[Fe([14]aneS_4)]$ unit can adopt a *cis* geometry, to allow the binding of a bidentate ligand such as dppe. Compounds have been reported where dppe can bridge between two metal centres[330,331] but to our knowledge, these generally are complexes which are square-planar, metal-metal bonded or contain other bridging ligands. For dppe to bridge between two octahedral metal centres in the axial sites would be unusual and sterically unfavourable; the polymerised product might be expected to have low solubility as well. We therefore tentatively propose that $[Fe([14]aneS_4)(dppe)](BF_4)_2$ is composed of discrete $[Fe([14]aneS_4)(dppe)]^{2+}$ cations, with the diphosphine P-donors bound in adjacent sites. The U.V./visible spectrum of $[Fe([14]aneS_4)(dppe)](BF_4)_2$ in CH_2Cl_2 ($\lambda_{max.}$ = 540 and 266nm.) is also very similar to that of $[Fe([12]aneS_4)(dppe)](BF_4)_2$ ($\lambda_{max.}$ = 521 and 270nm), which suggests that both have similar, *cis* co-ordinated dppe ligands.

7.2.5: The Synthesis of $[Fe([12]aneS_4)(dppm)](BF_4)_2$

The reaction of equimolar amounts of $[Fe([12]aneS_4)(CH_3CN)_2](BF_4)_2$ and dppm as CH_3NO_2 solutions under N_2 gave a purple air-sensitive solution. Addition of anhydrous diethyl ether gave a purple precipitate that was recrystallised from CH_2Cl_2/diethyl ether. The purple solid decomposed slowly in air but rapidly hydrolysed in H_2O. The f.a.b. mass spectrum of the

purple solid shows peaks at M^+ = 385, 680 and 767, which are assigned as $[dppmH]^+$, $[Fe([12]aneS_4)(dppm)]^+$ and $[Fe([12]aneS_4)(dppm)](BF_4)^+$ respectively. This data, together with the i.r. spectrum confirm the product as $[Fe([12]aneS_4)(dppm)](BF_4)_2$. The elemental analytical data is not in agreement with the proposed formulation and reflects the instability of this compound.

The U.V./visible spectrum of $[Fe([12]aneS_4)(dppm)](BF_4)_2$ in CH_2Cl_2 shows two bands at $\lambda_{max.}$ = 523 ($\epsilon_{max.}$ = $300M^{-1}cm^{-1}$) and 266 (7,000), which are assigned as a d → d transition and charge-transfer band respectively. The positions of the bands relative to $[Fe([12]aneS_4)(dppe)](BF_4)_2$ are similar, but the extinction coefficient of the charge-transfer band is significantly smaller. The ^1H n.m.r. spectrum of $[Fe([12]aneS_4)(dppm)](BF_4)_2$ in CD_3NO_2, shown in Figure 7.3, shows signals in the region 2.90-3.60, at 5.00 (triplet) and in the region 7.50-7.70p.p.m. These are assigned as $C\underline{H}_2$(macrocycle), P-$C\underline{H}_2$-P and aromatic-$\underline{H}$ protons respectively with the correct integrations. The triplet at 5.00p.p.m. is due to the $C\underline{H}_2$ protons of the methylene group coupling to two equivalent ^{31}P nuclei (J = 11Hz). The ^{13}C DEPT n.m.r. spectrum of $[Fe([12]aneS_4)(dppm)](BF_4)_2$ in CD_3NO_2, shows $\underline{C}H_2$ resonances at 35.91 (triplet) and 42.98p.p.m. and $\underline{C}H$ resonances at 128.86, 130.74 and 131.12p.p.m. and these are assigned to P-$\underline{C}H_2$-P, $\underline{C}H_2$(macrocycle), and three $\underline{C}$-H from the phenyl rings respectively. The coupling constant of the triplet is J = 25Hz, due to coupling of the ^{13}C nucleus to two equivalent ^{31}P nuclei. The ^{31}P n.m.r. of $[Fe([12]aneS_4)(dppm)](BF_4)_2$ in CD_3NO_2 shows one peak at 3.23p.p.m.

Figure 7.3 ^{1}H n.m.r. spectrum of $[Fe([12]aneS_4)(dppm)](BF_4)_2$ in CD_3NO_2

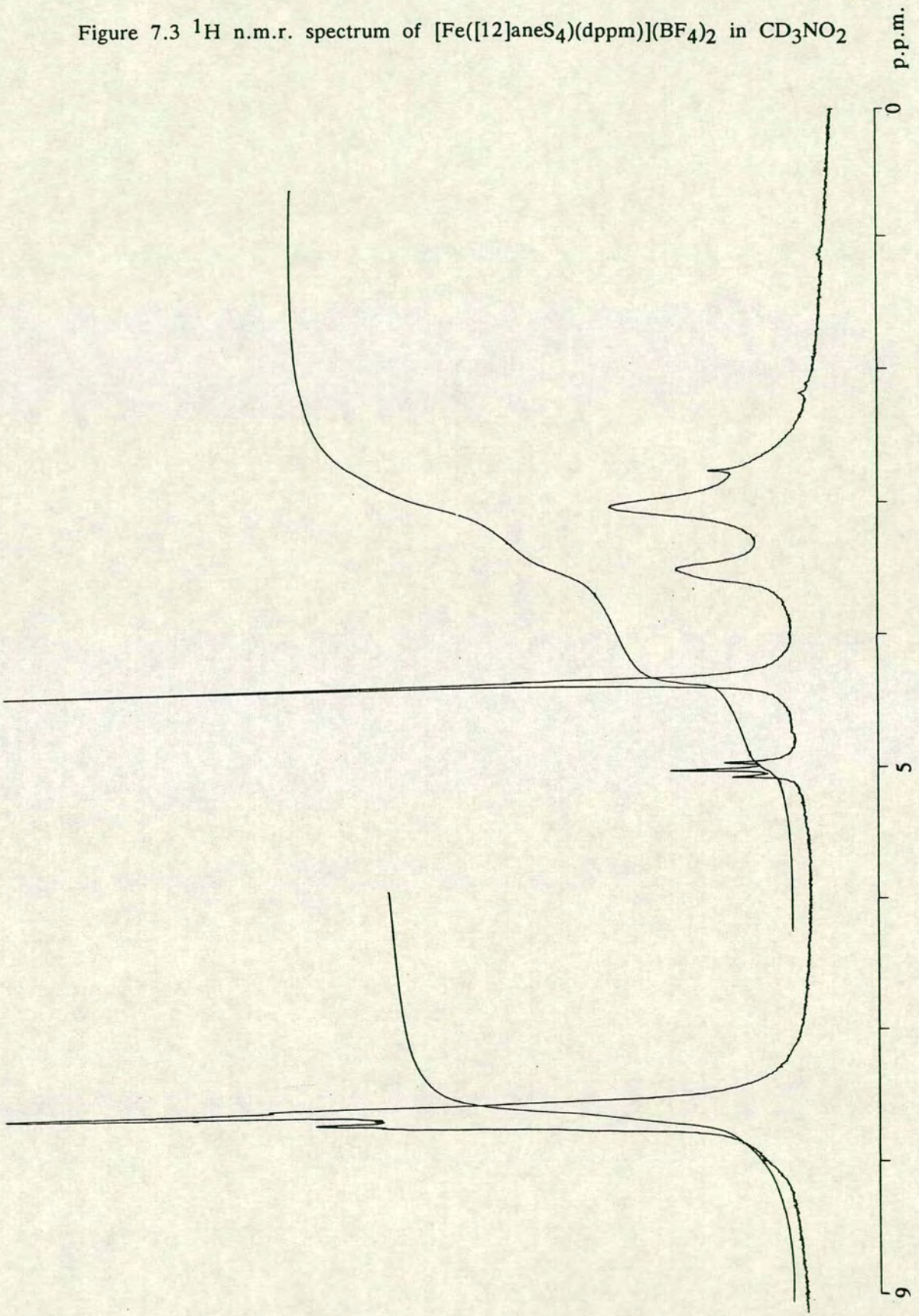

7.2.6: The Synthesis of $[Fe([12]aneS_4)(dppv)](BF_4)_2$

The reaction of equimolar amounts of $[Fe([12]aneS_4)(CH_3CN)_2](BF_4)_2$ and dppv as CH_3NO_2 solutions under N_2 gave a purple air-sensitive solution. Addition of anhydrous diethyl ether gave a purple precipitate that was recrystallised from CH_2Cl_2/diethyl ether. The purple solid was air-stable but rapidly hydrolysed in H_2O. The f.a.b. mass spectrum of the purple solid shows peaks at M^+ = 471, 664, 692, 711, 779, 848 and 867 which are assigned to $[Fe(dppv)(H_3O)]^+$, $[Fe([12]aneS_4-C_2H_4)(dppv)]^+$, $[Fe([12]aneS_4)(dppv)]^+$, $[Fe([12]aneS_4)(dppv)](H_3O)^+$, $[Fe([12]aneS_4)(dppv)](BF_4)^+$, $[Fe(dppv)_2]^+$ and $[Fe(dppv)_2(H_3O)]^+$ respectively. This data, together with the i.r. spectrum and elemental analytical data confirm the product as predominantly $[Fe([12]aneS_4)(dppv)](BF_4)_2$. It was not possible to prepare a pure sample of $[Fe([12]aneS_4)(dppv)](BF_4)_2$ without contamination with small amounts of the bis(diphosphine) complex $[Fe(dppv)_2(CH_3CN)_2](BF_4)_2$ (see Section 7.2.9). The impurity of $[Fe(dppv)_2(CH_3CN)_2]^{2+}$ was detected in the ^{31}P n.m.r. and f.a.b. mass spectra of the product. The U.V./visible spectrum of $[Fe([12]aneS_4)(dppv)](BF_4)_2$ in CH_2Cl_2 shows two absorptions at $\lambda_{max.}$ = 502 ($\epsilon_{max.}$ = $450M^{-1}cm^{-1}$) and 267nm. (17,000) which are assigned as a d → d transition and charge-transfer band respectively.

The ^1H n.m.r. spectrum of $[Fe([12]aneS_4)(dppv)](BF_4)_2$ in CD_3NO_2 gives some important evidence for the assignment of these $[Fe([12]aneS_4)(diphosphine)]^{2+}$ complexes and is shown in Figure 7.4. Normal signals in the region 7.45-8.30 and at 7.01p.p.m. are observed and are assigned to aromatic-H and P-CH= protons respectively. The macrocyclic proton resonances, though, are observed as four discrete resonances, showing two triplets of doublets at 1.49 and 2.96p.p.m. and two doublets of doublets at 3.20 and 3.48p.p.m. All four resonances give integrations corresponding to

4 H. We propose that a well-defined spectrum for the protons of [12]aneS$_4$ is observed because of the lack of flexibility in the dppv ligand, which then fixes the macrocyclic ligands into a specific conformation. In addition, the resonance at 1.49p.p.m. is shifted significantly from the expected region for macrocyclic protons because the four protons assigned to this peak are interacting with the phenyl rings of the dppv ligand. We have constructed molecular models for [Fe([12]aneS$_4$)(dppv)](BF$_4$)$_2$ and these show four equivalent protons on the the folded macrocycle are directed towards the centres of the aromatic rings (see Figure 7.5). Electronic ring currents at the centre of aromatic rings cause extra shielding of protons[332] and therefore the protons located above the centre of the phenyl rings resonate at higher applied magnetic fields and are observed at lower chemical shifts. This is good evidence that the dppv and [12]aneS$_4$ ligands are in close proximity and therefore bonded to the same metal centre. The interactions of the macrocyclic protons with the dppv ligand cause each proton in each S-CH$_2$-CH$_2$-S group to become inequivalent, which gives the four separate signals observed in the ^{1}H n.m.r. spectrum. The coupling constants and signal shapes imply that each CH$_2$CH$_2$ unit is in a staggered conformation.

The broad-band ^{13}C n.m.r. of [Fe([12]aneS$_4$)(dppv)](BF$_4$)$_2$ in CD$_3$NO$_2$ shows resonances at 33.47, 42.26, 128.77, 129.20, 129.60, 130.87, 131.17, 131.57 and 149.97 (doublet of doublets) p.p.m., which are assigned as two S-$\underline{C}$H$_2$-, six $\underline{C}$ from the phenyl rings and the P-$\underline{C}$H= carbons respectively. The coupling constants for the doublet of doublets are equivalent (J = 35Hz) caused by the ^{13}C nucleus coupling to two ^{31}P nuclei. The ^{31}P n.m.r. spectrum of [Fe([12]aneS$_4$)(dppv)](BF$_4$)$_2$ in CD$_3$NO$_2$ shows two peaks at 68.38 and 64.35p.p.m. in an approximate ratio of 12 : 1. The larger peak is assigned to the equivalent ^{31}P nuclei in [Fe([12]aneS$_4$)(dppv)](BF$_4$)$_2$, while the other is assigned to the equivalent ^{31}P nuclei in the

Figure 7.4 ^{1}H n.m.r. spectrum of $[Fe([12]aneS_4)(dppv)](BF_4)_2$ in CD_3NO_2

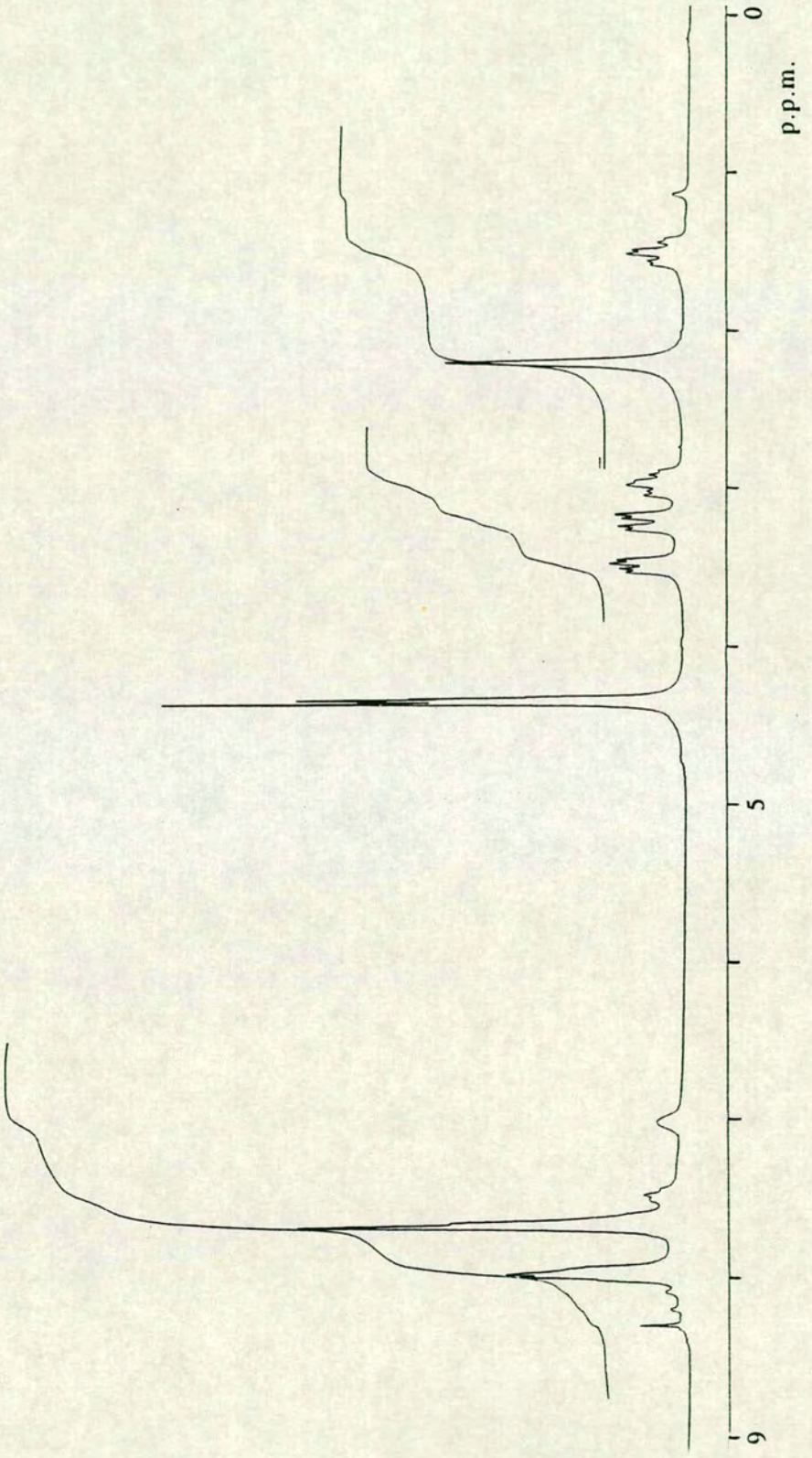

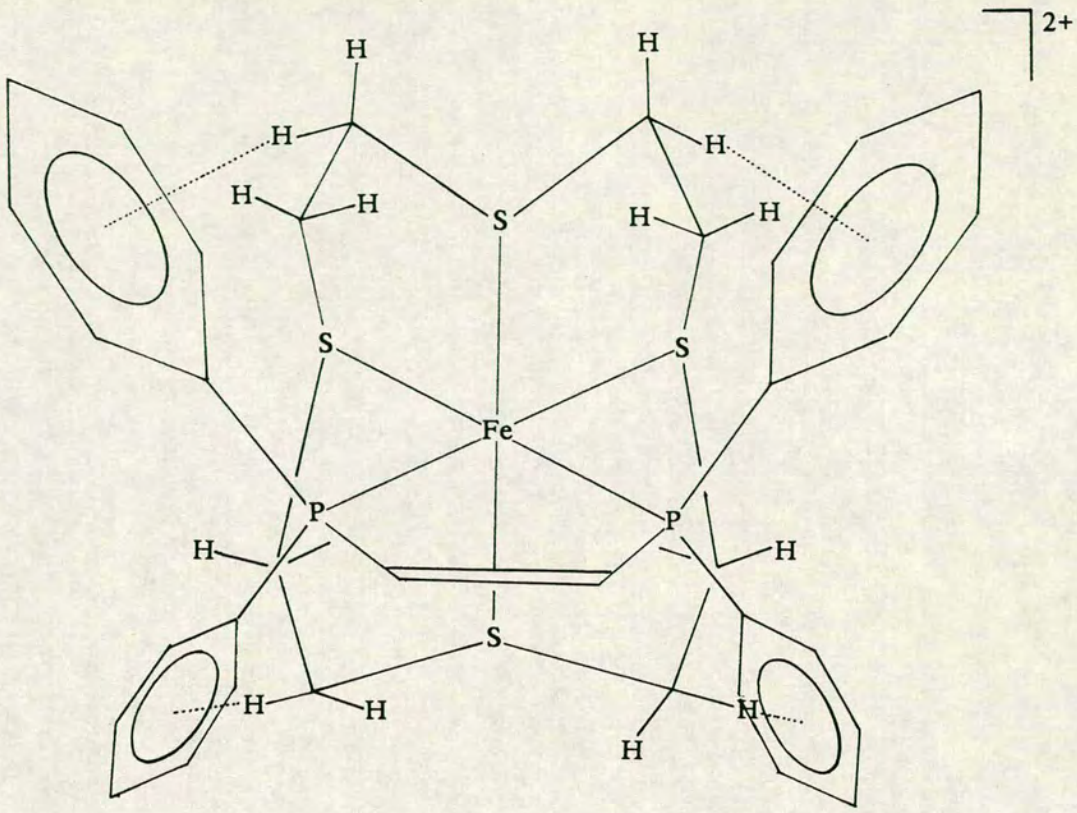

Figure 7.5 Proposed structure of $[Fe([12]aneS_4)(dppv)](BF_4)_2$ in CD_3NO_2 solution

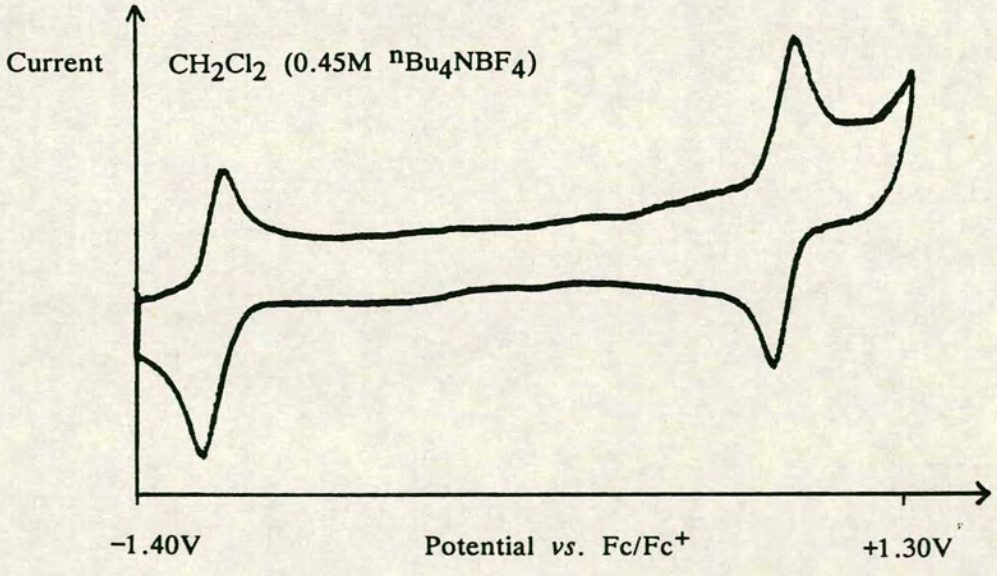

Figure 7.6 Cyclic voltammogram of $[Fe([12]aneS_4)(dppe)](BF_4)_2$

$[Fe(dppv)_2(CH_3CN)_2](BF_4)_2$ impurity (see above).

7.2.7: An Electrochemical Study of $[Fe([12]aneS_4)(dppe)](BF_4)_2$, $[Fe([12]aneS_4)(dppm)](BF_4)_2$ and $[Fe([12]aneS_4)(dppv)](BF_4)_2$ in CH_2Cl_2

Cyclic voltammetry of $[Fe([12]aneS_4)(dppe)](BF_4)_2$ measured at 298K in CH_2Cl_2 (0.45M $Bu^n_4NBF_4$ supporting electrolyte) at Pt electrodes shows one reversible oxidation at $E_{\frac{1}{2}}$ = +0.80V *vs.* Fc/Fc^+ and one reversible reduction at $E_{\frac{1}{2}}$ = −1.23V *vs.* Fc/Fc^+. These redox processes are shown in Figure 7.6.

A quantitative investigation of the oxidation process was undertaken. Coulometry of $[Fe([12]aneS_4)(dppe)](BF_4)_2$, measured at +1.01V *vs.* Fc/Fc^+, 298K in CH_2Cl_2 (0.45M $Bu^n_4NBF_4$ supporting electrolyte) at a Pt basket, confirmed that the oxidation corresponds to a one-electron process (n = 0.95 electrons). During bulk electrolysis the solution changed from a purple to an orange/brown colour. No signal is observed in the e.s.r. spectrum (measured at 77K, CH_2Cl_2 glass) of the orange/brown solution. This evidence is not inconsistent with the formation of a low spin Fe(III) species, since these species can be difficult to observe at temperatures above 4.2K, due to short spin-lattice relaxation times. Controlled potential electrolysis at 298K, +0.50V regenerated the original Fe(II) starting material quantitatively.

To investigate the nature of the product from the oxidation of $[Fe([12]aneS_4)(dppe)](BF_4)_2$, the one-electron oxidation was followed at +1.13V *vs.* Fc/Fc^+, 248K in CH_2Cl_2 by *in situ* U.V./visible spectroscopy using an O.T.T.L.E. system. The oxidation occurs isosbestically (λ_{iso} = 296nm.), with the loss of intensity of the absorption band at $\lambda_{max.}$ = 270nm and concommitant growth of a new band at $\lambda_{max.}$ = 336nm. The electronic spectrum observed during the oxidation is shown in Figure 7.7. Regeneration of the Fe(II) starting material at 0.0V, 248K occurs quantitatively. Assuming that the oxidation is metal-based, corresponding to

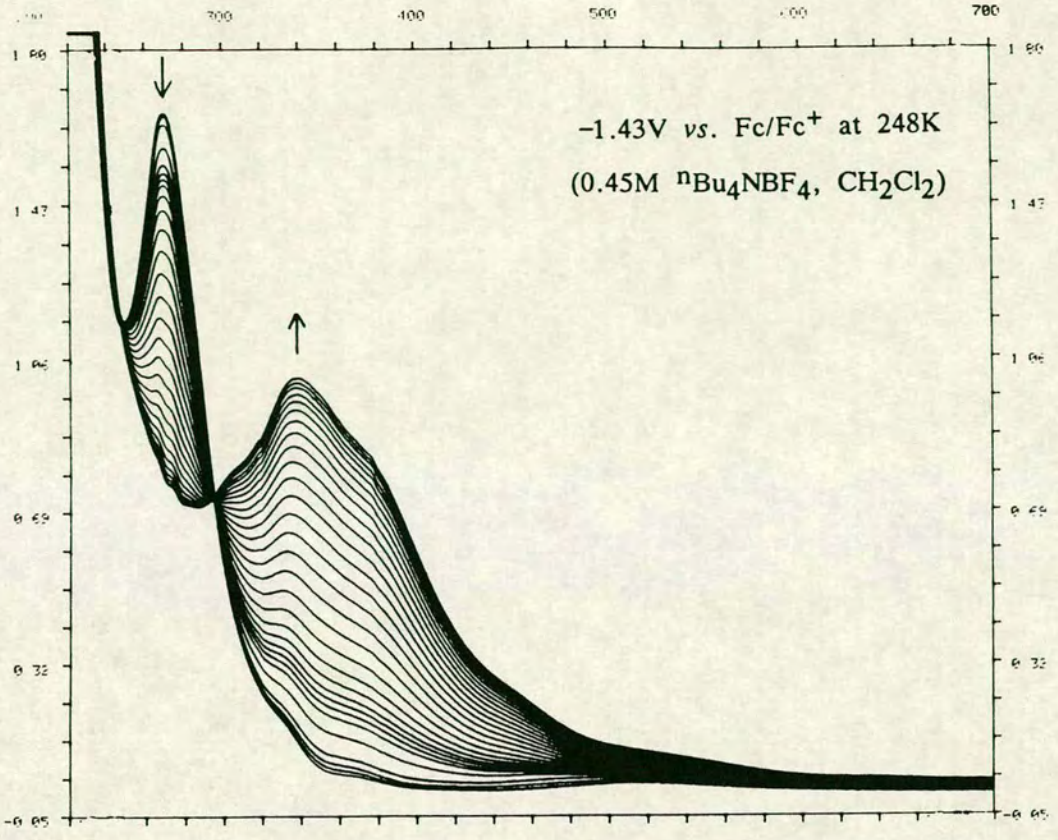

Figure 7.7 Electronic spectrum showing oxidation of $[Fe([12]aneS_4)(dppe)](BF_4)_2$

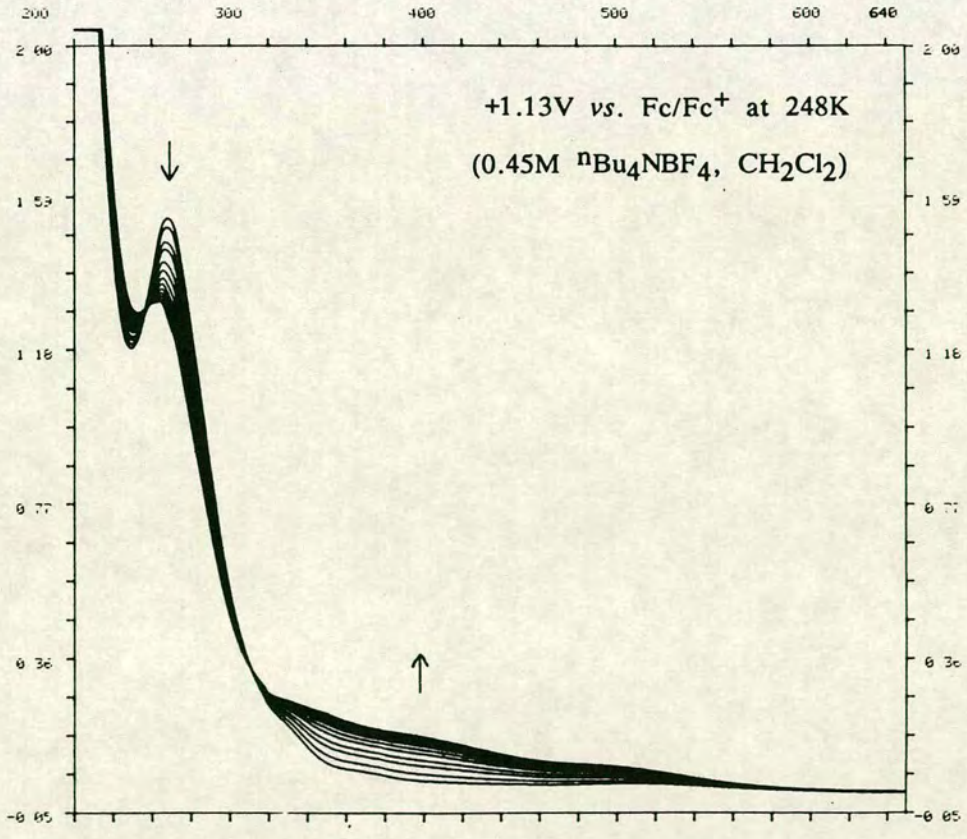

Figure 7.8 Electronic spectrum showing reduction of $[Fe([12]aneS_4)(dppe)](BF_4)_2$

the oxidation state change Fe(II) → Fe(III), the shift of the charge-transfer band to higher wavelengths (270 → 336nm.) leads us to assign the absorption band as due to metal-to-ligand charge-transfer.

A quantitative investigation of the reduction of $[Fe([12]aneS_4)(dppe)](BF_4)_2$ ($E_{\frac{1}{2}}$ = −1.23V *vs.* Fc/Fc^+) was also attempted. Coulometry of $[Fe([12]aneS_4)(dppe)](BF_4)_2$, measured at −1.43V *vs.* Fc/Fc^+, 298K in CH_2Cl_2 (0.45M $Bu^n_4NBF_4$ supporting electrolyte) at a Pt basket, gave inconsistent results (n = 1.44–1.75 electrons) and could not be rationalised. This behaviour was also observed at 248K. During bulk electrolysis a colour change from purple to colourless was observed in the solution and the e.s.r spectrum (measured at 77K, CH_2Cl_2 glass) of the colourless solution showed no signal. It was not possible to regenerate the $[Fe([12]aneS_4)(dppe)](BF_4)_2$ starting material from the colourless solution. This suggests that the product of the reduction of $[Fe([12]aneS_4)(dppe)](BF_4)_2$ is not stable at these temperatures and on the coulometric time-scale. However, considering that the peak heights of the oxidation and reduction processes are approximately equal, we tentatively propose that the reduction is a one-electron transfer.

In an attempt to obtain more data on this reductive process, the reduction was followed at −1.43V *vs.* Fc/Fc^+, 248K in CH_2Cl_2 by *in situ* U.V./visible spectroscopy using an O.T.T.L.E. system. The reduction occurs isosbestically (λ_{iso} = 252 and 316nm.), with the loss of intensity of the absorption band at $\lambda_{max.}$ = 270nm to give a new band at $\lambda_{max.}$ = 262nm. The electronic spectra observed during the reduction is shown in Figure 7.8. The shift of the band at 270nm to lower wave lengths on reduction reaffirms our assignment that this band is due to metal-to-ligand charge-transfer. The spectra also show the growth of a broad range of new bands in the region 300 → 550nm., which are of the appropriate magnitude for d → d transitions

($\epsilon_{max.}$ = c.500$M^{-1}cm^{-1}$). Partial regeneration of the Fe(II) starting material does occur at 0.0V *vs.* Fc/Fc^+, 248K but repeated cycling between the Fe(II) and reduced species leads to gradual decomposition of the complex. We have been unable to determine the nature of the reduced species, due to its overall instability; however, the reduced product is partially stable at 248K and on the timescale of the *in situ* electrogeneration experiment (in this case, 2–3 hours).

Cyclic voltammetry of $[Fe([12]aneS_4)(dppm)](BF_4)_2$ measured at 298K in CH_2Cl_2 (0.45M $Bu^n{}_4NBF_4$ supporting electrolyte) at Pt electrodes, shows one reversible oxidation at $E_{\frac{1}{2}}$ = +0.86V *vs.* Fc/Fc^+ and one irreversible reduction at E_{pc} = −1.36V *vs.* Fc/Fc^+ (scan rate = 0.50Vs^{-1}). The irreversibility of the reduction did not change on cooling of the solution to 253K. We attempted to investigate these redox processes both by coulometry and by *in situ* spectroscopy using an O.T.T.L.E. system, but decomposition of the complex always occurred. This is an illustration of the decreased stability of $[Fe([12]aneS_4)(dppm)](BF_4)_2$ as compared to $[Fe([12]aneS_4)(dppe)](BF_4)_2$ and $[Fe([12]aneS_4)(dppv)](BF_4)_2$.

Cyclic voltammetry of $[Fe([12]aneS_4)(dppv)](BF_4)_2$ measured at 298K in CH_2Cl_2 (0.45M $Bu^n{}_4NBF_4$ supporting electrolyte) at Pt electrodes, shows one reversible oxidation at $E_{\frac{1}{2}}$ = +0.92V *vs.* Fc/Fc^+ and one reversible reduction at $E_{\frac{1}{2}}$ = −1.28V *vs.* Fc/Fc^+. These redox processes are shown in Figure 7.9. and since the peak heights of each wave are approximately equal, we tentatively propose that each process corresponds to a one–electron transfer. The redox chemistry of $[Fe([12]aneS_4)(dppv)](BF_4)_2$ was not examined further due to a shortage of time.

A comparison of the electrochemical properties of $[Fe([12]aneS_4)(dppe)](BF_4)_2$, $[Fe([12]aneS_4)(dppm)](BF_4)_2$ and $[Fe([12]aneS_4)(dppv)](BF_4)_2$ reveals that each complex shows one oxidation

Table 7.1: Electrochemical data for [Fe([12]aneS$_4$)(diphosphine)](BF$_4$)$_2$

	Oxidation E (V)	Reduction E (V)
[Fe([12]aneS$_4$)(dppe)](BF$_4$)$_2$	+0.80(r)	-1.23(r)
[Fe([12]aneS$_4$)(dppm)](BF$_4$)$_2$	+0.86(r)	-1.36(i)
[Fe([12]aneS$_4$)(dppv)](BF$_4$)$_2$	+0.92(r)	-1.28(r)

r = reversible, i = irreversible (scan rate = 0.50Vs^{-1}). All *vs.* Fc/Fc$^+$

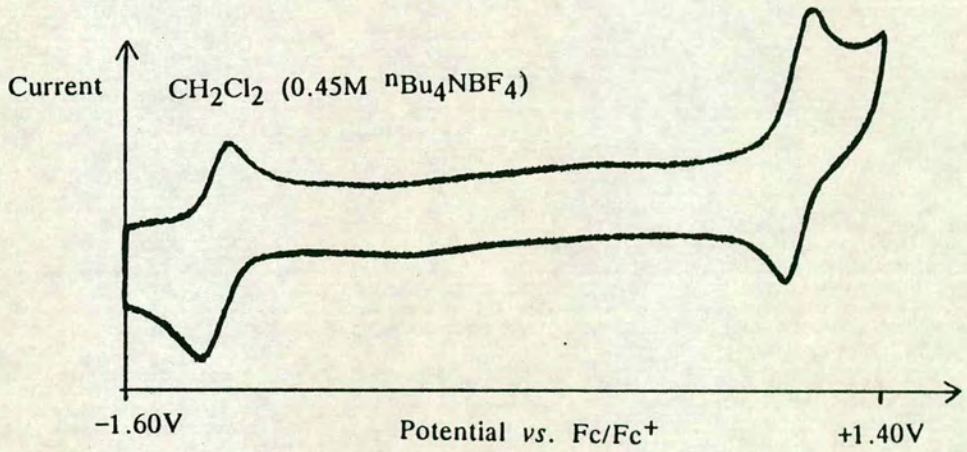

Figure 7.9 Cyclic voltammogram of [Fe([12]aneS$_4$)(dppv)](BF$_4$)$_2$

and reduction, at potentials which are roughly similar. This data is summarised in Table 7.1. All the redox processes are reversible, except for the reduction of $[Fe([12]aneS_4)(dppm)](BF_4)_2$, which is irreversible at all operating scan rates and temperatures above 253K. If the reduction of these $[Fe([12]aneS_4)(diphosphine)](BF_4)_2$ complexes is metal-based, corresponding to a Fe(II) → Fe(I) conversion, we expect that the reduction step will be accompanied by an increase in size of the metal centre. Therefore, the irreversibility of the reduction for $[Fe([12]aneS_4)(dppm)](BF_4)_2$ can be explained in terms of the smaller chelate ring-size of dppm not being able to accommodate the new stereochemical requirements of the Fe(I) centre. This results in an irreversible step occurring after the metal reduction.

It is noteworthy that although the $[Fe([12]aneS_4)(diphosphine)](BF_4)_2$ complexes do show electrochemical activity, both the oxidation and reduction occur at quite extreme potentials, with a difference of approximately 2.0V between the two processes. We propose therefore that the Fe(II) oxidation state for the complexes is significantly stabilised with respect to either oxidation or reduction.

7.2.8: Further Reactions of $[Fe([12]aneS_4)(CH_3CN)_2](BF_4)_2$

The reactions of $[Fe([12]aneS_4)(CH_3CN)_2](BF_4)_2$ with bidentate phosphines have been described above, where the $[Fe([12]aneS_4)]^{2+}$ unit is stabilised by the chelating ligand. A number of other reactions were attempted, with other bidentate and monodentate ligands which were less successful at giving products that were isolatable and characterisable in air. The general procedure for the reactions was to add the auxilliary ligand (preferably as a CH_3NO_2 solution) to a stirring solution of $[Fe([12]aneS_4)(CH_3CN)_2](BF_4)_2$ in CH_3NO_2. The products of the reactions were isolated by the addition of diethyl ether to the reaction mixture and

characterised, where possible, by i.r., f.a.b. mass spectroscopy and elemental analysis.

The outcomes of the reactions could be divided into three groups:

i) the added ligand displaced the macrocycle and precipitation of the macrocycle was observed on cooling;

ii) no reaction was observed;

iii) the auxilliary ligand appeared to co-ordinate to the $[Fe([12]aneS_4)]^{2+}$ unit, but the product decomposed in air.

Details of the attempted reactions are given in Sections 7.4.11-31. The ligands pyridine, 2,2-bipyridine, $[S_2CN(C_2H_5)_2]^-$, SCN^-, $C_6H_5S^-$ or Cl^- all caused replacement of the $[12]aneS_4$ macrocycle. Addition of imidazole, methylhydrazine, dppp, NO, CO or $CH_3CO_2^-$ to $[Fe([12]aneS_4)(CH_3CN)_2](BF_4)_2$ gave a colour change in the solution and no precipitate of $[12]aneS_4$ was observed on cooling the reaction solution. Attempted isolation of the products gave solids which rapidly deliquesced on exposure to the atmosphere. The dppp ligand gave a purple air-sensitive solution similar to the other $[Fe([12]aneS_4)(diphosphine)](BF_4)_2$ analogues, but the proposed complex $[Fe([12]aneS_4)(dppp)](BF_4)_2$ was unstable in air. No reactions were observed between solutions of $[Fe([12]aneS_4)(CH_3CN)_2](BF_4)_2$ in CH_3NO_2 with C_6H_5CN, Ph_3P, $(C_6H_{11})_3P$, $(C_6H_{11})_2PC_2H_4P(C_6H_{11})$, $Ph_2AsC_2H_4AsPh_2$, O_2, 1,3,5-trithiane and Na[2,4,6-tri(isopropyl)thiophenol].

7.2.9: The Synthesis of $[Fe(dppe)_2(CH_3CN)_2](BF_4)_2$

The reaction of $[Fe(CH_3CN)_6](BF_4)_2$ in CH_3NO_2 with a solution of two equivalents of dppe in CH_3NO_2 gave a red solution. Addition of excess diethyl ether gave a red crystalline precipitate which was recrystallised from CH_2Cl_2/diethyl ether. The f.a.b. mass spectrum of the red solid shows peaks

at M^+ = 399, 454, 473, 852 and 871, which are assigned to $[dppeH]^+$, $[Fe(dppe)]^+$, $[Fe(dppe)(H_3O)]^+$, $[Fe(dppe)_2]^+$ and $[Fe(dppe)_2(H_3O)]^+$ respectively. The i.r. spectrum of the red solid shows strong bands at 1434 and 1060cm^{-1}, which are assigned to P–C and B–F stretching vibrations respectively. There is also a weak absorption at 2200cm^{-1}, which is tentatively assigned to a co-ordinated C≡N stretching vibration. This evidence, together with elemental analytical data, confirm the product as $[Fe(dppe)_2(CH_3CN)_2](BF_4)_2$.

$[Fe(dppe)_2(CH_3CN)_2](BF_4)_2$ was identical to the red solids that were obtained from the decomposed solutions of $[Fe([12]aneS_4)(dppe)](BF_4)_2$ on exposure to the atmosphere. Similarly, $[Fe([12]aneS_4)(dppv)](BF_4)_2$ and $[Fe([12]aneS_4)(dppm)](BF_4)_2$ decomposed on exposure to the atmosphere to $[Fe(dppv)_2(CH_3CN)_2](BF_4)_2$ and $[Fe(dppm)_2(CH_3CN)_2](BF_4)_2$ respectively. $[Fe(dppe)_2(CH_3CN)_2](BF_4)_2$ is also a side-product in the synthesis of $[Fe([14]aneS_4)(dppe)](BF_4)_2$. We tentatively propose, on the evidence given above, that the mechanism of decomposition of $[Fe([12]aneS_4)(diphosphine)](BF_4)_2$ occurs by substitution of the macrocycle by H_2O from the atmosphere, followed by formation of $[Fe(dppe)_2(CH_3CN)_2](BF_4)_2$. It is surprising that the CH_3CN molecules in solution are co-ordinated preferentially to H_2O, but compounds of the form $[Fe(diphosphine)_2(CH_3CN)_2]^{2+}$ have been well-documented in the literature[333–337] and appear to be thermodynamically favoured products. $[Fe(dppe)_2(CH_3CN)_2](BF_4)_2$ has been reported previously[335] and the electrochemical behaviour has been extensively investigated[335]. $[Fe(dppe)_2(CH_3CN)_2](ClO_4)_2$ in CH_3CN shows one reversible one-electron oxidation (at $E^{\bullet}_{\frac{1}{2}}$ = 1.06V) and two reversible one-electron reductions ($E^{\bullet}_{\frac{1}{2}}$ = −1.36 and 1.78V)[335]. The Mössbauer spectrum of $[Fe(dppe)_2(CH_3CN)_2]I_2$ has also been reported[333]. However, the single crystal

X-ray structure of $[Fe(dppe)_2(CH_3CN)_2](BF_4)_2$ has not been previously determined and in order to compare this structure with those of analogous $[Fe(diphosphine)_2(CH_3CN)_2]^{2+}$ structures[334,336,337], the single crystal X-ray structure of $[Fe(dppe)_2(CH_3CN)_2](BF_4)_2$ was undertaken.

7.2.10: The Single Crystal X-Ray Structure of $[Fe(dppe)_2(CH_3CN)_2](BF_4)_2$

Details of the structure solution and refinement are given in the Experimental Section. Tables of relevant bond lengths, angles and torsions are given in Tables 7.2, 7.3 and 7.4 respectively. A view of the cation $[Fe(dppe)_2(CH_3CN)_2]^{2+}$ is shown in Figure 7.10.

The single crystal X-ray structure of $[Fe(dppe)_2(CH_3CN)_2](BF_4)_2$ shows that the Fe(II) ions are octahedrally co-ordinated and there are no significant interactions between the dication, the BF_4^- counterions and the included CH_2Cl_2 solvent molecules. The four P-donors in the cation form a rectangular equatorial plane, with the two CH_3CN ligands mutually *trans*. The Fe atom of $[Fe(dppe)_2(CH_3CN)_2](BF_4)_2$ is located on an inversion centre, so the two dppe ligands are in identical conformations. The Fe-P bond lengths are 2.3203(25) and 2.342(3)Å, which are standard values for low spin $[Fe(diphosphine)_2(CH_3CN)_2]^{2+}$ complexes[334,336,337]. The dppe ligands have a normal *gauche* conformation with a P(1)-C(1)-C(2)-P(2) torsion angle of 40.0(8)°. The Fe-N-C-CH_3 group is virtually linear [∠Fe-N(1)≡C(1A) = 177.9(8)°] and perpendicular to the equatorial plane [∠P(1)-Fe-N(1) = 86.26(25), ∠P(2)-Fe-N(1) = 86.21(25)°].

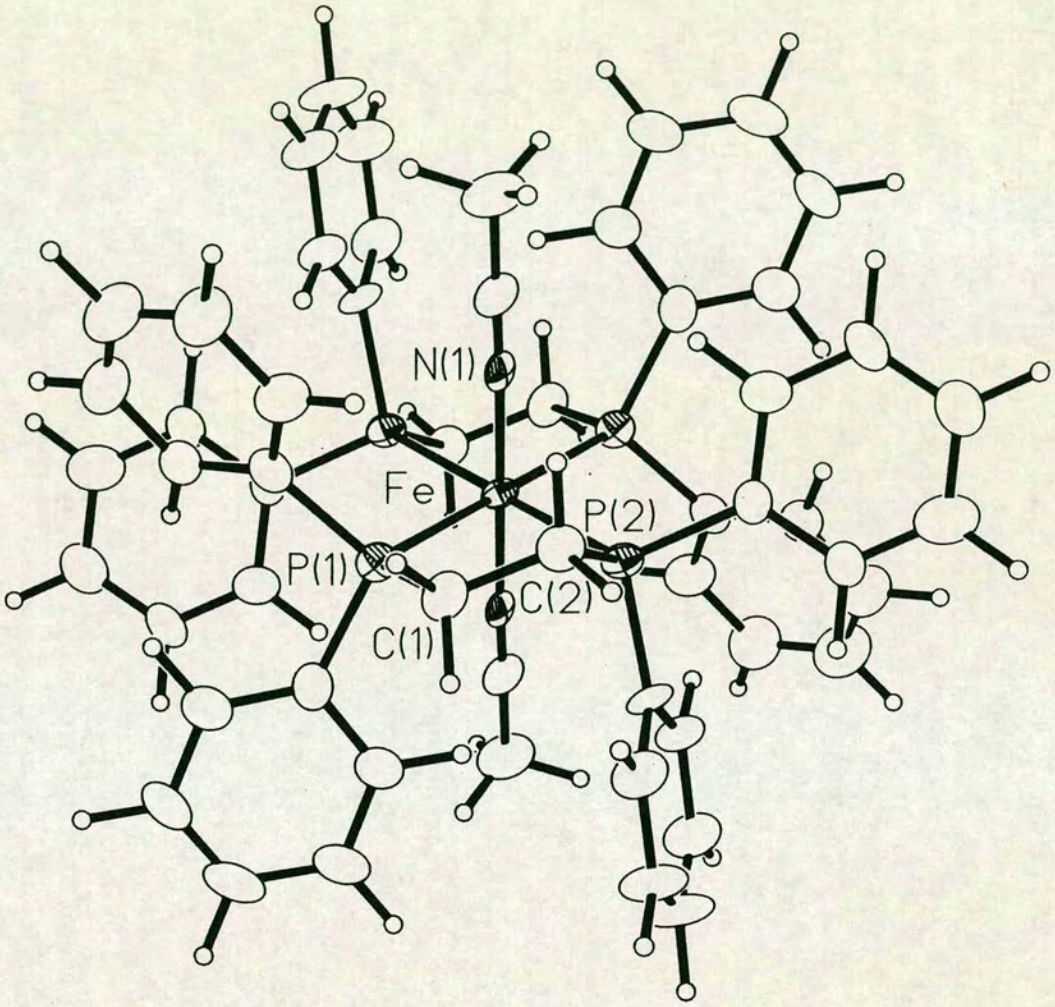

Figure 7.10 View of the single crystal X-ray structure of

$[Fe(dppe)_2(CH_3CN)_2]^{2+}$

Table 7.2 Selected bond lengths (Å) of $[Fe(dppe)_2(CH_3CN)_2]^{2+}$

Fe	- P(1)	2.342(3)			
Fe	- P(2)	2.3203(25)	P(2)	-C(21)	1.820(10)
Fe	- N(1)	1.913(8)	P(2)	- C(2)	1.833(10)
P(1)	- C(3)	1.837(10)	C(15)	-C(16)	1.403(14)
P(1)	- C(9)	1.827(10)	C(15)	-C(20)	1.396(14)
P(1)	- C(1)	1.871(10)	C(16)	-C(17)	1.374(16)
C(3)	- C(4)	1.413(14)	C(17)	-C(18)	1.410(17)
C(3)	- C(8)	1.373(14)	C(18)	-C(19)	1.389(16)
C(4)	- C(5)	1.377(15)	C(19)	-C(20)	1.383(15)
C(5)	- C(6)	1.403(16)	C(21)	-C(22)	1.385(16)
C(6)	- C(7)	1.371(16)	C(21)	-C(26)	1.419(15)
C(7)	- C(8)	1.393(15)	C(22)	-C(23)	1.395(19)
C(9)	-C(10)	1.398(14)	C(23)	-C(24)	1.360(21)
C(9)	-C(14)	1.400(15)	C(24)	-C(25)	1.376(20)
C(10)	-C(11)	1.381(16)	C(25)	-C(26)	1.378(17)
C(11)	-C(12)	1.356(19)	C(1)	- C(2)	1.519(14)
C(12)	-C(13)	1.375(19)	N(1)	-C(1A)	1.141(14)
C(13)	-C(14)	1.397(17)	C(1A)	-C(2A)	1.468(17)
P(2)	-C(15)	1.816(10)			

Table 7.3 Selected bond angles (°) of $[Fe(dppe)_2(CH_3CN)_2]^{2+}$

P(1)	- Fe	- P(2)	83.20(9)	Fe	- P(2)	-C(21)	116.6(3)
P(1)	- Fe	- N(1)	86.26(25)	Fe	- P(2)	- C(2)	104.5(3)
P(2)	- Fe	- N(1)	86.21(25)	C(15)	- P(2)	-C(21)	103.9(5)
Fe	- P(1)	- C(3)	121.3(3)	C(15)	- P(2)	- C(2)	101.9(4)
Fe	- P(1)	- C(9)	114.7(3)	C(21)	- P(2)	- C(2)	104.1(5)
Fe	- P(1)	- C(1)	108.3(3)	P(2)	-C(15)	-C(16)	121.3(7)
C(3)	- P(1)	- C(9)	106.1(5)	P(2)	-C(15)	-C(20)	121.0(7)
C(3)	- P(1)	- C(1)	100.3(5)	C(16)	-C(15)	-C(20)	117.7(9)
C(9)	- P(1)	- C(1)	103.8(5)	C(15)	-C(16)	-C(17)	121.5(10)
P(1)	- C(3)	- C(4)	116.5(7)	C(16)	-C(17)	-C(18)	120.6(11)
P(1)	- C(3)	- C(8)	126.3(8)	C(17)	-C(18)	-C(19)	117.8(10)
C(4)	- C(3)	- C(8)	117.2(9)	C(18)	-C(19)	-C(20)	121.5(10)
C(3)	- C(4)	- C(5)	121.8(10)	C(15)	-C(20)	-C(19)	120.8(9)
C(4)	- C(5)	- C(6)	118.9(10)	P(2)	-C(21)	-C(22)	122.9(8)
C(5)	- C(6)	- C(7)	120.3(11)	P(2)	-C(21)	-C(26)	119.0(8)
C(6)	- C(7)	- C(8)	119.5(10)	C(22)	-C(21)	-C(26)	118.1(10)
C(3)	- C(8)	- C(7)	122.2(10)	C(21)	-C(22)	-C(23)	120.0(11)
P(1)	- C(9)	-C(10)	121.7(8)	C(22)	-C(23)	-C(24)	121.2(13)
P(1)	- C(9)	-C(14)	119.7(8)	C(23)	-C(24)	-C(25)	119.8(14)
C(10)	- C(9)	-C(14)	118.4(9)	C(24)	-C(25)	-C(26)	120.6(12)
C(9)	-C(10)	-C(11)	119.5(10)	C(21)	-C(26)	-C(25)	120.2(10)
C(10)	-C(11)	-C(12)	122.0(12)	P(1)	- C(1)	- C(2)	112.0(7)
C(11)	-C(12)	-C(13)	120.0(13)	P(2)	- C(2)	- C(1)	110.5(7)
C(12)	-C(13)	-C(14)	119.7(12)	Fe	- N(1)	-C(1A)	177.9(8)
C(9)	-C(14)	-C(13)	120.4(10)	N(1)	-C(1A)	-C(2A)	179.1(12)
Fe	- P(2)	-C(15)	123.3(3)				

Table 7.4 Selected torsion angles (°) of $[Fe(dppe)_2(CH_3CN)_2]^{2+}$

C(9)	P(1)	C(3)	C(4)	-178.3(8)	C(21)	P(2)	C(15)	C(20)	175.2(8)
C(9)	P(1)	C(3)	C(8)	-1.9(11)	C(2)	P(2)	C(15)	C(16)	104.1(9)
C(1)	P(1)	C(3)	C(4)	-70.5(9)	C(2)	P(2)	C(15)	C(20)	-76.8(9)
C(1)	P(1)	C(3)	C(8)	105.9(10)	C(15)	P(2)	C(21)	C(22)	98.3(10)
C(3)	P(1)	C(9)	C(10)	-47.7(9)	C(15)	P(2)	C(21)	C(26)	-82.9(9)
C(3)	P(1)	C(9)	C(14)	137.0(8)	C(2)	P(2)	C(21)	C(22)	-8.1(10)
C(1)	P(1)	C(9)	C(10)	-153.0(8)	C(2)	P(2)	C(21)	C(26)	170.7(8)
C(1)	P(1)	C(9)	C(14)	31.8(9)	C(15)	P(2)	C(2)	C(1)	-179.3(7)
C(3)	P(1)	C(1)	C(2)	139.2(7)	C(21)	P(2)	C(2)	C(1)	-71.5(8)
C(9)	P(1)	C(1)	C(2)	-111.2(7)	P(2)	C(15)	C(16)	C(17)	176.7(9)
P(1)	C(3)	C(4)	C(5)	177.7(8)	C(20)	C(15)	C(16)	C(17)	-2.5(15)
C(8)	C(3)	C(4)	C(5)	0.9(15)	P(2)	C(15)	C(20)	C(19)	-178.4(8)
P(1)	C(3)	C(8)	C(7)	-178.4(8)	C(16)	C(15)	C(20)	C(19)	0.7(15)
C(4)	C(3)	C(8)	C(7)	-2.0(15)	C(15)	C(16)	C(17)	C(18)	1.4(17)
C(3)	C(4)	C(5)	C(6)	1.2(16)	C(16)	C(17)	C(18)	C(19)	1.4(17)
C(4)	C(5)	C(6)	C(7)	-2.4(17)	C(17)	C(18)	C(19)	C(20)	-3.1(17)
C(5)	C(6)	C(7)	C(8)	1.3(17)	C(18)	C(19)	C(20)	C(15)	2.1(16)
C(6)	C(7)	C(8)	C(3)	0.9(17)	P(2)	C(21)	C(22)	C(23)	174.6(10)
P(1)	C(9)	C(10)	C(11)	-174.3(9)	C(26)	C(21)	C(22)	C(23)	-4.3(17)
C(14)	C(9)	C(10)	C(11)	1.0(15)	P(2)	C(21)	C(26)	C(25)	-174.6(9)
P(1)	C(9)	C(14)	C(13)	173.8(9)	C(22)	C(21)	C(26)	C(25)	4.2(16)
C(10)	C(9)	C(14)	C(13)	-1.6(16)	C(21)	C(22)	C(23)	C(24)	1.3(20)
C(9)	C(10)	C(11)	C(12)	-0.1(18)	C(22)	C(23)	C(24)	C(25)	1.9(22)
C(10)	C(11)	C(12)	C(13)	-0.1(20)	C(23)	C(24)	C(25)	C(26)	-2.0(21)
C(11)	C(12)	C(13)	C(14)	-0.6(20)	C(24)	C(25)	C(26)	C(21)	-1.1(19)
C(12)	C(13)	C(14)	C(9)	1.4(18)	P(1)	C(1)	C(2)	P(2)	-40.0(8)
C(21)	P(2)	C(15)	C(16)	-3.9(9)					

7.3: Conclusions

The complexation of Fe(II) with tetra-, penta- and hexa-thioether macrocycles has been achieved, using the anhydrous starting material $[Fe(CH_3CN)_6](BF_4)_2$ and anhydrous reaction conditions. The complexes of Fe(II) with [12]aneS_4, [14]aneS_4 and [16]aneS_4 were difficult to characterise due to their instability with respect to hydrolysis, particularly from H_2O in the atmosphere. Air-stable solids were only obtained on reaction of $[Fe([12]aneS_4)(CH_3CN)_2](BF_4)_2$ with the bidentate diphosphines dppe, dppv and dppm. The complexes $[Fe([12]aneS_4)(diphosphine)](BF_4)_2$ (diphosphine = dppe, dppv and dppm) were purple solids that decomposed when in solution on exposure to air to the appropriate $[Fe(diphosphine)_2(CH_3CN)_2](BF_4)_2$ species, which are a well-known series of compounds. The redox activity of the $[Fe([12]aneS_4)(diphosphine)](BF_4)_2$ complexes was investigated and all three complexes showed an oxidation and reduction, which are assigned as one-electron steps. The oxidation and reduction of $[Fe([12]aneS_4)(dppe)](BF_4)_2$ were investigated by coulometry and by *in situ* U.V./visible spectroscopy. The reduction product of $[Fe([12]aneS_4)(dppe)](BF_4)_2$ was very unstable, even at 248K, and the Fe(II) starting material could not be regenerated quantitatively after generating the reduction product. The oxidation product could be generated reversibly, but from the evidence obtained overall, we suggest that for this thioether-phosphine S_4P_2-donor set, the Fe(II) oxidation state is overwhelmingly favoured. We have been unable to grow single crystals of the $[Fe([12]aneS_4)(diphosphine)](BF_4)_2$ complexes that would be suitable for an X-ray diffraction study, but the single crystal X-ray structure of the decomposition product of $[Fe([12]aneS_4)(dppe)](BF_4)_2$, $[Fe(dppe)_2(CH_3CN)_2](BF_4)_2$, has been determined.

The Fe(II) complexes of [15]aneS_5 and [18]aneS_6 have also been

synthesized, but both $[Fe([15]aneS_5)(CH_3CN)](BF_4)_2$ and particularly $[Fe([18]aneS_6)](BF_4)_2$ show low solubilities in organic solvents. $[Fe([18]aneS_6)](ClO_4)_2$ has also been prepared and is also an insoluble solid.

7.4: Experimental

All the procedures below were carried out in Schlenk apparatus and under N_2 unless otherwise stated. N.m.r. samples were prepared and solids were isolated in an Aldrich Glove-bag under N_2. CH_3CN was distilled under N_2 over P_2O_5, CH_2Cl_2 was distilled under N_2 over CaH_2 and diethyl ether was dried with Na wire before use. $[Fe(CH_3CN)_6](BF_4)_2$ was prepared by the method of Underhill *et al.*[219] and as described in Section 6.4.10.

7.4.1: Synthesis of $[Fe([12]aneS_4)(CH_3CN)_2](BF_4)_2$

To a solution of $[Fe(CH_3CN)_6](BF_4)_2$ in CH_3NO_2 ($1cm^3$ of 0.144M solution, 0.14mmol), a solution of $[12]aneS_4$ (35.0mg, 0.14mmol) in degassed CH_3NO_2 ($5cm^3$) was added. A clear blue solution was formed immediately. Evaporation of the solvent to approximately $2cm^3$ and addition of dried diethyl ether gave a blue, H_2O-sensitive solid. The blue solid was washed with dried diethyl ether and dried *in vacuo* and could be stored under N_2 for 8 weeks before decomposing. Yield = ca.100%. I.r. spectrum (HCBD mull): 2960w, 2928w, 2285vw, 2265vw, 1454w, 1433m, 1421w, 1270w and 1060s br cm^{-1}. U.V./vis. spectrum (CH_3NO_2): $\lambda_{max.}$ = 590nm. ($\varepsilon_{max.}$ = $120M^{-1}cm^{-1}$).

7.4.2: Synthesis of $[Fe([14]aneS_4)(CH_3CN)_2](BF_4)_2$

Method as for 7.4.1, using $[14]aneS_4$ (38.7mg, 0.14mmol). A purple solution was obtained, which gave a purple solid on addition of dried diethyl ether. The solid could be stored under N_2 for 4 weeks before decomposing.

Yield = ca.100%. I.r. spectrum (HCBD mull): 3010w, 2950w, 2930w, 2330–2250w br, 1440w, 1430m, 1420w and 1060s br cm^{-1}. U.V./vis. spectrum (CH_3NO_2) $\lambda_{max.}$ = 537nm. ($\varepsilon_{max.}$ = $300M^{-1}cm^{-1}$), 394 (140).

7.4.3: Synthesis of $[Fe([16]aneS_4)(CH_3CN)_2](BF_4)_2$

Method as for 7.4.1, using [16]aneS$_4$ (42.7mg, 0.14mmol). A blue/green solution was obtained, which gave a blue/green solid on addition of dried diethyl ether. The solid could be stored under N_2 for 1 day before decomposing. Yield = ca.100%. An i.r. spectrum of this compound could not be obtained due to its instability. U.V./vis. spectrum (CH_3NO_2): $\lambda_{max.}$ = 581nm. ($\varepsilon_{max.}$ = $50M^{-1}cm^{-1}$), 426 (40).

7.4.4: Synthesis of $[Fe([15]aneS_5)(CH_3CN)](BF_4)_2$

Method as for 7.4.1, using [15]aneS$_5$ (43.3mg, 0.14mmol). A purple solution was obtained, which gave a purple solid on addition of dried diethyl ether. The solid could be stored under N_2 for many weeks before decomposing. Yield = ca.100%. I.r. spectrum (KBr disc): 2985w, 2945w, 2910w, 2100–2060br w, 1436m, 1285w, 1173w, 1094s, 1060s, 1032s, 1002w, 954w, 801w, 630w and 522w cm^{-1}. U.V./vis. spectrum (CH_3NO_2): $\lambda_{max.}$ = 531nm. ($\varepsilon_{max.}$ = $230M^{-1}cm^{-1}$), 400 (230).

7.4.5: Synthesis of $[Fe([18]aneS_6)](BF_4)_2$

Method as for 7.4.1, using [18]aneS$_6$ (52.0mg, 0.14mmol). A pale purple precipitate was obtained immediately which was insoluble in all common solvents. Yield = 80mg, 94%. Elemental analysis: found C = 25.3; H = 4.22%. Calculated for $[Fe(C_{12}H_{24}S_6)](BF_4)_2$: C = 24.4; H = 4.10%. F.a.b. mass spectrum (3–NOBA matrix): only matrix peaks found. I.r. spectrum (KBr disc): 2945w, 2850w, 1550w, 1435m, 1060s br and 812w cm^{-1}.

7.4.6: Synthesis of $[Fe([18]aneS_6)](ClO_4)_2$

$Fe(ClO_4)_3.9H_2O$ (57.3mg, 0.11mmol) and $[18]aneS_6$ (40.0mg, 0.11mmol) were refluxed in dry CH_3OH under N_2 for 6 hours to give a cloudy suspension. On standing and cooling, a fine purple solid was obtained that was filtered, washed with CH_2Cl_2 and diethyl ether and dried *in vacuo*. Yield = 55mg, 80%. Elemental analysis: found C = 22.9; H = 4.01%. Calculated for $[Fe(C_{12}H_{24}S_6)](ClO_4)_2$: C = 23.4; H = 3.93%. F.a.b. mass spectrum (3-NOBA matrix): found peaks for matrix only. I.r. spectrum (KBr disc): 2983w, 2941w, 1435s, 1281w, 1175m, 1085br s, 1004m, 956m, 835w, 810w, 620s and 380w cm^{-1}.

7.4.7: Synthesis of $[Fe([12]aneS_4)(dppe)](BF_4)_2$

To a blue solution of $[Fe([12]aneS_4)(CH_3CN)_2](BF_4)_2$ (0.21mmol) in CH_3NO_2 ($5cm^3$), a colourless solution of dppe (75.0mg, 0.19mmol) in degassed CH_3NO_2 ($10cm^3$) was added dropwise. The solution rapidly became purple in colour with stirring. The volume of solvent was reduced to $5cm^3$ and diethyl ether was layered on top of the clear purple solution. On standing for a week at 253K, a purple, crystalline solid was obtained. The solid was filtered, washed with diethyl ether, recrystallised from CH_2Cl_2/diethyl ether and dried *in vacuo*. Yield = 124mg, 75%. Elemental analysis: found C = 43.5; H = 4.51; N = 2.43%. Calculated for $[Fe(C_8H_{16}S_4)(C_{26}H_{24}P_2)](BF_4)_2.2CH_3NO_2$: C = 43.6; H = 4.68; N = 2.82%. F.a.b. mass spectrum (3-NOBA matrix): found M^+ = 666, 694, 713, 781. Calculated for: $[^{56}Fe(C_8H_{16}S_4)(C_{26}H_{24}P_2)-(C_2H_4)]^+$, M^+ = 666; $[^{56}Fe(C_8H_{16}S_4)(C_{26}H_{24}P_2)]^+$, M^+ = 694, $[^{56}Fe(C_8H_{16}S_4)(C_{26}H_{24}P_2)](H_3O)^+$, M^+ = 713; $[^{56}Fe(C_8H_{16}S_4)(C_{26}H_{24}P_2)](BF_4)^+$, M^+ = 781. I.r. spectrum (KBr disc): 3420br, 3058w, 2990w, 2960w, 2920w, 2850w, 1585w, 1572w, 1480w, 1457w, 1433m, 1421w, 1283w, 1266w, 1060br s, 960w, 935w, 878w, 842w,

824w, 755m. 745m, 701m, 672w, 650w, 526m, 517m, 495w, 423w and 376w cm^{-1}. U.V./vis. spectrum (CH_2Cl_2): $\lambda_{max.}$ = 521nm. ($\varepsilon_{max.}$ = $270M^{-1}cm^{-1}$), 270 (16,000). ^1H n.m.r. spectrum (200.13MHz, CD_3NO_2, 298K): δ = 2.09p.p.m. (br s, P-C<u>H</u>$_2$-C, 4H); 2.90-3.40 (br m, S-C<u>H</u>$_2$-C, 16H); 7.62 and 7.78 (s, Ar-<u>H</u>, 20H). ^{13}C DEPT n.m.r. spectrum (50.32MHz, CD_3NO_2, 298K): δ = 27.69p.p.m. (dd, J = 13.5Hz, P-<u>C</u>H_2-); 32.21 (S-<u>C</u>H_2-CH_2-S); 42.79 (S-CH_2-<u>C</u>H_2-S); 128.74, 131.10 and 131.44 (Aromatic <u>C</u>). ^{31}P n.m.r. spectrum (36MHz, CD_3NO_2, 298K): δ = 57.28p.p.m.

<u>7.4.8</u>: Synthesis of [Fe([14]aneS$_4$)(dppe)](BF$_4$)$_2$

Method as for 7.4.7, using [Fe([14]aneS$_4$)(CH_3CN)$_2$](BF$_4$)$_2$ (0.17mmol) in CH_3NO_2 ($5cm^3$) and dppe (75mg, 0.16mmol) in CH_3NO_2 ($10cm^3$). The product was a microcrystalline purple solid. Yield = 65mg, 45%. Elemental analysis: found C = 48.3; H = 4.73%. Calculated for [Fe($C_8H_{16}S_4$)($C_{26}H_{24}P_2$)](BF$_4$)$_2$: C = 48.2; H = 4.95%. F.a.b. mass spectrum (3-NOBA matrix): found M^+ = 722, 741, 809, 852, 871. Calculated for: [Fe($C_8H_{16}S_4$)($C_{26}H_{24}P_2$)]$^+$, M^+ = 722; [Fe($C_8H_{16}S_4$)($C_{26}H_{24}P_2$)](H_3O)$^+$, M^+ = 741; [Fe($C_8H_{16}S_4$)($C_{26}H_{24}P_2$)](BF$_4$)$^+$, M^+ = 809; [Fe($C_{26}H_{24}P_2$)$_2$]$^+$, M^+ = 852; [Fe($C_{26}H_{24}P_2$)$_2$(H_3O)]$^+$, M^+ = 871. I.r. spectrum (KBr disc): 3400br, 3050w, 2920w, 1586w, 1572w, 1483w, 1433m, 1414w, 1306w, 1060br s, 877w, 820w, 749m, 703s, 674w, 656w, 528m, 498w, 424w and 381w cm^{-1}. U.V./vis. spectrum (CH_2Cl_2): $\lambda_{max.}$ = 540nm. ($\varepsilon_{max.}$ = $320M^{-1}cm^{-1}$), 266 (15,000).

7.4.9: Synthesis of [Fe([12]aneS$_4$)(dppm)](BF$_4$)$_2$

Method as for 7.4.7, using [Fe([12]aneS$_4$)(CH$_3$CN)$_2$](BF$_4$)$_2$ (0.21mmol) in CH_3NO_2 (5cm^3) and dppm (73mg, 0.19mmol) in CH_3NO_2 (10cm^3). The product was a microcrystalline purple solid. Yield = 101mg, 62%. Elemental analysis: found C = 33.9; H = 3.90%. Calculated for [Fe($C_8H_{16}S_4$)($C_{25}H_{22}P_2$)](BF$_4$)$_2$: C = 46.4; H = 4.48%. F.a.b. mass spectrum (3-NOBA matrix): found M^+ = 385, 680, 767. Calculated for: $[C_{25}H_{23}P_2]^+$, M^+ = 385; $[^{56}Fe(C_8H_{16}S_4)(C_{25}H_{22}P_2)]^+$, M^+ = 680; $[^{56}Fe(C_8H_{16}S_4)(C_{25}H_{22}P_2)](BF_4)^+$, M^+ = 767. I.r. spectrum (KBr disc): 3400br, 3050w, 2919w, 2848w, 1550w, 1482w, 1433m, 1376w, 1060br s, 842w, 790w, 743w, 697w, 675w, 531w, 519w, 506w and 477w cm^{-1}. U.V./vis. spectrum (CH_2Cl_2): $\lambda_{max.}$ = 523nm. ($\epsilon_{max.}$ = 300M^{-1}cm^{-1}), 266 (7,000). ^{1}H n.m.r. spectrum (200.13MHz, CD_3NO_2, 298K): δ = 2.90-3.60p.p.m. (br m, S-C<u>H</u>$_2$-, 16H); 5.00 (t, J = 11Hz, P-C<u>H</u>$_2$-P, 2H); 7.50-7.70 (m, Ar-<u>H</u>, 20H). ^{13}C DEPT n.m.r. spectrum (50.32MHz, CD_3NO_2, 298K): δ = 35.92p.p.m. (t, J = 25Hz, P-<u>C</u>H$_2$-P); 42.98 (S-<u>C</u>H$_2$-); 128.86, 130.74 and 131.12 (Aromatic <u>C</u>). ^{31}P n.m.r. spectrum (36MHz, CD_3NO_2, 298K): δ = 3.23p.p.m.

7.4.10: Synthesis of [Fe([12]aneS$_4$)(dppv)](BF$_4$)$_2$

Method as for 7.4.7, using [Fe([12]aneS$_4$)(CH$_3$CN)$_2$](BF$_4$)$_2$ (0.16mmol) in CH_3NO_2 (5cm^3) and dppv (63.0mg, 0.16mmol) in CH_3NO_2 (10cm^3). The product was a microcrystalline purple solid. Yield = 105mg, 75%. Elemental analysis: found C = 47.8; H = 4.62%. Calculated for [Fe($C_8H_{16}S_4$)($C_{26}H_{22}P_2$)](BF$_4$)$_2$: C = 47.1; H = 4.42%. F.a.b. mass spectrum (3-NOBA matrix): found M^+ = 471, 664, 692, 711, 779, 848, 867. Calculated for: $[^{56}Fe(C_{26}H_{22}P_2)(H_3O)]^+$, M^+ = 471; $[^{56}Fe(C_8H_{16}S_4)(C_{26}H_{22}P_2)-(C_2H_4)]^+$, M^+ = 664;

$[^{56}Fe(C_8H_{16}S_4)(C_{26}H_{22}P_2)]^+$, M^+ = 692; $[^{56}Fe(C_8H_{16}S_4)(C_{26}H_{22}P_2)](H_3O)^+$, M^+ = 711; $[^{56}Fe(C_8H_{16}S_4)(C_{26}H_{22}P_2)](BF_4)^+$, M^+ = 779; $[^{56}Fe(C_{26}H_{22}P_2)_2]^+$, M^+ = 848; $[^{56}Fe(C_{26}H_{22}P_2)_2](H_3O)^+$, M^+ = 867 or $[^{56}Fe(C_8H_{16}S_4)(C_{26}H_{22}P_2)+(H)](BF_4)_2$, M^+ = 866. I.r. spectrum (KBr disc): 3406br, 3054w, 3013w, 1481w, 1458w, 1435m, 1278w, 1264w, 1096s, 1054s, 996m, 958w, 844w, 769m, 704m, 693m, 559m, 526m, 497w, 473w and 457w cm^{-1}. U.V./vis. spectrum (CH_3NO_2): $\lambda_{max.}$ = 502nm. ($\epsilon_{max.}$ = $450M^{-1}cm^{-1}$), 267 (17,000). ^1H n.m.r. spectrum (200.13MHz, CD_3NO_2, 298K): δ = 1.49p.p.m. (td, J(t) = 14Hz, J(d) = 5Hz, S-CH<u>H</u>-CHH-S, 4H); 2.96 (td, J(t) = 13Hz, J(d) = 5Hz, S-<u>H</u>H-CHH-S, 4H); 3.20 (dd, J = 15Hz, J = 5Hz, S-CHH-C<u>H</u>H-S, 4H); 3.48 (dd, J = 12Hz, J = 5Hz, S-CHH-CH<u>H</u>-S, 4H); 7.01 (br, P-C<u>H</u>=, 2H); 7.45-8.30 (m, Ar-<u>H</u>, 20H). ^{13}C n.m.r. spectrum (50.23MHz, CD_3NO_2, 298K): δ = 33.47p.p.m. (S-<u>C</u>H_2-CH_2-S); 42.26 (S-CH_2-<u>C</u>H_2-S); 128.77, 129.20, 129.60, 130.87, 131.17, 131.57 (all aromatic <u>C</u>); 149.97 (dd, J = 35Hz, P-<u>C</u>H=). ^{31}P n.m.r. spectrum (36MHz, CD_3NO_2, 298K): δ = 64.35p.p.m.; 68.38 (ratio 1 : 12).

Reactions of $[Fe([12]aneS_4)(CH_3CN)_2](BF_4)_2$ with other ligands

The following reactions were attempted, but gave either unstable or unidentifiable products or no reaction was observed. The synthetic procedure was to add the dry reagent (in equivalents as shown) as a CH_3NO_2 solution or solid to a solution of $[Fe([12]aneS_4)(CH_3CN)_2](BF_4)_2$ in CH_3NO_2 under N_2. The solid products were isolated by adding an excess of diethyl ether to the CH_3NO_2 solution, filtering and drying *in vacuo*.

	Reagent	Products
7.4.11:	Excess pyridine$_{(l)}$	[12]aneS$_4$ precipitated
7.4.12:	2xpyridine$_{(l)}$	[12]aneS$_4$ precipitated
7.4.13:	1x2,2-bipyridine	Red [Fe(2,2-bipy)$_3$](BF$_4$)$_2$
7.4.14:	2ximidazole (CH_3NO_2)	Green air-sensitive solid
7.4.15:	Excess $CH_3NHNH_{2(l)}$	Red air-sensitive solid
7.4.16:	2x$C_6H_5CN_{(l)}$	Blue air-sensitive solid
7.4.17:	PPh_3 (CH_3NO_2)	No reaction
7.4.18:	$P(C_6H_{11})_3$ (CH_3NO_2)	No reaction
7.4.19:	dppp (CH_3NO_2)	Purple air-sensitive solid
7.4.20:	dcpe (CH_3NO_2)	No reaction
7.4.21:	$Ph_2AsC_2H_4AsPh_2$ (CH_3NO_2)	No reaction
7.4.22:	$NO_{(g)}$	Green air-sensitive solid
7.4.23:	$O_{2(g)}$	No reaction
7.4.24:	$CO_{(g)}$	Decomposition in few minutes
7.4.25:	$(NH_4)[S_2CN(C_2H_5)_2]$	Dark green {Fe[$S_2CN(C_2H_5)_2$]$_2$}
7.4.26:	2xKSCN	Purple $K_n[Fe(SCN)_m]$ and [12]aneS$_4$ precipitated
7.4.27:	1,3,5-trithiane	No reaction
7.4.28:	$[(C_3H_7)_3C_6H_2S]_2$	No reaction
7.4.29:	$Na(SC_6H_5)$	[12]aneS$_4$ precipitated
7.4.30:	$NBu^n{}_4CH_3CO_2$ (CH_3NO_2)	Green air-sensitive solid
7.4.31:	NEt_4Cl	[12]aneS$_4$ precipitated

Apart from when indicated, the products obtained could not be identified due to their instability in air. The solids decomposed by absorbing H_2O from the air, deliquescing rapidly with a colour change. The demetallated [12]aneS$_4$ ligands were identified by i.r. spectra. {Fe[$S_2CN(C_2H_5)_2$]$_2$}, $K_n[Fe(SCN)_m]$

and $[Fe(bipy)_3](BF_4)_2$ were characterised by i.r., f.a.b. mass spectra and U.V./visible spectroscopy.

7.4.32: Synthesis of $[Fe(dppe)_2(CH_3CN)_2](BF_4)_2$

$[Fe(CH_3CN)_6](BF_4)_2$ (50.0mg, 0.10mmol) in CH_3NO_2 ($5cm^3$) was added dropwise with stirring to a CH_3NO_2 solution ($10cm^3$) of dppe (83.8mg, 0.21mmol). The solution immediately acquired a red coloration. The volume of solvent was reduced to ca.$5cm^3$ and diethyl ether was layered on top of the red solution. A red crystalline precipitate was obtained after 4 days at 253K, that was filtered, washed with diethyl ether and dried *in vacuo*. The red product was recrystallised from CH_2Cl_2/diethyl ether. Yield = 72mg, 62%. Elemental analysis: found C = 59.4; H = 5.05; N = 2.75%. Calculated for $[Fe(C_{26}H_{24}P_2)_2(CH_3CN)_2](BF_4)_2$: C = 60.7; H = 4.91; N = 2.53%. F.a.b. mass spectrum (3-NOBA matrix): found M^+ = 399, 454, 473, 852, 871. Calculated for: $[C_{26}H_{25}P_2]^+$, M^+ = 399; $[^{56}Fe(C_{26}H_{24}P_2)]^+$, M^+ = 454; $[^{56}Fe(C_{26}H_{24}P_2)(H_3O)]^+$, M^+ = 473; $[^{56}Fe(C_{26}H_{24}P_2)_2]^+$, M^+ = 852; $[^{56}Fe(C_{26}H_{24}P_2)_2(H_3O)]^+$, M^+ = 871. I.r. spectrum (KBr disc): 3058w, 2986w, 2962w, 2938w, 2882w, 2200w, 1586w, 1553m, 1485m, 1457w, 1434s, 1377w, 1317w, 1306w, 1284w, 1060br s, 1000m, 869w, 813w, 802w, 751s, 703s, 665w, 654w, 527s, 511m, 497w, 480w, 455w, 423w and 379w cm^{-1}.

7.4.33: Single Crystal X-ray Structure of $[Fe(C_{26}H_{24}P_2)_2(CH_3CN)_2](BF_4)_2.2CH_2Cl_2$

Vapour diffusion of diethyl ether into a solution of the complex in CH_2Cl_2 gave red crystals of crystallographic quality. The crystal was coated in nujol film to prevent solvent loss and mounted on a glass fibre.

Crystal Data:

$[Fe(C_{26}H_{24}P_2)_2(CH_3CN)_2](BF_4)_2.2CH_2Cl_2$ M = 1108.42. Triclinic, space group $P\bar{1}$, a = 10.355(9), b = 12.045(9), c = 13.220(11)Å, α = 63.74(6), β = 85.62(6), γ = 80.15(3)°, V = 1456.9Å^3 (by least-squares refinement on diffraction angles for 23 reflections measured at $\pm\omega$ [$24 < 2\theta < 26°$, λ = 0.71073Å]), Z = 1, D_c = 1.457gcm^{-3}, T = 173K. Crystal dimensions 0.10 x 0.19 x 0.35mm^3, μ(Mo-Kα) = 0.615mm^{-1}, F(000) = 656.

Data Collection and Processing:

Stöe STADI-4 four-circle diffractometer, ω-2θ scan mode using the learnt-profile method[199]. Graphite-monochromated Mo-Kα radiation; 4270 reflections measured ($2\theta_{max.}$ = 45°, h -11 → 11, k -11 → 12, l 0 → 14), 3441 unique data (R_{int} = 0.11), giving 2554 with $F > 6\sigma(F)$. Crystal decay = 3%, no absorption correction.

Structure Analysis and Refinement:

The Fe atom was located using a Patterson synthesis[201], and successive cycles of least-squares refinement and difference Fourier synthesis[201] identified the positions of all other atoms. The crystal lattice was found to contain two CH_2Cl_2 molecules per cation and during refinement some disorder of these CH_2Cl_2 molecules was observed. One of the Cl atoms was spread over two sites, so the refined site occupancies of Cl(2S) and Cl(3S) were 39.2% and 60.8% respectively. The hydrogen atoms in the CH_2Cl_2 solvates were not located. Anisotropic thermal parameters were refined for all Fe, P, N, C, B, F and Cl atoms. H atoms were located from a difference map and included in fixed, calculated positions. The weighting scheme $w^{-1} = \sigma^2(F) + 0.000300F^2$ gave satisfactory agreement analyses. At final convergence, R = 0.080, R_w = 0.999, S = 1.518 for 371 independent

parameters, and the final difference Fourier synthesis showed no feature above +0.809 or below $-0.677 e\text{Å}^{-3}$.

Atomic scattering factors were inlaid[201], except for Fe[254], molecular geometry calculations utilised *CALC*[202] and figures were produced by *SHELXTL PC*[255].

APPENDIX

Experimental Techniques

Figure A.1 Thioether ligands used in this thesis

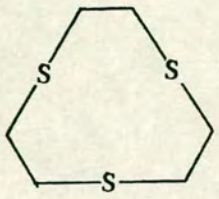

[9]aneS$_3$

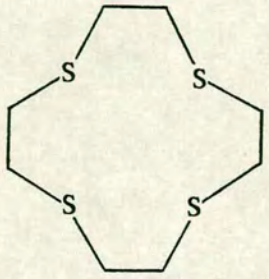

[12]aneS$_4$

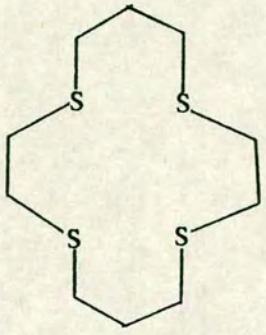

[14]aneS$_4$

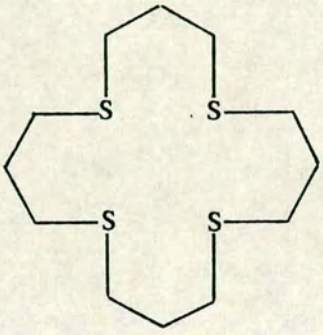

[16]aneS$_4$

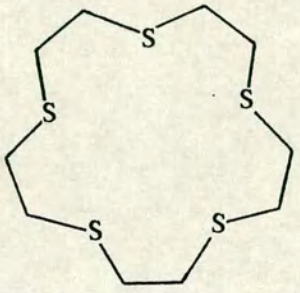

[15]aneS$_5$

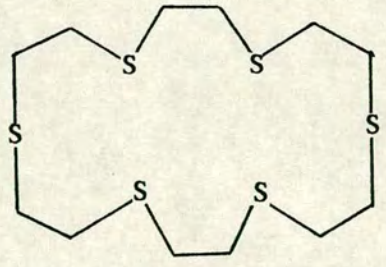

[18]aneS$_6$

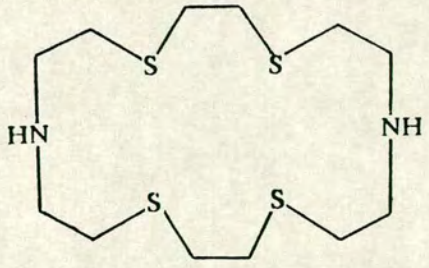

[18]aneN$_2$S$_4$

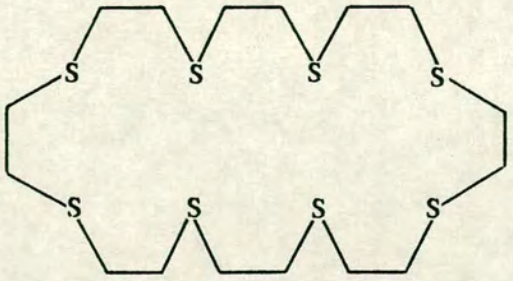

[24]aneS$_8$

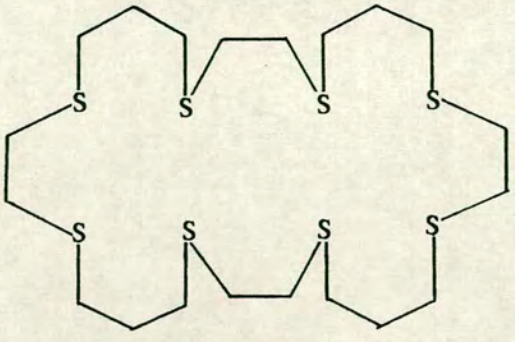

[28]aneS$_8$

Materials and Methods

All solvents were purified according to standard procedures. HPLC grade CH_3CN (Aldrich), HPLC grade CH_2Cl_2 (Fisons) and DMSO (BDH) were used in the electrochemical experiments. Commercial $RhCl_3$, $PdCl_2$, $[Pd(CH_3CO_2)_2]_3$ and $PtCl_2$ (Johnson Matthey p.l.c.) were used as supplied. $[Ni(H_2O)_6](BF_4)_2$ was dried in a Büchi Kügelrohr before use. The following were used as supplied: $NOBF_4$ (Lancaster Synthesis); $(CH_3)_2NCSCl$, *p*-cresol, 1,2-diaminoethane, 1,3-diaminopropane, 1,4-diaminobutane, NaH, 1,8-bis(dimethylamino)naphthalene, Pd sponge, DABCO, CH_3NHNH_2 (all Aldrich) and $[Fe(CH_3CO_2)_2]$ (Strem). All thioether and phosphine ligands were used without further purification: [9]aneS_3, [12]aneS_4, [14]aneS_4, [16]aneS_4, [15]aneS_5, [18]aneS_6, dppm, dppe, dppv, dppp, PPh_3 (Aldrich), triphos, dcpe and $P(C_6H_{11})_3$ (Strem). Tetrabutylammonium hexafluorophosphate ($^nBu_4NPF_6$) and tetrabutylammonium tetrafluoroborate ($^nBu_4NBF_4$) were prepared by the neutralisation of 40% $^nBu_4NOH$ (Aldrich) with 60% HPF_6 (Strem) and 48% HBF_4 (Aldrich) respectively, followed by recrystallisation from CH_3OH.

I.r. spectra were recorded on a Perkin-Elmer 1600 Series FTIR spectrometer (4000-450cm^{-1}) or on a Perkin-Elmer 598 spectrometer (4000-250cm^{-1}) using the KBr method. ^1H n.m.r. spectra were measured on Brucker WP80 and Brucker WP200 instruments operating at 80.13MHz and 200.13MHz respectively. ^{13}C n.m.r. spectra were run on a Brucker WP200 machine operating at 50.32MHz. F.a.b. mass spectra were run on a Kratos MS 50TC spectrometer and electonic spectra run on a Perkin-Elmer Lambda-9 U.V./vis./N.I.R. spectrophotometer using quartz cells. X-band e.s.r. measurements were recorded using a Brucker ER-200D spectrmeter using 100KHz field modulation. A quartz flat cell was employed for the solution

samples and frozen glass and powder samples were taken using quartz tubes (4mm O.D., 3mm I.D.).

Electrochemical measurements were recorded on a Brucker 310 Universal Modular Polarograph. Cyclic voltammetric studies were undertaken using a three electrode potentiostat system, with platinum button microelectrodes used as the working and auxilliary electrodes and a Ag/AgCl electrode as the reference. All test solutions were purged with a stream of dry argon gas prior to their study. A three compartment cell together with a three electrode system (Pt basket and Pt gauze as the working and auxilliary electrodes) were used for coulometry and electrolysis experiments.

Spectroelectrochemical studies were carried out using an Optically Transparent Thin Layer Electrode (O.T.T.L.E.) cell which was designed and built at Edinburgh. The cell consists of a fine Pt grid gauze working electrode (transparency $\simeq$ 40%) fitted into a standard Infrasil quartz cell of 0.5mm. pathlength. A quartz extension fitted to the top of the cell functioned as a reservoir and contains a Pt wire auxilliary electrode and Ag/Ag^+ reference electrode both of which are separated from the bulk solution by porous glass frits. This unit was fitted into a PTFE cell block and located in a Perkin-Elmer Lambda-9 spectrophotometer. Control of the temperature was maintained by the passage of pre-cooled N_2 around the assembly. Solutions of the complexes were degassed with Ar, then electrolysed at the working electrode in the cell situated in the beam of the spectrophotometer. The progress of the electrolysis was monitored both spectroscopicallly and by decay of the current to a constant residual value. The potential was then reversed to monitor whether the process was chemically reversible.

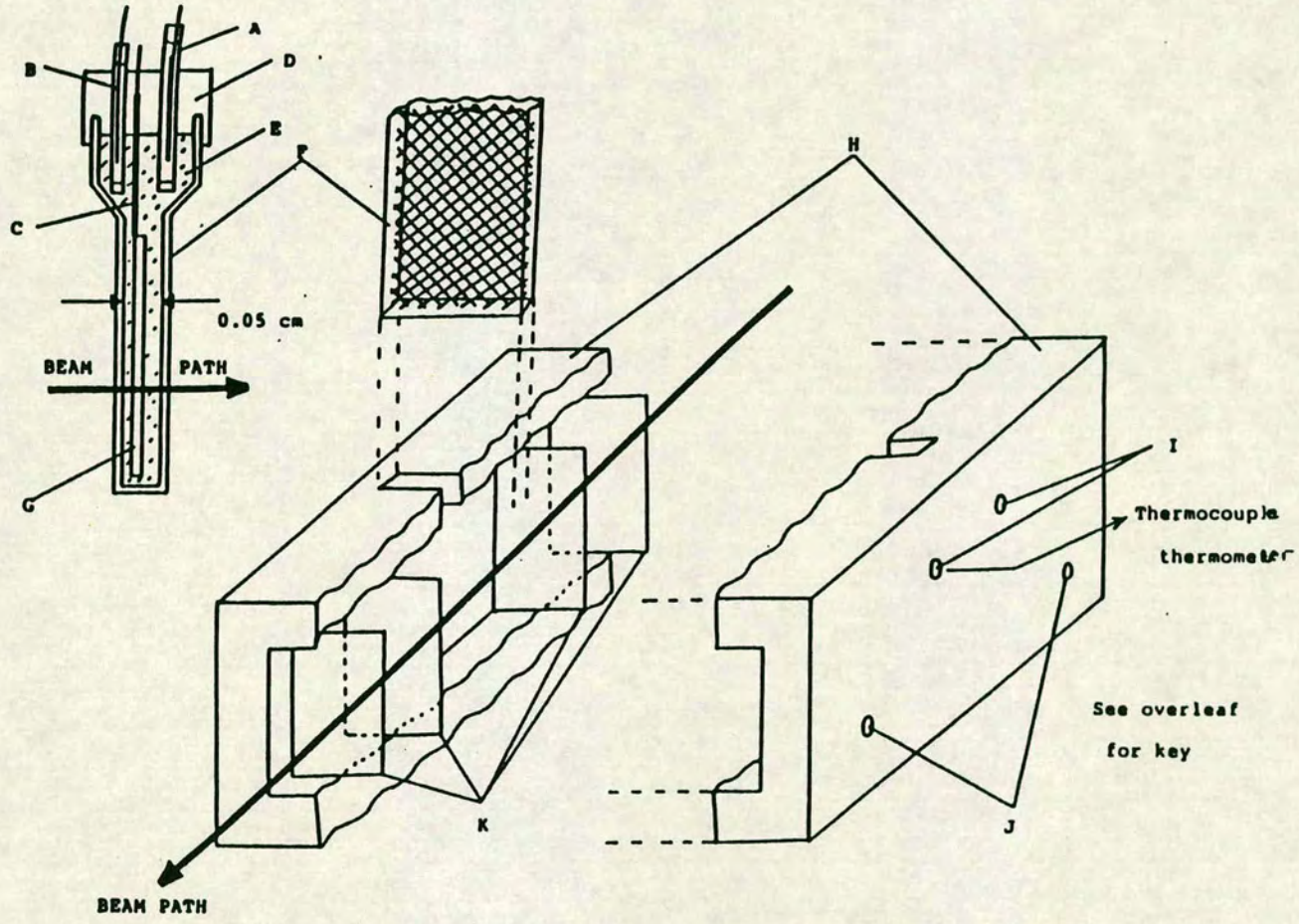

Figure A.2 The optically transparent electrode (O.T.T.L.E) system

Key to Figure A.2:

A. Counter electrode

B. Reference electrode

C. Working electrode connection protected from bulk solution by PTFE sleeve

D. PTFE cell cap

E. Degassed complex solution

F. 0.5mm. quartz cell containing Pt grid working electrode

G. Pt grid working electrode

H. PTFE block

I. Variable temperature N_2 inlet ports

J. Dry N_2 inlet ports

K. Quartz cell block windows

REFERENCES

1. "Coordination Chemistry of Macrocyclic Compounds", Ed. G.A.Melson, Plenum, New York 1979.
2. "The Chemistry of Macrocyclic Ligand Compounds", L.F.Lindoy, C.U.P., Cambridge 1989.
3. J-M.Lehn, *Angew.Chem., Intl.Ed.Engl.*, 1988, 27, 89.
4. D.J.Cram, *Angew.Chem., Intl.Ed.Engl.*, 1988, 27, 1009.
5. C.J.Pederson, *Angew.Chem., Intl.Ed.Engl.*, 1988, 27, 1021.
6. A.J.Blake and M.Schröder, *Adv.Inorg.Chem.*, 1990, 35, 1.
7. P.Chaudhuri and K.Wieghardt, *Prog.Inorg.Chem.*, 1987, 35, 329 and refs. within.
8. V.L.Goedken, in "Coordination Chemistry of Macrocyclic Compounds", Ch.10, "Natural Product Systems", 603, and references within.
9. L.Que and A.E.True, *Prog.Inorg.Chem.*, 1990, 38, 97.
10. D.E.Fenton, *Advances in Inorganic and Bioinorganic Mechanisms*, Academic Press, London, 1983, 2, 187.
11. T.M.Sorrel, *Tetrahedron*, 1989, 45, 3.
12. See for example, R.Motekaitis and A.E.Martel, *Inorg.Chem.*, 1991, 30, 694 and refs within.
13. Y.LeMest, M.L'Her, J.Courtot-Coupez, J.P.Collman, E.R.Evitt and C.S.Benscosme, *J.Chem.Soc., Chem.Commun.*, 1983, 1286.
14. R.R.Durand, C.S.Benscosme, J.P.Collman and F.C.Anson, *J.Am.Chem.Soc.*, 1983, 105, 2710.
15. J.A.R.Van Veen and J.F.Van Baar, *Rev.Inorg.Chem.*, 1982, 4, 293.
16. M.Schröder, *Pure Appl.Chem.*, 1988, 60, 517.
17. R.W.Hay, "Bio-inorganic Chemistry", Ellis Horwood, Chichester 1984.
18. J.M.Rifkind, in "Inorganic Biochemistry", Ed. G.L.Eichhorn, Elsevier,

Amsterdam, Ch.25, "Haemoglobin and Myoglobin", 832.

19. S.Ferguson-Miller, D.L.Brautigen and E.Margoliash, in "The Porphyrins", Ed. D.Dolphin, Academic Press, London, Vol.VI, Ch.4, 149-240, "The Electron Transfer Function of Cytochrome *c*".

20. J.J.Katz, in "Inorganic Biochemistry", Ch.29, "Chlorophyll", 1022.

21. O.T.G.Jones, in "The Porphyrins", Vol.VI, Ch.3, 179, "Chlorophyll Biosynthesis".

22. H.A.O.Hill, in "Inorganic Biochemistry", Ch.30, "Corrinoids", 1067.

23. J.M.Pratt, *Chem.Soc.Rev.*, 1985, 14, 161.

24. K.S.Suslick and T.J.Reinert, *J.Chem.Educ.*, 1985, 62, 974.

25. D.K.Cabbiness and D.W.Margerum, *J.Am.Chem.Soc.*, 1969, 91, 6540.

26. D.K.Cabbiness and D.W.Margerum, *J.Am.Chem.Soc.*, 1970, 92, 2151.

27. D.H.Busch, K.Farmery, V.Goedken, V.Katovic, A.C.Melnyk, C.R.Sperati and N.Tokel, *Adv.Chem.Ser.*, 1971, 100, 44.

28. L.Fabbrizzi, P.Paoletti and A.B.P.Lever, *Inorg.Chem.*, 1976, 15, 1502.

29. R.D.Hancock and A.E.Martell, *Comments Inorg.Chem.*, 1988, 6, 237.

30. H.J.Buschmann, in "Stereochemical and Stereophysical Behaviour of Macrocycles", Ed. I.Bernal, Elsevier, Amsterdam, Ch.2, 103, "Thermodynamic and Stereochemical Aspects of the Macrocyclic and Cryptate Effects".

31. D.Hinz and D.Margerum, *Inorg.Chem.*, 1974, 13, 2941.

32. R.M.Clay, S.Corr, G.Keenan and W.V.Steele, *J.Am.Chem.Soc.*, 1983, 105, 2070.

33. D.J.Cram, T.Kaneda, R.C.Helgeson, S.B.Brown, C.B.Knobler, E.Maverick and K.N.Trueblood, *J.Am.Chem.Soc.*, 1985, 107, 3645.

34. G.Wipff, P.Weiner and P.Kollman, *J.Am.Chem.Soc.*, 1982, 104, 3249.

35. H.Zhang and D.V.Dearden, *J.Am.Chem.Soc.*, 1992, 114, 2754 and refs. within.

39. R.S.Glass, G.S.Wilson and W.N.Setzer, *J.Am.Chem.Soc.*, 1980, 102, 5068.

36. R.E.DeSimone and M.D.Glick, *J.Am.Chem.Soc.*, 1976, 98, 762.

37. N.W.Alcock, N.Herron and P.Moore, *J.Chem.Soc., Dalton Trans.*, 1978, 394.

38. R.E.DeSimone and M.D.Glick, *J.Am.Chem.Soc.*, 1975, 97, 942.

39. R.S.Glass, G.S.Wilson and W.N.Setzer, *J.Am.Chem.Soc.*, 1980, 102, 5068.

40. R.J.P.Williams, *J.Mol.Catal.*, 1986, 1 (review issue).

41. H.Sigel (Ed.), "Metal Ions In Biological Systems", Dekker, 1981, New York, Vol.13, "Copper Proteins".

42. C.D.Garner and P.M.Harrison, *Chem.Br.*, 1982, 18, 173.

43. A.G.Sykes, *Adv.Inorg.Chem.*, 1990, 36, 377.

44. S.M.Nelson, *Inorg.Chim.Acta.*, 1982, 62, 39.

45. J.E.Bulkowski, P.L.Burk, J-L.Ludmann and J.A.Osborn, *J.Chem.Soc., Chem.Commun.*, 1977, 498.

46. S.M.Nelson, A.Lavery and M.G.B.Drew, *J.Chem.Soc., Dalton Trans.*, 1986, 911.

47. H.Adams, N.A.Bailey, M.J.S.Dwyer, D.E.Fenton, P.C.Hellier and P.D.Hempstead, *J.Chem.Soc., Chem.Commun.*, 1991, 1297.

48. P.L.Burk, J.A.Osborn, M.T.Youinou, Y.Agnus, R.Louis and R.Weiss, *J.Am.Chem.Soc.*, 1981, 103, 1273.

49. K.Wieghardt, I.Tolksdorf and W.Herrmann, *Inorg.Chem.*, 1985, 24, 1230.

50. D.E.Fenton, Perspectives in Co-ordination Chemistry, Ed. A.F.Williams, C.Floriani and A.E.Merbach, Verlag Helvetica Chimica Acta, Basel, 1992, 203.

51. J.P.Collman, R.R.Gagne, C.A.Reed, T.R.Halbert, G.Lang and

W.T.Robinson, *J.Am.Chem.Soc.*, 1975, 97, 1427.

52. J.P.Collman, J.I.Brauman, K.M.Doxsee, J.L.Sessler, R.M.Morris and Q.H.Gibson, *Inorg.Chem.*, 1983, 22, 1427.

53. J.Lindsey, *J.Org.Chem.*, 1980, 45, 5215.

54. T.G.Traylor and R.Popovitz-Biro, *J.Am.Chem.Soc.*, 1988, 110, 239.

55. M.Shimizu, F.Basolo, M.N.Vallejo and J.E.Baldwin, *Inorg.Chim.Acta.*, 1984, 91, 247.

56. J.Almog, J.E.Baldwin, M.J.Crosley, J.F.Debernardis, R.L.Dyer, J.R.Huff and M.K.Peters, *Tetrahedron*, 1981, 37, 3589.

57. J.P.Collman, J.I.Brauman, T.J.Collins, B.Iverson and J.L.Sessler, *J.Am.Chem.Soc.*, 1981, 103, 2450.

58. K.D.Karlin and Y.Gultneh, *Prog.Inorg.Chem.*, 1987, 35, 219.

59. J.B.Vincent, G.L.Olivier-Lilley and B.A.Averill, *Chem.Rev.*, 1990, 90, 1447.

60. R.G.Wilkins, *Chem.Soc.Rev.*, 1992, 21, 171.

61. E.Kimura, T.Shiota, T.Koike, M.Shiro and M.Kodama, *J.Am.Chem.Soc.*, 1990, 112, 5805.

62. Y.Pocker and J.T.Stone, *J.Am.Chem.Soc.*, 1965, 87, 5497.

63. Y.Pocker and T.L.Deits, *J.Am.Chem.Soc.*, 1982, 104, 2424.

64. K.K.Kannen, M.Petef, K.Fridborg, H.Cid-Dresdner and S.Lovgren, *FEBS Letters,* 1977, 73, 115.

65. T.Koike and E.Kimura, *J.Am.Chem.Soc.*, 1991, 113, 8935.

66. B.Fischer and R.Eisenberg, *J.Am.Chem.Soc.*, 1980, 102, 7361.

67. S.Meshitsuka, M.Ichikawa and K.Tamura, *J.Chem.Soc., Chem.Commun.*, 1974, 158.

68. M.Beley, J.P.Collin, R.Ruppert and J.P.Sauvage, *J.Chem.Soc., Chem.Commun.*, 1984, 1315.

69. M.Beley, J.P.Collin, R.Ruppert and J.P.Sauvage, *J.Am.Chem.Soc.*,

1986, 108, 7461.

70. D.A.Gangi and R.R.Durrand, *J.Chem.Soc., Chem.Commun.*, 1986, 697.

71. J.Y.Becker, B.Vainas, R.Eger and L.Kaufman, *J.Chem.Soc., Chem.Commun.*, 1985, 1471.

72. S.Matsuoka, K.Yamamoto, T.Ogata, M.Kusaba, N.Nakashima, E.Fujita and S.Yanagida, *J.Am.Chem.Soc.*, 1993, 115, 601.

73. B.B.Wayland and H.W.Bosch, *J.Chem.Soc., Chem.Commun.*, 1986, 900.

74. J.P.Collman, J.E.Hutchison, P.S.Wagenknecht, N.S.Lewis, M.A.Lopez and R.Guilard, *J.Am.Chem.Soc.*, 1990, 112, 8206.

75. P.J.Brothers and J.P.Collman, *Acc.Chem.Res.*, 1986, 19, 209.

76. L.L.Efros, H.H.Thorp, G.W.Brudwig and R.H.Crabtree, *Inorg.Chem.*, 1992, 31, 1722.

77. J.P.Collman, P.S.Wagenknecht, J.E.Hutchinson, N.S.Lewis, M.A.Lopez, R.Guilard, M.L'Her, A.A.Bothner-By and P.K.Mishra, *J.Am.Chem.Soc.*, 1992, 114, 5654.

78. J.P.Collman, P.S.Wagenknecht and N.S.Lewis, *J.Am.Chem.Soc.*, 1992, 114, 5665.

79. I.Taniguchi, T.Shimpuku, K.Yamashita and H.Ohtaki, *J.Chem.Soc., Chem.Commun.*, 1990, 915.

80. M.J.Camenzind, D.Dolphin and B.R.James, *J.Chem.Soc., Chem.Commun.*, 1986, 1814.

81. J.P.Collman, J.E.Hutchison, M.A.Lopez, R.Guilard and R.A.Reed, *J.Am.Chem.Soc.*, 1991, 113, 2794.

82. T.Yoshida, T.Adachi, M.Kaminaka, T.Ueda and T.Higuchi, *J.Am.Chem.Soc.*, 1988, 110, 4872.

83. J.P.Collman, J.E.Hutchison, M.A.Lopez and R.Guilard, *J.Am.Chem.Soc.*, 1992, 114, 8066.

84. J.P.Collman, J.E.Hutchison, M.S.Ennis, M.A.Lopez and R.Guilard,

J.Am.Chem.Soc., 1992, 114, 8074.

85. J.P.Collman and K.Kim, *J.Am.Chem.Soc.*, 1986, 108, 7847.

86. J.P.Collman, P.Denisevich, M.Marroco, C.Koval and F.C.Anson, *J.Am.Chem.Soc.*, 1980, 102, 6027–36.

87. D.Sazou, C.Araullo–McAdams, B.C.Han, M.M.Franzen and K.M.Kadish, *J.Am.Chem.Soc.*, 1990, 112, 7879.

88. P.Vasudevan, Santosh, N.Mann and S.Tyagi, *Transition Met.Chem.*, 1990, 15, 81.

89. A.Van Putten, A.Elzing, W.Visscher and E.Barendrecht, *J.Electroanal.Chem.*, 1987, 221, 95.

90. K.Wiesener, D.Ohms, V.Neumann and R.Franke, *Materials Chemistry and Physics*, 1989, 22, 457.

91. K.Hasegawa, T.Imamura and M.Fujimoto, *Inorg.Chem.*, 1986, 25, 2154.

92. R.Karaman, S.Jeon, Ö.Almarsson and T.C.Bruice, *J.Am.Chem.Soc.*, 1992, 114, 4899.

93. C.Shi and F.C.Anson, *Inorg.Chem.*, 1992, 31, 5078.

94. N.Kobayashi, P.Janda and A.B.P.Lever, *Inorg.Chem.*, 1992, 31, 5172.

95. T.Yoshida, T.Adachi and T.Ueda, 14th International Symposium on Macrocyclic Compounds, Abstract P77/M, Townsville, Australia, July 1989.

96. S.E.Groh, *Isr.J.Chem.*, 1977, 15, 277.

97. R.Robson and N.H.Pilkington, *Aust.J.Chem.*, 1970, 23, 2225.

98. D.E.Fenton, M.Mercer, N.S.Poonia and M.R.Truter, *J.Chem.Soc., Chem.Commun.*, 1972, 66.

99. K.Travis and D.H.Busch, *J.Chem.Soc., Chem.Commun.*, 1970, 1041.

100. A.C.Braithwaite, C.E.F.Rickard and T.N.Waters, *Aust.J.Chem.*, 1981, 34, 2665.

101. K.Saito, Y.Masudo and E.Sekido, *Anal.Chim.Acta.*, 1983, 151, 447.

102. D.Sevdić and H Meider, *J.Inorg.Nucl.Chem.*, 1977, 39, 1403.

103. A.J.Blake, A.Taylor and M.Schröder, *Polyhedron*, 1990, 9, 2911–18.

104. A.Taylor, Ph.D. Thesis, University of Edinburgh, 1991.

105. S.M.Nelson, *Pure Appl.Chem.*, 1980, 52, 2461.

106. D.E.Fenton, *Pure Appl.Chem.*, 1986, 58, 1437.

107. Y.Agnus, R.Louis and R.Weiss, *J.Am.Chem.Soc.*, 1979, 101, 3381–84.

108. R.Hotzelmann, K.Wieghardt, J.Ensling, H.Romstedt, P.Gütlich, E.Bill, U.Flörke and H.J.Haupt, *J.Amer.Chem.Soc.*, 1992, 114, 9470 and refs. within.

109. M.A.Halcrow, Ph.D. Thesis, University of Edinburgh, 1991.

110. A.J.Blake, M.A.Halcrow and M.Schröder, *Acta Cryst.Sect.C*, 1992, C48, 1844.

111. A.J.Blake, S.A.Ross and M.Schröder, unpublished results.

112. "Advanced Inorganic Chemistry", Ed. F.A.Cotton and G.Wilkinson, 5th. Edn., p.1224, Wiley, London, 1988 and refs. within.

113. B.F.Hoskins, N.J.McLeod and H.A.Schaap, *Aust.J.Chem.*, 1976, 29, 515.

114. S.K.Mandal, L.K.Thompson, M.J.Newlands and E.J.Gabe, *Inorg.Chem.*, 1989, 28, 3707.

115. B.F.Hoskins and G.A.Williams, *Aust.J.Chem.*, 1975, 28, 2607.

116. B.F.Hoskins, R.Robson and G.A.Williams, *Inorg.Chim.Acta*, 1976, 16, 121.

117. B.F.Hoskins and G.A.Williams, *Aust.J.Chem.*, 1975, 28, 2593.

118. G.A.Williams and R.Robson, *Aust.J.Chem.*, 1981, 34, 65.

119. H.Okawa and S.Kida, *Bull.Chem.Soc.Jpn.*, 1972, 45, 1759.

120. D.N.Hendrickson and S.L.Lambert, *Inorg.Chem.*, 1979, 18, 2683.

121. C.L.Spiro, S.L.Lambert, T.J.Smith, E.N.Duesler, R.R.Gagné and D.N.Hendrickson, *Inorg.Chem.*, 1981, 20, 1229.

122. A.W.Addison, *Inorg.Nucl.Chem.Lett.*, 1976, 12, 899.

123. R.R.Gagné, C.A.Koval, T.J.Smith and M.C.Cimolino, *J.Am.Chem.Soc.*, 1979, 101, 4571.

124. R.R.Gagné, L.M.Henling and T.J.Kistenmacher, *Inorg.Chem.*, 1980, 19, 1226.

125. P.Zanello, S.Tamburini, P.A.Vigato and G.A.Mazzochin, *Co-ord.Chem.Rev.*, 1987, 77, 165.

126. R.R.Gagné, C.A.Koval and T.J.Smith, *J.Am.Chem.Soc.*, 1977, 99, 8367.

127. S.K.Mandal and K.Nag, *J.Chem.Soc., Dalton Trans.*, 1983, 2429.

128. R.C.Long and D.N.Hendrickson, *J.Am.Chem.Soc.*, 1983, 105, 1513.

129. S.K.Mandal, B.Adhikary and K.Nag, *J.Chem.Soc., Dalton Trans.*, 1986, 1175.

130. P.Lacroix, O.Kahn, F.Theobald, J.Le Roy and C.Wakselman, *Inorg.Chim.Acta*, 1988, 142, 129.

131. P.Zanello, A.Cinquantini, P.Guerriero, S.Tamburini and P.Vigato, *Inorg.Chim.Acta*, 1986, 117, 91.

132. S.K.Mandal, L.K.Thompson and K.Nag, *Inorg.Chim.Acta*, 1988, 149, 247.

134. M.B.Robin and P.Day, *Adv.Inorg.Radiochem.*, 1967, 10, 247.

135. R.R.Gagné and C.L.Spiro, *J.Am.Chem.Soc.*, 1980, 102, 1443.

136. R.R.Gagné, C.L.Spiro, T.J,Smith, C.A.Hamann, W.R.Thies and A.K.Shiemke, *J.Am.Chem.Soc.*, 1981, 103, 4073.

137. S.K.Mandal, L.K.Thompson, M.J.Newlands, E.J.Gabe and K.Nag, *Inorg.Chem.*, 1990, 29, 1324.

138. K.Wieghardt, *Angew.Chem., Intl.Ed.Engl.*, 1989, 28, 1153.

139. G.Christou, *Acc.Chem.Res.*, 1989, 22, 328.

140. G.W.Brudwig and R.H.Crabtree, *Prog.Inorg.Chem.*, 1989, 37, 99.

141. G.C.Dismukes, *Chem.Scr.*, 1988, 28A, 99.

142. G.Renger, *Angew.Chem., Intl.Ed.Engl.*, 1987, 26, 643.

143. H.Diril, H-R.Chang, X.Zhang, S.K.Larsen, J.A.Potenza, C.G.Pierpont, H.J.Schugar, S.S.Isied and D.N.Hendrickson, *J.Am.Chem.Soc.*, 1987, 109, 6207.

144. H.R.Chang, S.K.Larsen, P.D.W.Boyd, C.G.Pierpont and D.N.Hendrickson, *J.Am.Chem.Soc.*, 1988, 110, 4565.

145. S.K.Mandal, L.K.Thompson, K.Nag, J-P.Charland and E.J.Gabe, *Inorg.Chem.*, 1987, 26, 1391.

146. H.Okawa, M.Tadokoro, H.Sakiyama, N.Matsumoto and S.Kida, *Bull.Chem.Soc.Jpn.*, 1990, 63, 3337.

147. H.Okawa, M.Tadokoro, N.Matsumoto, M.Koikawa and S.Kida, *J.Chem.Soc., Dalton Trans.*, 1991, 1657.

148. S.K.Mandal and K.Nag, *J.Chem.Soc., Dalton Trans.*, 1984, 2141.

149. I.E.Dickson and R.Robson, *Inorg.Chem.*, 1974, 13, 1301.

150. S.K.Mandal, L.K.Thompson, K.Nag, J-P.Charland and E.J.Gabe, *Can.J.Chem.*, 1987, 65, 2815.

151. D.C.Olsen and J.Vasilevskis, *Inorg.Chem.*, 1971, 10, 463.

152. R.Das and K.Nag, *Inorg.Chem.*, 1991, 30, 2831.

153. K.K.Nanda, R.Das, M.J.Newlands, R.Hynes, E.J.Gabe and K.Nag, *J.Chem.Soc., Dalton Trans.*, 1992, 897.

154. H.Okawa, M.Honda and S.Kida, *Chem.Lett.*, 1972, 1027.

155. S.K.Mandal, L.K.Thompson, M.J.Newlands, A.K.Biswas, B.Adhikary, K.Nag, E.J.Gabe and F.L.Lee, *Can.J.Chem.*, 1989, 67, 662.

156. M.D.Timken, W.A.Marritt, D.N.Hendrickson, R.R.Gagné and E.Sinn, *Inorg.Chem.*, 1985, 24, 4202.

157. R.E.Marsh and W.P.Schaefer, *Inorg.Chem.*, 1986, 25, 3661.

158. N.A.Bailey, D.E.Fenton, P.B.Roberts and A.M.Walford, *J.Chem.Soc., Dalton Trans.*, 1987, 1865.

159. J.E.Huheey,"Inorganic Chemistry", 2nd Edition, Harper and Row, New York, 1978.

160. V.McKee and S.S.Tandon, *J.Chem.Soc., Dalton Trans.*, 1989, 19.

161. S.S.Tandon, L.K.Thompson, J.N.Bridson, V.McKee and A.J.Downard, *Inorg.Chem.*, 1992, 31, 4635.

162. D.Luneau, J.M.Savariault, P.Cassoux and J-P.Tuchagues, *J.Chem.Soc., Dalton Trans.*, 1988, 1225.

163. M.Tadokoro, H.Sakiyama, N.Matsumoto, M.Kodera, H.Okawa and S.Kida, *J.Chem.Soc., Dalton Trans.*, 1992, 313.

164. V.McKee and S.S.Tandon, *J.Chem.Soc., Chem.Commun.*, 1988, 385.

165. V.McKee and S.S.Tandon, *Inorg.Chem.*, 1989, 28, 2901.

166. V.Mckee and S.S.Tandon, *J.Chem.Soc., Dalton Trans.*, 1991, 221.

167. V.McKee and S.S.Tandon, *J.Chem.Soc., Chem.Commun.*, 1988, 1334.

168. S.S.Tandon, L.K.Thompson and J.N.Bridson, *J.Chem.Soc., Chem.Commun.*, 1992, 911.

169. M.Bell, A.J.Edwards, B.F.Hoskins, E.H.Kachab and R.Robson, *J.Am.Chem.Soc.*, 1989, 111, 3603.

170. B.F.Hoskins, R.Robson and P.Smith, *J.Chem.Soc., Chem.Commun.*, 1990, 488.

171. A.J.Edwards, B.F.Hoskins, E.H.Kachab, A.Markiewicz, K.S.Murray and R.Robson, *Inorg.Chem.*, 1992, 31, 3585.

172. M.J.Grannas, B.F.Hoskins and R.Robson, *J.Chem.Soc., Chem.Commun.*, 1990, 1644.

173. W.D.Carlisle, D.E.Fenton, D.C.Mulligen, P.B.Roberts, P.A.Vigato and S.Tamburini, *Inorg.Chim.Acta*, 1987, 126, 233.

174. H.Okawa, H.Sakiyawa, K.Motoda and S.Kida, *Chem.Lett.*, 1991, 1133.

175. K.Motoda, H.Sakiyama, N.Matsumoto, H.Okawa and S.Kida, *Bull.Chem.Soc.Jpn.*, 1992, 65, 1176.

176. R.Manif, A.E.Martell, P.J.Squattrito and A.Clearfield, *Inorg.Chem.*, 1990, 29, 4723.

177. See, for example, F.Fages, J.P.Desvergne, H..Bouas-Laurent, J.M.Lehn, J.P.Konopelski, P.Marsau and Y.Barrens, *J.Chem.Soc., Chem.Commun.*, 1990, 655 and refs. within.

178. See, for example, V.Bulach, D.Mandon and R.Weiss, *Angew.Chem., Intl.Ed.Engl.*, 1991, 30, 572 and refs. within.

179. G.Reid, Ph.D. Thesis, University of Edinburgh, 1989.

180. D.Parker, J.M.Lehn and J.Rimmer, *J.Chem.Soc., Chem.Commun.*, 1985, 1517.

181. D.Parker, *J.Chem.Soc., Chem.Commun.*, 1985, 1129.

182. G.Ferguson, K.E.Matthes and D.Parker, *J.Chem.Soc., Chem.Commun.*, 1987, 1350.

183. K.E.Matthes, D.Parker and G.Ferguson, *Angew.Chem., Intl.Ed.Engl.*, 1987, 26, 1162.

184. I.M.Helps, K.E.Matthes, D.Parker and G.Ferguson, *J.Chem.Soc., Dalton Trans.*, 1989, 915.

185. G.A.Lawrance, M.Maeder, T.M.Manning, M.A.O'Leary, B.W.Skelton and A.H.White, *J.Chem.Soc., Dalton Trans.*, 1990, 2491.

186. See, for example, A.J.Blake, T.I.Hyde, R.S.E.Smith and M.Schröder, *J.Chem.Soc., Chem.Commun.*, 1986, 334.

187. "Advanced Inorganic Chemistry", Ed. F.A.Cotton and G.Wilkinson, 5th. Edn., p.288, Wiley, London, 1972.

188. P.G.Owston, R.Peters, E.Ramsammy, P.A.Tasker and J.Trotter, *J.Chem.Soc., Chem.Commun.*, 1980, 1218.

189. N.A.Bailey, M.M.Eddy, D.E.Fenton, G.Jones, S.Mass and A.Mukhopadhyay, *J.Chem.Soc., Chem.Commun.*, 1981, 628.

190. N.W.Alcock, R.G.Kingston, P.Moore and C.Pierpont, *J.Chem.Soc.,*

Dalton Trans., 1984, 1937.

191. J.Zagwinski, J-M.Lehn, R.Meric and J.P.Vigneron, *Tetrahedron Lett.*, 1987, 28, 3489.

192. D.MacDowell and J.Nelson, *Tetrahedron Lett.*, 1988, 29, 385.

193. M.G.B.Drew, D.MacDowell and J.Nelson, *Polyhedron*, 1988, 7, 2229.

194. N.A.Bailey, D.E.Fenton, M.G.Williams and D.J.Winter, *J.Chem.Soc., Dalton Trans.*, 1989, 1727.

195. H.Adams, N.A.Bailey, D.E.Fenton, R.J.Good, R.Moody, O.Cecilia and R.de Barbarin, *J.Chem.Soc., Dalton Trans.*, 1988, 207.

196. M.G.B.Drew, J.Nelson and S.M.Nelson, *J.Chem.Soc., Dalton Trans.*, 1981, 1678.

197. W.D.Carlisle, D.E.Fenton, P.B.Roberts, U.Casellato, P.A.Vigato and R.Graziani, *Transition Met.Chem.*, 1986, 11, 292.

198. F.Ullmann and K.Brittner, *Chem.Ber.*, 1909, 42, 2539.

199. W.Clegg, *Acta Cryst.*, 1981, A37, 22.

200. *SHELXS*-86, program for crystal structure solution, G.M.Sheldrick, University of Göttingen, Germany, 1986.

201. *SHELX*-76, program for crystal structure refinement, G.M.Sheldrick, University of Cambridge, England, 1976.

202. *CALC*, program for molecular geometry calculations, R.O.Gould and P.Taylor, University of Edinburgh, Scotland, 1985.

203. *ORTEP*-II, interactive version, P.D.Mallinson and K.W.Muir, *J.Appl.Cryst.*, 1985, 18, 51.

204. R.H.Holm, G.W.Everett and A.Chakravorty, *Prog.Inorg.Chem.*, 1966, 7, 83-214.

205. J.B.Willis and D.P.Mellor, *J.Am.Chem.Soc.*, 1947, 69, 1237.

206. H.C.Clark and A.L.Odell, *J.Chem.Soc.*, 1955, 3431.

207. F.Basolo and W.R.Mataush, *J.Am.Chem.Soc.*, 1953, 75, 5663.

208. G.Maki, *J.Chem.Phys.*, 1958, 29, 1129.

209. C.J.Ballhausen and A.D.Liehr, *J.Am.Chem.Soc.*, 1959, 81, 538.

210. R.H.Holm, *J.Am.Chem.Soc.*, 1961, 83, 4683.

211. H.C.Clark and R.J.O'Brien, *Can.J.Chem.*, 1962, 40, 822.

212. I.Sotofte, R.Gronbaer and S.E.Rasmussen, *Acta Cryst.Sect.B*, 1976, 32, 1692.

213. Comprehensive Co-ordination Chemistry, Vol.(II), "Ligands", 262, Ed. G.Wilkinson, Pergamon, Oxford, 1987.

214. J.A.S.Howell, J.Y.Saillard, A.Le Beuze and G.Jaouen, *J.Chem.Soc., Dalton Trans.*, 1982, 2533.

215. V.McKee and W.B.Shepard, *J.Chem.Soc., Chem.Commun.*, 1985, 158.

216. S.Brooker, V.McKee, W.B.Shepard and L.K.Pannell, *J.Chem.Soc., Dalton Trans.*, 1987, 2555.

217. V.McKee and J.Smith, *J.Chem.Soc., Chem.Commun.*, 1983, 1465.

218. N.A.Bailey, D.E.Fenton, R.Moody, C.O.Rodriguez de Barbarin, I.N.Sciambarella, J.M.Latour, D.Limosin and V.McKee, *J.Chem.Soc., Dalton Trans.*, 1987, 2519.

219. B.J.Hathaway, D.G.Holah and A.E.Underhill, *J.Chem.Soc.*, 1962, 2444.

220. K.Nakamoto, "Infrared and Raman Spectra of Inorganic and Co-ordination Compounds", 4th Ed., Wiley, Chichester, 1986.

221. R.Robson, *Aust.J.Chem.*, 1970, 23, 2217.

222. J.A.Bertrand and D.G.Caine, *J.Am.Chem.Soc.*, 1964, 86, 2298.

223. G.N.Schrauzer and J.Kohnle, *Chem.Ber.*, 1964, 97, 1727.

224. K.A.Burkov, L.S.Lilic and L.G.Sillen, *Acta.Chem.Scand.*, 1965, 19, 14.

225. J.E.Andrew and A.B.Blake, *Chem.Comm.*, 1967, 1174.

226. J.E.Andrew and A.B.Blake, *J.Chem.Soc.(A)*, 1969, 1456.

227. A.G.Krüger and G.Winter, *Aust.J.Chem.*, 1970, 23, 1.

228. J.A.Bertrand, A.P.Ginsberg, R.I.Kaplan, C.E.Kirkwood, R.L.Martin and

R.C.Sherwood, *Inorg.Chem.*, 1971, 10, 240.

229. A.P.Ginsberg, *Inorg.Chim.Acta Rev.*, 1971, 5, 45.

230. H.Ohtaki and G.Biedermann, *Bull.Chem.Soc.Jpn.*, 1971, 44, 1822.

231. K.A.Burkov, N.J.Zinevich and L.S.Lilich, *Russ.J.Inorg.Chem.(Engl.Transl.)*, 1971, 16, 927.

232. J.A.Barnes and W.E.Hatfield, *Inorg.Chem.*, 1971, 10, 2355.

233. B.W.Clare and D.L.Kepert, *Aust.J.Chem.*, 1975, 28, 1489.

234. B.Aurivillius, *Acta Chem.Scand.Ser.A.*, 1977, 501.

235. J.A.Bertrand, C.Marabella and D.G.Van Derveer, *Inorg.Chim.Acta.*, 1978, 26, 113.

236. W.L.Gladfelter, M.W.Lynch, W.P.Schaefer, D.N.Hendrickson and H.B.Gray, *Inorg.Chem.*, 1981, 20, 2390.

237. Y.A.Simonov, A.A.Dvorkin, G.S.Matuzenko, M.A.Yampolskaya, T.S.Gifeisman, N.V.Gerbeleu and T.I.Malinovski, *Koord.Khim.*, 1984, 10, 1247.

238. F.Paap, E.Bouwman, W.L.Driessen, R.A.G.de Graaff and J.Reedijk, *J.Chem.Soc., Dalton Trans.*, 1985, 737.

239. K.Bizilj, S.G.Hardin, B.F.Hoskins, P.J.Oliver, E.R.T.Kiekink and G.Winter, *Aust.J.Chem.*, 1986, 39, 1035.

240. B.F.Hoskins, R.Robson and D.G.Vince, *J.Chem.Soc., Chem.Commun.*, 1973, 392.

241. R.Robson and D.G.Vince, *Inorg.Chim.Acta.*, 1977, 25, 191.

242. R.R.Thomas and A.Sen, *Inorg.Synth.*, 1989, 26, 128.

243. T.Hyde, Ph.D.Thesis, 1987, University of Edinburgh.

244. J.G.Stark and H.G.Wallace, "Chemistry Data Book", J.Murray, London, 1984.

245. P.Braunstein, R.Bender and J.Jud, *Inorg.Synth.*, 1989, 26, 345.

246. E.Kimura, Y.Lin, R.Machida and H.Zenda, *J.Chem.Soc.*,

Chem.Commun., 1986, 1020.

247. R.J.Cozens, K.S.Murray and B.O.West, *Chem.Comm.*, 1970, 1262.

248. R.J.Cozens, K.S.Murray and B.O.West, *J.Organomet.Chem.*, 1972, 38, 391.

249. C.A.Rogers and B.O.West, *J.Organomet.Chem.*, 1974, 70, 445.

250. S.Calmotti and A.Pasini, *Inorg.Chim.Acta.*, 1984, 85, L55.

251. S.N.Gamage, R.H.Morris, S.J.Rettig and B.R.James, *J.Organomet.Chem.*, 1986, 309, C59.

252. S.N.Gamage, R.H.Morris, S.J.Rettig, D.C.Thrackray, I.S.Thorburn and B.R.James, *J.Chem.Soc., Chem.Commun.*, 1987, 894.

253. J.Cosier and A.M.Glazer, *J.Appl.Cryst.*, 1986, 19, 105.

254. D.T.Cromer and J.B.Mann, *Acta Cryst.*, 1968, A24, 321.

255. *SHELXTL PC* version 4.2, G.M.Sheldrick, University of Göttingen, Germany, 1990. Siemens Analytical X-ray Instrumentation, Inc., Madison, Wisconsin, U.S.A.

256. P.J.Blower and J.R.Dilworth, *Coord.Chem.Rev.*, 1987, 76, 121 and refs.within.

257. G.Christou, C.D.Garner and F.E.Mabbs, *J.Chem.Soc., Chem.Commun.*, 1978, 740.

258. G.Christou, R.V.Hageman and R.H.Holm, *J.Am.Chem.Soc.*, 1980, 102, 7601.

259. R.E.Palermo, P.P.Power and R.H.Holm, *Inorg.Chem.*, 1982, 21, 173.

260. I.K.Adzamli, K.Libson, J.D.Lydon, R.C.Elder and E.Deutsch, *Inorg.Chem.*, 1979, 18, 303.

261. D.Leaver, J.Smoliez and W.H.Stafford, *J.Chem.Soc.*, 1962, 740.

262. M.F.Corrigan and B.O.West, *Aust.J.Chem.*, 1976, 29, 1413.

263. M.F.Corrigan, I.D.Rae and B.O.West, *Aust.J.Chem.*, 1978, 31, 587.

264. M.F.Corrigan, K.S.Murray, B.O.West and J.R.Pilbrow, *Aust.J.Chem.*,

1977, 30, 2455.

265. P.J.Marini, K.S.Murray and B.O.West, *J.Chem.Soc., Dalton Trans.*, 1983, 143.

266. R.C.Coombes, J.P.Costes and D.E.Fenton, *Inorg.Chim.Acta*, 1983, 77, 173.

267. T.Yamamura, M.Tadokoro and R.Kuroda, *Chem.Lett.*, 1989, 1245.

268. G.D.Fallon, B.M.Gatehouse, P.J.Marini, K.S.Murray and B.O.West, *J.Chem.Soc., Dalton Trans.*, 1984, 2733.

269. P.J.Marini, K.J.Berry, K.S.Murray and B.O.West, *J.Chem.Soc., Dalton Trans.*, 1983, 879.

270. M.F.Corrigan, K.S.Murray and B.O.West, *J.Chem.Soc., Dalton Trans.*, 1977, 1478.

271. P.J.Marini, K.S.Murray and B.O.West, *J.Chem.Soc., Chem.Commun.*, 1981, 726.

272. W.Shin and P.A.Lindahl, *J.Am.Chem.Soc.*, 1992, 114, 9718 and refs. within

273. I.Bertini, L.Sacconi and G.P.Speroni, *Inorg.Chem.*, 1972, 11, 1323.

274. J.G.Hughes and R.Robson, *Inorg.Chim.Acta*, 1979, 35, 87.

275. P.Iliopoulos, K.S.Murray, R.Robson, J.C.Wilson and G.A.Williams, *J.Chem.Soc., Dalton Trans.*, 1987, 1585.

276. A.M.Bond, M.Haga, I.S.Creece, R.Robson and J.C.Wilson, *Inorg.Chem.*, 1989, 28, 559.

277. B.F.Hoskins, R.Robson, G.A.Williams and J.C.Wilson, *Inorg.Chem.*, 1991, 30, 4160.

278. B.F.Hoskins, C.J.MacKenzie, R.Robson and L.Zhenrong, *J.Chem.Soc., Dalton Trans.*, 1990, 2637.

279. P.Krautil and R.Robson, *J.Coord.Chem.*, 1980, 10, 7.

280. M.Louey, P.D.Nichols and R.Robson, *Inorg.Chim.Acta*, 1980, 47, 87.

281. R.H.Holm, R.B.King and F.G.A.Stone, *Inorg.Chem.*, 1963, 2, 219.

282. R.Zanella, R.Ros and M.Graziani, *Inorg.Chem.*, 1973, 12, 2736.

283. M.S.Newman and H.A.Karnes, *J.Org.Chem.*, 1966, 31, 3980.

284. R.Robson, personal communication, 1992.

285. *DIFABS*, program for empirical absorption correction, N.Walker and D.Stuart, *Acta Cryst.*, 1983, A39, 158.

286. A.J.Blake, R.O.Gould, A.J.Holder, T.I.Hyde and M.Schröder, *J.Chem.Soc., Dalton Trans.*, 1988, 1861.

287. S.C.Rawle, R.Yagbasan, K.Prout and S.R.Cooper, *J.Amer.Chem.Soc.*, 1987, 109, 6181.

288. A.J.Blake, A.J.Holder, T.I.Hyde, Y.V.Roberts, A.J.Lavery and M.Schröder, *J.Organomet.Chem.*, 1987, 323, 261.

289. A.J.Blake, A.J.Holder, T.I.Hyde and M.Schröder, *J.Chem.Soc., Chem.Commun.*, 1987, 987.

290. A.J.Blake, R.O.Gould, A.J.Holder, T.I.Hyde, M.O.Odulate, A.J.Lavery and M.Schröder, *J.Chem.Soc., Chem.Commun.*, 1987, 118.

291. S.G.Murray and F.R.Hartley, *Chem.Rev*, 1981, 81, 365.

292. A.J.Blake, A.J.Holder, T.I.Hyde and M.Schröder, *J.Chem.Soc., Chem.Commun.*, 1989, 1433.

293. W.N.Setzer, C.A.Ogle, G.S.Wilson and R.S.Glass, *Inorg.Chem.*, 1983, 22, 266.

294. M.N.Bell, A.J.Blake, H.J.Küppers, M.Schröder and K.Wieghardt, *Angew.Chem., Intl.Ed.Engl.*, 1987, 26, 250.

295. See "Comprehensive Organometallic Chemistry" and refs. within.

296. See S.G.Davies, *Aldrichimica Acta*, 1990, 23, 31 and refs. within.

297. A.J.Blake, R.D.Crofts, G.Reid and M.Schröder, *J.Organomet.Chem.*, 1989, 359, 371.

298. K.Wieghardt, H.J.Küppers and J.Weiss, *Inorg.Chem.*, 1985, 24, 3067.

299. R.M.Christie, Ph.D.Thesis, University of Edinburgh, 1989.

300. Y.V.Roberts, Ph.D.Thesis, University of Edinburgh, 1991.

301. M.J.Sullivan, Ph.D.Thesis, University of Edinburgh, to be published, 1993.

302. M.A.Halcrow, Ph.D.Thesis, University of Edinburgh, 1991.

303. See "Advanced Inorganic Chemistry", F.A.Cotton and G.A.Wilkinson, 5th Edn., 885, Wiley, London, 1988.

304. J.C.A.Boeyens, A.G.S.Forbes, R.D.Hancock and K.Wieghardt, *Inorg.Chem.*, 1985, 24, 2926.

305. H.J.Meyer and J.Pickardt, *Z.Anorg.Allg.Chem.*, 1988, 560, 185.

306. R.C.Elder, G.J.Kennard, M.Payne and E.Deutsch, *Inorg.Chem.*, 1978, 17, 1296.

307. M.E.Garcia Posse, M.A.Juri, P.Y.Aymonino, O.E.Piro, H.A.Negri and E.E.Castellano, *Inorg.Chem.*, 1984, 23, 948.

308. B.N.Figgis, B.W.Skelton and A.H.White, *Aust.J.Chem.*, 1978, 31, 57.

309. A.Zalkin, D.H.Templeton and T.Ueki, *Inorg.Chem.*, 1973, 12, 1641.

310. J.Baker, L.M.Engelhardt, B.N.Figgis and A.H.White, *J.Chem.Soc., Dalton Trans.*, 1975, 531.

311. R.D.Hancock, *Prog.Inorg.Chem.*, 1989,37, 187.

312. W.D.Horrocks, G.R.Van Hecke and D.D.Hall, *Inorg.Chem.*, 1967, 6, 694.

313. C.N.Sethulakshmi and P.T.Manoharan, *Inorg.Chem.*, 1981, 20, 2533.

314. V.M.Miskowski, J.L.Robbins, G.S.Hammond and H.B.Gray, *J.Amer.Chem.Soc.*, 1976, 98, 2477.

315. J.K.Stalick, P.W.R.Corfield and D.W.Meek, *J.Amer.Chem.Soc.*, 1972, 94, 6194.

316. A.J.Blake, R.O.Gould, M.A.Halcrow, A.J.Holder, T.I.Hyde and M.Schröder, *J.Chem.Soc., Dalton Trans.*, 1992, 3427.

317. A.J.Blake, M.A.Halcrow and M.Schröder, *J.Chem.Soc., Dalton Trans.*, 1992, 2803.

318. A.J.Blake, A.J.Holder, A.Taylor and M.Schröder, *New J.Chem.*, 1991, 15, 511.

319. G.Reid and M.Schröder, *Chem.Soc.Rev.*, 1990, 19, 239.

320. M.N.Bell, A.J.Blake, R.M.Christie, R.O.Gould, A.J.Holder, T.I.Hyde, M.Schröder and L.J.Yellowlees, *J.Chem.Soc., Dalton Trans.*, 1992, 2977.

321. N.Atkinson, A.J.Blake, M.G.B.Drew, G.Forsyth, R.O.Gould, A.J.Lavery, G.Reid and M.Schröder, *J.Chem.Soc., Dalton Trans.*,1992, 2993.

322. A.J.Blake, M.A.Halcrow and M.Schröder, *J.Chem.Soc., Chem.Commun.*, 1991, 253.

323. A.J.Blake, R.M.Christie, Y.V.Roberts, M.J.Sullivan, M.Schröder and L.J.Yellowlees, *J.Chem.Soc., Chem.Commun.*, 1992, 848.

324. See for example, R.H.Holm, S.Ciurli and J.A.Weigel, *Prog.Inorg.Chem.*, 1990, 38, 1.

325. J.C.Dabrowiak, P.H.Merrell, J.A.Stone and D.H.Busch, *J.Amer.Chem.Soc.*, 1973, 95, 6613.

326. D.L.Hughes, M.Jimenez-Tenorio, G.J.Leigh, A.Houlton and J.Silver, *J.Chem.Soc., Dalton Trans.*, 1992, 2033.

327. A.Hills, D.L.Hughes, M.Jimenez-Tenorio, G.J.Leigh, A.Houlton and J.Silver, *J.Chem.Soc., Chem.Commun.*, 1989, 1774.

328. D.S.C.Black and I.A.McLean, *Aust.J.Chem.*, 1971, 24, 1401.

329. "Advanced Inorganic Chemistry", F.A.Cotton and G.Wilkinson, 3rd Edn., 885, Wiley, London, 1972.

330. "Advanced Inorganic Chemistry", F.A.Cotton and G.Wilkinson, 5th Edn., 434, Wiley, London, 1988 and refs. within.

331. R.Puddephatt, *Chem.Soc.Rev.*, 1983, 99.

332. "Spectroscopic Methods in Organic Chemistry", D.H.Williams and I.Fleming, 3rd Edn., 85, McGraw-Hill, London, 1980.

333. J.E.Barclay, G.J.Leigh, A.Houlton and J.Silver, *J.Chem.Soc., Dalton Trans.*, 1988, 2865.

334. J.E.Barclay, A.Hills, D.L.Hughes and G.J.Leigh, *J.Chem.Soc., Dalton Trans.*, 1988, 2871.

335. G.Zotti, S.Zecchin and G.Pilloni, *J.Organomet.Chem.*, 1979, 181, 375.

336. A.R.Barron, G.Wilkinson, M.Motevalli and M.B.Hursthouse, *Polyhedron*, 1987, 1089.

337. A.F.Williams, *Acta Cryst.C*, 1988, 44, 1895.

List of Abbreviations

($\underline{1}H_2$)	11,23-dimethyl-3,7,15,19-tetraazatricyclo[19.3.1.$1^{9,13}$] hexacosa-2,7,9,11,13(26),14,19,21(25),22,24-decaene-25,26-diol, ($C_{24}H_{28}N_4O_2$) (for other ligands, see Chapter 2)
[9]aneN_3	1,4,7-triazacyclononane
Me_3[9]aneN_3	*N,N',N''*-trimethyl-1,4,7-triazacyclononane
[9]aneS_3	1,4,7-trithiacyclononane
[12]aneS_4	1,4,7,10-tetrathiacyclododecane
[14]aneS_4	1,4,8,11-tetrathiacyclotetradecane
[16]aneS_4	1,5,9,13-tetrathiacyclohexadecane
[15]aneS_5	1,4,7,10,13-pentathiacyclopentadecane
[18]aneS_6	1,4,7,10,13,16-hexathiacyclohexadecane
[24]aneS_8	1,4,7,10,13,16,19,22-octathiacyclotetracosane
[28]aneS_8	1,4,8,11,15,18,22,25-octathiacyclooctacosane
[18]aneN_2S_4	1,4,10,13-tetrathia-7,16-diazacyclooctadecane
br	broad
$^nBu_4N$	tetra-^{n}butylammonium
dcpe	1,2-bis(dicyclohexylphosphino)ethane
DEPT	distortionless enhancement by polarisation transfer
DMF	*N,N*-dimethylformamide
DMSO	dimethylsulphoxide
dppe	1,2-bis(diphenylphosphino)ethane
dppm	bis(diphenylphosphino)methane
dppp	1,3-bis(diphenylphosphino)propane
dppv	*cis*-1,2-bis(diphenylphosphino)ethylene

e.i.	electron impact
e.s.d.	estimated standard deviation
e.s.r.	electron spin resonance
Et	ethyl
f.a.b.	fast atom bombardment
Fc/Fc^+	ferrocene/ferrocenium
i.r.	infra red
m	medium
M^+	molecular ion peak
Me	methyl
MHz	megahertz
N.H.E.	normal hydrogen electrode
n.m.r.	nuclear magnetic resonance
3-NOBA	3-nitrobenzylalcohol
Ph	phenyl
p.p.m.	parts per million
s	strong
sh	shoulder
THF	tetrahydrofuran
Ts	tosyl (*p*-toluenesulphonyl)
U.V./vis.	ultra-violet/visible
w	weak

LECTURE COURSES AND MEETINGS ATTENDED

1. Departmental Inorganic Colloquia and Friday Discussion Group (3 years).
2. University of Strathclyde Inorganic Club Conferences, 1990, 1991, 1992.
3. R.S.C. Scottish Dalton Group Meeting, Glasgow, 1990.
4. Butler Postgraduate Electrochemistry Meeting, Edinburgh 1990, 1991.
5. U.K. Macrocyclic Symposium, Warwick, 1989, Manchester, 1991, Oxford, 1993.
6. R.S.C. Annual Chemical Congress, Belfast, 1990.
7. IV International Platinum Group Metals Conference, Cambridge, 1990.
8. I.C.C.C., Lausanne, Switzerland, 1992.
9. X-ray Crystallography - Structure Solution and Refinement, Drs. A.J.Blake and R.O.Gould, Edinburgh.
10. Medicinal Inorganic Chemistry, Dr. S.Chapman, Edinburgh.
11. E.s.r. Spectroscopy, Dr. R.E.P.Winpenny, Edinburgh.
12. Short Course on E.s.r. Spectroscopy, P.H.Rieger, Edinburgh.
13. Current Advamces in Inorganic Chemistry, Drs. S.Chapman, M.Schröder and R.E.P.Winpenny, Edinburgh.
14. Aspects and Applications of N.m.r. Spectroscopy, 1992, Drs. D. Reed and I.H.Sadler, Edinburgh.

Zeitschrift für Kristallographie 199, 287–289 (1992)

Crystal structure of trans-bis(acetonitrile)-bis(1,2-bis(diphenylphosphino)ethane)iron(II)-bis-(tetrafluoroborate) bis(dichloromethane), $(CH_3CN)_2(C_{26}H_{24}P_2)_2Fe(BF_4)_2(CH_2Cl_2)_2$

A. J. Blake, A. J. Atkins, R. O. Gould and M. Schröder

Department of Chemistry, The University of Edinburgh,
West Mains Road, Edinburgh EH9 3JJ, Scotland

(Received June 24, 1991)

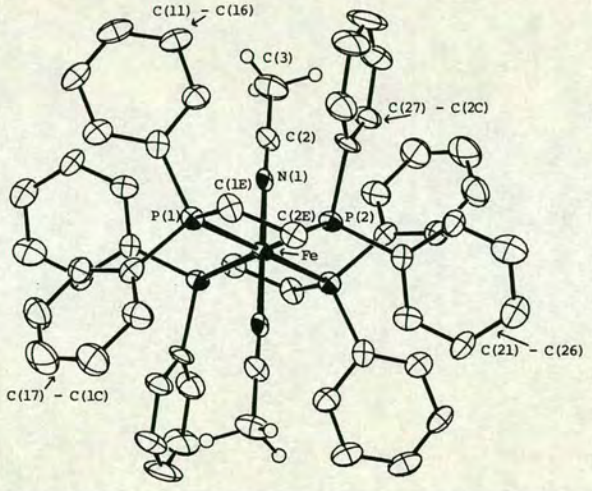

Source of material: By reaction of $[(CH_3CN)_6Fe](BF_4)_2$ (see ref. 1) with 1,2-bis(diphenylphosphino)ethane in CH_3NO_2, followed by recrystallisation from CH_2Cl_2-Et_2O.

For cell refinement, reflection centres were measured at $\pm\ \omega$. Data collection used the learnt-profile method of Clegg (see ref. 2). The dichloromethane solvates are disordered in that one of the chlorine atoms is spread over two sites, dichloromethane H's were not determined. The structure is analogous to that of previously reported complexes containing bidentate, chelating diphosphines (see ref. 3).

Triclinic, $P\bar{1}$ (no 2), $a = 10.355(9)$, $b = 12.045(9)$, $c = 13.22(1)$ Å, $\alpha = 63.74(6)°$, $\beta = 85.62(6)°$, $\gamma = 80.15(3)°$, $V = 1456.9$ Å^3, $Z = 1$, $R = 0.080$.

Table 1. Parameters used for the X-ray data collection

Diffractometer type:	Stoë Stadi-4	Number of unique reflections:	3826
Wave length:	Mo K_α radiation (0.7107 Å)	Criterion for unobserved reflections:	$F_o < 6\sigma(F_o)$
Crystal characteristics:	red lath, size $0.10 \times 0.20 \times 0.35$ mm	Number of refined parameters:	371
Temperature of measurement:	173 K	Scan mode:	ω-2Θscan
$2\theta_{max}$:	45°	μ:	4.5 cm^{-1}
		Structure solution program used:	SHELX

Table 2. Final atomic coordinates and displacement parameters (in $Å^2$)

Atom	x	y	z	U_{iso}/U_{11}	U_{22}	U_{33}	U_{12}	U_{13}	U_{23}
Fe	0.5	0.5	0.5	0.019(1)	0.023(1)	0.018(1)	−0.0070(8)	−0.0025(8)	−0.0070(8)
P(1)	0.2962(2)	0.5192(2)	0.5855(2)	0.020(1)	0.031(1)	0.026(1)	−0.009(1)	0.002(1)	−0.012(1)
C(11)	0.1749(9)	0.6617(9)	0.5226(8)	0.021(5)	0.034(6)	0.040(6)	−0.017(4)	0.008(4)	−0.022(5)
C(12)	0.1491(9)	0.7074(9)	0.4064(8)	0.024(6)	0.041(6)	0.044(7)	−0.005(5)	−0.003(5)	−0.019(5)
H(12)	0.2032(9)	0.6599(9)	0.3600(8)	0.05					
C(13)	0.0568(9)	0.8109(9)	0.3507(9)	0.020(6)	0.037(6)	0.056(7)	−0.006(5)	−0.006(5)	−0.015(6)
H(13)	0.0374(9)	0.8431(9)	0.2623(9)	0.05					
C(14)	−0.012(1)	0.874(1)	0.411(1)	0.019(6)	0.040(7)	0.066(8)	−0.001(5)	−0.006(5)	−0.014(6)
H(14)	−0.081(1)	0.957(1)	0.368(1)	0.05					
C(15)	0.0101(9)	0.8299(9)	0.5240(9)	0.022(6)	0.030(6)	0.063(8)	−0.003(5)	0.003(5)	−0.023(5)
H(15)	−0.0441(9)	0.8773(9)	0.5705(9)	0.05					
C(16)	0.1025(9)	0.7238(9)	0.5786(9)	0.021(5)	0.039(6)	0.049(6)	−0.010(5)	−0.000(5)	−0.019(5)
H(16)	0.1177(9)	0.6892(9)	0.6681(9)	0.05					
C(17)	0.3041(9)	0.4814(8)	0.7350(8)	0.022(5)	0.026(5)	0.035(6)	−0.006(4)	0.006(4)	−0.012(5)
C(18)	0.3158(9)	0.572(1)	0.7710(8)	0.024(6)	0.044(6)	0.033(6)	−0.003(5)	0.006(4)	−0.017(5)
H(18)	0.3114(9)	0.669(1)	0.7107(8)	0.05					
C(19)	0.333(1)	0.537(1)	0.8843(9)	0.048(7)	0.074(9)	0.039(7)	−0.010(6)	0.007(6)	−0.029(7)
H(19)	0.342(1)	0.608(1)	0.9114(9)	0.05					
C(1A)	0.339(1)	0.416(1)	0.963(1)	0.067(9)	0.08(1)	0.029(7)	−0.010(8)	0.010(6)	−0.016(7)
H(1A)	0.352(1)	0.392(1)	1.051(1)	0.05					
C(1B)	0.327(1)	0.325(1)	0.9300(9)	0.076(9)	0.055(8)	0.031(7)	−0.008(7)	0.010(6)	−0.008(6)
H(1B)	0.333(1)	0.228(1)	0.9920(9)	0.05					
C(1C)	0.308(1)	0.357(1)	0.8162(8)	0.031(6)	0.063(8)	0.030(6)	−0.007(6)	0.007(5)	−0.012(6)
H(1C)	0.297(1)	0.285(1)	0.7907(8)	0.05					
P(2)	0.3994(2)	0.3855(2)	0.4355(2)	0.019(1)	0.028(1)	0.025(1)	−0.008(1)	−0.002(1)	−0.010(1)
C(21)	0.4870(9)	0.2562(8)	0.4099(7)	0.026(5)	0.025(5)	0.030(5)	−0.010(4)	0.005(4)	−0.014(4)
C(22)	0.4589(9)	0.2397(9)	0.3157(8)	0.027(6)	0.036(6)	0.049(7)	−0.004(5)	−0.003(5)	−0.027(5)
H(22)	0.3801(9)	0.3021(9)	0.2599(8)	0.05					
C(23)	0.529(1)	0.146(1)	0.293(1)	0.026(6)	0.066(8)	0.056(7)	−0.017(6)	−0.003(5)	−0.022(6)
H(23)	0.507(1)	0.137(1)	0.219(1)	0.05					
C(24)	0.631(1)	0.061(1)	0.366(1)	0.028(6)	0.046(7)	0.069(8)	−0.011(5)	0.002(6)	−0.034(6)
H(24)	0.688(1)	−0.012(1)	0.347(1)	0.05					
C(25)	0.6547(9)	0.0742(9)	0.4613(9)	0.029(6)	0.033(6)	0.053(7)	0.001(5)	0.002(5)	−0.023(5)
H(25)	0.7286(9)	0.0077(9)	0.5205(9)	0.05					
C(26)	0.5860(9)	0.1707(9)	0.4826(8)	0.024(6)	0.036(6)	0.035(6)	−0.010(5)	−0.000(5)	−0.010(5)
H(26)	0.6094(9)	0.1801(9)	0.5565(8)	0.05					
C(27)	0.2935(9)	0.4750(9)	0.3129(7)	0.026(6)	0.051(6)	0.021(5)	−0.002(5)	−0.012(4)	−0.016(5)
C(28)	0.163(1)	0.463(1)	0.3135(9)	0.032(7)	0.071(8)	0.043(7)	−0.011(6)	−0.002(5)	−0.027(6)

Table 2. (Continued)

Atom	x	y	z	U_{iso}/U_{11}	U_{22}	U_{33}	U_{12}	U_{13}	U_{23}
H(28)	0.121(1)	0.393(1)	0.3864(9)	0.05					
C(29)	0.084(1)	0.542(1)	0.220(1)	0.029(7)	0.11(1)	0.064(9)	0.005(7)	−0.025(6)	−0.042(8)
H(29)	−0.018(1)	0.534(1)	0.222(1)	0.05					
C(2A)	0.134(1)	0.630(1)	0.126(1)	0.055(9)	0.11(1)	0.040(8)	0.019(8)	−0.031(7)	−0.019(8)
H(2A)	0.071(1)	0.692(1)	0.055(1)	0.05					
C(2B)	0.265(1)	0.639(1)	0.1214(9)	0.07(1)	0.068(8)	0.023(6)	0.009(7)	−0.013(6)	−0.009(6)
H(2B)	0.306(1)	0.706(1)	0.0459(9)	0.05					
C(2C)	0.346(1)	0.5624(9)	0.2124(8)	0.034(6)	0.050(7)	0.030(6)	−0.003(5)	−0.011(5)	−0.016(5)
H(2C)	0.449(1)	0.5691(9)	0.2074(8)	0.05					
C(1E)	0.2021(9)	0.4007(9)	0.5835(8)	0.026(6)	0.043(6)	0.035(6)	−0.018(5)	0.006(4)	−0.021(5)
H(1E1)	0.1225(9)	0.4488(9)	0.5240(8)	0.05					
H(1E2)	0.1629(9)	0.3509(9)	0.6668(8)	0.05					
C(2E)	0.2875(9)	0.3068(8)	0.5496(7)	0.025(5)	0.032(5)	0.028(5)	−0.015(4)	0.008(4)	−0.009(4)
H(2E1)	0.3439(9)	0.2367(8)	0.6216(7)	0.05					
H(2E2)	0.2257(9)	0.2625(8)	0.5212(7)	0.05					
N(1)	0.5434(7)	0.3460(7)	0.6320(6)	0.022(4)	0.032(5)	0.031(5)	−0.007(4)	−0.004(4)	−0.025(4)
C(2)	0.567(1)	0.256(1)	0.7127(8)	0.042(7)	0.036(6)	0.025(6)	−0.010(5)	−0.003(5)	−0.013(5)
C(3)	0.598(1)	0.139(1)	0.8154(9)	0.08(1)	0.054(8)	0.028(6)	0.003(7)	−0.014(6)	−0.003(6)
H(3A)	0.588(1)	0.162(1)	0.8858(9)	0.05					
H(3B)	0.701(1)	0.108(1)	0.8050(9)	0.05					
H(3C)	0.543(1)	0.065(1)	0.8313(9)	0.05					
B	0.751(2)	−0.006(2)	0.109(1)	0.14(2)	0.06(1)	0.05(1)	−0.02(1)	−0.03(1)	−0.015(9)
F(1)	0.643(1)	0.0815(9)	0.0758(7)	0.23(1)	0.089(7)	0.058(6)	0.012(8)	−0.021(7)	−0.021(5)
F(2)	0.773(1)	−0.053(1)	0.0322(7)	0.156(9)	0.148(8)	0.059(5)	0.014(7)	−0.003(5)	−0.053(6)
F(3)	0.735(1)	−0.0981(7)	0.2115(6)	0.32(2)	0.059(5)	0.040(5)	−0.061(7)	−0.003(6)	−0.010(4)
F(4)	0.843(2)	0.056(1)	0.116(1)	0.26(2)	0.21(1)	0.18(1)	−0.17(1)	−0.06(1)	−0.03(1)
C(1S)	0.078(1)	0.167(2)	0.144(1)	0.043(9)	0.13(1)	0.09(1)	0.013(9)	−0.023(7)	−0.04(1)
Cl(1S)	0.2114(4)	0.1203(4)	0.2339(3)	0.066(2)	0.118(3)	0.071(2)	−0.015(2)	−0.010(2)	−0.041(2)
Cl(2S)	−0.063(2)	0.229(2)	0.170(1)	0.11(1)	0.21(2)	0.10(1)	0.07(2)	−0.04(1)	−0.10(1)
Cl(3S)	0.017(1)	0.329(1)	0.1205(7)	0.095(7)	0.112(7)	0.085(5)	0.022(6)	−0.018(5)	−0.062(5)

Site occupation: Cl(25): 0.392, Cl(35): 0.608

Further details of the structure determination (e.g. structure factors) have been deposited within the relevant database and can be accessed as Collection No. 320282 or ordered from the Fachinformationszentrum Karlsruhe, D-7514 Eggenstein-Leopoldshafen.

References:

1. Hathaway, B.J., Holah, D.G., Underhill, A.E.: The Preparation and Properties of Some Bivalent Transition-metal Tetrafluoroborate-Methyl Cyanide Complexes. J. Chem. Soc. **(1962)** 2444–2448.
2. Clegg, W.: Faster Data Collection Without Loss of Precision: An Extension of the Learnt Profile Method. Acta Crystallogr. **A37** (1981) 22–28.
3. Barclay, J.E., Hills, A., Hughes, D.L., Leigh, G.J.: Crystal and Molecular Structures of Four Bis(diphosphine) Complexes of Iron(II). J. Chem. Soc. Dalton Trans. **(1988)** 2871–2877.

Synthesis of Binuclear Platinum Metal N_4O_2-Compartmental Complexes: the Structures of the Protonated Metal-free Macrocycle $[LH_4](PF_6)_2 \cdot MeNO_2$ and of $[Pd_2(L)](BF_4)_2 \cdot 2MeNO_2$

Andrew J. Atkins, Alexander J. Blake and Martin Schröder*

Department of Chemistry, University of Edinburgh, West Mains Road, Edinburgh EH9 3JJ, Scotland, UK

Reaction of $[LH_4](PF_6)_2$, formed by condensation of 1,3-diaminopropane and 2,6-diformyl-4-methylphenol in the presence of HBr followed by addition of NH_4PF_6, with platinum metal salts in the presence of base affords $[M_2(L)]^{2+}$ (M = Pd, Pt) and $[M_2Cl_4(L)]$ (M = Rh); the structure of $[LH_4](PF_6)_2 \cdot MeNO_2$ shows a folded conformation incorporating both inter- and intra-molecular π–π interactions between phenyl rings; in contrast, the structure of $[Pd_2(L)](BF_4)_2 \cdot 2MeNO_2$ shows the binucleating macrocycle to be planar with intermolecular π-ring stacking.

In 1970, Robson and Pilkington reported the template synthesis of L^{2-}† around a series of first row transition metal ions.[1] Since then a wide range of metal complexes of L^{2-} and related compartmental ligands have been reported, their syntheses being based on *in situ* template condensation of dialdehydes and diamines in the presence of labile transition metal and main group metal ions.[2–5] Particular emphasis has been placed on the synthesis of polynuclear complexes of biological importance.[4] We wished to develop routes to platinum metal complexes of L^{2-}. In general, however, the

† L^{2-} is the dianion of 11.23-dimethyl-3.7.15.19-tetraazatricyclo[19.3.1.1^{9,13}]hexacosa-2.7.9.11.13(26).14.19.21(25).22.24-decaene-25.26-diol.

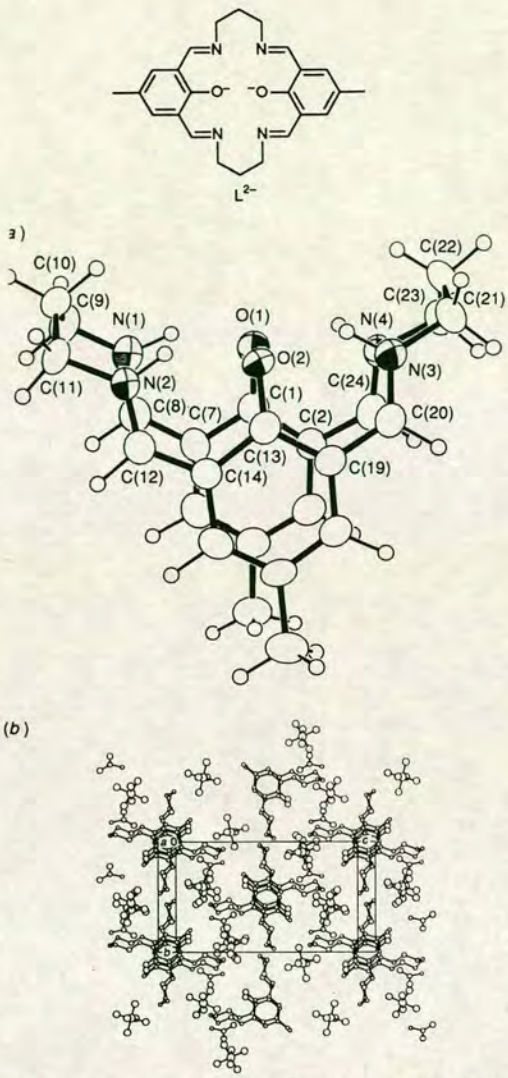

Fig. 1 (*a*) Structure of $[LH_4]^{2+}$ with numbering scheme adopted. (*b*) Packing diagram of $[LH_4](PF_6)_2 \cdot MeNO_2$.

synthesis of Schiff-base macrocyclic complexes incorporating relatively inert metal ions requires metal insertion into a preformed ligand.[6] We report herein the preparation of the metal-free compartmental ligand $[LH_4]^{2+}$ and the synthesis of a range of platinum metal complexes.

Reaction of 1,3-diaminopropane and 2,6-diformyl-4-methylphenol[7] in MeOH in the presence of 48% HBr followed by addition of Br_2[3] affords the insoluble salt $[LH_4](Br_3)_2$. Metathesis of this salt with NH_4PF_6 or $NaBF_4$ in MeOH affords the protonated 2 + 2 condensation species $[LH_4](PF_6)_2$ or $[LH_4](BF_4)_2$‡ as orange products. Red crystals of $[LH_4](PF_6)_2$ were grown from $MeNO_2$.§ The single crystal X-ray structure of $[LH_4](PF_6)_2$ shows [Fig. 1(*a*)] the protonated Schiff-base macrocycle to adopt a highly unusual folded conformation with the two phenyl rings involved in inter- and intra-molecular [Fig. 1(*b*)] stacking interactions. The conformation of $[LH_4]^{2+}$ is reminiscent of that of calixarenes[8] and related Schiff-base macrocycles[5] with the ring folded downwards to leave the N- and O-donor atoms on an exposed face.

$[LH_4](PF_6)_2$ and $[LH_4](BF_4)_2$ are useful starting materials for the synthesis of complexes of inert metal ions such as those of the platinum metal group. Thus, reaction of $[LH_4](BF_4)_2$ with MCl_2 (M = Pt, Pd) or $[Pd(OAc)_2]_3$ in the presence of a tenfold molar excess of Et_3N in MeCN affords $[M_2(L)]^{2+}$ (M = Pd, Pt) in up to 75% yield. Reaction with $RhCl_3 \cdot 3H_2O$ with one molar equivalent of $TlPF_6$ under the same conditions affords $[Rh_2Cl_4(L)]$.‡ Crystals of $[Pd_2(L)](BF_4)_2 \cdot 2MeNO_2$ were grown from $MeNO_2$–Et_2O and a single crystal X-ray structural determination undertaken.¶ The structure of the complex shows [Fig. 2(*a*)] each square planar Pd^{II} centre bound to two O-donors, Pd–O(1) 2.016(4), Pd–O(1a) 2.014(4) Å, and to two N-donors, Pd–N(1) 1.981(4), Pd–N(2) 1.993(4) Å, <O(1)–Pd–N(1) 93.30(17), <O(1)–Pd–N(2) 170.34(17), <N(1)–Pd–N(2) 96.36(18), <O(1)–Pd–O(1a) 77.13(15), <Pd–O(1)–Pd(a) 102.88(16)°. The Pd–Pd(a) distance is 3.1511(6) Å. In contrast to the folded conformation of the protonated ligand $[LH_4]^{2+}$, the macrocycle in $[Pd_2(L)]^{2+}$ is highly planar, thus removing the possibility of intramolecular π–π interaction between phenyl rings.

‡ Products have been characterised by elemental analyses, and by NMR, IR, electronic and FAB (fast atom bombardment) mass spectroscopy.

§ *Crystal data* for: $C_{24}H_{30}N_4O_2^{2+}2PF_6^- \cdot MeNO_2$, M = 757.35, monoclinic, space group $P2_1/c$, a = 14.4770(6), b = 11.2662(12), c = 20.0823(20) Å, β = 97.213(7)°, V = 3250 Å^3 [from 2θ values of 26 reflections measured at ±ω (2θ = 24–26°, $\bar{\lambda}$ = 0.71073 Å), T = 298 K], Z = 4, D_c = 1.548 g cm^{-3}, μ(Mo-Kα) = 0.235 mm^{-1}. A red block (0.36 × 0.28 × 0.24 mm) was mounted on a Stoë Stadi-4 four-circle diffractometer. Data collection using Mo-Kα X-radiation ($\bar{\lambda}$ = 0.71073 Å), ω–2θ scans and the learnt-profile method[9] gave 5313 reflections ($2\theta_{max}$ 45°), 4250 unique (R_{int} 0.074), of which 2833 with $F \geq 4\sigma(F)$ were used in all calculations. Following solution by automatic direct methods,[10] the structure was refined by full-matrix least-squares (on F), with anisotropic thermal parameters for all non-H atoms; methyl groups were treated as rigid entities, while other H atoms were included in fixed, calculated positions.[11] At final convergence, R = 0.0578, R_w = 0.0791, S = 1.337 for 455 parameters and the final ΔF synthesis showed no feature above 0.43 e Å^{-3}.

¶ *Crystal data* for $C_{24}H_{26}N_4O_2Pd_2^{2+}2BF_4^- \cdot 2MeNO_2$, M = 911.03, triclinic, space group $P\bar{1}$, a = 7.545(4), b = 8.566(4), c = 13.057(7) Å, α = 101.30(4), β = 94.82(3), γ = 102.92(3)°, V = 799.2 Å^3 [from 2θ values of 26 reflections measured at ±ω (2θ = 24–28°, $\bar{\lambda}$ = 0.71073 Å), T = 150.0(1) K], Z = 1 (implying that each dication lies across a crystallographic inversion centre), D_c = 1.892 g cm^{-3}, μ(Mo-Kα) = 1.205 mm^{-1}. A brown tablet (0.23 × 0.19 × 0.12 mm) was mounted on a Stoë Stadi-4 four-circle diffractometer equipped with an Oxford Cryosystems low-temperature device.[12] Data collection using Mo-Kα X-radiation ($\bar{\lambda}$ = 0.71073 Å), ω–2θ scans and the learnt-profile method[9] gave 2700 reflections ($2\theta_{max}$ 45°), 2045 unique (R_{int} 0.024), of which 1950 with $F \geq 4\sigma(F)$ were used in all calculations. Following identification of the Pd position from a Patterson synthesis, iterative cycles of least-squares refinement and difference Fourier synthesis located the remaining non-H atoms. Slight disorder in the anion was modelled by refining two idealised BF_4^- tetrahedra with a common B-atom (major occupancy 0.89, minor occupancy 0.11). The structure was refined by full-matrix least-squares (on F), with anisotropic thermal parameters for all non-H atoms except the F atoms with the minor occupancy; methyl H atoms were treated as part of rigid groups while other H atoms were included in calculated positions.[11] At final convergence, R = 0.0348, R_w = 0.0423, S = 1.131 for 238 parameters and the final ΔF synthesis showed no feature above 1.21 e Å^{-3}. Atomic coordinates, bond lengths and angles, and thermal parameters for both compounds have been deposited at the Cambridge Crystallographic Data Centre. See Notice to Authors, Issue No. 1.

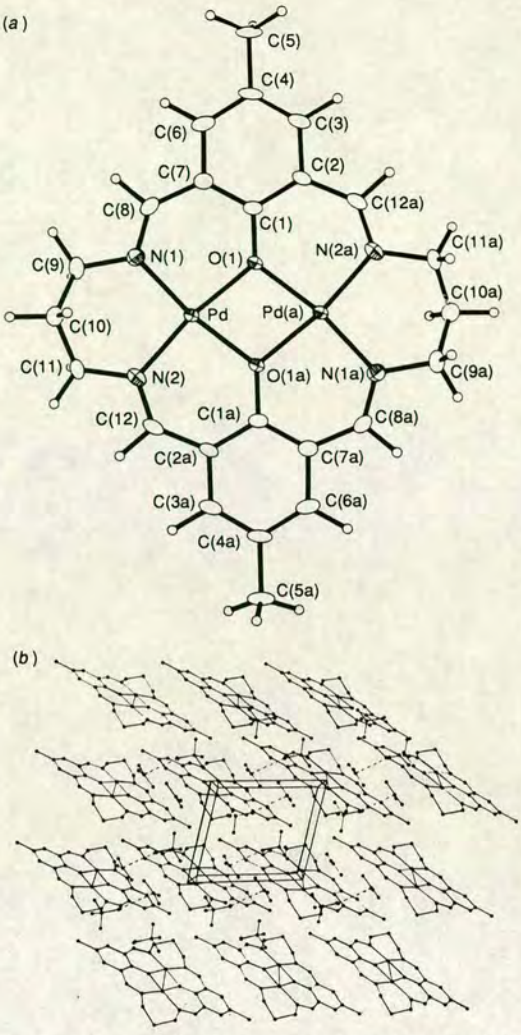

Fig. 2 (*a*) Structure of $[Pd_2(L)]^{2+}$ with numbering scheme adopted. (*b*) Packing diagram of $[Pd_2(L)](BF_4)_2 \cdot 2MeNO_2$.

However, intermolecular stacking of the phenyl rings occurs in the solid state to give a staggered array of cations [Fig. 2(b)].

The salt $[LH_4](Br_3)_2$ is not as useful a starting material for the preparation of these complexes as the PF_6^- or BF_4^- salts owing to its relative insolubility and competition reactions with Br^- ion during metal insertion reactions. However, direct condensation of 1,3-diaminopropane with 2,6-diformyl-4-methylphenol in thf (tetrahydrofuran) affords a yellow product containing the free binucleating ligand $[LH_2]$. However, some free aldehydic and free amine containing impurities are usually observed in these readily hydrolysed materials. Current work is aimed at an investigation of the redox properties of the binuclear complexes of L.

We thank the SERC for support, Johnson-Matthey Plc and the SERC for a CASE Award (to A. J. A.), and the Royal Society of Edinburgh and Scottish Office Education Department for a Support Research Fellowship (to M. S.). We thank Professor H. Okawa (Kyushu University), Professor R. Robson (University of Melbourne) and Dr P. Chaudhuri (Ruhr Universität, Bochum) for helpful discussions and for communicating unpublished results to us.

Received, 26th October 1992; Com. 2/05693C

References

1 N. H. Pilkington and R. Robson, *Aust. J. Chem.*, 1970, **23**, 2225.
2 For example see: H. Okawa and S. Kida, *Bull. Chem. Soc. Jpn.*, 1972, **45**, 1759; B. F. Hoskins and G. A. Williams, *Aust. J. Chem.*, 1975, **28**, 2607; 1975, **28**, 2593; R. R. Gagné, L. M. Henling and T. J. Kistenmacher, *Inorg. Chem.*, 1980, **19**, 1226; R. R. Gagné, C. L. Spiro, T. J. Smith, C. A. Hamann, W. R. Thies and A. K. Shiemke, *J. Am. Chem. Soc.*, 1981, **103**, 4073; C. L. Spiro, S. L. Lambert, T. J. Smith, E. N. Duesler, R. R. Gagné and D. N. Hendrickson, *Inorg. Chem.*, 1981, **20**, 1229; R. C. Long and D. N. Hendrickson, *J. Am. Chem. Soc.*, 1983, **105**, 1513; S. K. Mandal, L. K. Thompson, K. Nag, J.-P. Charland and E. J. Gabe, *Inorg. Chem.*, 1987, **26**, 1391; D. Luneau, J.-M. Savariault, P. Cassoux and J.-P. Tuchagues, *J. Chem. Soc., Dalton Trans.*, 1988, 1225; V. McKee and S. S. Tandon, *J. Chem. Soc., Chem. Commun.*, 1988, 385; M. Tadokoro, H. Sakiyama, N. Matsumoto, H. Okawa and S. Kida, *Bull. Chem. Soc. Jpn.*, 1990, **63**, 3337; M. Tadokoro, H. Okawa, N. Matsumoto, M. Koikawa and S. Kida, *J. Chem. Soc., Dalton Trans.*, 1991, 1657; M. Tadokoro, H. Sakiyama, N. Matsumoto, M. Kodera, H. Okawa and S. Kida, *J. Chem. Soc., Dalton Trans.*, 1992, 313; K. K. Nanda, R. Das, M. J. Newlands, R. Hynes, E. J. Gabe and K. Nag, *J. Chem. Soc., Dalton Trans.*, 1992, 897 and references cited therein.
3 B. F. Hoskins, R. Robson and G. A. Williams, *Inorg. Chim. Acta*, 1976, **16**, 121.
4 D. E. Fenton, in *Perspectives in Coordination Chemistry*, ed. A. F. Williams, C. Floriani and A. E. Merbach, VCH Publishers, Weinheim, 1992, p. 203; D. E. Fenton, *Advances in Inorganic and Bioinorganic Mechanisms*, ed. A. G. Sykes, Academic Press, London, 1983, p. 1492. For example see: H. Adams, N. A. Bailey, M. J. S. Dwyer, D. E. Fenton, P. C. Hellier and P. D. Hempstead, *J. Chem. Soc., Chem. Commun.*, 1991, 1297.
5 N. A. Bailey, D. E. Fenton, P. B. Roberts and A. M. Walford, *J. Chem. Soc., Dalton Trans.*, 1987, 1865; S. S. Tandon and V. McKee, *J. Chem. Soc., Dalton Trans.*, 1989, 19; 1991, 221.
6 For example: A. J. Blake, T. I. Hyde, R. S. E. Smith and M. Schröder, *J. Chem. Soc., Chem. Commun.*, 1986, 334.
7 F. Ullman and K. Brittner, *Berichte*, 1909, **42**, 2539.
8 *Calixarenes*, ed. C. D. Gutsche, Royal Society of Chemistry, Cambridge, UK, 1989.
9 W. Clegg, *Acta Crystallogr., Sect. A.*, 1981, **37**, 22.
10 SHELX86, G. M. Sheldrick, University of Göttingen, Germany, 1986.
11 SHELX76, G. M. Sheldrick, University of Cambridge, England, 1976.
12 J. Cosier and A. M. Glazer, *J. Appl. Crystallogr.*, 1986, **19**, 105.